BIOGEOCHEMISTRY OF MARINE DISSOLVED ORGANIC MATTER: MOLECULAR COMPOSITION, REACTIVITY AND NEW METHODS

Dissertation zur Erlangung eines

Doktors der Naturwissenschaften

– Dr. rer. nat. –

vorgelegt von

Oliver J. Lechtenfeld

am 22.10.2012

an der Universität Bremen

im Fachbereich Biologie/Chemie.

Gutachter:

1. Prof. Dr. Gerhard Kattner

2. Prof. Dr. Allan Cembella

Kolloquium: 16.11.2012

ACKNOWLEDGEMENTS

I am truly indebted and thankful to my doctoral advisors Prof. Gerhard Kattner and Prof. Boris Koch. They introduced me to a highly exciting and demanding scientific topic: marine organic and inorganic chemistry. They opened up the opportunities for me to broaden my expertise as an analytical chemist by working on and with state-of-the art techniques. The application of these techniques to a fascinating topic within environmental sciences was new for me and I thank Gerhard and Boris for offering me this opportunity.

Both my doctoral advisors always offered their time and support whenever I needed them to help and discuss scientific questions on and outside of my work topic. Moreover, they gave me the freedom to pursue my own ideas and realizations. In my opinion such preconditions are essential for being able to successfully accomplish a dissertation in natural sciences.

I also wish to thank Prof. Allan Cembella to accept without hesitation reviewing my dissertation thesis. His input broadened the overall scope of my work by highlighting the bio-ecological perspective. Moreover, I would like to thank Prof. Wolfram Thiemann for being part of my dissertation committee.

My special thanks go to my PhD colleague Ruth Flerus. Together, we spent a lot of time in various offices, labs, and on ships; discussing data, struggling with experiments or with science as a whole during New Years Eve night CTD shifts – Chococino always lifted our mood.

Furthermore, I am much obliged to all my colleagues from the “Marine Chemistry” working group at the Alfred-Wegener-Institute in Bremerhaven, namely Steffi Baßler, Claudia Burau, Ivan Dubinenkov, Ruth Flerus, Martin Graeve, Dieter (DJ) Janssen, Gerhard Kattner, Mandy Kiel, Boris Koch, Kai-Uwe (KUL) Ludwichowski, Kevin Völker, Marthi Wolff and Ying Wu. They all supported me with their expertise, reliability and helpfulness and hence have a great share of the completion and outcome of this thesis. But what counts just as much for me is the

great fun we had during the last couple of years. It was a wonderful time working with you and I thank you all for that!

This dissertation would not have been possible without the help of many people outside my own working group. In particular, I appreciate Ingrid Stimac and Matthias Witt for their dedication to and help with the ICP-MS and FT-ICR MS and Walter Geibert and Michiel Rutgers van der Loeff for always having answers to my frequent questions and setting new impulses and inspirations to my work.

Last but not least, I am grateful for the efforts of Jelle Bijma, Dörte Burhop, Claudia Hanfland, and Claudia Sprengel as representatives of the graduate school POLMAR. It is definitely an invaluable program for any PhD student. There is also a world outside!

My dissertation was funded by the “Deutsche Forschungsgemeinschaft”, DFG, within the priority program “Antarctic Research”.

TABLE OF CONTENTS

ABSTRACT

Dissolved organic matter (DOM) is an ultimate chemical product of all life on earth. It integrates energy, carbon dioxide and nutrients into a vast compositional and structural variety of molecules — further modified by biological, chemical, and physical processes. In the ocean, organic matter production depends mainly on the photosynthetic activity of autotrophs and most of it is immediately consumed and respired by heterotrophs. Some of this fresh organic matter, however, escapes immediate turnover and accumulates in dissolved form in the entire water column. During isopycnal transport and seasonal convective overturn, microbial, photochemical, and physical processes remove most of the fresh DOM. The remaining organic matter is an old, chemically poorly characterized heterogeneous mixture of small, partially oxidized and unsaturated molecules: refractory DOM.

The main topic of this thesis is the chemical characterization of DOM: elemental composition and reactivity with regard to environmental boundary conditions as well as causalities of persistence. All studies involved substantial chemical and physical gradients of temperature, pressure, salinity, irradiation, biological communities, and nutrients. These gradients allowed for testing the main research hypotheses with different end members to obtain functional relationships between the physico-chemical variables and the observed properties of DOM. Different methods were applied to achieve these aims. High resolution inorganic and organic mass spectrometry, chromatography, statistical analysis and modeling were performed on samples obtained from oceanic research cruises. Additional seasonal surveys in an estuarine system and experimental setups addressed the influence of the various physico-chemical boundary conditions on the chemical composition and phase distribution of DOM. The most comprehensive study of this work included more than 200 samples from the tropical to the polar open ocean and from the surface to the seafloor and represents the so far largest consolidated dataset for ultrahigh resolution organic mass spectrometry in the ocean.

A method was established that enabled for the first time separation and quantification of organic phosphorus and sulfur in marine DOM in a coupled chromatography – mass spectrometry system. It was shown that the compositional diversity of DOM, i.e., the contributions from the heteroatoms phosphorus and sulfur, was reflected in the chemical properties of the molecules as revealed by polarity separation. Further, the method was shown to be applicable for determining metal ions that are also part of the chemical entity of DOM. However, not all investigated metal ions showed a strong and selective affinity for organic matter, e.g., uranium. A rare isotope of uranium, ^{236}U, determined for the first time in an oceanic depth profile, was demonstrated to be a suitable transient tracer in oceanographic studies, reflecting an anthropogenic marker for water mass circulation.

Very different compounds, surface active sulfonic acids, were identified as part of the total DOM pool in a sea surface microlayer study. Although sulfonic acids are widely known as potential contaminants in surface waters, this study demonstrated the analytical capability of ultrahigh resolution organic mass spectrometry and fragmentation to study thousands of DOM molecules and their responses to changing physico-chemical conditions, e.g., the ionic strength of the aqueous phase. An even deeper insight into the composition and long-term transformation of DOM was achieved by comparing the molecular signatures of DOM samples from the East Atlantic and Southern Ocean. Using statistical tools, it was demonstrated that distinct patterns of mass peak magnitude changes could be related to the consecutive ageing of this mixture of molecules. A modeling of the degradation rates of individual DOM molecules demonstrated that the chemical composition of the bulk DOM changes with age towards a proposed “island of stability”. The broad distribution of these degradation rates is proposed as an extension of the contemporary perception of marine DOM cycling and reworking.

Bringing together inorganic and organic biogeochemistry as well as (molecular) microbiology to study the complex biogeochemical interactions in the ocean will be an important future research direction in marine sciences. The combined efforts from multidisciplinary research groups are a prerequisite to resolve the unanswered questions on the response of the microbial communities, the fate of anthropogenic carbon dioxide, the chemical processes and equilibria in the ocean, and their crucial feedback mechanisms in a changing climate.

ZUSAMMENFASSUNG

Gelöstes organisches Material (DOM) ist ein chemisches Endprodukt aller Lebensformen auf diesem Planeten. Energie, CO_2 und Nährstoffe werden zu einer enormen molekularen Vielfalt an Verbindungen und Strukturen verbunden, die durch biologische, chemische und physikalische Prozesse wieder modifiziert werden. Die Produktion von organischem Material im Ozean wird durch die Photosynthese-aktivität von autotrophen Organismen gesteuert wobei der überwiegende Teil des frischen organischen Materials unmittelbar von heterotrophen Lebewesen veratmet und verstoffwechselt wird. Eine kleine Menge DOM entgeht jedoch der sofortigen Umsetzung und akkumuliert in gelöster Form in der gesamten Wassersäule. Während des konvektiven Transports oder saisonaler Durchmischung im Meer bauen mikrobielle, photochemische und physikalische Prozesse den größten Teil des frischen DOMs ab. Das übrig bleibende Material besteht aus einer chemisch schlecht charakterisierten, heterogenen Mischung aus kleinen, teilweise oxidierten und ungesättigten Molekülen, dem refraktären DOM.

Im Mittelpunkt dieser Arbeit steht daher die chemische Charakterisierung von DOM: Elementzusammensetzung und Reaktivität unter Berücksichtigung der natürlichen Rahmenbedingungen sowie Ursachen von Persistenz. Alle Studien umfassen erhebliche chemische und physikalische Gradienten wie Temperatur, Druck, Salinität, solare und radioaktive Strahlung, biologische Gemeinschaften und Nährstoffangebot. Diese Gradienten ermöglichten es, dass die grundlegenden Hypothesen dieser Arbeit an verschiedenen Endgliedern getestet werden konnten, um dadurch funktionale Beziehungen zwischen den physikalisch-chemischen Variablen und den beobachteten Eigenschaften des DOM zu erhalten. Zu diesem Zweck wurden Proben auf Forschungsausfahrten gesammelt und mit diversen analytischen Methoden vermessen und ausgewertet, z.B. hochauflösende anorganische und organische Massenspektrometrie, Chromatographie, Statistik und Modellierung. Zusätzliche saisonale Studien in einem Ästuarsystem und weitere Laborexperimente unterstützten die Untersuchungen zur chemischen

Zusammensetzung des DOM sowie zur Partitionierung innerhalb unterschiedlicher physikalischer Phasen, in denen DOM im Ozean und angrenzender Bereiche vorkommen kann. Die umfangreichste Studie dieser Arbeit beinhaltete mehr als 200 Proben vom tropischen bis hin zum polaren offenen Ozean sowie von der Oberfläche bis zum Meeresboden und stellt damit den bis dato größten zusammenhängenden Datensatz von ultrahochauflösender organischer Massenspektrometrie im Ozean dar.

Die Entwicklung einer neuen, gekoppelten Chromatographie – Massenspektrometrie Methode ermöglichte erstmalig die Trennung und Quantifizierung von organischem Phosphor und Schwefel im DOM. Durch eine polaritätsbasierte Trennung konnte gezeigt werden, dass sich die molekulare Zusammensetzung des DOM, vor allem die Beiträge der Heteroatome Phosphor und Schwefel, in den chemischen Eigenschaften der DOM-Fraktionen widerspiegelt. Dies beeinflusste auch das chemische Verhalten gegenüber anderen Teilen des DOM, wie z.B. Metallionen, die mit der neuen Methode ebenfalls für biogeochemische Analysen zugänglich werden. Ein seltenes Uranisotop, ^{236}U, wurde zum ersten Mal in einem ozeanischen Tiefenprofil bestimmt und konnte als geeigneter „transient tracer“ (Spurenstoff mit zeitabhängiger Konzentration) für z.B. Wassermassenzirkulation verwendet werden.

Andere Stoffe wie z.B. oberflächenaktive Sulfonsäuren wurden als Teil des gesamten DOMs in einer Studie zu organischen Oberflächenfilmen identifiziert. Obwohl diese Stoffe weithin als mögliche Kontaminationen von Oberflächenwasser bekannt sind, zeigte diese Studie auch das Potential von ultrahochauflösender organischer Massenspektrometrie mit zusätzlicher Fragmentierung für die Untersuchung von tausenden von DOM Molekülen auf. Unterschiedliche physikalisch-chemische Bedingungen, wie z.B. die Ionenstärke der wässrigen Phase, beeinflusste die Partitionierung von verschiedenen Stoffklassen zwischen hydrophobem Oberflächenfilm und hydrophilem Wasserkörper. Ein noch tieferer Einblick in die Zusammensetzung und die langfristigen Veränderungen von DOM gelang durch einen Vergleich der molekularen Signaturen vom östlichen Atlantik und dem Südozean. Mit Hilfe statistischer Methoden konnte gezeigt werden, dass bestimmte Muster von molekularen Veränderungen mit der fortlaufenden Alterung der Mischung korrelieren. Eine Modellierung der Abbauraten einzelner DOM

Moleküle zeigte weiterhin, dass sich die chemische Zusammensetzung des gesamten DOM mit zunehmendem Alter hin zu einer möglichen „Insel der Stabilität“ verändert. Die kontinuierliche Verteilung der Abbauraten des DOM stellt eine Erweiterung des aktuellen Konzepts vom DOM-Kreislauf im Ozean dar.

Eine zukünftige Entwicklung in der meereswissenschaftlichen Forschung wird die Kombination und Integration von anorganischer und organischer Biogeochemie sowie (molekularer) Mikrobiologie sein, um die komplexen Interaktionen im Ozean untersuchen zu können. Die gemeinsamen Anstrengungen multidisziplinärer Forschungsgruppen sind eine wichtige Voraussetzung, um die ungelösten Fragen in Bezug auf den Klimawandel und dessen Auswirkungen auf mikrobielle Gemeinschaften, den Verbleib des anthropogenen CO_2, die chemischen Prozesse und Gleichgewichte im Ozean sowie aller wichtigen Rückkopplungsmechanismen zu beantworten.

ABBREVIATION LIST

16S rRNA	16S ribosomal ribonucleic acid
AABW	Antarctic Bottom Water
AAIW	Antarctic Intermediate Water
AASW	Antarctic Surface Water
ACC	Antarctic Circumpolar Current
AMS	Accelerator mass spectrometry
AOM	Atmospheric organic matter
APPI	Atmospheric pressure photo ionization
AR	Agulhas ring
BATS	Bermuda Atlantic Time-series Study
BGE	Bacterial growth efficiency
BP	Bacterial production
CDOM	Colored dissolved organic matter
CDW	Circumpolar Deep Water
CE	Capillary electrophoresis
CFC	Chlorofluorocarbon
CHO	Carbohydrate
CID	Collision induced dissociation
CLIVAR	Climate Variability and Predictability
CPI	Carbon Preference Index
CRAM	Carboxyl-rich alicyclic molecules
CSV-CLE	Competing ligand equilibration - cathodic stripping voltammetry
CTD	Conductivity temperature depth
D(C/F)AA	Dissolved (combined/free) amino acids
DAD	Diode array detector
DBE	Double bond equivalent
DIC	Dissolved inorganic carbon
DIP	Dissolved inorganic phosphorus

DMS	Dimethyl sulfide
DMSO	Dimethyl sulfoxide
DMSP	Dimethylsulfoniopropionate
DOC/N/P/S	Dissolved organic carbon / -nitrogen / -phosphorus / -sulfur
(L-/SL-/SR-/R-) DOM	(Labile / semi-labile / semi-refractory / refractory) dissolved organic matter
DPM	Disintegrations per minute
DSR	Deep sea reference standard
DWBC	Deep Western Boundary Current
EA	East Atlantic
EF	Enrichment factor
EPS	Extracellular polymeric substances
ESI	Electrospray ionization
FLD	Fluorescence detector
FT-ICR MS	Fourier transform ion cyclotron resonance mass spectrometry
GC	Gas chromatography
GDGT	Glycerol dibiphytanyl glycerol tetraethers
GEOSECS	Geochemical Ocean Section Study
GMR	Geometric Mean Regression
GPP	Gross (or global) primary production
HNLC	High nutrient - low chlorophyll
HOT	Hawaii Ocean Time-series
ICP-MS	Inductively coupled plasma mass spectrometry
I_{DEG}	Degradation state index
IDMS	Isotope dilution mass spectrometry
IODW	Indian Ocean Deep Water
IOIW	Indian Ocean Intermediate Water
IOS	Island of stability
KHP/PHP	Potassium hydrogen phthalate
LAS	Linear alkylbenzenesulfonate
LCDW	Lower Circumpolar Deep Water
LD-PE	Low density polyethylene
LPS	Lipopolysaccharide

LSSW	Low salinity shelf water
MCP	Microbial carbon pump
MUC	Molecular uncharacterized component
(H/L) MW	(High / low) molecular weight
N(E)ADW	North (East) Atlantic Deep Water
NCP	North Central Pacific
NEG	$\Delta^{14}C$ negatively correlating peaks
NMR	Nuclear magnetic resonance
NMWC	Nominal molecular weight cutoff
NOM	Natural organic matter
NPP	Net primary production
NSW	North Sea Water
PAR	Photosynthetically active radiation
PCA	Principal component analysis
PDB	Pee Dee Belemnite
PDW	Pacific Deep Water
PEEK	Polyether ether ketone
PETM	Paleocene-Eocene Thermal Maximum
(N/S) PF	(North/South of the) Polar Front
PFA	Perfluoroalkoxy copolymer
POC/M/N	Particulate organic carbon/matter/nitrogen
POS	$\Delta^{14}C$ positively correlation peaks
PTFE	Polytetrafluoroethylene
(RP-) HPLC	(Reversed phase-) high performance liquid chromatography
(R-)SD	(Relative-) standard deviation
SACW	South Atlantic Central Water
SAMW	Subantarctic Mode Water
SAR	South Atlantic Region
SAS	Surface active substances
SCOR	Scientific Committee on Oceanic Research
SEC	Size exclusion chromatography
SML	Surface Mixed Layer / Surface Microlayer
SO	Southern Ocean
SOUR	Southern Ocean Ultra-Refractory compounds

SPE	Solid phase extraction
SST	Sea surface temperature
TDP	Total dissolved phosphorus
TEP	Transparent exopolymer particles
TEX_{86}	Tetraether index
THAA	Total hydrolysable amino acids
THAS	Total hydrolysable amino sugars
THC	Thermohaline circulation
THNS	Total hydrolysable neutral sugars
TOC/N	Total organic carbon / -nitrogen
TOM	Terrestrial organic matter
UDOM	Ultrafiltered dissolved organic matter
ULW	Underlying water
WDW	Warm Deep Water
WG	Weddell Gyre
WOCE	World Ocean Circulation Experiment
WSDW	Weddell Sea Deep Water

I INTRODUCTION

Chemical characterization and biogeochemical transformation of dissolved organic matter (DOM) is the main research focus within this thesis. DOM needs to be thoroughly defined as many definitions have been used in the past to describe this heterogeneous mixture of matter. The introductory chapter puts the topic in a general context and aims at giving basic definitions of the most important terminology used throughout this work.[1] The second chapter sorts existing definitions according to chemical and physical measures. This categorization will be partially overruled with the discussion of the various sources and sinks in Chapter III. A summary of key questions in DOM research are presented in Chapter IV followed by the main objectives for this thesis in Chapter V. As amendment to the five publications, a general discussion and outlook are rounding off this thesis. Due to the large body of work in the field of DOM, only the subjectively most important aspects are compiled for the introductory chapters with a focus on the most recent literature.

[1] Many definitions for substances or compound classes which are adopted by environmental scientists have a somewhat broader range of definition than usually accepted in other chemistry disciplines. Wherever possible, a concretization of terminology is provided.

What is dissolved organic matter and why does it matter?

Organic compounds are generally defined as any chemical compound of carbon and hydrogen with other non-metals that form covalent bonds. Excluded from this definition are therefore carbon-containing salts, such as carbonates (e.g., $CaCO_3$) and simple oxides (e.g., CO_2, COS), although this distinction is more historic than systematic. Natural organic matter (NOM) comprises organic compounds that were initially formed by life but may have undergone multiple alterations and degradation processes.[2] The most important carbon source for the formation of NOM is carbon dioxide (CO_2) and the energy for the breakage of the C-O bonds is supplied by sunlight (i.e., the photosynthetically active radiation, PAR), although other sources of carbon and energy exist. NOM may therefore be classified into photoautotrophic organic matter (from $CO_2 + h \times v$)[3] and chemo-autotrophic organic matter ("dark" organic matter) and is often referred to as "reduced carbon", as the carbon atoms in NOM have on average a lower oxidation state than the CO_2 carbon.

For quantitative purposes, the carbon content of NOM is referred to as organic carbon (OC) and normalized to moles of carbon per volume or weight unit ($mol \times L^{-1} = M$ or $mol \times kg^{-1}$).[4] Although carbon and hydrogen are the specifying and structure-determining elements of NOM, molecules typically incorporate other elements that are covalently bound to carbon (generally referred to as heteroatoms). NOM is therefore a generic term comprising *inter alia* OC, organic nitrogen (ON), organic sulfur (OS), organic phosphorus (OP) and metals. The latter often form "metal-organic complexes" where a metal atom or ion is covalently bound to an organic ligand. It is obvious that all of the sub-pools of NOM greatly overlap and a single molecule can contribute to, e.g., OC and ON.

NOM can further be classified according to the source (e.g., from land plants: terrestrial NOM, or from ocean phytoplankton: marine NOM) or environmental

[2] An intermediate compound class between organic and inorganic is kerogen, found in sedimentary rocks. Its source is clearly living biomass but it has encountered geologic forces for extended periods of time, resulting in the formation of "geopolymers" (Killops and Killops 2005).

[3] Reducing here the enormous complexity of the photosynthetic carbon fixation, the actual reduction of CO_2 is realized in the Calvin cycle (Bassham et al. 1950). The reaction mechanism is "light-independent", but controlled by the light-depended oxidation of water and is therefore only active when light is available.

[4] In most mathematical formulas within this thesis the "×" is used as mathematical symbol for algebraic multiplication. The typeset of units is instead a juxtaposition.

compartment (e.g., atmospheric, soil, and sediment NOM), defining distinct pools of organic carbon. It is important to emphasize that all carbon pools are interconnected through the carbon cycle (Figure II.1-1). The links (i.e., fluxes) are composed of CO_2, natural organic matter and geologic processes (plate tectonics, catagenesis) on short, intermediate and long time scales.

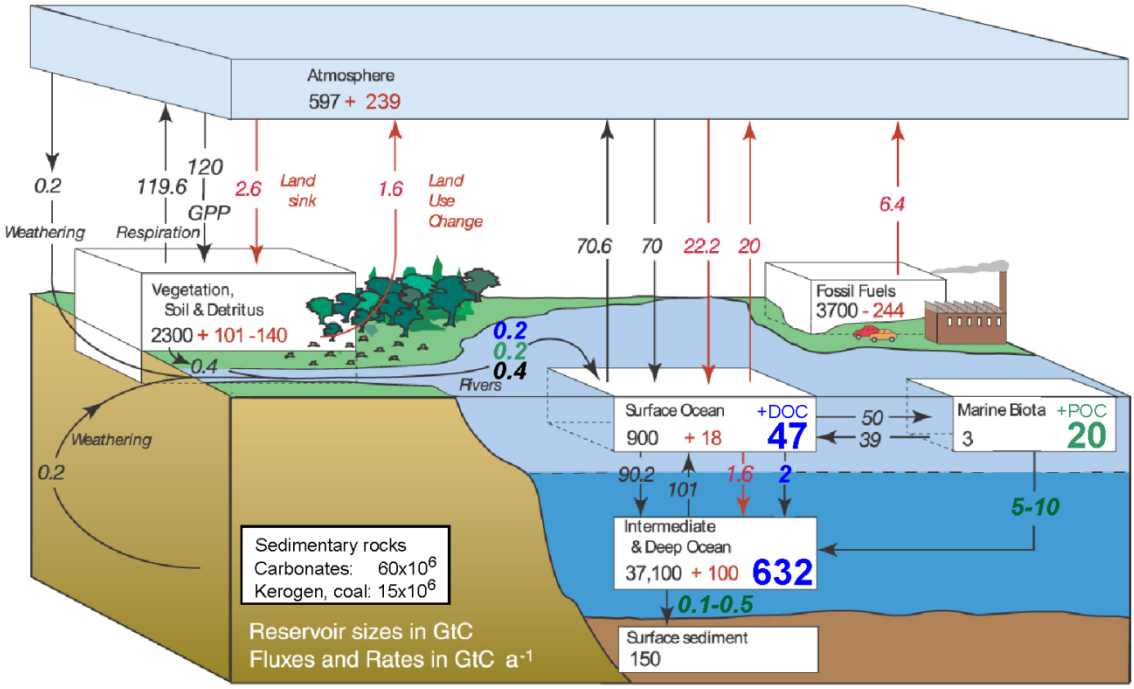

Figure II.1-1. The global carbon cycle.
The global carbon cycle at the end of the 1990's with preindustrial reservoir (pool) sizes, annual fluxes (black) and anthropogenic changes since ~ 1750 (red). Illustration modified from the 2007 IPCC report (Denman et al. 2007, their Figure 7.3). All reservoir size values are Gt carbon (Gt C) and fluxes are Gt C a^{-1}. Note that various numbers for all values exist in the literature and especially the rates of oceanic primary production and respiration differ greatly among different studies (e.g., Del Giorgio and Duarte 2002). Not included in the original figure was the "ocean organic carbon cycle" and important dissolved organic carbon (DOC) and particulate organic carbon (POC) fluxes and reservoirs are highlighted in blue and green (based on values from Berner (1989), Hedges (1992), Hedges et al. (1997), Gardner et al. (2006), Dunne et al. (2007), and Hansell et al. (2009)). Because of the reported uncertainties (not shown), the non-steady state of the system and different approaches to determine exact values, not all fluxes add to zero. For the transformation of organic carbon in the ocean interior see Figure III.3-1. In July 2012, the atmospheric inventory of CO_2 reached ≈ 836 Gt C (calculated from global mean of 392.4 ppmv CO_2 (Conway and Tans 2012) and a conversion factor of 2.13 (Clark 1982)). GPP = gross (terrestrial) primary production.

An operational definition divides NOM into “dissolved” and “particulate” phases where the differentiation between the two phases/pools is determined by the filter/membrane pore size (typically 0.1 – 1 µm). Due to the dominant categorization in the scientific community between dissolved and particulate forms, DOM will be generally referred to as the fraction of marine NOM that passes a filter of 0.7 µm nominal pore size.

Since atmospheric CO_2 and its role as greenhouse gas is nowadays of overwhelming importance for natural and social sciences,[5] much effort has been put into the understanding of the cycling of carbon between the various pools (Figure II.1-1). Especially the long-term deviation of carbon fluxes caused by anthropogenic perturbation is a focus of research.[6] In this context, the pool size of dissolved organic carbon (DOC: 662 ± 32 Pg, Hansell et al. 2012) is often compared with the atmospheric CO_2 content (Figure II.1-1) or the living biomass on land and in water (600 – 1000 Pg C, Falkowski et al. 2000). While this analogy certainly demonstrates the comparable size of the three pools, it is more an exemplification of the mere volume of the oceans rather than a useful basis for mass flux calculations. The significance of the marine organic matter pool is better highlighted with its property as an exchangeable pool of organic carbon. As such, it couples the quickly interchanging atmospheric CO_2 pool (the atmospheric lifetime of a single molecule is approximately 4 – 10 a, Craig 1957)[7] with the slow sedimentary organic carbon pool that cycles on geological timescales (millennia to millions of years). Interconnection of these pools in the ocean occurs predominantly in the surface ocean, where CO_2 rapidly exchanges between atmosphere and marine organic matter, but also at the water sediment interface, where part of the organic matter is stored for geological times and transported with the oceanic crust towards subduction zones.

The role of the ocean DOC inventory in the geological history of the earth (i.e., millions of years) is difficult to reconstruct simply because of the lack of (direct)

[5] The term “climate change” links to more than 6,000 articles in the scientific publication database “Web of Knowlegde[SM]”, and 114 million hits in the World Wide Web (search with Google, 06.09.2012).

[6] For a recent compilation of the scientific findings on the magnitudes and projections of global climate change see the Copenhagen Diagnosis (Allison et al. 2009). Note that the term “dissolved organic carbon/matter” does not even appear in this compilation, much alike the IPCC AR4 WG1 report (2007).

[7] The lifetime of a single molecule is different from the lifetime/residence time of additional anthropogenic CO_2 (perturbations) which is difficult to determine (e.g., Archer et al. 2009).

geological records.[8] Examples of proposed, though controversially discussed, causes for, e.g., the PETM (Paleocene-Eocene Thermal Maximum), and other more rapid warming events in the Eocene (56 – 34 Ma ago) include the massive release of greenhouse gases from permafrost soils or deep ocean reservoirs (DeConto et al. 2012) or the rapid and substantial remineralization of the ocean DOC inventory (Sexton et al. 2011). To trigger global temperature rises of up to 4 °C it is necessary that the ocean DOC pool was several times larger than today (see also Rothman et al. 2003; Ridgwell 2011). But still today, perturbations in the production and remineralization rates of the ocean organic carbon pools can have significant effects for the global carbon cycle with unknown climate feedback mechanisms (Falkowski et al. 1998; del Giorgio and Duarte 2002; Hopkinson and Vallino 2005).

Therefore, within the intermediate exchange rate of marine organic matter, DOM necessitates crucial reconsideration of its importance for the global carbon cycle. Besides small allochthonous sources (e.g., rivers and dust), autochthonous production of NOM in the surface ocean is dominated by photoautotrophs (marine phytoplankton), with minor contributions from photosynthetic heterotrophs and diazotrophs (mostly cyanobacteria). At a total annual new production of 7.2 pg OC, only ≈ 5 – 25% are estimated to resist immediate turnover (i.e., respiration of organic matter back to CO_2, Hansell and Carlson 1998b) and account for a production of new DOM in the surface ocean (Figure II.1-2). Advection and eventual downward transport of this DOM (with deep/bottom water formation or during seasonal convective overturn) removes a part of this fraction from contact with the atmosphere. Hence, apart from the physical/solubility carbon pump (i.e., downwelling of dissolved CO_2 at high latitudes) and the biological carbon pump (remineralization of sinking organic matter at depth), this DOM export mechanism in conjunction with a possible long-term sequestration as refractory components is being continuously discussed as a potential buffer for increased atmospheric CO_2 (Toggweiler 1988; Siegenthaler and Sarmiento 1993; Jiao et al. 2010). Whether the exportable fraction of DOM will increase (fast enough) with the expected global changes and compensate for the anticipated loss in buffer capacity of the oceans carbonate system (Sabine et al. 2004) is currently not known.

[8] The size of ancient ocean DOC pools is estimated from sedimentary carbonate ($\delta^{13}C$) isotopic mass balance.

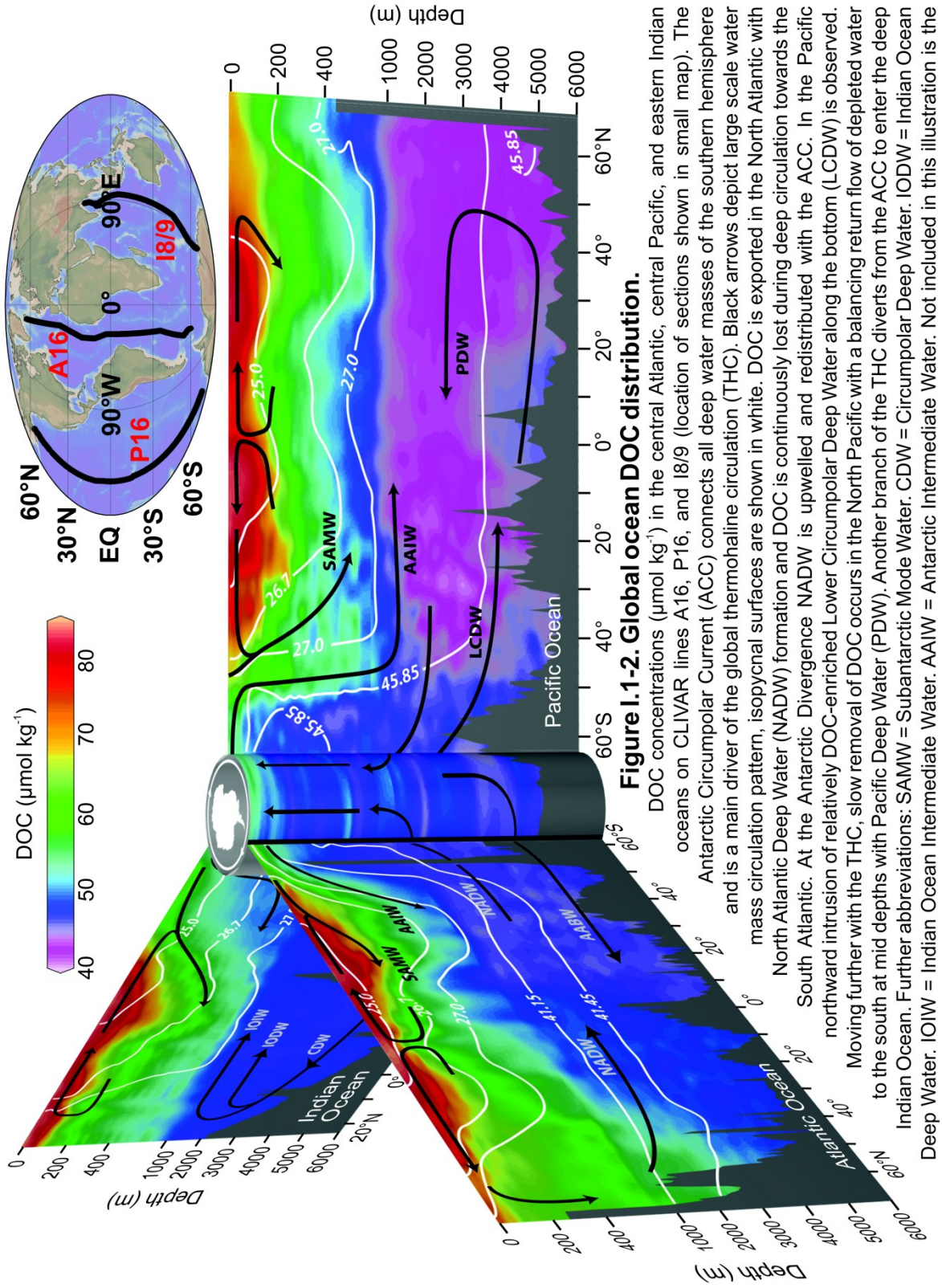

Figure I.1-2. Global ocean DOC distribution.
DOC concentrations (µmol kg^{-1}) in the central Atlantic, central Pacific, and eastern Indian oceans on CLIVAR lines A16, P16, and I8/9 (location of sections shown in small map). The Antarctic Circumpolar Current (ACC) connects all deep water masses of the southern hemisphere and is a main driver of the global thermohaline circulation (THC). Black arrows depict large scale water mass circulation pattern, isopycnal surfaces are shown in white. DOC is exported in the North Atlantic with North Atlantic Deep Water (NADW) formation and DOC is continuously lost during deep circulation towards the South Atlantic. At the Antarctic Divergence NADW is upwelled and redistributed with the ACC. In the Pacific northward intrusion of relatively DOC-enriched Lower Circumpolar Deep Water along the bottom (LCDW) is observed. Moving further with the THC, slow removal of DOC occurs in the North Pacific with a balancing return flow of depleted water to the south at mid depths with Pacific Deep Water (PDW). Another branch of the THC diverts from the ACC to enter the deep Indian Ocean. Further abbreviations: SAMW = Subantarctic Mode Water. CDW = Circumpolar Deep Water. IODW = Indian Ocean Deep Water. IOIW = Indian Ocean Intermediate Water. AAIW = Antarctic Intermediate Water. Not included in this illustration is the circulation in the Arctic Ocean. Adapted from Hansell et al. (2009) with permission from The Oceanography Society.

A major reason for this uncertainty is related to the mechanisms that transform primary production into DOM that resists further (rapid) reworking and remineralization. Remineralization usually refers to heterotrophic respiration, i.e., the complete oxidation of all carbon to CO_2. From the compositional heterogeneity and for stoichiometric reasons it is obvious that other products must be formed, e.g., nitrate, phosphate and ammonium. An incomplete remineralization may be termed “degradation” and is mostly accompanied with a loss of mass and chemical information. Reworking or alteration is a general term, if mechanisms and products of the transformation are unknown.

Although heterotrophic activity has been identified as the dominant mediator of NOM reworking (Azam et al. 1983; Azam 1998; Jiao et al. 2010), enzymatic pathways remain puzzling (Ogawa et al. 2001; Arnosti 2011; Kattner et al. 2011). From today’s perspective, it is the lack of knowledge about the chemical constituents that hinders the elucidation of transformation mechanisms. In other words: How should a (bio-)chemical pathway be identified, if neither the educt nor the product is known? It is this enigmatic nature of marine DOM that has challenged the scientific community since decades.

II PHYSICAL AND CHEMICAL PROPERTIES OF DOM

From the short and general description of the term “dissolved organic matter” in the introductory chapter, it is evident that DOM is an extremely complex, heterogeneous mixture of compounds and properties, spanning a wide range of sizes, energy contents and concentrations. None of these physical parameters are easily correlated, mainly because biological activity ultimately determines the distribution of matter within this pool. In this chapter, a formal classification of physical and chemical properties is compiled. Typical ranges of DOM for each property are given, together with a discussion of major problems encountered with each classification.

II.1 Mass and size

From a physical point of view, mass as a property of DOM is probably the easiest to define, as the mass of a molecule is the sum of the masses of its basic constituents, the atoms. However, measuring the mass of a single molecule requires substantial analytical effort — favorably accomplished with mass spectrometric techniques, where the mass to charge ratio of an ion is determined. Unfortunately, this analytical principle does not allow parallel collection of analytes, i.e., it cannot be used to fractionate a sample. A physical property which is closely related to mass is the size of a molecule, as every atom has a volume expansion, modified by the chemical binding in which it is integrated (here: the molecular volume in an electrolyte solution).

Figure II.1-1 shows the continuum of sizes of organic matter encountered in seawater. The upper limit for the size of DOM and the lower limit for the particulate phase (POC/POM) are determined by the pore size of the applied filter, typically 0.1 – 1 µm. The filter pore size is nominal, resulting in an upper size range. The particle retention specification of the widely used 0.7 µm Whatman™ GF/F filters is in a

range between 0.6 – 0.8 µm (98% retention level).[9] However, the dynamic pore size in the course of a filtration process can change substantially (Johnson and Wangersky 1985). The relatively large pore size of the borosilicate glass microfiber GF/F filters restricts the exact definition of DOM. First, almost all viruses and considerable amounts of bacteria and archaea are smaller than 0.7 µm and would be more efficiently retained at a pore size below 0.1 µm (e.g., Gasol and Moran 1999). However, the prokaryotic biomass, expressed as moles of carbon, is small compared to the total DOC and likely disintegrates as a result of acidification or organic solvent usage during sample treatment. Nevertheless, specific compound classes are enriched in e.g., bacteria (D-amino acids, muramic acid), and thus may bias the interpretation of dissolved constituents.

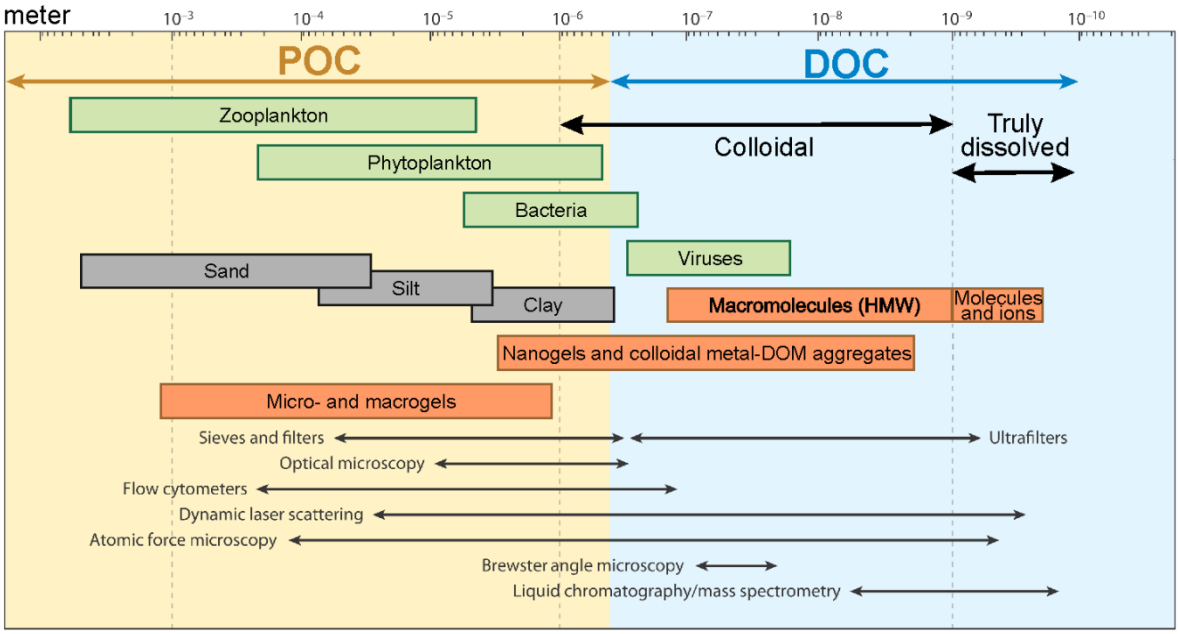

Figure II.1-1. Mass and size ranges.
Size ranges and scales in meters for different kinds of matter found in seawater. Living matter (green boxes), inorganic material (grey) and organic compounds (red) all overlap in the nano- to millimeter size range. Only single small molecules and ions occupy the low end of the scale. Operationally defined size classifications separate the continua of sizes into discrete fractions, where the colloidal and "truly" dissolved substances and smallest living cells are subsumed as the DOC fraction. The lower size limit for high molecular weight (HMW-) DOM is 1 nm or approximately 1000 Da. Gels are self-assembling aggregates of organic matter of various sizes and also incorporate nutrient- and metal ions. Common methods to separate or analyze the size fractions are shown in the lower part of the figure. Adapted from Verdugo et al. (2004) with permission from Elsevier and modified after Hedges (2002).

[9] http://www.whatman.com/GlassMicrofiberBinderFree.aspx.

Ultrafiltration techniques are used to distinguish DOM, depending on the membrane pore size, into a high molecular weight (HMW) and a low molecular weight (LMW) fraction (e.g., Benner et al. 1992; Kaiser and Benner 2009; Young and Ingall 2010). In this context, it is important to notice that although it is common practice to discriminate molecules in ultrafiltration techniques in Da (a non-SI unit of molecular mass), the true retention is defined by the specific volume of molecules. Thus, a nominal molecular weight cut-off (NMWC) of, e.g., 1000 Da refers to the size of a globular protein, of which 90% is retarded by the membrane after a twofold concentration.[10] For DOM molecules comprising a substantial structural heterogeneity, this definition may be less applicable.

Also, by definition, colloids span a size range of 1 nm to 1 µm, thus being part of the DOM fraction. The definition of colloids overlaps with HMW-DOM from ultrafiltration (with a pore size of 1 nm). However, colloids are better defined by their physical characteristics rather than their size, hence excluding HMW-DOM (Gustafsson and Gschwend 1997). The role of colloids is not well understood, especially those of metals associated with organic matter (e.g., Guo et al. 2000a; Stolpe et al. 2010). Colloids are intermediate phases between “truly” dissolved and particulate, and thus they can act as a mass flux mediator, adsorption and reaction surface and aggregation center. Further, they are considered to comprise a substantial fraction of the dissolved trace metal phase, and by that can determine the bioavailability of e.g., iron to phytoplankton (Schlosser and Croot 2008; Boye et al. 2010; Thuroczy et al. 2010).

The lower limit of DOM size/mass is restricted to the smallest compounds that can be recognized as organic molecules (e.g., monomeric biomolecules, such as amino acids or carbohydrates, typically > 100 Da).[11] However, only a small fraction of DOM can be identified as small monomers and the concentration of free amino acids, free sugars, etc. is in the nM range (Benner 2002; Bronk 2002). Other small molecules are either dissolved gases (methane, carbonylsulfide) or volatile compounds (e.g., dimethylsulfide, methanethiol) that are usually not considered as part of DOM.

[10] http://www.pall.com/main/Biopharmaceuticals/Literature-Library-Details.page?id=52194.
[11] Only two amino acid monomers have a molar mass < 100 g mol^{-1}: glycine and alanine.

Separation of DOM with ultrafiltration (1000 Da NMWC) yields approximately 60 – 75% of surface ocean DOC and 75 – 80% of deep ocean DOC in the LMW fraction, representing the major contribution to the total DOC pool. Mass spectrometric investigations further suggest that the major part of marine DOM is found between 200 and 1000 Da, which is in accordance with the constraints from the small monomers and the LMW fraction. The LMW fraction is consequently restricted to oligopeptides containing, for example, between 5 tyrosine and 13 glycine monomers or oligosaccharides containing between 5 glucose and 6 xylose units. However, the majority of oligopeptides and oligosaccharides (that are measured as total hydrolysable amino acids, THAA, and total hydrolysable neutral sugars, THNS) is found in the HMW fraction, accounting for almost three times the carbon yield compared to unfiltered DOM (Benner 2002). Since it is difficult to designate a maximum mass of HMW-DOM compounds (after filtration through 0.7 µM), the number of monomeric units in oligopeptides and oligosaccharides can be substantially higher.

All size separation techniques are strongly influenced by the bulk phase composition. Gravity or vacuum filtration result in a time and sample dependent clogging of the filter pores, hence reducing the effective filtration pore size or DOC can be lost through adsorption on the activated silica surface (see e.g., Kremling and Brügmann, 1999). Ultrafiltration may retain small molecules as well, but this effect is partly compensated by an exact control of the ultrafiltration process (i.e., tangential flow, diafiltration, concentration factor: Guo et al. 2000b; Walker et al. 2011). Size exclusion and gel permeation chromatography is also used for DOM analysis but was originally developed for the analysis of average molecular weight and polydispersity of chemically homogenous polymers. Due to the broad range of functional groups and polarity in DOM, these techniques discriminate also by analyte – stationary phase interactions (Specht and Frimmel 2000; Janos 2003). Electrostatic interactions with the saline sample matrix influence the hydrodynamic volume of DOM molecules as well (Engebretson and von Wandruszka 1994; Hutta et al. 2011). Thus, the apparent size distribution can change with the salt content (Kruger et al. 2011).

II.2 Age

One of the most puzzling properties of marine DOM is its average age and its age distribution. The “age” of a molecule can only be determined, if it contains or is associated with a radiometric clock. Most commonly used is the cosmogenic radionuclide of carbon, ^{14}C (half-life: 5,730 ± 40 a, Godwin 1962),[12] as carbon is — besides hydrogen — the most abundant atom in DOM and its radionuclide half-life is suitable to reconstruct the age of most DOM components. The ^{14}C content of a substance is generally reported as relative to an accepted standard (oxalic acid traceable to a piece of wood grown in 1890) and normalized for isotope fractionation effects and can be converted to a “conventional radiocarbon age” or “years before present” (Stuiver and Polach 1977). The constant equilibrium between atmospheric CO_2 (containing ≈ 1 ppt $^{14}CO_2$) and seawater CO_2 results in a continuous integration of radiocarbon into living organic matter. Once an organic molecule enters the dissolved phase its ^{14}C content changes only due to radioactive decay, starting the clock (precisely: the “average” ^{14}C content of all same molecules, because radioactive decay is a statistical process).[13] Thus, the age of DOM is the amount of time that has passed since the molecule was released into the dissolved phase. Severe complications arise from the fact that the natural equilibrium of ^{14}C was disrupted by burning of radiocarbon depleted fossil fuels (the Suess-Effect, Suess 1955; Stuiver and Quay 1981) and surface nuclear bomb testing in the 1960s and 1970s of the past millennium, introducing enhanced levels of ^{14}C into the ocean carbon cycle (Levin and Hesshaimer 2000). Further, alteration of DOM can significantly change its chemical composition and structure, yet mostly conserving its age. This process is most obvious when heterotrophic activity partially assimilates “old” DOM in the surface ocean, releasing again a mixture of old and young DOM (Cherrier et al. 1999; Hansman et al. 2009). This process is thought to, at least partially, account for the striking difference in surface ocean $DO^{14}C$ and inorganic/particulate ^{14}C content (Williams and Druffel 1987; Bauer et al. 1992).

[12] In reporting radiocarbon data as conventional radiocarbon age, the out-of-date, wrong “Libby half-life” of 5,568 a is still used (Stuiver and Polach 1977).

[13] Recent developments in “clumped isotope” geochemistry suggest that heavy isotopes tend to have a higher degree of intramolecular order than predicted from their pure statistical distribution (Eiler 2007). Moreover, site-specific carbon-isotopic fractionations within a molecule can be related to biological mechanisms under which these molecules are formed (Schouten et al. 2008). These effects have also potential implications for isotopic studies of DOM.

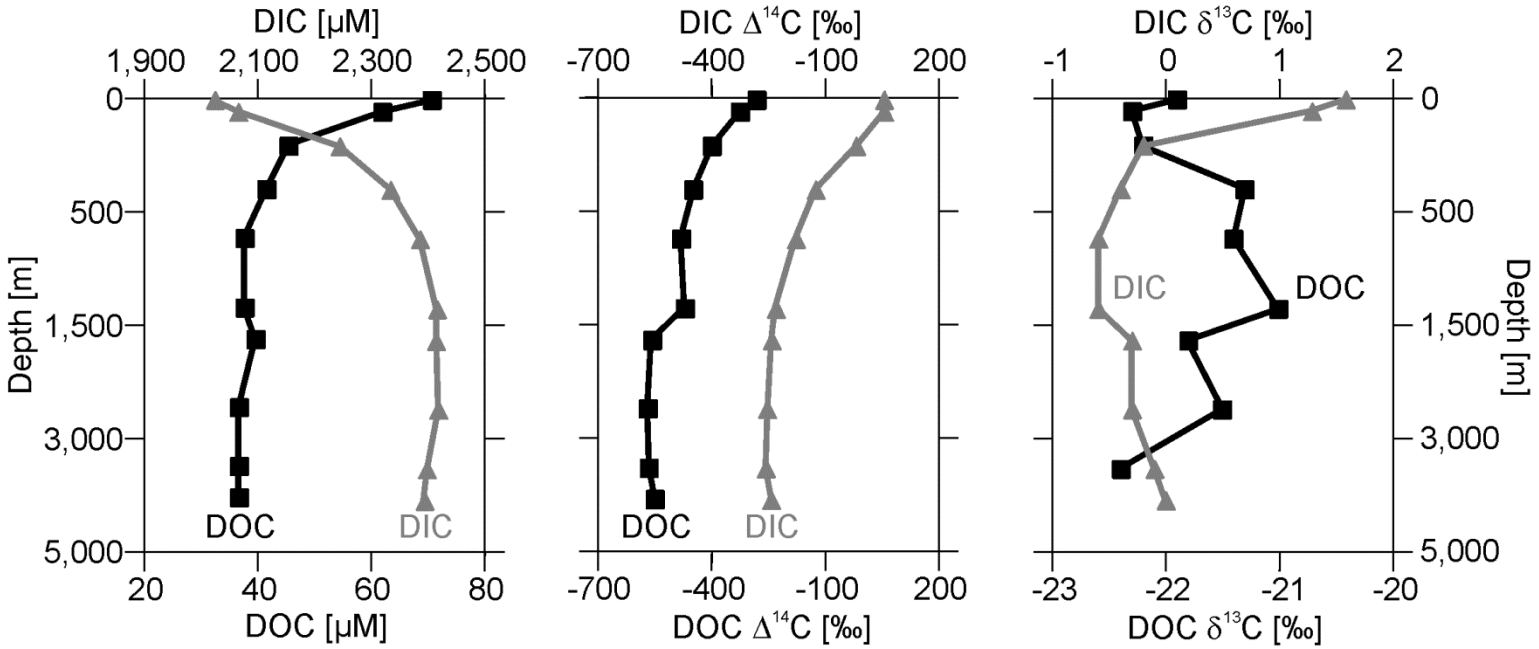

Figure II.2-1. DOC and DIC concentration and isotope ratios.

Representative open ocean depth profiles of dissolved organic (DOC, black) and inorganic (DIC, grey) carbon concentration, radiocarbon (DOC $\Delta^{14}C$, DIC $\Delta^{14}C$) and stable carbon isotope values (DOC $\delta^{13}C$, DIC $\delta^{13}C$) from station M in the eastern North Pacific (34°50' N 123°00' W). Data reproduced from Bauer et al. (1998) with permission from Elsevier. Standard deviations of the data values are generally smaller than data points and omitted for the figure.

A simplified explanation for the shape of the profiles is that DIC concentration, ^{14}C and ^{13}C reflect primary production in the surface and remineralization of organic matter at depth whereas DOC concentration and radiocarbon reflect secondary production (i.e., the microbial loop) both in the surface and at depth. Hence, the concentration profiles mirror each other. The radiocarbon profiles have an offset of ≈ 300‰ reflecting the slower turnover of DOC compared to DIC (which is near isotopic equilibrium with the atmosphere). The assimilation of CO_2 or HCO_3^- by primary producers discriminates against the heavier isotopes, reflected in the positive DIC $\delta^{13}C$ values in the surface and negative DOC $\delta^{13}C$ values. (Heterotrophic) degradation fractionation is low, and DOC $\delta^{13}C$ is relative invariant (Bauer 2002) with depth. It is general practice to normalize the radiocarbon data to the isotopic fractionation of ^{13}C, hence the Δ-notation for ^{14}C (Stuiver and Polach 1977).

Similar oceanic depth profiles for DOC concentration and DOC age (Figure II.2-1) have led to the suggestion that the overall DOM pool consists of two fractions, one old, refractory component that is equally distributed throughout the whole ocean and a young, labile component that is added in the surface ocean and remineralizes with depth (Williams and Druffel 1987; Mortazavi and Chanton 2004; Beaupré and Aluwihare 2010). The intriguing finding, however, was that the apparent age of deep ocean DOM (4,000 – 6,000 a, Bauer et al. 1992) by far exceeds the calculated deep ocean water replacement time determined from inorganic ^{14}C (≈ 500 a, Stuiver et al. 1983). Further, the deep ocean water transit time, determined from dissolved inorganic radiocarbon (DI^{14}C), between the major ocean basins in the Atlantic and Pacific is shorter than the apparent age difference of DO^{14}C (Bauer 2002), placing severe constraints on the conservative properties of DOC. Druffel et al. (1992) calculated that approximately 80% of the deep ocean DOC is recycled with each ocean mixing cycle.

Fraction and compound-specific analyses of organic radiocarbon partly resolved the mystery, as a continuous range of DOM ages was found, foremost suggesting a multi-component system with different age ranges for different compound classes. The full range from modern (i.e., containing bomb-^{14}C) to almost radiocarbon-dead compound classes was found (e.g., Loh et al. 2004). Specifying ages for individual compound classes allows the calculation of residence times, valuable information for the assessment of the reactivity of these compounds (*vide infra*). The apparently younger age of HMW-DOM compared to the bulk DOC inspired the suggestion of a size-age relationship (Guo et al. 1996; Walker et al. 2011) in accordance with the previously proposed size-reactivity continuum (Amon and Benner 1994).

Different information may be obtained from long-lived isotopes or isotope pairs: e.g., the U-Th series disequilibrium may be used to infer the removal rates of particulate organic matter from production sites (Buesseler 1991; Buesseler et al. 2007). DOM also plays a critical role in (radioactive) metal sorption characteristics (Quigley et al. 2001; Trenfield et al. 2011).

II.3 Isotopic composition

The second stable carbon isotope – ^{13}C – is another frequently used proxy for determining sources and pathways of organic and inorganic carbon transformation. The natural abundance of ^{13}C is 1.1078% (Bohlke et al. 2005) and due to its higher mass compared to the major isotope ^{12}C (+8.4%, De Laeter et al. 2003), it is involved in thermodynamic (e.g., evaporation) and kinetic (e.g., enzymatic) fractionation processes. It is important to note that the ^{14}C activity of a substance is normalized to its ^{13}C fractionation value to correct for the influence of natural isotopic fractionation.[14] However, the approach assumes that the isotopic fractionation of ^{14}C is just twice the fractionation of ^{13}C and for some applications reservoir age corrections have to be made (Stuiver and Polach 1977).

Other stable isotopes of abundant elements in DOM are used to study the biogeochemical properties of the organic material. ^{15}N is used to measure nitrogen assimilation rates via isotopic labeled compounds (ammonium, nitrate, and urea) and to study the transformation of inorganic nitrogen to dissolved organic nitrogen (DON: e.g., Bronk et al. 1994; Mahaffey et al. 2004) or the different fate of particulate organic nitrogen (PON) in comparison to POC (Benner et al. 1997; Knapp et al. 2012). Seldom used isotopes for DOM analysis are ^{2}H, ^{18}O and ^{34}S (e.g., Alling et al. 2008). An overview of the stable isotopic composition of organic matter is presented in Figure II.3-1.

[14] The international standard for ^{13}C measurements was Pee Dee Belemnite (PDB, a Cretaceous mineral, now replaced by secondary standards) and the isotopic fractionation of ^{14}C is normalized to a value of $\delta^{13}C$ = -25‰.

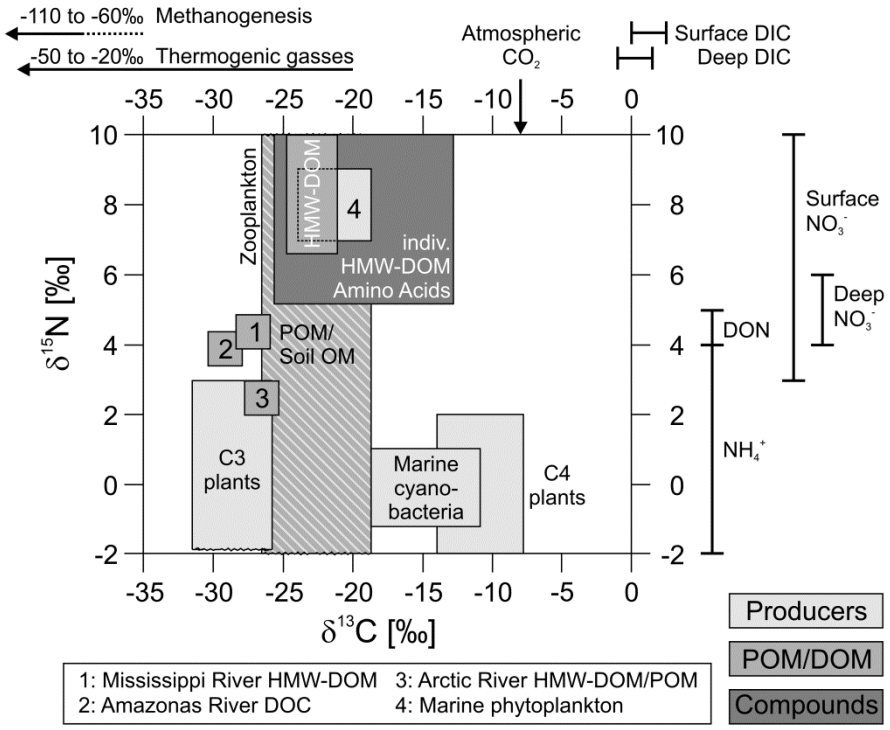

Figure II.3-1. Stable C and N isotope composition of organic matter.

Stable carbon and nitrogen isotopic composition of marine dissolved organic matter and selected sources. Scales are $\delta^{13}C$ and $\delta^{15}N$. Land plants have distinct isotopic source patterns (e.g., C3 vs. C4 photosynthetic pathway) which is also reflected in their lignin $\delta^{13}C$ values which tend to be isotopically lighter than cellulose (Benner et al. 1987). River sources of POM and DOM reflect the vegetation type in the watershed but both soil and marine POM have a large range of isotopic values. Atmospheric CO_2 $\delta^{13}C$ values decreased from a preindustrial value of -7‰ to -8‰ due to the Suess effect (Battle et al. 2000), followed by the DIC pool (McNichol et al. 2000). The ocean nitrogen isotope balance is mainly influenced by upwelling of nitrate and the contribution of N_2-fixing cyanobacteria. Few measurements exist for compound-specific stable isotopes in DOM, but HMW-amino acid isolates show a large scatter around bulk HMW $\delta^{13}C$ and $\delta^{15}N$ values (McCarthy et al. 2004, 2007) and marine zooplankton (Schell et al. 1998). Methane and other hydrocarbon gases enter the ocean with extremely depleted ^{13}C content due to large kinetic fractionation processes but in general, decomposition induces smaller fractionation than assimilation. Further sources: Peterson and Fry (1987), Checkley and Miller (1989), Melillo et al. (1989), Benner et al. (1997), Hedges et al. (1997), Wu et al. (1999), Lobbes et al. (2000), Sigman et al. (2000), Montoya et al. (2002), Guo et al. (2003), Benner et al. (2005), Knapp et al. (2005), Chen et al. (2006), Meador et al. (2007), Guo et al. (2009), Hoefs (2009), Kodina (2010), and Knapp et al. (2012).

II.4 Chemical compound classes of DOM

The ultimate source of DOM is living biomass, which is dominated by bacteria and phytoplankton contributing to the particulate organic matter (Pomeroy et al. 2007).[15] Major constituents of marine plankton (and most other life forms) are the main biochemical compound classes, proteins, carbohydrates,[16] and lipids, that account for > 80% of the organic carbon in phytoplankton (Wakeham et al. 1997). It is common practice in seawater analysis (of dissolved and particulate matter) that the polymeric biochemicals are hydrolyzed into their monomeric constituents, amino acids, amino sugars, monosaccharides, and fatty acids prior to measurement (see e.g., Skoog and Benner 1997; Kaiser and Benner 2000, 2005). Hence, amino acids, neutral and amino sugars together with lipids represent the identifiable carbon pool in POM together with small contributions of e.g., pigments and nucleic acid fragments. This ratio changes drastically, once the POM is released from its source. In the order surface POM, deep-sea POM, surficial sediment OM (both particulate and dissolved), and subsurface sediment OM, the fraction of uncharacterized OM constantly increases, accounting finally for more than 80% of the total carbon in subsurface sediment OM (Wakeham et al. 1997). A comparison with the dissolved phase that is expected to undergo immediate and substantial reworking after dissolution (e.g., Smith et al. 1992) reveals that the fraction of identifiable DOM is much lower, e.g., for surface (4 – 11% C and 7 – 14% N) and deep DOM (1 – 4% C and 4 – 9% N; Benner 2002; Kaiser and Benner 2009).[17] Figure II.4-1 presents an overview of the different compound classes of DOM and POM and their relative carbon yields.

[15] The phytoplankton biomass of ≈ 1 Pg accounts for only 0.2% of the global photosynthetic active biomass but contributes about half of the annual primary production (Falkowski et al. 1998, Carr et al. 2006).

[16] Carbohydrate in marine sciences is a general term for heterooligo and heteropolysaccharides, comprising very different compound and size classes, e.g., lipopolysaccharides (LPS), extracellular polymeric substances (EPS) or transparent exopolymer particles (TEP).

[17] Note that a similar fraction of organic nitrogen (60 – 80%) in phytoplankton can be accounted for by amino acids (Cowie and Hedges 1992), whereas the yield of amino acids in DON ("identifiable nitrogen") is larger than the yield of identifiable amino acid carbon in DOC (Benner 2002).

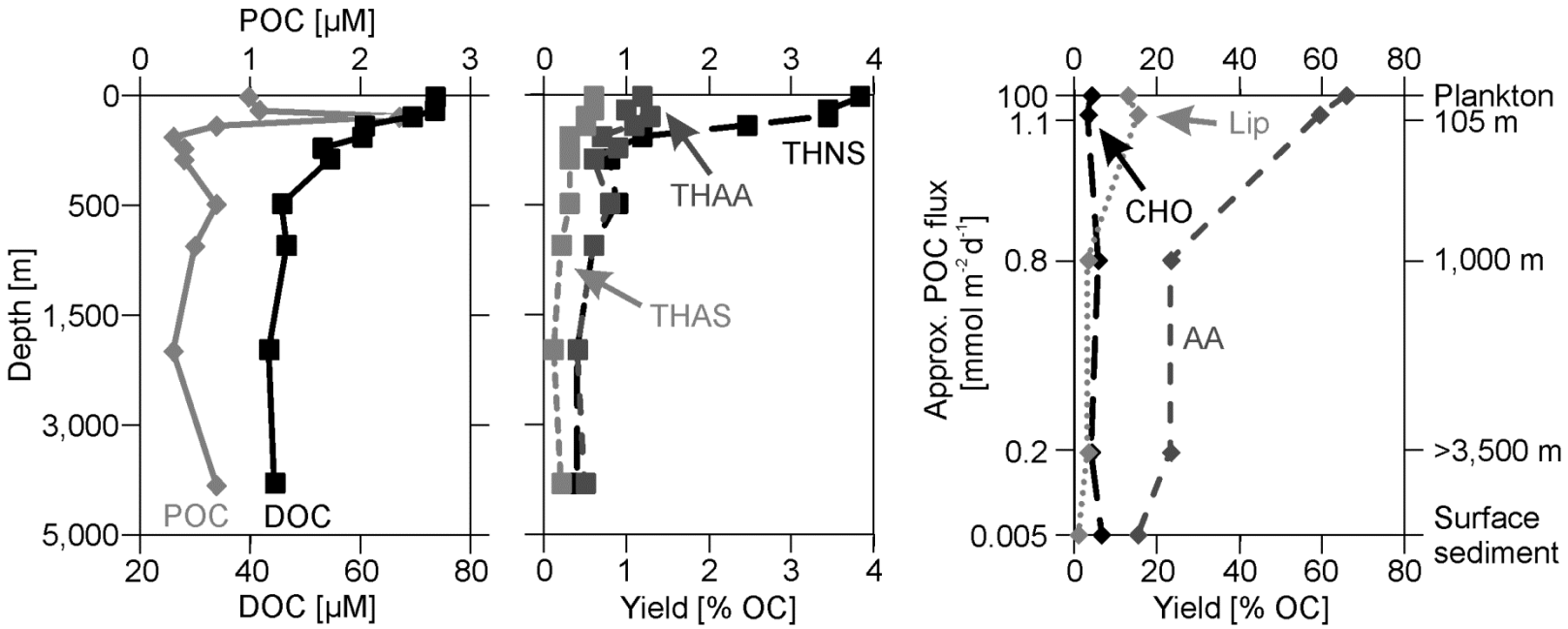

Figure II.4-1. Chemical composition of DOM and POM.

Representative profiles of dissolved and particulate organic carbon concentration and biochemical composition. The concentration of dissolved (DOC, squares) and particulate (POC, approx. 1 – 3% of DOC concentration, diamonds) organic carbon decreases with depth (left). The organic carbon yields of the main chemical compound classes of DOM (middle, THNS = total hydrolysable neutral sugars, THAA = total hydrolysable amino acids, THAS = total hydrolysable amino sugars) decrease faster than bulk DOC, reflecting a higher proportion of molecular uncharacterized components (MUC) at depth. The ratio MUC vs. biomolecules is smaller in particulate matter (right, CHO = carbohydrates, AA = amino acids, Lip = lipids), although it largely increases from phytoplankton (< 20%) and sinking POM to surficial sediment POM (> 75%). The organic carbon flux [mmol m^{-2} d^{-1}] attenuation of sinking particles is more than five orders of magnitude. Note that compared to the dissolved phase, amino acids are the dominant biomolecules in particulate organic matter and dissolved lipids are in the sub-nanomolar range. “Biomolecules” refer to monomeric “chemical compound classes” representing the building blocks of larger (hetero-)polymers. Data are from the Bermuda Atlantic Time Series (BATS) station and the equatorial Pacific (right) and are reproduced from Kaiser and Benner (2009) and Wakeham et al. (1997) with permissions from Elsevier.

Amino Acids

Proteinogenic amino acids are the dominant identifiable constituents of living biomass and POM and the main contributor to the DON pool. Their relative abundance in surface water DOM immediately reflects biological activity and is typically in the nM range (≈ 100 – 500 nM or 1 – 3% of DOC and 4 – 12% of DON; Cowie and Hedges 1994; Benner 2002; Davis et al. 2009). Free amino acids are highly reactive (typical concentration in the low nM range) and enhanced concentrations of amino acids are only sustained during continuous input from primary producers (Hammer and Kattner 1986; Keil and Kirchman 1999; Simon and Rosenstock 2007). Due to their high nitrogen-yield (C:N ratio of individual amino acids ≈ 2 – 8, compared to 15 – 20 for average ocean DOM, Bronk 2002) they are preferentially utilized by heterotrophs (e.g., Keil and Kirchman 1999; Zubkov et al. 2008). ^{3}H labeled leucine incorporation by bacteria (Smith and Azam 1992) is commonly used to estimate the overall bacterial production (e.g., Kirchman et al. 2009; Flerus et al. 2012; Friedline et al. 2012). The composition of individual amino acids is further used as a biochemical indicator for the quality and degradation state of (D)OM (Cowie and Hedges 1994; Dauwe and Middelburg 1998; Davis et al. 2009). The relative contribution of amino acid stereoisomers in DOM allows inferring the relative degree of heterotrophic bacterial reworking (Fitznar et al. 1999; Kaiser and Benner 2008; Kaiser and Benner 2012).

Carbohydrates

In contrast to amino acids in living biomass, carbohydrates and their hydrolyzation products are the largest fraction of identifiable biomolecules in the dissolved phase (Benner 2002). Although carbohydrates are preferentially lost in the mesopelagic zone (Pakulski and Benner 1994; Goldberg et al. 2010), their unfavorable C:N ratio compared to amino acids results in a relatively higher residence time in the dissolved phase. Carbohydrate concentrations vary between ocean basins and depend for instance on the nutrient availability (Goldberg et al. 2011; Kaiser and Benner 2012). However, the turnover of the combined carbohydrate pool is high compared to the bulk DOC and the residence times are in the order of minutes to days (Rich et al. 1996; Amon et al. 2001; Goldberg et al. 2009), resulting in mostly low concentrations in surface waters (0.2 – 2 µM or 2 – 6%

of total DOC; Benner 2002; Engbrodt and Kattner 2005; Goldberg et al. 2010). However, surface ocean concentrations of carbohydrates may be as high as ≈ 30% of the DOC pool for some regions (Pakulski and Benner 1994) and/or phytoplankton bloom conditions (Kirchman et al. 2001). Carbohydrates are assimilated by heterotrophs and the bacterial glucose uptake is a measure of the contribution of carbohydrates to bacterial production, which in turn controls the substrate abundance. The yields and monomer distribution of carbohydrates have been used to infer the diagenetic state of DOM (e.g., Cowie and Hedges 1994; Skoog and Benner 1997; Repeta and Aluwihare 2006).

Bacterial and archaeal lipid biomarkers

In addition to D-amino acids, muramic acid is an unambiguous marker for bacterial activity that can be identified with chromatographic methods in the dissolved phase (Mimura and Romano 1985; Kawasaki and Benner 2006). N-acetylmuramic acid is an integrative part of peptidoglycan, a cell wall biopolymer unique to bacteria (Schleifer and Kandler 1972; Benner and Kaiser 2003). Peptidoglycan itself is more stable than other proteins when released to the dissolved phase (Kitayama et al. 2007) but of the two main components, the peptide degrades three times faster than the polysaccharide moiety (Nagata et al. 2003), which is expected for these different biomolecules (*vide supra*). Other bacterial biomarkers include diaminopimelic acid and 3-hydroxy fatty acids (Jørgensen et al. 2003; Wakeham et al. 2003).

Archaeal cell wall membranes can be distinguished from their bacterial counterparts because they lack muramic acid. Examples are the crenarchaeols, e.g., the C_{86} glycerol dibiphytanyl glycerol tetraethers (GDGT). Archaeal ether lipids have not been detected in the dissolved phase, likely because of their high molecular weight and high degree of saturation. However, they are transported with sinking particles to the sediment where they serve as biomarkers to reconstruct paleo sea-surface temperatures (TEX_{86} index: Damste et al. 2002; Schouten et al. 2002).

Phytoplankton biomarkers

In conjunction with the release of amino acids and carbohydrates, other metabolic products from primary producers are released to the dissolved phase.

Among them are thiol-bearing molecules like phytochelatin and glutathione which are produced in response to metal stress (Ahner et al. 2002; Kawakami et al. 2006b) and considered as important metal chelators (Ammann 2002; Hirose 2006). Photosynthetic pigments and their degradation products as well as lipids and sterols are more abundant in the POM fraction (Wakeham et al. 1997). Some of them can also be identified in the dissolved phase (e.g., Mühlebach and Weber 1998; Mannino and Harvey 1999; McCallister et al. 2006). All these compounds are highly labile and only found in extremely low concentrations in ocean surface waters. The unsaturation pattern of two unbranched C_{37}-ketones produced from marine algae is sensitive to the surface water temperature. They are preserved in sediments and their abundance ratio is used as a proxy for paleo sea-surface temperature ($U^{K'}_{37}$: Brassell et al. 1986; Prahl and Wakeham 1987).

Terrestrial biomarkers

Every year, ≈ 250 Tg of dissolved and ≈ 150 Tg of particulate organic carbon is delivered to the oceans by rivers (Figure II.1-1), enough to replenish the total dissolved organic oceanic carbon pool in about 2,500 a (Hedges et al. 1997; Schlünz and Schneider 2000). However, it is estimated that 50 – 90% of the terrestrial OM is remineralized on the coastal shelves, the remainder eventually being exported to the sediment or advected to the pelagic ocean (e.g., Hedges and Keil 1995; Schlünz and Schneider 2000; Burdige 2005).[18] Hence, the coastal ocean may also be a source of atmospheric CO_2 (especially estuaries, whereas shelf areas are a major sink; Cai 2011) and the contribution of terrestrial components to the oceanic DOM pool is only minor (Meyers-Schulte and Hedges 1986; Opsahl and Benner 1997). Proof is derived from ^{13}C, ^{14}C and ^{34}S isotopic composition, C:N ratios and spectroscopic properties (*vide infra*).

Moreover, lignin, a terrestrial vascular plant biomarker, has generally only low concentrations in the open ocean and deep waters. Lignin can be hydrolyzed and analyzed with chromatographic methods and the distribution of the lignin phenols can be used for organic matter source tracing (Opsahl and Benner 1995, 1997; Kaiser

[18] This high percentage should not be confused with the fraction of global carbon burial occurring in coastal sediments (≈ 90%), since it comprises both, terrestrial OM and OM which is autochthonously produced in the coastal margin (e.g., Berner 1989; Burdige 2005).

and Benner 2011). Pelagic ocean surface concentrations of lignin phenols are 10 – 30 ng L^{-1} (Opsahl and Benner 1997). A prominent exception is the Arctic Ocean, where surface concentration of lignin phenols can reach values > 300 ng L^{-1} due to the large terrestrial organic matter input (TOM; Hernes and Benner 2006). Other terrestrial biomarkers are e.g., leaf waxes that are preserved in marine sediments and provide information about vegetation sources and paleoclimate conditions (Eglinton and Eglinton 2008).

Black Carbon

The distribution of this highly condensed, aromatic substance class is not well understood but sources in the deep sea (Dittmar and Koch 2006) as well as on land (Kim et al. 2004) have been identified. It was shown that black carbon comprises very old carbon (Ziolkowski and Druffel 2010) but it is subject to photochemical transformation in surface waters (Stubbins et al. 2012). It is estimated that ≈ 2% of the total DOM pool is black carbon (Dittmar and Koch 2006; Dittmar and Paeng 2009).

Other compounds of the DON and DOP pool

Although many examples of nitrogen containing molecules of the DOM pool have been presented in the previous sections, some remarks concerning the DON and dissolved organic phosphorus (DOP) pool in contrast to the DOC pool are required and some examples of nitrogen and phosphorus compounds are presented in Figure II.4-2.

DON comprises many substance classes: proteins, peptides, urea, free amino acids, nucleic acids, “humic” substances, and hundreds of yet to be characterized molecules (as inferred from the number of N-containing peaks in ultra high resolution mass spectrometric studies). The dominant structural component of (HMW-) DON is the amide-N-form with contributions from amine-N in surface waters (McCarthy et al. 1997; Aluwihare et al. 2005). Organic nitrogen is relatively enriched in ^{15}N compared to nitrate and the total organic nitrogen (TON) $\delta^{15}N$ isotopic values are ≈ 1 – 4‰ in surface waters (Knapp et al. 2005) with higher values of 4 – 10‰ for HMW-DON (Benner et al. 1997; Knapp et al. 2012, see also: Figure II.3-1). Nitrogen

fixation by the cyanobacterium *Trichodesmium* spp. tends to decrease the $\delta^{15}N$ values of OM (Carpenter et al. 1997).

Examples of DOP compounds are phospholipids, phosphonates, nucleic acids, vitamins with individual C:P ratios ranging between about 3 and 40. In contrast to nitrogen compounds, only few phosphorus bearing molecules have been detected in ultrahigh resolution mass spectrometric studies, mainly due to non-ambiguous molecular formula assignments. The (HMW-) DOP pool is dominated by phosphate-ester structures, with a relatively constant contribution from phosphonates (≈ 25%, Kolowith et al. 2001; Sannigrahi et al. 2006) and polyphosphates (Young and Ingall 2010).

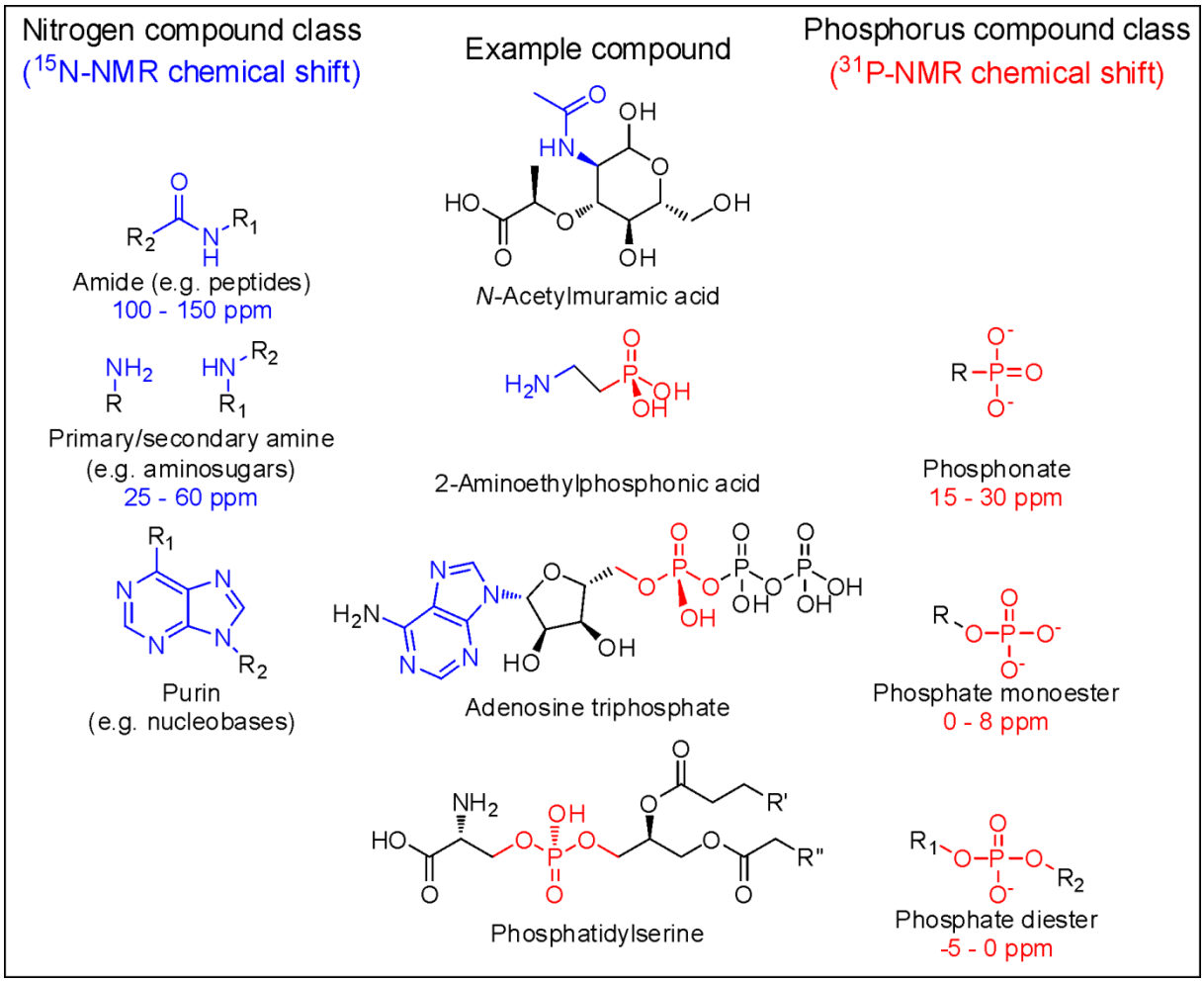

Figure II.4-2. Examples for DON and DOP compounds.
Naturally occurring important dissolved organic nitrogen (DON) and phosphorus (DOP) compound classes and example molecules. These compounds are either detected in seawater or found in culture exudates and are thus likely present in seawater. The largest DON fraction is comprised of amides and to a small extent of amines. The dominant DOP species are phosphate ester and phosphonates. The approximate ^{15}N- and ^{31}P-NMR chemical shift ranges for the major compound classes in (HMW-) DOM samples are included. Note that inorganic forms of nitrogen and phosphorus are also present, resulting in additional NMR peaks. Chemical shift values are from Aluwihare et al. (2005) and Sannigrahi et al. (2006).

The range of DON concentrations in surface waters is 0.8 – 13 µM N and decreases to deep ocean concentrations of < 5 µM N (e.g., Bronk 2002; Bronk et al. 2007; Torres-Valdes et al. 2009). The DOP concentrations range from ≈ 200 nM P in surface to < 100 nM P in deep waters (e.g., Karl and Björkman 2002; Björkman and Karl 2003; Mather et al. 2008). From the molar C:N and C:P ratios of any DOM pool (terrestrial, marine, living, etc) it is obvious that the DON pool is smaller than the DOC pool, with DOP even less abundant (labile DOM C:N:P ratio = 199:20:1; deep ocean (refractory) ratio = 3511:202:1, Hopkinson and Vallino 2005). Both ratios are higher than the canonical Redfield ratios for phytoplankton (106:16:1, Redfield 1958) and indicate a preferential utilization of the DON and DOP pools by secondary producers.[19] As a consequence of the exhausted inorganic sources of nitrogen and especially phosphorus in oligothrophic ocean systems, the organic nutrients DON and DOP cycle rapidly as well. Accordingly, also organic nitrogen and phosphorus are utilized to fuel primary production (e.g., Mahaffey et al. 2004; Bronk et al. 2007; Mather et al. 2008; Torres-Valdes et al. 2009) and the flux of matter through the DON and DOP pools in surface waters is higher than the flux of matter through the DOC pool. This is e.g., expressed in high turnover rates of dissolved combined amino acids (DCAA) and dissolved free amino acids (DFAA, Carlson 2002) and DOP (Benitez-Nelson and Buesseler 1999).

[19] The “mixing” of the refractory and labile DOM pools in surface waters thus lead to a mean surface C:N:P ratio of 374:27:1 (C:N ≈ 14).

II.5 Reactivity

The property of DOM that is probably most difficult to assess is its “reactivity”. Reactivity is neither purely physical nor biological, it is the sum of all processes that alter concentration, molecular composition/structure or phase distribution of a substance. Therefore, it is useful to distinguish different kinds of reactivity playing major roles in the ocean DOM cycle: Biological reactivity, photo-reactivity and particle reactivity are the most important aspects. In most cases, reactivity is synonymous for at least a partial loss of the substance from the system under consideration. For reasons of conservation of mass, this loss must be balanced by a gain of matter in a coupled system. E.g., heterotrophic respiration of DOM in the deep ocean leads to a decrease in DOC and oxygen concentration but an increase in dissolved inorganic carbon (DIC) and nutrients (Aristegui et al. 2002; Carlson et al. 2010). A certain type of reactivity can initiate or limit another, resulting in complex reaction mechanisms. If the DOM reactivity is experimentally determined, these complex couplings are usually eliminated by the choice of the experimental parameters. Although this is probably seldom successful for all interactions, it is an approach to assess the different types of reactivity and estimate their overall contribution to an observed phenomenon. An overview scheme of the different processes acting on oceanic organic matter is presented in Figure II.5-1.

Biological reactivity

Biological reactivity refers to the extent and rate of which a substance is utilized by living organisms. As a source of nutrients and energy, DOM is of special importance for heterotrophs.[20] Although POM is not directly available to bacteria, estimates for the bacterial consumption of total primary production are in the order of 50% (Kaiser and Benner 2009), thus half of the primary production is channeled through the DOM-heterotroph pathway.[21] Bacterial uptake mechanisms require that assimilated molecules are smaller than ≈ 600 Da (Weiss et al. 1991). To break down the larger POM or HMW-DOM molecules, heterotrophs have developed a suite of

[20] Using only DOM as carbon and energy source, bacteria and archea are heterotrophic osmotrophs.

[21] This estimate is based on the rough calculation that 10 – 20% of the oceanic primary production is bacterial production and that the bacterial growth efficiency is around 15 – 30% (see reviews by Carlson 2002, Benner 2002, Kirchman et al. 2009).

specific extracellular hydrolytic enzymes (Smith et al. 1992; Azam 1998) that are surface bound on the cells or released to the environment.[22]

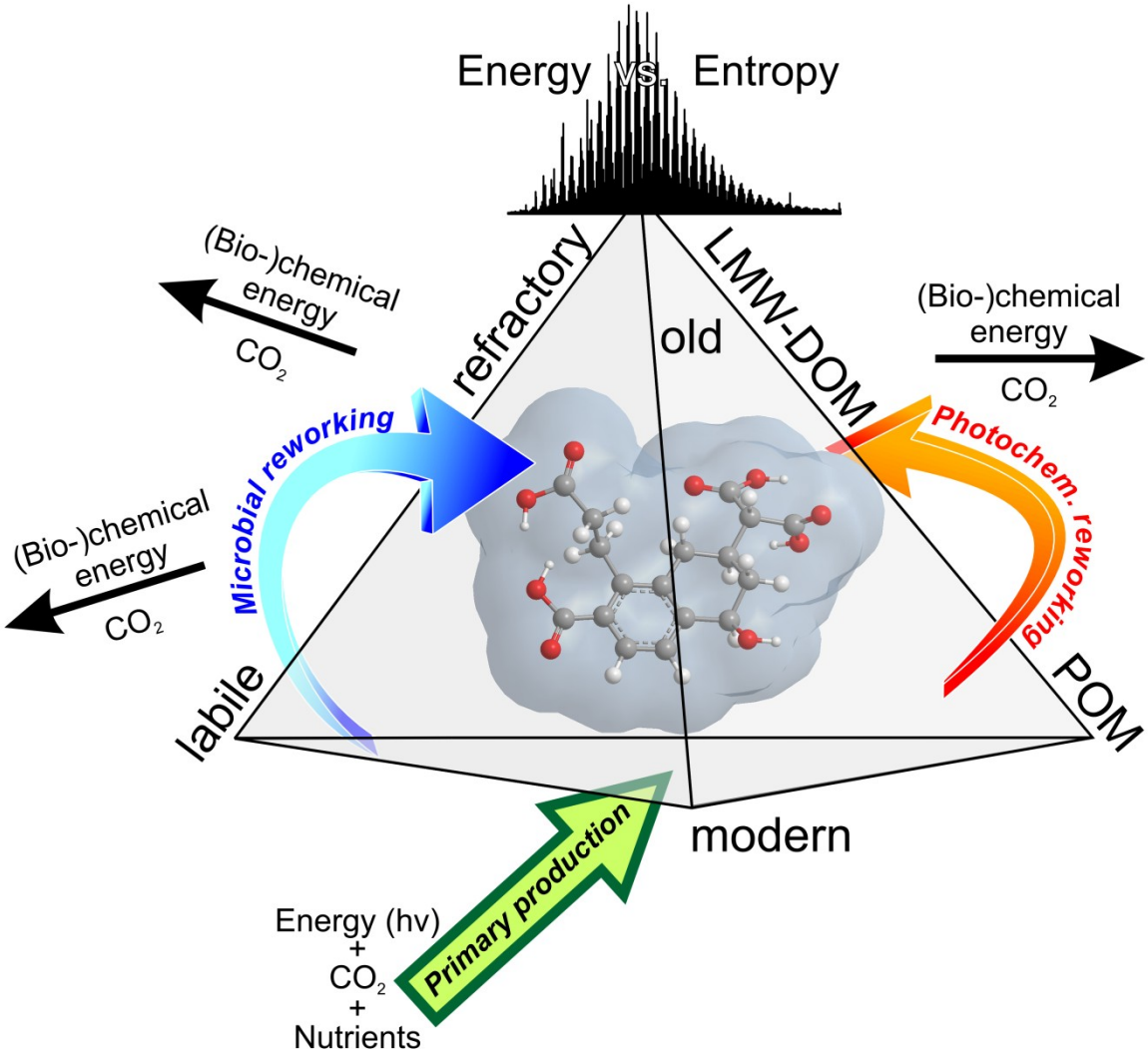

Figure II.5-1. Organic matter reactivity in the ocean.
Conceptual scheme of the contemporary view of the property continua in marine organic matter. Primary production relies predominantly on the availability of sunlight, CO_2 and nutrients which are biochemically transformed into (modern) organic matter. The photosynthetic energy is transferred into chemical energy that is stored in labile molecules. This (bio-)chemical energy is accessed by microbes, resulting in the breakdown of larger molecules (POM) and the remineralization of organic matter into CO_2 and nutrients. With the decrease of the nutritive value and concentration (e.g., with higher oxygen and lower nitrogen and phosphorus content) further utilization rate slows down, reflected in the old apparent age and low reactivity (refractory character) of LMW-DOM. Photochemical processes in the surface waters also degrade organic matter but the mechanisms are physico-chemically driven. The analytical observation is a superposition of all processes and is a result of energy and entropy constraints on organic matter.

[22] Particles and aggregates (“marine snow”) are known to be biological “hot spots” in the marine environment, because they contain the highest concentrations of bacteria (compared to the free living counterparts, e.g., Azam and Long (2001)). Microbial community members may thus profit from each other (“quorum sensing”, Gram et al. (2002) or “cheating”, Velicier (2003)).

In the context of biochemical tools evolved in marine prokaryotes and eukaryotes, it is important to recognize that in many regions of the pelagic ocean, marine life (including phytoplankton) is limited by the availability of trace metals, foremost iron (Martin and Fitzwater 1988; Tortell et al. 1996). Iron limitation thus in turn determines primary and secondary production, e.g., in the Southern Ocean (de Baar et al. 1995; Buesseler et al. 2004), and hence also DOM turnover in these regions. Therefore besides acquiring carbon, nitrogen and phosphorus, an even stronger pressure exists to satisfy the micronutrient demands (Morel and Price 2003). Similar to hydrolytic enzymes, specialized siderophores with strong iron affinity, were discovered and shown to influence the cycling of inorganic and organic moieties (Martinez et al. 2000; Barbeau et al. 2001; Gledhill et al. 2004; Velasquez et al. 2011).

Organic carbon from phytoplankton is released as a continuum of sizes and different reactivity. Particulate matter and HMW-DOM are preferentially consumed, which led to the concept of a size-reactivity continuum for DOM (Amon and Benner 1994), that was later also extended to other systems (Hedges and Oades 1997; Burdige and Gardner 1998; Loh et al. 2004). The most reactive form of organic carbon is POM, in agreement with the very high proportion of characterizable biomolecules (Wakeham et al. 1997). However, it was recently recognized from isotopic studies that a different pathway acts on organic nitrogen degradation and a direct release of LMW-DON from POM is likely to occur (Knapp et al. 2012).

The apparent old age of DOM suggests, in combination with the relatively homogenous deep water DOC concentrations, that not all fractions of DOM are similar in their biological reactivity. The huge differences in ages for different size and substance classes together with the broad range of concentrations also imply that certain fractions of DOM are preferentially utilized. The rate of biologically DOM utilization was historically distinguished between labile (LDOM, turnover within minutes to days), semi-labile (SLDOM, turnover within days to years) and a refractory/recalcitrant fraction (RDOM, turnover within centuries to millennia), although it is recently recognized that a continuum of reactivities exists, which is strongly dependent on the environmental parameters (nutrient-limitation, community structure, e.g., Carlson et al. 2000; Arnosti et al. 2011). Therefore, it is likely that the “affinity” of the microbial community towards certain substance classes determines

the “reactivity” of the DOM pools. The factors controlling a higher or lower affinity are not all evident, but it is presumably a combination of the concentration and chemical structure of the DOM molecules, nutritive (energetic) value (Kattner et al. 2011) and availability of co-metabolizing compounds.[23]

Examples for LDOM are the free monomers of amino acids or monosaccharides. Despite their very low concentrations, the total flux of DOC through the labile pool is expected to be very high (Carlson 2002). SLDOM compounds are e.g., combined amino acids or carbohydrates responsible for the vertical gradients in DOC concentration and accounting for the exportable DOC fraction. On the other end of the reactivity scale, RDOM or even ultra-refractory DOM (URDOM, Hansell 2013) compounds have high radiocarbon ages and cycle on average several times with the ocean circulation. From the deep sea gradient in DOC concentration and age, a very slow removal of (U)RDOM can be deduced although there may also exist in situ sources (Hansell and Carlson 1998a; Hansell et al. 2012).

The impacts of climate change on marine food web dynamics may also alter the reactivity of DOM pools (Jiao et al. 2010). Different source composition for e.g., terrestrial OM is expected (Vonk et al. 2010; Gustafsson et al. 2011; Stedmon et al. 2011) and a different response of the microbial community towards the available DOM with changing community structure (Arnosti et al. 2011; Giovannoni and Vergin 2012) is anticipated.

Abiotic processes: radiation and particle reactivity

Apart from the biologically mediated transformation processes, photochemical reactions and adsorption onto and desorption from particles (as a consequence of boundary layer equilibria) lead to changes in DOM concentration, composition and structure. Important implications of abiotic reactivity are generally discussed in the context of biological reactivity.

[23] The effect of a “priming” of the degradation of refractory DOM by additional “labile” compounds is well known in soil science and may also play a role in the marine environment, see Bianchi 2011.

It was recognized, that photochemical transformation of RDOM results in biologically available compounds (Kieber et al. 1989; Moran and Zepp 1997), although other studies suggested an at least ambivalent effect of solar radiation on bioavailability (Obernosterer et al. 1999; Kramer and Herndl 2004). However, photo- and biodegradation of DOM can overlap (Amon and Benner 1996b; Obernosterer and Benner 2004; Rontani et al. 2011) and substantial changes in optical and molecular properties of DOM are a result of photodegradation (e.g., Gonsior et al. 2009; Stubbins et al. 2010). Many reactive intermediate compounds from the photolytic cleavage of water (Mopper and Zhou 1990) result in highly reactive inorganic and organic radicals.

Photochemically produced LMW-DOM (Zhou and Mopper 1997; de Bruyn et al. 2011) and volatile organic compounds (Pos et al. 1998; Cutter et al. 2004) are consequently found in surface waters. Depending on the concentration of DOM, the occurrence of organic radical intermediates can principally also promote the formation of new compounds being larger and more complex (Amrani et al. 2007; Stubbins et al. 2010). Thus, photochemical reactions are quasi random – bidirectional reactions, adding a substantial statistical process to DOM transformation mechanisms.

In situ experimental approaches on the influence of solar radiation on DOM degradation in marine organic surface films revealed that secondary effects need to be considered, e.g., an uncoupling of production and respiration (Obernosterer et al. 2005). Photoautotrophic production is inhibited by high UV-B insolation in the surface layer (Williams et al. 1986) but release of potentially protective transparent exopolymer particles (TEP) molecules is enhanced (Ortega-Retuerta et al. 2009).

Despite photochemically induced radical reactions of DOM molecules, radioactive decay also provides enough energy for lysis reactions. The source of energy (decay of radionuclides, sunlight) is less important in this respect, likewise the mode of radioactive decay. But in contrast to photoreactions, natural radioactivity affects the whole water column (where ^{40}K is the dominant source of (β-) radiation energy) and the sediments (here, the α-decay of ^{230}Th and ^{40}K are the major

contributors to radioactivity).[24] The energy doses accumulating over hundreds of years in the deep ocean or even over millions of years in sedimentary layers have a large potential for structural alterations of organic matter by secondary reactions (Goldstone et al. 2002; Kreller et al. 2005).

Biogenic or mineral particles on the other hand can shield intrinsically labile DOM from biologic (enzymatic) access (Keil et al. 1994; Hedges et al. 2001; Sannigrahi et al. 2005) or oxidation (Hedges and Keil 1995; Nguyen et al. 2003). Colloidal mineral surfaces are catalytic sites for chemical reactions (Collins et al. 1995) or aggregation nuclei (Mayer 1999; McCarthy et al. 2008), similar to polysaccharide molecules in marine gel processes (Passow 2002; Engel et al. 2004).

II.6 The molecularly uncharacterized fraction of DOM

Substantial research effort has been undertaken in the past to resolve the conundrum of the molecular uncharacterized component (MUC) of DOM (Hedges et al. 2000). MUC is accessible through extraction, solubilization or hydrolyzation protocols and mostly operationally defined. Different isolation strategies result in differing conceptual definitions of MUC and there are some disparities concerning the nomenclature of MUC, and synonyms are often used (refractory OM, non-hydrolyzable OM, marine humics). A common term, marine humics, refers to the similar solubility in acid/base treatments of marine DOM and soil organic matter.[25] This similarity and photochemical properties have led to the assumption that marine humics have a terrestrial source (“Gelbstoffe”, Kalle 1937). But carbon isotopic composition and the high reactivity of terrestrial DOC in the coastal zone later precluded this theory (Sieburth and Jensen 1968; Nissenbaum and Kaplan 1972; Berner 1989). A different approach suggests that similar (trans-)formation mechanisms are responsible for the chemical analogy between marine and terrestrial humics (Harvey et al. 1984).

[24] Due to the high concentration of potassium in seawater, the natural radioisotope ^{40}K has an approximate activity of 12 Bq L^{-1} whereas the uranium and thorium decay chain radionuclides only contribute less than 2% to the total dose rate (Geibert et al. unpublished). In sediments however, the actual activity is strongly dependent on the uranium content which is spatially variable (Kretschmer et al. 2010).

[25] Note, however, that terrestrial humic substance production is e.g., characterized by “humification” processes, an abiotic heteropolycondensation reaction (Harvey et al. 1984), which is unlikely to occur in seawater due to the low concentrations.

It is generally accepted that the majority of MUC are refractory DOC compounds, although intrinsically bioreactive material may be physically shielded from degradation, due to pseudo-micellar microorganization of DOM (Engebretson and von Wandruszka 1994), sorption to or incorporation in a mineral matrix or organic particles (Keil et al. 1994; Nguyen et al. 2003). On the other hand, some refractory DOM is at least partially characterized. It has been shown with high-resolution molecular methods that carboxylic-rich alicyclic molecules (CRAM) make up a large fraction of deep sea (refractory) DOM (Hertkorn et al. 2006; Hertkorn et al. 2012). On the other hand, it was inferred from isotopic studies that the non-hydrolyzable DOM is composed of lipid-like material (Hwang and Druffel 2003; Hwang et al. 2006a; Roland et al. 2008), contradicting the hypothesis of non-selective preservation as obtained from nuclear magnetic resonance (NMR) studies of POM (Hedges et al. 2001) and chemical representativeness of ultrafiltrates (Sannigrahi et al. 2005).

Marine MUC/RDOM is therefore a mixture of saturated, polycarboxylated carbocycles (Hertkorn et al. 2006) with amide-nitrogen functionalities (e.g., McCarthy et al. 1997). Marine MUC is extensively branched and interlinked (e.g., Hedges et al. 1992) and has an average H:C ratio of 1.4 and O:C ratio of 0.7 (deep East Atlantic solid-phase extracted (SPE-) DOM, values determined from NMR mixing model; Hertkorn et al. 2012), with a C:N ratio of ≈ 15 (Bronk 2002).[26] Other components are highly aromatic, presumably thermo- or petrogenic derived and partly oxidized compounds (e.g., Dittmar and Koch 2006) and a lipid-like fraction (Hwang and Druffel 2003). Marine MUC is at least 4,000 a old (Bauer et al. 1992) and may contain much older sub-fractions (Loh et al. 2004). Only recently, more information on MUC has been obtained using Fourier transform ion cyclotron resonance mass spectrometry (FT-ICR MS) for marine DOM analyses (e.g., Koch et al. 2005; Hertkorn et al. 2006; Flerus et al. 2012).

[26] The elemental compositions and ratios are average deep sea values, supposedly indicative of refractory and uncharacterized DOM.

III SOURCES AND SINKS

A common approach to understand the cycling of carbon through the marine DOM pool is to assess the various sources and sinks of DOM and to quantify the flux of carbon through the DOM pool. Although the largest part of the ocean is assigned to the pelagic realm, the sources and sinks are neither ubiquitous nor constant. Besides the regional differentiation into coastal zone, continental margin and pelagic ocean, especially the seasonal effects in the temperate climate zones, but also in the polar oceans play important roles in determining the relative contributions of the different sources and sinks.

A distinctive feature of organic carbon sources is the place of production. The majority of organic matter in the ocean is produced from in situ sources, hence being autochthonous carbon. It can be distinguished into primary produced carbon and heterotrophic (secondary) carbon. A descriptive comparison of the relative abundances of different cell types in the ocean, responsible for production and/or reworking of organic matter, is presented by Azam and Malfatti (2007): On average, one microliter of seawater contains 10,000 viruses, 1000 bacteria, 100 *Prochlorococcus* cells, 10 *Synechococcus* cells, 10 eukaryotic algae, and 10 protists.[27]

The sinks of DOM can also be divided according to the chemical form of carbon, when it is removed from the DOM pool. This can be inorganic carbon (CO_2) and the general mechanism of this removal is referred to as remineralization. A different mechanism removes DOM as organic carbon from the ocean (e.g., depositing as sediment), which can be summarized as carbon burial.

[27] *Prochlorococcus* and *Synechococcus* are photosynthetic marine cyanobacteria. Protists are a group of unicellular eukaryotic microorganisms.

III.1 Sources: autochthonous carbon

The terrestrial and ocean biospheres contribute almost equally to the global annual net primary production (NPP), about 50 pg C a^{-1} each (Field et al. 1998; Carr et al. 2006b). [28] The NPP is defined as the difference between autotrophic photosynthesis and respiration. This definition includes regenerated production (using ammonium as nitrogen source) and new production (using nitrate). Ammonium derives from immediate remineralization of organic matter and thus regenerated production turns over organic carbon as well. The ratio of new versus regenerated production is described by the f-ratio (Eppley and Peterson 1979). In the ocean, phytoplankton and photoautotrophic bacteria assimilate CO_2 to build up organic matter but unless it enters the dissolved phase, it is not considered as DOM. Several release mechanisms can be distinguished, including extracellular release (either by diffusion or "overflow"; Carlson 2002), grazing by metazoans and protozoans (excretory release, egestion, "sloppy feeding"), [29] cell lysis (via bacterial or viral infection) and solubilization of sinking particles (mostly from dead phytoplankton or "marine snow").

Heterotrophic bacteria are key elements in the oceanic carbon cycle. Approximately 5×10^8 cells L^{-1} in the ocean contribute about 2.2 Pg C (Whitman et al. 1998), assuming ≈ 20 fg C $cell^{-1}$ (Lee and Fuhrman 1987). [30] Although heterotrophic bacteria are primarily considered as a sink of organic carbon (and a source of CO_2), they also produce (i.e., release) DOM. Bacterial production (BP) can be a significant fraction of the photosynthetic primary production, estimated to be 10 – 20% (Ducklow 1999; Kirchman et al. 2009). BP is a measure of the amount of DOC that is converted into bacterial biomass and as such spatially and temporally variable (Kirchman et al. 2009). Together with a determination of the bacterial growth efficiency (BGE), estimates of the net flux of DOC through bacteria can be

[28] However, the net uptake and thus the sink of (anthropogenic) CO_2 is calculated to be only ≈ 2 ± 1 Pg C a^{-1} (Quay et al. 1992; Gruber et al. 2005; Bruwiler et al. 2011).

[29] Protozoa are unicellular eukaryotes, e.g., flagellates, and often referred to as protists whereas metazoans are multicellular "animals". Spanning a huge range of sizes, both groups are part of the zooplankton.

[30] In the past, up to 95% of the open ocean bacterial cells have been considered as "free living" cells, the rest attached to sinking or suspended particles (Cho and Azam 1988; Turley and Mackie 1994). However, this ratio strongly depends on the ocean regime and sinking particles are now recognized as microbial "hot spots", due to their favorable microenvironment (e.g., Simon et al. 2002).

established. BGE in the open ocean is around 15% (Robinson 2008), the remainder of assimilated DOM is either remineralized (and thus serves as heterotrophic metabolic energy source) or lost due to grazing or viral infection (*vide supra*). Although the bacterial DOM originates from an external carbon source, when it is again released to the water phase, it has been imprinted by the bacterial metabolism and is considered as autochthonous DOM. Prominent examples are the unique bacterial cell wall polymer peptidoglycan, the stereoselective production of D-amino acids or the specific 16S rRNA of bacteria.

Other key players in the oceanic carbon cycle are viruses (especially bacteriophages), which are also recognized as being part of the microbial loop. According to the present state of knowledge, viruses are the most abundant life-form in the ocean, with ≈ 10^{10} cells L^{-1} (Bergh et al. 1989). Their biomass is ≈ 200 Tg C, likely standing for the second largest pool of living matter in the ocean (Suttle 2005). Although they do not directly produce significant amounts of DOM, the lysis of bacterial and archaeal cells results in LDOM being released to the dissolved phase. This “viral shunt” is estimated to channel 25% of the photosynthetically produced carbon through this lysis pathway (Wilhelm and Suttle 1999), thus contributing to the redistribution of DOM in the surface and the deep ocean and promoting the production of RDOM (Weinbauer et al. 2011).

Chemoautotrophically derived carbon from bacteria and archaea[31] in the deep sea or in the vicinity of hydrothermal sources are another autochthonous source of carbon in the ocean. This source is less constrained but small compared to the primary production in surface waters (< 1 Pg C a^{-1}, Middelburg 2011). However, it is assumed that chemoautotrophy has an influence on the carbon, oxygen and nutrient balance in the deep sea (Hansman et al. 2009; McCarthy et al. 2011; Wakeham et al. 2012).

[31] The pelagic ocean hosts ≈ 10^{28} archaea (Karner et al. 2001), thus roughly 10^{7} cells L^{-1}.

III.2 Sources: allochthonous carbon

Allochthonous carbon is produced on land and transported via rivers or the atmosphere to the oceans or it originates from geologic sources such as deep sea hydrocarbon seeps or sediment redistribution.

TOM and also atmospheric organic matter (AOM) are as diverse as marine organic matter and similarly difficult to explore (Goldstein and Galbally 2007; Hertkorn et al. 2007). The primary source of TOM in the oceans is riverine transport. An annual flux of ≈ 0.4 Pg OC is estimated globally (Hedges et al. 1997; Schlünz and Schneider 2000), including the major Arctic rivers, contributing as much as 10 – 13% of the global river discharge (Dittmar and Kattner 2003a), carrying 25 – 36 Tg OC a^{-1} (Raymond et al. 2007). The TOM is composed of various age fractions, from recently fixed (modern) organic carbon, pre-aged and remobilized soil organic carbon to kerogen carbon. Especially the old carbon that is mobilized by thawing Arctic permafrost soils and subsequently delivered to the shelves is expected to change the carbon budget at least in the Arctic Ocean (Benner et al. 2004; Woods et al. 2011).

Less constrained but expected to be of minor importance are other allochthonous organic carbon sources like atmospheric wet and dry deposition although these sources can be seasonally and regionally large (e.g., Andreae and Crutzen 1997). Other sources are hydrocarbon seepage (Wang et al. 2001; Pohlman et al. 2011), sediment pore water diffusion (Bauer et al. 1995; Guo and Santschi 2000; Lahajnar et al. 2005) and lateral export of sediment POC (Bauer and Druffel 1998).

III.3 Sinks: the biological pump

The major pathway for the transfer of organic carbon from the CO_2 equilibrated surface waters to the deep ocean is the concurrent biological pump/microbial loop (Figure III.3-1). This concept was developed by Pomeroy (1974) and Azam et al. (1983) and is a main process of carbon sequestration. Photoautotrophically fixed carbon in the surface layer is transported as dead sinking material to greater depth where it is remineralized to CO_2, maintaining a vertical gradient of CO_2 in the ocean's interior.[32] It is estimated that ≈ 5 – 10 Pg POC and ≈ 0.5 Pg $CaCO_3$-C are exported annually from the surface ocean (Dunne et al. 2007; Henson et al. 2011).[33] Bacteria are not able to take up POM directly but have a suite of ecto- and exoenzymes to hydrolyze POM and HMW-DOM to LMW-DOM, which they assimilate via osmosis (Weiss et al. 1991; Arnosti 2011). Archaea are increasingly recognized as DOM consumers, yet their importance as DOM sink is not well known (Robinson and Ramaiah 2011). POM and DOM that is remineralized to CO_2 in the ocean's interior is sequestered until the water parcel comes into contact with the atmosphere again (Aristegui et al. 2002). This occurs via upwelling (coastal, equatorial or in the Southern Ocean) or diapycnal mixing from the ocean's interior. Therefore the biological (and physical) pump only sequesters carbon on relatively short time scales, in the order of the ocean turnover time (Stuiver et al. 1983; Buesseler et al. 2007).

[32] The second pathway for the maintenance of the CO_2/DIC gradient of approx 350 µmol kg^{-1} between surface and the deep ocean is the physical/solubility pump that transports CO_2 enriched cold waters to the deep ocean with the thermohaline circulation (THC). The amount of carbon transported to the deep sea is balanced by the diffusive exchange and upwelling of deep waters and the relative contributions of the different pumps to the overall DIC difference is still being discussed (see e.g., Siegenthaler and Sarmiento 1993; Toggweiler et al. 2003; Cameron et al. 2005).

[33] The final amount of organic matter that is stored in sediments is about 0.1 – 0.5 Pg C a^{-1} and thus less than 1% of the annual global NPP (Hedges and Keil 1995; Boyd and Trull 2007; Dunne et al. 2007).

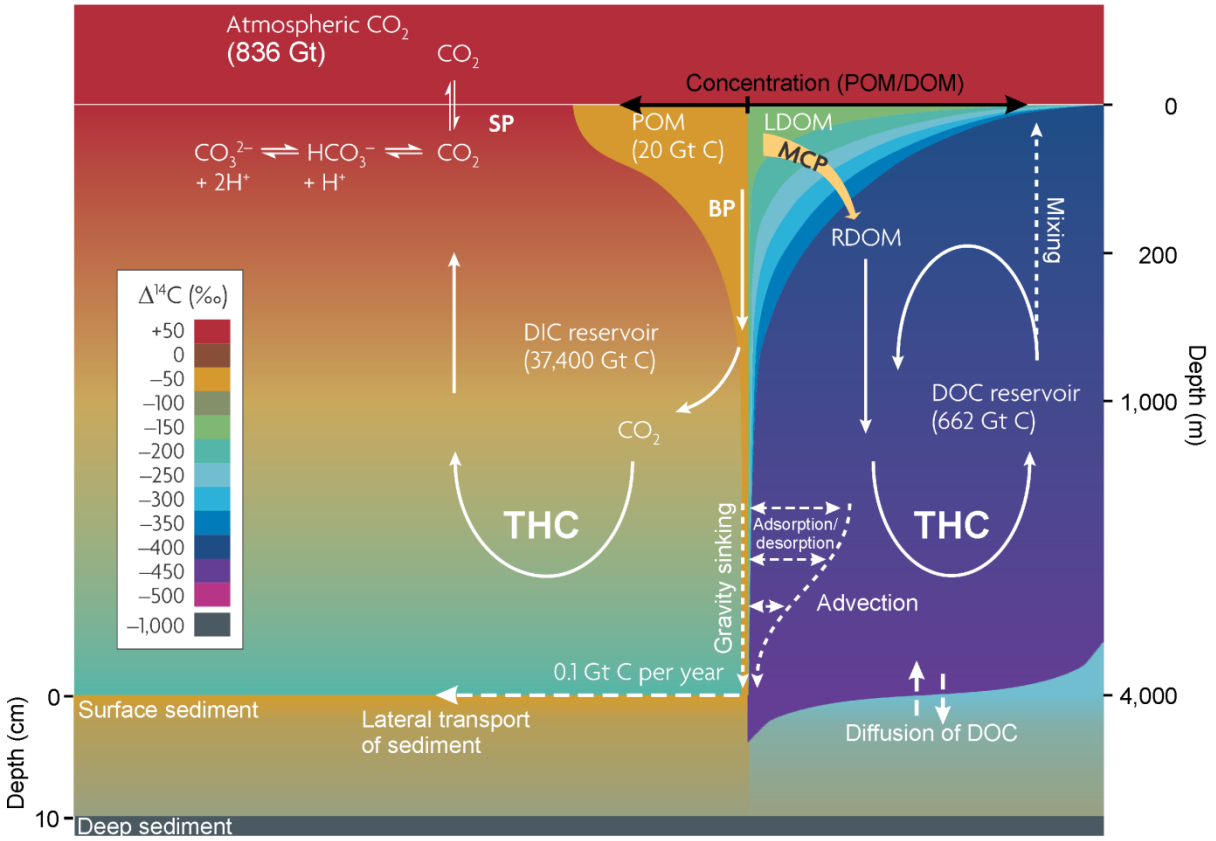

Figure III.3-1. The microbial carbon pump (MCP).

Schematic representation of the major processes determining the fate and age of different carbon species in the ocean. The left hand side of the figure represents particulate and sedimentary carbon and CO_2, the right hand side dissolved (pore water) carbon. Figure adapted from Jiao et al. (2010) with permissions from Nature Publishing Group and modified for sedimentary processes after Bauer et al. (1995).

Atmospheric CO_2 is in dynamic equilibrium with DIC (TCO_2, the sum of all inorganic carbon species) and transported via the “solubility pump” (SP) to depth at high latitudes (not shown) and is distributed with the thermohaline circulation (THC), maintaining a concentration and age gradient. Part of the DIC carbon in the surface is incorporated via photosynthesis into particulate organic matter (POM) and some of it is transported to depth via the biological pump (BP) where most of it is remineralized in the meso and bathypelagic ocean. Some of the POM that is solubilized as (labile, L-) DOM is reworked by microbes (the MCP) and may end as persistent (refractory, R-) DOM in the ocean interior, where it is subject to various physical processes (mixing, advection, ad- and desorption and diffusive exchange with sediment DOC). LDOM may also derive from direct release mechanisms and is only observable in the surface ocean, although reworking and remineralization of sinking POM also occurs in the ocean interior. The small amount of POM that reaches the surface sediment imprints there a younger age than the overlying DIC and DOC and is eventually laterally transported with e.g., bottom currents. Deep sediments are radiocarbon depleted and eventually contribute to the deep sea DOM via point sources (not shown). Generally, the POM pool is the youngest carbon pool, followed by the DIC and DOC pools.

III.4 Sinks: abiotic processes

Photoremineralization of DOM occurs in the photic zones and is expected to be a dominant sink for refractory DOM (Mopper et al. 1991; Moran and Zepp 1997; Riemer et al. 2000). Another physical process is the sorption of DOM onto sinking particles (scavenging, Hwang et al. 2006b) and subsequent deposition to the sediment (Armstrong et al. 2002). The ratio of the sinking material that is sequestered and the time scale of burial depend on the further fate of the organic matter in the sediment. It can be remineralized within the sediment (Bauer et al. 1995; Schmidt et al. 2011), redistributed (important for high sedimentation rate regions and continental margins; Santschi et al. 1999; Francois et al. 2004) or be enclosed in the sediment for geologic time scales. The cycling of seawater though hydrothermal systems is estimated to be a minor removal mechanism of DOM from deep waters (Lang et al. 2006).

IV MAJOR RESEARCH QUESTIONS

Most research in the past decades on the role of the oceanic carbon pool in the global carbon cycle was driven by considerations of climate change. Overarching questions in this context were and are: How does the anthropogenically caused increase of atmospheric CO_2 distribute within the environmental compartments and what are possible (future) carbon sinks that mitigate the impact of increased atmospheric CO_2?[34] Is the strength of recent and emerging sinks well constrained and what are possible feedback mechanisms? How will the ocean respond to warming, enhanced stratification and acidification? Regarding the interactive effects of enhanced ocean acidification with increased atmospheric CO_2, much effort is being expended to understand the chemical and biological responses of the ocean and its inhabitants (e.g., Riebesell et al. 2009; Boyce et al. 2010; Beaufort et al. 2011). In this context, it was recognized that the marine biota, besides the physical response of the oceans, play important roles although even the direction of its influence is not well understood (e.g., del Giorgio and Duarte 2002; Riebesell et al. 2007; Brewer and Peltzer 2009). This chapter will only focus on research questions that are directly related to DOM in the marine context and analytical challenges, as this is a main topic of this thesis.

[34] Although it was assumed earlier that the ocean does not serve as a sink for anthropogenic CO_2 (Keeling 1960), this view has been revised and the ocean was recognized as the dominant CO_2 sink, resulting in a dramatic decrease of the pH ('ocean acidification'). The increase in atmospheric CO_2 content is balanced by a net ocean uptake of ≈ 110 Pg C between 1800 and 1994, accounting for about half of the CO_2 induced by anthropogenic fossil fuel burning and cement production (Sabine et al. 2004).

IV.1 What is the chemical nature of DOM?

It has already been highlighted in the previous chapters that the identification of the exact constituents of DOM is crucial in order to understand its reactivity. Bulk elemental ratios, isotope mass balance and identifiable compounds have been used to infer the distribution and cycling of DOM in the ocean. The molecular complexity of DOM (and likewise terrestrial and atmospheric OM) precludes chromatographic resolution of single compounds from bulk mixtures and hampers identification of new compounds. Biochemical marker substances, accessible through rigorous sample preparation protocols from limnic (lignin, etc), atmospheric (leaf waxes, etc) and autochthonous sources (amino acids, lipids, carbohydrates, pigments, small sulfur compounds, nucleic acids) all comprise the set of known DOM molecules. Since the advent of FT-ICR MS (Senko et al. 1996; Marshall et al. 1998) and its application in marine sciences (Koch et al. 2005), the number of known DOM compounds has increased immensely and there are certainly a lot more to discover (Hertkorn et al. 2008). Simultaneously, unique compounds (similar to biochemical markers) for marine and terrestrial OM have been proposed on the basis of presence or absence of molecular formulas (Koch et al. 2005; Kujawinski et al. 2009). In more detailed studies, changes of NOM composition along physical gradients (mainly salinity) have been explained on a molecular level (Gonsior et al. 2011; Liu et al. 2011; Schmidt et al. 2011; Schmitt-Kopplin et al. 2012). However, mass spectrometric compound identifications are restricted to masses only (resulting in proposed molecular formulas with a given set of elements, Koch et al. 2007). Thus, a major topic in DOM research is the structural identification of these NOM compounds, e.g., through fragmentation experiments (Reemtsma et al. 2008b; Witt et al. 2009; Liu et al. 2011; LeClair et al. 2012). However, isomeric interferences of ions at the same nominal mass cannot be completely resolved so far.

Support for the structural characterization of DOM is mainly derived from NMR studies. In contrast to FT-ICR MS, this technique is at least partially quantitative (Hertkorn et al. 2012) and provides information about functional groups and binding properties of e.g., carbon (e.g., Benner et al. 1992; Hedges et al. 1992; Hedges et al. 2001; Sannigrahi et al. 2005), hydrogen (e.g., Aluwihare et al. 2002; Gogou and

Repeta 2010), nitrogen (e.g., McCarthy et al. 1997; Aluwihare et al. 2005) and phosphorus (e.g., Clark et al. 1998; Young and Ingall 2010).

Thus, of utmost priority for the chemical characterization of DOM is a detailed molecular and structural analysis of the major constituents. In the context of carbon cycling, a major constituent refers either to its relative abundance (compound C-yield) or the absolute rate of formation/degradation, which better describes the biological and biogeochemical relevance of a compound. New concepts are needed to obtain a most representative fraction of DOM for state-of-the art analytical techniques, such as combined extraction methods (e.g., reversed osmosis – electrodialysis, Koprivnjak et al. 2009; Chen et al. 2011; Mao et al. 2012; Tfaily et al. 2012 or coupled ultrafiltration – solid-phase extraction, Simjouw et al. 2005). Concurrently, only the development of unbiased quantification approaches for present high resolution techniques will exploit their full power for the application in NOM research.

IV.2 What are the mechanisms of production and degradation?

Tightly related to the identification of chemical compounds in marine DOM is the quest to understand the underlying mechanism from which DOM is produced, transformed and finally degraded. Autotrophs are the main source for DOM; prokaryotes and other heterotrophs consume, utilize and respire DOM and release a reworked material. Many studies focused on the boundary conditions under which biological production and degradation of DOM occurs, namely energy, nutrient availability, trophic food web interactions, microbial community structure and possible impacts of projected changes in ocean pH, warming, enhanced stratification and related effects.

Production of DOM is ultimately related to autotrophic fixation of carbon (and nitrogen by diazotrophs) mainly via oxidative photosynthesis. Several pathways exist for the release of biomolecules from plankton to the dissolved phase, where immediate transformation takes place. The rates of bulk DOM degradation and microbial consumption are relatively well constrained. However, enzymatic metabolic pathways for the uptake and utilization of DOM by osmotrophic heterotrophs are not well understood yet (Azam and Worden 2004; Arnosti 2011). Observing the changes in chemical composition induced by microbial reworking of simple substrates (Ogawa

et al. 2001; Gruber et al. 2006; Kawasaki and Benner 2006) provided valuable insights into the complexity of the transformation mechanisms. This has also been observed in many studies from incubated surface and deep waters (Kähler et al. 1997; Gruber et al. 2006; Yamashita and Tanoue 2008) or high resolution oceanic depth profiles (Davis et al. 2009; Goldberg et al. 2011; Kaiser and Benner 2012).

Different processes are responsible for the photochemical transformation of DOM. For these photochemical reactions, several possible mechanisms have already been proposed, including photo-assisted radical production (e.g., Mopper and Zhou 1990; Goldstone et al. 2002), trace metal speciation changes and redox reactions (e.g., Barbeau et al. 2001; Powell and Wilson-Finelli 2003; Laglera and van den Berg 2006) and remineralization (e.g., Mopper et al. 1991; White et al. 2010). Well studied are the processes that affect small sulfur-organic molecules, such as dimethyl sulfide (DMS), dimethyl sulfoxide (DMSO) and dimethylsulfoniopropionate (DMSP) because they are strongly coupled to atmospheric effects (Lomans et al. 2002; Yoch 2002).[35] A more complex mechanism involves the sequential photochemical – microbial degradation of DOM (Kieber et al. 1989; Obernosterer et al. 1999; Stedmon and Markager 2005).

Research on the relative rates of production and degradation is related to the different time scales on which these processes occur. Fast microbial reworking in the epipelagic ocean and the mechanisms of transformation are one major topic and much of it is related to the elemental stoichiometry of production and consumption (Redfield 1958; Tyrrell 1999; Raimbault et al. 2008). This addresses also the contribution of DOM accumulation to atmospheric CO_2 drawdown which is not well understood (Carlson et al. 1994; Kähler and Koeve 2001; del Giorgio and Duarte 2002). Similarly, it is not clear under which conditions a tight coupling or an uncoupling of organic matter production and microbial respiration occurs. Uncoupling of production and removal leads to a temporarily accumulation of DOM in surface waters which is later available for the export to the mesopelagic with seasonal convective overturn (Hansell and Carlson 2001; Hopkinson and Vallino 2005; Carlson et al. 2010; Goldberg et al. 2010) or with deep water formation in the North Atlantic

[35] DMS is the major volatile reduced sulfur species in surface waters (Stefels et al. 2007). Through photooxidation in the atmosphere to sulfuric acid, it serves as precursor for cloud condensation nuclei, thus influencing the earth's radiative balance (Bentley et al. 2004).

(Hansell et al. 2002; Hansell et al. 2012). Different climatic regimes cause also different partitioning of the primarily produced organic carbon into DOC and POC pools (Hansell and Carlson 1998b; Karl et al. 1998) but the underlying regulatory mechanisms also need to be identified.

IV.3 What causes a compound to be refractory?

Following the fast microbial utilization, the much slower degradation of the immediate transformation products has led to the concept of a microbial carbon pump (Jiao et al. 2010). As a third arch of the organic carbon sink in the oceans, the microbial pump transfers LDOM into RDOM, which resists subsequent fast turnover (Ogawa et al. 2001). This RDOM accumulates in the ocean as a “background” concentration with apparently old age.

Previous studies have shown that also the RDOM pool undergoes slow degradation, although it is predominantly based on remineralization of DOC (i.e., removal; e.g., Hansell and Carlson 1998a; Aristegui et al. 2002; Hansell et al. 2012) or isotopic mass balances (e.g., Bauer and Druffel 1998; Loh et al. 2004; Mortazavi and Chanton 2004; Hwang et al. 2006b; Beaupré and Aluwihare 2010) and to a minor extent on compositional or structural modifications (e.g., Hwang et al. 2006b; Yamashita and Tanoue 2008) of this refractory material. Only recently, this became available with the introduction of high resolution techniques (e.g., Hertkorn et al. 2006; Reemtsma et al. 2008a; Flerus et al. 2012; Hertkorn et al. 2012).

As highlighted in the previous chapters, accessing the chemical information of the refractory compounds (i.e., the composition and structure) is of major scientific importance. Only then, elucidation of the biological, kinetic or thermodynamic mechanisms that lead to the formation of this RDOM is feasible. No conceptual model exists so far describing whether a common mechanism exists that transfers chemical compounds into the RDOM pool or if this pool is a result of randomly occurring transformations. Accumulation of the RDOM pool could then just arise from the unfavorable composition or structure of these compounds. Possible explanations have been proposed for both hypotheses (e.g., Hedges et al. 2000; Benner and Herndl 2011) and it is likely that the accumulation of RDOM is a superposition of multiple mechanisms. Even more puzzling is the extremely slow rate of RDOM

decomposition/removal in the deep ocean. Possible explanations have been proposed but remain to be verified. These include abiotic removal (attachment to sinking particles, Druffel and Williams (1990)), hydrothermal cycling, (Lang et al. 2006), and biotic pathways (Tamburini et al. 2009; Weinbauer et al. 2011). The contribution of each mechanism to RDOM degradation is completely undetermined. Also, it was hypothesized that the low concentration of individual RDOM compounds in the deep ocean falls below the chemoreceptive threshold for substrate uptake and that the low energy yield from relatively high oxidized compounds makes consumption of RDOM disadvantageous for prokaryotes (Kattner et al. 2011).

IV.4 What is the impact of DOM on trace metal complexation?

It is widely accepted that trace metals (in particular Fe, Co, Zn, etc.) play a promote role in controlling primary productivity (Behrenfeld et al. 1996; Falkowski et al. 1998; Jickells et al. 2005). Especially their low concentrations in surface waters of most world oceans hinder phytoplankton growth and hence reduce the potential for carbon fixation and storage within deep waters (de Baar et al. 1995; Blain et al. 2007; Pollard et al. 2009).

The depth profiles of bioactive trace metals show a nutrient-type shape, with extreme depletion in most pelagic surface waters (Wu et al. 2001). Although dissolved ligand concentrations generally correlate with the abundance of dissolved trace metals, the underlying mechanisms that control the chemical composition of natural organic ligands are different. The molecular nature of organic molecules is determined by photochemical breakdown in the surface, release by cell lysis and remineralization (Boye et al. 2006). The high co-variance with phytoplankton and chlorophyll abundance suggests a biological source of natural organic ligands and hence a biological control on trace metal concentrations in the ocean (Gerringa et al. 2006).

Autotrophs and heterotrophs have developed a suite of mechanisms to sustain their high demand of trace metals and to maintain e.g., a million fold enrichment of iron inside the cell compared to environmental conditions (Morel and Price 2003). At present, one focus is on the production and excretion of natural organic molecules that exhibits extreme affinity and selectivity for trace metals. The

binding of trace metals to ligands ensures a higher ratio of (bio-) available trace metals in solution which otherwise would attach to particles or precipitate from seawater. On the other hand, highly specialized outer membrane receptor proteins can recognize and bind the metal – ligand complex and therefore enable metal transport into the cell (Armstrong et al. 2004)

In the context of global change and its consequences to oceanic primary production and carbon sequestration efficiency it is crucial to understand e.g., the effect of enhanced Fe-input to the high nutrient – low chlorophyll (HNLC) regions (Martin and Fitzwater 1988; Jickells et al. 2005). Much of the overall effect will be dependent on the ability of phytoplankton to keep the metals in solution (Boyd and Ellwood 2010). Here, the increased acidity of the ocean will counteract the complexation affinity of the natural ligands (Millero et al. 2009; Shi et al. 2010).

In the past, isolates from bacterial cultures revealed a set of natural organic ligands which could be molecularly characterized (e.g., desferrioxamines, Martinez et al. (2000) and phytochelatins, Kawakami et al. (2006)). However, the nature and fate of these ligands under natural conditions is still unclear. Electrochemical methods (mainly competing ligand equilibration – cathodic stripping voltammetry, CSV-CLE)[36] are suitable to collect information about concentrations and conditional stability constants of natural organic ligands, but provide little information on the chemical diversity and composition (Bruland 1989; Witter and Luther 1998; Vraspir and Butler 2009). Some attempts have been made to quantify and characterize metal – ligand interactions on an organo-chemical basis (e.g., Yang and van den Berg 2009; Stolpe et al. 2010; Laglera et al. 2011). Molecular level techniques to identify metal-ligands and to investigate biochemical processes on the production and transformation of these ligands will hence be a major upcoming research focus.

[36] CSV-CLE is an electrochemical method to determine conditional complex stability constants and complexing capacities (concentrations) of metals and their ligands. The method was adapted to seawater trace metal (Fe, Cu, Zn and Ni) analysis by e.g., Donat et al. (1994); Gledhill et al. (1994). An example for a competing ligand in iron speciation experiments is e.g., 2-(2-thiazolylazo)-4-methylphenol (TAC; Croot and Johannson 2000).

V OBJECTIVES AND MOTIVATION

This chapter describes the main research objectives related to this work. As already discussed in the previous chapters there are multifaceted key questions in DOM research and only few of them can be addressed within the frame of this work. In the past decades, research on marine, terrestrial and other DOM subclasses could be divided into two main directions, subsumed as an analytic and a holistic approach.

The analytic approach utilizes the detailed study of chemically characterizable constituents in order to understand mechanistic processes that lead to the occurrence and transformation patterns of this set of substances (Hedges et al. 2000). However, there was only little success in identifying new compounds from bulk DOM. This constraint was partly revoked with the introduction of ultrahigh resolution mass spectrometry into marine DOM studies (Koch et al. 2005; Hertkorn et al. 2006; Koch and Dittmar 2006), although this technique is still limited to a few elements only. Additionally, due to the large analytical effort required for the new high resolution methods, the spatial and temporal resolution in previous studies was generally low. A second branch of the analytical approach is culture and incubation experiments with e.g., phytoplankton or bacterial inocula. These experiments were used to infer the turnover rates of defined organic and inorganic precursor molecules and to trace the transformation and fate of these substances over a limited time frame and under controlled conditions (e.g., Ogawa et al. 2001; Kawasaki and Benner 2006). Microbiology and genomics are also increasingly recognized in marine DOM research with enhanced availability of techniques (Jiao et al. 2010; Kujawinski 2011; Weinbauer et al. 2011). Consequently, integrated research efforts, such as the SCOR working group “Microbial Carbon Pump in the Ocean” have been realized in the last few years.

The holistic approach tries to obtain unbiased information and spatial and temporal high resolution on bulk parameters of DOM. Much of what we know about DOM in the ocean’s carbon cycle, in terms of quantities and residence times, was directly derived from the observations of bulk properties, mainly the concentration

and mean age of DOC, the main contributor to DOM. Rates of production or degradation are usually normalized to the change in DOC concentration or age. Two implementations of the holistic approach can be differentiated. Long-term observations of (bulk) DOM parameters at selected ocean sites, so called time-series stations (e.g., BATS, HOT, but also the Sargasso Sea or North Central Pacific) that were continuously sampled for some parameters gave highly valuable insights into the seasonal dynamics of DOM and the coupling mechanisms with e.g., convective water column mixing and nutrient availability (e.g., Carlson et al. 1994; Goldberg et al. 2009).[37] On the other hand, basin wide, spatially high resolution transects (e.g., GEOSECS, CLIVAR, WOCE) illuminated the oceanographic, climatological, and ecological aspects of the distribution of DOM in the surface and deep ocean (Longhurst 2007; Carlson et al. 2010).

[37] The value for Society of continuous time series data is best demonstrated by the success of the Montreal protocol, a 1987 treaty regulating the phasing out of halogenated hydrocarbons, after they have been identified to cause the strong depletion of stratospheric ozone. An insistent plea for long term observation was held by Paul J. Crutzen in his Nobel Lecture. (http://www.nobelprize.org/nobel_prizes/chemistry/laureates/1995/crutzen-lecture.pdf).

V.1 The analytical approach: learning about constituents

The first part of this thesis deals with in depth analysis of the “MUC” fraction of DOM. The goal was to obtain molecular and chemical information and concentrations of individual constituents that were new to or at least underrepresented in DOM research. The benefits from high resolution techniques for the study of DOM compounds and related constituents are highlighted in the first three chapters. In continuation of the success of element specific inductively coupled plasma mass spectrometry (ICP-MS) analysis of (bulk) seawater, an extension to the organic fraction was pursued. Moreover, the frequently demanded implementation of organic and inorganic marine biogeochemistry was aimed to accomplish with the inclusion of metals into the set of simultaneously investigated elements. This first research topic is connected with two main hypotheses of biogeochemical relevance:

- DOP and DOS as relatively unexploited sub-fractions of DOM have distinguishable chemical properties from the bulk DOM. These fractions can be resolved and examined with hyphenated techniques.

- Heteroatoms play a significant role for trace metal – DOM interactions due to their versatile binding properties. Qualitative chemical statements (such as size, polarity, etc.) are accessible through previous separation.

Connected with the first two hypotheses was the aim to develop a quantitative method that provides a basis for mass balance calculations. The applicability of the method that is described in Chapter VI.1 for organic geochemical analysis of the dissolved phase was tested for the “rare” elements P and S that require both high sensitivity and low detection limits. Chemical information is readily accessible due to the versatile character of the hyphenation method which allows easy exchange of the chromatographic system or the extension of the ICP-MS detector to other elements. This combination of properties, i.e., chemical information on minor constituents and quantification capabilities will be of great benefit for trace metal – (DOM-) ligand interaction studies.

In geochemical studies of uranium in seawater, three isotopes are generally considered: ^{238}U, which is the most abundant isotope with a half-life $t_{½} = 4.5 \times 10^{9}$ a.

^{235}U ($t_{½}$ = 7.0 × 10^{8} a) and ^{234}U ($t_{½}$ = 2.5 × 10^{6} a) are the second and third most abundant isotopes and precise measurements of the oceanic isotope ratio $^{234}U/^{238}U$ revealed an extremely constant relationship in space (≈ 1.147) and time (Chen et al. 1986; Henderson 2002). So far, the potential of ^{236}U ($t_{½}$ = 2.3 × 10^{7} a) to serve as a tracer in oceanographic studies has been overlooked, mainly due to the extremely low concentration.[38] With the advance of analytical skills in accelerator mass spectrometry (AMS) even the least abundant isotopes can now be explored for their suitability as geochemical tracers. Calculations have shown that the instrumental detection limit are adequate to measure ^{236}U under natural conditions (Steier et al. 2008; Vockenhuber et al. 2011), but no measured oceanic depth profile existed so far.

- The first objective is therefore to assess if sampling for ^{236}U is possible onboard a research vessel, where other radioisotope sampling and sample handling is performed. The main concern is the use of radioisotope spikes onboard.

- Associated with the delicate sample handling and measurement procedures is the question of wheter or not ^{236}U can serve as a conservative tracer for water mass circulation. This depends strongly on the advance of the anthropogenic ^{236}U signal with deep water circulation.

Both objectives were tested on a research cruise with RV *Pelagia* to the West Atlantic within the Dutch GEOTRACES contribution. The organic ligand interactions and its implications for the biogeochemistry of uranium are discussed in Chapter VI.1. Two depth profiles of ^{236}U were sampled and measurement and modeling results presented in Chapter VI.2.

A different objective, although addressed via an analytic approach, is the study of sea-surface microlayers. A chemical fractionation of compounds is imposed

[38] The global inventory of ^{236}U the upper 1,000 m of the earth's crust is estimated to be only 35 kg. This reservoir is outranged by five orders of magnitude by the amount of anthropogenic ^{236}U that was (and is) released during nuclear bomb testing and nuclear reprocessing plants, although the latter are considered as point sources.

by the occurrence of a hydrophobic organic phase (the “microlayer”) at the sea surface. This allows studying the response of compounds to this induced difference in chemical potential under natural conditions. Much can be learned about the chemical properties of compounds, their “surface activity”, if the system is investigated with ultrahigh resolution organic mass spectrometry, i.e., FT-ICR MS. It allows the calculation of molecular formulas that can be related to chemical properties. Further hypotheses to be tested within this objective also include biogeochemical aspects:

- The bulk chemical composition of source waters influences the phase fractionation of DOM. This phenomenon is accessible through the study of multiphase systems, such as the sea-surface microlayers and may be applied to other multiphase systems, e.g., particle scavenging.

- In multiphase systems, different dominant processes determine the production and fate of DOM substance classes. Biological and abiotic effects are superimposed and determine each other.

- The phase modification by sea salts, i.e., the change in ionic strength, further determines the composition of the organic matter in both phases.

The microtidal estuary of the karstic river Krka (Croatia) was the suitable place to test the hypotheses (Chapter VI.3). In contrast to other estuaries which are dominated by terrestrial organic matter, sufficiently similar samples could be collected to reduce the influence of allochthonous organic matter input, which would likely obscure the effects of surface film fractionation. The effect of the salinity gradient in the estuary for molecular composition of the microlayer and the underlying bulk water was studied and considered in terms of chemical properties. Moreover, fragmentation experiments on selected ions led to proposed molecular structures of anthropogenic contaminants and a distribution of these molecules was inferred from pseudo-homologues.

V.2 The holistic approach: interpreting molecular trends

Compared to commonly applied holistic approaches that targets at measuring bulk properties of DOM such as average bulk elemental concentrations and ratios or mean ages, observed trends in bulk characteristics are here described as the sum of several hundred individual molecular patterns of the DOM constituents. Compared to the analytical approach, individual compounds and their elemental composition and detailed chemical properties are considered as part of larger patterns, thus partly omitting explicit information that can be obtained with ultrahigh resolution mass spectrometry. Based on the chemical information derived from in-depth molecular analysis of DOM and the implementation of multivariate statistical tools, exploitation of large datasets for spatial or temporal extensive sample sets are now feasible. Thus, an unprecedented view on the bulk matter and underlying chemical trends can be achieved. The approach includes several hypotheses connected with the use of FT-ICR MS technique that require thorough testing:

- The fraction of DOM obtained with common extraction methods is representative for the bulk material and invariant to the system boundary conditions (depth, temperature, primary production, climate regime).

- Trends in molecular composition and signal response are unbiased by the measurement or can be sufficiently normalized, hence being representative for diagenetic alteration between samples.

- If the first two hypotheses hold true, then the trends observed from many samples are descriptive of the diagenetic transformation of DOM.

Moreover, broader biogeochemical hypotheses also accompany this approach:

- The release of DOM in the surface results in a rapid and extensive reworking of the organic matter, leading to a molecular pattern that is very similar to the refractory background (Koch and Kattner 2012).

- Diagenetic patterns are intrinsically similar between the system boundary conditions and only dependent on the age of the DOM. Thus, diagenetic alterations can be calibrated with the age of the DOM.

Clearly, the last two hypotheses strongly depend on the verification of the first and second. Only if satisfactory control of the methodological aspects is achieved, the large datasets produced with FT-ICR MS can be reasonably mined.[39] Although it is generally desirable to develop quantitative and qualitative measures for environmental parameters, the toolbox of organic biochemists comprises a wealth of proxies and biomarkers only describing ratios (i.e., relative trends).[40] Hence, the methodological restrictions of FT-ICR MS analysis of SPE-DOM samples do not preclude the use of this technique as a biogeochemical tool. The so far largest dataset of marine FT-ICR MS samples was used to test these hypotheses.[41] Samples were collected on a two month research cruise of RV *Polarstern* and span from low to high latitude, from surface to deep waters and from oligotrophic to eutrophic conditions. In conjunction with supporting data, the description and interpretation of the results are divided into two chapters (VI.4 and VI.5) that are nonetheless interrelated. The huge FT-ICR MS dataset of roughly 10^6 data points was mined for relations with biogeochemical parameters and several correlations were found. A trend of increasing and decreasing peak intensities with the bulk DOM age led to a development of a degradation index and a calibration of DOM age. This functional relationship was further used to describe the ageing of DOM on a molecular level, supported with chemical information. The molecular patterns of DOM could then be related to oceanographic features and used to explain biogeochemical characteristics of the Southern Ocean.

[39] The word mining already implies that although the biogeochemical research questions set the framework (“where do we want to go?”) the direction of exploitation (“which way do we take?”) is not fixed a priori – characteristics of a classical bottom up approach.

[40] Examples are the carbon-number preference index (CPI) applied to the analysis of long chain alkanes from plant waxes in sediments (Bray and Evans 1961, Marzi et al. 1993) or the marine algae alkenone index $U^{K'}_{37}$ and archaeal lipid ether index TEX_{86} to reconstruct paleo sea surface temperatures.

[41] Comprising more than 130 samples, the dataset from manuscript 4 (Chapter VI.4) is to the best of my knowledge, also the largest published FT-ICR MS dataset in environmental science.

Both approaches, the analytic and the holistic, can be viewed as coherent and complementary, although they will be described in separate chapters and applied to different systems. Basically all of the above mentioned objectives try to shed light on the question of why some dissolved organic matter is “refractory” at all. The finding that a relative constant concentration of 37 – 45 µM DOC with a remarkable age of 4,000 – 6,000 a is found throughout the world’s oceans requires substantial resistance to degradation processes for almost geological timescales. This is directly related to predicted responses of the biogeochemical system in the ocean to global climate change. Tackling this question demands a multidisciplinary effort as microbial, photochemical, and physical processes are all capable to disintegrate and remineralize organic molecules into its basic constituents CO_2 and H_2O. Within this work, the analytical and chemical perspective of this topic is highlighted and the following chapters are intended to propose compositional information on DOM as well as chemical interpretations for the refractory character of DOM. Methods were developed, applicable in future studies on DOM that offer access to new aspects of the chemical characteristics of DOM. The overall aim is to broaden our view on the nature of DOM and its interrelation in the global biogeochemical cycling of elements and strengthen much of the present knowledge that was inferred from previous studies and using different techniques.

VI CUMULATIVE MANUSCRIPTS

The following five chapters are reprints of independent manuscripts of three published and two submitted research articles. All articles were submitted to international peer-reviewed journals and are thematically ordered. The content is unchanged and the style adapted to the general format. The references are included in the complete list at the end of the thesis. Original reprints of the three published manuscripts can be found as addendum to this thesis.

1. Lechtenfeld, O.J., B.P. Koch, W. Geibert, K.-U. Ludwichowski, and G. Kattner (2011). Inorganics in organics: Quantification of organic phosphorus and sulfur and trace element speciation in natural organic matter using HPLC-ICPMS. *Anal Chem* **83**(23): 8968-8974. doi: 10.1021/ac201765a

2. Christl, M., J. Lachner, C. Vockenhuber, O. Lechtenfeld, I. Stimac, M.R. van der Loeff, and H.-A. Synal (2012). A depth profile of uranium-236 in the Atlantic Ocean. *Geochim Cosmochim Acta* **77**(0): 98-107. doi: 10.1016/j.gca.2011.11.009

3. Lechtenfeld, O.J., B.P. Koch, B. Gasparovic, S. Frka, M. Witt, and G. Kattner (in press). Molecular and optical properties of the sea surface microlayer in a stratified estuary. *Mar Chem.*

4. Flerus, R., O.J. Lechtenfeld, B.P. Koch, S.L. McCallister, P. Schmitt-Kopplin, R. Benner, K. Kaiser, and G. Kattner (2012). A molecular perspective on the ageing of marine dissolved organic matter. *Biogeosciences* **9**(6): 1935-1955. doi: 10.5194/bg-9-1935-2012

5. Lechtenfeld, O.J., B.P. Koch, R. Flerus, S.L. McCallister, P. Schmitt-Kopplin, and G. Kattner (in preparation). Molecular transformation and degradation of refractory dissolved organic matter and role of the Weddell Sea for global carbon cycling. *Geochim Cosmochim Acta.*

VI.1 Manuscript 1[42]

Inorganics in organics: quantification of organic phosphorus and sulfur and trace element speciation in natural organic matter using HPLC-ICP-MS

Oliver J. Lechtenfeld,[1,*] Boris P. Koch,[1,2] Walter Geibert,[3,4] Kai-Uwe Ludwichowski,[1] and Gerhard Kattner[1]

1 Alfred Wegener Institute for Polar and Marine Research, Am Handelshafen 12, 27570 Bremerhaven, Germany

2 University of Applied Sciences, An der Karlstadt 8, 27568 Bremerhaven, Germany

3 School of GeoSciences, The University of Edinburgh, Edinburgh EH9 3JW, UK

4 Scottish Association for Marine Science (SAMS), Scottish Marine Institute, Oban, Argyll PA37 1QA, UK

* Corresponding author. Phone: +49 471 4831 2238. E-mail: oliver.lechtenfeld@awi.de

[42] This manuscript has been published in *Analytical Chemistry* in October 12, 2011. I developed the method, collected the samples, conducted the experiments, performed the evaluation and wrote the article. Reprint with permission from the American Chemical Society.

VI.1.1 Abstract

A method is presented for the chemical characterization of natural organic matter (NOM). We combined reversed-phase chromatographic separation of NOM with high resolution inductively coupled plasma mass spectrometry. A desolvation technique was used to remove organic solvent derived from the preceding chromatographic separation. We applied our method to solid-phase extracted marine dissolved organic matter samples from South Atlantic Surface Water and Antarctic Surface Water. The method provided a direct and quantitative determination of dissolved organic phosphorus and sulfur in fractions of differing polarity and also allowed simultaneous speciation studies of trace elements. Dissolved organic carbon:phosphorus and carbon:sulfur ratios for the different chromatographic fractions of our two samples ranged between 341 – 3,025 for C:P and 11 – 1,225 for C:S. Differences in elemental distribution between the fractions were attributed to different biochemical environments of the samples. Sulfur was exclusively found in one hydrophilic fraction, while uranium showed a strong affinity to the hydrophobic fractions. Our method was designed to be easily adapted to other separation techniques. The elemental information will deliver valuable information for ultrahigh resolution molecular analyses.

VI.1.2 Introduction

Natural organic matter (NOM) is degraded biomass that occurs in soils, sediments and water. Its composition is highly complex and polydisperse — the major reason which hinders a comprehensive molecular chemical characterization. In the past ten years, the application of ultrahigh resolution Fourier transform ion cyclotron resonance mass spectrometry (FT-ICR MS) allowed important insights in the molecular composition of thousands of NOM compounds (Kujawinski et al. 2002; Stenson et al. 2003; Koch et al. 2007; Sleighter and Hatcher 2007; Hertkorn et al. 2008; Koch et al. 2008; Witt et al. 2009). However, FT-ICR MS analyses of NOM is not quantitative and the unequivocal identification of molecules containing sulfur and phosphorus is particularly difficult (Koch et al. 2007).

Dissolved organic phosphorus (DOP) can be a limiting element for phytoplankton growth in the ocean (Benitez-Nelson 2000). DOP contains a considerable number of monomeric and polymeric phosphate esters, phosphonates and other N and S containing compounds (nucleotides, vitamins, etc.; Karl and Björkman 2002; Young and Ingall 2010). The chemical knowledge of dissolved organic sulfur (DOS) in marine organic matter is scarce and mainly restricted to small sulfur containing compounds such as dimethyl sulfide, dimethylsulfoniopropionate and methanethiol (Yoch 2002; Bentley and Chasteen 2004). Other thiols, e.g., phytochelatins are known to be important metal chelators (Wei and Ahner 2005), although their abundance in open ocean seawater is very low (Ahner et al. 1998). Few FT-ICR MS studies revealed a set of additional DOS compounds in marine NOM in the deep sea and in brine samples (Kujawinski et al. 2009; D'Andrilli et al. 2010b).

Organic metal speciation is of great interest in environmental science, because it affects bioaccumulation and toxicity (e.g., Cr, Hg, Cd; Ullrich et al. 2001; Luoma and Rainbow 2005; Rainbow 2007), bioavailability (e.g., Fe, Zn; Morel and Price 2003; Hirose 2006) and transport and distribution of trace metals (e.g., Mn, Th; Hirose 1996; Llewelyn et al. 2002). Many trace metals in seawater are essential constituents for a number of enzymes, and therefore their remineralization indirectly controls bioproductivity and species composition in the ocean.

In seawater, the analysis of trace concentrations of organic compounds (µg to mg L^{-1} range) and transition metals (ng to µg L^{-1} range) is especially demanding

due to the high salt concentration (35 g L^{-1}). To prevent interferences of sea salts, many analytical techniques require preceding enrichment and desalting procedures such as ultrafiltration, reversed osmosis or solid phase extraction (SPE). For speciation studies, the application of such extraction methods introduces an additional analytical challenge because the requirements for sample preparation (filter materials, storage bottles, acidification steps, etc.) in organic and inorganic studies often diverge. However, it is known that the retention of trace metals on e.g., C18 adsorber material (Mackey 1982, 1983; Donat et al. 1986; Kaczynski and Kieber 1994; Otero-Romani et al. 2005) and octanol partitioning (Turner and Mawji 2004) is considerable, and a large fraction of these metals exists in organic complexes rather than in a free ionic form in marine NOM (Macrellis et al. 2001; Morel and Price 2003; Laglera and van den Berg 2009). In the last years, research on the structure of organic ligands for trace metals in seawater intensified (Mawji et al. 2008; Manceau and Matynia 2010), but little is known about the organic complexation of uranium in seawater (Mann and Wong 1993; Alberti et al. 2007).

High resolution inductively coupled plasma sector field mass spectrometry (ICP-MS) is a favorable technique for the quantification of elements in NOM. ICP-MS is highly sensitive and allows for multi-element and even multi-isotope analyses. Hyphenation with separation techniques also enables speciation studies. Vogl and Heumann, for example, combined size exclusion chromatography (SEC) with isotope dilution ICP-MS to determine the dissolved organic carbon (DOC) content of humic substances fractions (Vogl and Heumann 1998). It has been previously shown that P could be detected in reversed-phase high performance liquid chromatography (RP-HPLC) fractions with ICP-MS in derivatized carboxylic acids (Cartwright et al. 2005) and phosphorylated proteins at very low concentrations (nM to pM; Wind et al. 2001a). To our knowledge, for marine DOP, similar applications have not been realized so far. Speciation of organic sulfur with HPLC-ICP-MS was carried out for phosphorylated peptides (Lindemann et al. 2007). Wang et al. developed a method for protein quantification via sulfur isotope dilution analysis in a coupled SEC-ICP-MS system (Wang et al. 2007). To our knowledge, no speciation study of marine DOS using LC-ICP-MS exists in the literature. ICP-MS in combination with SEC has also been applied to study speciation of trace metals in fresh water (Rottmann and Heumann 1994a); a different approach uses flow field-flow fractionation coupled to ICP-MS to separate colloidal size classes of trace meta – dissolved organic matter

(DOM) complexes (Stolpe et al. 2010). The use of silica based RP-HPLC separation for trace metal speciation studies is known to introduce artifacts (Mackey 1983; Mackey and Higgins 1988), and a careful investigation of metal recoveries is crucial (Mackey 1985).

The overall aim of this study is to establish a simultaneous determination of trace organic compounds and trace metals and to merge the analytical potentials of advanced polarity separation and ICP-MS. Our goal is to provide quantitative elemental information on different fractions of highly complex – low concentrated NOM in seawater. Simultaneous online ICP-MS detection of P and S provides a new approach to chemically assess DOP and DOS. This will be a prerequisite to improve molecular studies which are based on the analyses of chromatographic fractions by FT-ICR MS (Koch et al. 2008). In addition, the chromatographic separation of U is exemplarily discussed to demonstrate the capability of the method as a tool for trace metal speciation studies.

VI.1.3 Experimental section

Samples. Two surface water samples (2 m depth) were collected using a towed fish sampler (Sarthou et al. 2003) during the RV *Polarstern* cruises ANT-XXV/1 and ANT-XXV/2. One sample was collected in nutrient-poor surface waters of the Guinea Basin (South Atlantic Central Water, SACW); the other sample originates from the southern rim of the Antarctic Circumpolar Current (ACC) south of the Polar Front (Antarctic Surface Water, AASW) and was characterized by high nutrient and low DOC concentration. Samples were collected by pumping surface water with a Teflon membrane pump to the ship's lab, filtered with 0.2 µm cellulose acetate in-line filters (Sartolab P20, Sartorius) and acidified with hydrochloric acid (suprapur, Merck) to pH 2. DOM extraction was performed with 1 g solid phase extraction cartridges (PPL, Varian) according to Dittmar et al. (2008). A volume of 5.4 L and 4.85 L of the sample (SACW and AASW, respectively) was extracted and finally stored in 4.8 mL methanol (LiChrosolv, Merck) in precleaned LD-PE bottles at -20 °C. The cleaning procedures for sampling material was adapted from GEOTRACES (Cutter et al. 2011). There was also no significant contamination of DOC.

Chemicals and Reagents. Ultrapure water (18 MΩ) for diluting reagents and samples was always obtained from a two-step purification system (ElixS and Milli-Q Plus 185 with UV, Millipore). Nitric acid (analytical grade, OmniChem) was purified twofold in a quartz subboiling distillation apparatus. High purity methanol (LiChrosolv, Merck) was further purified by subboiling distillation in a quartz apparatus to reduce trace metal contributions. Standard solutions for calibration of the mass spectrometer were prepared from commercially available stock solutions (nonmetal multi-element standard for ICP-MS, VHG Labs; ICP-MS multi-element standard 23 solution, Merck).

HPLC system. Chromatographic separation was carried out according to Koch et al. (2008). The HPLC system (Hitachi/VWR) was equipped with a pump (L6200A), interface (D6600), autosampler (AS4000A), column oven (L5025), diode array detector (DAD, L4500) and fluorescence detector (FLD, F1050).

The separation was performed using a polar endcapped C18 reversed-phase column (4 µm Hydro-RP 80 Å, 250 × 4 mm, with AQ C18 Guard Column; Phenomenex, Synergi) running a gradient from 100% ultrapure water, adjusted to pH 7 (±0.05) with diluted NaOH (suprapur, Merck), to 100% methanol. The gradient was linearly increased from 0 to 100% methanol during a period from 6 to 20 min. In contrast to the original method, the HPLC-flow remained constant at 0.3 mL min^{-1} to avoid changes in the hydrodynamic conditions of the flow system. The column oven temperature was 25 °C. Both detectors were connected in series; absorbance was recorded between 200 and 400 nm, and the fluorescence signal was measured at 260 nm excitation and 430 nm emission wavelength (data not shown). Methanol reached the detector after ≈ 23 min. 30 µL and 40 µL of the extracts were injected for the SACW and AASW sample, respectively. The injection volume was adjusted to ensure similar extract DOC amounts (≈ 1 µmol) on the column for each chromatographic run.

Fraction collection. For DOC analysis, fractions were collected at the outflow of the fluorescence detector using a fraction collector (Foxy Jr., Teledyne Isco). The volume of 10 repeated injections were collected, then either freeze dried (aqueous fraction) or dried under N_2 gas (methanol fractions) and redissolved in 1 mL ultrapure water. The same injection volume as for the coupled analysis was used

since the column is sensitive to overloading for some fractions. Blank fractions were prepared without sample injection and were used to monitor the carbon contamination of the HPLC system.

Hyphenation between HPLC and ICP-MS. The system configuration (Figure VI.1-1) was adapted from Rottmann and Heumann (1994b). Compared to their original publication we used a reversed-phase column which introduces an organic solvent (methanol) into the inductively coupled plasma. Therefore following measures were taken to reduce the solvent loading of the combined flow and to stabilize the baseline of the ICP-MS signals: (i) reduction of the combined flow of 0.5 mL min^{-1} to about 0.05 mL min^{-1}, (ii) addition of 10% methanol to the postcolumn spike solution to make use of the solvent enhancement effect (Hu et al. 2004; Liu and Beauchemin 2006) and to reduce the large changes in matrix viscosity when introducing small amount of organic solvent into the nebulizer, (iii) desolvation of the sample aerosol to remove most of the methanol from the sample droplets and obtain a dried aerosol.

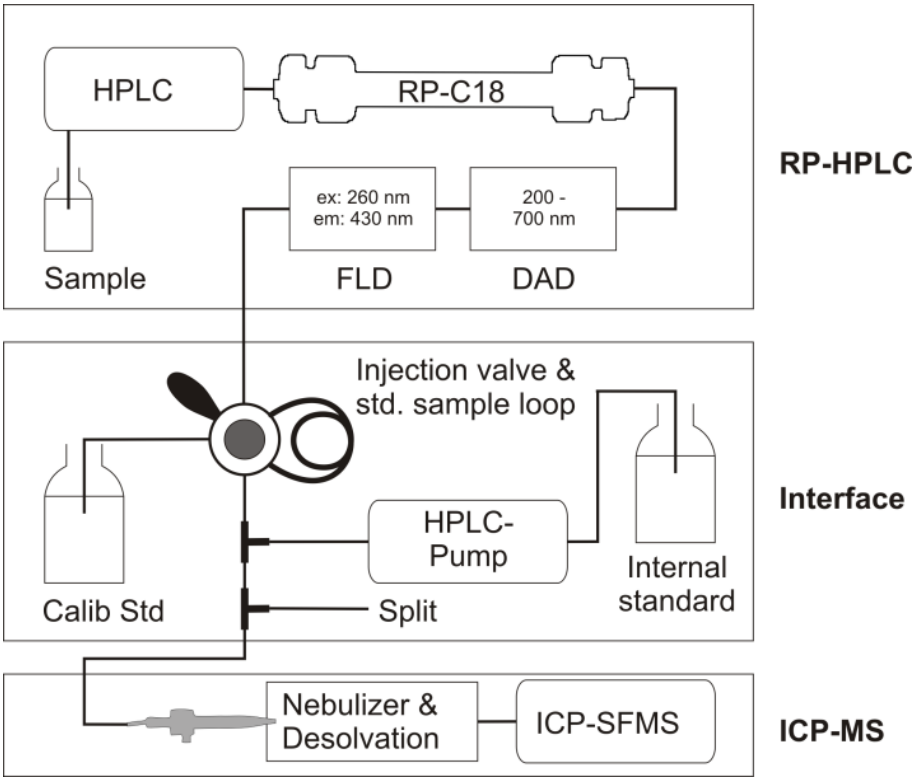

Figure VI.1-1. Hyphenation of RP-HPLC and ICP-MS.
Chromatographic column was a Synergi Hydro-RP C18 column. Diode array detector (DAD) recorded absorption between 200 and 700 nm whereas fluorescence detector (FLD) recorded fluorescence at 260 nm excitation and 430 nm emission.

The outlet of the fluorescence detector was connected with a PFA tubing (0.01 in inner diameter, ID) to a 6-port injection valve (Teflon, Upchurch Scientific), equipped with a 25 µL sample loop (0.4 ft × 0.02 in ID, PFA Hi Pur, Upchurch Scientific) for the addition of calibration standards. Standards were loaded by suction technique from a clean reservoir into the sample loop. Continuous addition of the internal standard (in 1 M nitric acid) to the HPLC-flow was achieved by a static mixing T-fitting (Upchurch Scientific). This flow was set to 0.2 mL min^{-1} using an HPLC-pump equipped with polyether ether ketone parts (PEEK, Alltech-Grace). Prior to nebulization the flow was reduced to 0.05 mL min^{-1} (micro-metering split valve, Upchurch Scientific) to lower the sample load in the plasma.

Samples were nebulized using an APEX-Q system (all quartz, Elemental Scientific) with a PFA micro-concentric nebulizer, a heated cyclonic spray chamber (100 °C), and a Peltier-cooled condenser (2 °C). Furthermore, a membrane desolvation unit (heated macro-porous PTFE, SPIRO-TMD, Elemental Scientific) was installed at the outlet of the APEX-Q for successive elimination of the matrix components of the aerosol, especially of methanol.

ICP-MS system. ICP-MS conditions are given in Table VI.1-1. A high resolution ICP mass spectrometer (Element 2, Thermo Fisher Scientific) equipped with a platinum guard electrode, nickel sampler and skimmer cones, was used. Data acquisition parameters were set for a full scan cycle within 2 s which was a compromise between time resolution (sampling frequency per peak) and counting statistics (dwell time per mass measurement and noise of the individual signal; Laborda et al. 2000) The instrument was tuned daily for optimized plasma conditions and accurate mass calibration with a multi-element tuning solution (≈ 0.1 ppb in 10% methanol, Merck). Signals of ^{31}P, ^{32}S, ^{238}U and ^{103}Rh were recorded in medium mass resolution (4,000 m/Δm). ^{103}Rh was used as internal standard with a concentration of ≈ 5 ppb in the spike solution. This Rh concentration resulted in an intensity of ≈ 5×10^4 cps at a split-ratio of 0.05/0.45 mL min^{-1}.

Data acquisition of the MS was triggered from the HPLC-system (TTL cable). The dead time between the fluorescence detector and MS was ≈ 60 s at a split-ratio of 0.05/0.45 mL min^{-1}.

Table VI.1-1. Instrumental ICP-MS conditions.

Plasma conditions	
RF power	1300 W
Ar sample gas	1.01 – 1.04 mL min^{-1}
Ar auxiliary gas	1.01 mL min^{-1}
Ar cool gas	16 mL min^{-1}
Ar sweep gas	6.5 bar
Data acquisition	
Scan mode	Peak hopping
Scan type	EScan
Samples per mass	12
Sample time	15 ms
Integration window	30%
Integration type	Average
Complete mass scan	2 s

DOC analysis. DOC was analyzed on a Shimadzu TOC-V_{CPN}+TNM-1 analyzer with external calibration with potassium hydrogen phthalate (PHP, Merck). Methanol extracts from solid-phase extracted samples (50 µL aliquots) were evaporated by N_2 gas flow to complete dryness and subsequently redissolved in 6.5 mL ultrapure water for DOC analysis. All samples (in duplicate) were acidified (0.1 M HCL suprapur, Merck) and purged with oxygen for > 5 min. HPLC fractions were injected directly on top of the catalyst tube using a manual injector (Shimadzu). Three to 5 replicates of 50 µL acidified sample were injected with a syringe (Hamilton). Performance of the instrument was recorded by daily analysis of in-lab PHP standard solutions and reference material (deep sea reference, DSR, Hansell research lab).

Data treatment. Raw data from the HPLC system and the mass spectrometer were analyzed with a home-built program. ICP-MS transient signals were treated with a smoothing algorithm (11 point quadratic; Savitzky and Golay 1964) prior to peak integration.

VI.1.4 Results and discussion

Separation mechanism. Prior to the coupling of HPLC and ICP-MS, a new assessment of our recent chromatographic method (Koch et al. 2008) was carried out at a constant flow of 0.3 mL min^{-1}. The injection of 50 µL methanol on the column led to an elution volume of 2.76 mL. After 6 min (= 1.8 mL) the gradient program started, and the start of the gradient was detected by the DAD (210 nm) at an elution volume of 6.96 mL. The difference of 2.4 mL is attributed to the gradient delay volume (i.e., the volume between mixing chamber and injection port). When injecting a DOM sample, the first peaks appeared already at 1.2 mL elution volume and hence ahead of the methanol matrix. This can be explained by a size separation mechanism since very large molecules are excluded from the 80 Å pore diameter of the RP column material. In addition, the clogging of the pores by molecules adsorbing at the rim of the pores (e.g., dimer or multimer formation of highly polar, carboxylic rich substances; Koch et al. 2008, potentially supported by a central metal ion) may reduce the effective pore diameter for subsequent molecules (Hearn and Aguilar 1987; Koch et al. 2008). This effect is known for humic acid fractions of NOM (Engebretson and von Wandruszka 1994; Piccolo 2001) and SEC analysis of DOM (Conte and Piccolo 1999; Dittmar and Kattner 2003b; Piccolo and Spiteller 2003).

DOC content of fractions. For the quantitative assessment of the different chromatographic fractions and their contribution to the total DOC in the sample we measured DOC in each fraction. Furthermore, we evaluated whether UV absorption can be applied as an estimate of DOC concentration in the chromatographic run. If using a DAD detection wavelength of 210 ± 5 nm absorption from $n \rightarrow \sigma^*$ (e.g., alcohols, ethers) and $\pi \rightarrow \pi^*$ electronic transitions (e.g., conjugated systems including carboxylic groups and partly aromatic systems) dominate. These chromophores usually compose the backbone of NOM molecules and therefore give a measure of the overall carbon content in the sample (Hertkorn et al. 2006). The DAD_{210nm} peak areas correlated highly significantly ($r^2 = 0.92$; $p < 0.001$; $n = 32$) with the DOC concentration of the fractions (Figure VI.1-2) suggesting that UV absorption can be reasonably applied as an approximation of the carbon amount in our samples.

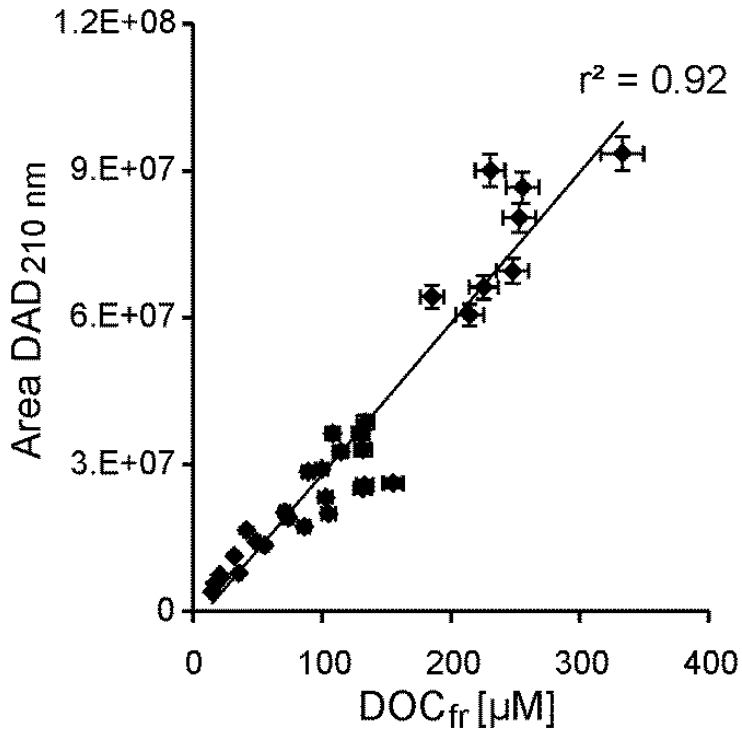

Figure VI.1-2. UV peak area versus DOC concentration.
UV peak area (diode array detection, DAD; [a.u.] = arbitrary unit) at 210 nm versus DOC concentrations (DOC_{fr}) of fractions F1 – F6 (see also Table VI.1-2). Marine surface water (SACW, AASW) and two additional deep water samples (data not shown furthermore) were measured as triplicates. Error bars indicate average relative standard deviation for both measurements (3.7% for DOC and 1.2% for DAD areas).

ICP-MS signal stability and influence of methanol. The use of organic solvents in a coupled HPLC-ICP-MS system influences the plasma stability by lowering the plasma temperature, by reducing the amount of Ar^+-species and finally by decreasing the intensity of the analytes at high organic solvent concentrations (Olesik and Moore 1990; Liu and Beauchemin 2006). The high vapor pressure of organic solvents can even extinguish the plasma. Another negative side effect is the buildup of perturbing amounts of carbon on the cones that leads to shifts in the signal intensity and resolution.

The ^{31}P and ^{32}S short term signal stability, calculated as the relative standard deviation (RSD) of the baseline (analyte signal between 0 and 4 min, where no substance is eluting), was in the range of 1 to 4% for the smoothed values. ^{238}U showed a much higher noise signal (RSD 20 – 40%), as the overall intensity was very low in medium resolution. However, sample peaks showed a U signal that was mostly higher by a factor of 10^2 to 10^3 than the baseline noise. Using the values

normalized to the internal standard, the RSD of the ratio did not change compared to the smoothed analyte signal.

A blank injection of 30 µL clean methanol led to an average loss of ^{103}Rh intensity of ≈ 20% between the gradient onset at 23 min and 100% methanol. A similar signal drift in the methanol gradient was observed for ^{31}P, ^{32}S and ^{238}U in the sample runs. Changing viscosity of the eluent as observed by an increasing backpressure of the second HPLC pump might contribute to the change in signal intensity. However, the decrease was not identical for all elements. We observed small deviations of the intensity ratios ^{31}P/^{103}Rh, ^{32}S/^{103}Rh and ^{238}U/^{103}Rh. Signal intensities also depend on the mass of the ions, their ionization potential and their extent/degree of oxide formation (Hu et al. 2004; Bendahl and Gammelgaard 2005) which in turn depend on the methanol concentration in the solvent. As a consequence, a daily sensitivity correction for each analyte was obtained from a blank run and applied to the sample measurements as suggested previously (Wind et al. 2001b).

Multiple injections of the same sample showed a highly significant correlation between the RSD values the DAD_{210nm} area and the RSD values of the ICP-MS signal area (r^2 = 0.75; p < 0.01, n = 8). Thus, the overall analytical precision is mainly influenced by the separation step rather than changing ICP conditions.

At the end of a chromatographic run (85 min) all signals returned to the initial value. Remnants of the organic solvent were rinsed with the nitric acid added postcolumn to the HPLC. Between two chromatographic runs, a correction for instrument mass drift was performed by running the Method Mass Offset measurement to support the “Auto Lock Mass” feature of the Element 2 in case the mass peaks shifted too much from the centroid mass during the 85 min analysis time. This procedure was necessary because of the small mass window that was chosen to increase the time resolution of the ICP signal.

Calibration and recovery. Calibration for P, S and U was carried out with a postcolumn injection of three calibration standards via the 25 µL sample loop into the HPLC flow (Figure VI.1-1). Due to the broad and nonsymmetrical peak shape in the sample runs we used peak areas rather than peak heights for quantification. The area of the blank (1 M HNO_3) was subtracted from each standard. The lowermost calibration level was 1.2 ng P, 0.25 ng S and 2.1 pg U. Limits of detection, as obtained by dividing three times the standard deviation (n = 4) of the lowermost calibration standard by the slope of the corresponding calibration function were 0.3 µM P, 0.01 µM S and 0.07 nM U.

To prove the suitability of the use of inorganic salts as standard solutions, a four point standard-addition of a methanol extract with calibration solutions was performed in the external sample loop. From the linear response of the P, S and U signals (r^2 > 0.995) we conclude that the chemical form of the calibration standards did not influence the ICP-MS response as the organic molecules in the sample should dissociate and ionize completely in the ICP.

The recovery of analytes during the HPLC separation was determined after replacing the column with a 100 cm × 0.02 in ID PEEK capillary. The total recovery by the HPLC was calculated as the amount of analyte eluting between 4 and 37 min compared to the concentration in the total extract (Table VI.1-2). For sample SACW and AASW, recoveries were 75 and 93% for P, 95 and 102% for S and 85 and 91% for U.

Table VI.1–2. Concentration and recovery of P, S in extract and fractions of samples SACW and AASW.[a]

		MeOH extract [b]	Fractions						Fractions [%] [c]	Total run [%] [d]
			F1	F2	F3	F4	F5	F6		
SACW	DOC [µM]	30966	1210	1913	5093	1383	7457	2870	64	102
	P [µM]	43	0.4	< 0.3	8	2	13	3	62	75
	S [µM]	132	4	16	27	6	38	7	74	95
	C:P	721	3025	-	614	751	595	848		
	C:S	234	309	123	190	215	196	395		
AASW	DOC [µM]	22340	653	1240	5207	1710	5667	1970	74	
	P [µM]	26	< 0.3	< 0.3	15	< 0.3	6	1	84	93
	S [µM]	176	4	116	23	3	17	2	93	102
	C:P	850	-	-	341	-	960	1921		
	C:S	127	181	11	224	545	333	1225		

[a] For values below the detection limit, no elemental ratio was calculated. Error estimates: Triplicate extraction of surface water resulted in a RSD of < 7% (DOC, P) and < 2% (S) for the total MeOH extracts; chromatographic separation of methanol extracts resulted in an average RSD of 4% (DOC; n = 8) and 9% (P, S; n = 3) for individual fractions. [b] Concentration as in unfractionated methanol extract. DOC in the original samples was 76.9 µM (SACW) and 51.8 µM (AASW). Extraction efficiency for C was 40% for both samples. [c] Fractions [%] calculated as sum of the six fractions F1 to F6. [d] Total run [%] represents the complete chromatogram between 4 and 37 min.

Analysis of DOP, DOS and U. Both sample chromatograms showed six peak-like regions, which were detected between 5 – 12 min and 23 – 32 min (Figure VI.1-3). The first small peak showed traces of P and S (F1, 4.7 – 5.8 min). The relative intensity of the second peak differed between the samples and was most pronounced in the S signal, whereas the DAD signal was only a small shoulder (F2, 5.8 – 7.0 min). The third peak was also variable in the two samples and highest in the DAD signal (F3, 7.0 – 9.7 min). The fourth peak was only pronounced in the SACW sample (F4, 10.0 – 11.2 min). Between the first and the second group of peaks no additional signals were detected for about 10 min. In other NOM samples (not shown) smaller additional peaks were found in this part of the chromatogram. The second group of peaks started with the methanol gradient and therefore resulted in a sharp peak. The DAD signal at 210 nm of this peak was always highest whereas the ICP signal varied between samples and elements (F5, 22.7 – 25.0 min). DAD, P and S showed a pronounced tailing as a result of the large number of components with very similar chemical properties which successively elute with increasing methanol content. U detection resulted in a second peak especially in the SACW sample (F6, 25.0 – 27.2 min). In the final part of the HPLC run (up to 37 min; 100% methanol) some smaller peaks appeared in the DAD detection but were not detected with the MS.

There was a remarkable difference in the relative amount of S in fraction F2 (70% in sample AASW and 16% in SACW) as well as P in fraction F3 (68% in AASW and 31% in SACW). According to the HPLC separation, P and S in sample AASW were incorporated in larger and more polar compounds. In fact, P and S are incorporated in large, polar biomolecules (e.g., phosphate esters, phosphonates). Such compounds can be quickly biodegraded, especially in regions where P is limiting the phyto- and bacterioplankton growth in surface waters (Mather et al. 2008). This indicates that DOM from AASW contains fresher (less degraded) material than from the SACW sample.

The stoichiometric elemental ratios C:P and C:S (as organic carbon, phosphorus and sulfur) potentially reflect the diagenetic state of DOM (Clark et al. 1998). This has been explained by different turnover rates of labile and refractory DOM and is reflected in a different C:P stoichiometry between surface and deep

ocean (C:P surface: 374 ± 59; C:P deep ocean: 3511 ± 1314; Hopkinson and Vallino 2005).

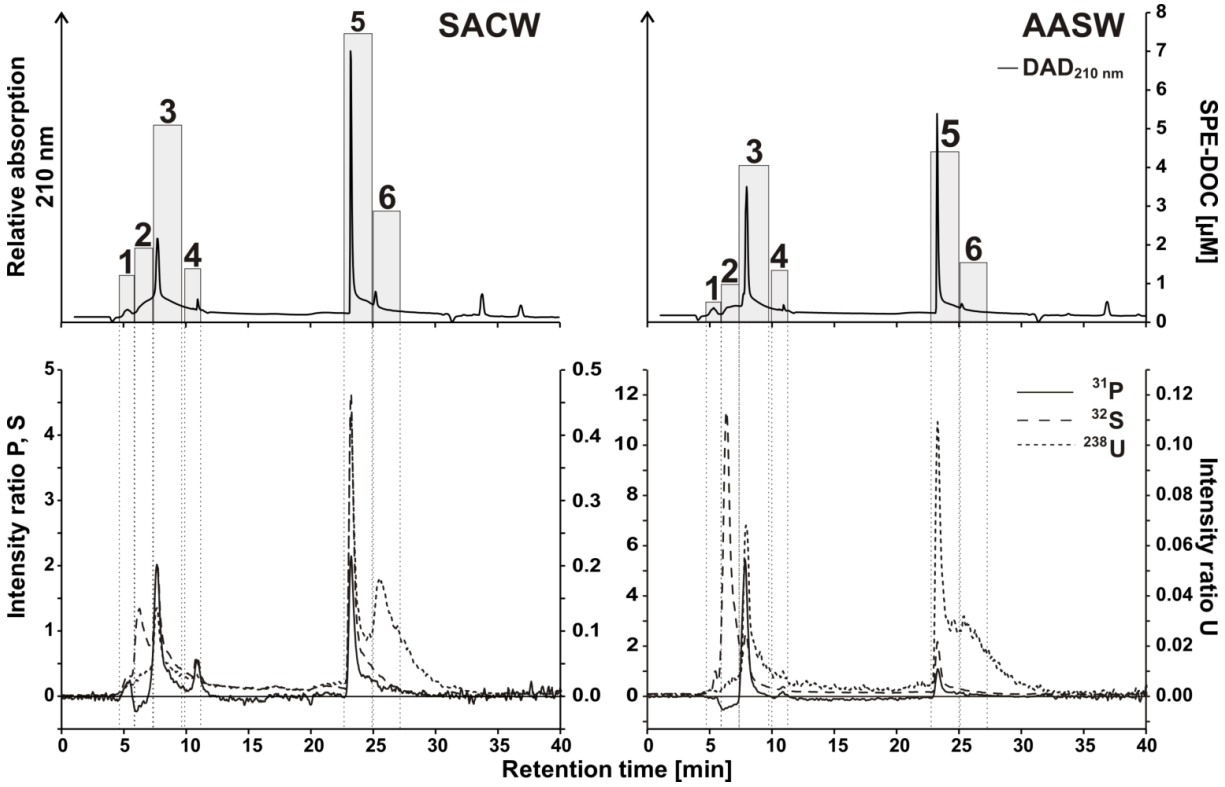

Figure VI.1-3. UV and ICP-MS chromatograms.
UV and mass chromatograms for two marine surface water extracts (SACW, AASW). The two upper chromatograms show the UV absorption from the DAD at 210 nm and the SPE-DOC concentration of the fractions (1 to 6; grey bars, right Y-axis). The two lower chromatograms show the related ICP-MS signals for P (solid line), S (dashed) and U (dotted, right Y-axis). They are displayed as intensity ratio (intensity analyte / intensity internal standard) after sensitivity correction as described in the text.

In macronutrient limited regions of the oceans, a dominant remineralization of P (and S) over C and N compounds occurs (Clark et al. 1998; Loh and Bauer 2000), leading to high C:P and C:S ratios compared to the average composition of marine algae (C:P = 106; Redfield 1958). The bulk SPE-DOM values for C:P found here (721 for SACW and 850 for AASW, Table VI.1-2) were higher than expected for surface water samples. This can be explained by a discrimination of very polar P-compounds by the extraction procedure, as it has been observed previously for N-compounds (Dittmar et al. 2008). Assuming that the extraction efficiency of P for both samples ranged between the C- and the N-extraction efficiency (40 and 15%, respectively), the SPE recovered P can be converted to an estimated DOP concentration in the original seawater of 0.11 – 0.29 µM P (SACW) and 0.07 – 0.18 µM P (AASW). The phosphate concentration of the SACW and AASW sample

was 0.05 and 1.79 µM P, respectively. This suggests that the dominant P pool in the oligotrophic SACW is of organic nature while in the phosphate rich AASW, DOP is only a minor component. The dominance of large and polar organic P-compounds in the nutrient poor water probably indicates enhanced DOP recycling. Our values are in good agreement with other studies, e.g., Mather et al. (2008), who found 0.15 – 0.3 µM DOP in the proximity of the equator in the central Atlantic Ocean in November. In the Drake Passage, Sanders and Jickells (2000) reported TOP values with a range from 0.07 to 0.2 µM P.

Studies involving DOS are very scarce. Alling et al. (2008) found C:S values in the Baltic Sea ranging from 219 to 282. In our study, C:S ratios were 234 and 127 for SACW and AASW, respectively. Assuming an S extraction efficiency between 15% and 40%, SPE-DOS concentration in the original seawater can thus be estimated to be 0.33 – 0.88 µM S (SACW) and 0.44 – 1.17 µM S (AASW). Cutter et al. (2004) reported Sargasso Sea surface water DOS concentrations in a range between 40 and 400 nM S. Although their values are lower than the DOS concentrations in this study, the agreement is reasonable considering the high seasonal-annual variability and the different study sites. The range of elemental ratios of the fractions scattered around the bulk values (C:P = 341 – 3025 and C:S = 11 – 1225, Table VI.1-2). Fraction ratios have a relatively high uncertainty (≈ 13% RSD) and depend on extraction efficiency and the separation mechanism on the column in addition to different sources of DOM.

Compared to P and S, U was less abundant in the water soluble fractions; most of the U eluted in the methanol part, indicating that the organic U complexes were more hydrophobic. The pronounced peak of U in the less polar fraction F6 was unique. For suspended organic matter it was proposed earlier that the organic binding sites for uranium are polydentate ligands (Hirose 1994). Together with a likely preference of the uranyl ion for carboxylic groups (as substitution for carbonate ions), we assume that chelate effects might be responsible for an apparently higher hydrophobicity of the U-DOM complex. We think that the distribution of U in the polarity gradient is interesting and contributes new information to the nature of U speciation — especially when compared with other trace elements such as Ni (data not shown).

However, due to the uncertainties in the extraction procedure, conclusions on the U distribution in the original seawater are difficult to draw without further assessment of U extraction efficiencies. The inorganic speciation of U strongly depends on pH (Djogic et al. 1986) and U-organic complex equilibriums are strongly affected as well (Li et al. 1980). Therefore, only stable (i.e., strongly bound) U complexes are amenable to analysis if the seawater sample is chemically modified.

VI.1.5 Conclusions

We described a novel analytical tool to measure and determine DOP and DOS compounds in seawater extracts by means of RP-HPLC hyphenated to ICP-MS. This method can be extended to trace metal detection, as shown here for U to obtain a new concept of natural ligand classes and to gain further insights into coupled biogeochemical cycles, e.g., Zn-Co-P (Jakuba et al. 2008; Trenfield et al. 2011). In particular, this technique can provide a tool to study the remineralization of phosphorus and organic-bound trace metals in the deeper ocean. Future applications of this method involve:

- Characterization, classification and quantification of DOP and DOS compounds in marine and other NOM samples;
- Speciation of trace metals according to chemical compound classes defined by the polarity of the NOM moieties;
- Refinement of molecular formula assignments in FT-ICR MS based on the abundance and distribution of organic phosphorus and sulfur compounds in NOM fractions;
- Without the restrictions evolving from the high salt content and low NOM concentration in seawater, the method can be applied even better to original samples of fresh water systems.

Acknowledgements

We thank the associate editor Reinhard Niessner and two anonymous reviewers for valuable comments and suggestions. We also thank the master and crew of RV *Polarstern* for their professional help. Analysis of the samples would not have been possible without allocation of the ICP-MS by Jana Friedrich and Ingrid

Stimac from Marine Geology department at AWI. We appreciate the expertise of Dieter Janssen and his help with the TOC analyzer. This work was financially supported by the Deutsche Forschungsgemeinschaft (DFG KO 2164/8-1) and the German Academic Exchange Service (DAAD PPP GB 50023021).

VI.2 Manuscript 2[43]

A depth profile of uranium-236 in the Atlantic Ocean

Marcus Christl,[1,*] Johannes Lachner,[1] Christof Vockenhuber,[1] Oliver Lechtenfeld,[2] Ingrid Stimac,[2] Michiel Rutgers van der Loeff,[2] and Hans-Arno Synal[1]

[1] Laboratory of Ion Beam Physics, ETH Zurich, Schafmattstr. 20, CH-8093 Zurich, Switzerland

[2] Alfred Wegner Institute, Am Handelshafen 12, 27570 Bremerhaven, Germany

* Corresponding author. Address: ETH Zurich, Schafmattstr. 20, HPK G23, CH-8093 Zurich, Switzerland. Tel.: +41 44 633 3884.

[43] This manuscript has been published in *Geochimica et Cosmochimica Acta* in January 15, 2012. I selected the sampling sites, collected the samples and commented on the manuscript. Reprint with permission from Elsevier.

VI.2.1 Abstract

In this study the first two oceanic depth profiles of ^{236}U sampled in the western equatorial Atlantic Ocean are presented. The measured $^{236}U/^{238}U$ ratios decrease from about 10^{-9} at the surface down to about 10^{-10}. Even the lowest ratios measured below 4,000 m depth are more than three orders of magnitude above the estimated natural $^{236}U/^{238}U$ level for the pre-anthropogenic ocean. This clearly indicates that anthropogenic ^{236}U already has reached the deep Atlantic Ocean. Three different conceptual models are applied to identify the relevant processes capable of transporting significant amounts of ^{236}U from the surface into the deep ocean. While the vertical transport of particulate U is excluded as a significant source, box model calculations suggest that North Atlantic Deep Water production with some minor contribution of ^{236}U from nuclear reprocessing as the most likely source for ^{236}U in the deep western equatorial Atlantic Ocean. Our results show that ^{236}U has a large potential as a new, conservative, and transient tracer in oceanography.

VI.2.2 Introduction

Uranium in the ocean is of special interest since its daughter nuclides are extensively used as tracers and chronometers in many (paleo) oceanographic studies (e.g., Ivanovich and Murray 1992; Henderson and Anderson 2003). In the ocean, the uranium concentration (≈ 3.3 ppb) and the activity ratio of $^{234}U/^{238}U$ (≈ 1.147) have been fairly constant in space and time (Chen et al. 1986; Henderson and Anderson 2003; Robinson et al. 2004; Andersen et al. 2010). For example, the $^{234}U/^{238}U$ ratio has not varied by more than 15‰ over the past 360 kyr[44] (Henderson 2002). The main source of U in the ocean is riverine input of continental waters with minor contributions from dust and groundwater (Ivanovich and Murray 1992). The main sinks for U in the ocean are suboxic and anoxic sediments (Sackett et al. 1973) as well as weathering of oceanic basalts (Bloch 1980). Within the large uncertainties of all the input and output fluxes the oceanic U budget is generally considered to be in balance (Henderson and Anderson 2003). Therefore, U in the ocean is used as a conservative tracer with a residence time of about 400 kyr (Mangini et al. 1979; Dunk et al. 2002). The conservative behavior is also reflected by the fact that salinity and U-content are tightly correlated in the open ocean. If the salinity of an open ocean water sample is known, the U-content can be predicted within less than 2% uncertainty (Pates and Muir 2007).

In contrast to the primordial U-isotopes (and the radiogenic daughter ^{234}U), uranium-236 ($T_{½}$ = 23.4 Myr) has not yet been used as an oceanic tracer although its potential as an environmental proxy has been well recognized recently (Steier et al. 2008). ^{236}U is almost exclusively produced from the abundant ^{235}U by neutron capture via an (n, γ)-reaction. The $^{236}U/^{238}U$ ratio, therefore, had been suggested early as a natural occurring neutron monitor (Purser et al. 1996).

On Earth, the majority of ^{236}U is produced by anthropogenic neutron flux e.g., during nuclear bomb explosions or in U-fission reactors. Only a very minor amount of ^{236}U is of cosmogenic origin (produced by galactic cosmic ray induced secondary neutrons) or nucleogenic origin (produced by neutrons originating from (α, n) reactions in the natural terrestrial environment).

[44] In contrast to the rest of this work “yr” is used throughout this manuscript a unit symbol for age.

The global inventory of ^{236}U was assessed recently (Steier et al. 2008). However, very few data about the distribution of ^{236}U in the environment exist. According to the above assessment the natural (nucleogenic and cosmogenic) ^{236}U inventory in the upper 1,000 m of the Earth's crust is about 35 kg (with about 10 kg of cosmogenic ^{236}U located in the upper few meters of the crust). In contrast, the amount of anthropogenic ^{236}U on Earth is estimated to be about 10^6 kg. Anthropogenic ^{236}U is mainly produced in nuclear reactors plus about 900 kg from atmospheric bomb tests (Sakaguchi et al. 2009). The latter number was derived from the average $^{236}U/^{239+240}Pu$ ratio measured in soil samples from the Japanese archipelago assuming a global deposition of 14.8 PBq $^{239+240}Pu$ on Earth. No uncertainty is reported for this ^{236}U inventory from fallout. It is, however, expected that this value represents a rather rough estimate since it does not consider the potentially different geochemical behavior of Pu and U in the environment that might change the Pu/U ratio recorded in the soil samples.

It is expected that only a very small fraction of the reactor produced ^{236}U has been or will be released into the environment either via nuclear reprocessing (Marsden et al. 2001) or during nuclear accidents like the Chernobyl disaster (Boulyga et al. 2000; Boulyga and Becker 2002). A few studies, however, indicate that young continental surface waters and sediments in particular in northwestern and central Europe are dominated by the presence of anthropogenic ^{236}U (Lee et al. 2008; Srncik et al. 2009).

To date no published dataset of ^{236}U in the open ocean exists. This is mainly due to the fact that the measurement of very low $^{236}U/^{238}U$ ratios even with modern mass spectrometers (e.g., TIMS, ICPMS) is limited by an abundance sensitivity in the order of 10^{-7} – 10^{-8} (Tanoue et al. ; Boulyga and Heumann 20062008a). Accelerator mass spectrometry (AMS) is currently the only technique that is able to determine naturally occurring $^{236}U/^{238}U$ ratios down to the 10^{-12} level (or even below) with sufficient efficiency (e.g., Zhao et al. 1994; Fifield 2008b; Steier et al. 2010).

This study presents the first depth profile of ^{236}U sampled in the western equatorial Atlantic Ocean. Our results show that anthropogenic ^{236}U is present at depths of more than 4,000 m. In the following, first the expected $^{236}U/^{238}U$ signal in the open ocean is estimated. Then, sample preparation and AMS measurement techniques are presented before the ^{236}U-data is discussed in detail. Finally, simple

conceptual models are applied to explain the observed ^{236}U data in the deep Atlantic Ocean.

VI.2.3 Natural and anthropogenic $^{236}U/^{238}U$ in the open ocean

Based on the above values for the global ^{236}U budget the contributions of the different ^{236}U-sources to the expected oceanic $^{236}U/^{238}U$ signal are calculated. Since the half-life of ^{236}U is much longer than its residence time, the oceans should have a $^{236}U/^{238}U$ ratio that reflects the inputs of ^{236}U. During the phase of atmospheric bomb testings (1945 – 1980) approximately 900 kg of ^{236}U had been released into the atmosphere (Sakaguchi et al. 2009). To assess the $^{236}U/^{238}U$ ratio in the modern ocean surface we assume that 70% (relative Earth's surface area covered by the oceans) of the globally released ^{236}U had been incorporated at once into the surface layer of the oceans (neglecting the atmospheric residence time of about 1 year (Buesseler and Sholkovitz 1987)). If we further assume that this amount (since then) has homogenously mixed with the upper 700 – 800 m (e.g., assessed from the average global penetration depth of anthropogenic CO_2 (Sabine et al. 2004)), a $^{236}U/^{238}U$ ratio of about 1×10^{-9} is calculated for modern ocean surface waters. Given the unknown but certainly large uncertainty of the global input value the above number is highly uncertain as well.

In addition to the ^{236}U from global fallout, significant amounts of anthropogenic radionuclides have been released into the North Sea region by nuclear reprocessing plants since 1952 (Sellafield) and 1966 (La Hague) (SEPA 2009). Measurements of $^{236}U/^{238}U$ in ocean water samples close to Sellafield (Irish Sea) document ratios at the order of 10^{-6} (Lee et al. 2008). Based on the available U release data (compiled by J. Herrmann, BSH-Hamburg, Germany based on the OSPAR Commission reports, e.g., Russ et al. 2009) it is suspected that in the 1980s the annual ^{238}U (producing ^{234}U) input had been about five times larger than in 2009. The maximum occurs in the 1980s because the $^{236}U/^{238}U$ release ratio still tends to increase (more reprocessed fuel is being used in the reactors) while the total U release decreases. Therefore, the ^{236}U input from nuclear reprocessing is significantly different from, for example, ^{129}I that reaches a maximum input around the year 2000 (Alfimov et al. 2006).

In contrast to the anthropogenic ^{236}U input that roughly started after 1945 the natural ^{236}U signal is expected to have reached steady state in the ocean. The natural signal of ^{236}U consists of two constituents. Both nucleogenic and cosmogenic ^{236}U are mobilized by continental weathering and enter the ocean via riverine input carrying the average $^{236}U/^{238}U$ ratio of the weathering components. Because the energy released in the (n, γ)-reaction producing ^{236}U is low compared to the α-decay of ^{236}U no preferential mobilization of ^{236}U compared to ^{235}U from the host rock is expected (in contrast to ^{234}U compared to ^{238}U).

The production of nucleogenic ^{236}U depends on the U concentration in the host rock itself. For example, in U-rich ores $^{236}U/^{238}U$ ratios of up to 2×10^{-10} have been measured (Wilcken et al. 2008). In contrast to the heterogeneous distribution of ^{236}U in the lithosphere, pre-anthropogenic ocean water is expected to reflect the global average of the natural $^{236}U/^{238}U$ signal. Following previous estimates (Steier et al. 2008) and using a global average U and Th concentration of 2 – 3 ppm in the weathering host rock leads to a very low average oceanic $^{236}U/^{238}U$ ratio at the order of 10^{-14} from nucleogenic ^{236}U production.

A quantitative assessment of the average cosmogenic $^{236}U/^{238}U$ signal in the ocean is complicated by the fact that the in situ production of cosmogenic nuclides strongly depends on geomagnetic latitude and atmospheric depth (i.e., elevation) (Lal 1988). As a rough estimate we use the analogy of cosmogenic ^{36}Cl production from ^{35}Cl. The average global production of cosmogenic ^{236}U is calculated from the average ^{36}Cl production given for different host rock compositions (Fabryka-Martin 1988) and using the relative difference in the respective cross sections for neutron capture. Assuming an average U concentration of a few ppm in the weathering host rock leads to an estimated oceanic $^{236}U/^{238}U$ ratio at the level of 10^{-13}. The uncertainty of this estimation is probably very large taking into account the number of rough assumptions made. Given that more than 50% of the global riverine U-flux into the ocean is carried by rivers transporting the weathering signal of the highly elevated and U-rich lithologies of the Himalayan region (Dunk et al. 2002; Singh et al. 2003) the above estimations might be systematically too low. Recently, a first experimental upper limit for the pre anthropogenic $^{236}U/^{238}U$ ratio was set to 4×10^{-12} (Winkler et al. 2011). In summary, the natural oceanic $^{236}U/^{238}U$ ratio is expected to be dominated by cosmogenic ^{236}U. Therefore, on a million year timescale, the average cosmogenic

$^{236}U/^{238}U$ ratio, as recorded in pre-anthropogenic ocean water, carries information about both, changes in the average continental erosion rate and/or relative changes in the U supply from different source regions to the ocean.

VI.2.4 Methods

Sampling location, hydrography. During the GEOTRACES cruise GA02 in 2010 two depth profiles (six samples of 13 – 22 kg seawater) were collected at stations 39 (latitude: 2°5′45.127″ N, longitude: 41°7′0.307″ W) and 40 (lat.: 1°1′47.228″ N, lon.: 39°6′86.035″ W) in the western equatorial Atlantic Ocean for ^{236}U-analysis (Table VI.2-1). The local hydrography at the selected location is reflected by the temperature and salinity (*T*–*S*) data (Figure VI.2-1). The surface waters are dominated by the westward flowing equatorial counter current with some contributions of low saline Amazon River water plumes. The salinity minimum at about 750 m depth reflects the northward flowing Antarctic Intermediate Waters (AAIW), the following salinity maximum at a depth of about 2,000 m is characteristic for the southward flowing North Atlantic Deep Water (NADW). A pronounced silicate maximum below about 4,000 m depth (not shown here) clearly indicates the presence of cold and less saline Antarctic Bottom Water (AABW) (Rijkenberg 2010). The water samples for ^{236}U were collected at 25, 2,500, and 4,250 m depth (Figure VI.2-1) and therefore should reflect the U-isotopic signatures of the local surface waters, of NADW, and of AABW in the western equatorial Atlantic Ocean. While the *T*–*S*-signature of the deep water samples (for corresponding depths) is virtually identical, the surface samples have a significantly different salinity probably caused by a varying admixture from the Amazon freshwater plumes (Figure VI.2-1).

Table VI.2–1. Water sample locations, hydrographic parameters, and measured ^{236}U-data.

Sample depth (m)	Sample mass (kg)	Potential temperature (°C)	Salinity	^{236}U concentration (at kg^{-1}) × 10^6	±1σ (at kg^{-1}) × 10^6	^{238}U concentration (µg g^{-1})	±1σ (µg g^{-1})	$^{236}U/^{238}U$ × 10^{-12}	±1σ × 10^{-12}
Station: 39, latitude (deg. min. milli): N 2°5′45.127″, longitude (deg. min. milli): W 41°7′0.307″									
25	21.695	28.8275	35.7933	6.33	0.33	3.37	0.07	683	25
2501	12.890	3.0682	34.9515	1.60	0.06	3.04	0.07	189	6
4252	18.135	1.5603	34.8117	1.15	0.12	3.14	0.09	128	9
Station: 40, latitude (deg. min. milli): N 1°1′47.228″, longitude (deg. min. milli): W 39°6′86.035″									
25	18.600	28.0224	36.2881	36.25	10.53	3.36	0.07	3567	678
2503	17.860	3.0389	34.9498	1.89	0.08	3.34	0.24	191	10
4247	21.025	1.5618	34.8112	0.80	0.09	3.32	0.16	91	5

Blanks	^{236}U (at) × 10^6	±1σ (at) × 10^6	^{238}U (µg)	±1σ (µg)
BL_1	1.7	0.2	0.16	0.07
BL_2	5.1	1.4	0.27	0.08

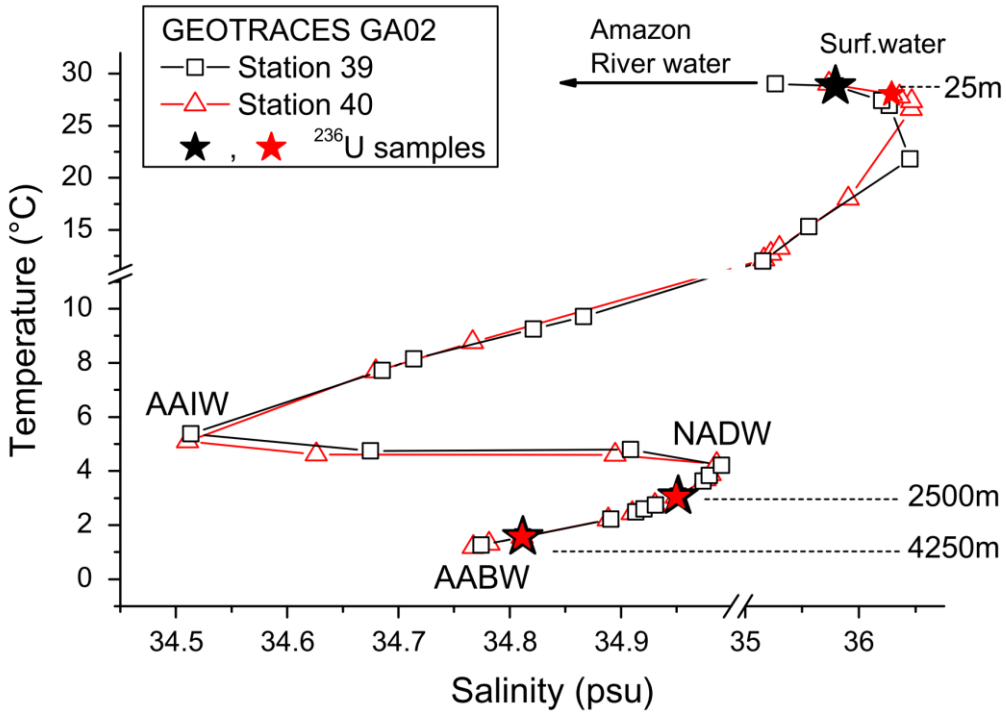

Figure VI.2-1. Hydrographic data.
Hydrographic data (temperature, *T* vs. salinity, *S*; bottle data) of stations 39 (open black squares) and 40 (open red triangles) in the western equatorial Atlantic Ocean sampled during GEOTRACES cruise GA02. The *T*–*S* data of the ^{236}U samples are marked with stars, the respective sampling depth is labeled on the right side of the diagram. Further, the characteristic water masses at this location are indicated (AAIW: Antarctic Intermediate Water, NADW: North Atlantic Deep Water, AABW: Antarctic Bottom Water).

Sample preparation and AMS measurement. The ^{236}U-samples were filtered (142 mm Nuclepore filter, 1 µm pore size) on board, transferred into 20 L polyethylene cubitainer® boxes and acidified with HNO_3. At AWI-Bremerhaven about 25 – 30 pg of a certified ^{233}U reference material (IRMM058) was added to the samples. The use of a ^{233}U spike allows determining the ratio of ^{236}U/^{238}U in the sample material and the concentration of both ^{236}U and ^{238}U during only one AMS-measurement. Details of sample preparation and AMS measurement will be described in a separate publication; here only the main points are summarized.

U was extracted from the seawater by a Fe-hydroxide co-precipitation that was followed by anion exchange cleaning step using UTEVA® resin. The cleaned U-sample was co-precipitated with Fe-hydroxide again, oxidized at 650 °C, mixed with Nb powder and finally pressed into the AMS target holders. The AMS measurements were performed at ETH-Zurich with the compact 0.5 MV AMS system TANDY (Synal et al. 2000; Stocker et al. 2005). The AMS system was recently upgraded and

equipped with an additional magnet on the high energy side (Müller et al. 2010). The performance of the upgraded AMS system for ^{236}U was thoroughly investigated and systematic background studies demonstrate that $^{236}U/^{238}U$ measurements in the 10^{-12} range are possible with a high detection efficiency of > 10^{-4} (Vockenhuber et al. 2011). In other words, the ^{236}U content of a 3 L seawater sample (approx. 10 µg U) with a $^{236}U/^{238}U$ ratio of 10^{-11} can be determined with an analytical precision of less than 10% (assuming 100% sample preparation efficiency). The compact ETH-TANDY system therefore ranges among three AMS facilities in the world that report a $^{236}U/^{238}U$ machine background of 10^{-12} and below (Steier et al. 2010).

The AMS measurement sequence, including the measurement of samples, standards and blanks, was repeated ten times (10 passes). From each pass the standard normalized and processing blank corrected values for the ^{236}U-conc., the ^{238}U-conc., and the $^{236}U/^{238}U$ ratio were calculated. The final values (Table VI.2-1) represent the blank corrected and error weighted mean of all 10 measurements including the 1σ-uncertainty.

The data were reported relative to the in house standard ZUTRI with a nominal $^{236}U/^{238}U$ ratio of $(4.05 \pm 0.10) \times 10^{-9}$ and a nominal $^{233}U/^{238}U$ ratio of $(3.32 \pm 0.08) \times 10^{-8}$. To control the machine background a diluted sample of the Vienna-KkU-standard (Steier et al. 2008) with a nominal $^{236}U/^{238}U$ ratio of $(69.8 \pm 3.2) \times 10^{-12}$ was measured during each run. For this sample, the U-oxide sample material was diluted with Nb powder to match the expected U-currents from the 20 L seawater samples (containing not more than 66 µg U). From these analyses and from the systematic background studies (Vockenhuber et al. 2011) we concluded that the AMS machine background was below 5×10^{-12} during all measurements (Figure VI.2-2). Using the average U-concentration in seawater the above value translates into a ^{236}U machine background of 0.04×10^{6} at kg^{-1} for this study. Two samples solely containing Nb powder were measured always directly after the ZUTRI-standard. The ^{236}U counting rates of these samples indicate that the maximum memory in the ion source was below 10^{-4} and therefore negligible.

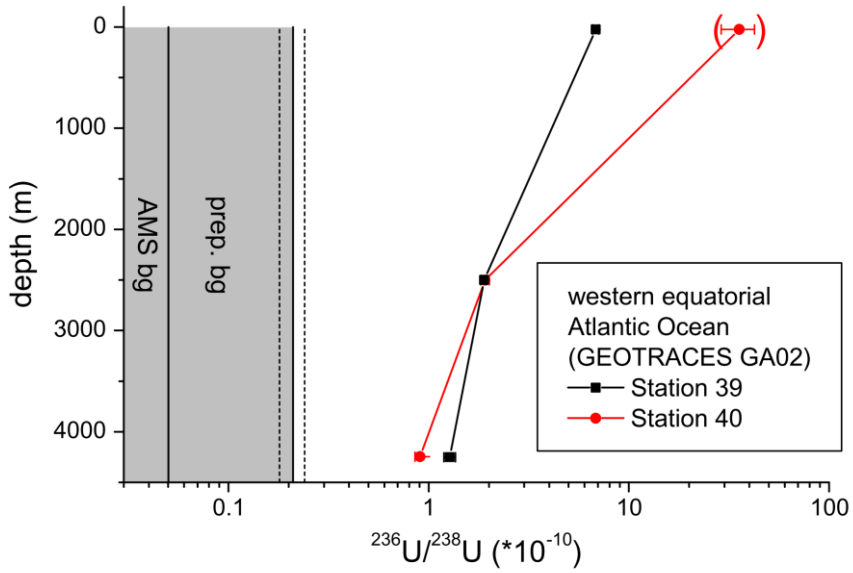

Figure VI.2-2. $^{236}U/^{238}U$ profiles.
The measured $^{236}U/^{238}U$ ratios plotted vs. depth at stations 39 (black squares) and 40 (red dots) in the western equatorial Atlantic Ocean on a logarithmic scale. The shaded regions indicate the machine background of the AMS system and the sample preparation background deduced from the blank measurements, respectively. The surface data point from station 40 is shown in brackets but excluded from the discussion because it showed clear indications for a contamination during the AMS measurements.

Blanks, background correction. Two processing blanks were prepared together with the samples (Table VI.2-1). A negligible amount of ^{236}U (about 3×10^3 at ^{236}U) is expected to be introduced with the ^{233}U spike ($^{236}U/^{233}U = 4.3 \times 10^{-8}$, IRMM058). However, a considerable amount of ^{236}U (weighted average: $(2.6 \pm 0.4) \times 10^6$ at/sample) was measured in the blanks (Table VI.2-1). This indicates that ^{236}U was picked up during the sample preparation. The origin of the contamination is not exactly known but we suspect that it was picked up in the AMS chemistry lab where a $^{236}U/^{233}U$ double spike material ($N(^{236}U) \approx 10^{12}$ at) had been processed before. Although the lab was carefully cleaned afterwards, an accidental contamination at the ppm level would explain the observed blank levels. For a 15 kg seawater sample, the average blank level translates into an average $^{236}U/^{238}U$ preparation background for this batch of samples of $(2.1 \pm 0.3) \times 10^{-11}$(prep. bg in Figure VI.2-2) corresponding to an average ^{236}U background concentration of $(0.17 \pm 0.03) \times 10^6$ at kg^{-1}. The average ^{238}U blank of 0.2 ± 0.1 µg $sample^{-1}$ causes background corrections for the ^{238}U-concentrations at the per mill level, which is well within the uncertainty of the ^{238}U-data. The data presented in this study (Table VI.2-1) includes all background corrections discussed above. The maximum relative

background corrections for ^{236}U are 13% and 16% for the two lowermost (4,250 m) samples.

VI.2.5 Data and discussion

^{236}U in the western equatorial Atlantic Ocean – data. Both ^{236}U concentration and $^{236}U/^{238}U$ ratio show a decreasing trend with depth of a factor of 6 – 7 (Table VI.2-1). The $^{236}U/^{238}U$ ratios decrease from 700×10^{-12} to about 100×10^{-12} (Figure VI.2-2), while the ^{236}U concentrations fall from 6×10^{6} at kg^{-1} at 25 m depth down to about 1×10^{6} at kg^{-1} at 4,250 m depth (Table VI.2-1). The surface sample from station 40 is shown but excluded from the following discussion because this AMS target showed strong indications for a particulate contamination with ^{236}U (largely varying counting rates during the measurement at almost constant ^{238}U current). Such a behavior was not observed with any of the other ^{236}U samples. We therefore exclude the possibility of such a contamination for the other samples. The good agreement of both ^{236}U-concentration and $^{236}U/^{238}U$ ratio between hydrographically identical samples (with respect to their temperature and salinity signature, Figure VI.2-1) further supports the good quality of the ^{236}U-data.

The measured $^{236}U/^{238}U$ ratios were all at least three orders of magnitude larger than the pre-anthropogenic signal estimated above. We therefore conclude that the whole water column down to 4,250 m is dominated by anthropogenic ^{236}U. The surface $^{236}U/^{238}U$ ratio of 0.7×10^{-9} was lower but still in agreement with the estimated signal from global fallout, especially when considering the large uncertainty of the global fallout inventory. It is also in rough agreement with a not further specified surface sample from the Atlantic Ocean ($^{236}U/^{238}U = (1.9 \pm 0.6) \times 10^{-9}$) recently presented by Eigl et al. (2011). At 2,500 m depth a $^{236}U/^{238}U$ signature of 2×10^{-10} was found for local NADW. Possible explanations involving deep water formation in the North Atlantic region and/or the transport of U with sinking particles are discussed in the following section.

At a depth of 4,250 m in the western equatorial Atlantic Ocean $^{236}U/^{238}U$ ratios of about 1×10^{-10} were found. At this location NADW entrains northward penetrating AABW. Hydrographical and phosphate data suggest a 50% NADW, 50% AABW mixing ratio below 4,000 m depth at this location (Broecker et al. 1998). The

assumption that a 50:50 binary mixing is also valid for the ^{236}U data suggests that pristine AABW does not contain any anthropogenic ^{236}U. This result is consistent with measured and modeled radiocarbon ages of > 300 yr for AABW in the equatorial Atlantic Ocean (Broecker and Peng 1982; Campin et al. 1999). We conclude that the observed $^{236}U/^{238}U$ ratio at 4,250 m depth results from a simple mixing of pristine (no anthropogenic ^{236}U) AABW with NADW. Therefore, the explanation of the local AABW signal is tightly connected with the explanation of the local NADW signal at 2,500 m depth (see Section 4.2).

Assuming that the ^{236}U concentration decreases exponentially with depth (r^2 = 0.95, not shown) a ^{236}U inventory of 1.1×10^9 at cm^{-2} is calculated. Extrapolating from these five data points to a global scale an oceanic input of about 1.5 t ^{236}U would be necessary to explain the observed inventory. If no other source of ^{236}U was involved, this number translates into an alternative assessment for the total amount of ^{236}U from global fallout, resulting in a value of about 2,100 kg. This is more than a factor of two higher than previous estimates (Sakaguchi et al. 2009). However, the uncertainty of this estimation is large because the calculated ^{236}U inventory strongly depends on the quality of one single surface data point as a representative for the global SML and because the calculated inventory also depends on the applied fit function. Additionally, the ^{236}U inventory might be systematically biased by ^{236}U transported by southward flowing NADW, which in turn might contain significant amounts of ^{236}U from nuclear reprocessing (see Section 4.2).

The measured ^{238}U concentrations at stations 39 and 40 (Figure VI.2-3, right axis) are in good agreement with the generally observed relation between U-concentration and salinity (Pates and Muir 2007; Owens et al. 2011) in the open ocean (black lines in Figure VI.2-3). The ^{236}U-concentration also exhibits a significant (r^2 = 0.997) but much steeper correlation with salinity (Figure VI.2-3, left axis, red dashed line). The tight correlation, however, is dominated by one (high saline) surface data point. On the base of the current data set it is not clear if the observed correlation is accidental. An apparent ^{236}U-salinity correlation could simply be caused by the fact that a two component mixing of a pre-anthropogenic and a single anthropogenic ^{236}U signal is observed.

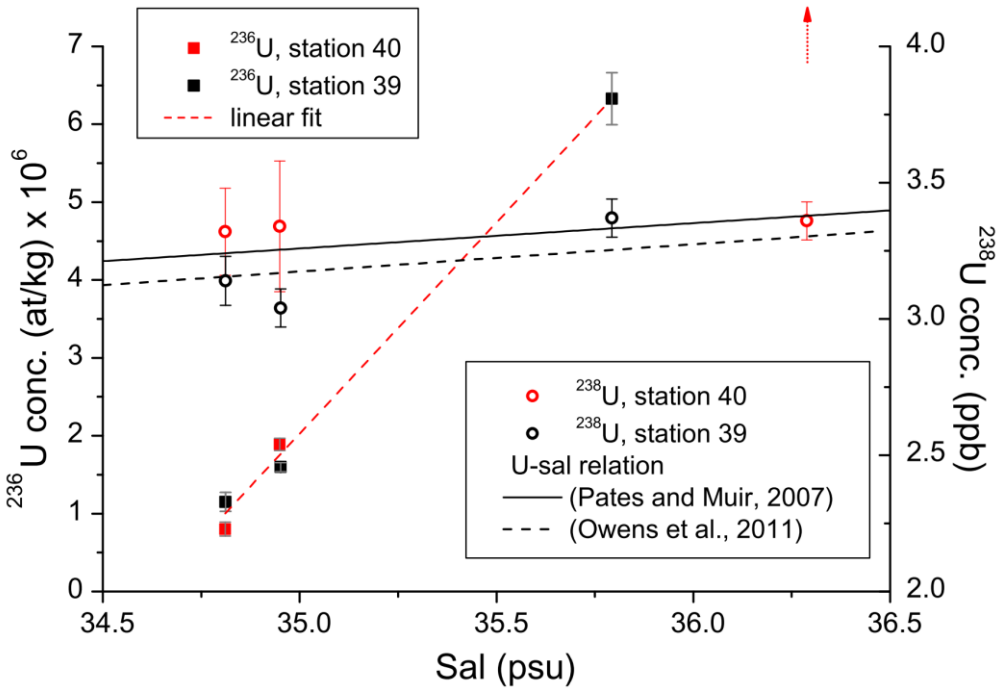

Figure VI.2-3. ^{236}U and ^{238}U concentration.
Measured ^{236}U concentration (filled squares) and ^{238}U concentration (open circles) vs. salinity at stations 39 (black symbols) and 40 (red symbols). Different U-salinity relations for the open ocean are shown: black straight line (Pates and Muir 2007), black dashed line (Owens et al. 2011). The red dashed line represents a linear fit to the ^{236}U data (r^2 = 0.997). The measured surface ^{236}U concentration at station 40 (indicated by the red dotted arrow) is regarded as an outlier and therefore neglected in the fit.

^{236}U in the western equatorial Atlantic Ocean – modeling results. A main conclusion from the ^{236}U data presented above is that the whole examined water column in the western equatorial Atlantic Ocean is influenced by anthropogenic ^{236}U. A major question therefore is: how has the anthropogenic ^{236}U signal propagated into the deep ocean over the past 50 – 60 yr? There are two different transport processes that may be involved. First, sinking particles may transport U from the biologically active surface layer into the deep ocean where it is released due to remineralization. Second, deep water production in the North Atlantic Ocean supplies fresh surface waters to the deep Atlantic Ocean via NADW formation. In the following, three simple conceptual models (Figure VI.2-4) are used to simulate particle flux and NADW production in order to identify the transport mechanism for ^{236}U into the deep ocean.

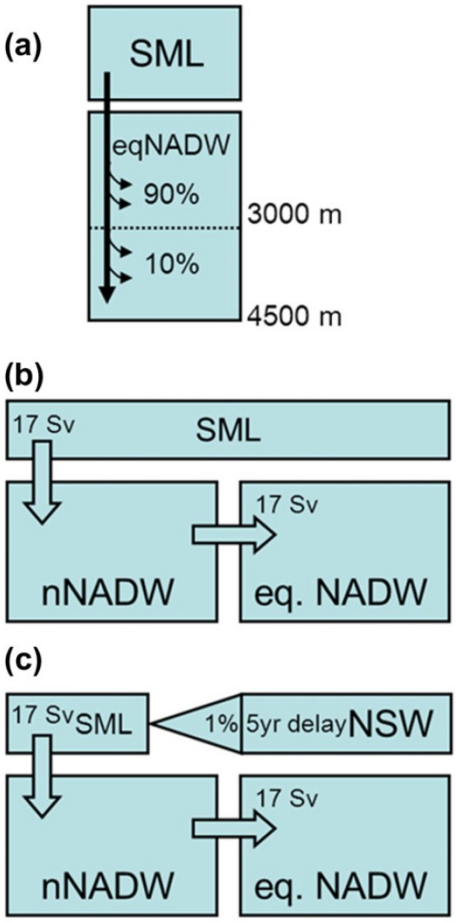

Figure VI.2-4. Box models.
Box models used for the different simulations; (a) three box model to investigate the effect of vertical transport of U with sinking particles (SML: surface mixed layer). The deep ocean box is divided at 3,000 m depth to separate eqNADW from AABW. In the simulation 90% of the particulate U is remineralized in the eqNADW box, with the remainder remineralizing in the AABW box; (b) three box model for the simulation of NADW formation and export, nNADW: northern NADW, eqNADW: equatorial NADW. The arrows indicate the flow direction, the labels give the volume rate; (c) the same model as in (b) with an additional and delayed input of 1% North Sea Water (NSW).

The input function: In all three box models ^{236}U is introduced into the surface mixed layer (SML) box (Figure VI.2-4). To estimate the $^{236}U/^{238}U$ level in the SML box including its temporal evolution it is assumed that 70% of the 900 kg ^{236}U, which were supposedly released during atmospheric bomb explosions, were at once deposited into the surface ocean in the year 1957 (roughly representing the median of the atmospheric bomb tests). In addition, the spatially heterogeneous deposition pattern of atmospheric fallout (southern vs. northern hemisphere = 1:3.8, (Hardy et al. 1973)) is considered. According to these assumptions more than 700 kg ^{236}U were deposited on the northern hemisphere, with 432 kg thereof directly entering the SML. Using this input value two different simulations are run assuming two different average SML depths (150 and 50 m; SML150 and SML50 in Figure VI.2-5). The SML

depths of 50 and 150 m represent typical minimal/maximal annual mean values for the subpolar and equatorial ocean (Monterey and Levitus 1997).

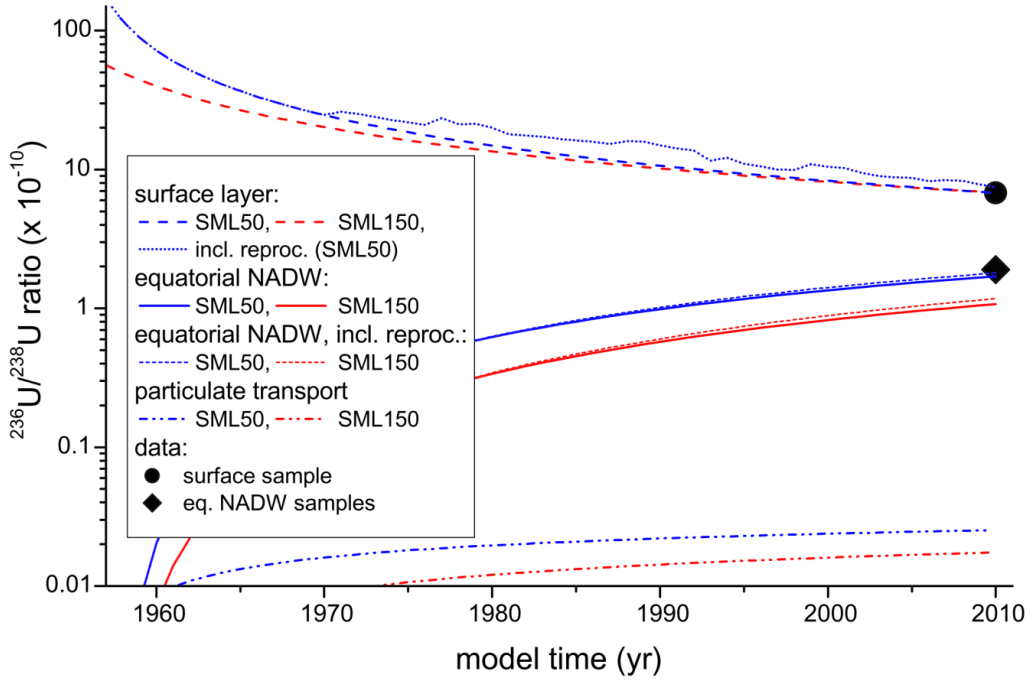

Figure VI.2-5. Simulated $^{236}U/^{238}U$ ratio.
The simulated $^{236}U/^{238}U$ ratio in the eqNADW given for different input scenarios and for different transport mechanisms on a logarithmic scale. Four different input scenarios are realized for the simulation of NADW production and export (upper dashed and dotted lines): (i) a transient $^{236}U/^{238}U$ scenario with an initial SML depth of 50 m (SML50, blue dashed line), (ii) a transient $^{236}U/^{238}U$ scenario with an initial SML depth of 150 m (SML150, red dashed line), (iii) and (iv) input scenarios (i) and (ii) plus an additional contribution of ^{236}U from nuclear reprocessing. For better visibility only one input scenario (iii): SML50 (blue dotted line) is shown that includes ^{236}U from reprocessing. The calculated $^{236}U/^{238}U$ ratios in the eqNADW-box for the four different input scenarios are indicated by the red and blue straight lines (without reprocessing) and by the red and blue short dotted lines (including reprocessing) in the middle of the plot. The color reflects the respective input scenario. The calculated $^{236}U/^{238}U$ ratio in the eqNADW box caused by the vertical transport of particulate U is indicated by the red and blue dashed-dotted lines in the lower part of the diagram. The filled circle and diamond mark the measured $^{236}U/^{238}U$ ratios (sampled in 2010) in the surface layer and in eqNADW, respectively.

The smaller the mixed layer in the model the higher is the calculated initial $^{236}U/^{238}U$ ratio. The SML50 scenario represents a maximum estimate for the modeled $^{236}U/^{238}U$ ratio in all simulations because in this scenario a higher $^{236}U/^{238}U$ ratio is always exported from the SML into the deep ocean than in the SML150 simulation. The above assumptions result in initial $^{236}U/^{238}U$ ratios (in the model year 1957) of 5.6×10^{-9} and 1.7×10^{-8} for the SML150 and SML50 scenarios, respectively.

In these transient scenarios it is further assumed that from year to year the initial ^{236}U signal in the SML penetrates deeper into the ocean where it then mixes

with water masses that do not contain anthropogenic ^{236}U. The average yearly penetration rate of the signal is determined under the assumption that the simulated $^{236}U/^{238}U$ ratio in the surface box (dashed lines in Figure VI.2-5) equals the measured $^{236}U/^{238}U$ ratio at 25 m depth in the year 2010 (filled circle in Figure VI.2-5). For a SML depth of 150 m (50 m) an average signal penetration rate of 20.7 m yr^{-1} (22.5 m yr^{-1}) is determined. This implies that in both input scenarios the calculated $^{236}U/^{238}U$ surface ratios decrease with time and per definition reach a value of 6.8×10^{-10} in the model year 2010. An average penetration rate of 21 m yr^{-1} further implies that in the model year 2010 the ^{236}U signal has homogenized with the uppermost 1,200 m of the water column. Further, an annual penetration length of L = 21 m corresponds to a vertical eddy diffusivity of D = 0.14 cm^2 s^{-1} (with $L = (Dt)^{½}$), which is well within the range of observational data (Gargett 1984).

Particle flux: In the surface waters of the open ocean dissolved U may be fixed to predominantly organic particles and exported to the bathypelagic layer (ca. 1,000 – 4,000 m) where it then remineralizes (Anderson 1982). In general, this process also transports ^{236}U from the surface layer into the deep ocean. To simulate the vertical transport of particulate U a simple conceptual model is applied (Figure VI.2-4a). In this model U is exported (e.g., by sinking particles) from the surface box and completely remineralized in the two deep ocean boxes below. For the surface layer we apply the two (SML50 and SML150) input scenarios described above. Measured export rates of particle bound bio-authigenic U range from 0.1 to 5.6 ng cm^{-2} yr^{-1} (Anderson 1982). A strict additional constraint for the maximum flux of particulate U is given by the U – salinity relation in the open ocean. Since no vertical gradient of the salinity normalized U-concentration is observed in the open ocean (Pates and Muir 2007) the flux of remineralized bio-authigenic U to the deep sea must be insufficient to measurably change the uranium concentration within the mixing time of the ocean (Anderson 1982).

To realize a maximum estimate of the vertical ^{236}U flux in the model it is assumed that 90% of the particulate U remineralizes in the eqNADW box. Under the restriction that the U concentration in this box is allowed to change by not more than 2% per 1000 yr a maximum U export flux of 20 ng cm^{-2} yr^{-1} is calculated. If particulate U export from the surface is the sole mechanism transporting ^{236}U into the deep ocean the above constraint implies that (assuming a constant $^{236}U/^{238}U$ ratio in the

SML) only 1.1‰ (i.e., 2% × 53 yr/1000 yr) of the $^{236}U/^{238}U$ signal at the surface reaches the deep ocean (the resulting $^{236}U/^{238}U$ ratio in eqNADW would not even be visible on the logarithmic scale of Figure VI.2-5). The non-steady state simulations use a transient $^{236}U/^{238}U$ signal as input function (SML50 and SML150). The results (blue and red dashed dotted lines in Figure VI.2-5) clearly indicate that the export and the subsequent remineralization of particulate U is not a significant source of ^{236}U in the deep ocean, neither in eqNADW nor in AABW.

We note that the $^{236}U/^{238}U$ signal in the deep ocean reacts much more sensitively to vertical transport processes than, for example, $^{234}U/^{238}U$ since the ^{236}U signal is not at steady state. It may therefore provide a powerful tool to quantify the particulate transport of U in oceanic regions where deep water formation does not play a significant role (e.g., the Pacific Ocean).

NADW formation: To simulate the temporal evolution of the $^{236}U/^{238}U$ ratio in the deep equatorial Atlantic Ocean a simple three box model was used (Figure VI.2-4b). In this model pristine (northern) nNADW is produced from the surface layer at a volume rate of 17 Sv, which is in accordance with estimates from hydrographic section data at 24° N (Roemmich and Wunsch 1985). Simulating the advective southward transport via the Deep Western Boundary Current (DWBC) the nNADW is transported into the equatorial NADW box (eqNADW) assuming the same volume rate (corresponding to a renewal time of 150 yr for each box). Since the modeled time period (53 yr) is much shorter than the oceanic mixing time (about 1000 yr) the box model does not conserve water (i.e., there is no return flux of water leaving the eqNADW box).

The results of the box model simulations (straight lines in Figure VI.2-5) show that only the SML50 simulation is able to explain the observed $^{236}U/^{238}U$ ratio in eqNADW quantitatively (filled diamond in Figure VI.2-5). The SML150 simulation produces $^{236}U/^{238}U$ ratios that are almost a factor of 2 lower than the measured data in eqNADW. Regarding all the assumptions made and the simplicity of the model the SML50 simulation is in reasonable agreement with the observations.

We are aware of the fact that the application of a box model to simulate the spatial propagation of a tracer signal a priori represents a maximum approach since no constraints for the maximal mixing lengths are given. To transport the

anthropogenic ^{236}U signal within about 50 yr from the region of deep water formation (Labrador and Nordic Seas) to the sampling location (6,000 – 8,000 km further south) a minimum average current velocity of 0.4 – 0.5 cm s^{-1} would be necessary. For the DWBC very variable velocities reaching values of up to 20 cm s^{-1} have been reported (Joyce et al. 1986).

Further, a rapid spreading of ^{236}U into the deep equatorial Atlantic Ocean is consistent with tritium and chlorofluorocarbon (CFC) data. For example, Jenkins and Rhines (1980) found a southward flowing tritium jet flow in the DWBC at 3,500 m depth (originating from nuclear weapons testing in the atmosphere). More recently, attempt has been made to access the transit time for the NADW pathway from the Labrador and Nordic Seas to the tropics using CFCs (Andrié et al. 2002). In this study a mean transit time of 25 yr (27 yr) was determined for upper (lower) NADW to reach the equatorial Atlantic Ocean.

All these results support the interpretation that, on a time scale of several decades, it is generally possible to transport significant amounts of anthropogenic ^{236}U from the SML into the deep western equatorial Atlantic Ocean via NADW formation.

NADW formation and nuclear reprocessing: A contribution of anthropogenic ^{236}U from the nuclear reprocessing plants in northwestern Europe might represent an additional source of ^{236}U in the eqNADW. Although the releases started more than 50 yr ago the spatial distance from the North Sea to the western equatorial Atlantic Ocean is even larger. Therefore it seems unlikely that much of the ^{236}U from nuclear reprocessing has reached the deep equatorial Atlantic Ocean. Yet on the other hand, even small contributions of North Sea Water (NSW) to the North Atlantic regions would significantly increase the $^{236}U/^{238}U$ ratio of the NADW forming surface waters. Furthermore, there is evidence for the presence of anthropogenic ^{129}I from nuclear reprocessing in the North East Atlantic Deep Water (NEADW) (Edmonds et al. 2001) and in the Deep Western Boundary Current (DWBC) (Santschi et al. 1996; Orre et al. 2010). Taking into account the different input functions (^{129}I releases peak around the year 2000 while the ^{236}U release peak was about 20 yr earlier) it might become possible that ^{236}U from nuclear reprocessing is already present in the eqNADW.

To test this assumption, a second simulation was run to assess the contribution of ^{236}U from nuclear reprocessing. The additional ^{236}U input is included in the model under the following two assumptions. The relative contribution of NSW to the deep water forming SML is 1% and the NSW signal arrives at the location of deep water formation (e.g., in the Greenland Sea) with a 5 yr time lag (Figure VI.2-4b). The above numbers are chosen arbitrarily to assess the sensitivity of the model to an additional input by nuclear reprocessing plants. The additional ^{236}U input is added to the SML50 and SML150 scenario, respectively (for better visibility only the SML50 plus reprocessing input is shown; blue short dotted line in Figure VI.2-5). The results of these simulations (short dashed lines in Figure VI.2-5) show that the incorporation of ^{236}U from nuclear reprocessing increases the $^{236}U/^{238}U$ ratio in eqNADW by not more than 10%. From this result we conclude that the incorporation of ^{236}U from nuclear reprocessing only marginally improves the agreement between data and simulation.

We note that all model simulations above were based on a global inventory of 900 kg ^{236}U from global fallout. As discussed above, this number is not well known and might reflect a source of systematic uncertainty for the simulations. A higher value, as suggested above, would improve the agreement between model and data, particularly for the SML 150 simulation. In summary, the box model simulations suggest that the distribution of ^{236}U in the deep western equatorial Atlantic Ocean most probably can be explained by deep water formation in the North Atlantic Ocean.

VI.2.6 Conclusion

The first two oceanic depth profiles of ^{236}U sampled in the western equatorial Atlantic Ocean have been presented and discussed in detail. The data show that anthropogenic ^{236}U is present throughout the water column down to more than 4,000 m depth. The local AABW samples and the 2,500 m eqNADW samples reflect a binary mixing with about 50% contribution of each water mass, which agrees well with other oceanographic data and tracers from that location.

Simple conceptual models were used to identify the mechanism transporting ^{236}U into the deep ocean. The model results suggest that deep water formation in the North Atlantic Ocean is the likeliest source of ^{236}U in the eqNADW, maybe with small

contributions of anthropogenic ^{236}U from nuclear reprocessing. According to the model simulations, the transport of U with sinking particles can be neglected as a significant source of ^{236}U in the deep open ocean.

^{236}U provides the transient twin isotope for natural U in the open ocean. Based on our results we conclude that ^{236}U has a large potential to become a new, transient, conservative, and therefore powerful tracer for future oceanic studies.

Acknowledgements

The authors want to thank Hendrik M. van Aken (NIOZ, Physical Oceanography Department) for providing and processing the hydrographic data, Michael Rüttimann (ETHZ) for carefully handling the ^{236}U samples in the chemistry lab, and Jürgen Herrmann (BSH-Hamburg) for compiling the ^{236}U release data. Gideon Henderson and three anonymous reviewers are acknowledged for their constructive comments that significantly improved the quality of the manuscript. This study used sample material from GEOTRACES section GA02. The Laboratory of Ion Beam Physics, ETH is partially supported by its consortium partners EAWAG, EMPA, and PSI.

VI.3 Manuscript 3[45]

The influence of salinity on the molecular and optical properties of surface microlayers in a karstic estuary

Oliver J. Lechtenfeld,[1] Boris P. Koch,[1,2,*] Blaženka Gašparović,[3] Sanja Frka,[3] Matthias Witt,[4] and Gerhard Kattner[1]

[1] Alfred Wegener Institute for Polar and Marine Research, Am Handelshafen 12, D-27570 Bremerhaven, Germany

[2] University of Applied Sciences, An der Karlstadt 8, D-27568 Bremerhaven, Germany

[3] Ruđer Bošković Institute, Bijenička cesta 54, HR-10000 Zagreb, Croatia

[4] Bruker Daltonik GmbH, Fahrenheitstrasse 4, D-28359 Bremen, Germany

[*] Corresponding author. Phone: +49 471 4831 1346. E-mail: boris.koch@awi.de

[45] This manuscript is accepted for publication in *Marine Chemistry*. I performed the data analysis and evaluation, and wrote the paper.

VI.3.1 Abstract

Sea-surface microlayers and the corresponding underlying waters of the karstic Krka Estuary (Croatia) were studied with respect to optical and molecular properties of dissolved organic matter (DOM). Solid-phase extracted DOM was separated by reversed-phase chromatography and analyzed with ultra-high resolution Fourier transform ion cyclotron resonance mass spectrometry (FT-ICR MS). The number and summed magnitudes of FT-ICR MS peaks, enriched in the microlayer, increased with increasing salinity along the estuary. The molecular hydrogen to carbon ratio (as a measure of polarity) of enriched compounds was higher for the low salinity samples than for a high salinity marine station, which we propose is a consequence of a salt-mediated separation mechanism. Absorption and fluorescence of all samples decreased along the estuary with the microlayer samples showing higher absorption than the underlying water. Chromatographic and FT-ICR MS data revealed a distinct shift towards a smaller molecular size in the microlayer compared to the underlying water. The redistribution of dissolved organic carbon within chromatographic fractions and the decrease in molecular size was interpreted to result from photo-degradation and/or microbial reprocessing. Collision induced dissociation of selected FT-ICR MS mass peaks revealed the presence of sulfur containing anthropogenic surfactants enriched in the microlayer. Molecular level investigation of estuarine surface microlayers will help to better understand the highly dynamic character of these systems, the accumulation of natural organic matter and anthropogenic pollutants and the role of surface microlayers for the sea-air energy exchange.

VI.3.2 Introduction

The surface microlayer is the phase-boundary between hydrosphere and atmosphere of aquatic systems (lakes, rivers, estuaries and oceans). Surface films are microhabitats, photochemical reactors, filters and physical membranes and control the gas exchange between air and water (Liss and Duce 1997). Various definitions exist for the microlayer, mainly defined operationally according to the sampling technique (glass plate, Garrett's screen, rotating drum) and the study subject (biological, chemical or physical properties). The vertical extent of the microlayer ranges from molecular monolayers up to millimeters (Hardy 1982). A visual representation of a coherent organic film at the sea surface is the sea slick, which appears quickly during calm wind conditions (Hunter and Liss 1981). Sea-surface microlayers (SML) are known to exist even at higher than global average wind speeds, potentially covering most of the ocean's surface at any time, hence they are of global importance (Wurl et al. 2011).

The SML consists generally of adsorbed surface active substances (SAS) that are amphiphilic molecules reducing the surface tension of the water-air interface. This includes a large variety of substances such as polysaccharides (Sieburth et al. 1976), transparent exopolymer particles (TEP, Wurl and Holmes 2008), polypeptides (Kuznetsova et al. 2004), lipid-like material (Kattner and Brockmann 1978; Gašparović et al. 1998; Lass and Friedrichs 2011) but also living bacteria (Cunliffe et al. 2011) and phytoplankton (Hardy and Apts 1984; Joux et al. 2006) and their exudates (e.g., Kattner et al. 1985). Many studies demonstrated that hydrophobic substances accumulate in the SML (e.g., Kattner et al. 1983), including anthropogenic pollutants such as hydrocarbons and trace metals (Wurl and Obbard 2004; Guitart et al. 2007). The chemical composition of the SML and the enrichment factors of individual substances vary widely in time and space, depending on the trophic state of the system, wind regime, seasonality and anthropogenic pollution. Differences in the composition of the SML and the underlying subsurface water are reflected in the dissolved organic matter (DOM) composition, e.g., amino acid concentrations (Kuznetsova et al. 2004), chromophoric dissolved organic matter (CDOM) distribution (Tilstone et al. 2010), physico-chemical properties (Zhang et al. 2003) and bacterial production and respiration (Reinthaler et al. 2008). However, an exact description of the SML lacks detailed and comprehensive molecular information

on the identity of the constituting substances, although some recent studies report high resolution mass spectrometry data (Frew et al. 2006; Morales-Cid et al. 2009; Schmitt-Kopplin et al. 2012).

For the chemical characterization of natural organic matter (NOM) salt-free and pre-concentrated extracts are obtained by e.g., solid-phase extraction (Dittmar et al. 2008). This is a prerequisite for many analytical techniques, such as reversed-phase chromatography, nuclear magnetic resonance spectroscopy or mass spectrometry. Ultra-high resolution Fourier transform ion cyclotron resonance mass spectrometry (FT-ICR MS) is an advanced analytical tool to study the extremely complex mixtures of NOM (Hertkorn et al. 2008; Xian et al. 2012). Due to its high mass resolution and accuracy, several thousands of molecular formulas per sample can be identified. Recent applications to investigate DOM include soil porewater (D'Andrilli et al. 2010a), groundwater (Longnecker and Kujawinski 2011), river and coastal water (Stubbins et al. 2010; Liu et al. 2011), open ocean and deep sea water (D'Andrilli et al. 2010b; Flerus et al. 2012), as well as sediment porewater (Schmidt et al. 2009). The information derived by FT-ICR MS is typically restricted to elemental composition and is non-quantitative. However, recent improvements of this technique included single mass fragmentation capabilities which lead to structural information on individual NOM molecules (Witt et al. 2009). By combining reversed-phase chromatographic separation with FT-ICR MS the molecular complexity of NOM samples can be reduced, which enhances the analytical resolving power and enables to chemically characterize sample moieties (Koch et al. 2008; Liu et al. 2011).

The Krka Estuary is particularly suitable to identify the chemical characteristics of the organic surface microlayer since constantly low terrestrial discharge results in relatively homogeneous organo-chemical conditions (Cauwet 1991). Therefore extraction and analytical biases due to the different chemical composition of samples along the estuary are potentially minimized. On the other hand, the strong horizontal salinity gradient und vertical stratification of the Krka Estuary allows studying microlayer versus underlying water composition under different ionic strength conditions and seasonal variations.

In our study, we present the first detailed chemical description of sea-surface microlayers compared with subsurface water with advanced molecular methods. Samples from the Krka Estuary were analyzed with FT-ICR MS and reversed-phase

high performance liquid chromatography (RP-HPLC) using absorption and fluorescence detection. This combination of methods was applied to identify so far chemically uncharacterized components of the microlayer and to study their distribution patterns. We aimed to derive insights into the molecular properties of the microlayer and the bulk subsurface water and the influence of increasing salt concentration on the chemical properties of microlayer-enriched substances. This molecular information will help to better describe the chemical processes leading to a phase transfer from underlying water into the microlayer.

VI.3.3 Methods

Sampling site and sample collection. Samples were collected in the highly stratified estuary of the Krka River in the Middle Eastern Adriatic Sea near the Croatian city of Šibenik. The hydrographic and biological features of this estuary are described in detail elsewhere (Vojvodić and Ćosović 1992; Legović et al. 1994; Svensen et al. 2007). For reasons of comparability we adopted station labels from these previous studies.

Surface microlayer (SML) and underlying water (ULW) samples were collected at three stations: In the upper estuary (Lake Prokljan, E3), characterized by low salinity and low anthropogenic impact (Vojvodić and Ćosović 1992), in the lower estuary, near the city of Šibenik (E4a) with the only significant anthropogenic influence on the estuary (Legović et al. 1994), and in the saline waters off the coast of Zlarin Island (C1). Samples were collected on September 9, 2008 (E4a only) and between May 18 and May 20, 2009 (E3, E4a and C1). It should be noted that the marine station C1 is located 4 km away from the mouth of the estuary, therefore only partly reflecting a parameter continuum. However, this station has been extensively used as reference station in the past.

SML samples (0.5 – 1 L) were derived with a Garrett-type screen made of stainless steel, with 1.03 mm^2 mesh size and 0.24 mm wire diameter and poured into a clean glass bottle. The screen was cleaned with dichloromethane and rinsed with sample water prior collection and glass bottles were cleaned with chromosulfuric acid and thoroughly rinsed with ultra pure water. The thickness of the sampled water layer was determined from the collected water volume being approximately 110 μm. ULW

(4 L) was collected directly with a clean glass bottle from 0.4 m depth. To avoid surface film contamination, the sampling bottle was slowly pushed underwater and opened at depth. All samples were GF/F filtered (≈ 0.7 µm nominal pore size, Whatman). Samples for nutrient analysis were poisoned and stored at 4 °C (Kattner 1999). Acidified samples (pH 2 with hydrochloric acid; suprapur, Merck) for DOC determinations were stored frozen at -20 °C and solid-phase extraction (SPE, 1 g; Mega Bond Elut, PPL, Varian) was performed according to Dittmar et al. (2008). Briefly, methanol (3 mL) and acidified (pH 2 with hydrochloric acid; suprapur) ultra pure water (3 mL) were used the clean and pre-condition the adsorbent. After applying the samples, remaining salt was rinsed with 3 mL acidified ultra-pure water and the cartridge bed dried with a N_2- flow. The eluted SPE samples (3 - 5 mL methanol, LichroSolv, Merck) with a nominal enrichment factor between 200 and 900 were stored at -20 °C until FT-ICR MS and RP-HPLC analysis.

DOC and nutrient analysis. DOC was determined by high temperature catalytic oxidation (TOC-V_{CPN} analyzer, Shimadzu). For external calibration potassium hydrogen phthalate (KHP, Merck) was used. Aliquots of the methanol extracts (50 µL) from the SPE samples were evaporated under N_2 gas flow to complete dryness and subsequently redissolved in 6.5 mL ultrapure water for DOC analysis (SPE-DOC). All samples (in duplicate) were acidified (0.1 M HCL suprapur, Merck) and purged with O_2 for > 5 min. Performance of the instrument was recorded by daily analysis of in-lab KHP standard solutions and reference samples (deep sea reference, DSR, Hansell research lab). The average instrument blank was 3.4 µM C (n = 11) and repeatability of the DSR was > 95%. The SPE efficiency [%] was calculated as 100 × SPE-DOC [µM] / (enrichment factor × DOC [µM]). Nutrient samples (nitrate, nitrite, phosphate, silicate) from the 2009 campaign were analyzed using an autoanalyzer (Evolution III, Alliance instruments) with standard seawater methods (Kattner and Becker 1991 and references therein).

HPLC measurements. An HPLC system (Hitachi/VWR) was used for the chromatographic separation of the SPE samples (Koch et al. 2008). The system consisted of a gradient pump (L-2130), autosampler (L-2200), column oven (L-2300), diode array detector (DAD, L-2450, optical path length: 1 cm) and fluorescence detector (FLD, L-2485). The separation was performed using a polar endcapped C18

reversed-phase column (4 µm Hydro-RP 80 Å, 250 × 4 mm, with AQ C18 Guard Column; Phenomenex, Synergi) running a linear gradient from 100% ultrapure water, adjusted to pH 7 (±0.05) with diluted NaOH (suprapur, Merck), to 100% methanol between 6 and 20 min. The flow increased in the same time period from 0.2 to 0.4 mL min^{-1}. The column oven temperature was 25 °C. Both detectors were connected in series; absorbance was recorded between 200 and 400 nm, and the fluorescence signal was measured at 260 nm excitation and 430 nm emission wavelength (ex260/em430). The excitation/emission pair used to monitor the fluorescence signal approximates the “peak A” of UV humic-like fluorescence. This peak was repeatedly found with excitation-emission-matrix spectroscopy of terrestrial organic matter and marine organic matter extracts (Coble 1996; Coble et al. 1998) and generally shows high fluorescence intensity. Methanol reached the detector after ≈ 22.5 min. 10 µL of each methanol extract were injected. The average relative standard deviation of the chromatogram peak areas were 2.4 ± 1.1% as determined from eight repeated injections of a DOM extract. DAD and FLD chromatograms were blank corrected (injection of 10 µL ultrapure water).

The main benefit of the chromatographic method was to induce a physico-chemical separation (as difference in polarity) of NOM components. Investigation of the distinct fractions (DOC content, optical or molecular properties) can reveal intrinsic differences between samples that are not accessible from bulk measurements. To maximize the separation effect, a gradient from 100% water (the matrix of the original sample) to 100% methanol (the extraction solvent) was applied. The distribution of peaks within this gradient therefore reflects the full polarity spectrum of all extracted compounds. However, also size effects need to be considered in the analysis of NOM samples with reversed-phase columns (Hutta et al. 2011; Lechtenfeld et al. 2011).

Absorbance at 210 nm was selected for the evaluation of the RP-HPLC-DAD spectra, according to the recently established relationship between DOC content and DOM absorption at this wavelength for individual chromatographic fractions (Lechtenfeld et al. 2011). As a first approximation, the average molar extinction coefficient ($\varepsilon_{210\,nm}$) was calculated for the total chromatogram according to equation 1:

$$\varepsilon_{210\ nm}\ [L\ mol^{-1}\ cm^{-1}] = \text{total peak area}\ [L] / DOC_{injected}\ [mol] \times 1\ cm^{-1} \quad (1)$$

where the total peak area refers to the integrated and blank-corrected absorbance of a sample between 4 and 36 min. $DOC_{injected}$ is the amount of DOC injected on the RP column. The approximate DOC amount for each peak (DOC_{calc}) was then calculated from equation 2:

$$DOC_{calc}\ [mol] = \text{peak area}\ [L] / \varepsilon_{210\ nm} \times 1\ cm \quad (2)$$

where peak area [L] is the integrated and blank-corrected absorbance of each chromatographic peak. . Absorbance at 355 nm wavelength is commonly used to characterize coastal and estuarine CDOM (Blough and del Vecchio 2002). To facilitate comparison with literature CDOM absorption coefficients (α(λ)), we estimated the absorption coefficients of the original sample, which were not measured, from equation 3:

$$\alpha(355\ nm)\ [m^{-1}] = 2.303 \times \varepsilon_{355\ nm} \times \text{SPE-DOC}\ [M] \times 100\ [cm\ m^{-1}] / \text{enrichment factor} \quad (3)$$

We used equation 1 to calculate the peak-area integrated extinction coefficient $\varepsilon_{355\ nm}$, not necessitating assumption on individual peak extinction coefficients. This approach yields only a lower limit for the CDOM absorption coefficients of the original sample because it does not consider CDOM extraction efficiencies.

FT-ICR MS measurements. DOM methanol extracts (1:1 diluted with ultrapure water) were analyzed with an FT-ICR mass spectrometer (Apex ultra, Bruker Daltonics, Billerica, MA) equipped with a 12 T refrigerated actively shielded superconducting magnet (Bruker Biospin, Wissembourg, France). An electrospay ionization (ESI) source was used in negative ion mode (capillary voltage: +4.4 kV) with a syringe pump for continuous infusion of the sample at a rate of ≈ 2 µL min^{-1}.

Fragmentation experiments via quadrupole isolation with a 1 Da isolation window and collision induced dissociation (qCID-MS/MS) in the hexapole collision cell with Argon as collision gas (-14.5 eV) were carried out. Dissociation products were further transferred into the ICR cell and detected in a mass to charge ratio (m/z) range of 147-2000. MS/MS mass spectra were acquired for two samples from 2009

on two high magnitude mass peaks (m/z m/z 311, C1, SML; m/z 325, E4a, SML). Although numerous peaks on a single nominal mass were detected, the high mass accuracy of FT-ICR MS allowed the calculation and therefore identification of dissociated small molecules from mass differences in the fragmentation spectra.

Five hundred scans were added for a full spectrum and 67 to 220 for a fragmentation spectrum. FT-ICR mass spectra were externally calibrated with arginine cluster and internally recalibrated with seven masses that were repeatedly found in marine DOM samples (Flerus et al. 2011). The standard deviation of the mass error of the calibration masses was below 0.03 ppm.

All peaks were singly charged ions and therefore the m/z ratio represents (molecular) mass [Da] of the compounds. Molecular formulas were calculated from the exact mass in the range of 200 – 700 Da with an accuracy ≤ ±0.5 ppm with a home-build algorithm, allowing for the following elemental compositions: $C_{0-\infty}H_{0-\infty}O_{0-\infty}N_{0-2}S_{0-2}$. For unambiguous elemental formula assignment the "nitrogen-rule" and elemental ratios O/C ≤ 1, N/C ≤ 1, H ≤ 2C+2+N (Koch et al. 2005; Koch et al. 2007) were applied and the elemental combination N_2S_2 was excluded to avoid ambiguous assignments. Usually the corresponding ^{13}C or ^{34}S isotope mass peak magnitudes were too low for verification of the molecular formula with the isotope peak abundances (relative abundance of ^{13}C and of ^{34}S is 1.1% and 4.2%, respectively). Remaining ambiguously assigned mass peaks were checked according to the homologous series, i.e., chemical building block approach (Koch et al. 2007). A molecular formula must be a member of a continuous "CH_2" and "CH_4-O" series and the number of O-atoms must be larger than the length of the "CH_4-O" series. To facilitate further comparison of sample pairs (SML vs ULW), we manually adjusted the lower relative peak magnitude limit (based on the highest peak of the NOM perimeter, see below) for samples E4a – 2008, ULW, C1 – 2009, SML and ULW (0.5% instead of 1%, signal to noise ratio always ≥ 4), resulting in comparable relative peak magnitude frequency distributions for all samples. This approach was necessary due to the deviating maximum peak magnitudes caused by either different total carbon content in the SPE samples or prominent "contaminant" peaks (identified as O_3S, O_4S- and O_5S-compounds, see Results section and Figure VI.3-1). A degradation index (I_{DEG}) was introduced by Flerus et al. (2012) using relative peak magnitudes of two quintuples of peaks ubiquitous found in FT-ICR MS samples. I_{DEG}

approximates the degradation state of solid-phase extracted DOM which is mainly dominated by heterotrophic and photochemical reworking. It is calculated according to equation 4 from the raw magnitudes of '$POS_{/DEG}$' ($C_{13}H_{18}O_7$, $C_{14}H_{20}O_7$, $C_{15}H_{22}O_7$, $C_{15}H_{22}O_8$, $C_{16}H_{24}O_8$) and '$NEG_{/DEG}$' ($C_{21}H_{26}O_{11}$, $C_{17}H_{20}O_9$, $C_{19}H_{22}O_{10}$, $C_{20}H_{22}O_{10}$, $C_{20}H_{24}O_{11}$) peaks, that showed a positive or negative correlation with the samples' $\Delta^{14}C$ values (Flerus et al. 2012):

$$I_{DEG} = \sum NEG_{/DEG} / \sum (NEG_{/DEG} + POS_{/DEG}) \quad (4)$$

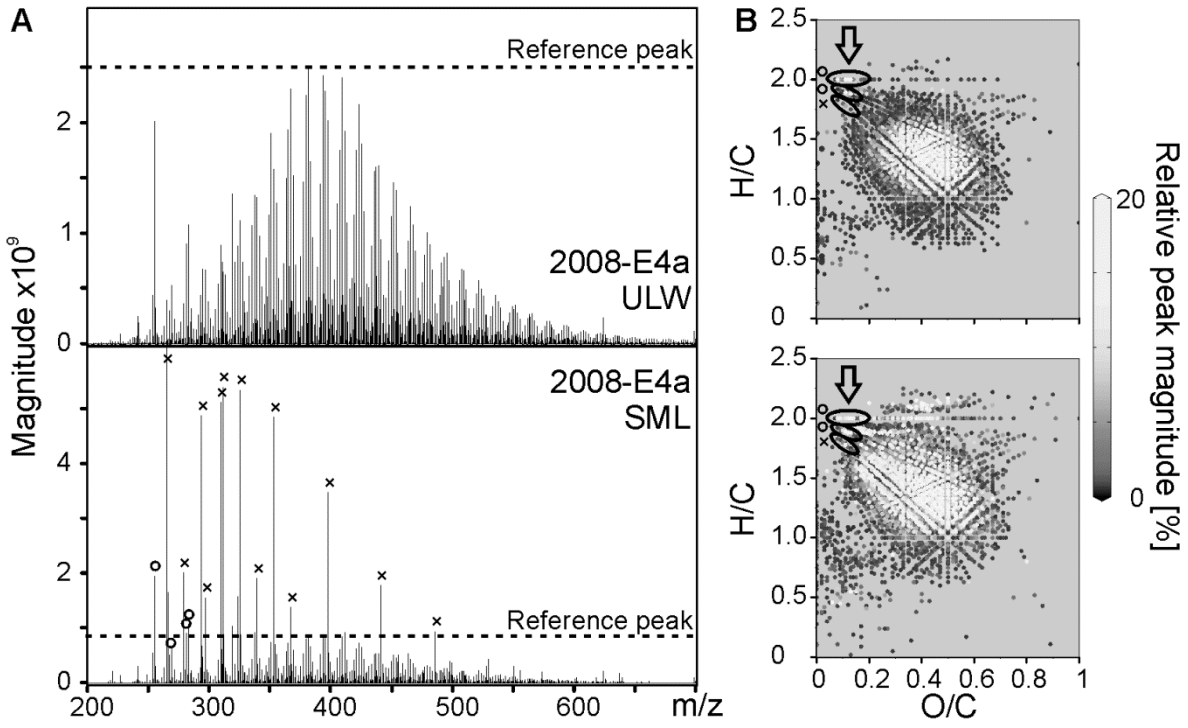

Figure VI.3-1. FT-ICR mass spectra of a SML/ULW sample pair.
A: Negative ESI FT-ICR mass spectra of a bulk water (ULW) and a microlayer sample (SML). SPE samples are from the middle station in the Krka estuary (E4a – 2008). B: Visual representation of all assigned molecular formulas for the ULW (n = 4,311) and the SML (n = 4,769) sample in a van Krevelen plot. Molecular hydrogen to carbon (H/C) vs. oxygen to carbon (O/C) ratios are plotted according to the relative peak magnitude. Prominent sulfur ("×") and $C_nH_{2n}COOH/C_nH_{2n-2}COOH$ ("o") peaks are indicated in the ULW sample and marked in the van Krevelen plots (black arrows and circles). Plots were prepared using Ocean Data View (R. Schlitzer, http://odv.awi.de).

A comparison with a surfactant database (http://www.terrabase-inc.com) revealed 71 molecular formulas in our samples that potentially represent anthropogenic surfactants. In the van Krevelen diagram, several series of homologous compounds from the database were identified that were enriched or exclusively found in the SML samples. Exclusion of method blank masses on a presence absence basis is to date the only possibility to exclude false positive

molecular formulas (e.g., contaminants) from a mass list. As this study was focused mainly on naturally occurring DOM, we consequently excluded all molecular formulas from the "terrabase-inc" database from the final FT-ICR MS dataset prior evaluation, considered to be the most conservative approach. Evidence for the presence of contaminant molecules in FT-ICR mass spectra can be obtained with fragmentation experiments of equivocal peaks, as demonstrated in this study.

Weighted average (wa) mass and elemental ratios were calculated from the relative peak magnitudes. Using weighted average parameter is a common way to facilitate comparison of FT-ICR MS spectra. Compared to the number-average approach, weighted averages do not imply equal concentrations of all NOM compounds and allow sample comparisons beyond a presence/absence basis. However, it is only a semi-quantitative approach assuming comparable ionization efficiencies and volatilities of the sample compounds in the ESI introduction system. Recent studies have demonstrated the applicability of the weighted-average approach for biogeochemical interpretations of FT-ICR MS data (Liu et al. 2011; Flerus et al. 2012; Schmitt-Kopplin et al. 2012).

The coarse shape of the spectra showed the almost Gaussian peak distribution that is characteristic for FT-ICR mass spectra of NOM (e.g., Koch et al. 2005; D'Andrilli et al. 2010b). The reference peak was defined as the highest magnitude peak within this perimeter, usually found between 380 and 450 Da (Figure VI.3-1). Occasionally the base peak of the spectrum was not the maximum of the typical NOM peak distribution (i.e., the reference peak), resulting in few peaks with relative magnitudes > 100% (typically S-compounds, Figure VI.3-1). Double bond equivalents (DBE, representing the sum of π-bonds and rings in a neutral molecule) were calculated according to the following equation 5:

$$DBE = 1 + ½(2C - H + N) \quad (5)$$

where C, H and N is the number of carbon, hydrogen and nitrogen atoms in a molecular formula.

To evaluate molecular differences between surface microlayers from different stations (and salinities), enrichment factors (EF) for each station (SML and ULW) were calculated according to equation 6:

$$EF_i = [X_i]_{SML} / [X_i]_{ULW} \quad (6)$$

where EF_i is the enrichment factor for a molecular formula "i" and $[X_i]_{SML}$, $[X_i]_{ULW}$ is the relative peak magnitude for this formula in the SML and corresponding ULW sample. Before classifying compounds as enriched or depleted, a threshold was set (enriched: EF ≥ 1.5; depleted: EF ≤ 0.67), taking into account the degree of mass peak magnitude repeatability of FT-ICR MS measurements (< 10% peak magnitude relative standard deviation for ESI negative full scan mode; Kido Soule et al. 2010). We did not assess the peak magnitude repeatability in this study, but the conservative EF thresholds require that the normalized magnitude of a compound in the SML (ULW) is at least 50% different from the ULW (SML).

Statistical analysis. For multivariate statistical analyses (Software "R", 2012) we used relative peak magnitudes of all molecular formulas (after exclusion of the doubly assigned peaks). Group average cluster analysis based on the Bray-Curtis dissimilarity (Bray and Curtis 1957) and Principal Component Analysis (PCA, Pearson 1901) were carried out. Significance tests for two groups of samples were either performed with the Mann-Whitney U-test or the Wilcox signed rank test (paired samples), based on the null hypothesis that both groups differ by less than "0" (i.e., they are equal). For *p*-values smaller than the significance level $\alpha = 0.05$ the null hypothesis was rejected (i.e., both groups differ). Variables were always heteroskedastic and non-normally distributed, as tested with the Bartlett- and Shapiro-Wilk-test ($\alpha = 0.05$).

VI.3.4 Results

Physico-chemical conditions and nutrients. The water temperatures were between 20 and 22 °C in May 2009 and 25 °C in September 2008. Surface layer salinity increased from the upper estuary towards the Adriatic Sea (Table VI.3-1) because of the wedge-shaped freshwater layer in the estuary. At the Šibenik station (E4a) salinity was much higher in 2008, reflecting the very low freshwater input in late summer. The SML had consistently higher DOC concentrations compared to the ULW (mean DOC-EF = 1.42 ± 0.29). DOC in the SML increased with salinity while macro nutrient concentrations were similar in all sample pairs (SML/ULW, relative

differences < 1%) and only ULW data are reported. In 2009, nitrate and silicate concentrations at the two estuary stations E3 and E4a were 15.6 ± 1.3 µM and 36.6 ± 3.6 µM, while at the marine site C1, concentrations were 1.4 µM and 4.4 µM, respectively. Nitrite and phosphate were always below 0.5 µM and 0.1 µM, respectively. Extraction efficiencies for the SPE recovered DOC varied between 22 and 33% (Table VI.3-1), with a significantly higher amount of DOC recovered from the SML samples (average SML: 29.5 ± 3.9%; average ULW: 23.8 ± 2.0%, $p < 0.04$). The reason for the lower extraction efficiency compared to Dittmar et al. (2008) is not clear. However, the extract C:N ratios (19.4 ± 3.5) were similar to reported values for PPL (Dittmar et al. 2008; Hertkorn et al. 2012) indicating a comparable extraction of NOM components.

Table VI.3-1. Overview and general data of all samples. SML: surface microlayer, ULW: underlying water, I_{DEG}: molecular degradation index after Flerus et al. (2012).

Sample	Location	Sample-type	Temperature [°C]	Salinity	DOC [µM]	SPE efficiency [%]	I_{DEG}
E4a - 2008	middle estuary	SML	25.0	30.0	181.3	26.8	0.36
		ULW	25.0	30.0	101.2	22.4	0.32
E3 - 2009	upper estuary	SML	21.3	1.9	89.3	33.6	0.21
		ULW	21.3	1.8	59.8	23.3	0.20
E4a - 2009	middle estuary	SML	22.0	6.3	97.1	31.9	0.23
		ULW	22.0	6.3	84.2	26.8	0.20
C1 - 2009	marine station	SML	20.3	34.9	174.5	25.6	0.21
		ULW	20.3	34.8	142.1	22.9	0.17

HPLC. The correlation between the total absorbance of the entire chromatograms (total peak area [L]) and the DOC concentration of the extract was significant for all samples ($r = 0.94$; $n = 8$, $p < 0.001$), although a non-zero y-intercept points towards some DOC fraction not absorbing at 210 nm. The average molar extinction coefficient $\varepsilon_{210\,nm}$ was highest for the samples from the middle station E4a and lowest for the marine station C1 (Table VI.3-2). The $\varepsilon_{210\,nm}$ (SML) / $\varepsilon_{210\,nm}$ (ULW) ratio as well as the calculated absorption coefficient $\alpha(\lambda = 210$ nm, 355 nm) for the original sample (i.e., considering the nominal enrichment factors of the extracts, Table VI.3-2) revealed an accumulation of CDOM in the SML samples (mean ratios α (SML) / α (ULW) = 1.9 ± 0.4 for $\lambda = 210$ nm and 2.4 ± 1.1 for $\lambda = 355$ nm).

Table VI.3-2. Extract average molar extinction coefficient $\varepsilon_{210\,nm}$ and calculated absorption coefficients $\alpha(\lambda)$. Total DOC normalized fluorescence (FLU) is relative to the sample with the most intense signal (100%) and normalized to the injected DOC amount.

Sample	Sample-type	$\varepsilon_{210\,nm}$ [L mol^{-1} cm^{-1}]	$\alpha(\lambda)$ in orig. sample [m^{-1}]		Ratio $\alpha(\lambda)$ SML / ULW		FLU [%]	Ratio FLU SML/ULW
			210 nm	355 nm	210 nm	355 nm		
E4a – 2008	SML	527.6	5.90	0.27	2.1	1.6	58.0	0.76
	ULW	548.4	2.86	0.18			73.2	
E3 – 2009	SML	488.7	3.52	0.27	2.3	4.0	78.4	0.78
	ULW	441.6	1.50	0.07			100.0	
E4a – 2009	SML	531.4	3.93	0.18	1.5	2.2	70.0	0.8
	ULW	456.0	2.48	0.08			87.9	
C1 – 2009	SML	424.2	4.47	0.13	1.7	1.8	23.0	0.94
	ULW	343.8	2.64	0.07			24.5	

In contrast, the DOC normalized peak area of the total fluorescence (ex260/em430) showed highest values for the upper estuary station E3 and lowest values for the marine station C1, as well as generally higher fluorescence values for all ULW samples (Table VI.3-2). The decrease in total DOC normalized fluorescence

is in accordance with the characteristics of the UV humic like “Peak A”, that is known to exhibit a linear negative correlation with salinity in estuaries (Coble 1996).

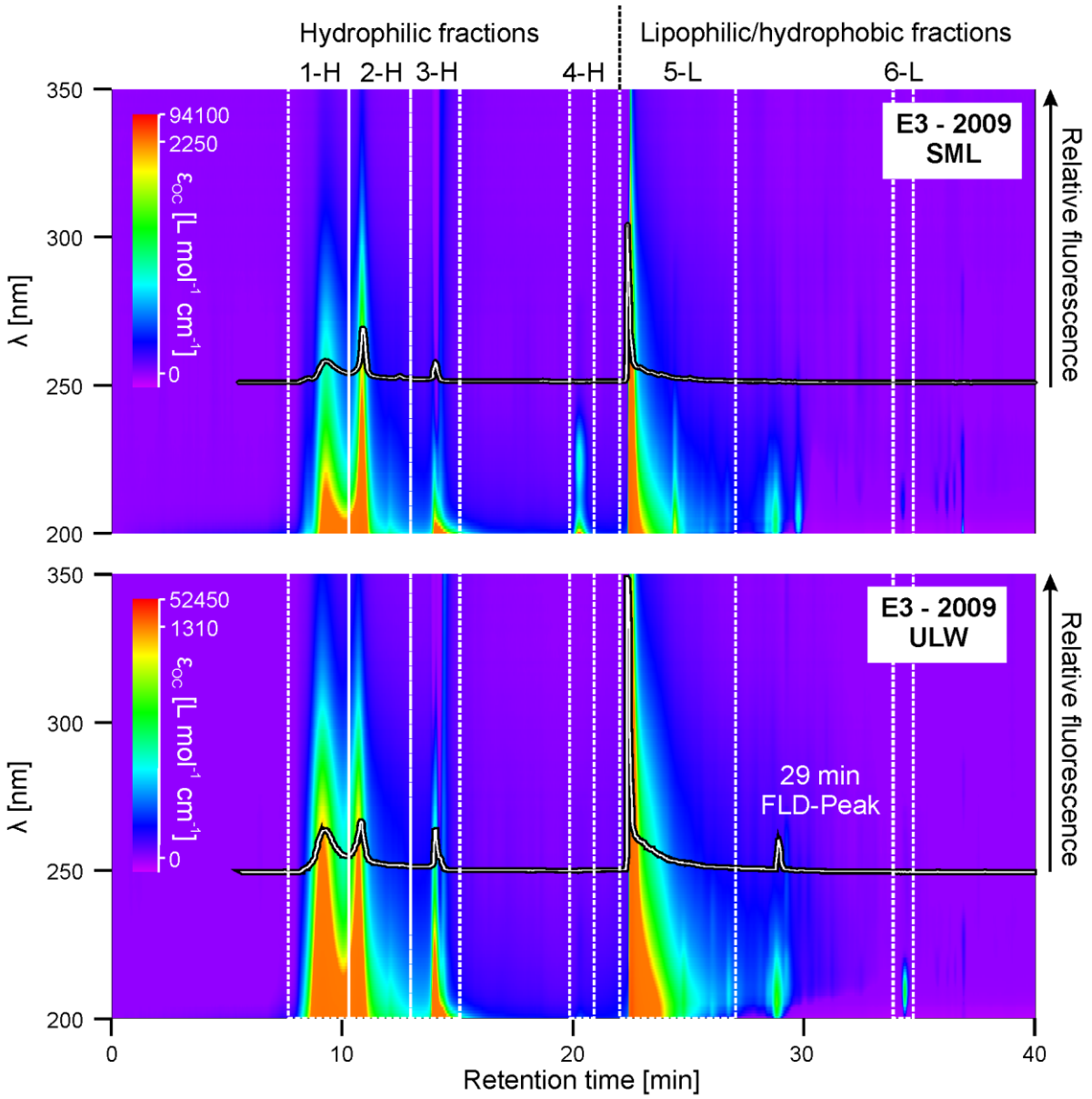

Figure VI.3-2. RP-HPLC with DAD and FLD of a SML/ULW sample pair.
Reversed phase high performance liquid chromatograms of microlayer and underlying water extracts (E3, SML and E3, ULW) with diode array (200 – 350 nm, left Y-axis) and relative fluorescence (FLD, ex260/em430 nm, black line, right Y-axis) signals. Diode array intensities were converted to molar extinction coefficient ε_{OC} and displayed as color scale for both samples. For peak labels, see text.

The $DAD_{210\ nm}$-chromatograms of all SML and ULW samples showed four major peaks while in some samples two additional small peaks appeared (Figure VI.3-2). Peaks were grouped as hydrophilic (-H) and lipophilic (-L). The main features of the SML samples were an additional peak at 20.43 ± 0.17 min (4-H, n = 3; not present in the 2008 sample) and a relatively higher absorbing peak at

10.73 ± 0.07 min (2-H, *n* = 3). Independent of the sample type, all samples (except E4a – 2008) showed a major contribution of very polar, water eluting components (fractions 1-H to 4-H versus 5-L and 6-L, $DAD_{210\,nm}$, $p < 0.02$). Fluorescence (ex260/em430) revealed a peak at 29.04 ± 0.04 min (*n* = 3) that was only present in the ULW samples with the exception of the E4a - 2008 sample.

FT-ICR MS. FT-ICR MS analyses resulted in 4,311 to 6,128 assigned molecular formulas per sample (number of total peaks per sample with S/N > 4 and 200 – 700 m/z: 11,435 – 13,702). Twenty-nine molecular formulas belonged to doubly assigned peaks with m/z > 550 Da and could not be unequivocally assigned according to the defined criteria. The summed peak magnitude of all doubly assigned peaks was only 0.01% of the total magnitude of all peaks. As a conservative approach, these peaks were removed from the final data set.

The general pattern of the molecular mass, O/C and H/C distribution of all samples (Figure VI.3-1) resembled that of solid-phase extracted marine surface waters, as found in other studies (Kujawinski et al. 2009; Gonsior et al. 2011). The mean elemental ratios were O/C = 0.438 ± 0.158 and H/C = 1.253 ± 0.357 (*n* = 41,953). Thirty-two percent of all formulas contained one or two nitrogen atoms, 17% contained one or two sulfur atoms and 4% contained nitrogen and sulfur (as compound classes N_1S_1, N_2S_1 or N_1S_2). The number of nitrogen, oxygen and sulfur peaks per sample did not show any clear trend (Table VI.3-3).

Comparing the weighted average elemental ratios of H/C and O/C (wa H/C, wa O/C) for all samples (Table VI.3-3), an increase of both ratios was found with increasing salinity and DOC concentration. The weighted average mass (wa mass) and number of peaks did not show any trend with salinity or DOC. Compared to ULW, the SML samples showed higher abundances of sulfur compounds (lower wa C/S ratio), higher saturation (higher wa H/C ratios and lower wa DBE values), and smaller wa mass. During the 2008 campaign all of these differences were particularly pronounced (Table VI.3-3).

Table VI.3-3. FT-ICR MS weighted average (wa) molecular parameters of the complete SPE sample set. H/C: hydrogen to carbon ratio, O/C: oxygen to carbon ratio, DBE: double bond equivalents. Number-percentage of CHO, CHNO, CHOS and CHNOS compounds to all detected ions.

Sample	Sample-type	Assigned formulas	wa H/C	wa O/C	wa mass [Da]	wa DBE	CHO peaks [%]	CHNO peaks [%]	CHOS peaks [%]	CHNOS peaks [%]
E4a – 2008	SML	4,769	1.440	0.364	415.71	7.03	49.5	27.1	19.9	3.4
	ULW	4,311	1.348	0.400	421.52	7.98	52.3	31.4	14.0	2.1
E3 – 2009	SML	5,420	1.231	0.461	452.32	9.45	47.5	33.1	16.4	2.9
	ULW	6,128	1.217	0.450	459.13	9.82	48.4	34.3	14.1	3.2
E4a – 2009	SML	5,247	1.251	0.467	448.25	9.11	47.0	32.0	18.3	2.7
	ULW	5,558	1.229	0.471	463.17	9.60	47.7	32.5	16.3	3.5
C1 – 2009	SML	5,530	1.266	0.484	457.11	9.00	42.5	33.7	19.4	4.5
	ULW	4,972	1.253	0.492	466.24	9.26	44.1	33.1	17.4	5.4

Cluster analysis based on all molecular formulas clearly separated all samples according to their salinities (Figure VI.3-3A). In addition, the SML samples separated from the ULW samples at the low salinity stations E3 and E4a (2009). The station E4a - 2008 showed a lower similarity to the 2009 samples and also less similarity between SML and ULW. For the samples from 2009, the PCA (Figure VI.3-3B) confirmed the clear separation between differences in salinity (PC1, 76% of variance) and between SML and ULW (PC2, 9.5% of variance).

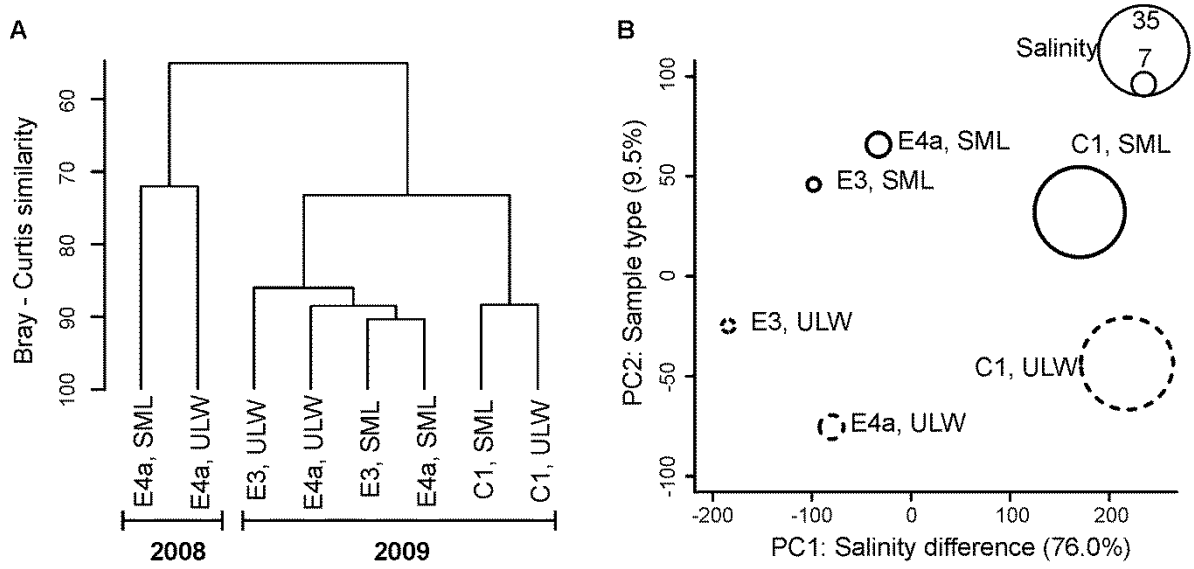

Figure VI.3-3. Multivariate statistics.
Multivariate statistical analysis of untransformed FT-ICR MS peak magnitudes of all molecular formulas (n = 41,953). A: cluster analysis (Bray-Curtis similarity) for all samples. B: principal component analysis (PCA) for the 2009 samples (SML = microlayer, solid lines; ULW = underlying water, dashed lines). The circle size specifies the salinity of each sample.

Out of all samples, 826 – 3,213 molecular formulas (accounting for 5 – 48% of the summed magnitude) were enriched or appeared uniquely in the SML samples, while 655 – 2,049 molecular formulas (3 – 13%) were enriched in or unique to the ULW samples (Table VI.3-4). For the 2009 samples the summed relative magnitude of enriched (depleted) compounds increased (decreased) with increasing salinity (Figure VI.3-4) and changed consistently with the number of enriched (depleted) molecular formulas. In 2008, a pronounced enrichment of compounds in the SML sample was observed. The “unique” peaks, belonging to SML or ULW in a sample pair, were equally distributed in the van Krevelen space and had low relative magnitudes (mean for all unique peaks: 1.33 ± 0.48). Therefore the corresponding peaks in the paired sample were likely below the magnitude threshold and thus not present in the evaluation data set. Figure VI.3-5 shows the EF values in a color

coded van Krevelen diagram for station E3 and C1 distinguishing between enriched and depleted compounds.

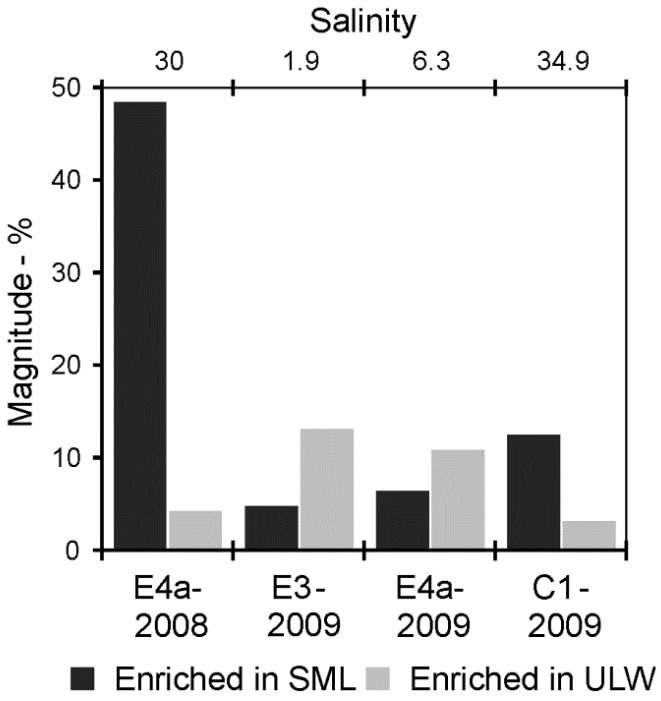

Figure VI.3-4. Summed magnitudes of enriched and depleted compounds.
Magnitude proportions of all molecular formulas that were enriched (EF > 1.5) or uniquely found in the microlayer (SML) or underlying water (ULW) sample of each station (ULW enriched corresponds to EF < 0.67) with the corresponding salinities.

On average, 20% of all molecular formulas in a sample and even 25 – 38% of all SML-enriched compounds contained at least one sulfur atom. The latter accounted for 28 – 44% of the summed magnitude of enriched peaks. Eight to 44% of all enriched compounds contained at least one nitrogen atom comprising 18 – 35% of the total enriched intensity. The average EF of the sulfur compound classes ("N_0S_{1-2}") was higher than for all molecular formulas, and it was lower for the nitrogen compound classes ("$N_{1-2}S_0$"). The highest EFs for N and S-compounds were found in the 2008 samples, while the average EF of all depleted compounds was similar regardless the compound class or the sample station (Table VI.3-4).

Table VI.3-4. Average enrichment factors (EF) for all, CHNO and CHOS compounds for the enriched (enr.) and depleted (depl.) compounds. Values in brackets are the number of respective peaks, not including the unique peaks. For E4a – 2008 depl., values were omitted (n.a.; only one peak below EF = 0.67). Unique peaks include all compound classes.

Sample	Sample-type	all compounds		CHNO compounds		CHOS compounds		unique peaks	
		enr.	depl.	enr.	depl.	enr.	depl.	enr.	depl.
E4a – 2008	SML	3.36	n.a.	2.14	n.a.	5.97	n.a.		
	ULW	(1,872)	n.a.	(386)	n.a.	(303)	n.a.	(1,341)	(882)
E3 – 2009	SML	2.16	0.58	1.72	0.61	2.57	0.57		
	ULW	(107)	(622)	(32)	(97)	(35)	(43)	(719)	(1,427)
E4a – 2009	SML	1.94	0.6	1.69	0.6	2.33	0.61		
	ULW	(204)	(497)	(66)	(75)	(55)	(95)	(679)	(990)
C1 – 2009	SML	1.97	0.58	1.78	0.54	2.73	0.6		
	ULW	(591)	(44)	(245)	(11)	(91)	(18)	(1,173)	(615)

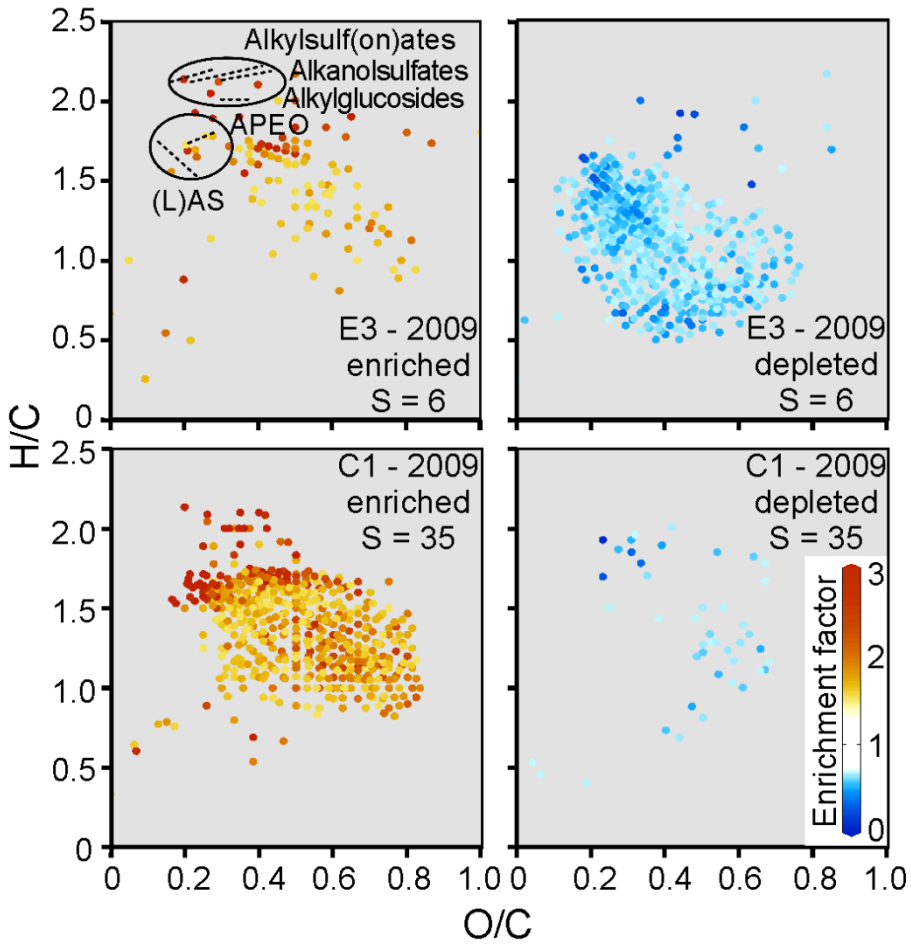

Figure VI.3-5. Van Krevelen plot of enriched and depleted compounds.
Van Krevelen visualization of FT-ICR MS derived molecular formulas that were enriched or depleted in the surface microlayer of a low salinity sample (E3, S = 6) and a high salinity sample (C1, S = 35), not including unique peaks for clarity. The enrichment factor for each peak is color coded (same scale for all panels). In the top left panel, the location of anthropogenic surfactant homologues from a database (http://www.terrabase-inc.com) are displayed as neutral molecules in the van Krevelen space (APEO = alkylphenol ethoxylates, (L)AS = (linear) alkylbenzenesulfonates). Plots were prepared using Ocean Data View (R. Schlitzer, http://odv.awi.de).

Fragmentation experiments. To elucidate the structure of some compounds identified by FT-ICR MS, collision induced dissociation (qCID-MS/MS) experiments were performed on two high magnitude nominal masses (m/z 311, 325) from different spectra. The fragmentation pattern for m/z 311.16864 (Figure VI.3-6, sample C1 - 2009, SML) strongly suggested that the oxygen was bound in a sulfonate group and not in a carboxylic group (SO_2 loss, but no loss of CO_2/H_2O, typically observed from CID fragmentation of carboxylic acids; Levsen et al. 2007; Witt et al. 2009). After the initial loss of C_2H_6 from the molecular ion $[M\text{-}H]^-$ repeated abstractions of $(CH_2)_n$-units were detected, resulting in the base peak at m/z 183 with the molecular formula $C_8H_8O_3S$ (DBE = 5). A benzene ring in the molecule is a reasonable assumption

(accounting for 4 DBE). Other low magnitude sulfur and non-sulfur ions were present in the full spectrum at nominal mass 311, and fragment ions of these were also detected (Figure VI.3-6). In contrast to the fragment ions, they were also present with a higher relative magnitude in the original spectrum. The fragmentation spectrum of nominal mass 325 (E4a - 2009, SML) showed fragment ions at the same mass differences but no detectable peak at m/z 170.

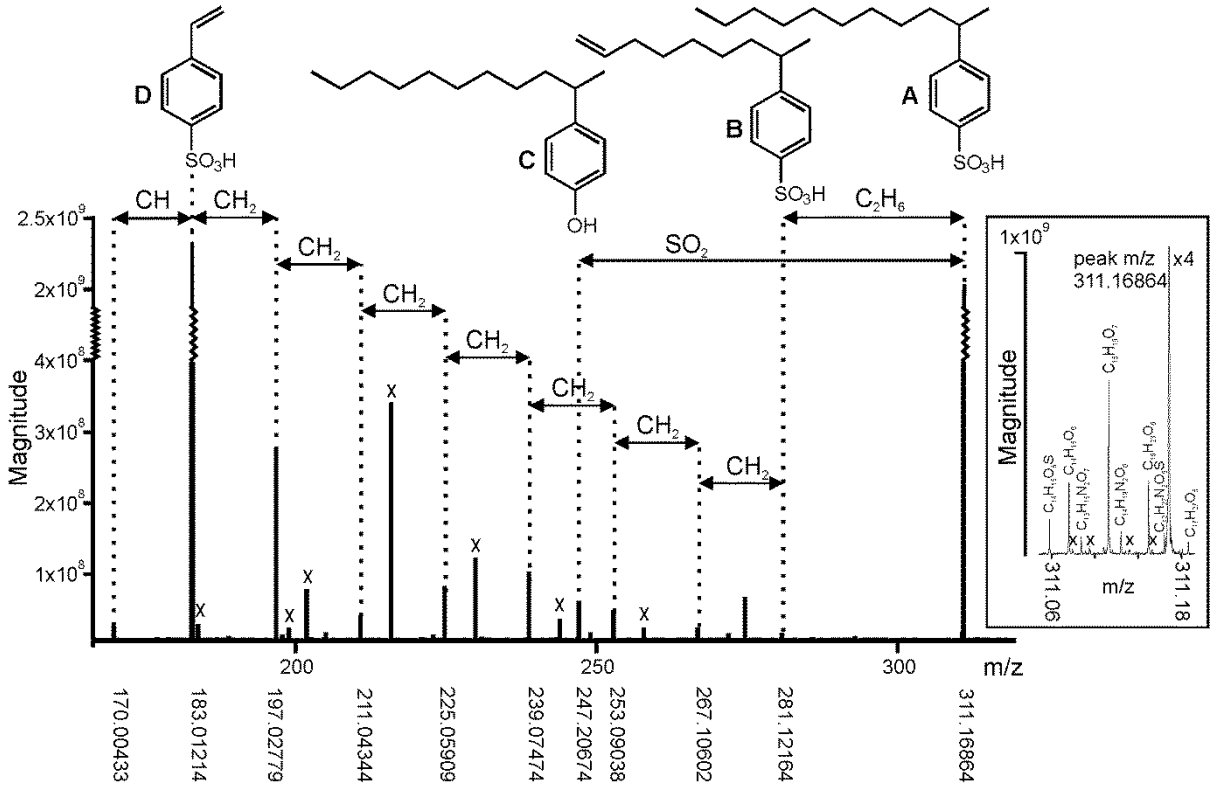

Figure VI.3-6. CID FT-ICR MS analysis of m/z 311.

Collision induced dissociation (qCID-MS/MS) spectrum of nominal mass 311 of a microlayer sample (C1 - 2009, SML) with exact m/z values for fragment ions. Fragments from calculated mass differences are displayed together with possible neutral structures of the major ions: undecylbenzenesulfonic acid (A, molecular ion peak), non-8-enylbenzenesulfonic acid (B), undecylphenol (C) and styrenesulfonic acid (D, base peak). "×" = major additional sulfur compounds (O_4S, O_5S), which possibly resulted from fragmentation of additional molecular ions at the isolation nominal mass. Other peaks present in the original spectrum C1 – 2009, SML at mass 311 are shown in the insert with assigned molecular formulas.

This approach strongly suggests that the molecular formulas of the base peaks at the nominal mass 311 and 325 (m/z 311.16864 and 325.18429) have only one major structural isomer and belong to the group of linear alkylbenzenesulfonates (LAS, which are widespread anthropogenic surfactant products). However, the exact substitution pattern and potential branching of the alkyl rest could not be resolved and might contribute to a higher degree of structural diversity for these peaks.

According to these results, we assume that the other molecular formulas that belonged to the same pseudo-homologous "CH_2"-series ($C_{13+k}H_{19+2k}O_3S$; k = 0 - 7) were true homologues and as well LAS compounds. In all samples most of the homologue molecular formulas of the LAS were also found, but with lower magnitudes. Enrichment factors for these mass peaks varied between EF = 1 and 17.

VI.3.5 Discussion

The Krka River Estuary is a well-studied biogeochemical system (see Marine Chemistry special issue 32, 1991) with low freshwater inflow and low terrestrial organic matter load (Cauwet 1991). The karstic catchment of the Krka River is reflected in low particulate organic matter carbon to nitrogen ratios (Svensen et al. 2007) suggesting mainly autochthonous production within the estuary. The persistent and strong halocline at the freshwater/saltwater interface in the microtidal estuary prevents exchange between surface brackish water and deep saline water. The halocline acts also as a barrier for autochthonous dissolved and particulate organic matter produced in the surface layer. Higher inflow of river water in May results in a shorter water residence time in the whole estuary as compared to September (Legović 1991).

Our bulk chemical data showed low DOC concentrations along the estuary transect increasing from the upper estuary to the marine station in May 2009. In the Krka Estuary non-conservative DOC mixing occurs, highlighting the importance of the autochthonous production (Sempere and Cauwet 1995; Louis et al. 2009). The very low phosphate concentrations throughout the whole estuary and lipid and fatty acid analysis (B. Gašparović et al. unpubl.) indicate growth limitation and point towards low production and post spring-bloom conditions. Compared to the upper estuary (station E3), nitrate was slightly elevated at the middle station E4a, which is closest to the only larger city along the estuary. Human activity may induce higher nutrient levels (Legović et al. 1994), although this was not observed in our phosphate data.

Chromatographic and optical properties. DOC and total absorbance (λ = 210 nm) were always higher in the microlayer than in the underlying water. The absorption coefficients α(355 nm) fell in the range of previously reported values for Adriatic Sea CDOM (Berto et al. 2010) and revealed high EFs for CDOM in the SML

ranging from 4.0 (station E3) to 1.8 (station C1) which is clearly higher than the enrichment of total DOC (mean EF of 1.42). Such high CDOM-EFs agree with data from slick samples (Blough 1997; Wurl et al. 2009), although visible surface slicks were not present at the sampling time. Considering enhanced photochemical degradation of CDOM in the SML a continuous CDOM enrichment has to occur in the SML (Wurl et al. 2009).

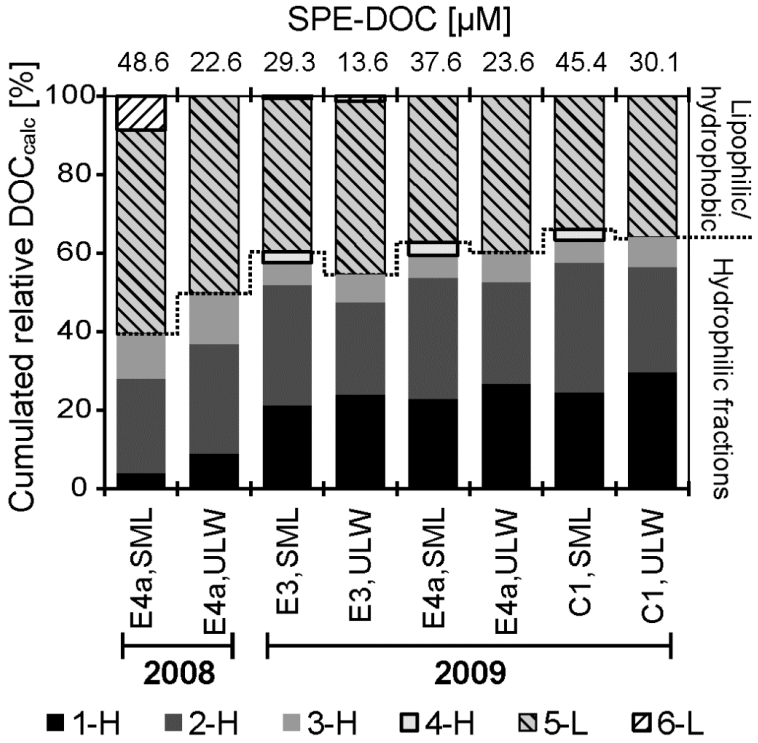

Figure VI.3-7. Calculated DOC concentration in RP-HPLC fractions.
Relative proportions of the calculated DOC amount (DOC_{calc}) for the chromatographic peaks for all samples with the corresponding total DOC concentration in the extract (SPE-DOC). For peak names refer to Figure VI.3-2. Peaks that do not appear in all samples are highlighted (4-H and 6-L, black boxes).

The first two peaks in the $DAD_{210\,nm}$ chromatograms (1-H, 2-H) showed the highest differences between SML and ULW samples. In addition to a pure polarity separation, the first two peaks partly reflect a size exclusion separation with a larger average molecular size for peak 1-H compared to peak 2-H (Hutta et al. 2011; Lechtenfeld et al. 2011). This is a result of the narrow average pore size diameter of the RP column with only 80 Å, resulting in an exclusion of the largest molecules or strongly bound aggregates. The peaks 1-H and 2-H therefore elute prior the dead volume of sample methanol and their separation resulted from a mixed mode separation mechanism preventing a direct correlation between hydrophobicity/molecular size and retention time. However, in all SML samples the

proportion of the calculated DOC content (%-DOC_{calc}) is higher in peak 2-H than in peak 1-H likely resulting from a higher contribution of lower molecular weight compounds in the SML (Figure VI.3-7). This is also supported by a smaller weighted average mass of SML compared to ULW compounds as detected by FT-ICR MS.

The trend of smaller average molecular size in the SML sample was especially evident from the 2008 samples from the middle station E4a. There, in the ULW sample, peaks 1-H and 2-H were shifted towards lower retention time (i.e., higher average size compared to the 2009 ULW samples). The E4a - 2009, SML sample showed in contrast a higher DOC_{calc} contribution and pronounced shift of peak 2-H to lower molecular size (compared to the 2008 ULW and 2009 SML samples). These results likely reflect an enhanced photochemical degradation of organic matter in the SML, presumably combined with enhanced microbial breakdown (Obernosterer et al. 2005). Hence, the pronounced accumulation of small breakdown products in the SML in September 2008 can be explained with the extended exposure to such degradation processes due to the longer water residence time in summer (Legović 1991). This is also supported by size-exclusion chromatography, which showed a unique peak of low molecular size compounds only appearing in the SML sample from 2008 (data not shown).

The total DOC normalized fluorescence decreased greatly from the freshwater E3 to the marine C1 station (on average 73% reduction for SML and ULW samples, Table VI.3-2). We assume that this change was due to differences in autochthonous production in the estuary (Ahel et al. 1996; Cetinic et al. 2006) and that the degradation of fluorophores during the transport from station E3 to C1 is responsible for the decrease in fluorescence. We further assume that the degradation of only small amounts of terrestrial humic-like material (Blough and del Vecchio 2002) from the karstic watershed of the Krka river is a minor contribution to the observed fluorescence decrease, in contrast to humic-rich river estuaries (Yamashita et al. 2008). Moreover, the DOC normalized total fluorescence ratio SML/ULW was always below one (Table VI.3-2). This indicates that fluorophores with either different quantum yield or higher abundance were present in the ULW samples, strong photobleaching in the SML took place or quenching effects due to the different compositions of both phases were dominant.

The occurrence of the unique fluorescence peak in the ULW samples at 29 min (not detected in the 2008 samples) presumably reflects fluorophores derived from primary production (Koch et al. 2008). The contribution of this peak to the total fluorescence was highest in the freshwater E3 sample and lowest in the marine C1 sample. This might be a discrimination effect in the microlayer enrichment mechanism (due to the changing ionic strength) or a consequence of degradation along the estuarine transport. However, this peak was also found in deeper water layers of the estuary (data not shown), suggesting that this fraction is also rapidly degraded in the SML.

Molecular characterization. FT-ICR MS analyses revealed that each SML sample had higher wa H/C (from +0.01 to +0.09) and lower wa mass (from -5.7 to -14.9 Da) compared to the ULW samples (Table VI.3-3). However, based on the complete sample set, there was no significant trend between these molecular parameters and salinity or DOC. Only the classification of all molecular formulas in each SML/ULW sample pair into “enriched/depleted in the SML” can explain these results in terms of microlayer chemical characteristics (Figure VI.3-5). Applying this approach, changes in numbers and proportional intensity of enriched/depleted compounds with increasing salinity were revealed in the estuary (Figure VI.3-4): At low salinities (i.e., low ionic strength) only compounds with very high H/C ratios were enriched in the SML. In contrast, at the high salinity marine station C1, the mean H/C ratio of compounds enriched in the SML and those enriched in the ULW were more similar (Table VI.3-5). The change in the H/C ratios of the enriched and depleted compounds points towards a separation mechanism of hydrophobic constituents at the phase transitiony between ULW and SML.

Table VI.3-5. Mean values and standard deviation for H/C, O/C, mass and DBE for all compounds that were enriched (enr.) or depleted (depl.) in the SML, not including the unique peaks. For E4a – 2008 depl., values were omitted (n.a.; only one peak below EF = 0.67).

Sample	Sample-type	H/C		O/C		mass [Da]		DBE	
		enr.	depl.	enr.	depl.	enr.	depl.	enr.	depl.
E4a – 2008	SML	1.454	n.a.	0.371	n.a.	405.3	n.a.	6.8	n.a.
	ULW	±0.295	n.a.	±0.152	n.a.	±103.4	n.a.	±3.5	n.a.
E3 – 2009	SML	1.476	1.117	0.487	0.382	401.6	483.9	6.3	11.9
	ULW	±0.363	±0.299	±0.186	±0.143	± 86.1	±131.6	±5.0	± 3.4
E4a – 2009	SML	1.462	1.113	0.521	0.497	386.3	566.0	5.9	12.9
	ULW	±0.311	±0.266	±0.186	±0.127	± 81.7	± 97.7	±3.5	± 4.1
C1 – 2009	SML	1.383	1.347	0.500	0.464	403.7	480.2	6.9	9.7
	ULW	±0.276	±0.425	±0.167	±0.165	± 88.9	±155.3	±3.1	± 8.1

The concept of “salting-out” of hydrophobic substances (Setschenov 1889) implies that the water solubility of hydrophobic molecules decreases with increasing ionic strength (Xie et al. 1997). Applied to the ULW/SML system, we assume that only at high ionic strength, the water-solubility of “moderately” hydrophobic (amphiphilic) substances is sufficiently reduced to accumulate in the SML. The salt-mediated, additional enrichment of compounds with intermediate H/C values therefore reduces the average H/C ratio of all enriched compounds at the marine station. Indications that the FT-ICR MS molecular H/C ratio can be interpreted as a measure of hydrophobicity of compounds (at constant O/C ratio) were derived from coupled RP-HPLC-FT-ICR MS experiments (Koch et al. 2008; Liu et al. 2011).

Consistent with the results from the HPLC analyses and the FT-ICR MS data from the total samples, the mean molecular mass of all SML enriched compounds was lower than for the total of all peaks and especially lower than for the ULW enriched compounds (i.e., depleted in the SML) in the corresponding paired sample (Table VI.3-5). This agrees with previous reports of photochemically produced and enriched low-molecular-weight compounds in surface microlayers (Zhou and Mopper 1997; Schmitt-Kopplin et al. 2012).

In addition, the contribution of S-compounds (on number and intensity basis) to all SML enriched molecular formulas was higher in the low salinity samples than in the high salinity samples, while the proportion of N-compounds increased slightly with salinity (Figure VI.3-8). Moreover, the difference in the H/C ratio and mass between the enriched and depleted N-compounds is always larger than the corresponding difference between the S-compounds. This suggests that, compared to nitrogen compounds, the size and polarity distribution of sulfur bearing compounds is more similar in SML and ULW. Thus, S-compounds are less influenced by the “salting out” effect along the estuary.

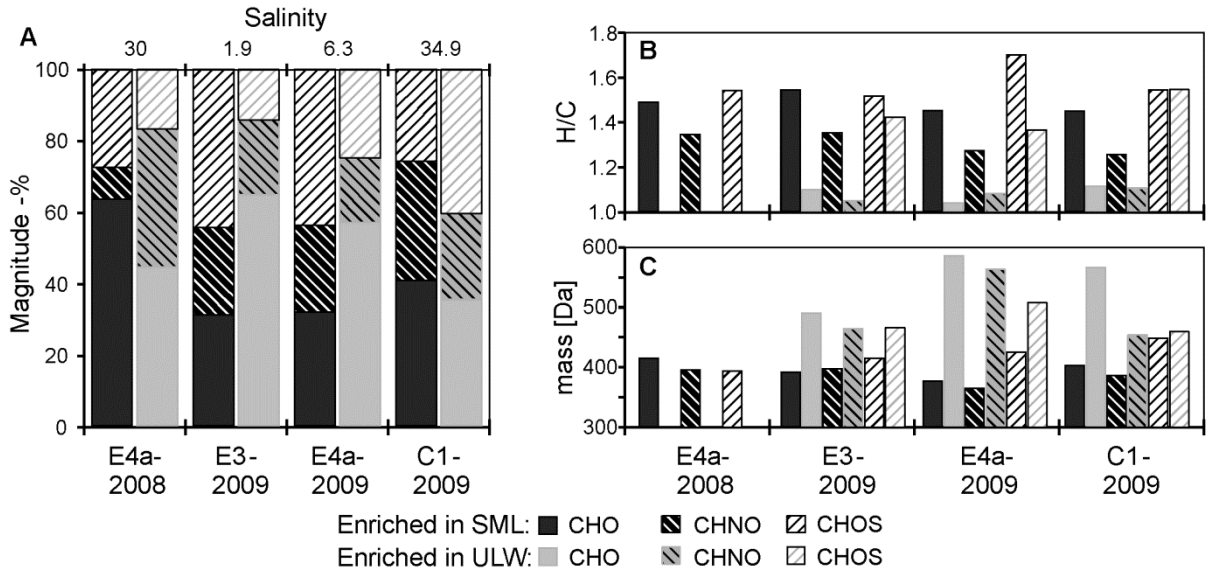

Figure VI.3-8. Summed magnitudes and molecular properties of enriched and depleted compounds.

Enrichment properties of different compound classes (CHO, CHNO, CHOS) for all stations. A: relative magnitude contribution to all enriched and unique compounds in the SML and ULW together with the salinity of the SML sample. B: mean molecular H/C ratio and C: mean molecular mass for the SML or ULW enriched compound classes. CHNOS as well as ULW enriched compounds for E4a – 2009 were omitted for this figure due to their low abundances. Mean ratios were used to highlight the differences in the molecular composition, as the peaks were selected by their EF and not their relative magnitude.

The variation between enriched and depleted compounds in the H/C dimension (the effect was less pronounced for the O/C ratios) was also demonstrated by the multivariate statistical analysis. The difference in the H/C ratios (Table VI.3-5) and the distance between SML and ULW samples on the PC2 axis (Figure VI.3-3B) reflect the difference in hydrophobicity. It should be noted that there is only little compositional overlap of the enriched/depleted substances between the four sample pairs, which can be attributed partly to the defined relative magnitude and EF thresholds.

Microlayer enriched compounds with a similar range of H/C and O/C ratios and low molecular mass were also found in the SML off the coast of Mallorca Island (Morales-Cid et al. 2009) and a study on the sea-air phase transfer of organic matter (Schmitt-Kopplin et al. 2012). Air bubbles mediate an enhanced transport of surface-active compounds from the bulk phase to the SML and further into the atmosphere. Active enrichment due to breaking waves is also the reason why at rough wind conditions, mean enrichment factors of surfactants can be even higher than at calm winds (Wurl et al. 2011). However, this did not influence the sample composition in our study, due to prevailing calm wind conditions during sampling.

The late summer 2008 sample from the middle station E4a could be described as a superposition of the high salinity sample C1 and the anthropogenically influenced middle estuary station from 2009. The different environmental conditions (longer water residence time, higher solar radiation dose, higher temperature) were likely reflected in the higher wa H/C, lower wa O/C ratios, wa mass and wa DBE values as well as high DOC concentration for both 2008 - E4a samples. Also, a set of high magnitude (> 5% relative peak magnitude), highly enriched (EF > 2.5) compounds was found (Figure VI.3-1), likely corresponding to saturated ($C_nH_{2n}COOH$) and mono unsaturated ($C_nH_{2n-2}COOH$) fatty acids, not present in the 2009 samples. If we consider that enrichment in the SML is dependent on the polarity of individual molecules (reflected by the H/C ratio) and the ionic strength of the medium, these results are in accordance with the proposed physico-chemical separation at the phase boundary. Frka et al. (2009) reported surface active substance concentrations at the Šibenik site that were three times higher in the SML and five times higher in the ULW in summer than in winter. These substances accumulate in the estuarine SML during the low run-off summer months, being more hydrophobic than in winter. Reports on the enrichment of hydrophobic lipid-like compounds or fatty acids (having high H/C and low O/C ratios) in SML samples are ambiguous (e.g., Gašparović et al. 2007; Lass and Friedrichs 2011). However, based on mass spectrometric analysis, Frew et al. (2006) reported an enrichment of surface-active lipids in slicked SML samples.

Seasonal differences were also reflected in very high EFs of some compounds in the September 2008 sample set compared to the May 2009 samples from the same station. The E4a – 2008 SML sample showed a clearly higher abundance of unique high magnitude, high H/C, and low O/C compounds which cannot be explained alone with the salinity-trend for the enrichment of substances. A set of high magnitude, sulfur bearing compounds contributed mainly to this enrichment.

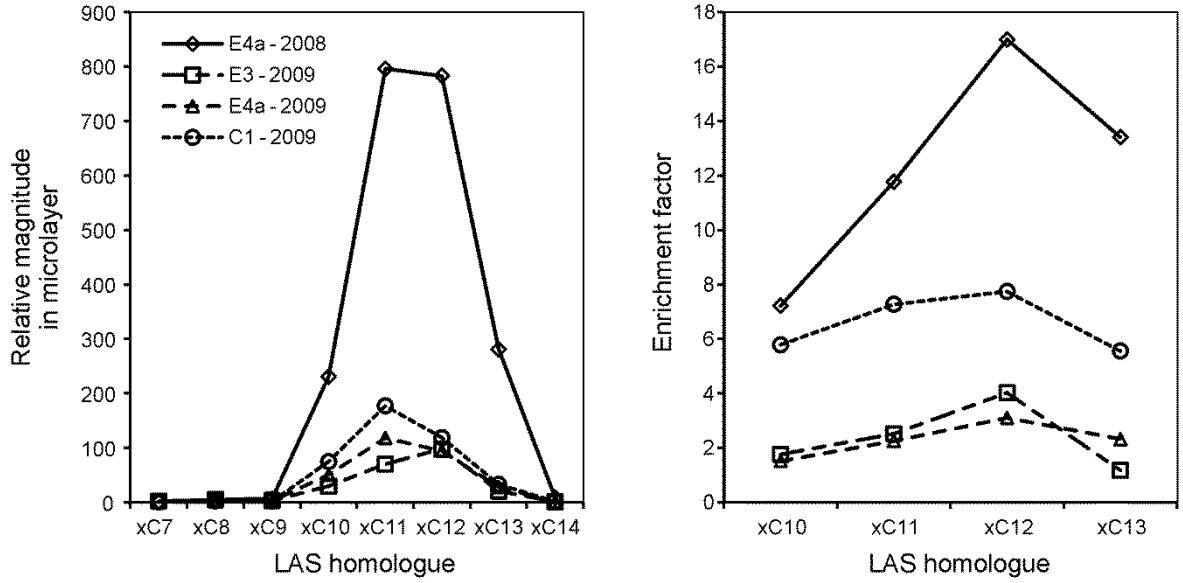

Figure VI.3-9. Magnitude distribution and enrichment factors of LAS homologues.

Relative peak magnitude distributions in the surface microlayer and enrichment factors for the proposed linear alkylbenzenesulfonate (LAS) homologues xC7 – xC14 in the Krka Esturay. The "x" indicates that the position of the benzene sulfonate group is unknown and the length of the alkyl rest is expressed as "C" and number. No enrichment factors were calculated for xC7 – xC9 and xC14 as the magnitudes for these homologues in the ULW samples were below the threshold.

Our fragmentation experiments revealed the occurrence of LAS in the SML, most pronounced in the 2008 sample close to the city of Šibenik, which is in agreement with earlier studies (Ahel and Terzic 2003). Calculation of concentrations of these substances was not possible, as FT-ICR MS data do not allow quantitative conclusions but the magnitude distribution of the LAS peaks in our samples (Figure VI.3-9) correspond well to the distribution determined by the industrial production process (Alzaga et al. 2003). A comparison of the relative peak magnitudes for each sample pair revealed a high enrichment in the SML for some LAS homologues for both high saline samples (E4a – 2008 and C1 – 2009; Figure VI.3-9). Relative magnitudes and enrichment were most pronounced in the 2008 sample, probably as a result of the longer water residence time in the estuary (Legović 1991). This strongly suggests enhanced enrichment of LAS in the microlayer with increasing salinity aided by the "salting-out" effect and suppression of the heterotrophic metabolic activity in higher saline waters (Terzic et al. 1992; Alzaga et al. 2003).

Other highly SML enriched sulfur compounds in the 2008 samples may also be passively or actively enriched from lower layers or may originate from autochthonous production in the surface layer. However, primary production was

unusually low during September (B. Gašparović et al. unpubl.). The contemporary view on the molecular structuring of SML (Cunliffe et al. 2011) requires a hydrated layer of a heterogeneous polymeric network. Carbohydrates (Williams et al. 1986; Kuznetsova et al. 2005) and TEP (Cunliffe et al. 2009; Wurl et al. 2009) are enriched in SML with a high fraction of sulfate ester groups (Wurl and Holmes 2008). However, high molecular weight, oxygen-rich compounds were not detected in our FT-ICR MS samples. Our findings based on FT-ICR MS fragmentation and database comparison hence necessitate very careful interpretation of sulfur containing molecular formulas as well as other potential non-ionic surfactant masses in future FT-ICR MS studies of solid-phase extracted NOM.

An approach to assess the general degradation state of an NOM sample is the degradation index (I_{DEG}, Eq. 4; Flerus et al. 2012). In our study the SML samples had generally higher I_{DEG}-values than the ULW samples, indicating a higher degree of degradation in the SML. Moreover, the 2008 samples had higher values than the 2009 samples. An explanation for the higher degree of degradation could be the enhanced photochemical and microbial reworking in the SML and the decoupling between autotrophic production and transformation of organic matter in this particular physico-chemical environment (as supported by the 29 min FLD peak, Obernosterer et al. 2005; Santos et al. 2011). Therefore, the I_{DEG} parameter might also be well applicable to characterize the degradation state of sea surface microlayers. Our ongoing research aims at understanding the molecular mechanisms and biogeochemical causes for the observed differences in the I_{DEG} parameter.

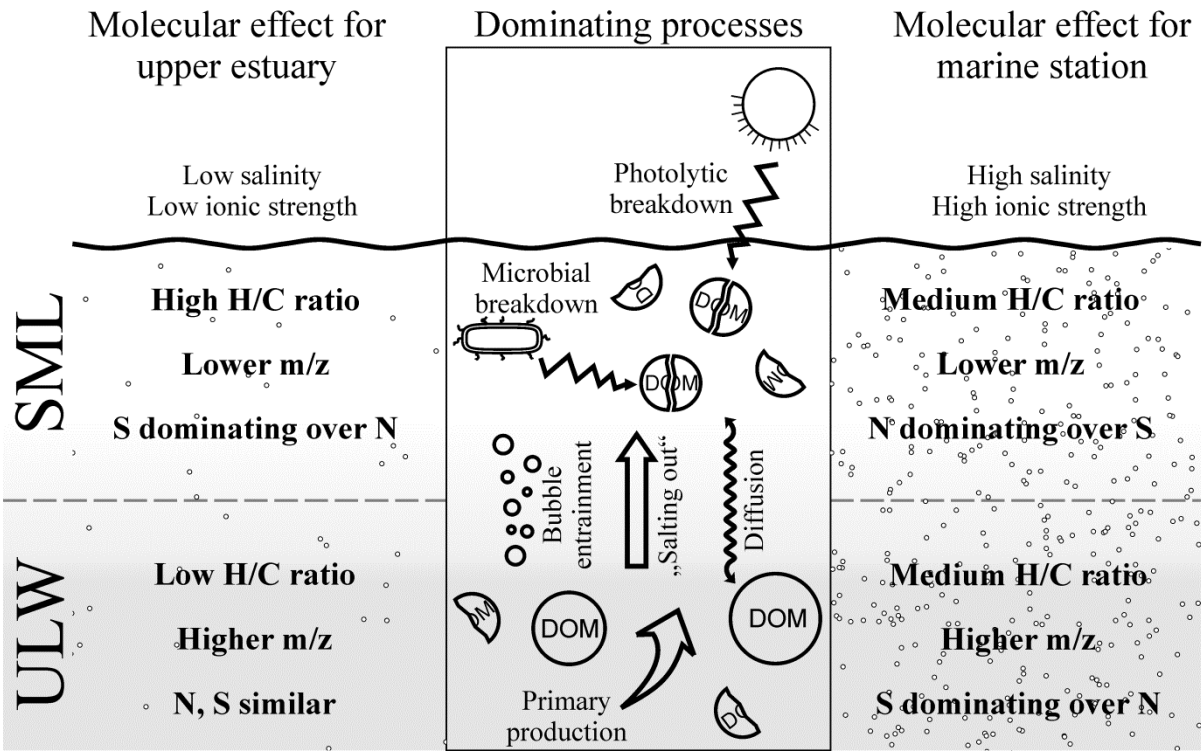

Figure VI.3-10. Sea-surface processes and observed molecular effects.
Summarizing sketch of the dominating processes in the SML and ULW and their consequences for the observed molecular characteristics of the DOM samples. Note that the "boundary" between ULW and SML is a transition layer (Zhang et al. 2003) but the molecular information is obtained from discrete samples.

Major processes that determine the molecular composition and hence the degradation state of NOM in the surface microlayer with respect to the bulk water phase are depicted in Figure VI.3-10: The SML is characterized by a strong enrichment of bacterial biomass (Sieburth et al. 1976) and predominating heterotrophic processes (Reinthaler et al. 2008; Santos et al. 2011). Together with the photoinhibition of photoautotrophs in the SML (due to high UV-B radiation) a decoupling of production and degradation can occur (Obernosterer et al. 2005). The pronounced exposure to sunlight in stratified estuaries and low wind conditions then favors the photochemical breakdown of DOM molecules in the SML (Tilstone et al. 2010). Physico-chemical processes further determine the composition of the SML and ULW, such as diffusion, bubble entrainment (Wurl et al. 2011), "salting-out" of hydrophobic molecules (Xie et al. 1997) and spontaneous vertical phase separation and horizontal segregation of surface active substances (Frka et al. 2012). However, sorption of organic compounds on suspended particles also changes the partitioning between water, solid phase and the hydrophobic surface microlayer (Gschwend and Schwarzenbach 1992; Brunk et al. 1997) and might lead to further molecular

fractionation between these phases in shelf waters (Boehm 1980). The chemical observations presented in this study are a superposition of all these effects, determining the equilibrium state of hydrophobic and hydrophilic substances between SML and ULW. Our current research aims at resolving the relative contribution of each effect on the molecular level distribution of compounds.

VI.3.6 Conclusions

Our ultra-high resolution mass spectrometry results on solid-phase extracted DOM from surface microlayers and underlying waters in the karstic Krka river estuary demonstrated that the SML is a layer with considerable compositional analogy to the ULW. However, specific differences in the molecular composition were attributable to the salinity gradient, a factor which is so far rarely considered in SML studies. In addition to the highly dynamic chemical and physical character of the SML, surface microlayers sampled in estuarine or coastal zones are particularly prone to anthropogenic influences. Hydrophobic and surface-active compounds released from ship traffic and wastewater discharge potentially influence the distribution of substances at the sea surface, which are not covered by the analytical window of conventional methods for surface microlayer studies. The presented study combines the benefits of high resolution molecular analysis of DOM with the potential to identify sampling site specific anthropogenic contributions. For a comprehensive understanding of the processes in the SML and their global significance for e.g., the accumulation and degradation of pollutants and the sea-air exchange of energy and matter, all of these factors need to be considered.

Acknowledgements

This work was funded by a grant of the bilateral collaboration between Croatia and Germany, from the Croatian Ministry of Science, Education and Sports, (project no. 098-0982934-2717), and the German Academic Exchange Service (DAAD project no. D/07/00068). O. J. L. was funded by the Deutsche Forschungsgemeinschaft (DFG KO 2164/8-1+2).

VI.4 Manuscript 4[46]

A molecular perspective on the ageing of marine dissolved organic matter

R. Flerus,[1,#] O.J. Lechtenfeld,[1,#] B.P. Koch,[1,2,#,*] S.L. McCallister,[3] P. Schmitt-Kopplin,[4,5] R. Benner,[6] K. Kaiser[6] and G. Kattner[1]

1 Alfred Wegener Institute for Polar and Marine Research, Ecological Chemistry, Bremerhaven, Germany

2 University of Applied Sciences, Bremerhaven, Germany

3 Virginia Commonwealth University, Department of Biology, Center for Environmental Studies, Richmond, VA, USA

4 Helmholtz Zentrum München, German Research Center for Environmental Health, Analytical BioGeoChemistry, Neuherberg, Germany

5 Chair of Analytical Food Chemistry, Technische Universität München, 85354 Freising-Weihenstephan, Germany

6 University of South Carolina, Marine Science Program, Columbia, SC, USA

# These authors equally contributed to this work.

* Correspondence to: B.P. Koch (Boris.Koch@awi.de)

[46] This manuscript has been published in *Biogeosciences* in June 01, 2012. I did parts of the sampling and measurements, performed parts of the data analysis, did the statistics, supported the interpretation and the editing of the manuscript resulting in equal contribution of the first three authors to the overall work.

VI.4.1 Abstract

Dissolved organic matter (DOM) was extracted by solid phase extraction (SPE) from 137 water samples from different climate zones and different depths along an eastern Atlantic Ocean transect. The extracts were analyzed with Fourier transform ion cyclotron resonance mass spectrometry (FT-ICR MS) with electrospray ionization (ESI). $\Delta^{14}C$ analyses were performed on subsamples of the SPE-DOM. In addition, the amount of dissolved organic carbon was determined for all water and SPE-DOM samples as well as the yield of amino sugars for selected samples. Linear correlations were observed between the magnitudes of 43% of the FT-ICR mass peaks and the extract $\Delta^{14}C$ values. Decreasing SPE-DOM $\Delta^{14}C$ values went along with a shift in the molecular composition to higher average masses (m/z) and lower hydrogen/carbon (H/C) ratios. The correlation was used to model the SPE-DOM $\Delta^{14}C$ distribution for all 137 samples. Based on single mass peaks a degradation index (I_{DEG}) was developed to compare the degradation state of marine SPE-DOM samples analyzed with FT-ICR MS. A correlation between $\Delta^{14}C$, I_{DEG}, DOC values and amino sugar yield supports that SPE-DOM analyzed with FT-ICR MS reflects trends of bulk DOM. DOM weighted normalized mass peak magnitudes were used to compare aged SPE-DOM and recent SPE-DOM semi-quantitatively regarding single mass peaks. The magnitude comparison showed a continuum of different degradation rates for the single compounds. A high proportion of the compounds should persist, possibly modified by partial degradation, throughout thermohaline circulation. Prokaryotic (bacterial) production, transformation and accumulation of this very stable DOM occurs probably primarily in the upper ocean. This DOM is an important contribution to very old DOM, showing that production and degradation are dynamic processes.

VI.4.2 Introduction

Marine dissolved organic matter (DOM) is one of the major active reservoirs of the global carbon cycle. The amount of marine dissolved organic carbon (DOC) is estimated to be 662 Gt, which is comparable to the amount of carbon in atmospheric CO_2 (Hedges 1992; Hansell et al. 2009; Conway and Tans 2012). Since the average age of bulk DOC below the thermocline is about 4,000 years in the Sargasso Sea and about 6,000 years in the central North Pacific, marine DOM plays an important role in long-term carbon storage and sequestration of atmospheric CO_2 (Williams and Druffel 1987; Bauer 2002). This older DOM pool represents a refractory background with concentrations of 35 – 45 µmol kg^{-1} (Hansell and Carlson 1998a; Ogawa et al. 1999) upon which labile and semi-labile pools of DOM are superimposed in the upper ocean. Numerous studies have examined the fluxes, remineralization and temporal variability of accumulated DOC (e.g., Goldberg et al. 2009; Hansell et al. 2009; Carlson et al. 2010). Jiao et al. (2010) proposed the concept of the microbial carbon pump as a potential process for the production of refractory DOM in surface waters. Hereby microbes produce the very stable DOM, which persists over very long time scales in the world oceans. However, the mechanisms of production, diagenesis and preservation of highly stable DOM are still unknown. The molecular analysis is particularly challenging as only a minor fraction of the DOM can be analyzed molecularly and identified as carbohydrates, lipids, amino acids and amino sugars (Benner 2002).

Ultrahigh resolution Fourier transform ion cyclotron resonance mass spectrometry (FT-ICR MS) with electrospray ionization (ESI) was successfully applied to distinguish thousands of compounds of different elemental compositions in ultra-filtered and solid-phase extracted marine DOM (SPE-DOM) (Koch et al. 2005; Hertkorn et al. 2006; Kujawinski et al. 2009). Ultrahigh resolution allows elemental formulas to be assigned for individual mass peaks (Stenson et al. 2003). Water samples of different spatial origin can be distinguished based on the molecular information from FT-ICR MS analysis. However, to date only a few samples have been compared with this technique, preventing a systematic comparison of FT-ICR MS data and additional analytical parameters.

Radiocarbon age and amino sugars are critical diagnostic parameters to assess the production of refractory DOM. The analysis of amino sugars in seawater

provides very valuable information on the early diagenesis of DOM (Benner and Kaiser 2003; Davis et al. 2009; Kaiser and Benner 2009). Radiocarbon age provides a timeline from carbon fixation in the upper ocean and its subsequent turnover and flux to the deep ocean for bulk DOC and individual components and compound classes (Druffel et al. 1992; Aluwihare et al. 1997; Loh et al. 2004; Repeta and Aluwihare 2006). Due to the analytical challenge of radiocarbon analysis of bulk DOC, the radiocarbon age has only been determined for a few samples at some locations including the Central North Pacific (Williams and Druffel 1987; Druffel et al. 1992), the Southern Ocean (Druffel and Bauer 2000) and the Sargasso Sea (Bauer et al. 1992; Druffel et al. 1992). A handful of additional studies have been performed on $\Delta^{14}C$ of marine DOM fractions of differing size or chemical components such as humic isolates, lipid extracts, carbohydrate-like DOM and protein-like DOM. The high molecular weight (> 10 kDa) DOM is of recent age suggesting greater lability and faster turnover, whereas the low molecular weight (< 1 kDa) DOM is apparently older (Santschi et al. 1995; Loh et al. 2004). Humic substances isolated with XAD-resins are similar to bulk C pools with radiocarbon ages only slightly older (Druffel et al. 1989). The oldest age (up to 17,000 years BP) was determined in lipid extracts (Loh et al. 2004). However, each DOM fraction still consists of multiple compounds with a continuum of ages, and consequently the bulk age of DOM represents an average of all the individual compounds. To date a direct linkage between radiocarbon age and DOM on a molecular level has not been reported.

The aim of this study was to investigate the ageing processes and associated molecular changes of DOM along an eastern Atlantic Ocean transect. Our combination of FT-ICR MS with radiocarbon age analysis of SPE-DOM from different depths and biogeochemical regions provided a unique opportunity to investigate the age-composition and related molecular signatures of a large ocean system. To discuss the data in a broader ecological and biogeochemical context, FT-ICR MS data were combined for the first time with environmental parameters, DOC, amino sugars and bacterial activity, each determined independently. Our ultimate goal was to elucidate molecular trends that are characteristic for the entire Atlantic Ocean.

VI.4.3 Materials and methods

Sampling. Water samples were collected along a transect from 50.2° N to 31.4° S in the eastern Atlantic Ocean in November 2008 during the cruise ANT-XXV/1 of RV *Polarstern*. Surface water was sampled 3 times per day with a fish sampler, which was fixed alongside the ship providing a continuous flow of surface water (≈ 2 m water depth). Water from 200 m and the fluorescence maximum was sampled daily with a rosette sampler connected to a CTD, as well as water from 7 selected stations from surface to bottom (Figure VI.4-1). Samples for the analysis of DOC and amino sugars were filtered through GF/F filters (Whatman, pre-combusted for 4 h, 450 °C) and stored in pre-combusted glass ampoules at -20 °C.

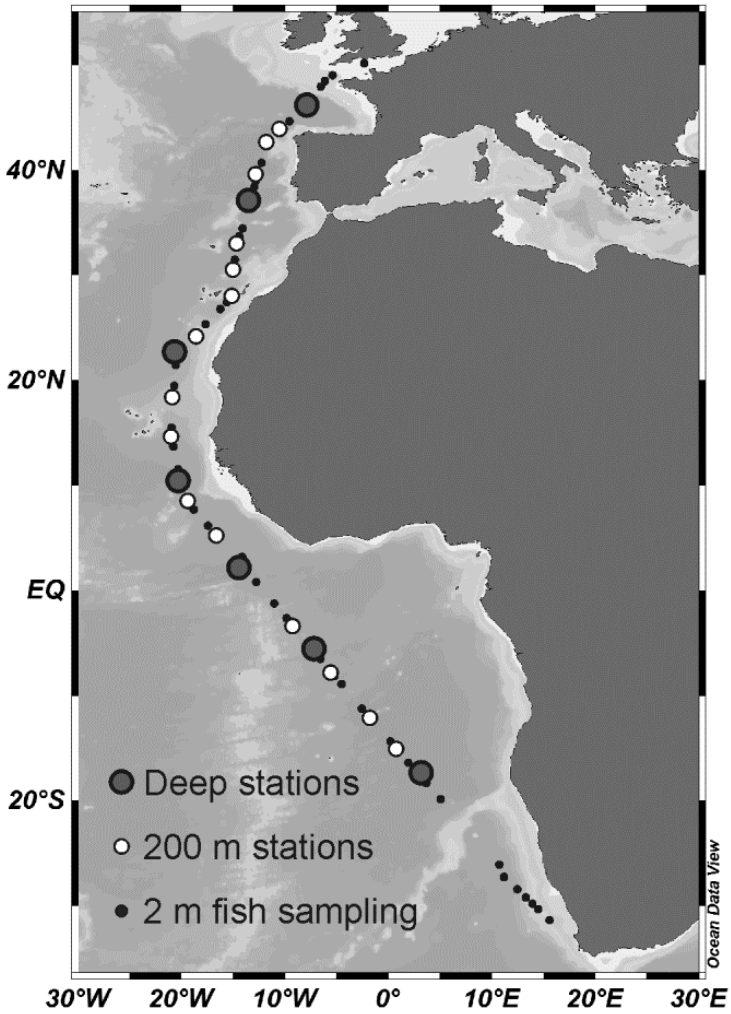

Figure VI.4-1. Sampling locations.
Map of the sampling locations on the cruise ANT-XXV/1 of RV Polarstern.

DOM Extraction. FT-ICR MS measurement requires the concentration and desalting of marine DOM. Therefore DOM was extracted on board using solid phase extraction (SPE) for which the term SPE-DOM will be used in the following. Filtered samples were acidified with HCl (hydrochloric acid, p.a. grade, Merck) to pH 2. The DOM was extracted using SPE cartridges (PPL, 1 g, Varian, Mega Bond Elut) according to Dittmar et al. (2008). The cartridges were rinsed with methanol (LiChrosolv; Merck), followed by acidified ultra-pure water (Milli-Q, pH 2, HCl) and then 5 L of seawater was gravity-passed through each cartridge. Subsequently remaining salt was removed with acidified ultra-pure water. After drying with nitrogen gas, DOM was eluted with 5 mL methanol into pre-combusted glass ampoules and stored at -20 °C.

Analyses. The DOC concentration was determined by high temperature catalytic oxidation with a Shimadzu TOC-V_{CPN} analyzer. Before analysis water samples were acidified in the auto-sampler and purged with O_2 for 5 min. The DOC content of the SPE-DOM was determined by evaporation of 50 µL methanol extract re-dissolved in 6.5 mL ultra-pure water.

Bacterioplankton production was estimated by ^{3}H-leucine uptake (Smith and Azam 1992). Triplicate subsamples (1.5 mL) and one trichloroacetic acid-killed control were amended with 5 nM ^{3}H-leucine (Amersham, specific activity 160 Ci mmol^{-1}) and incubated at in situ temperature (±2 °C) in the dark. Incubation time varied depending on depth: ≈ 2 h for upper waters (up to 200 m) and up to 12 h (below 200 m). Samples were processed according to Smith and Azam (1992) and radioassayed with a Wallac scintillation counter after addition of 1 mL of Ultima Gold AB scintillation cocktail. The disintegrations per minute (DPM) of the killed control were subtracted from the mean DPM of the corresponding duplicate samples and converted to leucine incorporation rates. A conversion factor of 3.1 kg C mol^{-1} was applied (Kirchman 1993).

Concentrations of galactosamine (GalN), mannosamine (ManN) and glucosamine (GlcN) were determined by high-performance anion-exchange chromatography coupled to a pulsed amperometric detector (Kaiser and Benner 2000). After hydrolysis in 3 M HCl (5 h, 100 °C) samples were neutralized with a self-absorbed ion retardation resin (AG11 A8, Biorad) and stored frozen until analysis.

Samples were desalted by solid-phase extraction using Biorad´s AG50 X8 resin in the Na^+-form before chromatographic separation. Subsequently, GalN, ManN and GlcN were separated isocratically on a Dionex PA20 anion-exchange column with 2 mM NaOH at a flow rate of 1 mL min^{-1}.

Subsamples of SPE-DOM (0.2 – 1 mg C) were quantitatively transferred to combusted (500 °C) quartz tubes (6 mm diameter), evaporated under a stream of N_2, sealed under vacuum and combusted at 900 °C to CO_2 using a CuO/Ag metal catalyst (Sofer 1980). The CO_2 from break-seals was subsequently reduced to graphite in an atmosphere of H_2 over a cobalt catalyst (Vogel et al. 1987). Graphite targets were analyzed at the Center for Accelerator Mass Spectrometry at Lawrence Livermore National Laboratory. $\Delta^{14}C$ is defined as the (per mil) deviation of a sample from the ^{14}C activity of a 1950 standard, corrected for fractionation according to Stuvier and Polach (1977). Total measurement uncertainties for $\Delta^{14}C$ analyses of these samples were typically ±4‰. A blank analysis of a SPE cartridge was determined before and no measurable amount of CO_2 was found (<1 µg).

FT-ICR MS analysis of 137 SPE-DOM samples was performed with an Apex Qe mass spectrometer (Bruker Daltonics) equipped with a 12 T superconducting magnet (Bruker Biospin) and an Apollo II Dual electrospray source (Bruker). Prior to analysis, SPE-DOM was adjusted to similar DOC concentrations by dilution with methanol (factor 3.1 – 9.7). The diluted extracts were analysed with ESI in negative ion mode (capillary voltage -4.2 kV, infusion flow rate 2 µL min^{-1}). Spectra were calibrated internally with compounds, which were repeatedly identified in marine DOM samples (339.10854, 369.11911, 411.12967, 469.13515, 541.15628 m/z; Schmidt et al. 2009; Flerus et al. 2011). 512 scans were added to acquire one spectrum. All ions were singly charged and the mass accuracy was below -0.2 ppm < mass accuracy < 0.2 ppm for the ions used for the internal calibration.

FT-ICR MS data evaluation. The mass spectra were evaluated in the range m/z 200 – 600. For each identified peak in the spectra (signal to noise > 3; Data analysis 3.4; Bruker Daltonics) elemental formulas were calculated in the mass accuracy range of ±0.5 ppm (e.g., Koch et al. 2005; Koch et al. 2007). The isotopes included for the formula calculation were as follows: ^{12}C (0 - ∞), ^{13}C (0 - 1), ^{1}H (0 - ∞), ^{16}O (0 - ∞), ^{14}N (0 - 2), ^{32}S (0 - 1). The average mass accuracy for all assigned peaks

was < ±0.2 ppm. For unambiguous elemental formula assignment the “nitrogen-rule” and following thresholds were applied: O/C ≤ 1.2 and H/C ≤ 2C + 2 + N (Koch et al. 2005). All formulas with ^{13}C isotopes were removed from the data set as they represent duplicates of the ^{12}C parent molecules.

Prior to mass spectra comparison, the mass peak magnitudes of each spectrum were normalized to the sum of all identified mass peak magnitudes of the respective spectrum. These relative peak magnitudes are presented in per mil (‰) and a magnitude cutoff of 0.05‰ was applied. All mass peaks present in less than 5 mass spectra were excluded from the final data set, in favor of identifying bulk trends. Since masses with low signal to noise ratios tend to show less mass accuracy, this procedure allowed an improved formula assignment. Ambiguously identified mass peaks were checked according to the “chemical building block” approach (Koch et al. 2007). Each oxygen atom in a molecular formula could be replaced with a CH_4-fragment, forming a pseudo-homologous series with a mass difference Δm = 36.4 mDa. Therefore, the number of oxygen atoms in a molecular formula must exceed the number of “CH_4-O” pseudo-homologous series members, otherwise it is considered as falsely assigned.

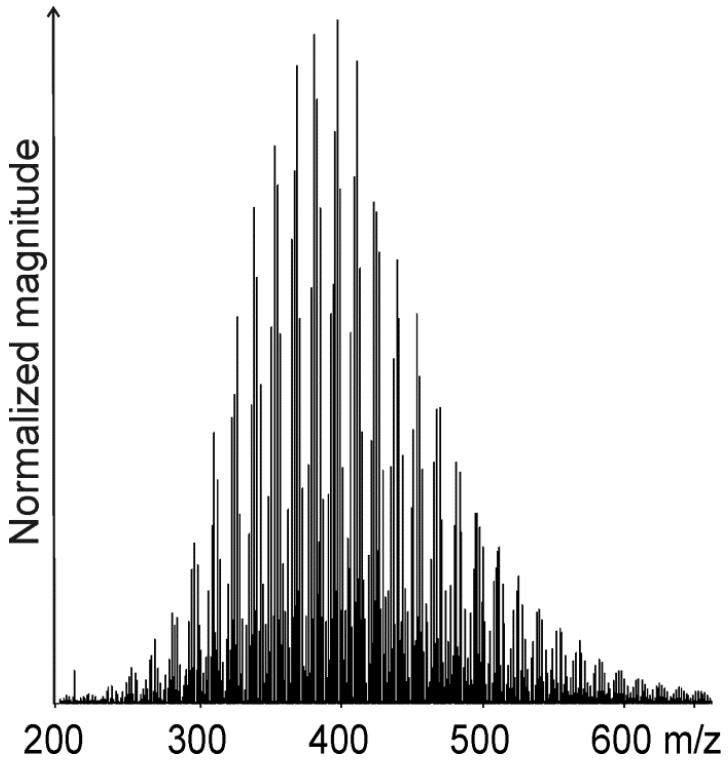

Figure VI.4-2. FT-ICR mass spectrum.
Negative ESI FT-ICR mass spectrum of a representative marine SPE-DOM sample from the eastern Atlantic Ocean.

Finally an evaluation data set was obtained showing 2,850 mass peaks with only few doubly assigned molecular formulas (average: 2 ± 1 double assignments per sample). On a presence-absence basis and the 0.05‰ cutoff, 54% of the detected molecular formulas were present in more than 135 samples, while 74% were present in at least 100 samples showing the typical peak magnitude distribution of marine SPE-DOM (Figure VI.4-2). Most mass peaks, which were not present in all samples, showed normalized magnitudes close to the cutoff limit. Due to the high degree of similarity between all samples, our data evaluation was based on normalized peak magnitudes instead of a presence/absence-based approach as previously applied for biomarker approaches in glacial or riverine DOM (Sleighter et al. 2008; Bhatia et al. 2010).

Statistical analysis. For statistical analysis we performed a non-parametric two-sided Mann-Whitney U-test for the comparison of weighted average parameters of SPE-DOM samples and two groups of peaks. The null hypothesis was that two groups differ by a location shift of “0” and the significance level α is 0.01.

VI.4.4 Results and discussion

$\Delta^{14}C$ values ranged from a maximum of -229‰ in surface water extracts (2 m) to -464‰ in deep water extracts (> 2,500 m, Figure VI.4-3). The highest surface $\Delta^{14}C$ values were comparable with the surface (3 m) $\Delta^{14}C$ value determined by Druffel and Bauer (1992) in the Sargasso Sea (-238‰). In comparison to the reported values from the Sargasso Sea, our $\Delta^{14}C$ values in deeper water (> 2 m) were slightly more negative, ranging between that of bulk DOC and XAD isolates (Bauer et al. 1992), and pointing to an almost representative extraction. However, from polarity-driven reversed phase chromatography and the lower extraction efficiency for organic nitrogen compared to organic carbon we know that the method discriminates against highly polar (and presumably small) compounds.

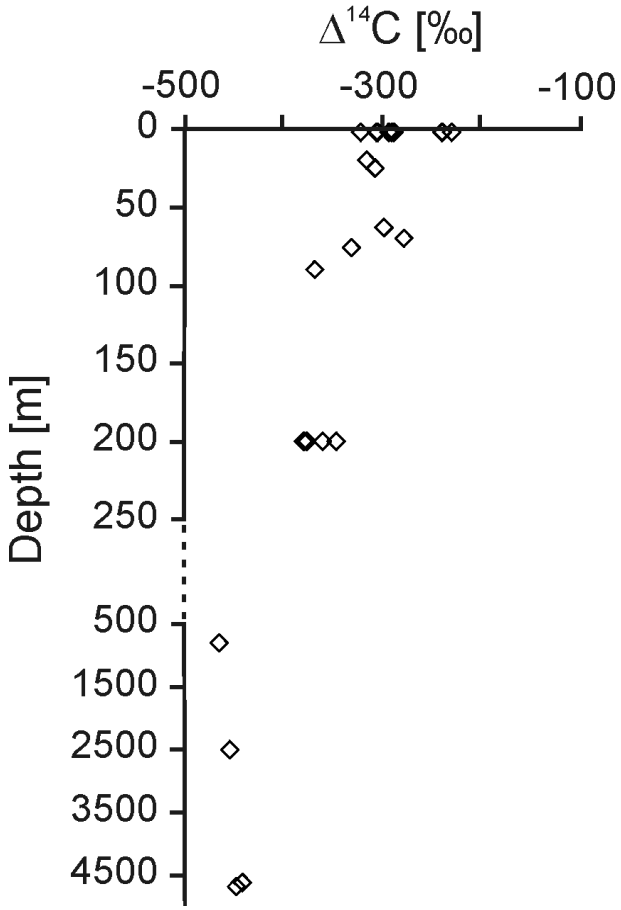

Figure VI.4-3. $\Delta^{14}C$ values of marine SPE-DOM from the eastern Atlantic Ocean.

Forty-three percent of the normalized FT-ICR mass peak magnitudes showed either a significantly linear positive (POS) or negative (NEG) correlation with $\Delta^{14}C$ ($R > 0.5$, $p < 0.01$) (elemental formulas are presented in Table A1 and A2[47] in the appendix). The magnitudes of all significantly POS and NEG correlating mass peaks were summed up separately (∑POS, ∑NEG), resulting in two average calibration functions (Figure VI.4-4a, b). The ∑POS and ∑NEG mass peaks account for 61 ± 1% of the summed magnitudes of all peaks in each spectrum, therefore representing a large and consistent fraction of peaks for the complete sample set. The two individual calibration functions were then used to calculate two different $\Delta^{14}C$ values for any of the 137 SPE-DOM samples, both resulting in almost identical $\Delta^{14}C$ values. Hence, the arithmetic mean of the two calculated $\Delta^{14}C$ values was used as the final $\Delta^{14}C$ value ($\Delta^{14}C_{Cal}$) for each sample. $\Delta^{14}C_{Cal}$ values for the upper 200 m are presented as depth-section (Figure VI.4-5), and for the few deep water samples as individual values in Table VI.4-1.

[47] Table A1 and A2 can be found as part of the addendum to this thesis.

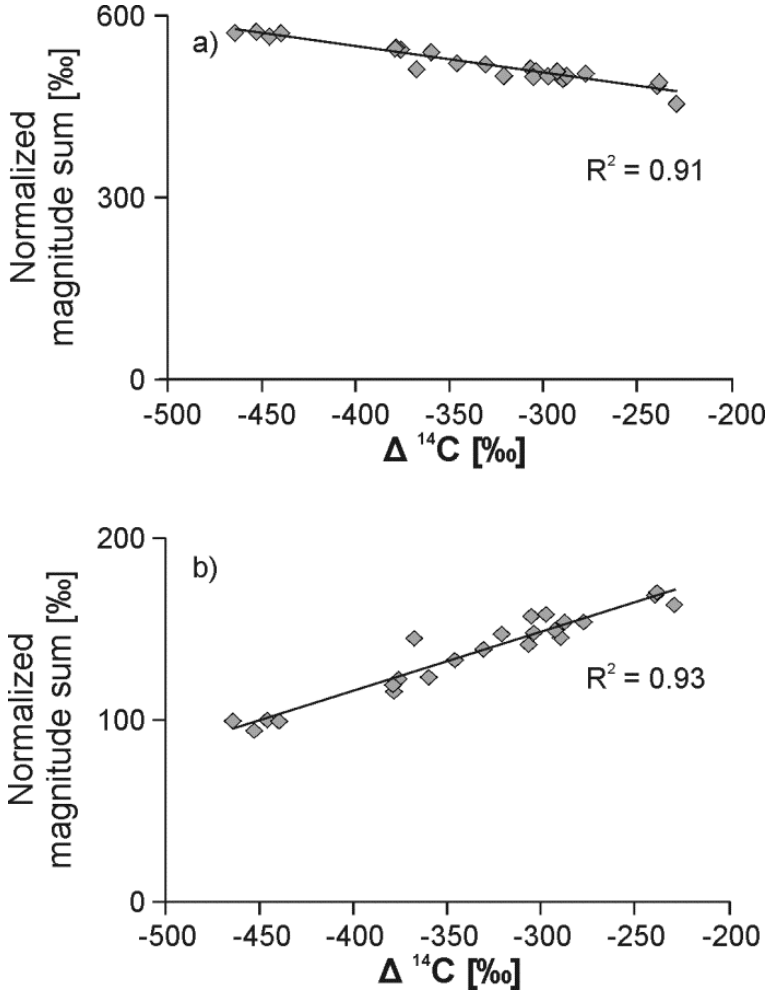

Figure VI.4-4. Peak magnitude vs. $\Delta^{14}C$ correlation.

Normalized magnitude sum [‰] of (a) negatively and (b) positively correlated FT-ICR mass peaks of eastern Atlantic Ocean SPE-DOM versus $\Delta^{14}C$ values of the SPE-DOM. The sums (∑NEG, ∑POS) were built by adding the normalized magnitudes of the single with $\Delta^{14}C$ highly negatively or positively correlating mass peaks for each sample.

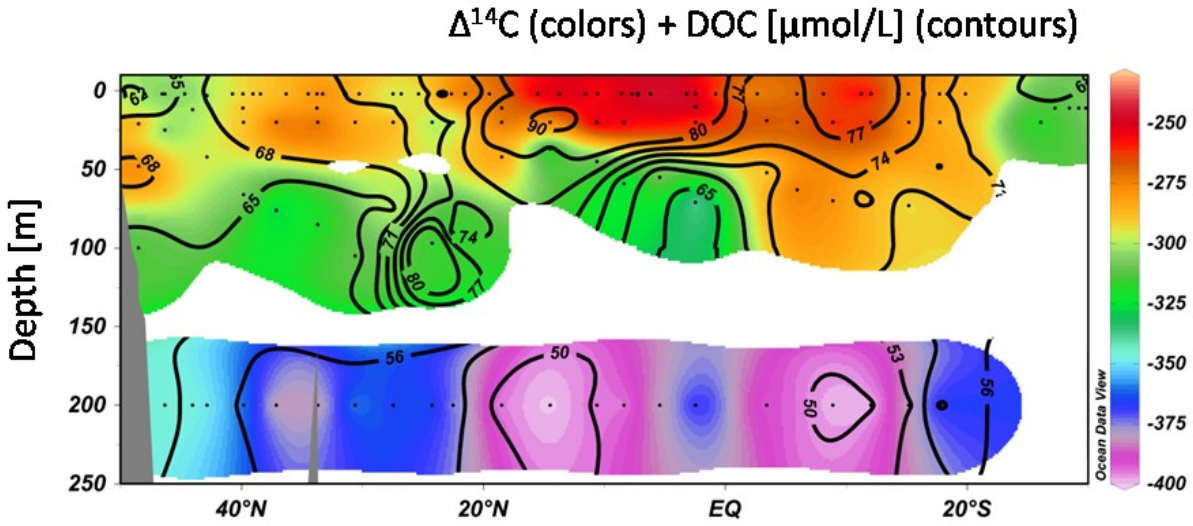

Figure VI.4-5. DOC and $\Delta^{14}C$ in the eastern Atlantic Ocean.

Calculated SPE-DOM $\Delta^{14}C$ values (colors) and measured bulk DOC concentrations (contours) in the upper 250 m of the water column in the eastern Atlantic Ocean. The $\Delta^{14}C_{cal}$ values and the DOC concentrations are significantly positively correlated.

Table VI.4-1. Calculated SPE-DOM $\Delta^{14}C_{cal}$ values [‰] and bulk DOC values [µM] in the deep water layers of the eastern Atlantic Ocean.

Depth [m]	Parameter	46° N 8° W	37° N 14° W	23° N 20° W	11° N 20° W	2° N 14° W	5° S 7° W	17° S 3° E	24° S 9° E
400 – 500	$\Delta^{14}C$ (‰)		-402						
800 – 900	$\Delta^{14}C$ (‰)				-456	-465	-448	-451	
1,100 – 1,800	$\Delta^{14}C$ (‰)		-436	-459				-449	
2,500	$\Delta^{14}C$ (‰)			-462					
4,000 – 5,000	$\Delta^{14}C$ (‰)	-443	-463	-456	-450	-451	-454		
400 – 500	DOC (µM)	56	58						
800 – 900	DOC (µM)				45	47	46	49	
1,100 – 1,800	DOC (µM)	50	48			52	54	47	
2,500	DOC (µM)	48		45					
4,000 – 5,000	DOC (µM)	48	45		47		41	47	45

This approach enabled us to apply calculated $\Delta^{14}C_{Cal}$ values for the whole sample set, allowing to define the groups of "recent" ($\Delta^{14}C_{Cal}$: > -280‰, n = 29) and "degraded" samples ($\Delta^{14}C_{Cal}$: < -450‰, n = 10). Within both groups, the peak magnitude distributions were similar. To obtain a semi-quantitative approach of the reactivity of individual DOM compounds in our Atlantic Ocean sample set, the normalized mass peak magnitudes were weighted by the respective bulk seawater DOC concentration. The relative changes in the magnitudes were calculated using a linear regression model (ordinary least squares, all 137 samples) resulting in predicted decreases of 22 – 167%. A rate of 100% or more is here defined as compounds with magnitudes falling below the 0.05‰ threshold. Since the 100 – 167% was a result of the definition and these compounds were still visible as very small mass peaks in the spectra we will use the term "highly degraded" for this group. The compounds with estimated decreases > 100% were yet observed to be highly degraded in the oldest SPE-DOM in the Atlantic Ocean. This applied for only 4% (number-%) of the compounds. The magnitude weighting resulted in the disappearance of the negative correlations of magnitudes with $\Delta^{14}C$. In fact, the NEG peaks now exhibited a positive correlation with $\Delta^{14}C$ as well, suggesting that both, POS and (formerly) NEG correlating compounds detected by FT-ICR MS decrease with age.

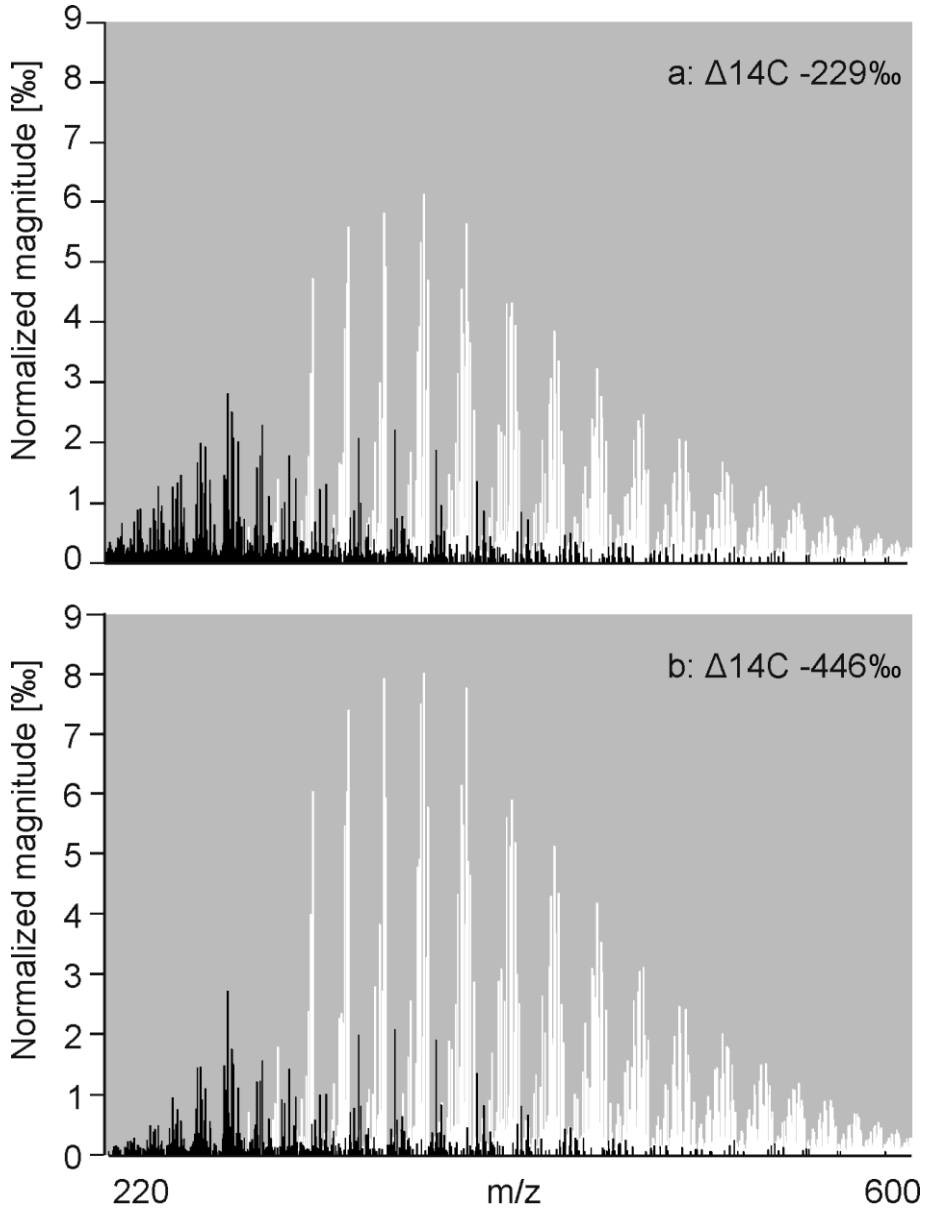

Figure VI.4-6. FT-ICR mass spectrum of young and old DOM.
Selected normalized FT-ICR mass peaks of eastern Atlantic Ocean SPE-DOM. The mass peaks show a significant linear correlation with $\Delta^{14}C$. (a) Surface sample extract with $\Delta^{14}C$ = -229‰ and (b) deep sea sample extract with $\Delta^{14}C$ = -446‰. The black colored masses are positively correlated with $\Delta^{14}C$ and are present in a higher proportion in the more recent SPE-DOM, whereas the white colored masses are negatively correlated with $\Delta^{14}C$ and present in a higher proportion in the aged SPE-DOM. The difference in the m/z between black and white masses is also reflected in the weighted average m/z of the whole SPE-DOM spectra and shifts from 407 (surface sample) to 413 (deep sea sample).

Molecular characteristics of DOM diagenesis. We observed clear differences in the molecular characteristics between POS and NEG compounds. The peak magnitudes of the POS compounds were generally much lower than those of the NEG compounds and the average m/z was inversely correlated with $\Delta^{14}C$ values (Figure VI.4-6). Comparing recent and aged samples revealed a highly significant difference (Mann-Whitney U-test; $p < 0.01$) in the weighted average m/z values of

11.1 Da. The magnitude averaged m/z therefore slightly increased from 407.8 ± 2.1 for recent to 417.9 ± 0.8 for aged SPE-DOM. Previous studies showed a decrease in molecular size from high molecular weight DOM (> 1 kDa) to low molecular weight DOM (< 1 kDa) as a result of increased diagenetic processing (Kaiser and Benner 2009) and a decreasing bioreactivity (Amon and Benner 1996a). Dittmar and Kattner (2003b) also suggested a comparatively higher refractory character for small DOM molecules. However, these previous results were obtained using size-related separations such as ultrafiltration and gel permeation chromatography. In contrast, we used absorbent enriched samples (SPE-DOM) preventing a direct comparison with the previous studies. Based on SPE-DOM samples Hertkorn et al. (2012) obtained results, which also suggested a similar trend of decreasing SPE-DOM molecular size with depth.

The van Krevelen diagram (Kim et al. 2003) showed differences in the elemental composition of the POS and NEG formulas (Figure VI.4-7). The majority of CHO compounds of the POS formulas showed high H/C ratios (1.53 ± 0.2), whereas the NEG CHO formulas showed medium to low H/C ratios (1.15 ± 0.2, Figure VI.4-7a,b). Within the region of H/C ≤ 1.4 of the van Krevelen diagram, the average mass for NEG and POS formulas was m/z 441 and m/z 300, respectively. Most of the POS formulas containing nitrogen (CHNO) showed higher H/C ratios (1.43 ± 0.2). CHNO compounds of NEG formulas occurred only in the low H/C region, similarly to the CHO compounds (1.16 ± 0.2, Figure VI.4-7c, d). The H/C ratio shift also affected the DBE, ranging between 2 and 11 for the POS formulas and between 7 and 14 for the NEG formulas.

Although it is well known that the efficiency of microbial degradation is often related to the polarity of the substrate, we did not observe a shift in the O/C ratios with increasing age of the samples. For both NEG and POS groups, CHO and CHNO compounds showed average O/C values of 0.48 ± 0.3 and 0.49 ± 0.2, respectively showing no significant differences. With the exception of two mass peaks CHOS compounds only occurred in the POS formulas having similar H/C values as the POS CHO and CHNO compounds (Figure VI.4-7e, f) with slightly higher O/C ratios (0.6 ± 0.2). However, only little is known about the role of CHOS compounds in DOM and a considerable contribution of anthropogenic input to these compounds cannot be excluded.

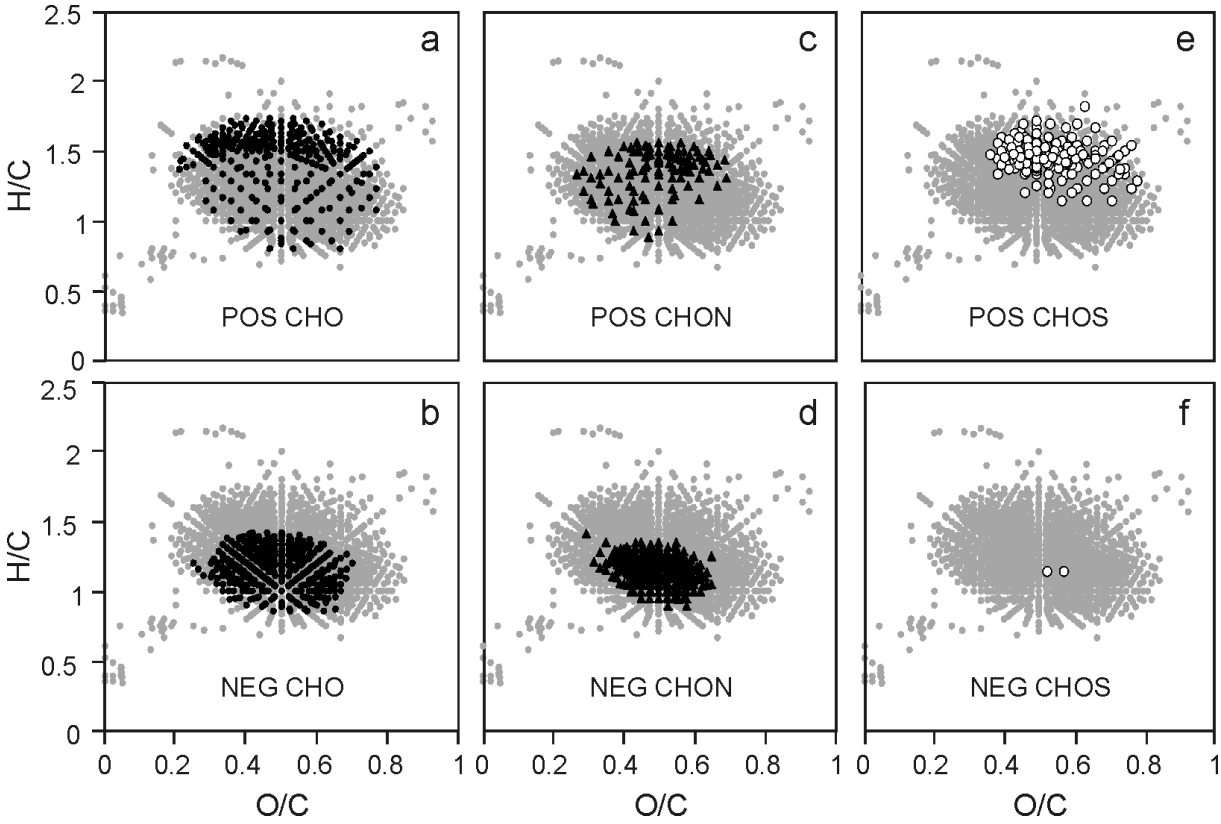

Figure VI.4-7. Van Krevelen diagrams of POS and NEG compound classes.
Van Krevelen diagrams of compounds in eastern Atlantic Ocean SPE-DOM that are significantly correlated with $\Delta^{14}C$ ($p < 0.01$): (a) positively with CHO compounds; (b) negatively with CHO compounds; (c) positively with CHNO compounds; (d) negatively with CHNO compounds; (e) positively with CHOS compounds; (f) negatively with CHOS compounds. The grey dots in the background show all compounds found in the majority of Atlantic Ocean water extracts.

The strong molecular similarity, as detected in this and other studies using FT-ICR MS, is considered to represent the refractory molecular background of marine DOM (Koch et al. 2005; Hertkorn et al. 2006; Gonsior et al. 2011). In our study, we observed depth and age related trends in the total average elemental composition of the spectra. These trends were similar to the trends observed for the POS and NEG formulas. We found a highly significant difference in the weighted average H/C ratios between recent and aged samples (Mann-Whitney U-test, $p < 0.01$). The magnitude averaged H/C ratios decreased from 1.268 ± 0.006 in recent to 1.245 ± 0.003 in aged SPE-DOM. Accordingly, the magnitude averaged DBE increased from 8.03 ± 0.06 in recent to 8.43 ± 0.03 in aged SPE-DOM. Again, no clear trend was found in the magnitude averaged O/C ratios, and we are currently examining potential reasons for this disparity.

Hertkorn et al. (2006) analysed surface and deep UDOM from the Pacific Ocean by NMR and FT-ICR MS. They identified carboxyl-rich alicyclic molecules

(CRAM) as a major constituent in surface and deep UDOM which was suggested to resist biodegradation. The region occupied by CRAM in the van Krevelen diagram corresponds well with the region of our NEG mass peaks, which are assumed to be compounds resistant to degradation. Hence, CRAM could also be a significant contributor to SPE-DOM. However, it has to be pointed out that the elemental composition can represent a large variety of possible structural isomers (Hertkorn et al. 2007). Nevertheless, a recent study by Witt et al. (2009) demonstrated that the structural variability represented by a single elemental formula in the FT-ICR mass spectra is probably not as high as expected for natural organic matter.

Table VI.4-2. Formulas utilized for magnitude summation in order to calculate the degradation index (I_{DEG}).

NEG correlating compounds	POS correlating compounds
$C_{21}H_{26}O_{11}$	$C_{13}H_{18}O_7$
$C_{17}H_{20}O_9$	$C_{14}H_{20}O_7$
$C_{19}H_{22}O_{10}$	$C_{15}H_{22}O_7$
$C_{20}H_{22}O_{10}$	$C_{15}H_{22}O_8$
$C_{20}H_{24}O_{11}$	$C_{16}H_{24}O_8$

East Atlantic Ocean DOM degradation state. The linear correlation between single mass peaks and SPE-DOM $\Delta^{14}C$ allows to compare SPE-DOM samples in terms of their degradation state. Since FT-ICR MS is increasingly used for marine DOM studies, we present a degradation index that can be easily used to estimate and compare the degradation state of marine SPE-DOM. To calculate the degradation index we selected 5 POS (POS_{IDEG}) and 5 NEG (NEG_{IDEG}) formulas (Table VI.4-2) with a particularly high correlation with the radiocarbon age. The 10 selected masses were also present in ≈ 400 previously analyzed samples from other locations and environments and therefore suitable to be implemented in a versatile index describing the relative degradation state of an individual sample within a given set of samples. The index I_{DEG} was calculated using the molecular formulas given in Table VI.4-2 and can be directly applied to the raw peak magnitudes:

$$I_{DEG} = \sum(\text{magnitudes } NEG_{IDEG}) / \sum(\text{magnitudes } (NEG_{IDEG} + POS_{IDEG}))$$

The value of I_{DEG} ranges between 0 – 1 and increases with the degradation state of the sample, because the magnitude contribution of NEG formulas increases. We observed, however, from our database that the absolute value of I_{DEG} is dependent on instrument, extraction technique and environment. For example, samples from soils and sediments had generally lower values for I_{DEG} than samples from ocean water (data not shown). If similar sample extracts are measured with the same instrument in series the I_{DEG} trends are comparable. However, since no comparable data exist, $\Delta^{14}C$ values should only be calculated using I_{DEG} in combination with measured reference $\Delta^{14}C$ values. Also, C18 extracted samples did not reliably show the respective peaks for the I_{DEG} calculation.

For our eastern Atlantic Ocean samples, I_{DEG} was in the range from 0.628 – 0.756 for the surface samples (Figure VI.4-8a) and 0.756 – 0.808 for deeper water > 200 m (Table VI.4-3). I_{DEG} showed a strong correlation with the $\Delta^{14}C$ values and the bulk DOC concentrations. In particular, in the upper 200 m changes in DOC concentrations were reflected in the I_{DEG}. The lowest I_{DEG} was found in the area with the youngest SPE-DOM in the upper 25 m between 2 – 12° N along with the highest DOC concentrations. This was the most stratified region with thermocline depths of 25 – 30 m. The accumulation of freshly produced DOC in highly stratified surface water was also reported by Carlson et al. (1994) and Goldberg et al. (2009). At 200 m depth the lowest I_{DEG} and the youngest SPE-DOM were calculated north of 40° N. The highest I_{DEG} as well as the oldest SPE-DOM and lowest bulk DOC concentrations matched with the tropical divergences around 15° N and 10° S which are upwelling areas. The location of the tropical divergences was obtained from CTD temperature profiles of the cruise. So far, the narrow range and small number of data points of $\Delta^{14}C$ values, DOC concentrations and FT-ICR MS spectra for deep (> 500 m) and bottom water samples circumvents a detailed oceanographic discussion of abyssal water masses in terms of DOM degradation.

To support the differentiation of fresh and old DOM, amino sugars were determined directly in bulk water samples as an independent measurement. Amino sugars are bioactive compounds and the DOC-normalized yield of amino sugars is an indicator for the degradation state of DOM (Benner and Kaiser 2003; Kaiser and Benner 2009). The significant correlation between $\Delta^{14}C_{Cal}$ and the yield of amino sugars is consistent with previous observations indicating that they are more reactive

than bulk DOC. These independent results are a good indication that our mass peak magnitude based $\Delta^{14}C$ calculation is reasonable (Figure VI.4-9). The exponential relation between the amino sugar yield and $\Delta^{14}C_{Cal}$ also suggests that a fraction of the youngest and most bioavailable compounds was not recovered by SPE or was not detected by FT-ICR MS analysis.

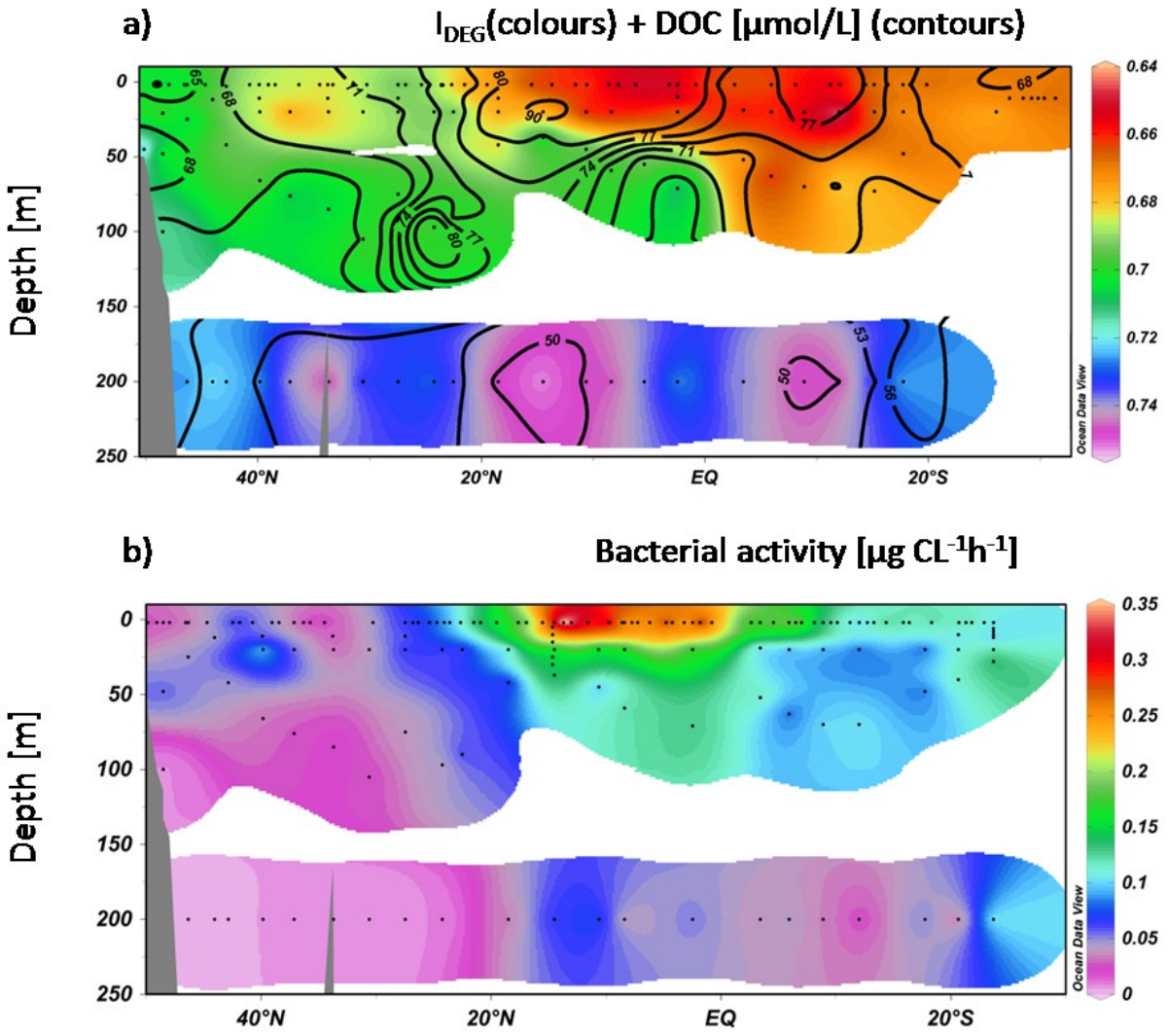

Figure VI.4-8. I_{DEG} and bacterial activity in the eastern Atlantic Ocean.
(a) Values of the degradation index I_{DEG} for SPE-DOM samples from the eastern Atlantic Ocean (colors) and bulk DOC concentrations (contours); (b) the bacterial activity determined as utilized µg C L^{-1} h^{-1} in the upper 250 m of the water column in the eastern Atlantic Ocean. I_{DEG} can be easily calculated and used to estimate and compare the degradation state of marine FT-ICR MS analyzed SPE-DOM. As higher the values of I_{DEG} as more degraded is the SPE-DOM. I_{DEG} and the DOC concentrations are significantly correlated. The bacterial activity maximum coincides with the lowest I_{DEG}, the DOC maximum and the youngest SPE-DOM (Figure VI.4-5).

Table VI.4-3. I_{DEG} values for deep water layers.

Depth [m]	46° N 8° W	37° N 14° W	23° N 20° W	11° N 20° W	2° N 14° W	5° S 7° W	17° S 3° E
400 – 500		0.756					
800 – 900				0.793	0.790	0.777	0.776
1,100 – 1,800		0.787	0.801				0.779
2,500			0.807				
4,000 – 5,000	0.798	0.808	0.805	0.787	0.785	0.788	

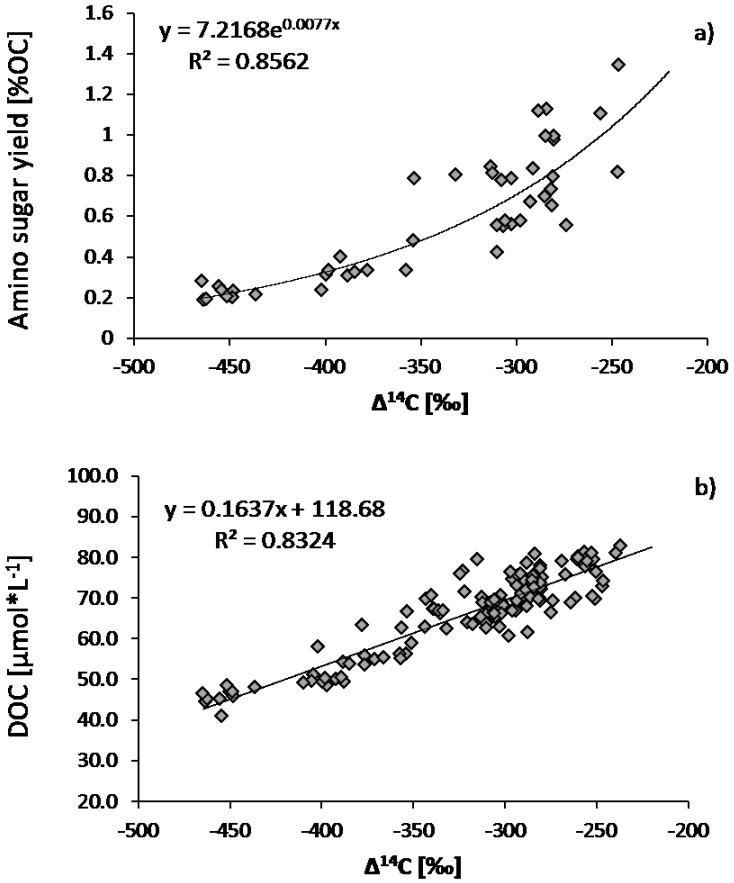

Figure VI.4-9. Amino sugar yield and DOC vs. $\Delta^{14}C$ correlation.
Correlation and equations of a) bulk amino sugar yields and b) bulk DOC concentrations of Atlantic Ocean water and calculated $\Delta^{14}C$ values of the corresponding SPE-DOM. The correlations indicate the reasonability of the trend in $\Delta^{14}C_{Cal}$. The exponential relation between the amino sugar yield and $\Delta^{14}C_{Cal}$ also suggests that a fraction of the youngest and most bioavailable compounds was not recovered by SPE or was not detected by FT-ICR MS analysis.

Degradation continuum and the microbial carbon pump. Several studies present strategies to explain mechanisms of redistribution of DOM in the water column based on their $\Delta^{14}C$ values and two or three component models (Williams

and Druffel 1987; Beaupré and Druffel 2009; Hansell et al. 2009; Beaupré and Aluwihare 2010). The models suggest a refractory DOM background fraction and labile or semi-labile fractions with distinct isotopic compositions. Beaupré and Druffel (2009) used 2-component Keeling plots to estimate the radiocarbon age of the background and the fresh DOM fractions. Applying the Keeling plot method to the SPE-DOM samples from the 7 deep stations, results in similar values for the fresh SPE-DOM fraction at every station (Table VI.4-4). The values are slightly lower than the values reported for the Sargasso Sea (Beaupré and Aluwihare 2010) but the variation is within the range of reported values for the Pacific Ocean (Beaupré and Druffel 2009). This provides further evidence that the trends in radiocarbon age of SPE-DOM are comparable to that for the bulk DOC. Beaupre and Druffel (2009) calculated $\Delta^{14}C$ for the background DOM, but since $\Delta^{14}C$ was too low for the oldest water sample they considered a multiple component system.

Table VI.4-4. Calculated $\Delta^{14}C$ values of excess SPE-DOM and corresponding Keeling slope values for the 7 deep stations of the East Atlantic Ocean.

Station		$\Delta^{14}C$ of excess SPE-DOM	Keeling slope
46° N	8° W	-121	-6,880
37° N	14° W	108	-11,394
23° N	20° W	17	-10,050
11° N	20° W	50	-9,938
2° N	14° W	68	-10,203
5° S	7° W	76	-10,550
17° S	3° E	44	-10,239

Our results indeed showed a wide spectrum of DOM reactivity represented by varying slopes of magnitude change with age, supporting our hypothesis of a continuum of DOM reactivity and age. As mentioned above, we assume that the compounds in the FT-ICR mass spectra have been degraded over time, but to varying extents. In the North Central Pacific Ocean (NCP) the lowest $\Delta^{14}C$ value of bulk DOC is -546‰ (Druffel et al. 1992), which is older than the oldest SPE-DOM in the Atlantic Ocean. Coinciding with the oldest water masses, the DOC concentration in the deep NCP is only ≈ 34 µmol kg^{-1} (Hansell et al. 2009), supporting the hypothesis of a very slow degradation (remineralization) of refractory DOC (Hansell

et al. 2012). Based on the correlation between $\Delta^{14}C_{Cal}$ of SPE-DOM and DOC concentration (Figure VI.4-9b) we estimated the $\Delta^{14}C$ values and molecular degradation trends of SPE-DOM during thermohaline circulation. Applying this correlation, the SPE-DOM $\Delta^{14}C$ in the NCP calculates to -518‰ which is in good agreement with the values reported (Williams and Druffel 1987; Druffel et al. 1992). To elucidate at which point during the thermohaline circulation a single compound would be highly degraded, we performed a rough estimate using the following assumptions: i) each mass peak either represents one compound or several compounds with similar degradation rates. This is based on a recent study by Witt et al. (2009) suggesting that the structural variability of a single elemental formula in the FT-ICR mass spectra is probably not as high as expected for natural organic matter; ii) a compound is regarded as highly degraded, when the relative magnitude falls below the cutoff of 0.05‰. Using the calibration functions resulting from the correlation between the bulk DOC weighted magnitudes and $\Delta^{14}C_{cal}$, a theoretical SPE-DOM $\Delta^{14}C$ limit ($\Delta^{14}C_{Lim}$) was calculated at which each compound is considered to be highly degraded. Thus, the proportion of mass peaks can be estimated, which will be highly degraded in the NCP. Since we were interested in general trends this calculation was performed for compounds which were present in 27 – 29 of all "young" samples. All compounds with $\Delta^{14}C_{Lim} > -518‰$ are expected to be highly degradable, as they are supposed not to be present in the NCP. This applied for 16% (number-%) of the compounds. Portions of the remaining compounds will persist for long periods of time (Figure VI.4-10) and are supposed to contribute to the high average age of DOM. The FT-ICR MS analyzed SPE-DOM represents a fraction of the marine DOM for which a high portion of 84% of the compounds (number-%) is expected to persist, possibly modified by partial degradation, during one or more thermohaline cycles through the global ocean circulation. At the same time the compounds are expected to degrade very slowly with a continuum of different rates in the range from 22 – 167% (Figure VI.4-10). The relative decreases were calculated using a linear regression model (ordinary least squares, all 137 samples), resulting in predicted decreases > 100% for some compounds. These compounds were yet observed to be highly degraded in the oldest SPE-DOM in the Atlantic Ocean.

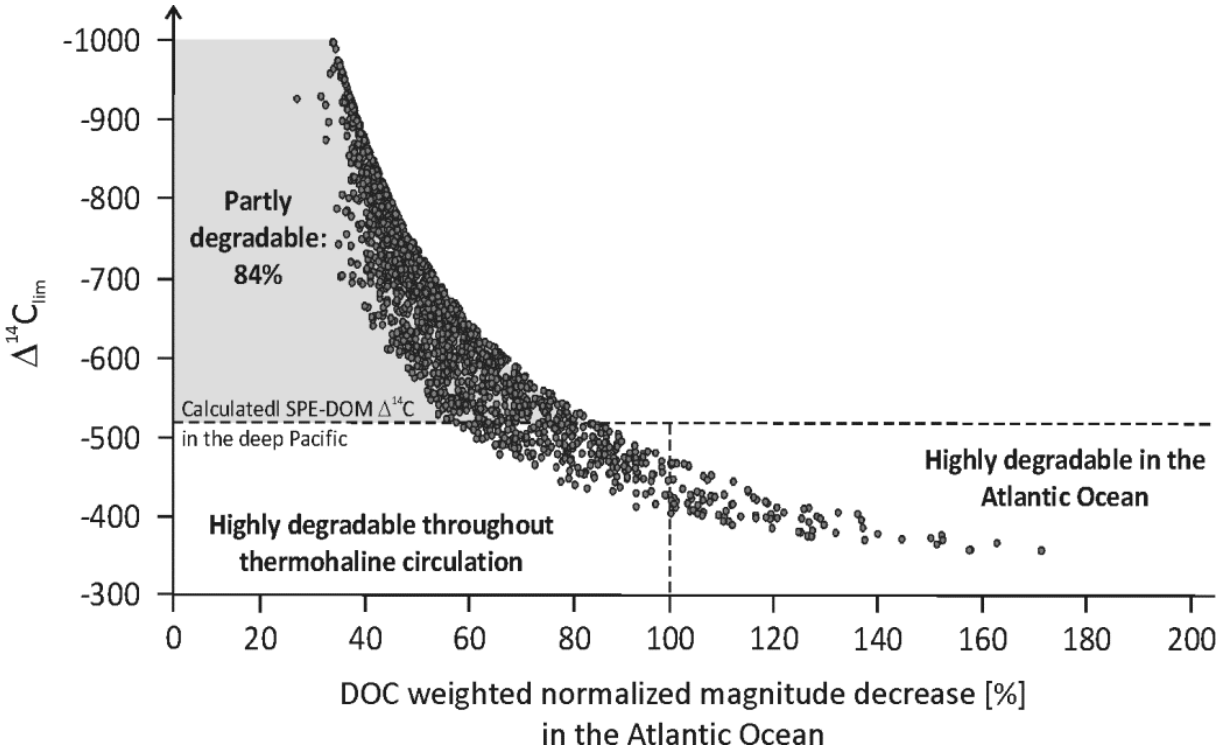

Figure VI.4-10. The degradation continuum.
Calculated limit of $\Delta^{14}C$ ($\Delta^{14}C_{Lim}$) for Atlantic Ocean SPE-DOM compounds represented by FT-ICR mass peaks versus the calculated DOC-weighted normalized magnitude decrease of SPE-DOM in the Atlantic Ocean (x-axis, [%]). All compounds are expected to decrease with increasing SPE-DOM age, but with different rates between 22 – 167%. The relative decreases were calculated using a linear regression model (ordinary least squares, all 137 samples), resulting in predicted decreases > 100% for some compounds. These compounds are yet observed to be highly degraded in the oldest SPE-DOM in the Atlantic Ocean. $\Delta^{14}C_{Lim}$ is a theoretical SPE-DOM $\Delta^{14}C$ value at which a compound is regarded to be highly degraded. All compounds with a $\Delta^{14}C_{Lim}$ > -518‰ (SPE-DOM $\Delta^{14}C$ value estimated for the CNP) are expected to be highly degraded in the oldest water masses. 84% (number-%) of the compounds should persist possibly modified by partial degradation throughout thermohaline circulation. The variability of decreasing rates as well as the $\Delta^{14}C_{Lim}$ values represents a continuum of different degradation rates for the individual compounds.

Our results support the hypothesis of a broad and continuous distribution of $\Delta^{14}C$ ages as proposed by Bauer et al. (1992). Since only few of the compounds were identified to be highly degraded in the oldest Atlantic Ocean SPE-DOM, compounds of moderate reactivity, which are degraded within month to decades and expected to be present in SPE-DOM, are potentially underrepresented in the FT-ICR mass spectra. Also the presence of an absolute refractory fraction (i.e., ^{14}C depleted), that is hidden in a mixture with degrading compounds, cannot be excluded. However, since the $\Delta^{14}C$ trends in SPE-DOM are similar to $\Delta^{14}C$ trends of bulk DOM we propose the degradation continuum shown for FT-ICR MS analysed SPE-DOM to be one important pathway in marine DOM degradation. Operational terms as “labile”, “semi-labile”, “refractory (recalcitrant)”, “background” or “excess”

DOM as used in different studies (Williams and Druffel 1987; Beaupré and Druffel 2009; Hansell et al. 2009; Beaupré and Aluwihare 2010; Jiao et al. 2010) are generally useful to distinguish among the reactivities of different DOM fractions, but the complexity of DOM reactivity is better described as a continuum.

The microbial carbon pump provides a conceptual framework for a better understanding of the role of microbial processes in the generation of recalcitrant DOM and carbon storage in the ocean (Ogawa et al. 2001; Jiao et al. 2010). It is hypothesized that the transformation of labile and semi-labile DOM through microbial processes leads to the accumulation of recalcitrant DOM in the ocean. Indeed, the highest bacterial activity as well as the maximum abundance of the reactive parameters, DOC, amino sugars and I_{DEG}, was determined in surface waters of the highly stratified region between 0 – 15° N (Figure VI.4-7b). The primary production was supposed to have only minor contribution. A comparison of I_{DEG} with the TChl-a fluorescence data from the discrete stations (Taylor et al. 2011) showed no clear relationship. Out of all mass peaks, the estimated fraction of the least reactive compounds is at least 61%, accounting for 94% of the summed magnitudes per sample. We hypothesize that this low reactivity fraction is produced and accumulates in the euphotic zone. Fresh and highly reactive DOM is rapidly consumed by prokaryotes (Carlson and Ducklow 1996) and partially converted to low reactivity DOM (Ogawa et al. 2001). These recently produced refractory and younger compounds mix with older refractory compounds of similar reactivity in the epipelagial. This mixture is then further degraded by bacterial activity (Ogawa and Tanoue 2003) and thereby aged during the thermohaline circulation.

VI.4.5 Conclusions

Trends in bulk DOC radiocarbon ages were reflected in the radiocarbon age determined from a correlation between selected FT-ICR mass peaks and SPE-DOM $\Delta^{14}C$ values. With this knowledge the degradation state of other marine DOM samples can be estimated by comparing FT-ICR mass peaks. Since this method was only applied for the Atlantic Ocean it is important to continue these studies in other oceanic regions. For this, the degradation index I_{DEG} was introduced as a simple tool to evaluate relative degradation states in a set of similarly treated samples. So far

I_{DEG} has only been applied for SPE-DOM samples (PPL extracts) from the Atlantic Ocean and thus has to be further verified.

We propose a degradation continuum of the compounds represented in the FT-ICR mass spectra, but only a minor portion of them are expected to be highly degraded during thermohaline circulation. Prokaryotic (bacterial) production, transformation and accumulation of the very stable DOM occurs probably primarily in the upper ocean (Benner and Herndl 2011). This DOM is an important contribution to very old DOM, showing that production and degradation are dynamic processes. Since bacterial growth, bacterial production or enzymatic activities are influenced by parameters as e.g., temperature or CO_2 (Piontek et al. 2009; Piontek et al. 2010) a change of these parameters could also influence the processes of refractory DOM production or degradation and as a consequence also the amount of DOM in the world oceans.

It is likely that the microbial carbon pump and the proposed degradation continuum of microbially produced DOM are parts of several processes taking place concurrently, resulting in the observed average age of DOM samples. To elucidate these complex processes it is important to further investigate sources, transformations and fates of DOM in the ocean. The FT-ICR MS data provide novel insights into the molecular composition of highly degraded DOM. Microbial degradation experiments and studies of aggregation processes combined with FT-ICR MS will help to gain a better understanding of DOM cycling in the ocean.

Acknowledgements

The authors gratefully acknowledge Anne Stuart for lab assistance, two anonymous reviewers for their helpful comments and the crew of the research vessel “Polarstern” for professional assistance during sample collection.

This work was partially funded by the German Academic Exchange Service (DAAD, project 50023021), the German Science Foundation (KO 2164/8-1), and a National Science Foundation-Ocean Sciences grant OCE-0825403 to S.L.M. and NSF 0713915.

VI.5 Manuscript 5[48]

Molecular transformation and degradation of refractory dissolved organic matter and role of the Weddell Sea for global carbon cycling

Oliver J. Lechtenfeld,[1] Boris P. Koch,[1,2,*] Ruth Flerus,[1,#] S. Leigh McCallister,[3] Philippe Schmitt-Kopplin,[4,5] and Gerhard Kattner[1]

[1] Alfred Wegener Institute for Polar and Marine Research, Ecological Chemistry, Am Handelshafen 12, D-27570 Bremerhaven, Germany

[2] University of Applied Sciences, An der Karlstadt 8, D-27568 Bremerhaven, Germany

[3] Virginia Commonwealth University, Department of Biology, Center for Environmental Studies, 1000 West Cary Street, Richmond, Virginia 23284, USA

[4] Helmholtz Zentrum München, German Research Center for Environmental Health, Analytical BioGeoChemistry, Ingolstädter Landstraße 1, D-85764 Neuherberg, Germany

[5] Technische Universität München, Chair of analytical food chemistry, Alte Akademie 10, D-85354 Freising, Germany

[#] Present address: GEOMAR Helmholtz Centre for Ocean Research, Biological Oceanography, Düsternbrooker Weg 20, D-24105 Kiel, Germany

[*] To whom correspondence should be addressed: E-mail: boris.koch@awi.de

[48] This manuscript is in preparation for *Geochimica et Cosmochimica Acta*. I did parts of the sampling and measurements, performed the data analysis and evaluation, and wrote the paper.

VI.5.1 Abstract

Dissolved organic matter (DOM) in the deep sea is of refractory nature with mean residence times of 4,000 – 6,000 years and it comprises almost 75% of the global ocean organic carbon inventory. Refractory DOM is a long-term buffer in the global carbon cycle but its chemical composition, structure, and biochemical formation and degradation mechanisms are still unresolved. Here we compiled the so far most comprehensive molecular data set of 197 Fourier transform ion cyclotron resonance mass spectrometry analyses from solid-phase extracted marine DOM covering two major oceans, the Atlantic sector of the Southern Ocean and the East Atlantic Ocean. Molecular trends and Δ^{14}C-dating of 34 DOM samples, ranging from -229 to -495‰, were combined to model an integrated degradation rate for bulk dissolved organic carbon (DOC) resulting in a predicted age of > 24 ka for the most persistent DOM fraction. First order kinetic degradation rates for 1,557 mass peaks indicate that numerous DOM molecules cycle on timescales much longer than the turnover of the bulk DOC pool resulting in estimated residence times of > 100 ka. In contrast to young DOM, these most persistent compounds encompass only a narrow range of elemental ratios H/C (1.17 ± 0.13), and O/C (0.52 ± 0.10) and molecular mass (360 ± 28 and 497 ± 51 Da) reflecting the most stable composition in the oceanic environment. In the Southern Ocean, we identified 339 mass peaks which likely contribute to an increased DOC concentration and potentially reflecting an accumulation or enhanced sequestration of refractory DOC.

VI.5.2 Introduction

The major part of marine dissolved organic carbon (DOC) is present in the deep-sea below 1,000 m and hosts 72% of the total organic carbon in the oceans, equivalent to about 477 Pg C (Hansell et al. 2009). This DOC is highly refractory with average residence times of 4,000 – 6,000 a and concentrations of 37 – 45 µM C (Druffel et al. 1992; Hansell et al. 2012). DOC is ultimately derived from primary producers using atmospheric CO_2 as their carbon source. It is directly released from photosynthetic plankton or heterotrophic processes into the oceans and also transported from land by rivers and dust. On the shelves and in the pelagic ocean the major amount of DOC is remineralized to CO_2 by heterotrophs (respiration from prokaryotes or higher trophic level organisms; Opsahl and Benner 1997; del Giorgio and Duarte 2002) and via photodegradation (Mopper et al. 1991; Moran and Zepp 1997), or it is transformed to a small fraction of degraded organic matter. As a consequence of the persistent nature of degraded DOC a large amount of carbon is stored in the ocean, circulates with the currents and serves as a buffer in the global organic carbon cycle. The molecular signatures of sources and degradation pathways of marine dissolved organic matter (DOM) is an ongoing focus in marine chemistry research (Jiao et al. 2010) because the amount of deep-sea DOC that can be described as a molecular characterizable chemical fraction is less than 5% (Kaiser and Benner 2009). Thus, the chemical identity of the large majority of refractory DOM compounds remains enigmatic.

To assess the various sources and fluxes between different pools of DOM, radiocarbon (^{14}C) dating of bulk DOC or of fraction/compound specific isolates of DOC is commonly applied (e.g., Loh et al. 2004; Repeta and Aluwihare 2006; Walker et al. 2011). These studies revealed a size-age relationship of DOM although distinct chemical fractions also cover a wide range of ages from modern to radiocarbon-depleted and hence of ocean residence times. Full depth profiles of $DO^{14}C$ demonstrated fundamentally different processes that determine the cycling of inorganic ($DI^{14}C$) and particulate ($PO^{14}C$) radiocarbon in contrast to $DO^{14}C$ (Druffel et al. 1992; Beaupré and Aluwihare 2010). Although similar in shape, the depth profiles of $DO^{14}C$ are typically depleted by about 300‰ relative to $DI^{14}C$ throughout the water column. Furthermore, the calculated transit time from the deep North Atlantic to the deep Pacific Ocean is ≈ 1,300 a for $DI^{14}C$ while it is ≈ 2,000 a for $DO^{14}C$ (Stuiver et

al. 1983; Bauer et al. 1992). This discrepancy highlights the different mechanisms of formation, removal and transformation of the dissolved organic carbon pool compared to the dissolved inorganic carbon pool.

The only published full depth profile of DO^{14}C from the Southern Ocean indicates that surface and deep waters of the Ross Sea are relatively depleted in radiocarbon (Druffel and Bauer 2000) compared to other open ocean sites. The authors found that the deep Southern Ocean DOC deviated from the degradation line between deep Atlantic and deep Pacific DOC. Furthermore, the surface DOC Δ^{14}C values are lower by about 160‰ compared to the Sargasso Sea (Bauer et al. 1992), but could be explained by vertical mixing processes of old, radiocarbon-depleted DOC and the small surplus of freshly produced surface DOC with a recent radiocarbon signature (Druffel and Bauer 2000). Despite intense spring phytoplankton blooms during winter sea-ice retreat (Lochte et al. 1997; Arrigo et al. 2008; Geibert et al. 2010), the Southern Ocean surface DOC concentrations are among the lowest in the global ocean (Ogawa et al. 1999; Hansell 2002) and only little seasonal accumulation has been observed in the Ross Sea (Carlson et al. 1998; Carlson et al. 2000) and the Weddell Sea (Kähler et al. 1997). This has been explained by enhanced partitioning of primary production into the POC pool (Carlson et al. 1998) and an efficient heterotrophic removal of the intra-seasonal generated, semi-labile DOC (Kähler et al. 1997), despite lower bacterial growth rates compared to temperate ocean regimes (Kirchman et al. 2009).

A different approach to investigate the various DOM transformation processes involves chemical signatures (e.g., Goldberg et al. 2011; Kaiser and Benner 2012). These signatures were either derived by direct analysis of biomolecules and their known degradation products in seawater (e.g., amino acids, carbohydrates) or via experimental degradation approaches (e.g., Gruber et al. 2006; Davis et al. 2009). The spatiotemporal variability of biomolecules and net removal rates of DOC or distinct fractions (e.g., Amon and Benner 1994; Loh et al. 2004; Kaiser and Benner 2009; Hansell 2013) corroborated the concepts of age-, size- and reactivity continua in which the microbial carbon pump (Jiao et al. 2010) plays a major role in transforming fresh into refractory organic matter. However, the (re-)circulation of DOC with the global thermohaline circulation prevents a direct study of the long-term decay of substances.

The advent of Fourier transform ion cyclotron resonance mass spectrometry (FT-ICR MS) has opened a new analytical window to compounds that cannot be recognized by standard analytical techniques (Hertkorn et al. 2006; Kujawinski et al. 2009). This technique helped to identify thousands of molecular formulas of marine DOM (Koch et al. 2005; Koch et al. 2008; D'Andrilli et al. 2010b). Currently, much effort is undertaken to overcome analytical restrictions of this technique (Kido Soule et al. 2010; Sleighter et al. 2010; Tfaily et al. 2011) and refine the data evaluation algorithms (Kujawinski and Behn 2006; Koch et al. 2007; Flerus et al. 2011; Tziotis et al. 2011; Sleighter et al. 2012). A particular drawback is that usually only small sample sets were analyzed, which hinders broader generalizations and investigations of molecular features within samples from different origins.

Recently, Flerus et al. (2012) published the so far largest FT-ICR MS dataset of marine SPE-DOM comprising 137 samples from surface to depth of the East Atlantic Ocean. Here we present a dataset for the Atlantic sector of the Southern Ocean (Weddell Sea) which allows extending and refining the concepts of the DOM age model, DOM degradation state and DOM degradation continuum. We aim at testing the applicability of the age model and degradation continuum for the hydrologically complex region of the Weddell Sea where substantial upwelling and mixing of aged water masses with surface waters occur. Further, we expect to access chemical information on the different sub-fractions of the total DOM pool by FT-ICR MS derived molecular formulas and compound degradation rates which is otherwise masked by bulk values. This highly detailed view on DOM will have implications for the Weddell Sea carbon cycling because it allows identification of compounds possibly contributing to the different biogeochemical properties of Southern Ocean DOM.

VI.5.3 Materials and methods

Sampling. Water samples were collected with a rosette sampler with mounted conductivity-temperature-depth (CTD) sensors in the Atlantic sector of the Southern Ocean in December 2008 during the RV *Polarstern* cruise ANT-XXV/2. Sampling stations are shown in Figure VI.5-1. Sample depths were 2 m, 20 m, fluorescence maximum, 200 m, 2,000 m and 55 m above seafloor.

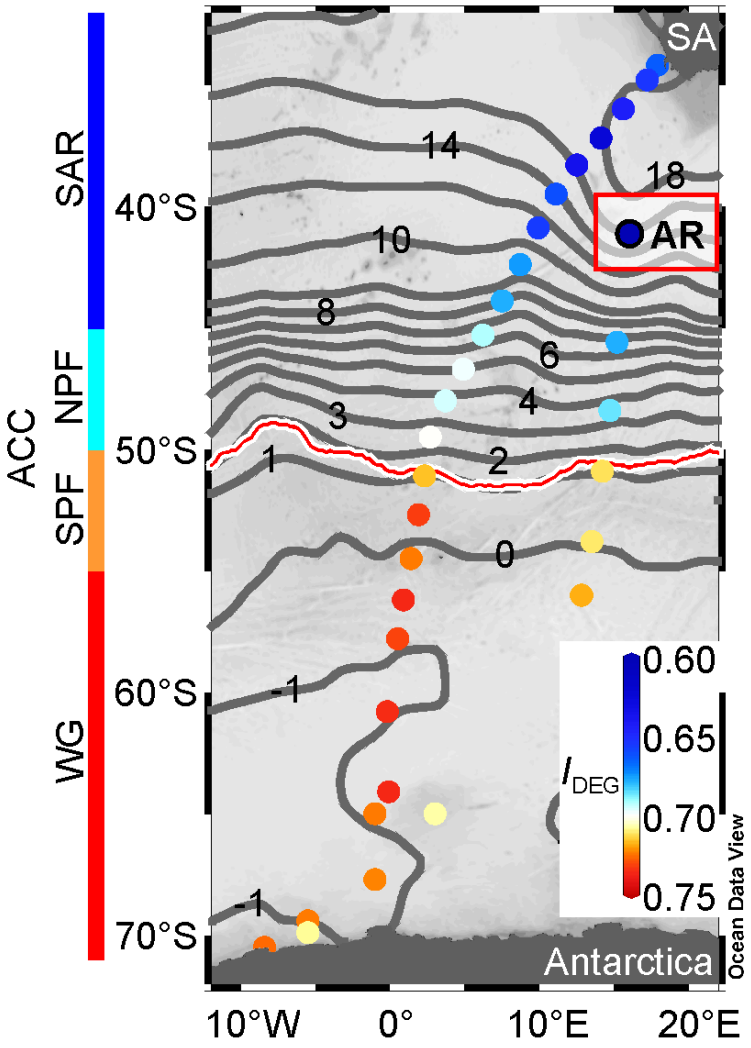

Figure VI.5-1. Sampling stations in the South-east Atlantic and Atlantic sector of the Southern Ocean.

Contour lines (grey) are the monthly means of sea surface temperature in °C (*Data from Dec, 2008,* http://www.esrl.noaa.gov/psd/). The red line indicates the approximate position of the Polar Front PF (Orsi et al. 1995). The color of the surface sample (11 m) between South Africa (SA) and Antarctica shows the DOM degradation index (I_{DEG}; Flerus et al. 2012). Left: geographical grouping of samples to SAR, NPF, SPF and WG (see text for abbreviations). The warm AR station is indicated by the red box.

Each sample was assigned by a geographical grouping ("water mass"). Samples from the Antarctic Circumpolar Current (ACC) were divided into north (NPF) and south (SPF) of the Polar Front (around 14.5° E and 50° S). Stations south of 55° S (corresponding to the southern boundary of the ACC) are defined as Weddell Gyre (WG) and were characterized by their water mass properties according to Foldvik et al. (1985) into Antarctic surface water (AASW), low salinity shelf water (LSSW), warm deep water (WDW) and Weddell Sea deep water (WSDW). Four samples were derived from the center of the warm Agulhas ring (AR). Other samples south of the African continent and north of -40° S were labeled South Atlantic Region (SAR).

All samples were filtered with GF/F filters (≈ 0.7 µm nominal pore size, Whatman). Samples for nutrient analysis were poisoned ($HgCl_2$) and stored at 4 °C (Kattner 1999). Acidified samples (pH 2 with hydrochloric acid; suprapur, Merck) for DOC determinations were stored frozen at -20 °C. Solid-phase extraction (SPE; 1 g Mega Bond Elut PPL, Varian) was performed according to Dittmar et al. (2008). The SPE samples (5 L water was extracted and eluted in 5 mL methanol; LichroSolv, Merck) were stored at -20 °C until FT-ICR MS analysis.

DOC and nutrient analysis. DOC was determined by high temperature catalytic oxidation (TOC-V_{CPN} analyzer, Shimadzu). For external calibration potassium hydrogen phthalate (KHP, Merck) was used. Aliquots of the methanol extracts (50 µL) from the SPE samples were evaporated under N_2 gas flow to complete dryness and subsequently redissolved in 6.5 mL ultrapure water for DOC analysis (SPE-DOC). All samples were acidified (0.1 M HCL suprapur, Merck) and purged with O_2 for >5 min. Performance of the instrument was recorded by daily analysis of in-lab KHP standard solutions and reference samples (deep sea reference, DSR, Hansell research lab). The average instrument blank was <1 µM C (n = 56) and repeatability of the DSR was >95% (n = 42). Nutrient samples (nitrate, nitrite, ammonium, phosphate, silicate) were analyzed using an autoanalyzer (Evolution III, Alliance instruments) with standard seawater methods (Kattner and Becker 1991).

^{14}C measurements. Subsamples of the SPE methanol extracts (0.2 mL) were quantitatively transferred to pre-combusted quartz tubes (500 °C, 6 mm diameter), the solvent evaporated under N_2 flow, and the DOM in vacuum sealed tubes combusted to CO_2 at 900 °C (with CuO/Ag; Sofer 1980). The CO_2 was subsequently reduced with H_2 to graphite over a Co catalyst (Vogel et al. 1987). Graphite targets were analyzed for ^{14}C at the Center for Accelerator Mass Spectrometry at Lawrence Livermore National Laboratory. Δ^{14}C values were reported according to the conventions of Stuiver and Polach (1977). SPE-DOC blanks did not yield any detectable amount of carbon.

FT-ICR MS measurements. Sixty SPE-DOM samples from the Southern Ocean were analyzed with a Fourier transform ion cyclotron resonance (FT-ICR)

mass spectrometer (Apex Qe, Bruker Daltonics, Billerica, MA), equipped with a 12 T refrigerated actively shielded superconducting magnet (Bruker Biospin, Wissembourg, France). An Apollo II dual electrospray source (ESI, Bruker) was used in negative ion mode (capillary voltage: -4,200 V, infusion flow rate: 2 µL min^{-1}). Prior to measurement, the extracts were diluted with methanol (LiChrosolv, Merck) to the same SPE-DOC concentrations for all samples. For one spectrum 512 scans were added in the mass range 147 – 2,000 m/z and the acquired spectra were externally calibrated with arginine cluster. To achieve an optimum in comparability of marine DOM analysis we internally recalibrated the spectra with masses that were repeatedly found in marine DOM samples (Koch et al. 2008; Flerus et al. 2011). The standard deviation of the mass error of the calibration masses was < 0.2 ppm. Samples were measured immediately following the samples from Flerus et al. (2012).

FT-ICR MS data evaluation. All ions were singly charged as confirmed by the spacing of the related $^{12}C_n$ and $^{13}C^{12}C_{n-1}$ mass peaks. The mass spectra were evaluated in the range 200 – 600 m/z according to Flerus et al. (2012). Briefly, molecular formulas were calculated from the ions m/z values with a home-build algorithm allowing for the elemental combinations $^{12}C_{0-50}{}^{13}C_{0-1}{}^{1}H_{0-120}{}^{14}N_{0-2}{}^{16}O_{0-35}{}^{34}S_{0-1}$ with a mass accuracy $|\Delta m| \leq 0.5$ ppm. The "nitrogen-rule" and elemental ratios O/C ≤ 1, N/C ≤ 1, H ≤ 2C+2+N (Koch et al. 2005; Koch et al. 2007) were applied to all molecular formulas and ambiguously assigned mass peaks were checked with the "chemical building block" approach (Koch et al. 2007). Due to the high degree of spectral similarity between samples (52% of mass peaks were present in at least 75% of all samples) detailed data evaluation was based on normalized magnitudes. The normalized magnitude values were calculated as mass peak magnitude divided by the summed magnitude of all mass peaks in a respective spectrum and expressed as percent. Furthermore, only mass peaks having a normalized magnitude ≥ 0.01% were considered for the evaluation, accounting on average for 96.1 ± 0.8% of the total intensity. This approach resulted in 1,391 ± 47 assigned mass peaks with only 1 ± 2 doubly assigned mass peaks for each of the 60 spectra from the Southern Ocean. The summed intensity of the double assigned mass peaks is equivalent to 0.002 ± 0.003% of the total intensity, therefore introducing only negligible effects on the average elemental ratios. For ease of reading, we refer to m/z only as "molecular mass" and to mass peak only as "peak".

The assigned molecular formulas can comprise an immense structural diversity (Hertkorn et al. 2008), making it impossible to designate chemical reactions as transformation pathways between molecular formulas. In this article, we refer to a calculated molecular formula as “compound”.

Intensity weighted average (wa) molecular masses and elemental ratios were calculated from the normalized peak magnitudes. Double bond equivalents (DBE, representing the sum of π-bonds and rings in a neutral molecule) were calculated according to the following equation: DBE = 1 + ½(2C – H + N) where C, H and N is the number of carbon, hydrogen and nitrogen atoms in a molecular formula.

Age model and degradation continuum concept. A representative subset of FT-ICR MS peaks from 24 samples from the East Atlantic Ocean (Flerus et al. 2012) was used to model the age of bulk SPE-DOM. Peak magnitudes which showed a significantly positive (POS) or negative (NEG) correlation with measured $\Delta^{14}C$ values ($\Delta^{14}C_{meas}$) were subsumed and implemented in a calibration function. This function was applied to the total FT-ICR MS data set, resulting in calculated $\Delta^{14}C$ values ($\Delta^{14}C_{calc}$) for 137 East Atlantic Ocean samples.

To assure statistical robustness of the SPE-DOM age model for the Southern Ocean (AM^{SO}) in this study, only those peaks were considered that appeared in all 10 Southern Ocean samples for which a $\Delta^{14}C$ value was determined. Further, a significant Pearson’s coefficient of correlation (r) between normalized peak magnitude and $\Delta^{14}C$ value was required ($|r| > 0.65$; $p < 0.05$) to include a peak in the calibration. For the subsequently applied combined age model (AM^{EA+SO}, based on a total of 34 $\Delta^{14}C$ measurements), we only considered peaks which were present in ≥ 25 samples showing a highly significant correlation with $\Delta^{14}C$ ($|r| \geq 0.5$; $p < 0.01$).

For the concept of a continuous degradation of DOM Flerus et al. (2012) used the intrinsic molecular signatures of 137 SPE-DOM samples from the East Atlantic Ocean analyzed with FT-ICR MS. Each peak from their set of samples for which an elemental composition could be determined (2,850 distinct molecular formulas) was analyzed for a statistic significant correlation with the age of the bulk SPE-DOM sample. The relative peak magnitude distribution within a sample represents the intrinsic degradation state of the respective sample. The degradation

state can be approximated with the degradation index (I_{DEG}) comprised of a small subset of compounds present in all samples: $I_{DEG} = \sum NEG_{IDEG}/\sum(NEG_{IDEG}+POS_{IDEG})$. Here, summed raw peak magnitudes of a quintuple of POS and NEG compounds are used. I_{DEG} provides an easy to use indicator of the overall biochemical boundary condition, from which the samples were derived. Higher I_{DEG} values generally correspond to a higher degree of degradation (Flerus et al. 2012). In this study, young and old DOM samples were defined by calculated radiocarbon ages of < 2,500 a and > 5,000 a, respectively.

Statistical analysis. For multivariate statistical analyses (Software "R"; 2012) we used principal component analysis (PCA; Pearson 1901) based on natural log transformed normalized magnitudes (to emphasize peaks with low magnitudes). Comparison of two sample means was performed with a Student's t-test and for more than two samples with a Tukey's honest significance difference test. If the sample distribution was not normally distributed (tested with the Kruskal-Wallis test), a Mann Whitney *U*-test (two independent samples) or Wilcoxon *T*-test (paired samples) was performed. Comparison of regression model subsets was performed with an *F*-test to account for different degrees of freedom. The Null hypothesis was rejected if the test's p-value was below the significance level $\alpha = 0.05$, unless otherwise stated.

VI.5.4 Results

Physico-chemical parameters and SPE-DOM $\Delta^{14}C$. In the top 100 m of the Weddell Sea, DOC concentrations ([DOC]) were in a small range of 46.3 ± 3.3 µM and not significantly different from the deep water DOC concentrations (> 100 m: 44.2 ± 4.0 µM). Local surface maxima of [DOC] were observed in the ACC zone between about 45 and 55° S (max: 67 µM). North of the Polar Front, increased sub-surface (20 – 100 m) DOC concentrations were found (54.9 ± 5.0 µM) in contrast to the SPF stations (45.4 ± 2.0 µM). Nutrient data and a section plot with temperature profiles and [DOC] distribution in the upper 500 m of the WG/ACC are presented in Table S1 and Figure S1 in the supporting information.[49] All SPE samples from the Southern Ocean (i.e., south of 45° S) revealed $\Delta^{14}C$ values in the

[49] The supporting information to this manuscript can be found as part of the addendum to this thesis.

range -408 to -490‰ (Table VI.5-1). These values reflect an average age of the SPE-DOM of ≈ 4,200 to 5,400 a.

Table VI.5-1. Radiocarbon values ($\Delta^{14}C_{meas}$ ± SD) and ages of Southern Ocean bulk SPE-DOM samples. $\Delta^{14}C_{calc}$ ± SEM values calculated from the combined age model **c** (AM^{EA+SO}). $\Delta^{14}C_{dev}$ is the relative difference between $\Delta^{14}C_{calc}$ and $\Delta^{14}C_{meas}$.

Latitude [°S]	Longitude [°E]	Depth [m]	water mass	$\Delta^{14}C_{meas}$ [‰]	Radiocarbon age BP [a]	$\Delta^{14}C_{calc}$ [‰]	$\Delta^{14}C_{dev}$ [%]
70.5	-8.4	20	AASW	-458 ± 12	4,850 ± 180	-468 ± 15	2.3
69.9	-5.5	800	WDW	-476 ± 9	5,130 ± 130	-477 ± 15	0.2
67.7	-1.0	4,500	WSDW	-455 ± 9	4,820 ± 130	-475 ± 15	4.3
67.7	-1.0	200	WDW	-440 ± 8	4,600 ± 110	-477 ± 15	8.5
65.0	-1.0	200	WDW	-443 ± 11	4,640 ± 150	-480 ± 15	8.3
56.0	12.8	200	WDW	-495 ± 15	5,420 ± 240	-467 ± 14	-5.7
56.0	12.8	3	AASW	-425 ± 15	4,390 ± 210	-441 ± 13	3.6
53.8	13.5	3	SPF	-453 ± 10	4,790 ± 150	-439 ± 13	-3.1
50.9	14.2	200	NPF	-432 ± 9	4,480 ± 130	-455 ± 14	5.3
48.4	14.7	200	NPF	-413 ± 10	4,210 ± 140	-419 ± 13	1.5

FT-ICR MS results from the Southern Ocean. A total number of 2,363 different molecular formulas were found in the 60 SPE-DOM samples, from which 678 formulas were present in all samples. On a presence/absence basis, no clear distinction between surface and deep water samples was found. Weighted average molecular mass, oxygen to carbon (wa O/C) and hydrogen to carbon (wa H/C) ratios were all confined to a very narrow range (404.7 ± 4.7 Da, 0.509 ± 0.004, 1.246 ± 0.007, respectively). No significant trend was observed for any station between the data from surface and 200 m water depth. Samples derived from NPF, SAR and AR showed higher wa H/C ratios, and the sample from the warm AR had a significantly smaller wa molecular mass (-11.5 Da, $p < 0.05$), accompanied with higher wa H/C ratios (+0.016, $p < 0.05$) compared to the samples south of 45° S. The PCA confirmed that essentially all samples from the southern Weddell Sea (including the shelf stations) had a similar molecular pattern (Figure VI.5-2). The average elemental ratios for these samples were also similar (Table S2). The first two

principal components (PC1 and PC2) explained 34.6% of the variability in the data. The scores from PC1 correlated significantly with wa molecular mass (r = 0.55), I_{DEG} (r = 0.92), age (r = 0.94) and latitude (r = -0.81) and scores from PC2 correlated with wa nitrogen to carbon ratio (N/C, r = -0.71). The absolute value of the PC2 scores correlated significantly with wa H/C (r = 0.77).

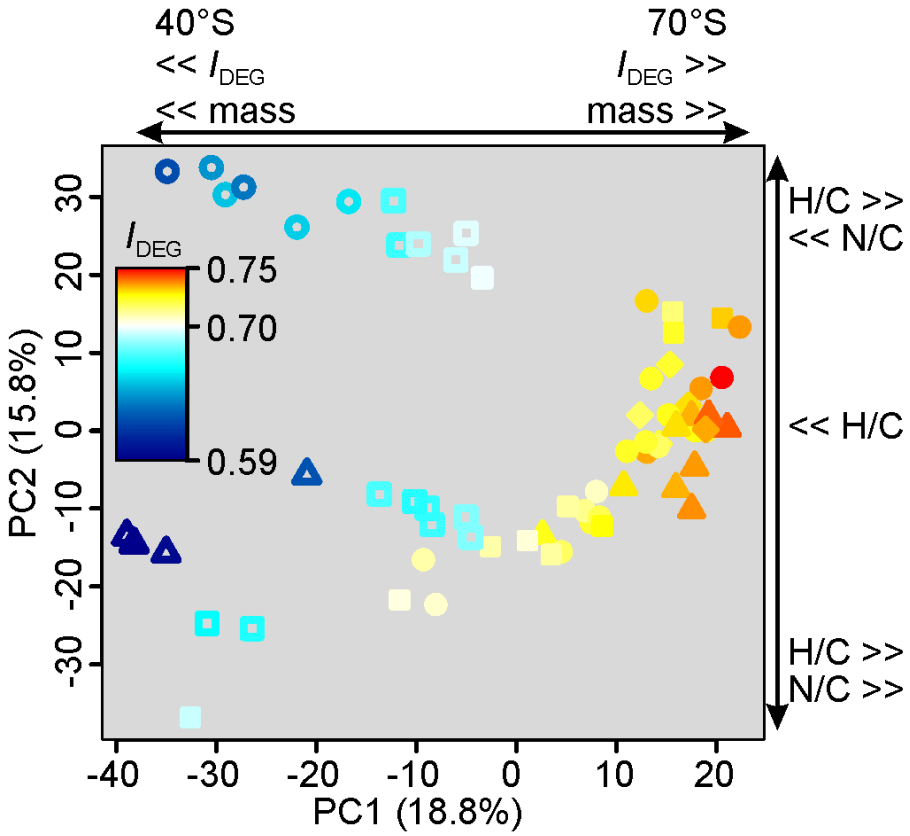

Figure VI.5-2. Principal component analysis for all Southern Ocean samples.
Number of samples (n_s = 60). PCA based on all peaks present in ≥ 25 samples. Samples north of the Polar Front (PF): open symbols (circles: SAR, triangles: AR, squares: NPF); south of the PF: filled symbols (squares: SPF, circles: AASW, diamonds: LSSW, triangles: WDW/WSDW). Colors represent the I_{DEG} value of each sample and the main correlations of FT-ICR MS parameters (H/C, N/C, molecular mass), I_{DEG} and latitude with the first principal components (PC1 and PC2) are indicated. Note the grouping of surface and deep DOM samples from the Weddell Sea.

The sharp zonal border at the Polar Front, as observed from the physico-chemical parameters was well reflected by I_{DEG} (Figure VI.5-1, Figure VI.5-2). Surface SPE-DOM samples (0 – 200 m) from the SPF had I_{DEG} values > 0.7, whereas samples from the NPF showed I_{DEG} values < 0.7. High I_{DEG} values (> 0.73) were found in the deeper waters of the Weddell Sea, which could be attributed to WDW and WSDW. In the return flow of the Weddell Gyre in the north (200 m), the highest I_{DEG} value (0.77) was calculated coinciding with the lowest measured $\Delta^{14}C$ value (-490‰). Notably, the three deep ocean samples (WSDW) had lower I_{DEG}

values than the WDW samples and the deepest sample from the Antarctic continental shelf. Also, the I_{DEG} values of the Weddell Gyre surface samples are higher than the East Atlantic Ocean values whereas they are lower at greater depth.

FT-ICR MS age model validation. We used three approaches (**a** – **c**) to construct and validate the SPE-DOM age model for the Southern Ocean samples:

a) Positive (POS) and negative (NEG) correlating peaks and $\Delta^{14}C$ values of 22 samples from the East Atlantic (EA, Flerus et al. 2012) were adopted and the calibration function applied to the new Southern Ocean data (AM^{EA}_{ext}). We used a higher peak magnitude threshold of 0.01% covering 43% of the original POS and 65% of the NEG peaks. We then compared the calculated $\Delta^{14}C$ values ($\Delta^{14}C_{calc}$) with the new set of measured Southern Ocean $\Delta^{14}C$ values ($\Delta^{14}C_{meas}$).

b) A completely new age model (resulting in a new set of 52 POS and 46 NEG peaks) for the Southern Ocean samples (AM^{SO}) was established based on 10 Southern Ocean $\Delta^{14}C_{meas}$ values from this study. All of these $\Delta^{14}C_{meas}$ values revealed a comparably higher age than the data set from the East Atlantic Ocean, thus extending the age model AM^{SO} towards older and presumably more degraded SPE-DOM samples.

c) All 34 $\Delta^{14}C_{meas}$ values were implemented to create a combined age model (comprising 187 POS and 633 NEG masses) covering the data from both the East Atlantic and the Southern Ocean (AM^{EA+SO}) and an age range from 2,000 to 5,500 a.

A detailed comparison of the different approaches is presented in Table S3 and Figure S2. In summary, all three approaches similarly reflected the trends in the $\Delta^{14}C_{meas}$ values. After inclusion of 10 additional $\Delta^{14}C$ values (**c**), 33% of the POS and 64% of the NEG masses from the original model AM^{EA} were covered in the new age model AM^{EA+SO} and span the complete range of O/C and H/C ratios found in all 60 Southern Ocean samples (Figure S3). As approach **c** also spanned the largest DOM age range and smallest relative standard errors of $\Delta^{14}C_{calc}$, we will subsequently focus on this approach. The POS and NEG peaks that were considered for the

calculation of $\Delta^{14}C_{calc}$ represent 35% of all different peaks found in the Southern Ocean samples but 64.5 ± 1.3% of the summed magnitudes.

VI.5.5 Discussion

SPE-DOM Δ^{14}C and DOC measurements in the Southern Ocean. The very low SPE-DOM Δ^{14}C surface water values in the Weddell Sea agree with previous observations in the Ross Sea (Druffel and Bauer 2000) and are considerably lower than surface DOC Δ^{14}C values from the North Central Pacific (NCP; Williams and Druffel 1987) or the Sargasso Sea (SS; Bauer et al. 1992). This can be explained by refractory DOM that is not accessible to microbes in the bathypelagic ocean. This DO^{14}C depleted DOM may be photochemically altered to become bioreactive in surface waters (Kieber et al. 1989) after upwelling with the WDW and redistribution in the Weddell Gyre (estimated residence time of Weddell Gyre surface waters: 2.5 – 3 a; Gordon and Huber 1990; Hoppema et al. 1999). This old DOM can be assimilated by bacteria (Cherrier et al. 1999) and after its release contributing to the high average DOM age of Southern Ocean surface waters.

SPE-DOM Δ^{14}C, DOC concentration and FT-ICR MS derived molecular features (wa H/C ratios, I_{DEG}) confirm independently that fresh organic matter contributed only little to the total Southern Ocean DOC concentration in austral spring. The low surface DOC concentrations agreed well with previously published DOC concentrations in the Southern Ocean, south of the PF (Kähler et al. 1997; Carlson et al. 1998; Loh and Bauer 2000; Zemmelink et al. 2008) and the wa H/C values were significantly lower compared to the East Atlantic Ocean surface DOM (-0.014, $p < 0.05$). Uniform depth distribution of [DOC] has been reported for the Southern Ocean (Wedborg et al. 1998; Wiebinga and de Baar 1998; Ogawa et al. 1999) and is consistent with constantly low wa H/C and high I_{DEG} values. The uniform wa H/C ratios are unusual for FT-ICR MS samples spanning from the surface to the deep ocean (Kujawinski et al. 2009; Flerus et al. 2012; Hertkorn et al. 2012) but have been also reported by Koch et al. (2005) for depth profiles in the southwestern Weddell Sea. Low H/C ratios and high I_{DEG} values in the deep East Atlantic Ocean compared to the surface waters have been interpreted as a signature of reworked and degraded organic matter (Flerus et al. 2012). Further indications for the

homogenous distribution of DOM in the Southern Ocean were obtained from PCA that showed similar chemical composition for the surface and deep Weddell Sea samples. We conclude that the majority of SPE accessible DOM in the Weddell Sea is of old age, biologically reworked and chemically degraded. However, during spring bloom events in the Ross Sea (Carlson et al. 2000) and Weddell Sea (Kähler et al. 1997) increased surface DOC concentrations have been observed, likely also temporally increasing the DOC $\Delta^{14}C$.

The 200 m samples showed a significant increase in measured SPE-DOM $\Delta^{14}C$ across the PF towards the north (from -495‰ to -413‰), being still lower than the 200 m SPE-DOM $\Delta^{14}C$ values reported for the East Atlantic Ocean (average: -367‰; Flerus et al. 2012). In addition to the significant increase in surface DOC concentration north of the PF (Doval et al. 2001 and this study, $p < 0.02$), the observed shift of DOM towards younger average age highlights the role of the ACC as a geo-ecological boundary (Longhurst 2007). However, especially in surface waters with high productivity, large temporal (daily and seasonal) variations in $DO^{14}C$ can occur, as observed for the eastern North Pacific (Bauer et al. 1998; Beaupré and Druffel 2009). The increase in surface DOC concentrations and decreasing average ages of the 200 m samples across the PF towards the north might be related to seasonally enhanced primary production (Geibert et al. 2010; Park et al. 2010; Korb et al. 2012) with subsequent bacterial degradation (Rosenstock et al. 2005; Dumont et al. 2011; Pearce et al. 2011) of the fresh organic matter. In the Southern Ocean, phytoplankton production is accompanied with enhanced POC export (Carlson et al. 1998; Carlson et al. 2000) compared to other ocean regimes. Furthermore, a shallow remineralization of the export production occurs in the WG and the ACC (Usbeck et al. 2002; Jacquet et al. 2011; van der Loeff et al. 2011) which is expected to result in increased subsurface DOC concentrations. However, this was not observed in our data, suggesting efficient and complete remineralization of new (dissolved) organic carbon in the WG/ACC subsurface waters.

Our SPE-DOM $\Delta^{14}C$ values for the WDW (average: -464 ± 26‰), which originates from the North Atlantic Deep water (NADW), agree with the values from the deep East Atlantic Ocean (-446 ± 7‰; Flerus et al. 2012) and are lower than in the deep Sargasso Sea (-394 ± 13‰; Beaupré and Druffel 2009). The age differences between these water masses are consistent with water mass transport

patterns in the deep East Atlantic Ocean and the different origins of deep water DOC (NADW and Antarctic Bottom Water). Assuming that the deep bulk DOC $\Delta^{14}C$ values in the Weddell Sea and the Ross Sea are similar (average: -500‰; Druffel and Bauer 2000), we can calculate the $\Delta^{14}C$ values of the SPE discriminated fraction X_{discr} (i.e., the DOM fraction not extracted with PPL) via simple isotopic mass balance. Using the average carbon extraction efficiency in the deep Weddell Sea (42 ± 6%, n_s = 7), we obtain $0.42 \times (-464‰) + 0.58 \times (X_{discr}\ \Delta^{14}C) = 1 \times (-500‰)$ and thus $X_{discr}\ \Delta^{14}C = -526‰$. This demonstrates that the SPE discriminated fraction X_{discr} is not primarily modern carbon. The difference of about 40‰ between deep Ross Sea DOC $\Delta^{14}C$ and our data can also be explained by the deep circumpolar water transit time of 85 a (Stuiver et al. 1983) and a temporal variability of (deep) $\Delta^{14}C$ values (Bauer et al. 1998).

Age model validation. The DOM age model (Flerus et al. 2012) relates the SPE-DOM $\Delta^{14}C$ values to the relative magnitudes of hundreds of peaks found in every FT-ICR MS analysis. For the selection of masses contributing to the age model only the overall coefficient of correlation is relevant, irrespective of the steepness of the slope. Moreover, the sum of hundreds of FT-ICR MS peaks used for the age model is less influenced by magnitude outliers of a few peaks, thus resulting in a more robust regression. For the same reason we did not use the DOC concentration to establish the age model as this approach is very sensitive to measurement errors. In contrast to the combined model AM^{EA+SO} (approach **c**), the AM^{SO} model (**b**) is biased towards a much higher age if applied to East Atlantic Ocean samples (not shown) and the AM^{EA} model (**a**) resulted in younger ages for the Southern Ocean samples than actually measured (Figure S2). We conclude from the age model validation steps that the inclusion of new reference ages (via discrete SPE-DOM $\Delta^{14}C$ measurements) refined the age model but did not substantially alter the general pattern and trends of model derived $\Delta^{14}C_{calc}$ values. The higher contribution of POS and NEG masses to the total summed intensity than to the total number of peaks showed that the magnitude dominating peaks are equally distributed throughout all samples and represent a consistent fraction of SPE-DOM. Thus, our modeling approach is a robust way to calibrate FT-ICR MS data with $\Delta^{14}C$ values.

Degradation rate of bulk DOC determined from SPE-DOM Δ^{14}C. As a prerequisite to apply our age model to bulk organic carbon calculations, the relation of DOC vs. SPE-DOM age was evaluated. The extraction efficiency for the complete data set was 42 ± 7% (n_s = 187 SPE-DOC measurements, see Text SI for a description of outliers), and no relation of the extraction efficiency with depth, latitude or bulk DOC concentration was observed. The best linear fit of a model II regression (geometric mean regression, GMR) of [DOC] vs. SPE-DOM age was obtained if we assume that the DOC decays and ages in an exponential manner with time, i.e., similar to a first order reaction rate. Indications, that the DOC decay/removal is not sufficiently described by a two-component linear mixing model (e.g., Keeling-regression of Δ^{14}C vs. 1/[DOC], Mortazavi and Chanton 2004) were already discussed by Beaupré and Aluwihare (2010) and Carlson et al. (2010). Ocean models accounting for DOC production and decay also consider an exponential decay of DOC fractions (Schlitzer 2007; Hansell et al. 2012). Hence, we apply equation 1 to describe the bulk DOC degradation:

$\ln([DOC]) = b + m \times t$ and with with $\exp(b) = a^0_{DOC}$ and $m = -k_{DOC}$:

$$[DOC] = a^0_{DOC} \times \exp(-k_{DOC} \times t) \quad (1)$$

where [DOC] is the concentration of bulk DOC, t_s represents the bulk SPE-DOM conventional radiocarbon age, a^0_{DOC} is the intercept of the GMR regression and equivalent to [DOC] at time t_s = 0 a, and k_{DOC} is the reaction/degradation rate.

GMR regression of all $\Delta^{14}C_{calc}$ (n_s = 187) values from the age model AM^{EA+SO} and the respective bulk DOC concentrations enables to determine an integrated bulk DOC degradation rate (Figure VI.5-3). Here we use conventional radiocarbon ages of SPE-DOM samples to obtain a DOC degradation rate, which is different from other approaches applying observed net losses of total [DOC] correlating with water mass tracers, mixing models of [DOC] or inverse modeling to derive decay rates (e.g., Hansell et al. 2009; Carlson et al. 2010; Hansell et al. 2012). The approach defines a lower limit for the decay rate as it includes decay of ^{14}C and preferential loss of young compounds. Further, our model can only resolve long-term DOC degradation rates that are limited by the accuracy of the Δ^{14}C measurements (≈ 200 a) and thus excludes the most labile fractions. However, considering only the DOM components

with low turnover rates (the “refractory” DOM; Hansell et al. 2012) our calculation still accounts for 72% of the global ocean DOC inventory (Hansell et al. 2009).

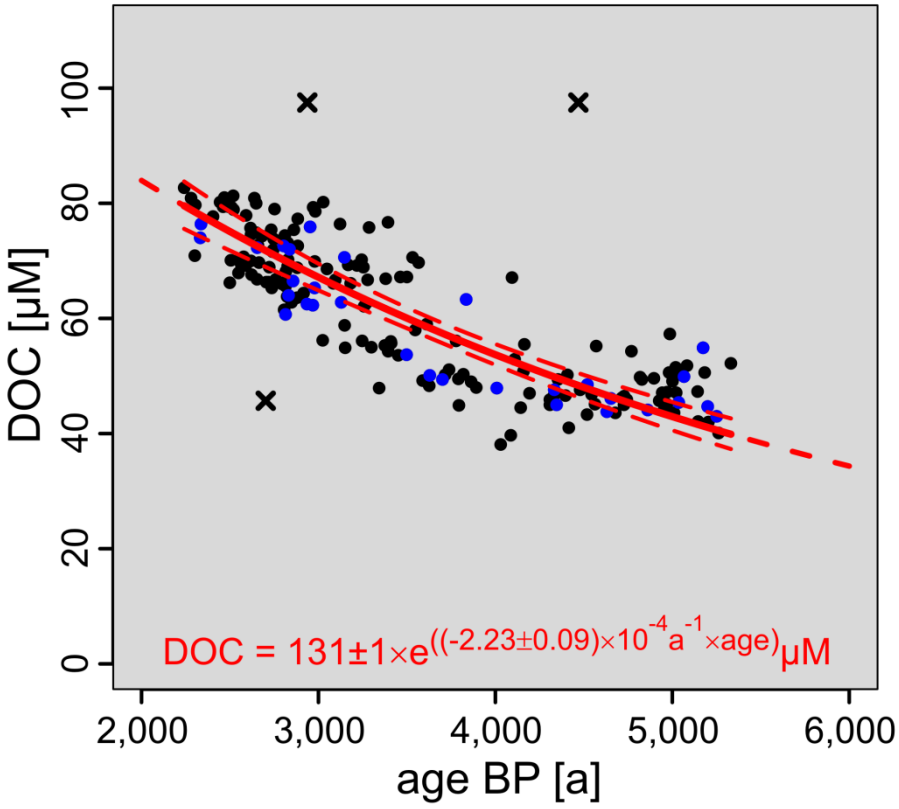

Figure VI.5-3. Bulk DOC concentration vs. calculated age of the SPE-DOM.
Number of samples n_s = 187, GMR regression, blue = $\Delta^{14}C_{meas}$ data. [DOC]-SD (mean: 5%) and $\Delta^{14}C_{calc}$-SEM (mean: 60 a) not shown for clarity. Data points marked with an ‘x’ were treated as outliers. Red curve: fitted exponential DOC degradation including confidence intervals.

The calculated degradation rate was extrapolated to the average deep North Central Pacific (NCP) DOC concentration (34 µM) resulting in a predicted DOC age of 6,410 ± 290 a (NCP SPE-DOM $\Delta^{14}C_{pred}$ = -553 ± 16‰). Comparing this estimate of NCP $\Delta^{14}C_{pred}$ with the analogous estimate using only the 34 $\Delta^{14}C_{meas}$ values resulted in a similar NCP SPE-DOM $\Delta^{14}C_{pred}$ of -549 ± 37‰ (Table S4). A complete remineralization of the bulk DOC was assumed at a threshold concentration < 1 µM, and the extrapolation of the DOC degradation rate to this concentration yields a DOC residence time (t_{DOC}) of 24,400 ± 1,100 a ($\Delta^{14}C_{pred}$ = -953 ± 7‰). This approach assumes that the observed degradation of DOC between apparent ages of 2,000 and 5,500 a can be extrapolated i.e., the mechanisms responsible for DOM transformation are in a steady state. Our “degradation rate” k_{DOC} is different from the “removal rate” by Hansell et al. (2012) who used inorganic radiocarbon as quasi-conservative tracer of water mass circulation and hence, time since surface export.

We use the intrinsic mean age of DOM and predict the age of DOM after degradation of the youngest fractions. This degradation occurs concurrently to water mass transport, i.e., decay of radiocarbon. Due to the lack of an independent age tracer the degradation observed from $DO^{14}C$ is a superposition of multiple mechanisms. However, if we assume that the global mechanisms for refractory DOM degradation are similar our approach enables to study samples from different origins and with different ages. Comparing the 16,000 a lifetime of the refractory DOC fraction from Hansell et al. (2012) with our predicted DOC residence time (≈ 24,000 a) sets a lower and upper limit for the bulk DOC degradation.

The DOM degradation continuum. Basically all chemically identifiable, naturally occurring compounds decrease with depth (age of water mass) and the proportion of chemically identifiable compounds in DOM decreases faster than bulk [DOC] (Kaiser and Benner 2009). Hence, we assume that all compounds detected by FT-ICR MS in SPE-DOM samples also decrease with age (Flerus et al. 2012). The consequence of the degradation continuum concept is that every sample has a distinct age and is characterized by a distribution of compounds with very different degradation rates. Applying this approach, semi-quantitative degradation rates for each FT-ICR MS identified compound can be calculated. As a first approximation, we assume that the relative decrease of each peak is linear proportional to the decrease in total DOC concentration which in turn follows a first order (exponential) degradation. Therefore, equation 2 is suitable to approximate the decrease of each peak.

$\ln(M_i \times [DOC]_s) = b_i + m_i \times t_s$, with $\exp(b_i) = a_i^0$ and $m_i = -k_i$:

$$M_i \times [DOC]_s = a_i^0 \times \exp(-k_i \times t_s) \quad (2)$$

where M_i is the normalized peak magnitude of the compound ‘i’ in sample ‘s’, $[DOC]_s$ is the DOC concentration in the original sample, a_i^0 is equivalent to the product of $M_i \times [DOC]_s$ at $t_s = 0$ a, and k_i is the apparent reaction/degradation rate constant for the compound ‘i’. The factor $M_i \times [DOC]_s$ is a semi-quantitative measure and can be referred to as “DOC normalized relative peak magnitude”. We only considered peaks detected in ≥ 25 samples, where the Pearson’s correlation coefficient is highly significant (n = 1,557, $p \leq 10^{-4}$), covering on average 84 ± 1% of

the total magnitude and 1,326 ± 82 peaks of each sample. The highest degradation rate is constrained by the age difference between the youngest 25 samples (≈ 400 a), thus compounds which are fully degraded prior this limit cannot be observed.

Due to the spectrum normalization procedure, only changes in peak intensity relative to the total spectrum intensity can be described, i.e., each peak is considered independently. The bulk DOC degrades with a known rate (k_{DOC}) and consequently the degradation of each peak can be viewed as relative to the bulk DOC degradation (k_i/k_{DOC}, Figure VI.5-4). The rates k_i are independent of the mean peak magnitudes and the highest rate k_i for an individual DOM compound was more than seven times the degradation rate of bulk DOC, while the lowest rate was only ≈ 30%. From the intercept a_i^0 and the decay rate k_i, we can calculate the theoretical time after which a single peak would be fully degraded ($M_i \times [DOC]_s < 0.01$ [% μM]), assuming that the observed degradation is in steady state. Due to the assumed linear relation between [DOC] and M_i and isotopic mass balance constraints we observe compounds with calculated residence times (t_R) longer than the residence time for bulk DOC (t_{DOC}). Our approach thus yields calculated t_R for a substantial subset of all compounds ranging from ≈ 6 – 117 ka (Figure VI.5-5), considering that it excludes by definition labile and semi-labile substances and the degradation rates are constrained by the rate k_{DOC}. The mean rate $\langle k_i \rangle = 2.64 \times 10^{-4}$ a^{-1} and residence time $\langle t_R \rangle$ = 28,800 a of all peaks were slightly higher than the values observed from the bulk DOC degradation, indicating that the high magnitude peaks may be overrepresented in the FT-ICR mass spectra.

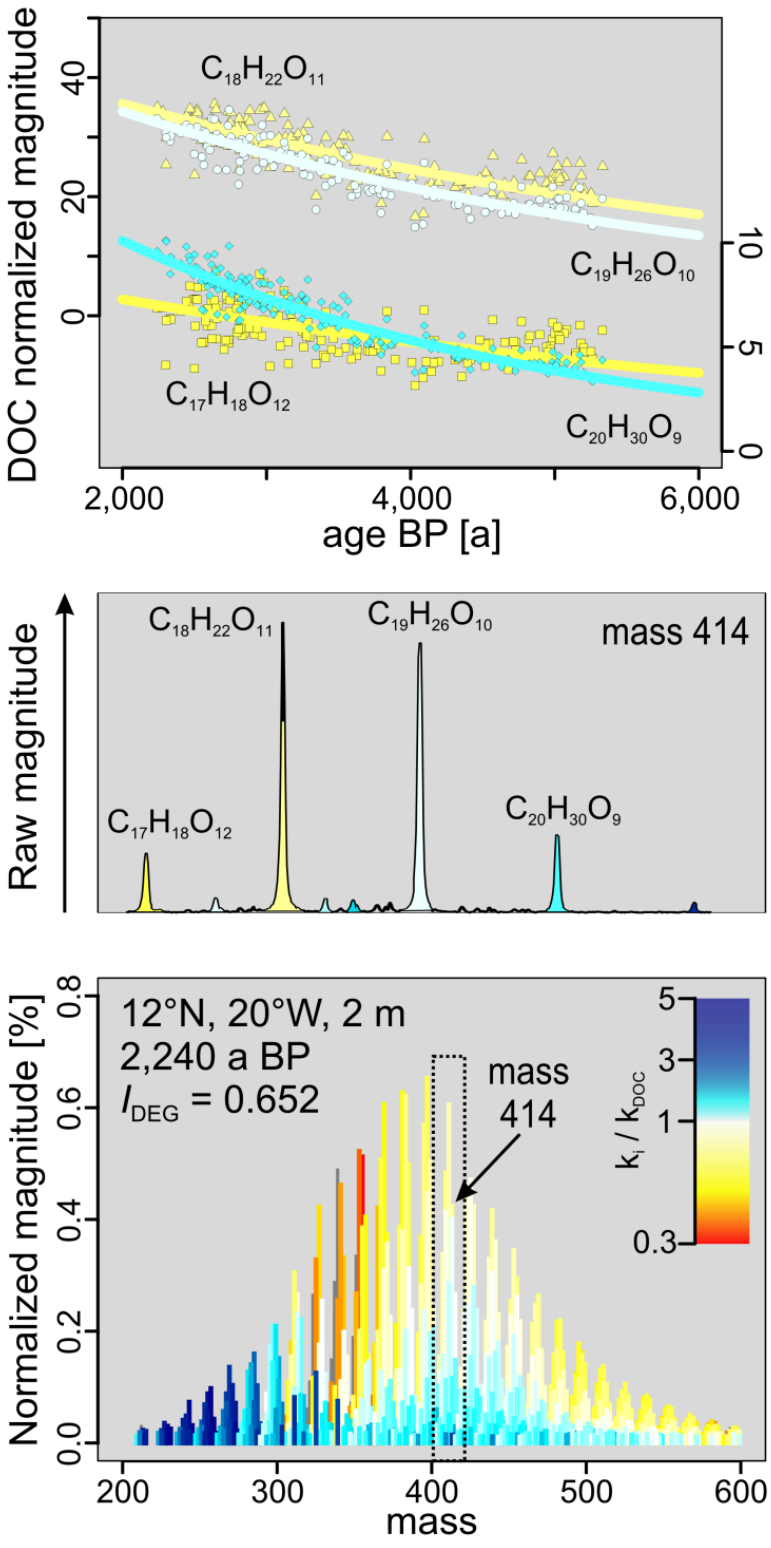

Figure VI.5-4. The degradation continuum of a young sample.
Top: examples of different slopes of the exponential regression of peaks at the molecular mass 414. Middle: the degradation rate (k_i) distribution of the four compounds at nominal mass 414 as present in a young surface sample. Bottom: The full FT-ICR MS spectrum with the typical peak magnitude distribution observed from negative mode ESI-FT-ICR MS analysis of marine DOM (Koch et al. 2005; D'Andrilli et al. 2010b; Gonsior et al. 2011). The colors refer to the ratio k_i/k_{DOC} and peaks without assigned k_i are shown in dark gray.

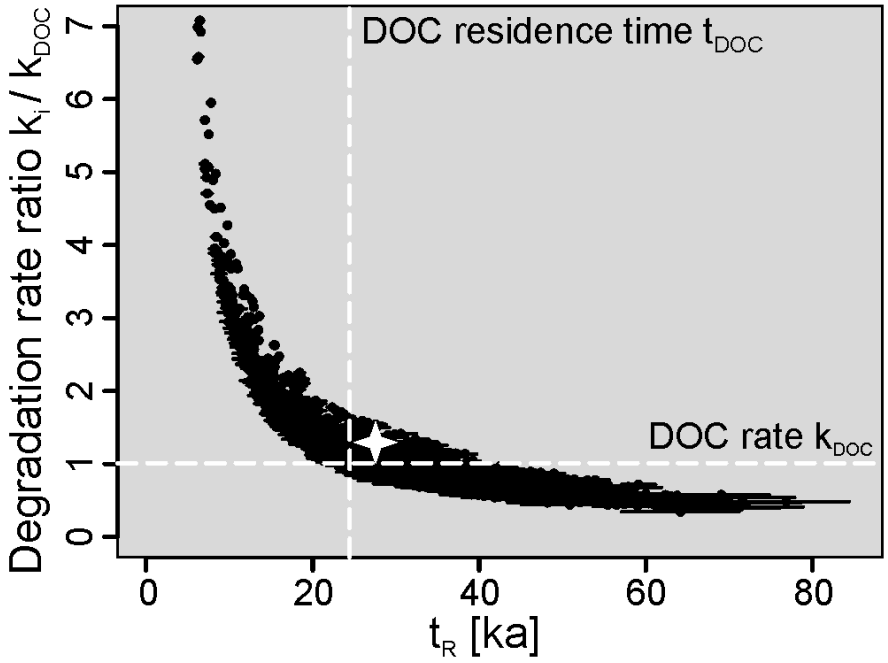

Figure VI.5-5. The degradation continuum.
Normalized degradation rates k_i/k_{DOC} vs. calculated residence time (t_R) for all peaks correlating highly significantly with age (n = 1,557). SEM error bars for t_R are ~5%. Peaks with a ratio $k_i/k_{DOC} > 1$ degrade faster than bulk DOC (n = 686) and peaks with $t_R > 3 \times t_{DOC}$ were excluded from the plot (n = 6). The white star indicates the mean peak degradation rate $\langle k_i \rangle$ and residence time $\langle t_R \rangle$ of all peaks.

Similar to rate calculations from bulk DOC, we only obtain net rates of degradation. Uncertainties in the rate calculation using masses and molecular formulas derive from possible structural isomers with individual degradation rates and molecular transformations within DOM that shift compounds along the molecular mass scale (and also along the H/C, O/C, etc. scale). Also, net rates do not account for different pathways of degradation, such as respiration in the mesopelagial and sorption/aggregation in the bathypelagial, leading to a potential superposition of two or more different degradation rates for a single peak.

We cannot finally decide on the fate of the total DOC pool nor single compounds since the oldest bulk DOC has been dated to ≈ 6,200 a (Williams and Druffel 1987). Druffel et al. (1992) calculated that 80% of the deep ocean DOC is recycled within every deep ocean mixing cycle, allowing for very long residence times of individual compounds. The presence of much older DOM fractions, such as lipid-like components (≈ -880‰; Loh et al. 2004) or black carbon (-918‰; Ziolkowski and Druffel 2010) imply much longer residence times for these components than the apparent mean age of the bulk DOC and already suggest a broad continuum of residence times and degradation rates.

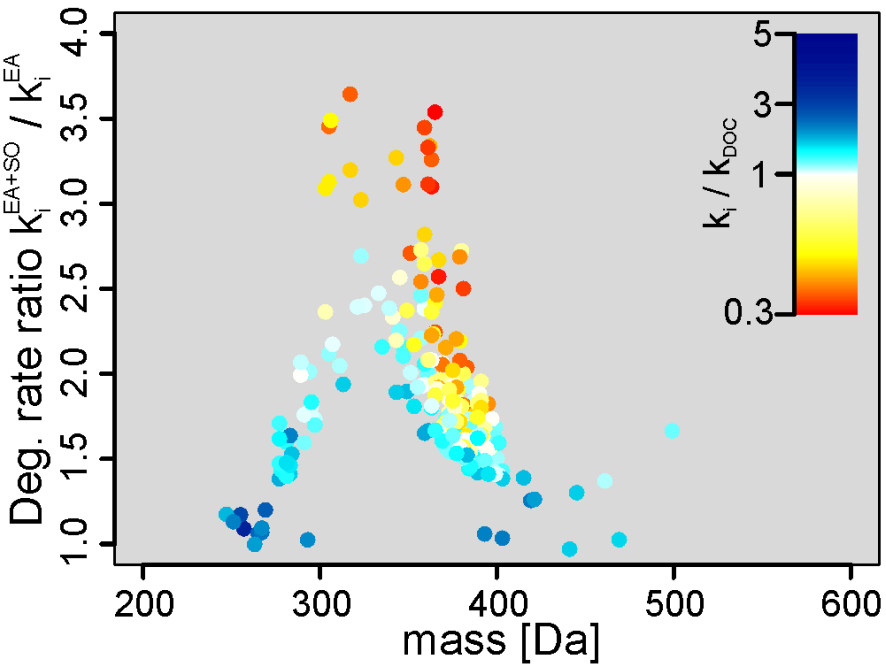

Figure VI.5-6. The SOUR compounds.
Enriched compounds in the Southern Ocean (SO) compared to the East Atlantic (EA). The ratio of the degradation rates k_i of both regressions modes (samples 'EA+SO' and 'EA only') indicates a most pronounced k_i deviation around molecular mass 300 – 370 Da (n = 225). The color refers to the calculated ratio k_i/k_{DOC} of the regression for all samples.

Is there too much DOC in the Southern Ocean? To account for the bio-ecological boundary of the ACC as observed from the bulk DOC age and [DOC], we compared the regression of $\ln(M_i \times [DOC]_s)$ vs. t_s for the complete dataset (n_s = 185, 'EA+SO') with just the sample set north of 45° S (n_s = 138, 'EA only'). Three hundred thirty-nine peaks were identified that significantly deviated from the regression line constructed for all samples (n = 225, $\alpha = 10^{-4}$) or correlated only with the samples north of 45° S (n = 114), representing 20% of all peaks for which a residence time was assigned. About half of the 225 peaks had low rates k_i/k_{DOC} (< 1). Removing the Southern Ocean samples from these 225 peaks, k_i increased and t_R decreased by as much as a factor of 3.5 for these compounds (Figure VI.5-6). Those peaks are referred to as Southern Ocean ultra refractory (SOUR) compounds and the summed normalized magnitude of all SOUR peaks was 31.7 ± 1.1% in the Southern Ocean samples. SOUR compounds were characterized by a lower mean molecular mass (360 ± 51 Da) compared other compounds (Figure VI.5-6, Table S5) but were not significantly different in elemental ratios. Using the mean age of all Southern Ocean samples, we calculated that about 5% of the total magnitude of the Southern Ocean samples was attributed to the increase in "DOC normalized relative peak magnitude"

of the SOUR peaks. We conclude that those peaks represent a degraded fraction of DOM and possibly contribute to additional DOC present in the Southern Ocean.

Our result is supported by Druffel and Bauer (2000) who found that radiocarbon measurements of deep Southern Ocean DOC from the Ross Sea deviates from the degradation line between deep Atlantic and deep Pacific in a DOC $\Delta^{14}C$ vs. [DOC] plot. Although the authors assumed a constant rate of degradation between the Sargasso Sea and the NCP they suggested that either the deep Southern Ocean DOC concentration was too high and/or the DOC $\Delta^{14}C$ values were too low. Accessing hundreds of peaks with FT-ICR MS enabled to identify possible compounds that eventually contribute to an “increased” DOC concentration in the Southern Ocean. Any deviation of the measured DOC concentration from the DOC degradation curve leads to a proportional deviation of the DOC normalized peak magnitudes but only the SOUR compounds reflected this deviation.

The statement that there is “additional” or “increased” DOC in the Southern Oceans seems a paradox, considering the very low surface and deep sea DOC concentration in Antarctic waters. The PCA (Figure VI.5-2) and I_{DEG} showed that the molecular characteristics of surface and deep Weddell Sea SPE-DOM are comparable suggesting only little contribution from recently produced DOM. Upwelling of large volumes of ^{14}C depleted deep waters with the WDW in the Weddell Gyre could favor assimilation and reworking of already old carbon (Cherrier et al. 1999). Together with the low annual primary production and substantial reworking of the fresh biomass (Kähler et al. 1997; Carlson et al. 1998), this mechanism could increase the DOC concentration but maintain the apparently old age. During repeated cycling within the ACC prior to export with deep/bottom water, accumulation of these substances can lead to the observed increase of the DOC normalized peak magnitude. Other sources (hydrothermal vents: Lang et al. 2006; Pohlman et al. 2011; chemoautotrophy: McCarthy et al. 2011; Middelburg 2011; black carbon: Dittmar and Koch 2006), and advection processes (transport from marginal sediments: Bauer and Druffel 1998; deep water formation: Hansell et al. 2002) may substantially increase the deep ocean concentration of some compounds and enter the Weddell Sea surface with entraining WDW. We cannot finally decide if the SOUR peaks are a result of an accumulation of compounds with mean age or the addition of older components from external sources because both mechanisms would

lead to the observed peak magnitude pattern. Our ongoing research focuses to explain the lower mean molecular mass of the SOUR peaks and a comparison of these findings with the Ross Sea.

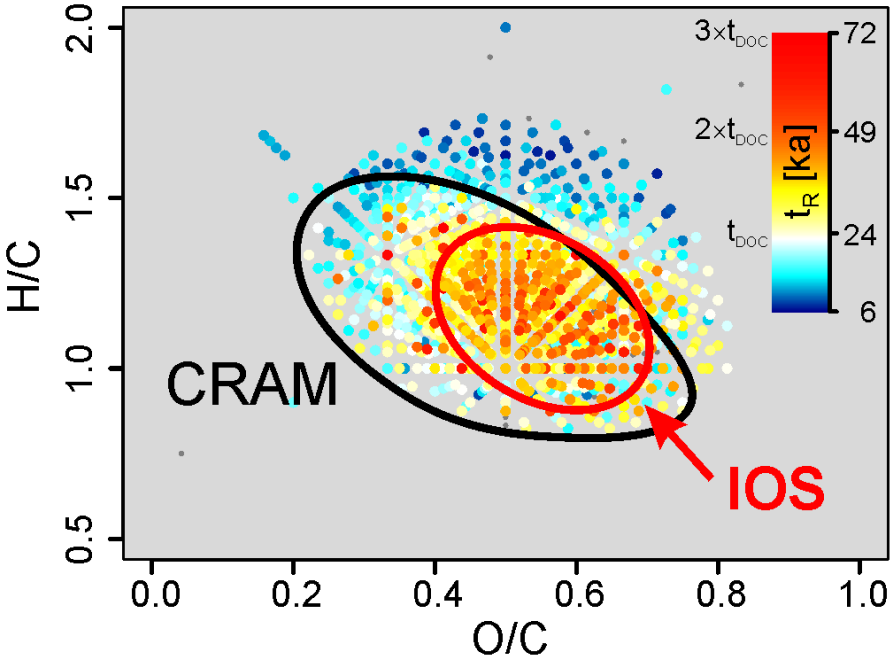

Figure VI.5-7. The island of stability (IOS).
Molecular formulas (n = 1,557) plotted according to their elemental ratios and residence times (t_R), where yellow and red compounds have the highest t_R. Compounds with no assigned t_R are displayed in dark gray. The approximate perimeter of CRAM-like compounds in our dataset is shown (black ellipse: DBE/C = 0.30–0.68; DBE/H = 0.20–0.95; DBE/O = 0.77–1.75, Hertkorn et al. 2006).

Chemical information on the most persistent DOM: the "island of stability". The assignment of molecular formulas to FT-ICR MS peaks allows deducing chemical information for the refractory DOM compounds and evaluating the trends for average elemental ratios and molecular mass with increasing residence time t_R of the compounds (Figure S4). Assuming that compounds with an assigned residence time are removed from the DOM pool at the time t_R, the average molecular H/C ratio decreases with DOM ageing, while the average O/C ratio increases, indicative of less saturated, higher oxygenated compounds. Only little changes in the H/C and O/C ratio, the DBE-O value and the mass of the "removed" compounds occur after $t_R \approx 25$ ka. This indicates that compounds with very long residence times are chemically invariant to further degradation process. This age limit coincides with the calculated residence time t_{DOC} for bulk DOC. The compounds with the longest residence times were confined to a narrow range of O/C and H/C ratios in the central area of the typical distribution of marine DOM (Figure VI.5-7). The elemental ratios

covered by compounds with $t_R > 1.5 \times t_{DOC}$ have a substantial overlap with the carboxyl-rich alicyclic molecules (CRAM), a major refractory component in marine DOM (Hertkorn et al.).

According to our results, we propose an “island of stability” (IOS), that is a set of compounds with H/C (1.17 ± 0.13), O/C (0.52 ± 0.10) and molecular mass (360 ± 28 and 497 ± 51 Da) ranges that comprise the most stable and likely also the most diverse combination of elements in marine DOM on very long timescales (longer than ≈ 2 times the mean residence time of DOC). Any molecule, once it enters the DOM pool, is biologically and/or (photo-)chemically modified until it is either fully remineralized or ends up in the IOS where it is subject to a much slower further degradation. A possible mechanism, modifying compounds towards the IOS can be radiolytic processes that do not substantially remineralize DOM but can alter the chemical composition of compounds towards higher oxygenation and lower saturation (Koch et al. 2012). Also, selective cleavage of side groups by exo-acting enzymes (Arnosti 2011) may reduce the subsequent reactivity of the products. Further, there is growing evidence, that part of the marine DOM is composed of old black carbon (Ziolkowski and Druffel 2010) with sources in the deep sea or from land-derived pyrogenic carbon (Dittmar and Koch 2006). Especially highly condensed compounds are photolabile and thought to degrade when exposed to UV-radiation at the surface ocean (Stubbins et al. 2012). The low contribution of nitrogen and sulfur to the IOS compounds (only 19% of the IOS compounds contain N compared to 31% for all peaks, and no S is present in any IOS compound) further suggests that these compounds are of lower nutritive value for heterotrophs.

The underlying mechanism that prevents or at least hinders further degradation of the IOS compounds is unclear. Kattner et al. (2011) hypothesized that the concentration of individual deep-sea refractory compounds are lower than the chemoreceptive threshold of prokaryotes or that at least the energetic yields from already highly oxygenated compounds are too low. However, the lowest calculated rates k_i are so low, that abiotic removal mechanisms seem likely to determine the ultimate fate of these compounds. Adsorption to particles and subsequent removal from the water column (Druffel and Williams 1990), pyrogenic transformation through hydrothermal systems (Lang et al. 2006) or diapycnal mixing into surface waters may be the rate determining steps for the decay of this persistent DOM fraction.

VI.5.6 Conclusions

Based on SPE-DOM, the concept of a DOM degradation continuum was confirmed, refined and extended covering now two major global oceans. The mean age of the SPE-DOM is reflected in the intrinsic molecular patterns and resulted in calculated radiocarbon ages which were in very good agreement with previous studies using bulk DOC data. The calculated mean degradation rate and residence time for this representative fraction of DOM agree well with the conceptual definition of refractory DOM obtained from experimental data and modelling studies. We assume that our approach is applicable to other oceans worldwide providing new information on the role of DOC in the marine carbon cycle. From a holistic perspective our data indicate that addition of freshly produced DOM to the background refractory DOM does not substantially influence the subsequent degradation mechanisms of this mixed pool of organic matter despite different geo-ecological boundary conditions (e.g., phytoplankton and microbial community structure, climate regime) and support the conceptual framework of the microbial carbon pump.

In contrast to bulk DOC and $\Delta^{14}C$ measurements, DOM degradation can now be studied on the molecular level allowing differentiating between compounds and compound classes of different lability and residence time. Radiocarbon dating and molecular information derived by FT-ICR MS provided molecular residence times much longer (> 24 ka) than any other residence time which has been proposed for an organic molecule in the ocean. The long residence times have implications for the distribution of refractory DOC in the water column and consequently for the global amount of the most refractory DOC fraction. We propose that the DOM degradation continuum provides an important enhancement for biogeochemical models using DOC as it sets chemical constraints on the degradability of DOM in the pelagic and deep ocean.

In the Southern Ocean, we identified a discrete group of compounds having an increased abundance. These findings are in agreement with results from Druffel and Bauer (2000) but contrast with the standard paradigm of radiocarbon age and DOC concentration relationship in the deep ocean and contemporary concepts of marine DOC cycling. These compounds are potentially indicative of an enhanced capability of the Southern Ocean to sequester organic carbon as refractory DOM and

thus long-term carbon storage. The underlying source and formation mechanism remain to be revealed and are likely related to the specific oceanographic conditions in the Weddell Sea. Studying the details of this surplus of old DOC will contribute substantially to an improved understanding of the marine DOC cycle.

Acknowledgements

The authors gratefully acknowledge the master and crew of the research vessel *Polarstern*, the chief scientist Olaf Boebel for professional assistance during sample collection and Lindsey Koren for radiocarbon sample preparation. We thank Stephan Frickenhaus, Mario Hoppema, and Michiel Rutgers van der Loeff for their helpful discussions. O. J. L. was funded by the German Science Foundation (DFG), grant KO 2164/8-1+2, as part of the DFG-Priority Program ‘Antarctic Research’.

VII GENERAL DISCUSSION

Here, a summarizing discussion of the previous chapters and conclusions for the objectives are presented with special focus on the methodological and biogeochemical aspects.

VII.1 Applicability of the methods

It is arguable to what extent solid-phase extraction only recovers a subfraction of the total DOM pool and discriminates e.g., versus very hydrophilic substances, elemental composition or small molecules.[50] Further, there is considerable discussion on whether the SPE recovered fraction is similar for different environmental settings (e.g., Dittmar et al. 2008; Kruger et al. 2011). However, SPE has two major advantages: First, it is a cheap and quick method that can be easily applied in the field and in the laboratory. The recovery of DOM on a carbon basis is almost as good as more laborious techniques such as ultrafiltration, reverse osmosis or electrodialysis, in addition to comparably small sample volumes (e.g., Chen et al. 2011; Tfaily et al. 2012). Second, the matrix transfer from the salty seawater to an organic solvent (usually methanol) allows easy and safe storage of the samples (e.g., Flerus et al. 2011). A desalted and water free sample is the prerequisite for the most advanced analytical techniques such as RP-HPLC, ICP-MS and FT-ICR MS.

The use of RP-HPLC as a chromatographic pre-separation of NOM still needs better physico-chemical characterization. Certainly, individual compounds of DOM cannot be resolved with chromatographic techniques (even those with much higher separation power such as gas chromatography or capillary electrophoresis). However, liquid chromatography was successfully applied to reduce the complexity of the mixture subsequently analyzed with e.g., FT-ICR MS (Koch et al. 2008;

[50] The commonly used term “representative” fraction cannot be easily applied to DOM extraction techniques as it strongly depends on the chemical or physical parameters that the extract is expected to represent.

Reemtsma et al. 2008b; Capley et al. 2010; Lechtenfeld et al. 2010). Using a predominant hydrophobic phase (e.g., Hydro-RP C18, Phenomenex) with a water – methanol gradient elution covers the full polarity range of solid-phase extracted marine DOM that was retained using an adsorber of intermediate polarity (e.g., Bond Elut PPL, Agilent) and methanol elution. The most hydrophilic and the most hydrophobic compounds are likely not retained with this approach as a simple consequence of the polarity choices.

An attempt to investigate the chemical properties of SPE-DOM was carried out within a master thesis of M. Einsporn from the University of Applied Sciences in Bremerhaven (Einsporn 2011). The aim of the thesis was to characterize the polarity of SPE-DOM with special focus on the RP-HPLC method (Koch et al. 2008). The results showed that similar to hydrophobic interaction effects in SEC (Specht and Frimmel 2000), also size effects influence the separation of DOM on a reversed phase column (Einsporn 2011; Hutta et al. 2011). A currently running master thesis work by T. Jendrossek is aimed to investigate the influence of different sample volumes and salt contents on the extraction efficiency and optical and chemical discrimination using various SPE sorbents.

Both high resolution mass spectrometric techniques that were used throughout this work encompass fundamentally different aspects: ICP-MS is a well established technique that provides quantitative results for the concentration or isotope ratios of elements. However, it relies strongly on the knowledge of the species, in which the element was bound, or it will just yield bulk values. Moreover, the use of a reversed-phase chromatographic technique to satisfactory separate organic fractions prior ICP-MS detection in DOM is largely hindered due to the need for organic solvents and is still in the early development stages (see reviews by e.g., Heumann 2004; Lobinski et al. 2006; Todoli and Mermet 2006; Profrock and Prange 2012). Apart from few speciation examples (e.g., Wu et al. 2004; Iwahata et al. 2008; Stolpe et al. 2010), the technique is new to the DOM community and needs to prove its eligibility.

Chapter VI.1 demonstrated that RP-HPLC-ICP-MS indeed is a promising approach to elucidate the full chemical composition of DOM as it combines non-targeted separation and quantitative determination of DOM species otherwise hard to accomplish. E.g., DOP and DOS were previously only amenable through difference

measurement of inorganic species. As an example, DOP is defined as the additional amount of phosphate obtained after oxidation of the organic phosphorus. This estimation of DOP is referred to as the total dissolved phosphorus/dissolved inorganic phosphorus (TDP/DIP) method (Karl and Björkman 2002; Kattner 2009). The hyphenation method introduced in Chapter VI.1 overcomes this restriction and unlocks the biogeochemical potential of DOP and DOS studies for the community by allowing direct measurements with greatly increased detection limit compared to established methods.

The exemplary work with uranium as target for metal speciation showed that the hyphenation of HPLC with ICP-MS offers great potential for the emerging field of trace metal – organic ligand analysis in biogeochemical studies. If uranium and very likely other metals are still present in the methanolic DOM extracts they must exhibit a large complex stability. This stability is also a prerequisite to keep metals with extremely low solubility in biologically utilizable amounts dissolved in seawater (Morel and Price 2003; Millero et al. 2009).

Certainly, more development work and modifications of the HPLC-ICP-MS method are needed in order to reduce the levels of contamination and to fully assess the recovery and reproducibility of this method for trace metal determinations. Especially the biological and geochemical important transition metals Fe, Co, Ni, etc. require enhanced levels of cleanliness. However, for investigation of DOP and DOS pools, the developed method already meets the requirements for a robust method and certainly enhances the accuracy and informative value of these sub-pools for the cycling of DOM in the ocean.

The developed method allows easy exchange of the chromatographic separation technique (i.e., choice of different column types, change between RP and SEC, etc.). Further, modification of the interface for use with isotope dilution mass spectrometry (IDMS) is easy to implement and first experiments have been conducted and showed promising results. Volatility and ionization efficiencies are largely influenced by the change in chromatographic conditions (Hu et al. 2004; Bendahl and Gammelgaard 2005; Carr et al. 2006a; Lokits et al. 2009) and blank correction algorithms are needed to account for these matrix changes (e.g., Wind et al. 2001b and Chapter VI.1). A postcolumn spike addition with an isotope of the analyte overcomes most of these difficulties. Thus, IDMS offers the potential of an

enhanced level of precision and accuracy for metal speciation studies which has already been recognized in the seminal works of Heumann and Rottmann (Heumann et al. 1994; Rottmann and Heumann 1994a; Rottmann and Heumann 1994b). However, IDMS was rarely adapted for marine DOM research and only few IDMS studies were carried out on other organic matter pools in the recent past (e.g., Vogl and Heumann 1998; Karlsson et al. 2007; Bai et al. 2011).

More work on the quantification of FT-ICR MS data is strongly demanded by the scientific community. The problem results from a lack of knowledge of the ionization properties of different compound classes due to the co-occurrence of thousands of substances that compete for charges as well as signal suppression in the ICR cell.[51] In addition, the lack of a suitable “DOM-standard” for FT-ICR MS precludes easy empirical approaches to quantify DOM compounds with this technique. Neither the use of mean values nor (intensity) weighted average elemental composition or mass sufficiently describes the mean elemental composition of a sample. The first approach implies that the abundance of all compounds in the sample is equal; the second assumes that all compounds have the same signal response and the intensity ratio represents the true ratio of compounds. A practical consequence for the application in DOM studies is that bulk elemental ratios, calculated from assigned molecular formulas deviate from the results of e.g., elemental analyzers. Nitrogen and sulfur are generally underrepresented in the FT-ICR mass spectra, resulting in higher C:N and C:S ratios. Unless an attempt is made to survey the ionization characteristics of the various DOM compound classes in ESI-negative and other ionization methods, this problem will persist. However, the application of strict rules to set limits on the calculated molecular formulas (in terms of ambiguity, elemental composition ranges, etc.; Kujawinski and Behn 2006; Koch et al. 2007; Tziotis et al. 2011) is an established procedure to internally constrain the spectra.

On the other hand, FT-ICR MS provides the community with a wealth of compounds newly identified in marine DOM that need to be further investigated. Only few known compounds have been identified in FT-ICR MS samples so far and results

[51] The problem of the different ionization properties can best be demonstrated, if different ionization techniques (ESI-positive, ESI-negative, APPI, etc) are used (Stenson et al. 2003; Hertkorn et al. 2008; Kido Soule et al. 2010, Podgorski et al. 2012).

are partly ambiguous in elemental composition and structure, highlighting the immense compositional diversity of DOM. Hence, FT-ICR MS enables studying of hundreds to thousands of compounds not accessible with other techniques. The outstanding resolution and mass accuracy of this technique allows differentiation of tens of mass peaks within one single nominal mass, not provided by any other mass spectrometric technique so far (Xian et al. 2012). Thus, FT-ICR MS is an ideal technique to study the highly complex organic mixtures in NOM samples. FT-ICR MS opens the analytical window to the “MUC” and refractory fractions of NOM (see e.g., Koch et al. 2005; Hertkorn et al. 2006; Flerus et al. 2012) and the potential for structural elucidation with fragmentation experiments is a valuable amendment to NMR studies (Witt et al. 2009 and Chapter VI.3).

Chapter VI.3 linked the quantitative aspect of DOS analyzed with the HPLC-ICP-MS method (Chapter VI.1) with the compositional and structural aspects available through FT-ICR MS. Organo-sulfur compounds showed a characteristic behavior in the two-phase system sea surface microlayer – underlying water. An enrichment of sulfur by means of FT-ICR MS signal intensities in the microlayer may be verified by a combination of the methods, facilitated by the similar requirements of sample preparation. It was further shown that FT-ICR MS is comparable to other mass spectrometric techniques to acquire structural information on compounds via fragmentation experiments that helped to identify contaminant species in the samples and may be further used in structural studies of DOM.

The holistic approach from Chapter VI.4 and VI.5 extended the range of application of FT-ICR MS to large scale studies of DOM and its degradation pathways, supported by independent parameters and statistical tools. The results presented in both chapters describe a fraction and (bio-) geochemical properties of MUC and RDOM which is not accessible by analyzing only small sample numbers. This approach is entirely new because there is currently no measure available to define compounds as belonging to the RDOM fraction (i.e., no identifiable compound is known to be “refractory”, although some compound classes have long apparent residence times)[52] and degradation experiments cannot cover the time scales under

[52] The preservation of biomarkers in sedimentary records has likely different causes than the recalcitrance of RDOM in seawater but is similar puzzling (Prahl and Wakeham 1987; Mollenhauer et al. 2008). A plausible thermodynamic explanation is provided by LaRowe and Van Capellen (2011).

consideration. Degradation rates can be predicted and fast and slow degrading compounds are chemically distinguishable. But the exact rates still need to be calibrated and extended to the most labile compounds.

VII.2 The biogeochemical perspective

Only few studies of open ocean concentrations of DOS exist in the literature (Cutter et al. 2004; Alling et al. 2008), in contrast to DOP related studies (e.g., Mather et al. 2008; Lomas et al. 2010). But almost no chemical differentiation within the DOS and DOP pools has been obtained in the past (except from the few ^{31}P-NMR studies by e.g., Clark et al. 1998; Kolowith et al. 2001; Young and Ingall 2010 and compound specific analysis of e.g., phosphonates, e.g., Cembella and Antia 1986; Dyhrman et al. 2009 or phytochelatins, e.g., Wei and Ahner 2005). Combining (quantitative) metal speciation with organic matter separation for marine DOM analysis was rarely achieved in the past and offers exciting insights into the biogeochemical cycling of elements, e.g., the remineralization of phosphorus at depth (where only few data exist due to the analytical restrictions of the TDP/DIP method, Karl and Björkman 2002). Even less is known about the biogeochemical cycling of DOS. Due to the large excess of inorganic sulfur, this pool is probably the least explored in the oceanic cycling of DOM.[53] Moreover, the ability to assess the complexation of essential trace metals with organic compounds has wide implications for biogeochemical cycles (Jakuba et al. 2008; Boyd and Ellwood 2010; Shi et al. 2010). Especially the molecular composition and structure of natural organic ligands (e.g., metal specific heteroatom distribution, e.g., Manceau and Matynia 2010) and their effect on trace element distribution in the marine realm is important to understand as it controls primary productivity and the microbial loop in micronutrient-poor ocean domains (Mills et al. 2004; Martinez-Garcia et al. 2011). Stimulated sequestration of atmospheric CO_2 and carbon storage by natural or anthropogenic iron inputs still fuels the debate on future global warming (Martin and Fitzwater 1988; Buesseler and Boyd 2003; Behrenfeld et al. 2006). On the other hand, projected decrease in ocean pH (Ocean Acidification) is expected to change the chemical speciation, and thus, the bioavailable fraction of trace metals (Millero et al. 2009; Shi et al. 2010). This could

[53] Sulfate outweighs DOS by five orders of magnitude, hence sulfur is often not being considered as a limiting nutrient, although it is actively assimilated by organisms (e.g., Giordano et al. 2005).

potentiate micronutrient limitation in large parts of the worlds ocean, alter phytoplankton productivity and change the phytoplankton and heterotrophic species composition (Saito et al. 2008).

Similar impacts for the biogeochemical cycling of organic carbon are expected to result from the proposed DOM degradation model. It was earlier assumed that the compounds of DOM represent a continuum of reactivities (Amon and Benner 1994; Kaiser and Benner 2009) and hence life-times in the ocean (Bauer 2002; Loh et al. 2004; Beaupré and Druffel 2009), but this could not be confirmed yet for the slowest degrading fraction of DOM. The presented studies of a large molecular DOM data set revealed indeed such a continuum. The broad range of degradation rates may be indicative of the microbial carbon pump operating at different speeds: after the conversion of LDOM and SLDOM to RDOM, further inhibited remineralization of this RDOM accumulates carbon in the DOM pool. Whether this is a result of the different microbial community assemblages (laterally and vertically) and their different ability to use the available carbon substrates remains to be elucidated (Schattenhofer et al. 2009; Jiao et al. 2010; Pearce et al. 2011). The response of the microbial community to substrate change will further determine, whether a future warmer ocean will be a source or a sink for carbon (Azam and Malfatti 2007; Arnosti et al. 2011; Luna et al. 2012).

Preliminary results on the influence of the energy release via radioactive decay of uranium and other radioisotopes on DOM in seawater and sediments showed the potential for a so far unconsidered reaction pathway. A direct hit of a DOM molecule by α and β radiation is very unlikely due to the low concentration of DOM, the low activity of radionuclides in seawater and the high absorption coefficient of seawater and its main constituents. However, especially secondary effects like radical reactions with water radiolysis products and DOM have an increased probability of occurrence. This was demonstrated with an experiment in cooperation with the University of Edinburgh (DAAD project with B.P. Koch, W. Geibert, R. Flerus and O.J. Lechtenfeld), where a high activity β-source was available. A direct remineralization was not observed with radiation doses relevant for seawater. However, increased oxygen to carbon and decreased hydrogen to carbon ratios are consistent with the assumption that secondary reactions with e.g., hydroxyl radical influence the chemical composition of DOM on long time scales (Koch et al. 2012).

VII.3 Conclusions

Chapter VI.1 and VI.2 were mostly addressing the development and application of analytical methods to study DOM composition and characteristics, thus belonging to the analytical approach as described in the objectives Chapter V.

- It was shown in Chapter VI.1 that the hyphenation of element specific and quantitative ICP-MS detector with chromatographic pre-separation yields new and accurate results for two sub-pools of DOM, the DOP and DOS fraction. These fractions were shown to exhibit different chemical characteristics, i.e., a distinct elution pattern of sulfur compared to phosphorus. Moreover, the chromatographic peaks showed differing elemental ratios suggestive of dissimilar chemical (polarity and size) characteristics. The results were explained with the different biogeochemical boundary conditions of the sample locations (i.e., oligotrophic tropical vs. macronutrient-rich polar conditions).

- The inclusion of uranium as an abundant and chemically versatile metal in the method development demonstrated the methods' applicability to investigate trace metal – DOM interactions. The chemical information (on organic moieties) provided from the chromatographic separation and the potential to quantify even the least abundant metals in seawater extracts highlights the performance capability of the method. Like the DOP and DOS fractions, different elution patterns and quantities of the metal(s) which are chemically bound to DOM ligands can be explained with the chemistry of the metals and ligands and will give exciting new insights into the chemical relations of inorganic ions and organic ligands in seawater and other NOM. However, further development of the method is required to test these findings for biochemically important trace metals.

- Uranium is generally considered to be a conservative tracer in (paleo-) oceanography due to the tight relation of U concentration and salinity (Owens et al. 2011). However, a small contribution of dissolved organic fractions of uranium in the ocean have been reported in the past (e.g., Sugimura and Mayeda 1980), but isotopic fractionation of uranium

isotopes in natural organic matter has not been observed. Therefore, the lateral transport of ^{236}U after North Atlantic Deep Water formation is not expected to be influenced by the chemical speciation of uranium. This property enables ^{236}U to be a potential transient but conservative tracer (with regard to ocean circulation), adding to the suite of e.g., chlorofluorocarbons or radioactive isotopes with short half-lives (e.g., ^{3}H). Although the measurement itself requires enormous analytical effort, the sampling for ^{236}U was shown to be realizable on board of research vessels.

- Insights into the different chemistry and physics of especially sulfur and nitrogen bearing DOM compounds could also be obtained from the sea-surface microlayer study in Chapter VI.3. It was shown that despite compositional overlap between both phases the response to a changing ionic strength in an estuarine salinity gradient was different, i.e., sulfur bearing compounds were predominantly enriched in the surface microlayer in brackish waters whereas nitrogen compounds were more abundant in the microlayer phase in high salinity waters. The change in ionic strength of the surface microlayer and the underlying bulk water resulted in a chemically consistent change for microlayer enriched compounds deduced from the molecular formulas detected with FT-ICR MS.

- The results of the surface microlayer study were explained with the bio- and photochemical consequences of the apparent phase separation along the phase boundary but certainly, more experiments are needed to address this topic. In addition, the influence of various proportions of autochthonous production and allochthonous sources and their subsequent transformation and the chemical composition of the microlayer and bulk phase needs further investigation.

- Already the interpretation of FT-ICR MS data of a single NOM sample is demanding and time consuming. Consequently, for the exploitation of large sample sets, statistical tools are needed and already proved its suitability for biogeochemical research questions (Dauwe and

Middelburg 1998; Kaiser and Benner 2009; Xue et al. 2011) and also FT-ICR MS studies (Sleighter et al. 2010). The data analysis from Chapters VI.4 and VI.5 developed this concept further to obtain sample age dependent characteristics of DOM (compounds). This was possible through reproducible extraction and enhanced normalization and calibration algorithms. The age of a sample was shown to be the biogeochemically determining parameter of the mass peak patterns of a large fraction of peaks across many samples, resulting in an age calibration and degradation function.

- The concepts of a continuous distribution of the stability of DOM compounds was adapted to the degradation behavior and resulted in a model of a degradation continuum (Chapter VI.4) with corresponding chemical characterization and biogeochemical implications (Chapter VI.5). The non-quantitative nature of FT-ICR MS analysis so far prevents a mass balance calculation which could constrain of the results. However, the semi-quantitative indicators of degradation developed in these two chapters are nonetheless valuable approaches to infer the intrinsic stability (or lability) of different DOM fractions. The study of SPE-DOM can only partly resolve the fast biochemical processes determining the fate of fresh DOM in surface waters. However, geo-ecological differences are imprinted as part of the water mass history and can be revealed with FT-ICR MS. The majority of compounds reflect a common degradation mechanism or pathway independent from the origin of the fresh DOM.

VIII OUTLOOK

The driving force for DOM research in the future will certainly be the question about the perturbations and impacts of global climate change on organic carbon fluxes and its feedback mechanisms. Yet, these projections on a global scale need to be accompanied by methodological and conceptual advances in the understanding of the cycling of elements and natural organic matter.

VIII.1 Methodological advances

The value of SPE techniques for molecular analysis of DOM has been already highlighted in the previous chapters. However, there are still many unsolved problems and a poor understanding of the factors influencing retention and separation of DOM on chemically modified solid phases. The continuous quest for a "representative" extraction (in terms of chemical composition, age, size, trace metal content, etc.) will likely get new impulses from combined extraction procedures (i.e., the use of multiple extraction phases, combined techniques, etc). A prerequisite to understand the chemical interactions of different NOM classes (marine vs. terrestrial, low vs. high salinity), combined applications of different techniques to fully constrain e.g., the size and polarity spectrum of DOM need to be considered.

Production and transformation of natural organic ligands are part of the complex physical, chemical and biological feedback mechanism that determine the implications of global warming, ocean acidification and permafrost degradation on primary productivity. Methodological and experimental advances in the field of trace metal – organic ligand composition, stability and biochemistry are expected in the near future (Vraspir and Butler 2009). The need to develop new techniques to understand the stability of trace metal – ligand complexes was recently highlighted with the foundation of a SCOR working group "Organic Ligands – A Key Control on

Trace Metal Biogeochemistry in the Ocean".[54] Coupled techniques such as the (HP)LC-ICP-MS method developed in Chapter VI.1 are gaining growing interest in the community (e.g., Gledhill et al. 2004; Mawji et al. 2008; Velasquez et al. 2011) and will certainly be part of the analytical tools used for these studies. In this context, studies of the applicability of the present extraction methods to obtain unbiased samples for organo-metal analysis and further improvements of the sensitivity and reproducibility of coupled techniques are required. Combined (micro-) biological and chemical experiments to investigate the influence of trace metal limitations for phytoplankton and bacterial production will certainly profit from the new methods presented here.

Integrating organic and inorganic chemistry in marine sciences will enhance our view on the global biogeochemical cycles. However, for appropriate reconciling and predicting fluxes of carbon, mechanistic details and responses have to be elucidated. Especially the nature of refractory material and its formation and degradation pathways need to be determined. High resolution mass spectrometry will help to shed light on the molecular composition of DOM fractions and single constituents (e.g., organic ligands, new biomarkers, etc.). Although the current view on the compositional aspects of NOM has greatly profited from the ultrahigh resolution of FT-ICR MS, the structural diversity is only partly resolved. Expanding the fragmentation capabilities of FT-ICR MS as a standard tool will allow insights into the structure of DOM and anthropogenic molecules and their degradation products as demonstrated in Chapter VI.3. In addition, the combination of (pre-) fractionation and a continuously lower requirement for NMR sample sizes will generate better insights into the structural dimension of natural organic matter. Further improvements in the sample preparation, measurement methods and evaluation procedures will enhance the analytical applicability of the high-precision frequency techniques like NMR and FT-ICR MS towards an unbiased and representative view on DOM.

Alongside structural aspects, especially the quantification capabilities of FT-ICR MS need to be improved. Promising approaches are e.g., the use of (internal) standards of known composition and concentration and studies of their signal responses with varying DOM matrix concentration, composition, etc. The thorough study of ionization efficiency and compound volatility will lead to a better match

[54] http://www.scor-int.org/Working_Groups/wg139.htm.

between calculated elemental ratios and those measured on the bulk samples. This also includes unambiguous identification of other heteroatoms in the molecular formula generation like phosphorus and implementation of a larger number of heteroatoms per molecular formula to account e.g., for oligopeptides.

VIII.2 Conceptual advances

Recent conceptual advances in understanding the functioning of the biological pump, e.g., the microbial carbon pump concept, have highlighted the complex interactions between DOM, heterotrophic activity and carbon sequestration. In this context a strengthening in the combined efforts of microbiology and biogeochemistry to resolve the functioning of the MCP has been demanded (Jiao et al. 2010; Kujawinski 2011). Thus, degradation experiments with molecular characterization (e.g., bacterial biomarkers) and community studies (metabolic activities, metabolomics, etc.) as continuation of the seminal work by Brophy and Carlson (1989) are promising ways to access the natural complexity of the biochemical interactions. These studies will greatly profit from the recent developments of FT-ICR MS and NMR techniques and their ability to unlock the molecularly characterized fraction of DOM. Further improvements in the sample preparation, measurement methods and evaluation procedures will enhance the analytical applicability of these techniques towards an unbiased and representative view on DOM. The ultimate aim is to obtain high resolution in time and high resolution of molecular changes during production, transformation and degradation of DOM under different environmental conditions.

The implementation of inventories and rates of production and removal of DOM fractions into biogeochemical and ecosystem models (e.g., Schlitzer 2007; Ye et al. 2009) can better reveal the importance of DOM for the global carbon cycle and enables to predict future changes. Here, the calculated degradation rates of hundreds of compounds in refractory SPE-DOM easily translate into an age-specific distribution of degradation rates that determine the biogeochemical character of a single sample. Hence, a sample can be sufficiently described by its age, carbon content and a parameterized degradation function. This degradation continuum concept has to be tested in other oceanic basins, sediments, estuaries and for permafrost organic matter and will profit from a calibration of the time scale with

independent, transient tracers like CFCs, DI^{14}C, etc. Biogeochemical models also include the interaction of organic matter with the cycling of trace metals but the analytical skills to produce concrete numbers of complex stability and complex composition are still poor. Substantial improvement for our understanding of the biogeochemical cycles is expected, if the chemical properties, the production pathways and the degradation rates of the organic ligands are better known.

A critical aspect in projected climate change scenarios is the large carbon reservoir in the circum-arctic permafrost soils[55] that eventually disintegrate and release (apart from large amounts of CO_2, methane and nitrous oxide; Schuur et al. 2009; Elberling et al. 2010) dissolved and particulate carbon to the Arctic Ocean (Dittmar and Kattner 2003a; Guo et al. 2007). Although there is some evidence that these released aquatic carbon pools are highly bioavailable (Raymond et al. 2007; Letscher et al. 2011; Mann et al. 2012), more research is needed which addresses seasonality of the carbon export (Holmes et al. 2008) to estimate the net effect for the global carbon cycle. The molecular characterization of the permafrost carbon and the application of degradation experiments and comparison with the marine degradation rates introduced in Chapters VI.4 and VI.5 may further help to illuminate this topic.

Compositional and structural elucidation of the whole DOM pool is not only of analytical interest but has also huge biogeochemical impacts. The vision for the future research is a combined understanding of both, the organic and inorganic biogeochemistry, where single molecules can be related to sources, a production and degradation pathway, a biochemical function and thermodynamic and kinetic properties determining the biological and abiotic fate in the oceanic environment under changing environmental conditions.

[55] The amount of carbon stored in the circum-arctic permafrost soil is estimated to be 1,672 Pg C, accounting for half of the global soil carbon (Tarnocai et al. 2009).

REFERENCES

Ahel, M., R.G. Barlow, and R.F.C. Mantoura (1996). Effect of salinity gradients on the distribution of phytoplankton pigments in a stratified estuary. *Mar Ecol Prog Ser* **143**(1-3): 289-295. doi: 10.3354/meps143289

Ahel, M. and S. Terzic (2003). Biogeochemistry of aromatic surfactants in microtidal estuaries. *Chimia* **57**(9): 550-555. doi: 10.2533/000942903777679019

Ahner, B.A., J.G. Lee, N.M. Price, and F.M.M. Morel (1998). Phytochelatin concentrations in the equatorial Pacific. *Deep Sea Res I* **45**(11): 1779-1796. doi: 10.1016/s0967-0637(98)00043-0

Ahner, B.A., L.P. Wei, J.R. Oleson, and N. Ogura (2002). Glutathione and other low molecular weight thiols in marine phytoplankton under metal stress. *Mar Ecol Prog Ser* **232**: 93-103. doi: 10.3354/meps232093

Alberti, G., R. Biesuz, and M. Pesavento (2007). Determination of the total concentration and speciation of uranium in natural waters by the resin titration method. *Microchem J* **86**(2): 166-173. doi: 10.1016/j.microc.2007.02.004

Alfimov, V., G. Possnert, and A. Aldahan (2006). Anthropogenic iodine-129 in the Arctic Ocean and Nordic Seas: Numerical modeling and prognoses. *Mar Pollut Bull* **52**(4): 380-385. doi: 10.1016/j.marpolbul.2005.09.025

Alling, V., C. Humborg, C.M. Morth, L. Rahm, and F. Pollehne (2008). Tracing terrestrial organic matter by delta S-34 and delta C-13 signatures in a subarctic estuary. *Limnol Oceanogr* **53**(6): 2594-2602. doi: 10.4319/lo.2008.53.6.2594

Allison, I., N.L. Bindoff, R.A. Bindschadler, P.M. Cox, N. de Noblet, M.H. England, J.E. Francis, N. Gruber, A.N. Haywood, D.J. Karoly, G. Kaser, C. Le Quéré, T.M. Lenton, M.E. Mann, B.I. McNeil, A.J. Pitman, S. Rahmstorf, E. Rignot, H.J. Schellnhuber, S.H. Schneider, S.C. Sherwood, R.C.J. Somerville, K. Steffen, E.J. Steig, M. Visbeck, and A.J. Weaver (2009). *The Copenhagen Diagnosis: Updating the world on the latest climate science*. The University of New South Wales Climate Change Research Centre (CCRC).

Aluwihare, L.I., D.J. Repeta, and R.F. Chen (1997). A major biopolymeric component to dissolved organic carbon in surface sea water. *Nature* **387**(6629): 166-169. doi: 10.1038/387166a0

——— (2002). Chemical composition and cycling of dissolved organic matter in the Mid-Atlantic Bight. *Deep Sea Res II* **49**(20): 4421-4437. doi: 10.1016/s0967-0645(02)00124-8

Aluwihare, L.I., D.J. Repeta, S. Pantoja, and C.G. Johnson (2005). Two chemically distinct pools of organic nitrogen accumulate in the ocean. *Science* **308**(5724): 1007-1010. doi: 10.1126/science.1108925

Alzaga, R., A. Pena, L. Ortiz, and J.M. Bayona (2003). Determination of linear alkylbenzensulfonates in aqueous matrices by ion-pair solid-phase microextraction-in-port derivatization-gas chromatography-mass spectrometry. *J Chromatogr, A* **999**(1-2): 51-60. doi: 10.1016/s0021-9673(03)00493-x

Ammann, A.A. (2002). Speciation of heavy metals in environmental water by ion chromatography coupled to ICP-MS. *Anal Bioanal Chem* **372**(3): 448-452. doi: 10.1007/s00216-001-1115-8

Amon, R.M.W. and R. Benner (1994). Rapid cycling of high-molecular-weight dissolved organic matter in the ocean. *Nature* **369**(6481): 549-552. doi: 10.1038/369549a0

——— (1996a). Bacterial utilization of different size classes of dissolved organic matter. *Limnol Oceanogr* **41**(1): 41-51

——— (1996b). Photochemical and microbial consumption of dissolved organic carbon and dissolved oxygen in the Amazon River system. *Geochim Cosmochim Acta* **60**(10): 1783-1792. doi: 10.1016/0016-7037(96)00055-5

Amon, R.M.W., H.-P. Fitznar, and R. Benner (2001). Linkages among the bioreactivity, chemical composition, and diagenetic state of marine dissolved organic matter. *Limnol Oceanogr* **46**(2): 287–297

Amrani, A., J.W. Turner, Q.S. Ma, Y.C. Tang, and P.G. Hatcher (2007). Formation of sulfur and nitrogen cross-linked macromolecules under aqueous conditions. *Geochim Cosmochim Acta* **71**(17): 4141-4160. doi: 10.1016/j.gca.2007.06.051

Andersen, M.B., C.H. Stirling, B. Zimmermann, and A.N. Halliday (2010). Precise determination of the open ocean (234)U/(238)U composition. *Geochem Geophys Geosyst* **11**(Q12003). doi: 10.1029/2010gc003318

Anderson, R.F. (1982). Concentration, vertical flux, and remineralization of particulate uranium in seawater. *Geochim Cosmochim Acta* **46**(7): 1293-1299. doi: 10.1016/0016-7037(82)90013-8

Andreae, M.O. and P.J. Crutzen (1997). Atmospheric aerosols: Biogeochemical sources and role in atmospheric chemistry. *Science* **276**(5315): 1052-1058. doi: 10.1126/science.276.5315.1052

Andrié, C., M. Rhein, S. Freudenthal, and O. Plahn (2002). CFC time series in the deep water masses of the western tropical Atlantic, 1990-1999. *Deep Sea Res I* **49**(2): 281-304. doi: 10.1016/s0967-0637(01)00053-x

Archer, D., M. Eby, V. Brovkin, A. Ridgwell, L. Cao, U. Mikolajewicz, K. Caldeira, K. Matsumoto, G. Munhoven, A. Montenegro, and K. Tokos (2009). Atmospheric lifetime of fossil fuel carbon dioxide. *Annu Rev Earth Planet Sci* **37**: 117-134. doi: 10.1146/annurev.earth.031208.100206

Aristegui, J., C.M. Duarte, S. Agusti, M. Doval, X.A. Alvarez-Salgado, and D.A. Hansell (2002). Dissolved organic carbon support of respiration in the dark ocean. *Science* **298**(5600): 1967-1967. doi: 10.1126/science.1076746

Armstrong, E., J. Granger, E.L. Mann, and N.M. Price (2004). Outer-membrane siderophore receptors of heterotrophic oceanic bacteria. *Limnol Oceanogr* **49**(2): 579-587

Armstrong, R.A., C. Lee, J.I. Hedges, S. Honjo, and S.G. Wakeham (2002). A new, mechanistic model for organic carbon fluxes in the ocean based on the quantitative association of POC with ballast minerals. *Deep Sea Res II* **49**(1-3): 219-236. doi: 10.1016/S0967-0645(01)00101-1

Arnosti, C. (2011). Microbial extracellular enzymes and the marine carbon cycle. *Ann Rev Mar Sci* **3**: 401-425. doi: 10.1146/annurev-marine-120709-142731

Arnosti, C., A.D. Steen, K. Ziervogel, S. Ghobrial, and W.H. Jeffrey (2011). Latitudinal gradients in degradation of marine dissolved organic carbon. *PLoS One* **6**(12). doi: 10.1371/journal.pone.0028900

Arrigo, K.R., G.L. van Dijken, and S. Bushinsky (2008). Primary production in the Southern Ocean, 1997-2006. *J Geophys Res-Oceans* **113**(C8004). doi: 10.1029/2007jc004551

Azam, F. (1998). Microbial control of oceanic carbon flux: The plot thickens. *Science* **280**(5364): 694-696. doi: 10.1126/science.280.5364.694

Azam, F., T. Fenchel, J.G. Field, J.S. Gray, L.A. Meyerreil, and F. Thingstad (1983). The ecological role of water-column microbes in the sea. *Mar Ecol Prog Ser* **10**(3): 257-263. doi: 10.3354/meps010257

Azam, F. and R.A. Long (2001). Oceanography - Sea snow microcosms. *Nature* **414**(6863): 495-498. doi: 10.1038/35107174

Azam, F. and F. Malfatti (2007). Microbial structuring of marine ecosystems. *Nat Rev Microbiol* **5**(10): 782-791. doi: 10.1038/nrmicro1747

Azam, F. and A.Z. Worden (2004). Microbes, molecules, and marine ecosystems. *Science* **303**(5664): 1622-1624. doi: 10.1126/science.1093892

Bai, J.L., H. Minami, H. Sakagami, K. Mantoku, I. Atsuya, N. Takahashi, A. Tanaka, K. Jin, and T. Kawai (2011). Development of determination method of trace nickel in natural water by ID-oxygen added nitrogen-MIP-MS with direct measurement of liquid-liquid extracted organic phase. *Int J Environ Anal Chem* **91**(9): 811-820. doi: 10.1080/03067311003782641

Barbeau, K., E.L. Rue, K.W. Bruland, and A. Butler (2001). Photochemical cycling of iron in the surface ocean mediated by microbial iron(III)-binding ligands. *Nature* **413**(6854): 409-413. doi: 10.1038/35096545

Bassham, J.A., A.A. Benson, and M. Calvin (1950). The path of carbon in photosynthesis. *J Biol Chem* **185**(2): 781-787

Bauer, J.E. (2002). Carbon isotopic composition of DOM, pp. 405-453, in D.A. Hansell and C.A. Carlson [eds.], *Biogeochemistry of marine dissolved organic matter*. Academic Press, Elsevier Science, San Diego, USA.

Bauer, J.E. and E.R.M. Druffel (1998). Ocean margins as a significant source of organic matter to the deep open ocean. *Nature* **392**(6675): 482-485. doi: 10.1038/33122

Bauer, J.E., E.R.M. Druffel, P.M. Williams, D.M. Wolgast, and S. Griffin (1998). Temporal variability in dissolved organic carbon and radiocarbon in the eastern North Pacific Ocean. *J Geophys Res-Oceans* **103**(C2): 2867-2881. doi: 10.1029/97jc02545

Bauer, J.E., C.E. Reimers, E.R.M. Druffel, and P.M. Williams (1995). Isotopic constraints on carbon exchange between deep ocean sediments and sea water. *Nature* **373**(6516): 686-689. doi: 10.1038/373686a0

Bauer, J.E., P.M. Williams, and E.R.M. Druffel (1992). C-14 activity of dissolved organic carbon fractions in the north-central Pacific and Sargasso Sea. *Nature* **357**(6380): 667-670. doi: 10.1038/357667a0

Beaufort, L., I. Probert, T. de Garidel-Thoron, E.M. Bendif, D. Ruiz-Pino, N. Metzl, C. Goyet, N. Buchet, P. Coupel, M. Grelaud, B. Rost, R.E.M. Rickaby, and C. de Vargas (2011). Sensitivity of coccolithophores to carbonate chemistry and ocean acidification. *Nature* **476**(7358): 80-83. doi: 10.1038/nature10295

Beaupré, S.R. and L. Aluwihare (2010). Constraining the 2-component model of marine dissolved organic radiocarbon. *Deep Sea Res II* **57**(16): 1494-1503. doi: 10.1016/j.dsr2.2010.02.017

Beaupré, S.R. and E.R.M. Druffel (2009). Constraining the propagation of bomb-radiocarbon through the dissolved organic carbon (DOC) pool in the northeast Pacific Ocean. *Deep Sea Res I* **56**(10): 1717-1726. doi: 10.1016/j.dsr.2009.05.008

Behrenfeld, M.J., A.J. Bale, Z.S. Kolber, J. Aiken, and P.G. Falkowski (1996). Confirmation of iron limitation of phytoplankton photosynthesis in the equatorial Pacific Ocean. *Nature* **383**(6600): 508-511. doi: 10.1038/383508a0

Behrenfeld, M.J., R.T. O'Malley, D.A. Siegel, C.R. McClain, J.L. Sarmiento, G.C. Feldman, A.J. Milligan, P.G. Falkowski, R.M. Letelier, and E.S. Boss (2006). Climate-driven trends in contemporary ocean productivity. *Nature* **444**(7120): 752-755. doi: 10.1038/nature05317

Bendahl, L. and B. Gammelgaard (2005). Sample introduction systems for reversed phase LC-ICP-MS of selenium using large amounts of methanol — comparison of systems based on membrane desolvation, a spray chamber and direct injection. *J Anal At Spectrom* **20**: 410-416. doi: 10.1039/b415717f

Benitez-Nelson, C.R. (2000). The biogeochemical cycling of phosphorus in marine systems. *Earth-Science Reviews* **51**(1-4): 109-135. doi: 10.1016/S0012-8252(00)00018-0

Benitez-Nelson, C.R. and K.O. Buesseler (1999). Variability of inorganic and organic phosphorus turnover rates in the coastal ocean. *Nature* **398**(6727): 502-505. doi: 10.1038/19061

Benner, R. (2002). Chemical composition and reactivity, pp. 59-90, in D.A. Hansell and C.A. Carlson [eds.], *Biogeochemistry of marine dissolved organic matter*. Academic Press, Elsevier Science, San Diego, USA.

Benner, R., B. Benitez-Nelson, K. Kaiser, and R.M.W. Amon (2004). Export of young terrigenous dissolved organic carbon from rivers to the Arctic Ocean. *Geophys Res Lett* **31**(L05305). doi: 10.1029/2003gl019251

Benner, R., B. Biddanda, B. Black, and M. McCarthy (1997). Abundance, size distribution, and stable carbon and nitrogen isotopic compositions of marine organic matter isolated by tangential-flow ultrafiltration. *Mar Chem* **57**(3-4): 243-263. doi: 10.1016/s0304-4203(97)00013-3

Benner, R. and G.J. Herndl (2011). Bacterially derived dissolved organic matter in the microbial carbon pump, pp. 46-48, in N. Jiao, F. Azam and S. Sanders [eds.], *Microbial carbon pump in the ocean*. Science/AAAS, Washington, DC.

Benner, R. and K. Kaiser (2003). Abundance of amino sugars and peptidoglycan in marine particulate and dissolved organic matter. *Limnol Oceanogr* **48**(1): 118-128

Benner, R., J.D. Pakulski, M. McCarthy, J.I. Hedges, and P.G. Hatcher (1992). Bulk chemical characteristics of dissolved organic matter in the ocean. *Science* **255**(5051): 1561-1564. doi: 10.1126/science.255.5051.1561

Bentley, R. and T.G. Chasteen (2004). Environmental VOSCs - formation and degradation of dimethyl sulfide, methanethiol and related materials. *Chemosphere* **55**(3): 291-317. doi: 10.1016/j.chemosphere.2003.12.017

Bergh, Ø., K.Y. Borsheim, G. Bratbak, and M. Heldal (1989). High abundance of viruses found in aquatic environments. *Nature* **340**(6233): 467-468. doi: 10.1038/340467a0

Berner, R.A. (1989). Biogeochemical cycles of carbon and sulfur and their effect on atmospheric oxygen over phanerozoic time. *Palaeogeogr Palaeoclimatol Palaeoecol* **75**(1-2): 97-122. doi: 10.1016/0031-0182(89)90186-7

Berto, D., M. Giani, F. Savelli, E. Centanni, C.R. Ferrari, and B. Pavoni (2010). Winter to spring variations of chromophoric dissolved organic matter in a temperate estuary (Po River, northern Adriatic Sea). *Mar Environ Res* **70**(1): 73-81. doi: 10.1016/j.marenvres.2010.03.005

Bhatia, M.P., S.B. Das, K. Longnecker, M.A. Charette, and E.B. Kujawinski (2010). Molecular characterization of dissolved organic matter associated with the Greenland ice sheet. *Geochim Cosmochim Acta* **74**(13): 3768-3784. doi: 10.1016/j.gca.2010.03.035

Bianchi, T.S. (2011). The role of terrestrially derived organic carbon in the coastal ocean: A changing paradigm and the priming effect. *Proc Natl Acad Sci USA* **108**(49): 19473-19481. doi: 10.1073/pnas.1017982108

Björkman, K.M. and D.M. Karl (2003). Bioavailability of dissolved organic phosphorus in the euphotic zone at station ALOHA, North Pacific Subtropical Gyre. *Limnol Oceanogr* **48**(3): 1049-1057

Blain, S., B. Queguiner, L. Armand, S. Belviso, B. Bombled, L. Bopp, A. Bowie, C. Brunet, C. Brussaard, F. Carlotti, U. Christaki, A. Corbiere, I. Durand, F. Ebersbach, J.L. Fuda, N. Garcia, L. Gerringa, B. Griffiths, C. Guigue, C. Guillerm, S. Jacquet, C. Jeandel, P. Laan, D. Lefevre, C. Lo Monaco, A. Malits, J. Mosseri, I. Obernosterer, Y.H. Park, M. Picheral, P. Pondaven, T. Remenyi, V. Sandroni, G. Sarthou, N. Savoye, L. Scouarnec, M. Souhaut, D. Thuiller, K. Timmermans, T. Trull, J. Uitz, P. van Beek, M. Veldhuis, D. Vincent, E. Viollier, L. Vong, and T. Wagener (2007). Effect of natural iron fertilization on carbon sequestration in the Southern Ocean. *Nature* **446**(7139): 1070-1074. doi: 10.1038/nature05700

Bloch, S. (1980). Some factors controlling the concentration of uranium in the world ocean. *Geochim Cosmochim Acta* **44**(2): 373-377. doi: 10.1016/0016-7037(80)90145-3

Blough, N.V. (1997). Photochemistry in the sea-surface microlayer, pp. 383-424, in P.S. Liss and R.A. Duce [eds.], *The sea surface and global change*. Cambrigde University Press, Cambridge, United Kingdom.

Blough, N.V. and R. del Vecchio (2002). Chromophoric DOM in the coastal environment, pp. 509-546, in D. Hansell and C.A. Carlson [eds.], *Biogeochemistry of marine dissolved organic matter*. Academic Press, Elsevier Science, San Diego, USA.

Boehm, P.D. (1980). Evidence for the decoupling of dissolved, particulate and surface microlayer hydrocarbons in Northwestern Atlantic continental shelf waters. *Mar Chem* **9**(4): 255-281. doi: 10.1016/0304-4203(80)90029-8

Bohlke, J.K., J.R. de Laeter, P. De Bievre, H. Hidaka, H.S. Peiser, K.J.R. Rosman, and P.D.P. Taylor (2005). Isotopic compositions of the elements, 2001. *J Phys Chem Ref Data* **34**(1): 57-67. doi: 10.1063/1.1836764

Boulyga, S.F. and J.S. Becker (2002). Isotopic analysis of uranium and plutonium using ICP-MS and estimation of burn-up of spent uranium in contaminated environmental samples. *J Anal At Spectrom* **17**(9): 1143-1147. doi: 10.1039/b202196j

Boulyga, S.F., J.S. Becker, J.L. Matusevitch, and H.J. Dietze (2000). Isotope ratio measurements of spent reactor uranium in environmental samples by using inductively coupled plasma mass spectrometry. *Int J Mass Spectrom* **203**(1-3): 143-154. doi: 10.1016/s1387-3806(00)00296-7

Boulyga, S.F. and K.G. Heumann (2006). Determination of extremely low U-236/U-238 isotope ratios in environmental samples by sector-field inductively coupled plasma mass spectrometry using high-efficiency sample introduction. *J Environ Radioact* **88**(1): 1-10. doi: 10.1016/j.jenvrad.2005.12.007

Boyce, D.G., M.R. Lewis, and B. Worm (2010). Global phytoplankton decline over the past century. *Nature* **466**(7306): 591-596. doi: 10.1038/nature09268

Boyd, P.W. and M.J. Ellwood (2010). The biogeochemical cycle of iron in the ocean. *Nature Geosci* **3**(10): 675-682. doi: 10.1038/ngeo964

Boyd, P.W. and T.W. Trull (2007). Understanding the export of biogenic particles in oceanic waters: Is there consensus? *Prog Oceanogr* **72**(4): 276-312. doi: 10.1016/j.pocean.2006.10.007

Boye, M., A. Aldrich, C.M.G. van den Berg, J.T.M. de Jong, H. Nirmaier, M. Veldhuis, K.R. Timmermans, and H.J.W. de Baar (2006). The chemical speciation of iron in the north-east Atlantic Ocean. *Deep Sea Res I* **53**(4): 667-683. doi: 10.1016/j.dsr.2005.12.015

Boye, M., J. Nishioka, P. Croot, P. Laan, K.R. Timmermans, V.H. Strass, S. Takeda, and H.J.W. de Baar (2010). Significant portion of dissolved organic Fe complexes in fact is Fe colloids. *Mar Chem* **122**(1-4): 20-27. doi: 10.1016/j.marchem.2010.09.001

Brassell, S.C., G. Eglinton, I.T. Marlowe, U. Pflaumann, and M. Sarnthein (1986). Molecular stratigraphy: a new tool for climatic assessment. *Nature* **320**(6058): 129-133. doi: 10.1038/320129a0

Bray, J.R. and J.T. Curtis (1957). An ordination of the upland forest communities of southern Wisconsin. *Ecological Monographs* **27**(4): 326-349

Brewer, P.G. and E.T. Peltzer (2009). Limits to marine life. *Science* **324**(5925): 347-348. doi: 10.1126/science.1170756

Broecker, W.S., S.L. Peacock, S. Walker, R. Weiss, E. Fahrbach, M. Schröder, U. Mikolajewicz, C. Heinze, R. Key, T.H. Peng, and S. Rubin (1998). How much deep water is formed in the Southern Ocean? *J Geophys Res-Oceans* **103**(C8): 15833-15843. doi: 10.1029/98jc00248

Broecker, W.S. and T.H. Peng (1982). *Tracers in the sea*. Lamont-Doherty Geological Observatory, Columbia University, Palisades, New York.

Bronk, D.A. (2002). Dynamics of DON, pp. 153-247, in D.A. Hansell and C.A. Carlson [eds.], *Biogeochemistry of marine dissolved organic matter*. Academic Press, Elsevier Science, San Diego, USA.

Bronk, D.A., P.M. Glibert, and B.B. Ward (1994). Nitrogen uptake, dissolved organic nitrogen release, and new production. *Science* **265**(5180): 1843-1846. doi: 10.1126/science.265.5180.1843

Bronk, D.A., J.H. See, P. Bradley, and L. Killberg (2007). DON as a source of bioavailable nitrogen for phytoplankton. *Biogeosciences* **4**(3): 283-296. doi: 10.5194/bg-4-283-2007

Brophy, J.E. and D.J. Carlson (1989). Production of biologically refractory dissolved organic carbon by natural seawater microbial populations. *Deep-Sea Research Part a-Oceanographic Research Papers* **36**(4): 497-507. doi: 10.1016/0198-0149(89)90002-2

Bruhwiler, L.M.P., A.M. Michalak, and P.P. Tans (2011). Spatial and temporal resolution of carbon flux estimates for 1983-2002. *Biogeosciences* **8**(5): 1309-1331. doi: 10.5194/bg-8-1309-2011

Bruland, K.W. (1989). Complexation of zinc by natural organic ligands in the Central North Pacific. *Limnol Oceanogr* **34**(2): 269-285

Brunk, B.K., G.H. Jirka, and L.W. Lion (1997). Effects of salinity changes and the formation of dissolved organic matter coatings on the sorption of phenanthrene: Implications for pollutant trapping in estuaries. *Environ Sci Technol* **31**(1): 119-125. doi: 10.1021/es9602051

Buesseler, K.O. (1991). Do upper-ocean sediment traps provide an accurate record of particle flux? *Nature* **353**(6343): 420-423. doi: 10.1038/353420a0

Buesseler, K.O., J.E. Andrews, S.M. Pike, and M.A. Charette (2004). The effects of iron fertilization on carbon sequestration in the Southern Ocean. *Science* **304**(5669): 414-417. doi: 10.1126/science.1086895

Buesseler, K.O. and P.W. Boyd (2003). Will ocean fertilization work? *Science* **300**(5616): 67-68. doi: 10.1126/science.1082959

Buesseler, K.O., C.H. Lamborg, P.W. Boyd, P.J. Lam, T.W. Trull, R.R. Bidigare, J.K.B. Bishop, K.L. Casciotti, F. Dehairs, M. Elskens, M. Honda, D.M. Karl, D.A. Siegel, M.W. Silver, D.K. Steinberg, J. Valdes, B. Van Mooy, and S. Wilson (2007). Revisiting carbon flux through the ocean's twilight zone. *Science* **316**(5824): 567-570. doi: 10.1126/science.1137959

Buesseler, K.O. and E.R. Sholkovitz (1987). The geochemistry of fallout plutonium in the North Atlantic: II. View the Pu-240/Pu-239 source ratios and their significance. *Geochim Cosmochim Acta* **51**(10): 2623-2637. doi: 10.1016/0016-7037(87)90144-x

Burdige, D.J. (2005). Burial of terrestrial organic matter in marine sediments: a re-assessment. *Global Biogeochem Cycles* **19**(Gb4011). doi: 10.1029/2004gb002368

Burdige, D.J. and K.G. Gardner (1998). Molecular weight distribution of dissolved organic carbon in marine sediment pore waters. *Mar Chem* **62**(1-2): 45-64. doi: 10.1016/S0304-4203(98)00035-8

Cai, W.-J. (2011). Estuarine and coastal ocean carbon paradox: CO2 sinks or sites of terrestrial carbon incineration? *Ann Rev Mar Sci* **3**(1). doi: 10.1146/annurev-marine-120709-142723

Cameron, D.R., T.M. Lenton, A.J. Ridgwell, J.G. Shepherd, R. Marsh, and A. Yool (2005). A factorial analysis of the marine carbon cycle and ocean circulation controls on atmospheric CO2. *Global Biogeochem Cycles* **19**(GB4027). doi: 10.1029/2005gb002489

Campin, J.M., T. Fichefet, and J.C. Duplessy (1999). Problems with using radiocarbon to infer ocean ventilation rates for past and present climates. *Earth Planet Sci Lett* **165**(1): 17-24. doi: 10.1016/s0012-821x(98)00255-6

Capley, E.N., J.D. Tipton, A.G. Marshall, and A.C. Stenson (2010). Chromatographic reduction of isobaric and isomeric complexity of fulvic acids to enable multistage tandem mass spectral characterization. *Anal Chem* **82**(19): 8194-8202. doi: 10.1021/ac1016216

Carlson, C.A. (2002). Production and removal processes, pp. 91-151, in D.A. Hansell and C.A. Carlson [eds.], *Biogeochemistry of marine dissolved organic matter*. Academic Press, Elsevier Science, San Diego, USA.

Carlson, C.A. and H.W. Ducklow (1996). Growth of bacterioplankton and consumption of dissolved organic carbon in the Sargasso Sea. *Aquat Microb Ecol* **10**(1): 69-85. doi: 10.3354/ame010069

Carlson, C.A., H.W. Ducklow, D.A. Hansell, and W.O. Smith (1998). Organic carbon partitioning during spring phytoplankton blooms in the Ross Sea polynya and the Sargasso Sea. *Limnol Oceanogr* **43**(3): 375-386

Carlson, C.A., H.W. Ducklow, and A.F. Michaels (1994). Annual flux of dissolved organic carbon from the euphotic zone in the northwestern Sargasso Sea. *Nature* **371**(6496): 405-408. doi: 10.1038/371405a0

Carlson, C.A., D.A. Hansell, N.B. Nelson, D.A. Siegel, W.M. Smethie, S. Khatiwala, M.M. Meyers, and E. Halewood (2010). Dissolved organic carbon export and subsequent remineralization in the mesopelagic and bathypelagic realms of the North Atlantic basin. *Deep Sea Res II* **54**(16): 1433-1445. doi: 10.1016/j.dsr2.2010.02.013

Carlson, C.A., D.A. Hansell, E.T. Peltzer, and W.O. Smith (2000). Stocks and dynamics of dissolved and particulate organic matter in the southern Ross Sea, Antarctica. *Deep Sea Res II* **47**(15-16): 3201-3225. doi: 10.1016/s0967-0645(00)00065-5

Carpenter, E.J., H.R. Harvey, B. Fry, and D.G. Capone (1997). Biogeochemical tracers of the marine cyanobacterium Trichodesmium. *Deep Sea Res I* **44**(1): 27-38. doi: 10.1016/s0967-0637(96)00091-x

Carr, J.E., K. Kwok, G.K. Webster, and J.W. Carnahan (2006a). Effects of liquid chromatography mobile phases and buffer salts on phosphorus inductively coupled plasma atomic emission and mass spectrometries utilizing ultrasonic nebulization and membrane desolvation. *J Pharm Biomed Anal* **40**(1): 42-50. doi: 10.1016/j.jpba.2005.06.033

Carr, M.E., M.A.M. Friedrichs, M. Schmeltz, M.N. Aita, D. Antoine, K.R. Arrigo, I. Asanuma, O. Aumont, R. Barber, M. Behrenfeld, R. Bidigare, E.T. Buitenhuis, J. Campbell, A. Ciotti, H. Dierssen, M. Dowell, J. Dunne, W. Esaias, B. Gentili, W. Gregg, S. Groom, N. Hoepffner, J. Ishizaka, T. Kameda, C. Le Quere, S. Lohrenz, J. Marra, F. Melin, K. Moore, A. Morel, T.E. Reddy, J. Ryan, M. Scardi, T. Smyth, K. Turpie, G. Tilstone, K. Waters, and Y. Yamanaka (2006b). A comparison of global estimates of marine primary production from ocean color. *Deep Sea Res II* **53**(5-7): 741-770. doi: 10.1016/j.dsr2.2006.01.028

Cartwright, A.J., P. Jones, J.C. Wolff, and E.H. Evans (2005). Detection of phosphorus tagged carboxylic acids using HPLC-SF-ICP-MS. *J Anal At Spectrom* **20**(2): 75-80. doi: 10.1039/b415962d

Cauwet, G. (1991). Carbon inputs and biogeochemical processes at the halocline in a stratified estuary: Krka River, Yugoslavia. *Mar Chem* **32**(2–4): 269-283. doi: 10.1016/0304-4203(91)90043-v

Cembella, A.D. and N.J. Antia (1986). The determination of phosphonates in seawater by fractionation of the total phosphorus. *Mar Chem* **19**(3): 205-210. doi: 10.1016/0304-4203(86)90023-x

Cetinic, I., D. Vilicic, Z. Buric, and G. Olujic (2006). Phytoplankton seasonality in a highly stratified karstic estuary (Krka, Adriatic Sea). *Hydrobiologia* **555**: 31-40. doi: 10.1007/s10750-005-1103-7

Chen, H.M., A. Stubbins, and P.G. Hatcher (2011). A mini-electrodialysis system for desalting small volume saline samples for Fourier transform ion cyclotron resonance mass spectrometry. *Limnol Oceanogr: Methods* **9**: 582-592. doi: 10.4319/lom.2011.9.582

Chen, J.H., R.L. Edwards, and G.J. Wasserburg (1986). U-238, U-234 and Th-232 in seawater. *Earth Planet Sci Lett* **80**(3-4): 241-251. doi: 10.1016/0012-821X(86)90108-1

Cherrier, J., J.E. Bauer, E.R.M. Druffel, R.B. Coffin, and J.P. Chanton (1999). Radiocarbon in marine bacteria: Evidence for the ages of assimilated carbon. *Limnol Oceanogr* **44**(3): 730-736

Cho, B.C. and F. Azam (1988). Major role of bacteria in biogeochemical fluxes in the ocean's interior. *Nature* **332**(6163): 441-443. doi: 10.1038/332441a0

Clark, L.L., E.D. Ingall, and R. Benner (1998). Marine phosphorus is selectively remineralized. *Nature* **393**(6684): 426-426. doi: 10.1038/30881

Coble, P.G. (1996). Characterization of marine and terrestrial DOM in seawater using excitation emission matrix spectroscopy. *Mar Chem* **51**(4): 325-346. doi: 10.1016/0304-4203(95)00062-3

Coble, P.G., C.E. Del Castillo, and B. Avril (1998). Distribution and optical properties of CDOM in the Arabian Sea during the 1995 Southwest Monsoon. *Deep Sea Res II* **45**(10-11): 2195-2223. doi: 10.1016/s0967-0645(98)00068-x

Collins, M.J., A.N. Bishop, and P. Farrimond (1995). Sorption by mineral surfaces: Rebirth of the classical condensation pathway for kerogen formation?

Geochim Cosmochim Acta **59**(11): 2387-2391. doi: 10.1016/0016-7037(95)00114-f

Conte, P. and A. Piccolo (1999). Conformational arrangement of dissolved humic substances. Influence of solution composition on association of humic molecules. *Environ Sci Technol* **33**(10): 1682-1690. doi: 10.1021/es9808604

Conway, T. and P. Tans (2012). *Recent Global CO2.* NOAA/ESRL, availabe from: www.esrl.noaa.gov/gmd/ccgg/trends/ (06.09.2012).

Cowie, G.L. and J.I. Hedges (1994). Biochemical indicators of diagenetic alteration in natural organic matter mixtures. *Nature* **369**(6478): 304-307. doi: 10.1038/369304a0

Craig, H. (1957). The natural distribution of radiocarbon and the exchange time of carbon dioxide between atmosphere and sea. *Tellus* **9**(1): 1-17. doi: 10.1111/j.2153-3490.1957.tb01848.x

Croot, P.L. and M. Johansson (2000). Determination of iron speciation by cathodic stripping voltammetry in seawater using the competing ligand 2-(2-thiazolylazo)-p-cresol (TAC). *Electroanalysis* **12**(8): 565-576. doi: 10.1002/(SICI)1521-4109(200005)12:8<565::AID-ELAN565>3.0.CO;2-L

Cunliffe, M., M. Salter, P.J. Mann, A.S. Whiteley, R.C. Upstill-Goddard, and J.C. Murrell (2009). Dissolved organic carbon and bacterial populations in the gelatinous surface microlayer of a Norwegian fjord mesocosm. *FEMS Microbiol Lett* **299**(2): 248-254. doi: 10.1111/j.1574-6968.2009.01751.x

Cunliffe, M., R.C. Upstill-Goddard, and J.C. Murrell (2011). Microbiology of aquatic surface microlayers. *FEMS Microbiol Rev* **35**(2): 233-246. doi: 10.1111/j.1574-6976.2010.00246.x

Cutter, G., P. Andersson, L. Codispoti, P.L. Croot, R. Francois, M. Lohan, H. Obata, and M.M.R. van der Loeff (2011). *Sampling and sample-handling protocols for GEOTRACES cruises*, GEOTRACES Standards and Intercalibration Committee.

Cutter, G.A., L.S. Cutter, and K.C. Filippino (2004). Sources and cycling of carbonyl sulfide in the Sargasso Sea. *Limnol Oceanogr* **49**(2): 555-565

D'Andrilli, J., J.P. Chanton, P.H. Glaser, and W.T. Cooper (2010a). Characterization of dissolved organic matter in northern peatland soil porewaters by ultra high resolution mass spectrometry. *Org Geochem* **41**(8): 791-799. doi: 10.1016/j.orggeochem.2010.05.009

D'Andrilli, J., T. Dittmar, B.P. Koch, J.M. Purcell, A.G. Marshall, and W.T. Cooper (2010b). Comprehensive characterization of marine dissolved organic matter by Fourier transform ion cyclotron resonance mass spectrometry with electrospray and atmospheric pressure photoionization. *Rapid Commun Mass Spectrom* **24**(5): 643-650. doi: 10.1002/rcm.4421

Damste, J.S.S., S. Schouten, E.C. Hopmans, A.C.T. van Duin, and J.A.J. Geenevasen (2002). Crenarchaeol: the characteristic core glycerol dibiphytanyl glycerol tetraether membrane lipid of cosmopolitan pelagic crenarchaeota. *J Lipid Res* **43**(10): 1641-1651. doi: 10.1194/jlr.M200148-JLR200

Dauwe, B. and J.J. Middelburg (1998). Amino acids and hexosamines as indicators of organic matter degradation state in North Sea sediments. *Limnol Oceanogr* **43**(5): 782-798

Davis, J., K. Kaiser, and R. Benner (2009). Amino acid and amino sugar yields and compositions as indicators of dissolved organic matter diagenesis. *Org Geochem* **40**(3): 343-352. doi: 10.1016/j.orggeochem.2008.12.003

de Baar, H.J.W., J.T.M. de Jong, D.C.E. Bakker, B.M. Loscher, C. Veth, U. Bathmann, and V. Smetacek (1995). Importance of iron for plankton blooms and carbon dioxide drawdown in the Southern Ocean. *Nature* **373**(6513): 412-415. doi: 10.1038/373412a0

de Bruyn, W.J., C.D. Clark, L. Pagel, and C. Takehara (2011). Photochemical production of formaldehyde, acetaldehyde and acetone from chromophoric dissolved organic matter in coastal waters. *J Photochem Photobiol, A* **226**(1): 16-22. doi: 10.1016/j.jphotochem.2011.10.002

De Laeter, J.R., J.K. Bohlke, P. De Bievre, H. Hidaka, H.S. Peiser, K.J.R. Rosman, and P.D.P. Taylor (2003). *Atomic weights of the elements: Review 2000 - (IUPAC technical report)*, Pure Appl Chem(75).

DeConto, R.M., S. Galeotti, M. Pagani, D. Tracy, K. Schaefer, T.J. Zhang, D. Pollard, and D.J. Beerling (2012). Past extreme warming events linked to massive carbon release from thawing permafrost. *Nature* **484**(7392): 87-91. doi: 10.1038/nature10929

del Giorgio, P.A. and C.M. Duarte (2002). Respiration in the open ocean. *Nature* **420**(6914): 379-384. doi: 10.1038/nature01165

Dittmar, T. and G. Kattner (2003a). The biogeochemistry of the river and shelf ecosystem of the Arctic Ocean: a review. *Mar Chem* **83**(3-4): 103-120. doi: 10.1016/S0304-4203(03)00105-1

Dittmar, T. and G. Kattner (2003b). Recalcitrant dissolved organic matter in the ocean: major contribution of small amphiphilics. *Mar Chem* **82**(1-2): 115-123. doi: 10.1016/s0304-4203(03)00068-9

Dittmar, T. and B.P. Koch (2006). Thermogenic organic matter dissolved in the abyssal ocean. *Mar Chem* **102**(3-4): 208-217. doi: 10.1016/j.marchem.2006.04.003

Dittmar, T., B.P. Koch, N. Hertkorn, and G. Kattner (2008). A simple and efficient method for the solid-phase extraction of dissolved organic matter (SPE-DOM) from seawater. *Limnol Oceanogr: Methods* **6**: 230-235. doi: 10.4319/lom.2008.6.230

Dittmar, T. and J. Paeng (2009). A heat-induced molecular signature in marine dissolved organic matter. *Nat Geosci* **2**(3): 175-179. doi: 10.1038/ngeo440

Djogic, R., L. Sipos, and M. Branica (1986). Characterization of uranium(VI) in seawater. *Limnol Oceanogr* **31**(5): 1122-1131

Donat, J.R., K.A. Lao, and K.W. Bruland (1994). Speciation of dissolved copper and nickel in South San Francisco Bay: a multi-method approach. *Anal Chim Acta* **284**(3): 547-571. doi: 10.1016/0003-2670(94)85061-5

Donat, J.R., P.J. Statham, and K.W. Bruland (1986). An evaluation of a C-18 solid phase extraction technique for isolating metal-organic complexes from central North Pacific Ocean waters. *Mar Chem* **18**(1): 85-99. doi: 10.1016/0304-4203(86)90078-2

Doval, M.D., X.A. Alvarez-Salgado, J.M. Gasol, L.M. Lorenzo, I. Miron, F.G. Figueiras, and C. Pedros-Alio (2001). Dissolved and suspended organic carbon in the Atlantic sector of the Southern Ocean. Stock dynamics in upper ocean waters. *Mar Ecol Prog Ser* **223**: 27-38. doi: 10.3354/meps223027

Druffel, E.R.M. and J.E. Bauer (2000). Radiocarbon distributions in Southern Ocean dissolved and particulate organic matter. *Geophys Res Lett* **27**. doi: 10.1029/1999gl002398

Druffel, E.R.M. and P.M. Williams (1990). Identification of a deep marine source of particulate organic carbon using bomb C-14. *Nature* **347**(6289): 172-174. doi: 10.1038/347172a0

Druffel, E.R.M., P.M. Williams, J.E. Bauer, and J.R. Ertel (1992). Cycling of dissolved and particulate organic matter in the open ocean. *J Geophys Res-Oceans* **97**(C10): 15639-15659. doi: 10.1029/92JC01511

Druffel, E.R.M., P.M. Williams, and Y. Suzuki (1989). Concentrations and radiocarbon signatures of dissolved organic matter in the Pacific Ocean. *Geophys Res Lett* **16**(9): 991-994. doi: 10.1029/GL016i009p00991

Ducklow, H.W. (1999). The bacterial component of the oceanic euphotic zone. *FEMS Microbiol Ecol* **30**(1): 1-10. doi: 10.1111/j.1574-6941.1999.tb00630.x

Dumont, I., V. Schoemann, S.H.M. Jacquet, F. Masson, and S. Becquevort (2011). Bacterial abundance and production in epipelagic and mesopelagic waters in the Subantarctic and Polar Front zones south of Tasmania. *Deep Sea Res II* **58**(21-22): 2212-2221. doi: 10.1016/j.dsr2.2011.05.024

Dunk, R.M., R.A. Mills, and W.J. Jenkins (2002). A reevaluation of the oceanic uranium budget for the Holocene. *Chem Geol* **190**(1-4): 45-67. doi: 10.1016/s0009-2541(02)00110-9

Dunne, J.P., J.L. Sarmiento, and A. Gnanadesikan (2007). A synthesis of global particle export from the surface ocean and cycling through the ocean interior and on the seafloor. *Global Biogeochem Cycles* **21**(Gb4006). doi: 10.1029/2006gb002907

Dyhrman, S.T., C.R. Benitez-Nelson, E.D. Orchard, S.T. Haley, and P.J. Pellechia (2009). A microbial source of phosphonates in oligotrophic marine systems. *Nat Geosci* **2**(10): 696-699. doi: 10.1038/ngeo639

Edmonds, H.N., Z.Q. Zhou, G.M. Raisbeck, F. Yiou, L. Kilius, and J.M. Edmond (2001). Distribution and behavior of anthropogenic I-129 in water masses ventilating the North Atlantic Ocean. *J Geophys Res-Oceans* **106**(C4): 6881-6894. doi: 10.1029/1999jc000282

Eglinton, T.I. and G. Eglinton (2008). Molecular proxies for paleoclimatology. *Earth Planet Sci Lett* **275**(1–2): 1-16. doi: 10.1016/j.epsl.2008.07.012

Eigl, R., M. Wallner, M. Srncik, P. Steier, and S. Winkler (2011). The suitability of 236U as an ocean tracer. *Mineral Mag* **75**(3): 802

Eiler, J.M. (2007). "Clumped-isotope" geochemistry - The study of naturally-occurring, multiply-substituted isotopologues. *Earth Planet Sci Lett* **262**(3-4): 309-327. doi: 10.1016/j.epsl.2007.08.020

Einsporn, M.H. (2011). *Polarity-related molecular characterization of (marine) dissolved organic matter*. Master thesis. University of Applied Sciences, Bremerhaven.

Elberling, B., H.H. Christiansen, and B.U. Hansen (2010). High nitrous oxide production from thawing permafrost. *Nat Geosci* **3**(5): 332-335. doi: 10.1038/ngeo803

Engbrodt, R. and G. Kattner (2005). On the biogeochemistry of dissolved carbohydrates in the Greenland Sea (Arctic). *Org Geochem* **36**(6): 937-948. doi: 10.1016/j.orggeochem.2004.12.007

Engebretson, R.R. and R. von Wandruszka (1994). Microorganization in dissolved humic acids. *Environ Sci Technol* **28**(11): 1934-1941. doi: 10.1021/es00060a026

Engel, A., S. Thoms, U. Riebesell, E. Rochelle-Newall, and I. Zondervan (2004). Polysaccharide aggregation as a potential sink of marine dissolved organic carbon. *Nature* **428**(6986): 929-932. doi: 10.1038/nature02453

Eppley, R.W. and B.J. Peterson (1979). Particulate organic matter flux and planktonic new production in the deep ocean. *Nature* **282**(5740): 677-680. doi: 10.1038/282677a0

Fabryka-Martin, J.T. (1988). *Production of radionuclides in the earth and their hydrologic significance, with emphasis on chlorine-36 and iodine-129*. Department of Hydrology and Water Resources, University of Arizona.

Falkowski, P., R.J. Scholes, E. Boyle, J. Canadell, D. Canfield, J. Elser, N. Gruber, K. Hibbard, P. Hogberg, S. Linder, F.T. Mackenzie, B. Moore, T. Pedersen, Y. Rosenthal, S. Seitzinger, V. Smetacek, and W. Steffen (2000). The global carbon cycle: A test of our knowledge of earth as a system. *Science* **290**(5490): 291-296. doi: 10.1126/science.290.5490.291

Falkowski, P.G., R.T. Barber, and V. Smetacek (1998). Biogeochemical controls and feedbacks on ocean primary production. *Science* **281**(5374): 200-206. doi: 10.1126/science.281.5374.200

Field, C.B., M.J. Behrenfeld, J.T. Randerson, and P. Falkowski (1998). Primary production of the biosphere: integrating terrestrial and oceanic components. *Science* **281**(5374): 237-240. doi: 10.1126/science.281.5374.237

Fifield, L.K. (2008). Accelerator mass spectrometry of long-lived heavy radionuclides, pp. 263-293, in P.P. Povinec [ed.], *Radioactivity in the Environment*. Analysis of Environmental Radionuclides.

Fitznar, H.P., J.M. Lobbes, and G. Kattner (1999). Determination of enantiomeric amino acids with high-performance liquid chromatography and pre-column derivatisation with o-phthaldialdehyde and N-isobutyrylcysteine in seawater and fossil samples (mollusks). *J Chromatogr, A* **832**(1-2): 123-132. doi: 10.1016/s0021-9673(98)01000-0

Flerus, R., B.P. Koch, P. Schmitt-Kopplin, M. Witt, and G. Kattner (2011). Molecular level investigation of reactions between dissolved organic matter and extraction solvents using FT-ICR MS. *Mar Chem* **124**(1-4): 100-107. doi: 10.1016/j.marchem.2010.12.006

Flerus, R., O.J. Lechtenfeld, B.P. Koch, S.L. McCallister, P. Schmitt-Kopplin, R. Benner, K. Kaiser, and G. Kattner (2012). A molecular perspective on the ageing of marine dissolved organic matter. *Biogeosciences* **9**(6): 1935-1955. doi: 10.5194/bg-9-1935-2012

Foldvik, A., T. Gammelsrød, and T. Tørresen (1985). Hydrographic observations from the Weddell Sea during the Norwegian Antarctic Research Expedition 1976/77. *Polar Res* **3**(2): 177-193

Francois, R., M. Frank, M.M.R. van der Loeff, and M.P. Bacon (2004). Th-230 normalization: An essential tool for interpreting sedimentary fluxes during the late Quaternary. *Paleoceanography* **19**(Pa1018). doi: 10.1029/2003pa000939

Frew, N., R.K. Nelson, and C.G. Johnson (2006). Sea slicks: variability in chemical composition and surface elasticity, pp. 45-56, in M. Gade, H. Hühnerfuss and G.M. Korenowski [eds.], *Marine surface films - chemical characteristics, influence on air-sea interactions and remote sensing*. Springer, Berlin Heidelberg.

Friedline, C.J., R.B. Franklin, S.L. McCallister, and M.C. Rivera (2012). Bacterial assemblages of the eastern Atlantic Ocean reveal both vertical and latitudinal biogeographic signatures. *Biogeosciences* **9**(6): 2177-2193. doi: 10.5194/bg-9-2177-2012

Frka, S., Z. Kozarac, and B. Ćosović (2009). Characterization and seasonal variations of surface active substances in the natural sea surface micro-layers of the coastal Middle Adriatic stations. *Estuar Coast Shelf S* **85**(4): 555-564. doi: 10.1016/j.ecss.2009.09.023

Frka, S., S. Pogorzelski, Z. Kozarac, and B. Ćosović (2012). Physicochemical signatures of natural sea films from Middle Adriatic stations. *J Phys Chem A*. doi: 10.1021/jp212430a

Gargett, A.E. (1984). Vertical eddy diffusivity in the ocean interior. *J Mar Res* **42**(2): 359-393. doi: 10.1357/002224084788502756

Gasol, J.M. and X.A.G. Moran (1999). Effects of filtration on bacterial activity and picoplankton community structure as assessed by flow cytometry. *Aquat Microb Ecol* **16**(3): 251-264. doi: 10.3354/ame016251

Gašparović, B., Z. Kozarac, A. Saliot, B. Ćosović, and D. Möbius (1998). Physicochemical characterization of natural and ex-situ reconstructed sea-surface microlayers. *J Colloid Interface Sci* **208**(1): 191-202. doi: 10.1006/jcis.1998.5792

Gašparović, B., M. Plavsic, B. Ćosović, and A. Saliot (2007). Organic matter characterization in the sea surface microlayers in the subarctic Norwegian fjords region. *Mar Chem* **105**(1-2): 1-14. doi: 10.1016/j.marchem.2006.12.010

Geibert, W., P. Assmy, D.C.E. Bakker, C. Hanfland, M. Hoppema, L.E. Pichevin, M. Schröder, J.N. Schwarz, I. Stimac, R. Usbeck, and A. Webb (2010). High productivity in an ice melting hot spot at the eastern boundary of the Weddell Gyre. *Global Biogeochem Cycles* **24**(Gb3007). doi: 10.1029/2009gb003657

Gerringa, L.J.A., M.J.W. Veldhuis, K.R. Timmermans, G. Sarthou, and H.J.W. de Baar (2006). Co-variance of dissolved Fe-binding ligands with phytoplankton characteristics in the Canary Basin. *Mar Chem* **102**(3-4): 276-290. doi: 10.1016/j.marchem.2006.05.004

Giordano, M., A. Norici, and R. Hell (2005). Sulfur and phytoplankton: acquisition, metabolism and impact on the environment. *New Phytol* **166**(2): 371-382. doi: 10.1111/j.1469-8137.2005.01335.x

Giovannoni, S.J. and K.L. Vergin (2012). Seasonality in ocean microbial communities. *Science* **335**(6069): 671-676. doi: 10.1126/science.1198078

Gledhill, M., P. McCormack, S. Ussher, E.P. Achterberg, R.F.C. Mantoura, and P.J. Worsfold (2004). Production of siderophore type chelates by mixed bacterioplankton populations in nutrient enriched seawater incubations. *Mar Chem* **88**(1-2): 75-83. doi: 10.1016/j.marchem.2004.03.003

Gledhill, M. and C.M.G. van den Berg (1994). Determination of complexation of iron(III) with natural organic complexing ligands in seawater using cathodic stripping voltammetry. *Mar Chem* **47**(1): 41-54. doi: 10.1016/0304-4203(94)90012-4

Godwin, H. (1962). Half-life of radiocarbon. *Nature* **195**(4845): 984-984. doi: 10.1038/195984a0

Gogou, A. and D.J. Repeta (2010). Particulate-dissolved transformations as a sink for semi-labile dissolved organic matter: Chemical characterization of high molecular weight dissolved and surface-active organic matter in seawater and in diatom cultures. *Mar Chem* **121**(1-4): 215-223. doi: 10.1016/j.marchem.2010.05.001

Goldberg, S.J., C.A. Carlson, B. Bock, N.B. Nelson, and D.A. Siegel (2010). Meridional variability in dissolved organic matter stocks and diagenetic state within the euphotic and mesopelagic zone of the North Atlantic subtropical gyre. *Mar Chem* **119**(1–4): 9-21. doi: 10.1016/j.marchem.2009.12.002

Goldberg, S.J., C.A. Carlson, M. Brzezinski, N.B. Nelson, and D.A. Siegel (2011). Systematic removal of neutral sugars within dissolved organic matter across ocean basins. *Geophys Res Lett* **38**(L17606). doi: 10.1029/2011gl048620

Goldberg, S.J., C.A. Carlson, D.A. Hansell, N.B. Nelson, and D.A. Siegel (2009). Temporal dynamics of dissolved combined neutral sugars and the quality of dissolved organic matter in the Northwestern Sargasso Sea. *Deep Sea Res I* **56**(5): 672-685. doi: 10.1016/j.dsr.2008.12.013

Goldstein, A.H. and I.E. Galbally (2007). Known and unexplored organic constituents in the earth's atmosphere. *Environ Sci Technol* **41**(5): 1514-1521. doi: 10.1021/es072476p

Goldstone, J.V., M.J. Pullin, S. Bertilsson, and B.M. Voelker (2002). Reactions of hydroxyl radical with humic substances: Bleaching, mineralization, and production of bioavailable carbon substrates. *Environ Sci Technol* **36**(3): 364-372. doi: 10.1021/es0109646

Gonsior, M., B.M. Peake, W.T. Cooper, D. Podgorski, J. D'Andrilli, and W.J. Cooper (2009). Photochemically induced changes in dissolved organic matter identified by ultrahigh resolution Fourier transform ion cyclotron resonance mass spectrometry. *Environ Sci Technol* **43**(3): 698-703. doi: 10.1021/es8022804

Gonsior, M., B.M. Peake, W.T. Cooper, D.C. Podgorski, J. D'Andrilli, T. Dittmar, and W.J. Cooper (2011). Characterization of dissolved organic matter across the Subtropical Convergence off the South Island, New Zealand. *Mar Chem* **123**(1-4): 99-110. doi: 10.1016/j.marchem.2010.10.004

Gordon, A.L. and B.A. Huber (1990). Southern Ocean winter mixed layer. *J Geophys Res* **95**(C7): 11655-11672. doi: 10.1029/JC095iC07p11655

Gram, L., H.P. Grossart, A. Schlingloff, and T. Kiorboe (2002). Possible quorum sensing in marine snow bacteria: Production of acylated homoserine lactones by Roseobacter strains isolated from marine snow. *Appl Environ Microbiol* **68**(8): 4111-4116. doi: 10.1128/aem.68.8.4111-4116.2002

Gruber, D.F., J.P. Simjouw, S.P. Seitzinger, and G.L. Taghon (2006). Dynamics and characterization of refractory dissolved organic matter produced by a pure bacterial culture in an experimental predator-prey system. *Appl Environ Microbiol* **72**(6): 4184-4191. doi: 10.1128/aem.02882-05

Gruber, N., M. Gloor, S.E.M. Fletcher, S.C. Doney, S. Dutkiewicz, M.J. Follows, M. Gerber, A.R. Jacobson, F. Joos, K. Lindsay, D. Menemenlis, A. Mouchet, S.A. Muller, J.L. Sarmiento, and T. Takahashi (2009). Oceanic sources, sinks, and transport of atmospheric CO2. *Global Biogeochem Cycles* **23**(Gb1005). doi: 10.1029/2008gb003349

Gschwend, P.M. and R.P. Schwarzenbach (1992). Physical chemistry of organic compounds in the marine environment. *Mar Chem* **39**(1–3): 187-207. doi: 10.1016/0304-4203(92)90101-f

Guitart, C., N. García-Flor, J.M. Bayona, and J. Albaigés (2007). Occurrence and fate of polycyclic aromatic hydrocarbons in the coastal surface microlayer. *Mar Pollut Bull* **54**(2): 186-194. doi: 10.1016/j.marpolbul.2006.10.008

Guo, L.D., C.L. Ping, and R.W. Macdonald (2007). Mobilization pathways of organic carbon from permafrost to arctic rivers in a changing climate. *Geophys Res Lett* **34**(L13603). doi: 10.1029/2007gl030689

Guo, L.D. and P.H. Santschi (2000). Sedimentary sources of old high molecular weight dissolved organic carbon from the ocean margin benthic nepheloid layer. *Geochim Cosmochim Acta* **64**(4): 651-660

Guo, L.D., P.H. Santschi, L.A. Cifuentes, S.E. Trumbore, and J. Southon (1996). Cycling of high-molecular-weight dissolved organic matter in the middle Atlantic bight as revealed by carbon isotopic (C-13 and C-14) signatures. *Limnol Oceanogr* **41**(6): 1242-1252

Guo, L.D., P.H. Santschi, and K.W. Warnken (2000a). Trace metal composition of colloidal organic material in marine environments. *Mar Chem* **70**(4): 257-275. doi: 10.1016/S0304-4203(00)00031-1

Guo, L.D., L.S. Wen, D.G. Tang, and P.H. Santschi (2000b). Re-examination of cross-flow ultrafiltration for sampling aquatic colloids: evidence from molecular probes. *Mar Chem* **69**(1-2): 75-90. doi: 10.1016/s0304-4203(99)00097-3

Gustafsson, O. and P.M. Gschwend (1997). Aquatic colloids: Concepts, definitions, and current challenges. *Limnol Oceanogr* **42**(3): 519-528

Gustafsson, O., B.E. van Dongen, J.E. Vonk, O.V. Dudarev, and I.P. Semiletov (2011). Widespread release of old carbon across the Siberian Arctic echoed by its large rivers. *Biogeosciences* **8**(6): 1737-1743. doi: 10.5194/bg-8-1737-2011

Hammer, K.D. and G. Kattner (1986). Dissolved free amino acids in the marine environment: a carbon to nitrogen ratio shift during diatom blooms. *Mar Ecol Prog Ser* **31**(1): 35-45. doi: 10.3354/meps031035

Hansell, D.A. (2002). DOC in the global ocean carbon cycle, pp. 685-715, in D.A. Hansell and C.A. Carlson [eds.], *Biogeochemistry of marine dissolved organic matter*. Academic Press, Elsevier Science, San Diego, USA.

Hansell, D.A. (2013). Recalcitrant dissolved organic carbon fractions. *Ann Rev Mar Sci* **5**(1): in press. doi: 10.1146/annurev-marine-120710-100757

Hansell, D.A. and C.A. Carlson (1998a). Deep-ocean gradients in the concentration of dissolved organic carbon. *Nature* **395**(6699): 263-266. doi: 10.1038/26200

——— (1998b). Net community production of dissolved organic carbon. *Global Biogeochem Cycles* **12**(3): 443-453. doi: 10.1029/98GB01928

——— (2001). Biogeochemistry of total organic carbon and nitrogen in the Sargasso Sea: control by convective overturn. *Deep Sea Res II* **48**(8-9): 1649-1667. doi: 10.1016/s0967-0645(00)00153-3

Hansell, D.A., C.A. Carlson, D.J. Repeta, and R. Schlitzer (2009). Dissolved organic matter in the ocean: A controversy stimulates new insights. *Oceanography* **22**(4): 202-211. doi: 10.5670/oceanog.2009.109

Hansell, D.A., C.A. Carlson, and R. Schlitzer (2012). Net removal of major marine dissolved organic carbon fractions in the subsurface ocean. *Global Biogeochem Cycles* **26**(GB1016). doi: 10.1029/2011gb004069

Hansell, D.A., C.A. Carlson, and Y. Suzuki (2002). Dissolved organic carbon export with North Pacific Intermediate Water formation. *Global Biogeochem Cycles* **16**. doi: 10.1029/2000gb001361

Hansman, R.L., S. Griffin, J.T. Watson, E.R.M. Druffel, A.E. Ingalls, A. Pearson, and L.I. Aluwihare (2009). The radiocarbon signature of microorganisms in the mesopelagic ocean. *Proc Natl Acad Sci USA* **106**(16): 6513-6518. doi: 10.1073/pnas.0810871106

Hardy, E.P., P.W. Krey, and H.L. Volchok (1973). Global inventory and distribution of fallout Plutonium. *Nature* **241**(5390): 444-445. doi: 10.1038/241444a0

Hardy, J.T. (1982). The sea-surface microlayer: Biology, chemistry and anthropogenic enrichment. *Prog Oceanogr* **11**(4): 307-328. doi: 10.1016/0079-6611(82)90001-5

Hardy, J.T. and C.W. Apts (1984). The sea-surface microlayer: phytoneuston productivity and effects of atmospheric particulate matter. *Mar Biol* **82**(3): 293-300. doi: 10.1007/bf00392409

Harvey, G.R., D.A. Boran, S.R. Piotrowicz, and C.P. Weisel (1984). Synthesis of marine humic substances from unsaturated lipids. *Nature* **309**(5965): 244-246. doi: 10.1038/309244a0

Hearn, M.T.W. and M.I. Aguilar (1987). High-performance liquid chromatography of amino acids, peptides and proteins: LXXIII. Investigations on the relationships between molecular structure, retention and band-broadening properties of polypeptides separated by reversed-phase high-performance liquid chromatography. *J Chromatogr, A* **397**: 47-70. doi: 10.1016/S0021-9673(01)84989-X

Hedges, J.I. (1992). Global biogeochemical cycles: progress and problems. *Mar Chem* **39**(1-3): 67-93. doi: 10.1016/0304-4203(92)90096-S

Hedges, J.I., J.A. Baldock, Y. Gelinas, C. Lee, M. Peterson, and S.G. Wakeham (2001). Evidence for non-selective preservation of organic matter in sinking marine particles. *Nature* **409**(6822): 801-804. doi: 10.1038/35057247

Hedges, J.I., G. Eglinton, P.G. Hatcher, D.L. Kirchman, C. Arnosti, S. Derenne, R.P. Evershed, I. Kogel-Knabner, J.W. de Leeuw, R. Littke, W. Michaelis, and J. Rullkötter (2000). The molecularly-uncharacterized component of nonliving organic matter in natural environments. *Org Geochem* **31**(10): 945-958. doi: 10.1016/S0146-6380(00)00096-6

Hedges, J.I., P.G. Hatcher, J.R. Ertel, and K.J. Meyers-Schulte (1992). A comparison of dissolved humic substances from seawater with Amazon River counterparts by 13C-NMR spectrometry. *Geochim Cosmochim Acta* **56**(4): 1753-1757. doi: 10.1016/0016-7037(92)90241-a

Hedges, J.I. and R.G. Keil (1995). Sedimentary organic matter preservation: an assessment and speculative synthesis. *Mar Chem* **49**(2-3): 81-115. doi: 10.1016/0304-4203(95)00008-f

Hedges, J.I., R.G. Keil, and R. Benner (1997). What happens to terrestrial organic matter in the ocean? *Org Geochem* **27**(5-6): 195-212. doi: 10.1016/S0146-6380(97)00066-1

Hedges, J.I. and J.M. Oades (1997). Comparative organic geochemistries of soils and marine sediments. *Org Geochem* **27**(7-8): 319-361

Henderson, G.M. (2002). Seawater (U-234/U-238) during the last 800 thousand years. *Earth Planet Sci Lett* **199**(1-2): 97-110. doi: 10.1016/s0012-821x(02)00556-3

Henderson, G.M. and R.F. Anderson (2003). The U-series toolbox for Paleoceanography. *Rev Mineral Geochem* **52**(1): 493-531. doi: 10.2113/0520493

Henson, S.A., R. Sanders, E. Madsen, P.J. Morris, F. Le Moigne, and G.D. Quartly (2011). A reduced estimate of the strength of the ocean's biological carbon pump. *Geophys Res Lett* **38**(L04606). doi: 10.1029/2011gl046735

Hernes, P.J. and R. Benner (2006). Terrigenous organic matter sources and reactivity in the North Atlantic Ocean and a comparison to the Arctic and Pacific oceans. *Mar Chem* **100**(1-2): 66-79. doi: 10.1016/j.marchem.2005.11.003

Hertkorn, N., R. Benner, M. Frommberger, P. Schmitt-Kopplin, M. Witt, K. Kaiser, A. Kettrup, and J.I. Hedges (2006). Characterization of a major refractory component of marine dissolved organic matter. *Geochim Cosmochim Acta* **70**(12): 2990-3010. doi: 10.1016/j.gca.2006.03.021

Hertkorn, N., M. Frommberger, M. Witt, B.P. Koch, P. Schmitt-Kopplin, and E.M. Perdue (2008). Natural organic matter and the event horizon of mass spectrometry. *Anal Chem* **80**(23): 8908-8919. doi: 10.1021/ac800464g

Hertkorn, N., M. Harir, B.P. Koch, B. Michalke, P. Grill, and P. Schmitt-Kopplin (2012). High field NMR spectroscopy and FTICR mass spectrometry: powerful discovery tools for the molecular level characterization of marine dissolved

organic matter from the South Atlantic Ocean. *Biogeosciences Discuss* **9**(1): 745-833. doi: 10.5194/bgd-9-745-2012

Hertkorn, N., C. Ruecker, M. Meringer, R. Gugisch, M. Frommberger, E.M. Perdue, M. Witt, and P. Schmitt-Kopplin (2007). High-precision frequency measurements: indispensable tools at the core of the molecular-level analysis of complex systems. *Anal Bioanal Chem* **389**: 1311-1327

Heumann, K.G. (2004). Isotope-dilution ICP-MS for trace element determination and speciation: from a reference method to a routine method? *Anal Bioanal Chem* **378**(2): 318-329. doi: 10.1007/s00216-003-2325-z

Heumann, K.G., L. Rottmann, and J. Vogl (1994). Elemental speciation with liquid chromatography-inductively coupled plasma isotope dilution mass spectrometry. *J Anal At Spectrom* **9**: 1351-1355. doi: 10.1039/ja9940901351

Hirose, K. (1994). Speciation of particulate uranium in seawater: Mass balance analysis of sequential leaching experiments. *J Radioanal Nucl Chem* **181**(1): 11-24. doi: 10.1007/BF02037543

——— (1996). Determination of a strong organic ligand dissolved in seawater: Thorium-complexing capacity of oceanic dissolved organic matter. *J Radioanal Nucl Chem* **204**(1): 193-204. doi: 10.1007/BF02060880

——— (2006). Chemical speciation of trace metals in seawater: a review. *Anal Sci* **22**(8): 1055-1063. doi: 10.2116/analsci.22.1055

Holmes, R.M., J.W. McClelland, P.A. Raymond, B.B. Frazer, B.J. Peterson, and M. Stieglitz (2008). Lability of DOC transported by Alaskan rivers to the Arctic Ocean. *Geophys Res Lett* **35**(L03402). doi: 10.1029/2007gl032837

Hopkinson, C.S. and J.J. Vallino (2005). Efficient export of carbon to the deep ocean through dissolved organic matter. *Nature* **433**(7022): 142-145. doi: 10.1038/nature03191

Hoppema, M., E. Fahrbach, M.H.C. Stoll, and H.J.W. de Baar (1999). Annual uptake of atmospheric CO2 by the Weddell Sea derived from a surface layer balance, including estimations of entrainment and new production. *J Mar Syst* **19**(4): 219-233. doi: 10.1016/s0924-7963(98)00091-8

Hu, Z.C., S.H. Hu, S. Gao, Y.S. Liu, and S.L. Lin (2004). Volatile organic solvent-induced signal enhancements in inductively coupled plasma-mass spectrometry: a case study of methanol and acetone. *Spectrochim Acta, Part B* **59**(9): 1463-1470. doi: 10.1016/j.sab.2004.07.007

Hunter, K.A. and P.S. Liss (1981). Organic sea surface films, pp. 259-298, in E.K. Duursma and R. Dawson [eds.], *Marine organic chemistry*. Elsevier Oceanography Series. Elsevier Scientific Publishing Company, Amsterdam.

Hutta, M., R. Gora, R. Halko, and M. Chalanyova (2011). Some theoretical and practical aspects in the separation of humic substances by combined liquid chromatography methods. *J Chromatogr, A* **1218**(49): 8946-8957. doi: 10.1016/j.chroma.2011.06.107

Hwang, J., E.R.M. Druffel, T.I. Eglinton, and D.J. Repeta (2006a). Source(s) and cycling of the nonhydrolyzable organic fraction of oceanic particles. *Geochim Cosmochim Acta* **70**(20): 5162-5168. doi: 10.1016/j.gca.2006.07.020

Hwang, J.S. and E.R.M. Druffel (2003). Lipid-like material as the source of the uncharacterized organic carbon in the ocean? *Science* **299**(5608): 881-884. doi: 10.1126/science.1078508

Hwang, J.S., E.R.M. Druffel, and J.E. Bauer (2006b). Incorporation of aged dissolved organic carbon (DOC) by oceanic particulate organic carbon (POC): An experimental approach using natural carbon isotopes. *Mar Chem* **98**(2-4): 315-322. doi: 10.1016/j.marchem.2005.10.008

Ivanovich, M. and A. Murray (1992). Spectroscopic methods, in M. Ivanovich and R.S. Harmon [eds.], *Uranium series disequilibrium: Applications to environmental problems*. Clarendon Press, Oxford.

Iwahata, D., K. Hirayama, and H. Miyano (2008). A highly sensitive analytical method for metal-labelled amino acids by HPLC/ICP-MS. *J Anal At Spectrom* **23**(8): 1063-1067. doi: 10.1039/b802862a

Jacquet, S.H.M., P.J. Lam, T. Trull, and F. Dehairs (2011). Carbon export production in the subantarctic zone and polar front zone south of Tasmania. *Deep Sea Res II* **58**(21–22): 2277-2292. doi: 10.1016/j.dsr2.2011.05.035

Jakuba, R.W., J.W. Moffett, and S.T. Dyhrman (2008). Evidence for the linked biogeochemical cycling of zinc, cobalt, and phosphorus in the western North Atlantic Ocean. *Global Biogeochem Cycles* **22**(GB4012). doi: 10.1029/2007GB003119

Janos, P. (2003). Separation methods in the chemistry of humic substances. *J Chromatogr, A* **983**(1-2): 1-18. doi: 10.1016/S0021-9673(02)01687-4

Jenkins, W.J. and P.B. Rhines (1980). Tritium in the deep North Atlantic Ocean. *Nature* **286**(5776): 877-880. doi: 10.1038/286877a0

Jiao, N., G.J. Herndl, D.A. Hansell, R. Benner, G. Kattner, S.W. Wilhelm, D.L. Kirchman, M.G. Weinbauer, T. Luo, F. Chen, and F. Azam (2010). Microbial production of recalcitrant dissolved organic matter: long-term carbon storage in the global ocean. *Nat Rev Microbiol* **8**(8): 593-599. doi: 10.1038/nrmicro2386

Jickells, T.D., Z.S. An, K.K. Andersen, A.R. Baker, G. Bergametti, N. Brooks, J.J. Cao, P.W. Boyd, R.A. Duce, K.A. Hunter, H. Kawahata, N. Kubilay, J. laRoche, P.S. Liss, N. Mahowald, J.M. Prospero, A.J. Ridgwell, I. Tegen, and R. Torres (2005). Global iron connections between desert dust, ocean biogeochemistry, and climate. *Science* **308**(5718): 67-71. doi: 10.1126/science.1105959

Johnson, B.D. and P.J. Wangersky (1985). Seawater filtration: particle flow and impaction considerations. *Limnol Oceanogr* **30**(5): 966-971

Jørgensen, N.O.G., R. Stepanaukas, A.G.U. Pedersen, M. Hansen, and O. Nybroe (2003). Occurrence and degradation of peptidoglycan in aquatic environments. *FEMS Microbiol Ecol* **46**(3): 269-280. doi: 10.1016/s0168-6496(03)00194-6

Joux, F., H. Agogue, I. Obernosterer, C. Dupuy, T. Reinthaler, G.J. Herndl, and P. Lebaron (2006). Microbial community structure in the sea surface microlayer at two contrasting coastal sites in the northwestern Mediterranean Sea. *Aquat Microb Ecol* **42**(1): 91-104. doi: 10.3354/ame042091

Joyce, T.M., C. Wunsch, and S.D. Pierce (1986). Synoptic Gulf Stream velocity profiles through simultaneous inversion of hydrographic and acoustic doppler data. *J Geophys Res-Oceans* **91**(C6): 7573-7585. doi: 10.1029/JC091iC06p07573

Kaczynski, S.E. and R.J. Kieber (1994). Hydrophobic C18 bound organic complexes of chromium and their potential impact on the geochemistry of Cr in natural waters. *Environ Sci Technol* **28**(5): 799-804. doi: 10.1021/es00054a009

Kähler, P., P.K. Bjørnsen, K. Lochte, and A. Antia (1997). Dissolved organic matter and its utilization by bacteria during spring in the Southern Ocean. *Deep Sea Res II* **44**(1-2): 341-353. doi: 10.1016/s0967-0645(96)00071-9

Kähler, P. and W. Koeve (2001). Marine dissolved organic matter: Can its C:N ratio explain carbon overconsumption? *Deep Sea Res I* **48**(1): 49-62. doi: 10.1016/S0967-0637(00)00034-0

Kaiser, K. and R. Benner (2000). Determination of amino sugars in environmental samples with high salt content by high performance anion exchange chromatography and pulsed amperometric detection. *Anal Chem* **72**(11): 2566-2572. doi: 10.1021/ac991407t

——— (2005). Hydrolysis-induced racemization of amino acids. *Limnol Oceanogr: Methods* **3**: 318-325

——— (2008). Major bacterial contribution to the ocean reservoir of detrital organic carbon and nitrogen. *Limnol Oceanogr* **53**(1): 99-112. doi: 10.4319/lo.2008.53.1.0099

——— (2009). Biochemical composition and size distribution of organic matter at the Pacific and Atlantic time-series stations. *Mar Chem* **113**(1-2): 63-77. doi: 10.1016/j.marchem.2008.12.004

Kaiser, K. and R. Benner (2011). Characterization of lignin by gas chromatography and mass spectrometry using a simplified CuO oxidation method. *Anal Chem* **84**(1): 459-464. doi: 10.1021/ac202004r

——— (2012). Organic matter transformations in the upper mesopelagic zone of the North Pacific: Chemical composition and linkages to microbial community structure. *J Geophys Res* **117**(C01023). doi: 10.1029/2011jc007141

Kalle, K. (1937). Meereskundliche chemische Untersuchungen mit Hilfe des Zeiss'schen Pulfrich Photometers. *Ann Hydrogr Berlin* **65**: 276-282

Karl, D.M. and K.M. Björkman (2002). Dynamics of DOP, pp. 249-366, in D.A. Hansell and C.A. Carlson [eds.], *Biogeochemistry of marine dissolved organic matter*. Academic Press, Elsevier Science, San Diego, USA.

Karl, D.M., D.V. Hebel, K. Björkman, and R.M. Letelier (1998). The role of dissolved organic matter release in the productivity of the oligotrophic North Pacific Ocean. *Limnol Oceanogr* **43**(6): 1270-1286

Karlsson, T., K. Elgh-Dalgren, E. Björn, and U. Skyllberg (2007). Complexation of cadmium to sulfur and oxygen functional groups in an organic soil. *Geochim Cosmochim Acta* **71**(3): 604-614. doi: 10.1016/j.gca.2006.10.011

Karner, M.B., E.F. DeLong, and D.M. Karl (2001). Archaeal dominance in the mesopelagic zone of the Pacific Ocean. *Nature* **409**(6819): 507-510. doi: 10.1038/35054051

Kattner, G. (1999). Storage of dissolved inorganic nutrients in seawater: poisoning with mercuric chloride. *Mar Chem* **67**(1-2): 61-66. doi: 10.1016/s0304-4203(99)00049-3

——— (2009). Dissolved organic and particulate nitrogen and phosphorous, pp. 179-190, in O. Wurl [ed.], *Practical guidelines for the analysis of seawater*. CRC Press Taylor & Francis Group.

Kattner, G. and H. Becker (1991). Nutrients and organic nitrogenous compounds in the marginal ice zone of the Fram Strait. *J Mar Syst* **2**(3–4): 385-394. doi: 10.1016/0924-7963(91)90043-t

Kattner, G. and U.H. Brockmann (1978). Fatty-acid composition of dissolved and particulate matter in surface films. *Mar Chem* **6**(3): 233-241. doi: 10.1016/0304-4203(78)90032-4

Kattner, G., K. Nagel, U.H. Brockmann, K.D. Hammer, and K. Eberlein (1983). Composition of natural surface films in the North Sea, pp. 662-670, in J. Sündermann and W. Lenz [eds.], *North Sea Dynamics*. Springer Verlag, Berlin, Heidelberg.

Kattner, G., K. Nagel, K. Eberlein, and K.D. Hammer (1985). Components of natural surface microlayers and subsurface water. *Oceanol Acta* **8**(2): 175-183

Kattner, G., M. Simon, and B.P. Koch (2011). Molecular characterization of dissolved organic matter and constraints for prokaryotic utilization, pp. 60-61, in N. Jiao, F. Azam and S. Sanders [eds.], *Microbial carbon pump in the ocean*. Science/AAAS, Washington, DC.

Kawakami, S.K., M. Gledhill, and E.P. Achterberg (2006a). Determination of phytochelatins and glutathione in phytoplankton from natural waters using HPLC with fluorescence detection. *TrAC, Trends Anal Chem* **25**(2): 133-142. doi: 10.1016/j.trac.2005.06.005

——— (2006b). Production of phytochelatins and glutathione by marine phytoplankton in response to metal stress. *Journal of Phycology* **42**(5): 975-989. doi: 10.1111/j.1529-8817.2006.00265.x

Kawasaki, N. and R. Benner (2006). Bacterial release of dissolved organic matter during cell growth and decline: molecular origin and composition. *Limnol Oceanogr* **51**(5): 2170-2180

Keeling, C.D. (1960). The concentration and isotopic abundances of carbon dioxide in the atmosphere. *Tellus* **12**(2)

Keil, R.G. and D.L. Kirchman (1999). Utilization of dissolved protein and amino acids in the northern Sargasso Sea. *Aquat Microb Ecol* **18**(3): 293-300. doi: 10.3354/ame018293

Keil, R.G., D.B. Montlucon, F.G. Prahl, and J.I. Hedges (1994). Sorptive preservation of labile organic matter in marine sediments. *Nature* **370**(6490): 549-552. doi: 10.1038/370549a0

Kido Soule, M.C., K. Longnecker, S.J. Giovannoni, and E.B. Kujawinski (2010). Impact of instrument and experiment parameters on reproducibility of ultrahigh resolution ESI FT-ICR mass spectra of natural organic matter. *Org Geochem* **41**(8): 725-733. doi: 10.1016/j.orggeochem.2010.05.017

Kieber, D.J., J. McDaniel, and K. Mopper (1989). Photochemical source of biological substrates in sea water: implications for carbon cycling. *Nature* **341**(6243): 637-639. doi: 10.1038/341637a0

Killops, S. and V. Killops (2005). *Introduction to Organic Geochemistry*, 2nd ed. Blackwell Science Ltd, Malden, USA.

Kim, S., L.A. Kaplan, R. Benner, and P.G. Hatcher (2004). Hydrogen-deficient molecules in natural riverine water samples - evidence for the existence of black carbon in DOM. *Mar Chem* **92**(1-4): 225-234. doi: 10.1016/j.marchem.2004.06.042

Kim, S., A.J. Simpson, E.B. Kujawinski, M.A. Freitas, and P.G. Hatcher (2003). High resolution electrospray ionization mass spectrometry and 2D solution NMR for the analysis of DOM extracted by C-18 solid phase disk. *Org Geochem* **34**(9): 1325-1335. doi: 10.1016/s0146-6380(03)00101-3

Kirchman, D.L. (1993). Leucine incorporation as a measure of biomass production by heterotrophic bacteria, pp. 509-512, in P.F. Kemp, J.J. Cole, B.F. Sherr and E.B. Sherr [eds.], *Handbook of Methods in Aquatic Microbial Ecology*. Lewis Publishers, New York.

Kirchman, D.L., B. Meon, H.W. Ducklow, C.A. Carlson, D.A. Hansell, and G.F. Steward (2001). Glucose fluxes and concentrations of dissolved combined neutral sugars (polysaccharides) in the Ross Sea and Polar Front Zone, Antarctica. *Deep Sea Res II* **48**(19-20): 4179-4197. doi: 10.1016/s0967-0645(01)00085-6

Kirchman, D.L., X.A.G. Moran, and H. Ducklow (2009). Microbial growth in the polar oceans - role of temperature and potential impact of climate change. *Nat Rev Microbiol* **7**(6): 451-459. doi: 10.1038/nrmicro2115

Kitayama, K., T. Hama, and K. Yanagi (2007). Bioreactivity of peptidoglycan in seawater. *Aquat Microb Ecol* **46**(1): 85-93. doi: 10.3354/ame046085

Knapp, A.N., D.M. Sigman, A.B. Kustka, S.A. Sañudo-Wilhelmy, and D.G. Capone (2012). The distinct nitrogen isotopic compositions of low and high molecular weight marine DON. *Mar Chem* **136–137**(0): 24-33. doi: 10.1016/j.marchem.2012.05.001

Knapp, A.N., D.M. Sigman, and F. Lipschultz (2005). N isotopic composition of dissolved organic nitrogen and nitrate at the Bermuda Atlantic time-series study site. *Global Biogeochem Cycles* **19**(Gb1018). doi: 10.1029/2004gb002320

Koch, B.P. and T. Dittmar (2006). From mass to structure: an aromaticity index for high-resolution mass data of natural organic matter. *Rapid Commun Mass Spectrom* **20**(5): 926-932. doi: 10.1002/rcm.2386

Koch, B.P., T. Dittmar, M. Witt, and G. Kattner (2007). Fundamentals of molecular formula assignment to ultrahigh resolution mass data of natural organic matter. *Anal Chem* **79**(4): 1758-1763. doi: 10.1021/ac061949s

Koch, B.P., W. Geibert, O.J. Lechtenfeld, M. Witt, and K. Fahl (2012). Natural radiation modifies the structure of organic matter in aqueous systems, *2012 Ocean Science Meeting* (Salt Palace Convention Center, Salt Lake City, Utah, USA).

Koch, B.P. and G. Kattner (2012). Sources and rapid biogeochemical transformation of dissolved organic matter in the Atlantic surface ocean. *Biogeosciences* **9**: 2597-2602. doi: 10.5194/bg-9-2597-2012

Koch, B.P., K.-U. Ludwichowski, G. Kattner, T. Dittmar, and M. Witt (2008). Advanced characterization of marine dissolved organic matter by combining reversed-phase liquid chromatography and FT-ICR-MS. *Mar Chem* **111**(3-4): 233-241. doi: 10.1016/j.marchem.2008.05.008

Koch, B.P., M. Witt, R. Engbrodt, T. Dittmar, and G. Kattner (2005). Molecular formulae of marine and terrigenous dissolved organic matter detected by electrospray ionization Fourier transform ion cyclotron resonance mass spectrometry. *Geochim Cosmochim Acta* **69**(13): 3299-3308. doi: 10.1016/j.gca.2005.02.027

Kolowith, L.C., E.D. Ingall, and R. Benner (2001). Composition and cycling of marine organic phosphorus. *Limnol Oceanogr* **46**(2): 309-320

Koprivnjak, J.F., P.H. Pfromm, E. Ingall, T.A. Vetter, P. Schmitt-Kopplin, N. Hertkorn, M. Frommberger, H. Knicker, and E.M. Perdue (2009). Chemical and spectroscopic characterization of marine dissolved organic matter isolated using coupled reverse osmosis-electrodialysis. *Geochim Cosmochim Acta* **73**(14): 4215-4231. doi: 10.1016/j.gca.2009.04.010

Korb, R.E., M.J. Whitehouse, P. Ward, M. Gordon, H.J. Venables, and A.J. Poulton (2012). Regional and seasonal differences in microplankton biomass, productivity, and structure across the Scotia Sea: Implications for the export of biogenic carbon. *Deep Sea Res II* **59–60**(0): 67-77. doi: 10.1016/j.dsr2.2011.06.006

Kramer, G.D. and G.J. Herndl (2004). Photo- and bioreactivity of chromophoric dissolved organic matter produced by marine bacterioplankton. *Aquat Microb Ecol* **36**(3): 239-246. doi: 10.3354/ame036239

Kreller, D.I., B.F. Turner, K. Namjesnik-Dejanovic, and P.A. Maurice (2005). Comparison of the effects of sonolysis and gamma-radiolysis on dissolved organic matter. *Environ Sci Technol* **39**(24): 9732-9737. doi: 10.1021/es051416l

Kretschmer, S., W. Geibert, M.M.R. van der Loeff, and G. Mollenhauer (2010). Grain size effects on Th-230(xs) inventories in opal-rich and carbonate-rich marine sediments. *Earth Planet Sci Lett* **294**(1-2): 131-142. doi: 10.1016/j.eps1.2010.03.021

Kruger, B.R., B.J. Dalzell, and E.C. Minor (2011). Effect of organic matter source and salinity on dissolved organic matter isolation via ultrafiltration and solid phase extraction. *Aquat Sci* **73**(3): 405-417. doi: 10.1007/s00027-011-0189-4

Kujawinski, E.B. (2011). The impact of microbial metabolism on marine dissolved organic matter. *Ann Rev Mar Sci* **3**: 567-599. doi: 10.1146/annurev-marine-120308-081003

Kujawinski, E.B. and M.D. Behn (2006). Automated analysis of electrospray ionization Fourier transform ion cyclotron resonance mass spectra of natural organic matter. *Anal Chem* **78**(13): 4363-4373. doi: 10.1021/ac0600306

Kujawinski, E.B., M.A. Freitas, X. Zang, P.G. Hatcher, K.B. Green-Church, and R.B. Jones (2002). The application of electrospray ionization mass spectrometry (ESI MS) to the structural characterization of natural organic matter. *Org Geochem* **33**(3): 171-180

Kujawinski, E.B., K. Longnecker, N.V. Blough, R.D. Vecchio, L. Finlay, J.B. Kitner, and S.J. Giovannoni (2009). Identification of possible source markers in marine dissolved organic matter using ultrahigh resolution mass spectrometry. *Geochim Cosmochim Acta* **73**(15): 4384-4399. doi: 10.1016/j.gca.2009.04.033

Kuznetsova, M., C. Lee, and J. Aller (2005). Characterization of the proteinaceous matter in marine aerosols. *Mar Chem* **96**(3-4): 359-377. doi: 10.1016/j.marchem.2005.03.007

Kuznetsova, M., C. Lee, J. Aller, and N. Frew (2004). Enrichment of amino acids in the sea surface microlayer at coastal and open ocean sites in the North Atlantic Ocean. *Limnol Oceanogr* **49**(5): 1605-1619. doi: 10.4319/lo.2004.49.5.1605

Laborda, F., J. Medrano, and J.R. Castillo (2000). Data acquisition of transient signals in inductively coupled plasma mass spectrometry. *Anal Chim Acta* **407**(1-2): 301-309

Laglera, L.M., G. Battaglia, and C.M.G. van den Berg (2011). Effect of humic substances on the iron speciation in natural waters by CLE/CSV. *Mar Chem* **127**(1-4): 134-143. doi: 10.1016/j.marchem.2011.09.003

Laglera, L.M. and C.M.G. van den Berg (2006). Photochemical oxidation of thiols and copper complexing ligands in estuarine waters. *Mar Chem* **101**(1-2): 130-140. doi: 10.1016/j.marchem.2006.01.006

——— (2009). Evidence for geochemical control of iron by humic substances in seawater. *Limnol Oceanogr* **54**(2): 610-619. doi: 10.4319/lo.2009.54.2.0610

Lahajnar, N., T. Rixen, B. Gaye-Haake, P. Schafer, and V. Ittekkot (2005). Dissolved organic carbon (DOC) fluxes of deep-sea sediments from the Arabian Sea and NE Atlantic. *Deep Sea Res II* **52**(14-15): 1947-1964. doi: 10.1016/j.dsr2.2005.05.006

Lal, D. (1988). Theoretically expected variations in the terrestrial cosmic-ray production rates of isotopes, p. 216, in G.C. Castagnoli [ed.], *Proceedings of the International School of Physics "Enrico Fermi", Course XCV* (Verenna on Lake Como, Villa Monastero). North-Holland Publishing Company, Amsterdam, The Netherlands.

Lang, S.Q., D.A. Butterfield, M.D. Lilley, H.P. Johnson, and J.I. Hedges (2006). Dissolved organic carbon in ridge-axis and ridge-flank hydrothermal systems. *Geochim Cosmochim Acta* **70**(15): 3830-3842. doi: 10.1016/j.gca.2006.04.031

LaRowe, D.E. and P. Van Cappellen (2011). Degradation of natural organic matter: A thermodynamic analysis. *Geochim Cosmochim Acta* **75**(8): 2030-2042. doi: 10.1016/j.gca.2011.01.020

Lass, K. and G. Friedrichs (2011). Revealing structural properties of the marine nanolayer from vibrational sum frequency generation spectra. *J Geophys Res-Oceans* **116**. doi: 10.1029/2010jc006609

Lechtenfeld, O.J., B.P. Koch, W. Geibert, K.-U. Ludwichowski, and G. Kattner (2011). Inorganics in organics: Quantification of organic phosphorus and sulfur and trace element speciation in natural organic matter using HPLC-ICPMS. *Anal Chem* **83**(23): 8968-8974. doi: 10.1021/ac201765a

Lechtenfeld, O.J., B.P. Koch, M. Witt, and G. Kattner (2010). Inorganics in organics: Tracking down the intrinsic equilibriums between organic molecules and trace elements in oceanic waters, *2010 AGU Fall Meeting* (San Francisco, California).

LeClair, J.P., J.L. Collett, and L.R. Mazzoleni (2012). Fragmentation analysis of water-soluble atmospheric organic matter using ultrahigh-resolution FT-ICR mass spectrometry. *Environ Sci Technol* **46**(8): 4312-4322. doi: 10.1021/es203509b

Lee, S. and J.A. Fuhrman (1987). Relationships between biovolume and biomass of naturally derived marine bacterioplankton. *Appl Environ Microbiol* **53**(6): 1298-1303

Lee, S.H., P.P. Povinec, E. Wyse, and M.A.C. Hotchkis (2008). Ultra-low-level determination of U-236 in IAEA marine reference materials by ICPMS and AMS. *Appl Radiat Isot* **66**(6-7): 823-828. doi: 10.1016/j.apradiso.2008.02.020

Legović, T. (1991). Exchange of water in a stratified estuary with an application to Krka (Adriatic Sea). *Mar Chem* **32**(2–4): 121-135. doi: 10.1016/0304-4203(91)90032-r

Legović, T., V. Žutić, Z. Gržetić, G. Cauwet, R. Precali, and D. Viličić (1994). Eutrophication in the Krka estuary. *Mar Chem* **46**(1–2): 203-215. doi: 10.1016/0304-4203(94)90056-6

Letscher, R.T., D.A. Hansell, and D. Kadko (2011). Rapid removal of terrigenous dissolved organic carbon over the Eurasian shelves of the Arctic Ocean. *Mar Chem* **123**(1-4): 78-87. doi: 10.1016/j.marchem.2010.10.002

Levin, I. and V. Hesshaimer (2000). Radiocarbon - A unique tracer of global carbon cycle dynamics. *Radiocarbon* **42**(1): 69-80

Levsen, K., H.-M. Schiebel, J.K. Terlouw, K.J. Jobst, M. Elend, A. Preiß, H. Thiele, and A. Ingendoh (2007). Even-electron ions: a systematic study of the neutral species lost in the dissociation of quasi-molecular ions. *J Mass Spectrom* **42**(8): 1024-1044. doi: 10.1002/jms.1234

Li, W.C., D.M. Victor, and C.L. Chakrabarti (1980). Effect of pH and uranium concentration on interaction of uranium(VI) and uranium(IV) with organic ligands in aqueous solutions. *Anal Chem* **52**(3): 520-523. doi: 10.1021/ac50053a033

Lindemann, T., J. Hinrichs, M. Hamester, and J. Wills (2007). *Simultaneous phosporus and sulfur speciation by HPLC interfaced with high resolution ICP-MS*, Application Note 30076. Thermo Fischer Scientific.

Liss, P.S. and R.A. Duce [eds.] (1997). *The sea surface and global change*. Cambrigde University Press, Cambridge, United Kingdom.

Liu, S. and D. Beauchemin (2006). Effect of methanol and sodium dodecylsulfate on radial profiles of ion abundance in inductively coupled plasma mass

spectrometry. *Spectrochim Acta, Part B* **61**(3): 319-325. doi: 10.1016/j.sab.2006.02.010

Liu, Z., R.L. Sleighter, J. Zhong, and P.G. Hatcher (2011). The chemical changes of DOM from black waters to coastal marine waters by HPLC combined with ultrahigh resolution mass spectrometry. *Estuar Coast Shelf S* **92**(2): 205-216. doi: 10.1016/j.ecss.2010.12.030

Llewelyn, J.M., W.M. Landing, A.G. Marshall, and W.T. Cooper (2002). Electrospray ionization Fourier transform ion cyclotron resonance mass spectrometry of dissolved organic phosphorus species in a treatment wetland after selective isolation and concentration. *Anal Chem* **74**(3): 600-606. doi: 10.1021/ac010909f

Lobinski, R., D. Schaumlöffel, and J. Szpunar (2006). Mass spectrometry in bioinorganic analytical chemistry. *Mass Spectrom Rev* **25**(2): 255-289. doi: 10.1002/mas.20069

Lochte, K., P.K. Bjørnsen, H. Giesenhagen, and A. Weber (1997). Bacterial standing stock and production and their relation to phytoplankton in the Southern Ocean. *Deep Sea Res II* **44**(1–2): 321-340. doi: 10.1016/s0967-0645(96)00081-1

Loh, A.N. and J.E. Bauer (2000). Distribution, partitioning and fluxes of dissolved and particulate organic C, N and P in the eastern North Pacific and Southern Oceans. *Deep Sea Res I* **47**(12): 2287-2316. doi: 10.1016/S0967-0637(00)00027-3

Loh, A.N., J.E. Bauer, and E.R.M. Druffel (2004). Variable ageing and storage of dissolved organic components in the open ocean. *Nature* **430**(7002): 877-881. doi: 10.1038/nature02780

Lokits, K.E., P.A. Limbach, and J.A. Caruso (2009). Interfaces for capillary LC with ICPMS detection: A comparison of nebulizers/spray chamber configurations. *J Anal At Spectrom* **24**(4): 528-534. doi: 10.1039/b820121h

Lomans, B.P., C. van der Drift, A. Pol, and H.J.M. Op den Camp (2002). Microbial cycling of volatile organic sulfur compounds. *Cell Mol Life Sci* **59**(4): 575-588. doi: 10.1007/s00018-002-8450-6

Lomas, M.W., A.L. Burke, D.A. Lomas, D.W. Bell, C. Shen, S.T. Dyhrman, and J.W. Ammerman (2010). Sargasso Sea phosphorus biogeochemistry: an important role for dissolved organic phosphorus (DOP). *Biogeosciences* **7**(2): 695-710

Longhurst, A. (2007). *Ecological geography of the sea*, 2nd ed. Academic Press, Burlington, San Diego, London.

Longnecker, K. and E.B. Kujawinski (2011). Composition of dissolved organic matter in groundwater. *Geochim Cosmochim Acta* **75**(10): 2752-2761. doi: 10.1016/j.gca.2011.02.020

Louis, Y., C. Garnier, V. Lenoble, S. Mounier, N. Cukrov, D. Omanovic, and I. Pizeta (2009). Kinetic and equilibrium studies of copper-dissolved organic matter complexation in water column of the stratified Krka River Estuary (Croatia). *Mar Chem* **114**(3-4): 110-119. doi: 10.1016/j.marchem.2009.04.006

Luna, G.M., S. Bianchelli, F. Decembrini, E. De Domenico, R. Danovaro, and A. Dell'Anno (2012). The dark portion of the Mediterranean Sea is a bioreactor of organic matter cycling. *Global Biogeochem Cycles* **26**(GB2017). doi: 10.1029/2011gb004168

Luoma, S.N. and P.S. Rainbow (2005). Why is metal bioaccumulation so variable? Biodynamics as a unifying concept. *Environ Sci Technol* **39**(7): 1921-1931. doi: 10.1021/es048947e

Mackey, D.J. (1982). An investigation of the suitability of amberlite XAD-1 resin for studying trace metal speciation in seawater. *Mar Chem* **11**(2): 169-181. doi: 10.1016/0304-4203(82)90040-8

——— (1983). Metal-organic complexes in seawater - An investigation of naturally occurring complexes of Cu, Zn, Fe, Mg, Ni, Cr, Mn and Cd using high-performance liquid chromatography with atomic fluorescence detection. *Mar Chem* **13**(3): 169-180. doi: 10.1016/0304-4203(83)90012-9

——— (1985). HPLC analyses of metal-organics in seawater - interference effects attributed to stationary-phase free silanols. *Mar Chem* **16**(2): 105-119. doi: 10.1016/0304-4203(85)90016-7

Mackey, D.J. and H.W. Higgins (1988). Reversed-phase chromatographic separation and analysis of marine metal--organic complexes. *J Chromatogr, A* **436**: 243-257. doi: 10.1016/S0021-9673(00)94582-5

Macrellis, H.M., C.G. Trick, E.L. Rue, G. Smith, and K.W. Bruland (2001). Collection and detection of natural iron-binding ligands from seawater. *Mar Chem* **76**(3): 175-187. doi: 10.1016/S0304-4203(01)00061-5

Mahaffey, C., R.G. Williams, G.A. Wolff, and W.T. Anderson (2004). Physical supply of nitrogen to phytoplankton in the Atlantic Ocean. *Global Biogeochem Cycles* **18**(Gb1034). doi: 10.1029/2003gb002129

Manceau, A. and A. Matynia (2010). The nature of Cu bonding to natural organic matter. *Geochim Cosmochim Acta* **74**(9): 2556-2580. doi: 10.1016/j.gca.2010.01.027

Mangini, A., C. Sonntag, G. Bertsch, and E. Muller (1979). Evidence for a higher natural uranium content in world rivers. *Nature* **278**(5702): 337-339. doi: 10.1038/278337a0

Mann, D.K. and G.T.F. Wong (1993). 'Strongly bound' uranium in marine waters: occurrence and analytical implications. *Mar Chem* **42**(1): 25-37. doi: 10.1016/0304-4203(93)90247-L

Mann, P.J., A. Davydova, N. Zimov, R.G.M. Spencer, S. Davydov, E. Bulygina, S. Zimov, and R.M. Holmes (2012). Controls on the composition and lability of dissolved organic matter in Siberia's Kolyma River basin. *J Geophys Res-Biogeosci* **117**(G01028). doi: 10.1029/2011jg001798

Mannino, A. and H.R. Harvey (1999). Lipid composition in particulate and dissolved organic matter in the Delaware Estuary: Sources and diagenetic patterns. *Geochim Cosmochim Acta* **63**(15): 2219-2235. doi: 10.1016/s0016-7037(99)00128-3

Mao, J.D., X.Q. Kong, K. Schmidt-Rohr, J.J. Pignatello, and E.M. Perdue (2012). Advanced solid-state NMR characterization of marine dissolved organic matter isolated using the coupled reverse osmosis/electrodialysis method. *Environ Sci Technol* **46**(11): 5806-5814. doi: 10.1021/es300521e

Marsden, O.J., F.R. Livens, J.P. Day, L.K. Fifield, and P.S. Goodall (2001). Determination of U-236 in sediment samples by accelerator mass spectrometry. *Analyst* **126**(5): 633-636. doi: 10.1039/b009764k

Marshall, A.G., C.L. Hendrickson, and G.S. Jackson (1998). Fourier transform ion cyclotron resonance mass spectrometry: a primer. *Mass Spectrom Rev* **17**(1): 1-35. doi: 10.1002/(SICI)1098-2787(1998)17:1<1::AID-MAS1>3.0.CO;2-K

Martin, J.H. and S.E. Fitzwater (1988). Iron deficiency limits phytoplankton growth in the north-east Pacific subarctic. *Nature* **331**(6154): 341-343. doi: 10.1038/331341a0

Martinez-Garcia, A., A. Rosell-Mele, S.L. Jaccard, W. Geibert, D.M. Sigman, and G.H. Haug (2011). Southern Ocean dust-climate coupling over the past four million years. *Nature* **476**(7360): 312-U141. doi: 10.1038/nature10310

Martinez, J.S., G.P. Zhang, P.D. Holt, H.T. Jung, C.J. Carrano, M.G. Haygood, and A. Butler (2000). Self-assembling amphiphilic siderophores from marine bacteria. *Science* **287**(5456): 1245-1247. doi: 10.1126/science.287.5456.1245

Mather, R.L., S.E. Reynolds, G.A. Wolff, R.G. Williams, S. Torres-Valdes, E.M.S. Woodward, A. Landolfi, X. Pan, R. Sanders, and E.P. Achterberg (2008). Phosphorus cycling in the North and South Atlantic Ocean subtropical gyres. *Nat Geosci* **1**(7): 439-443. doi: 10.1038/ngeo232

Mawji, E., M. Gledhill, J.A. Milton, G.A. Tarran, S. Ussher, A. Thompson, G.A. Wolff, P.J. Worsfold, and E.P. Achterberg (2008). Hydroxamate siderophores: occurrence and importance in the Atlantic Ocean. *Environ Sci Technol* **42**(23): 8675-8680. doi: 10.1021/es801884r

Mayer, L.M. (1999). Extent of coverage of mineral surfaces by organic matter in marine sediments. *Geochim Cosmochim Acta* **63**(2): 207-215. doi: 10.1016/s0016-7037(99)00028-9

McCallister, S.L., J.E. Bauer, and E.A. Canuel (2006). Bioreactivity of estuarine dissolved organic matter: A combined geochemical and microbiological approach. *Limnol Oceanogr* **51**(1): 94-100

McCarthy, J.F., J. Ilavsky, J.D. Jastrow, L.M. Mayer, E. Perfect, and J. Zhuang (2008). Protection of organic carbon in soil microaggregates via restructuring of aggregate porosity and filling of pores with accumulating organic matter. *Geochim Cosmochim Acta* **72**(19): 4725-4744. doi: 10.1016/j.gca.2008.06.015

McCarthy, M., T. Pratum, J. Hedges, and R. Benner (1997). Chemical composition of dissolved organic nitrogen in the ocean. *Nature* **390**(6656): 150-154. doi: 10.1038/36535

McCarthy, M.D., S.R. Beaupre, B.D. Walker, I. Voparil, T.P. Guilderson, and E.R.M. Druffel (2011). Chemosynthetic origin of C-14-depleted dissolved organic matter in a ridge-flank hydrothermal system. *Nat Geosci* **4**(1): 32-36. doi: 10.1038/ngeo1015

Meyers-Schulte, K.J. and J.I. Hedges (1986). Molecular evidence for a terrestrial component of organic matter dissolved in ocean water. *Nature* **321**(6065): 61-63. doi: 10.1038/321061a0

Middelburg, J.J. (2011). Chemoautotrophy in the ocean. *Geophys Res Lett* **38**(L24604). doi: 10.1029/2011gl049725

Millero, F.J., R. Woosley, B. Ditrolio, and J. Waters (2009). Effect of ocean acidification on the speciation of metals in seawater. *Oceanography* **22**(4): 72-85

Mills, M.M., C. Ridame, M. Davey, J. La Roche, and R.J. Geider (2004). Iron and phosphorus co-limit nitrogen fixation in the eastern tropical North Atlantic. *Nature* **429**(6989): 292-294. doi: 10.1038/nature02550

Mimura, T. and J.C. Romano (1985). Muramic acid measurements for bacterial investigations in marine environments by high-pressure liquid chromatography. *Appl Environ Microbiol* **50**(2): 229-237

Mollenhauer, G., T.I. Eglinton, E.C. Hopmans, and J.S.S. Damste (2008). A radiocarbon-based assessment of the preservation characteristics of crenarchaeol and alkenones from continental margin sediments. *Org Geochem* **39**(8): 1039-1045. doi: 10.1016/j.orggeochem.2008.02.006

Monterey, G. and S. Levitus (1997). *Seasonal variability of mixed layer depth for the world ocean.* US Dept. of Commerce, NOAA-NESDIS; Washington, availabe from: ftp://ftp.nodc.noaa.gov/pub/data.nodc/woa/PUBLICATIONS/Atlas14.pdf.

Mopper, K. and X.L. Zhou (1990). Hydroxyl radical photoproduction in the sea and its potential impact on marine processes. *Science* **250**(4981): 661-664. doi: 10.1126/science.250.4981.661

Mopper, K., X.L. Zhou, R.J. Kieber, D.J. Kieber, R.J. Sikorski, and R.D. Jones (1991). Photochemical degradation of dissolved organic carbon and its impact on the oceanic carbon cycle. *Nature* **353**(6339): 60-62. doi: 10.1038/353060a0

Morales-Cid, G., I. Gebefugi, B. Kanawati, M. Harir, N. Hertkorn, R. Rossello-Mora, and P. Schmitt-Kopplin (2009). Automated microextraction sample preparation coupled on-line to FT-ICR-MS: application to desalting and concentration of river and marine dissolved organic matter. *Anal Bioanal Chem* **395**(3): 797-807. doi: 10.1007/s00216-009-3025-0

Moran, M.A. and R.G. Zepp (1997). Role of photoreactions in the formation of biologically labile compounds from dissolved organic matter. *Limnol Oceanogr* **42**(6): 1307-1316

Morel, F.M.M. and N.M. Price (2003). The biogeochemical cycles of trace metals in the oceans. *Science* **300**(5621): 944-947. doi: 10.1126/science.1083545

Mortazavi, B. and J.P. Chanton (2004). Use of Keeling plots to determine sources of dissolved organic carbon in nearshore and open ocean systems. *Limnol Oceanogr* **49**(1): 102-108

Mühlebach, A. and K. Weber (1998). Origins and fate of dissolved sterols in the Weddell Sea, Antarctica. *Org Geochem* **29**(5-7): 1595-1607. doi: 10.1016/s0146-6380(98)00097-7

Müller, A.M., M. Christl, J. Lachner, M. Suter, and H.A. Synal (2010). Competitive Be-10 measurements below 1 MeV with the upgraded ETH-TANDY AMS facility. *Nucl Instrum Methods Phys Res, Sect B* **268**(17-18): 2801-2807. doi: 10.1016/j.nimb.2010.05.104

Nagata, T., B. Meon, and D.L. Kirchman (2003). Microbial degradation of peptidoglycan in seawater. *Limnol Oceanogr* **48**(2): 745-754

Nguyen, R.T., H.R. Harvey, X. Zang, J.D.H. van Heemst, M. Hetenyi, and P.G. Hatcher (2003). Preservation of algaenan and proteinaceous material during the oxic decay of Botryococcus braunii as revealed by pyrolysis-gas chromatography/mass spectrometry and C-13 NMR spectroscopy. *Org Geochem* **34**(4): 483-497. doi: 10.1016/s0146-6380(02)00261-9

Nissenbaum, A. and I.R. Kaplan (1972). Chemical and isotopic evidence for in-situ origin of marine humic substances. *Limnol Oceanogr* **17**(4): 570-582

Obernosterer, I. and R. Benner (2004). Competition between biological and photochemical processes in the mineralization of dissolved organic carbon. *Limnol Oceanogr* **49**(1): 117-124

Obernosterer, I., P. Catala, T. Reinthaler, G.J. Herndl, and P. Lebaron (2005). Enhanced heterotrophic activity in the surface microlayer of the Mediterranean Sea. *Aquat Microb Ecol* **39**(3): 293-302. doi: 10.3354/ame039293

Obernosterer, I., B. Reitner, and G.J. Herndl (1999). Contrasting effects of solar radiation on dissolved organic matter and its bioavailability to marine bacterioplankton. *Limnol Oceanogr* **44**(7): 1645-1654

Ogawa, H., Y. Amagai, I. Koike, K. Kaiser, and R. Benner (2001). Production of refractory dissolved organic matter by bacteria. *Science* **292**(5518): 917-920. doi: 10.1126/science.1057627

Ogawa, H., R. Fukuda, and I. Koike (1999). Vertical distributions of dissolved organic carbon and nitrogen in the Southern Ocean. *Deep Sea Res I* **46**(10): 1809-1826. doi: 10.1016/S0967-0637(99)00027-8

Ogawa, H. and E. Tanoue (2003). Dissolved organic matter in oceanic waters. *Journal of Oceanography* **59**(2): 129-147

Olesik, J.W. and A.W. Moore (1990). Influence of small amounts of organic solvents in aqueous samples on argon inductively coupled plasma spectrometry. *Anal Chem* **62**(8): 840-845. doi: 10.1021/ac00207a014

Opsahl, S. and R. Benner (1995). Early diagenesis of vascular plant tissues: Lignin and cutin decomposition and biogeochemical implications. *Geochim Cosmochim Acta* **59**(23): 4889-4904. doi: 10.1016/0016-7037(95)00348-7

——— (1997). Distribution and cycling of terrigenous dissolved organic matter in the ocean. *Nature* **386**(6624): 480-482. doi: 10.1038/386480a0

Orre, S., J.N. Smith, V. Alfimov, and M. Bentsen (2010). Simulating transport of I-129 and idealized tracers in the northern North Atlantic Ocean. *Environ Fluid Mech* **10**(1-2): 213-233. doi: 10.1007/s10652-009-9138-3

Orsi, A.H., T. Whitworth, and W.D. Nowlin (1995). On the meridional extent and fronts of the Antarctic Circumpolar Current. *Deep Sea Res I* **42**(5): 641-673. doi: 10.1016/0967-0637(95)00021-W

Ortega-Retuerta, E., U. Passow, C.M. Duarte, and I. Reche (2009). Effects of ultraviolet B radiation on (not so) transparent exopolymer particles. *Biogeosciences* **6**(12): 3071-3080. doi: 10.5194/bg-6-3071-2009

Otero-Romani, J., A. Moreda-Pineiro, A. Bermejo-Barrera, and P. Bermejo-Barrera (2005). Evaluation of commercial C18 cartridges for trace elements solid phase extraction from seawater followed by inductively coupled plasma-optical emission spectrometry determination. *Anal Chim Acta* **536**(1-2): 213-218. doi: 10.1016/j.aca.2004.12.046

Owens, S.A., K.O. Buesseler, and K.W.W. Sims (2011). Re-evaluating the U-238-salinity relationship in seawater: Implications for the U-238-Th-234 disequilibrium method. *Mar Chem* **127**(1-4): 31-39. doi: 10.1016/j.marchem.2011.07.005

Pakulski, J.D. and R. Benner (1994). Abundance and distribution of carbohydrates in the ocean. *Limnol Oceanogr* **39**(4): 930-940

Park, J., I.-S. Oh, H.-C. Kim, and S. Yoo (2010). Variability of SeaWiFs chlorophyll-a in the southwest Atlantic sector of the Southern Ocean: strong topographic effects and weak seasonality. *Deep Sea Res I* **57**(4): 604-620. doi: 10.1016/j.dsr.2010.01.004

Passow, U. (2002). Transparent exopolymer particles (TEP) in aquatic environments. *Prog Oceanogr* **55**(3-4): 287-333. doi: 10.1016/s0079-6611(02)00138-6

Pates, J.M. and G.K.P. Muir (2007). U-salinity relationships in the Mediterranean: Implications for Th-234-U-238 particle flux studies. *Mar Chem* **106**(3-4): 530-545. doi: 10.1016/j.marchem.2007.05.006

Pearce, I., A.T. Davidson, P.G. Thomson, S. Wright, and R. van den Enden (2011). Marine microbial ecology in the sub-Antarctic Zone: Rates of bacterial and phytoplankton growth and grazing by heterotrophic protists. *Deep Sea Res II* **58**(21-22): 2248-2259. doi: 10.1016/j.dsr2.2011.05.030

Pearson, K. (1901). On lines and planes of closest fit to systems of points in space. *Philosophical Magazine Series 6* **2**(11): 559-572. doi: 10.1080/14786440109462720

Piccolo, A. (2001). The supramolecular structure of humic substances. *Soil Sci* **166**(11): 810-832. doi: 10.1097/00010694-200111000-00007

Piccolo, A. and M. Spiteller (2003). Electrospray ionization mass spectrometry of terrestrial humic substances and their size fractions. *Anal Bioanal Chem* **377**(6): 1047-1059. doi: 10.1007/s00216-003-2186-5

Piontek, J., N. Händel, G. Langer, J. Wohlers, U. Riebesell, and A. Engel (2009). Effects of rising temperature on the formation and microbial degradation of marine diatom aggregates. *Aquat Microb Ecol* **54**(3): 305-318. doi: 10.3354/ame01273

Piontek, J., M. Lunau, N. Händel, C. Borchard, M. Wurst, and A. Engel (2010). Acidification increases microbial polysaccharide degradation in the ocean. *Biogeosciences* **7**(5): 1615-1624. doi: 10.5194/bg-7-1615-2010

Podgorski, D.C., A.M. McKenna, R.P. Rodgers, A.G. Marshall, and W.T. Cooper (2012). Selective ionization of dissolved organic nitrogen by positive ion atmospheric pressure photoionization coupled with Fourier transform ion cyclotron resonance mass spectrometry. *Anal Chem* **84**(11): 5085-5090. doi: 10.1021/ac300800w

Pohlman, J.W., J.E. Bauer, W.F. Waite, C.L. Osburn, and N.R. Chapman (2011). Methane hydrate-bearing seeps as a source of aged dissolved organic carbon to the oceans. *Nat Geosci* **4**(1): 37-41. doi: 10.1038/ngeo1016

Pollard, R.T., I. Salter, R.J. Sanders, M.I. Lucas, C.M. Moore, R.A. Mills, P.J. Statham, J.T. Allen, A.R. Baker, D.C.E. Bakker, M.A. Charette, S. Fielding, G.R. Fones, M. French, A.E. Hickman, R.J. Holland, J.A. Hughes, T.D. Jickells, R.S. Lampitt, P.J. Morris, F.H. Nedelec, M. Nielsdottir, H. Planquette, E.E. Popova, A.J. Poulton, J.F. Read, S. Seeyave, T. Smith, M. Stinchcombe, S. Taylor, S. Thomalla, H.J. Venables, R. Williamson, and M.V. Zubkov (2009). Southern Ocean deep-water carbon export enhanced by natural iron fertilization. *Nature* **457**(7229): 577-U581. doi: 10.1038/nature07716

Pomeroy, L.R. (1974). The ocean's food web, a changing paradigm. *Bioscience* **24**(9): 499-504. doi: 10.2307/1296885

Pomeroy, L.R., P.J.I. Williams, F. Azam, and J.E. Hobbie (2007). The Microbial Loop. *Oceanography* **20**(2): 28-33

Pos, W.H., D.D. Riemer, and R.G. Zika (1998). Carbonyl sulfide (OCS) and carbon monoxide (CO) in natural waters: evidence of a coupled production pathway. *Mar Chem* **62**(1-2): 89-101. doi: 10.1016/s0304-4203(98)00025-5

Powell, R.T. and A. Wilson-Finelli (2003). Photochemical degradation of organic iron complexing ligands in seawater. *Aquat Sci* **65**(4): 367-374. doi: 10.1007/s00027-003-0679-0

Prahl, F.G. and S.G. Wakeham (1987). Calibration of unsaturation patterns in long-chain ketone compositions for palaeotemperature assessment. *Nature* **330**(6146): 367-369. doi: 10.1038/330367a0

Profrock, D. and A. Prange (2012). Inductively coupled plasma-mass spectrometry (ICP-MS) for quantitative analysis in environmental and life sciences: A review of challenges, solutions, and trends. *Appl Spectrosc* **66**(8): 843-868. doi: 10.1366/12-06681

Purser, K.H., L.R. Kilius, A.E. Litherland, and X.L. Zhao (1996). Detection of U-236: A possible 100-million year neutron flux integrator. *Nucl Instrum Methods Phys Res, Sect B* **113**(1-4): 445-452. doi: 10.1016/0168-583x(95)01369-5

Quay, P.D., B. Tilbrook, and C.S. Wong (1992). Oceanic uptake of fossil fuel CO2: carbon-13 evidence. *Science* **256**(5053): 74-79. doi: 10.1126/science.256.5053.74

Quigley, M.S., P.H. Santschi, L.D. Guo, and B.D. Honeyman (2001). Sorption irreversibility and coagulation behavior of Th-234 with marine organic matter. *Mar Chem* **76**(1-2): 27-45. doi: 10.1016/S0304-4203(01)00045-7

R Development Core Team (2012) R: A Language and Environment for Statistical Computing (R Foundation for Statistical Computing, Vienna, Austria), http://www.R-project.org/.

Raimbault, P., N. Garcia, and F. Cerutti (2008). Distribution of inorganic and organic nutrients in the South Pacific Ocean - evidence for long-term accumulation of organic matter in nitrogen-depleted waters. *Biogeosciences* **5**(2): 281-298

Rainbow, P.S. (2007). Trace metal bioaccumulation: models, metabolic availability and toxicity. *Environment International* **33**(4): 576-582. doi: 10.1016/j.envint.2006.05.007

Raymond, P.A., J.W. McClelland, R.M. Holmes, A.V. Zhulidov, K. Mull, B.J. Peterson, R.G. Striegl, G.R. Aiken, and T.Y. Gurtovaya (2007). Flux and age of dissolved organic carbon exported to the Arctic Ocean: A carbon isotopic study of the five largest arctic rivers. *Global Biogeochem Cycles* **21**(Gb4011). doi: 10.1029/2007gb002934

Redfield, A.C. (1958). The biological control of chemical factors in the environment. *Am Sci* **46**: 205-221

Reemtsma, T., A. These, M. Linscheid, J. Leenheer, and A. Spitzy (2008a). Molecular and structural characterization of dissolved organic matter from the deep ocean by FTICR-MS, including hydrophilic nitrogenous organic molecules. *Environ Sci Technol* **42**(5): 1430-1437. doi: 10.1021/es7021413

Reemtsma, T., A. These, A. Springer, and M. Linscheid (2008b). Differences in the molecular composition of fulvic acid size fractions detected by size-exclusion chromatography-on line Fourier transform ion cyclotron resonance (FTICR-) mass spectrometry. *Water Res* **42**(1-2): 63-72. doi: 10.1016/j.watres.2007.06.063

Reinthaler, T., E. Sintes, and G.J. Herndl (2008). Dissolved organic matter and bacterial production and respiration in the sea-surface microlayer of the open Atlantic and the western Mediterranean Sea. *Limnol Oceanogr* **53**(1): 122-136. doi: 10.4319/lo.2008.53.1.0122

Repeta, D.J. and L.I. Aluwihare (2006). Radiocarbon analysis of neutral sugars in high-molecular-weight dissolved organic carbon: implications for organic carbon cycling. *Limnol Oceanogr* **51**(2): 1045-1053

Rich, J.H., H.W. Ducklow, and D.L. Kirchman (1996). Concentrations and uptake of neutral monosaccharides along 140 degrees W in the equatorial Pacific: Contribution of glucose to heterotrophic bacterial activity and the DOM flux. *Limnol Oceanogr* **41**(4): 595-604

Ridgwell, A. (2011). Evolution of the ocean's "biological pump". *Proc Natl Acad Sci USA* **108**(40): 16485-16486. doi: 10.1073/pnas.1112236108

Riebesell, U., A. Kortzinger, and A. Oschlies (2009). Sensitivities of marine carbon fluxes to ocean change. *Proc Natl Acad Sci USA* **106**(49): 20602-20609. doi: 10.1073/pnas.0813291106

Riebesell, U., K.G. Schulz, R.G.J. Bellerby, M. Botros, P. Fritsche, M. Meyerhofer, C. Neill, G. Nondal, A. Oschlies, J. Wohlers, and E. Zollner (2007). Enhanced biological carbon consumption in a high CO2 ocean. *Nature* **450**(7169): 545-U510. doi: 10.1038/nature06267

Riemer, D.D., P.J. Milne, R.G. Zika, and W.H. Pos (2000). Photoproduction of nonmethane hydrocarbons (NMHCs) in seawater. *Mar Chem* **71**(3-4): 177-198. doi: 10.1016/S0304-4203(00)00048-7

Rijkenberg, M.J.A. (2010). *RV Pelagia PE321 Cruise summary report*.

Robinson, C. (2008). Heterotrophic bacterial respiration, pp. 299-480, in D. Kirchman [ed.], *Microbial Ecology of the Oceans*. John Wiley & Sons, Hoboken, New Jersey.

Robinson, C. and N. Ramaiah (2011). Microbial heterotrophic rates constrain the microbial carbon pump, pp. 52-53, in N. Jiao, F. Azam and S. Sanders [eds.], *Microbial carbon pump in the ocean*. Sciens/AAAS, Washington, DC.

Robinson, L.F., N.S. Belshaw, and G.M. Henderson (2004). U and Th concentrations and isotope ratios in modern carbonates and waters from the Bahamas. *Geochim Cosmochim Acta* **68**(8): 1777-1789. doi: 10.1016/j.gca.2003.10.005

Roemmich, D. and C. Wunsch (1985). Two transatlantic sections: meridional circulation and heat flux in the subtropical North Atlantic Ocean. *Deep Sea Res I* **32**(6): 619-664. doi: 10.1016/0198-0149(85)90070-6

Roland, L.A., M.D. McCarthy, and T. Guilderson (2008). Sources of molecularly uncharacterized organic carbon in sinking particles from three ocean basins: A coupled delta C-14 and delta C-13 approach. *Mar Chem* **111**(3-4): 199-213. doi: 10.1016/j.marchem.2008.05.010

Rontani, J.F., N. Zabeti, and S.G. Wakeham (2011). Degradation of particulate organic matter in the equatorial Pacific Ocean: biotic or abiotic? *Limnol Oceanogr* **56**(1): 333-349. doi: 10.4319/lo.2011.56.1.0333

Rosenstock, B., W. Zwisler, and M. Simon (2005). Bacterial consumption of humic and non-humic low and high molecular weight DOM and the effect of solar irradiation on the turnover of labile DOM in the Southern Ocean. *Microb Ecol* **50**(1): 90-101. doi: 10.1007/s00248-004-0116-5

Rothman, D.H., J.M. Hayes, and R.E. Summons (2003). Dynamics of the Neoproterozoic carbon cycle. *Proc Natl Acad Sci USA* **100**(14): 8124-8129. doi: 10.1073/pnas.0832439100

Rottmann, L. and K.G. Heumann (1994a). Determination of heavy metal interactions with dissolved organic materials in natural aquatic systems by coupling a high-performance liquid chromatography system with an inductively coupled plasma mass spectrometer. *Anal Chem* **66**(21): 3709-3715. doi: 10.1021/ac00093a027

Rottmann, L. and K.G. Heumann (1994b). Development of an online isotope-dilution technique with HPLC ICP-MS for the accurate determination of elemental species. *Fresen J Anal Chem* **350**(4-5): 221-227. doi: 10.1007/BF00322473

Russ, B., M. Chartier, and A.-M. Hägg (2009). *Liquid discharges from nuclear installations in 2009*, Radioactive Substances Series. OSPAR Commission.

Sabine, C.L., R.A. Feely, N. Gruber, R.M. Key, K. Lee, J.L. Bullister, R. Wanninkhof, C.S. Wong, D.W.R. Wallace, B. Tilbrook, F.J. Millero, T.H. Peng, A. Kozyr, T. Ono, and A.F. Rios (2004). The oceanic sink for anthropogenic CO(2). *Science* **305**(5682): 367-371. doi: 10.1126/science.1097403

Sackett, W., T. Mo, R. Spalding, and M. Exner (1973). A revaluation of the marine geochemistry of uranium. *Int At Energy Agency Proc Ser*(IAEA SM-158/51): 757-769

Saito, M.A., T.J. Goepfert, and J.T. Ritt (2008). Some thoughts on the concept of colimitation: Three definitions and the importance of bioavailability. *Limnol Oceanogr* **53**(1): 276-290. doi: 10.4319/lo.2008.53.1.0276

Sakaguchi, A., K. Kawai, P. Steier, F. Quinto, K. Mino, J. Tomita, M. Hoshi, N. Whitehead, and M. Yamamoto (2009). First results on (236)U levels in global fallout. *Sci Total Environ* **407**(14): 4238-4242. doi: 10.1016/j.scitotenv.2009.01.058

Sanders, R. and T. Jickells (2000). Total organic nutrients in Drake Passage. *Deep Sea Res I* **47**(6): 997-1014. doi: 10.1016/s0967-0637(99)00079-5

Sannigrahi, P., E.D. Ingall, and R. Benner (2005). Cycling of dissolved and particulate organic matter at station Aloha: Insights from C-13 NMR spectroscopy coupled with elemental, isotopic and molecular analyses. *Deep Sea Res I* **52**(8): 1429-1444. doi: 10.1016/j.dsr.2005.04.001

——— (2006). Nature and dynamics of phosphorus-containing components of marine dissolved and particulate organic matter. *Geochim Cosmochim Acta* **70**(23): 5868-5882. doi: 10.1016/j.gca.2006.08.037

Santos, L., A.L. Santos, F. Coelho, N.C.M. Gomes, J.M. Dias, A. Cunha, and A. Almeida (2011). Relation between bacterial activity in the surface microlayer and estuarine hydrodynamics. *FEMS Microbiol Ecol* **77**(3): 636-646. doi: 10.1111/j.1574-6941.2011.01147.x

Santschi, P.H., L.D. Guo, M. Baskaran, S. Trumbore, J. Southon, T.S. Bianchi, B. Honeyman, and L. Cifuentes (1995). Isotopic evidence for the contemporary origin of high-molecular weight organic matter in oceanic environments. *Geochim Cosmochim Acta* **59**(3): 625-631. doi: 10.1016/0016-7037(94)00378-y

Santschi, P.H., L.D. Guo, I.D. Walsh, M.S. Quigley, and M. Baskaran (1999). Boundary exchange and scavenging of radionuclides in continental margin waters of the Middle Atlantic Bight: implications for organic carbon fluxes. *Cont Shelf Res* **19**(5): 609-636. doi: 10.1016/S0278-4343(98)00103-4

Santschi, P.H., D.R. Schink, O. Corapcioglu, S. Oktay-Marshall, U. Fehn, and P. Sharma (1996). Evidence for elevated levels of iodine-129 in the Deep Western Boundary current in the Middle Atlantic Bight. *Deep Sea Res I* **43**(2): 259-265. doi: 10.1016/0967-0637(96)00005-2

Sarthou, G., A.R. Baker, S. Blain, E.P. Achterberg, M. Boye, A.R. Bowie, P. Croot, P. Laan, H.J.W. de Baar, T.D. Jickells, and P.J. Worsfold (2003). Atmospheric iron deposition and sea-surface dissolved iron concentrations in the eastern Atlantic Ocean. *Deep Sea Res I* **50**(10-11): 1339-1352. doi: 10.1016/s0967-0637(03)00126-2

Savitzky, A. and M.J.E. Golay (1964). Smoothing and differentiation of data by simplified least squares procedures. *Anal Chem* **36**(8): 1627-1639. doi: 10.1021/ac60214a047

Schattenhofer, M., B.M. Fuchs, R. Amann, M.V. Zubkov, G.A. Tarran, and J. Pernthaler (2009). Latitudinal distribution of prokaryotic picoplankton populations in the Atlantic Ocean. *Environ Microbiol* **11**(8): 2078-2093. doi: 10.1111/j.1462-2920.2009.01929.x

Schleifer, K.H. and O. Kandler (1972). Peptidoglycan types of bacterial cell-walls and their taxonomic implications. *Bacteriol Rev* **36**(4): 407-477

Schlitzer, R. (2007). Assimilation of radiocarbon and chlorofluorocarbon data to constrain deep and bottom water transports in the world ocean. *J Phys Oceanogr* **37**(2): 259-276. doi: 10.1175/jpo3011.1

Schlosser, C. and P.L. Croot (2008). Application of cross-flow filtration for determining the solubility of iron species in open ocean seawater. *Limnol Oceanogr: Methods* **6**: 630-642

Schlünz, B. and R.R. Schneider (2000). Transport of terrestrial organic carbon to the oceans by rivers: re-estimating flux- and burial rates. *Int J Earth Sci* **88**(4): 599-606. doi: 10.1007/s005310050290

Schmidt, F., M. Elvert, B.P. Koch, M. Witt, and K.-U. Hinrichs (2009). Molecular characterization of dissolved organic matter in pore water of continental shelf

sediments. *Geochim Cosmochim Acta* **73**(11): 3337-3358. doi: 10.1016/j.gca.2009.03.008

Schmidt, F., B.P. Koch, M. Elvert, G. Schmidt, M. Witt, and K.U. Hinrichs (2011). Diagenetic transformation of dissolved organic nitrogen compounds under contrasting sedimentary redox conditions in the Black Sea. *Environ Sci Technol* **45**(12): 5223-5229. doi: 10.1021/es2003414

Schmitt-Kopplin, P., G. Liger-Belair, B.P. Koch, R. Flerus, G. Kattner, M. Harir, B. Kanawati, M. Lucio, D. Tziotis, N. Hertkorn, and I. Gebefügi (2012). Dissolved organic matter in sea spray: a transfer study from marine surface water to aerosols. *Biogeosciences* **9**(4): 1571-1582. doi: 10.5194/bg-9-1571-2012

Schouten, S., E.C. Hopmans, E. Schefuss, and J.S.S. Damste (2002). Distributional variations in marine crenarchaeotal membrane lipids: a new tool for reconstructing ancient sea water temperatures? *Earth Planet Sci Lett* **204**(1-2): 265-274. doi: 10.1016/s0012-821x(02)00979-2

Schouten, S., S. Ozdirekcan, M.T.J. van der Meer, P. Blokker, M. Baas, J.M. Hayes, and J.S.S. Damste (2008). Evidence for substantial intramolecular heterogeneity in the stable carbon isotopic composition of phytol in photoautotrophic organisms. *Org Geochem* **39**(1): 135-146. doi: 10.1016/j.orggeochem.2007.09.002

Schuur, E.A.G., J.G. Vogel, K.G. Crummer, H. Lee, J.O. Sickman, and T.E. Osterkamp (2009). The effect of permafrost thaw on old carbon release and net carbon exchange from tundra. *Nature* **459**(7246): 556-559. doi: 10.1038/nature08031

Sempere, R. and G. Cauwet (1995). Occurrence of organic colloids in the stratified estuary of the Krka Estuary (Croatia). *Estuar Coast Shelf S* **40**(1): 105-114. doi: 10.1016/0272-7714(95)90016-0

Senko, M.W., C.L. Hendrickson, L. PasaTolic, J.A. Marto, F.M. White, S.H. Guan, and A.G. Marshall (1996). Electrospray ionization Fourier transform ion cyclotron resonance at 9.4 T. *Rapid Commun Mass Spectrom* **10**(14): 1824-1828. doi: 10.1002/(sici)1097-0231(199611)10:14<1824::aid-rcm695>3.3.co;2-5

SEPA (2009). *Radioactivity in Food and the Environment*(15). Scottish Environment Protection Agency.

Setschenov, M. (1889). Über die Konstitution der Salzlösungen auf Grund Ihres Verhaltens zu Kohlensäure. *Z Phys Chem*(4): 117-128

Sexton, P.F., R.D. Norris, P.A. Wilson, H. Palike, T. Westerhold, U. Rohl, C.T. Bolton, and S. Gibbs (2011). Eocene global warming events driven by ventilation of oceanic dissolved organic carbon. *Nature* **471**(7338): 349-352. doi: 10.1038/nature09826

Shi, D.L., Y. Xu, B.M. Hopkinson, and F.M.M. Morel (2010). Effect of ocean acidification on iron availability to marine phytoplankton. *Science* **327**(5966): 676-679. doi: 10.1126/science.1183517

Sieburth, J.M. and A. Jensen (1968). Studies on algal substances in the sea. I. Gelbstoff (humic material) in terrestrial and marine waters. *J Exp Mar Biol Ecol* **2**(2): 174-189. doi: 10.1016/0022-0981(68)90008-7

Sieburth, J.M., P.J. Willis, K.M. Johnson, C.M. Burney, D.M. Lavoie, K.R. Hinga, D.A. Caron, F.W. French, P.W. Johnson, and P.G. Davis (1976). Dissolved organic matter and heterotrophic microneuston in the surface microlayer of the North Atlantic. *Science* **194**(4272): 1415-1418. doi: 10.1126/science.194.4272.1415

Siegenthaler, U. and J.L. Sarmiento (1993). Atmospheric carbon dioxide and the ocean. *Nature* **365**(6442): 119-125. doi: 10.1038/365119a0

Simjouw, J.P., E.C. Minor, and K. Mopper (2005). Isolation and characterization of estuarine dissolved organic matter: Comparison of ultrafiltration and C-18 solid-phase extraction techniques. *Mar Chem* **96**(3-4): 219-235. doi: 10.1016/j.marchem.2005.01.003

Simon, M., H.P. Grossart, B. Schweitzer, and H. Ploug (2002). Microbial ecology of organic aggregates in aquatic ecosystems. *Aquat Microb Ecol* **28**(2): 175-211. doi: 10.3354/ame028175

Simon, M. and B. Rosenstock (2007). Different coupling of dissolved amino acid, protein, and carbohydrate turnover to heterotrophic picoplankton production in the Southern Ocean in austral summer and fall. *Limnol Oceanogr* **52**(1): 85-95

Singh, S.K., T.K. Dalai, and S. Krishnaswami (2003). U-238 series isotopes and Th-232 in carbonates and black shales from the Lesser Himalaya: implications to dissolved uranium abundances in Ganga-Indus source waters. *J Environ Radioact* **67**(1): 69-90. doi: 10.1016/s0265-931x(02)00161-3

Skoog, A. and R. Benner (1997). Aldoses in various size fractions of marine organic matter: implications for carbon cycling. *Limnol Oceanogr* **42**(8): 1803-1813

Sleighter, R.L., H.M. Chen, A.S. Wozniak, A.S. Willoughby, P. Caricasole, and P.G. Hatcher (2012). Establishing a Measure of Reproducibility of Ultrahigh-Resolution Mass Spectra for Complex Mixtures of Natural Organic Matter. *Anal Chem* **84**(21): 9184-9191. doi: 10.1021/ac3018026

Sleighter, R.L. and P.G. Hatcher (2007). The application of electrospray ionization coupled to ultrahigh resolution mass spectrometry for the molecular characterization of natural organic matter. *J Mass Spectrom* **42**(5): 559-574. doi: 10.1002/jms.1221

Sleighter, R.L., Z.F. Lie, J.H. Xue, and P.G. Hatcher (2010). Multivariate statistical approaches for the characterization of dissolved organic matter analyzed by ultrahigh resolution mass spectrometry. *Environ Sci Technol* **44**(19): 7576-7582. doi: 10.1021/es1002204

Sleighter, R.L., G.A. McKee, Z. Liu, and P.G. Hatcher (2008). Naturally present fatty acids as internal calibrants for Fourier transform mass spectra of dissolved organic matter. *Limnol Oceanogr: Methods* **6**: 246-253

Smith, D.C. and F. Azam (1992). A simple, economical method for measuring bacterial protein synthesis rates in seawater using 3H-leucine. *Mar Microb Food Webs* **6**(2): 107-114

Smith, D.C., M. Simon, A.L. Alldredge, and F. Azam (1992). Intense hydrolytic enzyme activity on marine aggregates and implications for rapid particle dissolution. *Nature* **359**(6391): 139-142. doi: 10.1038/359139a0

Sofer, Z. (1980). Preparation of carbon dioxide for stable carbon isotope analysis of petroleum fractions. *Anal Chem* **52**(8): 1389-1391. doi: 10.1021/ac50058a063

Specht, C.H. and F.H. Frimmel (2000). Specific interactions of organic substances in size-exclusion chromatography. *Environ Sci Technol* **34**(11): 2361-2366. doi: 10.1021/es991034d

Srncik, M., P. Steier, and G. Wallner (2009). Determination of the isotopic ratio 236U/238U in Austrian water samples. *Nucl Instrum Methods Phys Res, Sect B* **268**(7-8): 1146-1149. doi: 10.1016/j.nimb.2009.10.120

Stedmon, C.A., R.M.W. Amon, A.J. Rinehart, and S.A. Walker (2011). The supply and characteristics of colored dissolved organic matter (CDOM) in the Arctic Ocean: Pan Arctic trends and differences. *Mar Chem* **124**(1–4): 108-118. doi: 10.1016/j.marchem.2010.12.007

Stedmon, C.A. and S. Markager (2005). Tracing the production and degradation of autochthonous fractions of dissolved organic matter by fluorescence analysis. *Limnol Oceanogr* **50**(5): 1415-1426

Stefels, J., M. Steinke, S. Turner, G. Malin, and S. Belviso (2007). Environmental constraints on the production and removal of the climatically active gas dimethylsulphide (DMS) and implications for ecosystem modelling. *Biogeochemistry* **83**(1-3): 245-275. doi: 10.1007/s10533-007-9091-5

Steier, P., M. Bichler, L.K. Fifield, R. Golser, W. Kutschera, A. Priller, F. Quinto, S. Richter, M. Srncikf, P. Terrasi, L. Wacker, A. Wallner, G. Wallner, K.M. Wilcken, and E.M. Wild (2008). Natural and anthropogenic (236)U in environmental samples. *Nucl Instrum Methods Phys Res, Sect B* **266**(10): 2246-2250. doi: 10.1016/j.nimb.2008.03.002

Steier, P., F. Dellinger, O. Forstner, R. Golser, K. Knie, W. Kutschera, A. Priller, F. Quinto, M. Srncik, F. Terrasi, C. Vockenhuber, A. Wallner, G. Wallner, and E.M. Wild (2010). Analysis and application of heavy isotopes in the environment. *Nucl Instrum Methods Phys Res, Sect B* **268**(7-8): 1045-1049. doi: 10.1016/j.nimb.2009.10.094

Stenson, A.C., A.G. Marshall, and W.T. Cooper (2003). Exact masses and chemical formulas of individual suwannee river fulvic acids from ultrahigh resolution electrospray ionization Fourier transform ion cyclotron resonance mass spectra. *Anal Chem* **75**(6): 1275-1284. doi: 10.1021/ac026106p

Stocker, M., M. Dobeli, M. Grajcar, M. Suter, H.A. Synal, and L. Wacker (2005). A universal and competitive compact AMS facility. *Nucl Instrum Methods Phys Res, Sect B* **240**(1-2): 483-489. doi: 10.1016/j.nimb.2005.06.224

Stolpe, B., L.D. Guo, A.M. Shiller, and M. Hassellov (2010). Size and composition of colloidal organic matter and trace elements in the Mississippi River, Pearl River and the northern Gulf of Mexico, as characterized by flow field-flow fractionation. *Mar Chem* **118**(3-4): 119-128. doi: 10.1016/j.marchem.2009.11.007

Stubbins, A., J. Niggemann, and T. Dittmar (2012). Photo-lability of deep ocean dissolved black carbon. *Biogeosciences* **9**(5): 1661-1670. doi: 10.5194/bg-9-1661-2012

Stubbins, A., R.G.M. Spencer, H.M. Chen, P.G. Hatcher, K. Mopper, P.J. Hernes, V.L. Mwamba, A.M. Mangangu, J.N. Wabakanghanzi, and J. Six (2010). Illuminated darkness: Molecular signatures of Congo River dissolved organic matter and its photochemical alteration as revealed by ultrahigh precision mass spectrometry. *Limnol Oceanogr* **55**(4): 1467-1477. doi: 10.4319/lo.2010.55.4.1467

Stuiver, M. and H.A. Polach (1977). Reporting of C-14 data - discussion. *Radiocarbon* **19**(3): 355-363

Stuiver, M. and P.D. Quay (1981). Atmospheric C-14 changes resulting from fossil fuel CO2 release and cosmic ray flux variability. *Earth Planet Sci Lett* **53**(3): 349-362. doi: 10.1016/0012-821x(81)90040-6

Stuiver, M., P.D. Quay, and H.G. Ostlund (1983). Abyssal water carbon-14 distribution and the age of the world oceans. *Science* **219**(4586): 849-851. doi: 10.1126/science.219.4586.849

Suess, H.E. (1955). Radiocarbon concentration in modern wood. *Science* **122**(3166): 415-417. doi: 10.1126/science.122.3166.415-a

Sugimura, Y. and M. Mayeda (1980). The uranium content and the activity ratio U-234/U-238 in sea water in the Pacific Ocean, pp. 211-246, in E.D. Goldberg and Y. Horibe [eds.], *Isotope Marine Chemistry*. Uchida Rokakuho, Tokyo.

Suttle, C.A. (2005). Viruses in the sea. *Nature* **437**(7057): 356-361. doi: 10.1038/nature04160

Svensen, C., D. Viličić, P. Wassmann, E. Arashkevich, and T. Ratkova (2007). Plankton distribution and vertical flux of biogenic matter during high summer stratification in the Krka Estuary (Eastern Adriatic). *Estuar Coast Shelf S* **71**(3-4): 381-390. doi: 10.1016/j.ecss.2006.07.022

Synal, H.A., S. Jacob, and M. Suter (2000). The PSI/ETH small radiocarbon dating system. *Nucl Instrum Methods Phys Res, Sect B* **172**: 1-7. doi: 10.1016/s0168-583x(00)00376-1

Tamburini, C., M. Garel, B. Al Ali, B. Merigot, P. Kriwy, B. Charriere, and G. Budillon (2009). Distribution and activity of bacteria and archaea in the different water masses of the Tyrrhenian Sea. *Deep Sea Res II* **56**(11-12): 700-712. doi: 10.1016/j.dsr2.2008.07.021

Tanoue, E., S. Nishiyama, M. Kamo, and A. Tsugita (1995). Bacterial membranes: possible source of a major dissolved protein in seawater. *Geochim Cosmochim Acta* **59**(12): 2643-2648. doi: 10.1016/0016-7037(95)00134-4

Taylor, B.B., E. Torrecilla, A. Bernhardt, M.H. Taylor, I. Peeken, R. Röttgers, J. Piera, and A. Bracher (2011). Bio-optical provinces in the eastern Atlantic Ocean and their biogeographical relevance. *Biogeosciences* **8**(12): 3609-3629. doi: 10.5194/bg-8-3609-2011

Terzic, S., D. Hrsak, and M. Ahel (1992). Primary biodegradation kinetics of linear alkylbenzenesulfonates in estuarine waters. *Water Res* **26**(5): 585-591. doi: 10.1016/0043-1354(92)90231-r

Tfaily, M., S. Hodgkins, D. Podgorski, J. Chanton, and W. Cooper (2012). Comparison of dialysis and solid-phase extraction for isolation and concentration of dissolved organic matter prior to Fourier transform ion cyclotron resonance mass spectrometry. *Anal Bioanal Chem* **404**(2): 447-457. doi: 10.1007/s00216-012-6120-6

Tfaily, M.M., D.C. Podgorski, J.E. Corbett, J.P. Chanton, and W.T. Cooper (2011). Influence of acidification on the optical properties and molecular composition of dissolved organic matter. *Anal Chim Acta* **706**(2): 261-267. doi: 10.1016/j.aca.2011.08.037

Thuroczy, C.E., L.J.A. Gerringa, M.B. Klunder, R. Middag, P. Laan, K.R. Timmermans, and H.J.W. de Baar (2010). Speciation of Fe in the Eastern North Atlantic Ocean. *Deep Sea Res I* **57**(11): 1444-1453. doi: 10.1016/j.dsr.2010.08.004

Tilstone, G.H., R.L. Airs, V. Martinez-Vicente, C. Widdicombe, and C. Llewellyn (2010). High concentrations of mycosporine-like amino acids and colored dissolved organic matter in the sea surface microlayer off the Iberian Peninsula. *Limnol Oceanogr* **55**(5): 1835-1850. doi: 10.4319/lo.2010.55.5.1835

Todoli, J.L. and J.M. Mermet (2006). Sample introduction systems for the analysis of liquid microsamples by ICP-AES and ICP-MS. *Spectrochim Acta, Part B* **61**(3): 239-283. doi: 10.1016/j.sab.2005.12.010

Toggweiler, J.R. (1988). Deep-sea carbon, a burning issue. *Nature* **334**(6182): 468-468. doi: 10.1038/334468a0

Toggweiler, J.R., A. Gnanadesikan, S. Carson, R. Murnane, and J.L. Sarmiento (2003). Representation of the carbon cycle in box models and GCMs: 1. Solubility pump. *Global Biogeochem Cycles* **17**(1026). doi: 10.1029/2001gb001401

Torres-Valdes, S., V.M. Roussenov, R. Sanders, S. Reynolds, X. Pan, R. Mather, A. Landolfi, G.A. Wolff, E.P. Achterberg, and R.G. Williams (2009). Distribution of dissolved organic nutrients and their effect on export production over the Atlantic Ocean. *Global Biogeochem Cycles* **23**(Gb4019). doi: 10.1029/2008gb003389

Tortell, P.D., M.T. Maldonado, and N.M. Price (1996). The role of heterotrophic bacteria in iron-limited ocean ecosystems. *Nature* **383**(6598): 330-332. doi: 10.1038/383330a0

Trenfield, M.A., S. McDonald, K. Kovacs, E.K. Lesher, J.M. Pringle, S.J. Markich, J.C. Ng, B. Noller, P.L. Brown, and R.A. van Dam (2011). Dissolved organic carbon reduces uranium bioavailability and toxicity. 1. Characterization of an aquatic fulvic acid and its complexation with uranium(VI). *Environ Sci Technol* **45**(7): 3075-3081. doi: 10.1021/es103330w

Turley, C.M. and P.J. Mackie (1994). Biogeochemical significance of attached and free-living bacteria and the flux of particles in the NE Atlantic Ocean. *Mar Ecol Prog Ser* **115**(1-2): 191-203. doi: 10.3354/meps115191

Turner, A. and E. Mawji (2004). Hydrophobicity and octanol-water partitioning of trace metals in natural waters. *Environ Sci Technol* **38**(11): 3081-3091. doi: 10.1021/es030151c

Tyrrell, T. (1999). The relative influences of nitrogen and phosphorus on oceanic primary production. *Nature* **400**(6744): 525-531. doi: 10.1038/22941

Tziotis, D., N. Hertkorn, and P. Schmitt-Kopplin (2011). Kendrick-analogous network visualisation of ion cyclotron resonance Fourier transform mass spectra: improved options for the assignment of elemental compositions and the classification of organic molecular complexity. *Eur J Mass Spectrom* **17**(4): 415-421. doi: 10.1255/ejms.1135

Ullrich, S.M., T.W. Tanton, and S.A. Abdrashitova (2001). Mercury in the aquatic environment: A review of factors affecting methylation. *Crit Rev Env Sci Tec* **31**(3): 241-293. doi: 10.1080/20016491089226

Usbeck, R., M.M.R. van der Loeff, M. Hoppema, and R. Schlitzer (2002). Shallow remineralization in the Weddell Gyre. *Geochem Geophys Geosyst* **3**. doi: 10.1029/2001gc000182

van der Loeff, M.M.R., P.H.H. Cai, I. Stimac, A. Bracher, R. Middag, M.B. Klunder, and S. van Heuven (2011). Th-234 in surface waters: Distribution of particle export flux across the Antarctic Circumpolar Current and in the Weddell Sea during the GEOTRACES expedition ZERO and DRAKE. *Deep Sea Res II* **58**(25-26): 2749-2766. doi: 10.1016/j.dsr2.2011.02.004

Velasquez, I., B.L. Nunn, E. Ibisanmi, D.R. Goodlett, K.A. Hunter, and S.G. Sander (2011). Detection of hydroxamate siderophores in coastal and Sub-Antarctic waters off the South Eastern Coast of New Zealand. *Mar Chem* **126**(1-4): 97-107. doi: 10.1016/j.marchem.2011.04.003

Velicer, G.J. (2003). Social strife in the microbial world. *Trends Microbiol* **11**(7): 330-337. doi: 10.1016/s0966-842x(03)00152-5

Vockenhuber, C., M. Christl, C. Hofmann, J. Lachner, A.M. Mueller, and H.-A. Synal (2011). Accelerator mass spectrometry of U-236 at low energies. *Nucl Instrum Methods Phys Res, Sect B* **269**(24): 3199-3203. doi: 10.1016/j.nimb.2011.04.026

Vogel, J.S., D.E. Nelson, and J.R. Southon (1987). C-14 background levels in an accelerator mass spectrometry system. *Radiocarbon* **29**(3): 323-333

Vogl, J. and K.G. Heumann (1998). Development of an ICP−IDMS method for dissolved organic carbon determinations and its application to

chromatographic fractions of heavy metal complexes with humic substances. *Anal Chem* **70**(10): 2038-2043. doi: 10.1021/ac971283p

Vojvodić, V. and B. Ćosović (1992). The hydrophobic fraction of organic matter in the Krka River Estuary. *Mar Chem* **39**(4): 251-267. doi: 10.1016/0304-4203(92)90012-y

Vonk, J.E., B.E. van Dongen, and O. Gustafsson (2010). Selective preservation of old organic carbon fluvially released from sub-Arctic soils. *Geophys Res Lett* **37**(L11605). doi: 10.1029/2010gl042909

Vraspir, J.M. and A. Butler (2009). Chemistry of marine ligands and siderophores. *Ann Rev Mar Sci* **1**(1): 43-63. doi: doi:10.1146/annurev.marine.010908.163712

Wakeham, S.G., C. Lee, J.I. Hedges, P.J. Hernes, and M.L. Peterson (1997). Molecular indicators of diagenetic status in marine organic matter. *Geochim Cosmochim Acta* **61**(24): 5363-5369. doi: 10.1016/s0016-7037(97)00312-8

Wakeham, S.G., T.K. Pease, and R. Benner (2003). Hydroxy fatty acids in marine dissolved organic matter as indicators of bacterial membrane material. *Org Geochem* **34**(6): 857-868. doi: 10.1016/s0146-6380(02)00189-4

Wakeham, S.G., C. Turich, F. Schubotz, A. Podlaska, X.N.N. Li, R. Varela, Y. Astor, J.P. Saenz, D. Rush, J.S.S. Damste, R.E. Summons, M.I. Scranton, G.T. Taylor, and K.U. Hinrichs (2012). Biomarkers, chemistry and microbiology show chemoautotrophy in a multilayer chemocline in the Cariaco Basin. *Deep Sea Res I* **63**: 133-156. doi: 10.1016/j.dsr.2012.01.005

Walker, B.D., S.R. Beaupré, T.P. Guilderson, E.R.M. Druffel, and M.D. McCarthy (2011). Large-volume ultrafiltration for the study of radiocarbon signatures and size vs. age relationships in marine dissolved organic matter. *Geochim Cosmochim Acta* **75**(18): 5187-5202. doi: 10.1016/j.gca.2011.06.015

Wang, M., W.Y. Feng, W.W. Lu, B. Li, B. Wang, M. Zhu, Y. Wang, H. Yuan, Y. Zhao, and Z.F. Chai (2007). Quantitative analysis of proteins via sulfur determination by HPLC coupled to isotope dilution ICPMS with a hexapole collision cell. *Anal Chem* **79**(23): 9128-9134. doi: 10.1021/ac071483t

Wang, X.C., R.F. Chen, J. Whelan, and L. Eglinton (2001). Contribution of "old" carbon from natural marine hydrocarbon seeps to sedimentary and dissolved organic carbon pools in the Gulf of Mexico. *Geophys Res Lett* **28**(17): 3313-3316. doi: 10.1029/2001gl013430

Wedborg, M., M. Hoppema, and A. Skoog (1998). On the relation between organic and inorganic carbon in the Weddell Sea. *J Mar Syst* **17**(1-4): 59-76. doi: 10.1016/S0924-7963(98)00029-3

Wei, L.P. and B.A. Ahner (2005). Sources and sinks of dissolved phytochelatin in natural seawater. *Limnol Oceanogr* **50**(1): 13-22

Weinbauer, M.G., F. Chen, and S.W. Wilhelm (2011). Virus-mediated redistribution and partitioning of carbon in the global Oceans, pp. 54-56, in N. Jiao, F. Azam and S. Sanders [eds.], *Microbial carbon pump in the ocean*. Sciens/AAAS, Washington, DC.

Weiss, M.S., U. Abele, J. Weckesser, W. Welte, E. Schiltz, and G.E. Schulz (1991). Molecular architecture and electrostatic properties of a bacterial porin. *Science* **254**(5038): 1627-1630. doi: 10.1126/science.1721242

White, E.M., D.J. Kieber, J. Sherrard, W.L. Miller, and K. Mopper (2010). Carbon dioxide and carbon monoxide photoproduction quantum yields in the Delaware Estuary. *Mar Chem* **118**(1-2): 11-21. doi: 10.1016/j.marchem.2009.10.001

Whitman, W.B., D.C. Coleman, and W.J. Wiebe (1998). Prokaryotes: the unseen majority. *Proc Natl Acad Sci USA* **95**(12): 6578-6583. doi: 10.1073/pnas.95.12.6578

Wiebinga, C.J. and H.J.W. de Baar (1998). Determination of the distribution of dissolved organic carbon in the Indian sector of the Southern Ocean. *Mar Chem* **61**(3-4): 185-201. doi: 10.1016/S0304-4203(98)00014-0

Wilcken, K.M., L.K. Fifield, T.T. Barrows, S.G. Tims, and L.G. Gladkis (2008). Nucleogenic Cl-36, U-236 and Pu-239 in uranium ores. *Nucl Instrum Methods Phys Res, Sect B* **266**(16): 3614-3624. doi: 10.1016/j.nimb.2008.06.009

Wilhelm, S.W. and C.A. Suttle (1999). Viruses and nutrient cycles in the sea - Viruses play critical roles in the structure and function of aquatic food webs. *Bioscience* **49**(10): 781-788. doi: 10.2307/1313569

Williams, P.M., A.F. Carlucci, S.M. Henrichs, E.S. Vanvleet, S.G. Horrigan, F.M.H. Reid, and K.J. Robertson (1986). Chemical and microbiological studies of sea-surface films in the Southern Gulf of California and off the West Coast of Baja California. *Mar Chem* **19**(1): 17-98. doi: 10.1016/0304-4203(86)90033-2

Williams, P.M. and E.R.M. Druffel (1987). Radiocarbon in dissolved organic matter in the Central North Pacific Ocean. *Nature* **330**(6145): 246-248. doi: 10.1038/330246a0

Wind, M., M. Edler, N. Jakubowski, M. Linscheid, H. Wesch, and W.D. Lehmann (2001a). Analysis of protein phosphorylation by capillary liquid chromatography coupled to element mass spectrometry with P-31 detection and to electrospray mass spectrometry. *Anal Chem* **73**(1): 29-35. doi: 10.1021/ac0009595

Wind, M., H. Wesch, and W.D. Lehmann (2001b). Protein phosphorylation degree: Determination by capillary liquid chromatography and inductively coupled plasma mass spectrometry. *Anal Chem* **73**(13): 3006-3010. doi: 10.1021/ac010066s

Winkler, S., J. Carilli, and P. Steier (2011). 100-year record of 236U/238U in coral as a step towards establishing 236U as oceanic tracer. *Mineral Mag* **75**(3): 2167

Witt, M., J. Fuchser, and B.P. Koch (2009). Fragmentation studies of fulvic acids using collision induced dissociation Fourier transform ion cyclotron resonance mass spectrometry. *Anal Chem* **81**(7): 2688-2694. doi: 10.1021/ac802624s

Witter, A.E. and G.W. Luther (1998). Variation in Fe-organic complexation with depth in the Northwestern Atlantic Ocean as determined using a kinetic approach. *Mar Chem* **62**(3-4): 241-258. doi: 10.1016/s0304-4203(98)00044-9

Woods, G.C., M.J. Simpson, B.G. Pautler, S.F. Lamoureux, M.J. Lafrenière, and A.J. Simpson (2011). Evidence for the enhanced lability of dissolved organic matter following permafrost slope disturbance in the Canadian High Arctic. *Geochim Cosmochim Acta* **75**(22): 7226-7241. doi: 10.1016/j.gca.2011.08.013

Wu, F., D. Evans, P. Dillon, and S. Schiff (2004). Molecular size distribution characteristics of the metal – DOM complexes in stream waters by high-performance size-exclusion chromatography (HPSEC) and high-resolution inductively coupled plasma mass spectrometry (ICP-MS). *J Anal At Spectrom* **19**: 979-983

Wu, J.F., E. Boyle, W. Sunda, and L.S. Wen (2001). Soluble and colloidal iron in the oligotrophic North Atlantic and North Pacific. *Science* **293**(5531): 847-849. doi: 10.1126/science.1059251

Wurl, O. and M. Holmes (2008). The gelatinous nature of the sea-surface microlayer. *Mar Chem* **110**(1-2): 89-97. doi: 10.1016/j.marchem.2008.02.009

Wurl, O., L. Miller, R. Röttgers, and S. Vagle (2009). The distribution and fate of surface-active substances in the sea-surface microlayer and water column. *Mar Chem* **115**(1-2): 1-9. doi: 10.1016/j.marchem.2009.04.007

Wurl, O. and J.P. Obbard (2004). A review of pollutants in the sea-surface microlayer (SML): a unique habitat for marine organisms. *Mar Pollut Bull* **48**(11-12): 1016-1030. doi: 10.1016/j.marpolbul.2004.03.016

Wurl, O., E. Wurl, L. Miller, K. Johnson, and S. Vagle (2011). Formation and global distribution of sea-surface microlayers. *Biogeosciences* **8**(1): 121-135. doi: 10.5194/bg-8-121-2011

Xian, F., C.L. Hendrickson, and A.G. Marshall (2012). High resolution mass spectrometry. *Anal Chem* **84**(2): 708-719. doi: 10.1021/ac203191t

Xie, W.H., W.Y. Shiu, and D. Mackay (1997). A review of the effect of salts on the solubility of organic compounds in seawater. *Mar Environ Res* **44**(4): 429-444. doi: 10.1016/s0141-1136(97)00017-2

Xue, J.H., C. Lee, S.G. Wakeham, and R.A. Armstrong (2011). Using principal components analysis (PCA) with cluster analysis to study the organic geochemistry of sinking particles in the ocean. *Org Geochem* **42**(4): 356-367. doi: 10.1016/j.orggeochem.2011.01.012

Yamashita, Y., R. Jaffé, N. Maie, and E. Tanoue (2008). Assessing the dynamics of dissolved organic matter (DOM) in coastal environments by excitation emission matrix fluorescence and parallel factor analysis (EEM-PARAFAC). *Limnol Oceanogr* **53**(5): 1900-1908. doi: 10.4319/lo.2008.53.5.1900

Yamashita, Y. and E. Tanoue (2008). Production of bio-refractory fluorescent dissolved organic matter in the ocean interior. *Nat Geosci* **1**(9): 579-582. doi: 10.1038/ngeo279

Yang, R.J. and C.M.G. van den Berg (2009). Metal complexation by humic substances in seawater. *Environ Sci Technol* **43**(19): 7192-7197. doi: 10.1021/es900173w

Ye, Y., C. Völker, and D.A. Wolf-Gladrow (2009). A model of Fe speciation and biogeochemistry at the Tropical Eastern North Atlantic Time-Series Observatory site. *Biogeosciences* **6**(10): 2041-2061. doi: 10.5194/bg-6-2041-2009

Yoch, D.C. (2002). Dimethylsulfoniopropionate: Its sources, role in the marine food web, and biological degradation to dimethylsulfide. *Appl Environ Microbiol* **68**(12): 5804-5815. doi: 10.1128/aem.68.12.5804-5815.2002

Young, C.L. and E.D. Ingall (2010). Marine dissolved organic phosphorus composition: Insights from samples recovered using combined electrodialysis/reverse osmosis. *Aquat Geochem* **16**(4): 563-574. doi: 10.1007/s10498-009-9087-y

Zemmelink, H.J., L. Houghton, J.W.H. Dacey, J. Stefels, B.P. Koch, M. Schröder, A. Wisotzki, A. Scheltz, D.N. Thomas, S. Papadimitriou, H. Kennedy, H. Kuosa, and T. Dittmar (2008). Stratification and the distribution of phytoplankton, nutrients, inorganic carbon, and sulfur in the surface waters of Weddell Sea leads. *Deep Sea Res II* **55**(8-9): 988-999. doi: 10.1016/j.dsr2.2007.12.011

Zhang, Z.B., L.S. Liu, C.Y. Liu, and W.J. Cai (2003). Studies on the sea surface microlayer - II. The layer of sudden change of physical and chemical properties. *J Colloid Interface Sci* **264**(1): 148-159. doi: 10.1016/s0021-9797(03)00390-4

Zhao, X.L., M.J. Nadeau, L.R. Kilius, and A.E. Litherland (1994). The first detection of naturally-occurring 236U with accelerator mass spectrometry. *Nucl Instrum*

Methods Phys Res, Sect B **92**(1-4): 249-253. doi: 10.1016/0168-583x(94)96014-3

Zhou, X.L. and K. Mopper (1997). Photochemical production of low-molecular-weight carbonyl compounds in seawater and surface microlayer and their air-sea exchange. *Mar Chem* **56**(3-4): 201-213. doi: 10.1016/s0304-4203(96)00076-x

Ziolkowski, L.A. and E.R.M. Druffel (2010). Aged black carbon identified in marine dissolved organic carbon. *Geophys Res Lett* **37**(L16601). doi: 10.1029/2010gl043963

Zubkov, M.V., G.A. Tarran, I. Mary, and B.M. Fuchs (2008). Differential microbial uptake of dissolved amino acids and amino sugars in surface waters of the Atlantic Ocean. *J Plankton Res* **30**(2): 211-220. doi: 10.1093/plankt/fbm091

ADDENDUM

This addendum to the thesis contains original reprints of the three published manuscripts (no. 1, 2 and 4) as well as the supplementary material to the submitted manuscript no. 5.

analytical chemistry

ARTICLE

pubs.acs.org/ac

Inorganics in Organics: Quantification of Organic Phosphorus and Sulfur and Trace Element Speciation in Natural Organic Matter Using HPLC-ICPMS

Oliver J. Lechtenfeld,[*,†] Boris P. Koch,[†,‡] Walter Geibert,[§,⊥] Kai-Uwe Ludwichowski,[†] and Gerhard Kattner[†]

[†]Alfred Wegener Institute for Polar and Marine Research, Am Handelshafen 12, 27570 Bremerhaven, Germany

[‡]University of Applied Sciences, An der Karlstadt 8, 27568 Bremerhaven, Germany

[§]School of GeoSciences, The University of Edinburgh, Edinburgh EH9 3JW, United Kingdom

[⊥]Scottish Association for Marine Science (SAMS), Scottish Marine Institute, Oban, Argyll PA37 1QA, United Kingdom

ABSTRACT: A method is presented for the chemical characterization of natural organic matter (NOM). We combined reversed-phase chromatographic separation of NOM with high resolution inductively coupled plasma mass spectrometry. A desolvation technique was used to remove organic solvent derived from the preceding chromatographic separation. We applied our method to solid-phase extracted marine dissolved organic matter samples from South Atlantic and Antarctic surface waters. The method provided a direct and quantitative determination of dissolved organic phosphorus and sulfur in fractions of differing polarity and also allowed simultaneous speciation studies of trace elements. Dissolved organic carbon/phosphorus and carbon/sulfur ratios for the different chromatographic fractions of our two samples ranged between 341−3025 for C/P and 11−1225 for C/S. Differences in elemental distribution between the fractions were attributed to different biochemical environments of the samples. Sulfur was exclusively found in one hydrophilic fraction, while uranium showed a strong affinity to the hydrophobic fractions. Our method was designed to be easily adapted to other separation techniques. The elemental information will deliver valuable information for ultrahigh resolution molecular analyses.

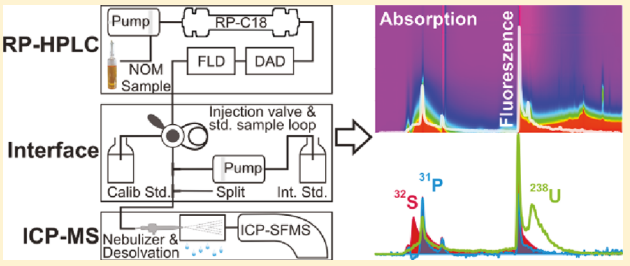

Natural organic matter (NOM) is degraded biomass that occurs in soils, sediments, and water. Its composition is highly complex and polydisperse, which are the major reasons a comprehensive molecular chemical characterization is hindered. In the past ten years, the application of ultrahigh resolution Fourier transform ion cyclotron resonance mass spectrometry (FT-ICR MS) allowed important insights in the molecular composition of thousands of NOM compounds.[1−7] However, FT-ICR MS analyses of NOM is not quantitative and the unequivocal identification of molecules containing sulfur and phosphorus is particularly difficult.[1]

Dissolved organic phosphorus (DOP) can be a limiting element for phytoplankton growth in the ocean.[8] DOP contains a considerable number of monomeric and polymeric phosphate esters, phosphonates, and other N and S containing compounds (nucleotides, vitamins, etc.).[9,10] The chemical knowledge of dissolved organic sulfur (DOS) in marine organic matter is scarce and mainly restricted to small sulfur containing compounds such as dimethyl sulfide, dimethylsulfoniopropionate, and methanethiol.[11,12] Other thiols, e.g., phytochelatins, are known to be important metal chelators,[13] although their abundance in open ocean seawater is very low.[14] Few FT-ICR MS studies revealed a set of additional DOS compounds in marine NOM in the deep sea and in brine samples.[15,16]

Organic metal speciation is of great interest in environmental science, because it affects bioaccumulation and toxicity[17−19] (e.g., Cr, Hg, Cd), bioavailability[20,21] (e.g., Fe, Zn), and transport and distribution of trace metals[22,23] (e.g., Mn, Th). Many trace metals in seawater are essential constituents for a number of enzymes, and therefore, their remineralization indirectly controls bioproductivity and species composition in the ocean.

In seawater, the analysis of trace concentrations of organic compounds (μg to mg L^{-1} range) and transition metals (ng to μg L^{-1} range) is especially demanding due to the high salt concentration (35 g L^{-1}). To prevent interferences of sea salts, many analytical techniques require preceding enrichment and desalting procedures such as ultrafiltration, reversed osmosis, or solid-phase extraction (SPE). For speciation studies, the application of such extraction methods introduces an additional analytical challenge because the requirements for sample preparation (filter materials, storage bottles, acidification steps, etc.) in organic and inorganic studies often diverge. However, it is known that the retention of trace metals on, e.g., C18 adsorber material[24−28] and octanol partitioning[29] is considerable, and a large fraction of

Received: July 8, 2011
Accepted: October 12, 2011
Published: October 12, 2011

these metals exists in organic complexes rather than in a free ionic form in marine NOM.[20,30,31] In the last years, research on the structure of organic ligands for trace metals in seawater intensified,[32,33] but little is known about the organic complexation of uranium in seawater.[34,35]

High resolution inductively coupled plasma sector field mass spectrometry (ICPMS) is a favorable technique for the quantification of elements in NOM. ICPMS is highly sensitive and allows for multielement and even multi-isotope analyses. Hyphenation with separation techniques also enables speciation studies. Vogl and Heumann, for example, combined size exclusion chromatography (SEC) with isotope dilution ICPMS to determine the dissolved organic carbon (DOC) content of humic substance fractions.[36] It has been previously shown that P could be detected in reversed-phase high performance liquid chromatography (RP-HPLC) fractions with ICPMS in derivatized carboxylic acids[37] and phosphorylated proteins[38] at very low concentrations (nM to pM). Speciation of organic sulfur with HPLC-ICPMS was carried out for phosphorylated peptides.[39] Wang et al. developed a method for protein quantification via sulfur isotope dilution analysis in a coupled SEC-ICPMS system.[40] To our knowledge, no speciation study of marine DOP and DOS using LC-ICPMS exists in the literature. ICPMS in combination with SEC has also been applied to study speciation of trace metals in fresh water;[41] a different approach uses flow field-flow fractionation coupled to ICPMS to separate colloidal size classes of trace metal-dissolved organic matter (DOM) complexes.[42] The use of silica based RP-HPLC separation for trace metal speciation studies is known to introduce artifacts,[24,43] and a careful investigation of metal recoveries is crucial.[44]

The overall aim of this study is to establish a simultaneous determination of trace organic compounds and trace metals and to merge the analytical potentials of advanced polarity separation and ICPMS. Our goal is to provide quantitative elemental information on different fractions of highly complex-low concentrated NOM in seawater. Simultaneous online ICPMS detection of P and S provides a new approach to chemically assess DOP and DOS. This will be a prerequisite to improve molecular studies which are based on the analyses of chromatographic fractions by FTICR-MS.[7] In addition, the chromatographic separation of U is exemplarily discussed to demonstrate the capability of the method as a tool for trace metal speciation studies.

EXPERIMENTAL SECTION

Samples. Surface water samples (2 m depth) were collected using a towed fish sampler[45] during the R/V *Polarstern* cruises ANT-XXV/1 and ANT-XXV/2. One sample was selected from nutrient-poor surface waters of the Guinea Basin (South Atlantic Central Water, SACW); the other sample originates from the southern rim of the Antarctic Circumpolar Current (ACC) south of the Polar Front (Antarctic Surface Water, AASW) and was characterized by high nutrient and low DOC concentration. Samples were collected by pumping surface water with a Teflon membrane pump to the ship's lab, filtered with 0.2 μm cellulose acetate in-line filters (Sartolab P20, Sartorius), and acidified with hydrochloric acid (suprapur, Merck) to pH 2. DOM extraction was performed with 1 g solid-phase extraction cartridges (PPL, Varian) according to Dittmar et al.[46] A volume of 5.4 and 4.85 L of sample (SACW and AASW, respectively) was extracted and finally stored in 4.8 mL of methanol (LiChrosolv, Merck) in precleaned LD-PE bottles at −20 °C. The cleaning procedures for sampling material was adapted from GEOTRACES.[47] There was also no significant contamination of DOC.

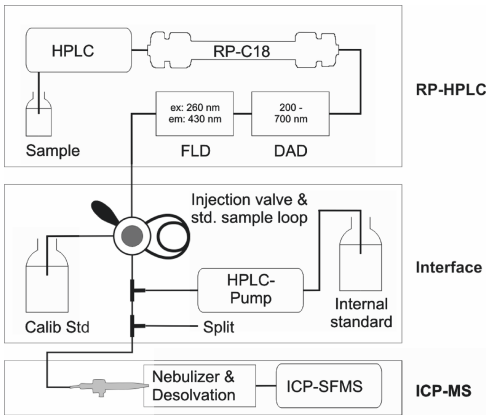

Figure 1. Hyphenation of RP-HPLC and ICPMS. Chromatographic column was a Synergi Hydro-RP C18 column. Diode array detector (DAD) recorded absorption between 200 and 700 nm whereas fluorescence detector (FLD) recorded fluorescence at 260 nm excitation and 430 nm emission.

Chemicals and Reagents. Ultrapure water (18 MΩ) for diluting reagents and samples was always obtained from a two-step purification system (ElixS and Milli-Q Plus 185 with UV, Millipore). Nitric acid (analytical grade, OmniChem) was purified 2-fold in a quartz subboiling distillation apparatus. High purity methanol (LiChrosolv, Merck) was further purified by subboiling distillation in a quartz apparatus to reduce trace metal contributions. Standard solutions for calibration of the mass spectrometer were prepared from commercially available stock solutions (nonmetal multielement standard for ICPMS, VHG Laboratories; ICPMS multielement standard 23 solution, Merck).

HPLC System. Chromatographic separation was carried out according to Koch et al.[7] The HPLC system (Hitachi/VWR) was equipped with a pump (L6200A), interface (D6600), autosampler (AS4000A), column oven (L5025), diode array detector (DAD, L4500), and fluorescence detector (FLD, F1050). The separation was performed using a polar end-capped C18-reversed-phase column (4 μm Hydro-RP 80 Å, 250 × 4 mm, with AQ C18 Guard Column; Phenomenex, Synergi) running a gradient from 100% ultrapure water, adjusted to pH 7 (±0.05) with diluted NaOH (suprapur, Merck), to 100% methanol. The gradient was linearly increased from 0 to 100% methanol during a period from 6 to 20 min. In contrast to the original method, the HPLC flow remained constant at 0.3 mL min^{-1} to avoid changes in the hydrodynamic conditions of the flow system. The column oven temperature was 25 °C. Both detectors were connected in series; absorbance was recorded between 200 and 400 nm, and the fluorescence signal was measured at 260 nm excitation and 430 nm emission wavelength (data not shown). Methanol reached the detector after ∼23 min. Thirty and 40 μL of the extracts were injected for the SACW and AASW sample, respectively. The injection volume was adjusted to ensure similar extract DOC amounts (∼1 μmol) on the column for each chromatographic run.

Fraction Collection. For DOC analysis, fractions were collected at the outflow of the fluorescence detector using a fraction collector (Foxy Jr., Teledyne Isco). The volume of 10 repeated

Table 1. Instrumental ICPMS Conditions

Plasma Conditions	
RF power	1300 W
Ar sample gas	1.01−1.04 mL min^{-1}
Ar auxiliary gas	1.01 mL min^{-1}
Ar cool gas	16 mL min^{-1}
Ar sweep gas	6.5 bar
Data Acquisition	
scan mode	peak hopping
scan type	EScan
samples per mass	12
sample time	15 ms
integration window	30%
integration type	average
complete mass scan	2 s

injections were collected and then either freeze-dried (aqueous fraction) or dried under N_2 gas (methanol fractions) and redissolved in 1 mL of ultrapure water. The same injection volume as for the coupled analysis was used since the column is sensitive to overloading for some fractions. Blank fractions were prepared without sample injection and were used to monitor the carbon contamination of the HPLC system.

Hyphenation between HPLC and ICPMS. The system configuration (Figure 1) was adapted from Rottmann and Heumann.[48] Compared to their original publication, we used a reversed-phase column which introduces an organic solvent (methanol) into the inductively coupled plasma. Therefore, the following measures were taken to reduce the solvent loading of the combined flow and to stabilize the baseline of the ICPMS signals: (i) reduction of the combined flow of 0.5 mL min^{-1} to about 0.05 mL/min, (ii) addition of 10% methanol to the postcolumn spike solution to make use of the solvent enhancement effect[49,50] and to reduce the large changes in matrix viscosity when introducing a small amount of organic solvent into the nebulizer, and (iii) desolvation of the sample aerosol to remove most of the methanol from the sample droplets and obtain a dried aerosol.

The outlet of the fluorescence detector was connected with a PFA tubing (0.01 in. inner diameter, ID) to a 6-port injection valve (Teflon, Upchurch Scientific), equipped with a 25 μL sample loop (0.4 ft x 0.02 in ID, PFA Hi Pur, Upchurch Scientific) for the addition of calibration standards. Standards were loaded by suction technique from a clean reservoir into the sample loop. Continuous addition of the internal standard (in 1 M nitric acid) to the HPLC flow was achieved by a static mixing T-fitting (Upchurch Scientific). This flow was set to 0.2 mL min^{-1} using an HPLC-pump equipped with polyether ether ketone parts (PEEK, Alltech-Grace). Prior to nebulization, the flow was reduced to 0.05 mL min^{-1} (micro metering split valve, Upchurch Scientific) to lower the sample load in the plasma.

Samples were nebulized using an APEX-Q system (all quartz, Elemental Scientific) with a PFA microconcentric nebulizer, a heated cyclonic spray chamber (100 °C), and a Peltier-cooled condenser (2 °C). Furthermore, a membrane desolvation unit (heated macro-porous PTFE, SPIRO-TMD, Elemental Scientific) was installed at the outlet of the APEX-Q for successive elimination of the matrix components of the aerosol, especially of methanol.

ICPMS System. ICPMS conditions are given in Table 1. A high resolution ICP mass spectrometer (Element 2, Thermo Fisher Scientific) equipped with a platinum guard electrode, nickel sampler, and skimmer cones was used. Data acquisition parameters were set for a full scan cycle within 2 s which was a compromise between time resolution (sampling frequency per peak) and counting statistics (dwell time per mass measurement and noise of the individual signal).[51] The instrument was tuned daily for optimized plasma conditions and accurate mass calibration with a multielement tuning solution (~0.1 ppb in 10% methanol, Merck). Signals of ^{31}P, ^{32}S, ^{238}U, and ^{103}Rh were recorded in medium mass resolution (4000 m/Δm). ^{103}Rh was used as internal standard with a concentration of ~5 ppb in the spike solution. This Rh concentration resulted in an intensity of ~5×10^4 cps at a split ratio of 0.05/0.45 mL min^{-1}.

Data acquisition of the MS was triggered from the HPLC-system (TTL cable). The dead time between the fluorescence detector and MS was ~60 s at a split ratio of 0.05/0.45 mL min^{-1}.

DOC Analysis. DOC was analyzed on a Shimadzu TOC-V_{CPN}+TNM-1 analyzer with external calibration with potassium hydrogen phthalate (PHP, Merck). Methanol extracts from solid-phase extracted samples (50 μL aliquots) were evaporated by N_2 gas flow to complete dryness and subsequently redissolved in 6.5 mL of ultrapure water for DOC analysis. All samples (in duplicate) were acidified (0.1 M HCL suprapur, Merck) and purged with oxygen for >5 min. HPLC fractions were injected directly on top of the catalyst tube using a manual injector (Shimadzu). Three to 5 replicates of 50 μL of acidified sample were injected with a syringe (Hamilton). Performance of the instrument was recorded by daily analysis of in-lab PHP standard solutions and reference material (deep sea reference, DSR, Hansell research lab).

Data Treatment. Raw data from the HPLC system and the mass spectrometer were analyzed with a home-built program. ICPMS transient signals were treated with a smoothing algorithm (Savitzky-Golay; 11 point quadratic[52]) prior to peak integration.

RESULTS AND DISCUSSION

Separation Mechanism. Prior to the coupling of HPLC and ICPMS, a new assessment of our recent chromatographic method[7] was carried out using a constant flow of 0.3 mL min^{-1}. The injection of 50 μL of methanol on the column led to an elution volume of 2.76 mL. After 6 min (=1.8 mL), the gradient program started, and the start of the gradient was detected by the DAD (210 nm) at an elution volume of 6.96 mL. The difference of 2.4 mL is attributed to the gradient delay volume (i.e., the volume between mixing chamber and injection port). When injecting a DOM sample, the first peaks appeared already at a 1.2 mL elution volume and hence ahead of the methanol matrix. This can be explained by a size separation mechanism since very large molecules are excluded from the 80 Å pore diameter of the RP column material. In addition, the clogging of the pores by molecules adsorbing at the rim of the pores (e.g., dimer or multimer formation of highly polar, carboxylic rich substances,[7] potentially supported by a central metal ion) may reduce the effective pore diameter for subsequent molecules.[7,53] This effect is known for humic acid fractions of NOM[54,55] and SEC analysis of DOM.[56−58]

DOC Content of Fractions. For the quantitative assessment of the different chromatographic fractions and their contribution

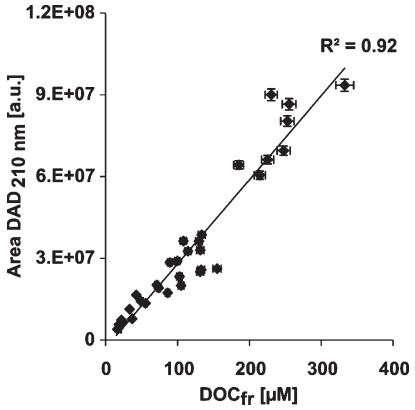

Figure 2. UV peak area (diode array detection, DAD; [a.u.] = arbitrary unit) at 210 nm versus DOC concentrations (DOC_{fr}) of fractions F1−F6 (see also Table 2). Marine surface water (SACW, AASW) and two additional deep water samples (data not shown furthermore) were measured as triplicates. Error bars indicate average relative standard deviation for both measurements (3.7% for DOC and 1.2% for DAD areas).

to the total DOC in the sample, we measured DOC in each fraction. Furthermore, we evaluated whether UV absorption can be applied as an estimate of DOC concentration in the chromatographic run. Using a DAD detection wavelength of 210 ± 5 nm, absorption from $n \rightarrow \sigma^*$ (e.g., alcohols, ethers) and $\pi \rightarrow \pi^*$ electronic transitions (e.g., conjugated systems including carboxylic groups and partly aromatic systems) dominate. These chromophores usually compose the backbone of NOM molecules and therefore give a measure of the overall carbon content in the sample.[59] The $DAD_{210\ nm}$ peak areas correlated highly significantly (r^2 = 0.92; p < 0.001; n = 32) with the DOC concentration of the fractions (Figure 2) suggesting that UV absorption can be reasonably applied as an approximation of the carbon amount in our samples.

ICPMS Signal Stability and Influence of Methanol. The use of organic solvents in a coupled HPLC-ICPMS system influences the plasma stability by lowering the plasma temperature, by reducing the amount of Ar^+-species and finally by decreasing the intensity of the analytes at high organic solvent concentrations.[50,60] The high vapor pressure of organic solvents can even extinguish the plasma. Another negative side effect is the buildup of perturbing amounts of carbon on the cones that leads to shifts in the signal intensity and resolution.

The ^{31}P and ^{32}S short-term signal stability, calculated as the relative standard deviation (RSD) of the baseline (analyte signal between 0 and 4 min, where no substance is eluting), was in the range of 1−4% for the smoothed values. ^{238}U showed a much higher noise signal (RSD 20−40%), as the overall intensity was very low in medium resolution. However, sample peaks showed a U signal that was mostly higher by a factor of 10^2 to 10^3 than the baseline noise. Using the values normalized to the internal standard, the RSD of the ratio did not change compared to the smoothed analyte signal.

A blank injection of 30 µL of clean methanol led to an average loss of ^{103}Rh intensity of ∼20% between the gradient onset at 23 min and 100% methanol. A similar signal drift in the methanol gradient was observed for ^{31}P, ^{32}S, and ^{238}U in the sample runs. Changing viscosity of the eluent as observed by an increasing backpressure of the second HPLC pump might contribute to the change in signal intensity. However, the decrease was not identical for all elements. We observed small deviations of the intensity ratios $^{31}P/^{103}Rh$, $^{32}S/^{103}Rh$, and $^{238}U/^{103}Rh$. Signal intensities also depend on the mass of the ions, their ionization potential, and their extent/degree of oxide formation[49,61] which in turn depend on the methanol concentration in the solvent. As a consequence, a daily sensitivity correction for each analyte was obtained from a blank run and applied to the sample measurements as suggested previously.[62]

Multiple injection of the same sample showed a highly significant correlation between the RSD values the $DAD_{210\ nm}$ area and the RSD values of the ICPMS signal area (r^2 = 0.75; p < 0.01, n = 8). Thus, the overall analytical precision is mainly influenced by the separation step rather than changing ICP conditions.

At the end of a chromatographic run (85 min), all signals returned to the initial value. Remnants of the organic solvent were rinsed with nitric acid added postcolumn to the HPLC. Between two chromatographic runs, a correction for instrument mass drift was performed by running the Method Mass Offset measurement to support the "Auto Lock Mass" feature of the Element 2 in case the mass peaks shifted too much from the centroid mass during the 85 min analysis time. This procedure was necessary because of the small mass window that was chosen to increase the time resolution of the ICP signal.

Calibration and Recovery. Calibration for P, S, and U was carried out with a postcolumn injection of three calibration standards via the 25 µL sample loop into the HPLC flow (Figure 1). Due to the broad and nonsymmetrical peak shape in the sample runs, we used peak areas rather than peak heights for quantification. The area of the blank (1 M HNO_3) was subtracted from each standard. The lowermost calibration level was 1.2 ng P, 0.25 ng S, and 2.1 pg U. Limits of detection, as obtained by dividing three times the standard deviation (n = 4) of the lowermost calibration standard by the slope of the corresponding calibration function, were 0.3 µM P, 0.01 µM S, and 0.07 nM U.

To prove the suitability of the use of inorganic salts as standard solutions, a four point standard addition of a methanol extract with calibration solutions was performed in the external sample loop. From the linear response of the P, S, and U signals (r^2 > 0.995), we conclude that the chemical form of the calibration standards did not influence the ICPMS response as the organic molecules in the sample should dissociate and ionize completely in the ICP.

The recovery of analytes during the HPLC separation was determined after replacing the column with a 100 cm × 0.02 in. ID PEEK capillary. The total recovery by the HPLC was calculated as the amount of analyte eluting between 4 and 37 min compared to the concentration in the total extract (Table 2). For sample SACW and AASW, recoveries were 75 and 93% for P, 95 and 102% for S, and 85 and 91% for U.

Analysis of DOP, DOS, and U. Both sample chromatograms showed six peak-like regions, which were detected between 5−12 min and 23−32 min (Figure 3). The first small peak showed traces of P and S (F1, 4.7−5.8 min). The relative intensity of the second peak differed between samples and was most pronounced in the S signal, whereas the DAD signal was only a small shoulder (F2, 5.8−7.0 min). The third peak was also variable in the two samples and highest in the DAD signal (F3, 7.0−9.7 min). The fourth peak was only pronounced in the SACW sample (F4, 10.0−11.2 min). Between the first and the second group of peaks, no additional signals were detected for about 10 min. In other NOM samples (not shown), smaller

Table 2. Concentration and Recovery of P and S in Extract and Fractions of Samples SACW and AASW[a]

			fractions							
		MeOH extract[b]	F1	F2	F3	F4	F5	F6	fractions [%][c]	total run [%][d]
SACW	DOC [μM]	30966	1210	1913	5093	1383	7457	2870	64	102
	P [μM]	43	0.4	<0.3	8	2	13	3	62	75
	S [μM]	132	4	16	27	6	38	7	74	95
	C/P	721	3025		614	751	595	848		
	C/S	234	309	123	190	215	196	395		
AASW	DOC [μM]	22340	653	1240	5207	1710	5667	1970	74	
	P [μM]	26	<0.3	<0.3	15	<0.3	6	1	84	93
	S [μM]	176	4	116	23	3	17	2	93	102
	C/P	850			341		960	1921		
	C/S	127	181	11	224	545	333	1225		

[a] For values below the detection limit, no elemental ratio was calculated. Error estimates: Triplicate extraction of surface water resulted in a RSD of <7% (DOC, P) and <2% (S) for the total MeOH extracts; chromatographic separation of methanol extracts resulted in an average RSD of 4% (DOC; $n = 8$) and 9% (P, S; $n = 3$) for individual fractions. [b] Concentration as in unfractionated methanol extract. DOC in the original samples was 76.9 μM (SACW) and 51.8 μM (AASW). Extraction efficiency for C was 40% for both samples. [c] Fractions [%] calculated as sum of the six fractions F1 to F6. [d] Total run [%] represents the complete chromatogram between 4 and 37 min.

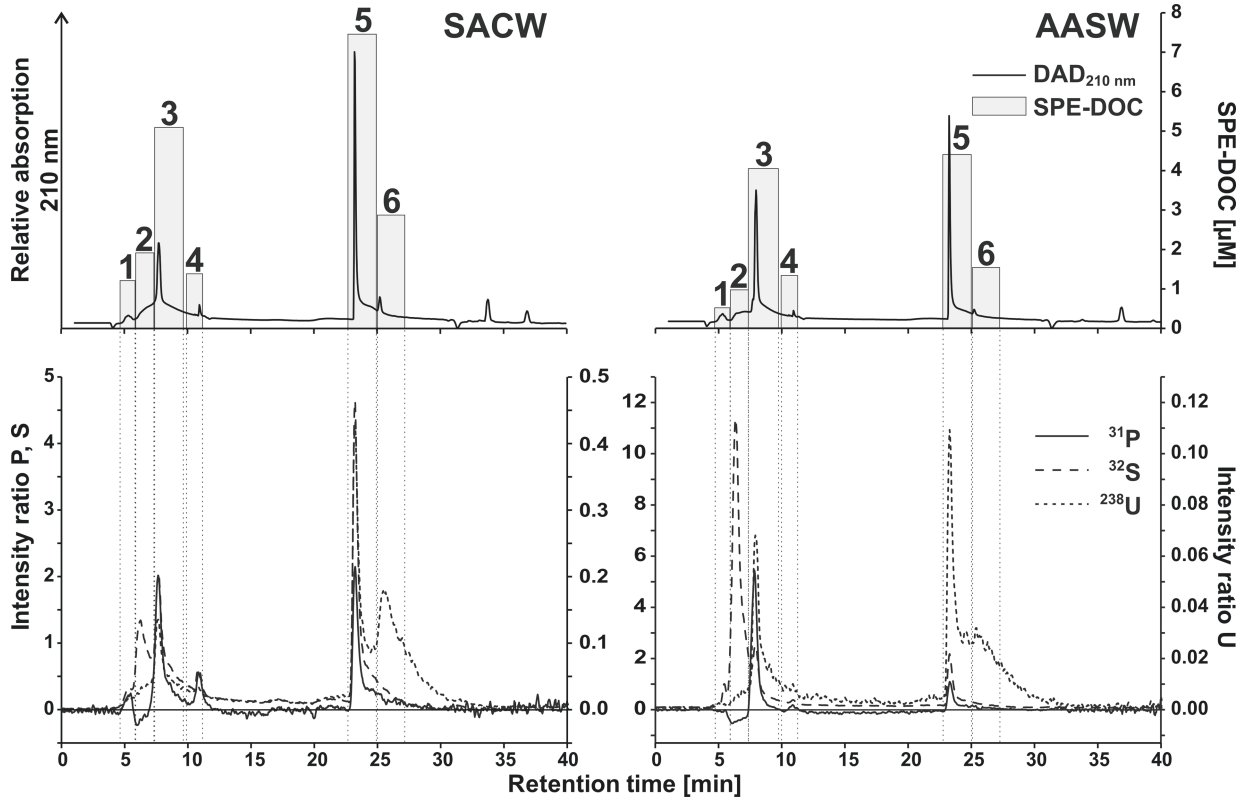

Figure 3. UV and mass chromatograms for two marine surface water extracts (SACW, AASW). The two upper chromatograms show the UV absorption from the DAD at 210 nm and the SPE-DOC concentration of the fractions (1 to 6; gray bars, right *Y*-axis). The two lower chromatograms show the related ICPMS signals for P (solid line), S (dashed line), and U (dotted line, right *Y*-axis). They are displayed as intensity ratio (intensity analyte/intensity internal standard) after sensitivity correction as described in the text.

additional peaks were found in this part of the chromatogram. The second group of peaks started with the methanol gradient and therefore resulted in a sharp peak. The DAD signal at 210 nm of this peak was always highest whereas the ICP signal varied between samples and elements (F5, 22.7−25.0 min). DAD, P, and S showed a pronounced tailing as a result of the large number of components with very similar chemical properties which successively elute with increasing methanol content. U detection resulted in a second peak especially in the SACW sample (F6, 25.0−27.2 min). In the final part of the HPLC run (up to 37 min; 100% methanol), some smaller peaks appeared in the DAD detection but were not detected with the MS.

dx.doi.org/10.1021/ac201765a |*Anal. Chem.* 2011, 83, 8968–8974

There was a remarkable difference in the relative amount of S in fraction F2 (70% in sample AASW and 16% in SACW) as well as P in fraction F3 (68% in AASW and 31% in SACW). According to the HPLC separation, P and S in sample AASW were incorporated in larger and more polar compounds. In fact, P and S are incorporated in large, polar biomolecules (e.g., phosphate esters, phosphonates). Such compounds can be quickly biodegraded, especially in regions where P is limiting the phyto- and bacterioplankton growth in surface waters.[63] This indicates that DOM from AASW contains fresher (less degraded) material than from the SACW sample.

The stoichiometric elemental ratios C/P and C/S (as organic carbon, phosphorus, and sulfur) potentially reflect the diagenetic state of DOM.[64] This has been explained by different turnover rates of labile and refractory DOM and is reflected in a different C/P stoichiometry between surface and deep ocean (C/P surface: 374 ± 59; C/P deep ocean: 3511 ± 1314).[65]

In macronutrient limited regions of the oceans, a dominant remineralization of P (and S) over C and N compounds occurs,[64,66] leading to high C/P and C/S ratios compared to the average composition of marine algae (C/P = 106).[67] The bulk SPE-DOM values for C/P found here (721 for SACW and 850 for AASW, Table 2) were higher than expected for surface water samples. This can be explained by a discrimination of very polar P compounds by the extraction procedure, as it has been observed previously for N compounds.[46] Assuming that the extraction efficiency of P for both samples ranged in between the C- and the N-extraction efficiency (40 and 15%, respectively), the SPE recovered P can be converted to an estimated DOP concentration in the original seawater of 0.11−0.29 μM P (SACW) and 0.07−0.18 μM P (AASW). The phosphate concentration of the SACW and AASW sample was 0.05 and 1.79 μM P, respectively. This suggests that the dominant P pool in the oligotrophic SACW is of organic nature while, in the phosphate rich AASW, DOP is only a minor component. The dominance of large and polar organic P compounds in the nutrient poor water probably indicates enhanced DOP recycling. Our values are in good agreement with other studies, e.g., Mather et al., who found 0.15−0.3 μM DOP in the proximity of the equator in the central Atlantic Ocean in November.[63] In the Drake Passage, Sanders and Jickells reported TOP values with a range from 0.07 to 0.2 μM P.[68]

Studies involving DOS are very scarce. Alling et al. found C/S values in the Baltic Sea ranging from 219 to 282.[69] In our study, C/S ratios were 234 and 127 for SACW and AASW, respectively. Assuming an S extraction efficiency between 15% and 40%, SPE-DOS concentration in the original seawater can thus be estimated to be 0.33−0.88 μM S (SACW) and 0.44−1.17 μM S (AASW). Cutter et al. reported Sargasso Sea surface water DOS concentrations in a range between 40 and 400 nM S.[70] Although their values are lower than the DOS concentrations in this study, the agreement is reasonable considering the high seasonal-annual variability and the different study sites. The range of elemental ratios of the fractions scattered around the bulk values (C/P = 341−3025 and C/S = 11−1225, Table 2). Fraction ratios have a relatively high uncertainty (~13% RSD) and depend on extraction efficiency and the separation mechanism on the column in addition to different sources of DOM.

Compared to P and S, U was less abundant in the water-soluble fractions; most of the U eluted in the methanol part, indicating that the organic U complexes were more hydrophobic. The pronounced peak of U in the less polar fraction F6 was unique. For suspended organic matter, it was proposed earlier that the organic binding sites for uranium are polydentate ligands.[71] Together with a likely preference of the uranyl ion for carboxylic groups (as substitution for carbonate ions), we assume that chelate effects might be responsible for an apparently higher hydrophobicity of the U-DOM complex. We think that the distribution of U in the polarity gradient is interesting and contributes new information to the nature of U speciation, especially when compared with other trace elements such as Ni (data not shown).

However, due to the uncertainties in the extraction procedure, conclusions on the U distribution in the original seawater are difficult to draw without further assessment of U extraction efficiencies. The inorganic speciation of U strongly depends on pH,[72] and U-organic complex equilibriums are strongly affected as well.[73] Therefore, only stable (i.e., strongly bound) U complexes are amenable to analysis if the seawater sample is chemically modified.

CONCLUSIONS

We described a novel analytical tool to measure and determine DOP and DOS compounds in seawater extracts by means of RP-HPLC hyphenated to ICPMS. This method can be extended to trace metal detection, as shown here for U to obtain a new concept of natural ligand classes and to gain further insights into coupled biogeochemical cycles, e.g., Zn−Co−P.[74,75] In particular, this technique can provide a tool to study the remineralization of phosphorus and organic-bound trace metals in the deeper ocean. Future applications of this method involve (1) characterization, classification, and quantification of DOP and DOS compounds in marine and other NOM samples; (2) speciation of trace metals according to chemical compound classes defined by the polarity of the NOM moieties; (3) refinement of molecular formula assignments in FT-ICR MS based on the abundance and distribution of organic phosphorus and sulfur compounds in NOM fractions. Additionally, without the restrictions evolving from the high salt content and low NOM concentration in seawater, the method can be even better applied to original samples of fresh water systems.

AUTHOR INFORMATION

Corresponding Author

*Phone: +49 471 4831 2238. E-mail: oliver.lechtenfeld@awi.de.

ACKNOWLEDGMENT

We thank the associate editor Reinhard Niessner and two anonymous reviewers for valuable comments and suggestions. We also thank the master and crew of R/V *Polarstern* for their professional help. Analysis of the samples would not have been possible without allocation of the ICPMS by Jana Friedrich and Ingrid Stimac from Marine Geology department at AWI. We appreciate the expertise of Dieter Janssen and his help with the TOC analyzer. This work was financially supported by the Deutsche Forschungsgemeinschaft (DFG KO 2164/8-1) and the German Academic Exchange Service (DAAD PPP GB 50023021).

REFERENCES

(1) Koch, B. P.; Witt, M.; Kattner, G.; Dittmar, T. *Anal. Chem.* **2007**, *79*, 1758–1763.

(2) Sleighter, R. L.; Hatcher, P. G. *J. Mass Spectrom.* **2007**, *42*, 559–574.
(3) Kujawinski, E. B.; Freitas, M. A.; Zang, X.; Hatcher, P. G.; Green-Church, K. B.; Jones, R. B. *Org. Geochem.* **2002**, *33*, 171–180.
(4) Stenson, A. C.; Marshall, A. G.; Cooper, W. T. *Anal. Chem.* **2003**, *75*, 1275–1284.
(5) Hertkorn, N.; Frommberger, M.; Witt, M.; Koch, B. P.; Schmitt-Kopplin, P.; Perdue, E. M. *Anal. Chem.* **2008**, *80*, 8908–8919.
(6) Witt, M.; Fuchser, J.; Koch, B. P. *Anal. Chem.* **2009**, *81*, 2688–2694.
(7) Koch, B. P.; Ludwichowski, K.-U.; Kattner, G.; Dittmar, T.; Witt, M. *Mar. Chem.* **2008**, *111*, 233–241.
(8) Benitez-Nelson, C. R. *Earth-Sci. Rev.* **2000**, *51*, 109–135.
(9) Young, C. L.; Ingall, E. D. *Aquat. Geochem.* **2010**, *16*, 563–574.
(10) Karl, D. M.; Bjorkman, K. M. Dynamics of DOP. In *Biogeochemistry of Marine Dissolved Oragnic Matter*; Hansell, D., Carlson, C.A., Eds.; Academic Press, Elsevier Science: San Diego, USA, 2002.
(11) Yoch, D. C. *Appl. Environ. Microbiol.* **2002**, *68*, 5804–5815.
(12) Bentley, R.; Chasteen, T. G. *Chemosphere* **2004**, *55*, 291–317.
(13) Wei, L. P.; Ahner, B. A. *Limnol. Oceanogr.* **2005**, *50*, 13–22.
(14) Ahner, B. A.; Lee, J. G.; Price, N. M.; Morel, F. M. M. *Deep-Sea Res. I* **1998**, *45*, 1779–1796.
(15) D'Andrilli, J.; Dittmar, T.; Koch, B. P.; Purcell, J. M.; Marshall, A. G.; Cooper, W. T. *Rapid Commun. Mass Spectrom.* **2010**, *24*, 643–650.
(16) Kujawinski, E. B.; Longnecker, K.; Blough, N. V.; Vecchio, R. D.; Finlay, L.; Kitner, J. B.; Giovannoni, S. J. *Geochim. Cosmochim. Acta* **2009**, *73*, 4384–4399.
(17) Luoma, S. N.; Rainbow, P. S. *Environ. Sci. Technol.* **2005**, *39*, 1921–1931.
(18) Rainbow, P. S. *Environ. Int.* **2007**, *33*, 576–582.
(19) Ullrich, S. M.; Tanton, T. W.; Abdrashitova, S. A. *Crit. Rev. Environ. Sci. Technol.* **2001**, *31*, 241–293.
(20) Morel, F. M. M.; Price, N. M. *Science* **2003**, *300*, 944–947.
(21) Hirose, K. *Anal. Sci.* **2006**, *22*, 1055–1063.
(22) Hirose, K. *J. Radioanal. Nucl. Chem.-Articles* **1996**, *204*, 193–204.
(23) Santschi, P. H.; Guo, L.; Walsh, I. D.; Quigley, M. S.; Baskaran, M. *Cont. Shelf Res.* **1999**, *19*, 609–636.
(24) Mackey, D. J. *Mar. Chem.* **1983**, *13*, 169–180.
(25) Kaczynski, S. E.; Kieber, R. J. *Environ. Sci. Technol.* **1994**, *28*, 799–804.
(26) Donat, J. R.; Statham, P. J.; Bruland, K. W. *Mar. Chemistry* **1986**, *18*, 85–99.
(27) Otero-Romani, J.; Moreda-Pineiro, A.; Bermejo-Barrera, A.; Bermejo-Barrera, P. *Anal. Chim. Acta* **2005**, *536*, 213–218.
(28) Mackey, D. J. *Mar. Chemistry* **1982**, *11*, 169–181.
(29) Turner, A.; Mawji, E. *Environ. Sci. Technol.* **2004**, *38*, 3081–3091.
(30) Macrellis, H. M.; Trick, C. G.; Rue, E. L.; Smith, G.; Bruland, K. W. *Mar. Chem.* **2001**, *76*, 175–187.
(31) Laglera, L. M.; van den Berg, C. M. G. *Limnol. Oceanogr.* **2009**, *54*, 610–619.
(32) Mawji, E.; Gledhill, M.; Milton, J. A.; Tarran, G. A.; Ussher, S.; Thompson, A.; Wolff, G. A.; Worsfold, P. J.; Achterberg, E. P. *Environ. Sci. Technol.* **2008**, *42*, 8675–8680.
(33) Manceau, A.; Matynia, A. *Geochim. Cosmochim. Acta* **2010**, *74*, 2556–2580.
(34) Alberti, G.; Biesuz, R.; Pesavento, M. *Microchem. J.* **2007**, *86*, 166–173.
(35) Mann, D. K.; Wong, G. T. F. *Mar. Chem.* **1993**, *42*, 25–37.
(36) Vogl, J.; Heumann, K. G. *Anal. Chem.* **1998**, *70*, 2038–2043.
(37) Cartwright, A. J.; Jones, P.; Wolff, J. C.; Evans, E. H. *J. Anal. At. Spectrom.* **2005**, *20*, 75–80.
(38) Wind, M.; Edler, M.; Jakubowski, N.; Linscheid, M.; Wesch, H.; Lehmann, W. D. *Anal. Chem.* **2001**, *73*, 29–35.
(39) Lindemann, T.; Hinrichs, J.; Hamester, M.; Wills, J. *Simultaneous Phosporus and Sulfur Speciation by HPLC Interfaced with High Resolution ICP-MS*; Thermo Fischer Scientific: Bremen, Germany, 2007.
(40) Wang, M.; Feng, W. Y.; Lu, W. W.; Li, B.; Wang, B.; Zhu, M.; Wang, Y.; Yuan, H.; Zhao, Y.; Chai, Z. F. *Anal. Chem.* **2007**, *79*, 9128–9134.
(41) Rottmann, L.; Heumann, K. G. *Anal. Chem.* **1994**, *66*, 3709–3715.
(42) Stolpe, B.; Guo, L. D.; Shiller, A. M.; Hassellov, M. *Mar. Chem.* **2010**, *118*, 119–128.
(43) Mackey, D. J.; Higgins, H. W. *J. Chromatogr., A* **1988**, *436*, 243–257.
(44) Mackey, D. J. *Mar. Chem.* **1985**, *16*, 105–119.
(45) Sarthou, G.; Baker, A. R.; Blain, S.; Achterberg, E. P.; Boye, M.; Bowie, A. R.; Croot, P.; Laan, P.; de Baar, H. J. W.; Jickells, T. D.; Worsfold, P. J. *Deep-Sea Res. I* **2003**, *50*, 1339–1352.
(46) Dittmar, T.; Koch, B. P.; Hertkorn, N.; Kattner, G. *Limnol. Oceanogr.: Methods* **2008**, *6*, 230–235.
(47) Cutter, G.; Andersson, P.; Codispoti, L.; Croot, P. L.; Francois, R.; Lohan, M.; Obata, H.; Rutgers van der Loeff, M. *Sampling and Sample-handling Protocols for GEOTRACES Cruises.* 2010 GEOTRACES Standards and Intercalibration Committee. [Online] December 2010 http://www.obs-vlfr.fr/GEOTRACES/libraries/documents/Intercalibration/Cookbook.pdf. (accessed October 7, 2011).
(48) Rottmann, L.; Heumann, K. G. *Fresenius J. Anal. Chem.* **1994**, *350*, 221–227.
(49) Hu, Z. C.; Hu, S. H.; Gao, S.; Liu, Y. S.; Lin, S. L. *Spectrochim. Acta, Part B* **2004**, *59*, 1463–1470.
(50) Liu, S.; Beauchemin, D. *Spectrochim. Acta, Part B* **2006**, *61*, 319–325.
(51) Laborda, F.; Medrano, J.; Castillo, J. R. *Anal. Chim. Acta* **2000**, *407*, 301–309.
(52) Savitzky, A.; Golay, M. J. E. *Anal. Chem.* **1964**, *36*, 1627–1639.
(53) Hearn, M. T. W.; Aguilar, M. I. *J. Chromatogr., A* **1987**, *397*, 47–70.
(54) Piccolo, A. *Soil Sci.* **2001**, *166*, 810–832.
(55) Engebretson, R. R.; Vonwandruszka, R. *Environ. Sci. Technol.* **1994**, *28*, 1934–1941.
(56) Dittmar, T.; Kattner, G. *Mar. Chem.* **2003**, *82*, 115–123.
(57) Piccolo, A.; Spiteller, M. *Anal. Bioanal. Chem.* **2003**, *377*, 1047–1059.
(58) Conte, P.; Piccolo, A. *Environ. Sci. Technol.* **1999**, *33*, 1682–1690.
(59) Hertkorn, N.; Benner, R.; Frommberger, M.; Schmitt-Kopplin, P.; Witt, M.; Kaiser, K.; Kettrup, A.; Hedges, J. I. *Geochim. Cosmochim. Acta* **2006**, *70*, 2990–3010.
(60) Olesik, J. W.; Moore, A. W. *Anal. Chem.* **1990**, *62*, 840–845.
(61) Bendahl, L.; Gammelgaard, B. *J. Anal. At. Spectrom.* **2005**, *20*, 410–416.
(62) Wind, M.; Wesch, H.; Lehmann, W. D. *Anal. Chem.* **2001**, *73*, 3006–3010.
(63) Mather, R. L.; Reynolds, S. E.; Wolff, G. A.; Williams, R. G.; Torres-Valdes, S.; Woodward, E. M. S.; Landolfi, A.; Pan, X.; Sanders, R.; Achterberg, E. P. *Nat. Geosci.* **2008**, *1*, 439–443.
(64) Clark, L. L.; Ingall, E. D.; Benner, R. *Nature* **1998**, *393*, 426–426.
(65) Hopkinson, C. S.; Vallino, J. J. *Nature* **2005**, *433*, 142–145.
(66) Loh, A. N.; Bauer, J. E. *Deep-Sea Res. I* **2000**, *47*, 2287–2316.
(67) Redfield, A. C. *Am. Sci.* **1958**, *46*, 205–221.
(68) Sanders, R.; Jickells, T. *Deep-Sea Res. I* **2000**, *47*, 997–1014.
(69) Alling, V.; Humborg, C.; Morth, C. M.; Rahm, L.; Pollehne, F. *Limnol. Oceanogr.* **2008**, *53*, 2594–2602.
(70) Cutter, G. A.; Cutter, L. S.; Filippino, K. C. *Limnol. Oceanogr.* **2004**, *49*, 555–565.
(71) Hirose, K. *J. Radioanal. Nucl. Chem.-Articles* **1994**, *181*, 11–24.
(72) Djogic, R.; Sipos, L.; Branica, M. *Limnol. Oceanogr.* **1986**, *31*, 1122–1131.
(73) Li, W. C.; Victor, D. M.; Chakrabarti, C. L. *Anal. Chem.* **1980**, *52*, 520–523.
(74) Saito, M. A.; Goepfert, T. J.; Ritt, J. T. *Limnol. Oceanogr.* **2008**, *53*, 276–290.
(75) Jakuba, R. W.; Moffett, J. W.; Dyhrman, S. T. *Global Biogeochem. Cycles* **2008**, *22*, GB4012, DOI: 10.1029/2007GB003119.

Available online at www.sciencedirect.com

SciVerse ScienceDirect

Geochimica et Cosmochimica Acta 77 (2012) 98–107

Geochimica et Cosmochimica Acta

www.elsevier.com/locate/gca

A depth profile of uranium-236 in the Atlantic Ocean

Marcus Christl [a,*], Johannes Lachner [a], Christof Vockenhuber [a], Oliver Lechtenfeld [b], Ingrid Stimac [b], Michiel Rutgers van der Loeff [b], Hans-Arno Synal [a]

[a] *Laboratory of Ion Beam Physics, ETH Zurich, Schafmattstr. 20, CH-8093 Zurich, Switzerland*
[b] *Alfred Wegner Institute, Am Handelshafen 12, 27570 Bremerhaven, Germany*

Received 30 June 2011; accepted in revised form 17 October 2011

Abstract

In this study the first two oceanic depth profiles of ^{236}U sampled in the western equatorial Atlantic Ocean are presented. The measured $^{236}U/^{238}U$ ratios decrease from about 10^{-9} at the surface down to about 10^{-10}. Even the lowest ratios measured below 4000 m depth are more than three orders of magnitude above the estimated natural $^{236}U/^{238}U$ level for the pre-anthropogenic ocean. This clearly indicates that anthropogenic ^{236}U already has reached the deep Atlantic Ocean. Three different conceptual models are applied to identify the relevant processes capable of transporting significant amounts of ^{236}U from the surface into the deep ocean. While the vertical transport of particulate U is excluded as a significant source, box model calculations suggest that North Atlantic Deep Water production with some minor contribution of ^{236}U from nuclear reprocessing as the most likely source for ^{236}U in the deep western equatorial Atlantic Ocean. Our results show that ^{236}U has a large potential as a new, conservative, and transient tracer in Oceanography.

1. INTRODUCTION

Uranium in the ocean is of special interest since its daughter nuclides are extensively used as tracers and chronometers in many (paleo) oceanographic studies (e.g. Ivanovich and Harmon, 1992; Henderson and Anderson, 2003). In the ocean, the uranium concentration (~3.3 ppb) and the activity ratio of $^{234}U/^{238}U$ (~1.147) have been fairly constant in space and time (Chen et al., 1986; Henderson and Anderson, 2003; Robinson et al., 2004: Andersen et al., 2010). For example, the $^{234}U/^{238}U$ ratio has not varied by more than 15‰ over the past 360 kyr (Henderson, 2002). The main source of U in the ocean is riverine input of continental waters with minor contributions from dust and groundwater (Ivanovich and Harmon, 1992). The main sinks for U in the ocean are suboxic and anoxic sediments (Sackett et al., 1973) as well as weathering of oceanic basalts (Bloch, 1980). Within the large uncertainties of all the input and output fluxes the oceanic U budget is generally considered to be in balance (Henderson and Anderson, 2003). Therefore, U in the ocean is used as a conservative tracer with a residence time of about 400 kyr (Mangini et al., 1979; Dunk et al., 2002). The conservative behavior is also reflected by the fact that salinity and U-content are tightly correlated in the open ocean. If the salinity of an open ocean water sample is known, the U-content can be predicted within less than 2% uncertainty (Pates and Muir, 2007).

In contrast to the primordial U-isotopes (and the radiogenic daughter ^{234}U), uranium-236 ($T_{½} = 23.4$ Myr) has not yet been used as an oceanic tracer although its potential as an environmental proxy has been well recognized recently (Steier et al., 2008). ^{236}U is almost exclusively produced from the abundant ^{235}U by neutron capture via an (n, γ)-reaction. The $^{236}U/^{238}U$ ratio, therefore, had been suggested early as a natural occurring neutron monitor (Purser et al., 1996).

On Earth, the majority of ^{236}U is produced by anthropogenic neutron flux e.g. during nuclear bomb explosions or in U-fission reactors. Only a very minor amount of ^{236}U is of cosmogenic origin (produced by galactic cosmic ray

* Corresponding author. Address: ETH Zurich, Schafmattstr. 20, HPK G23, CH-8093 Zurich, Switzerland. Tel.: +41 44 633 3884.
E-mail address: mchristl@phys.ethz.ch (M. Christl).

0016-7037/$ - see front matter © 2011 Elsevier Ltd. All rights reserved.
doi:10.1016/j.gca.2011.11.009

induced secondary neutrons) or nucleogenic origin (produced by neutrons originating from (α, n) reactions in the natural terrestrial environment).

The global inventory of ^{236}U was assessed recently (Steier et al., 2008). However, very few data about the distribution of ^{236}U in the environment exist. According to the above assessment the natural (nucleogenic and cosmogenic) ^{236}U inventory in the upper 1000 m of the Earth's crust is about 35 kg (with about 10 kg of cosmogenic ^{236}U located in the upper few meters of the crust). In contrast, the amount of anthropogenic ^{236}U on Earth is estimated to be about 10^6 kg. Anthropogenic ^{236}U is mainly produced in nuclear reactors plus about 900 kg from atmospheric bomb tests (Sakaguchi et al., 2009). The latter number was derived from the average $^{236}U/^{239+240}Pu$ ratio measured in soil samples from the Japanese archipelago assuming a global deposition of 14.8 PBq $^{239+240}Pu$ on Earth. No uncertainty is reported for this ^{236}U inventory from fallout. It is, however, expected that this value represents a rather rough estimate since it does not consider the potentially different geochemical behavior of Pu and U in the environment that might change the Pu/U ratio recorded in the soil samples.

It is expected that only a very small fraction of the reactor produced ^{236}U has been or will be released into the environment either via nuclear reprocessing (Marsden et al., 2001) or during nuclear accidents like the Chernobyl disaster (Boulyga et al., 2000; Boulyga and Becker, 2002). A few studies, however, indicate that young continental surface waters and sediments in particular in northwestern and central Europe are dominated by the presence of anthropogenic ^{236}U (Lee et al., 2008; Srncik et al., 2009).

Up to date no published dataset of ^{236}U in the open ocean exists. This is mainly due to the fact that the measurement of very low $^{236}U/^{238}U$ ratios even with modern mass spectrometers (e.g. TIMS, ICPMS) is limited by an abundance sensitivity at the order of 10^{-7}–10^{-8} (Boulyga and Heumann, 2006; Fifield, 2008b). Accelerator mass spectrometry (AMS) is currently the only technique that is able to determine naturally occurring $^{236}U/^{238}U$ ratios down to the 10^{-12} level (or even below) with sufficient efficiency (e.g. Zhao et al., 1994; Fifield, 2008a; Steier et al., 2010).

This study presents the first depth profile of ^{236}U sampled in the western equatorial Atlantic Ocean. Our results show that anthropogenic ^{236}U is present at depths of more than 4000 m. In the following, first the expected $^{236}U/^{238}U$ signal in the open ocean is estimated. Then, sample preparation and AMS measurement techniques are presented before the ^{236}U-data is discussed in detail. Finally, simple conceptual models are applied to explain the observed ^{236}U data in the deep Atlantic Ocean.

2. NATURAL AND ANTHROPOGENIC $^{236}U/^{238}U$ IN THE OPEN OCEAN

Based on the above values for the global ^{236}U budget the contributions of the different ^{236}U-sources to the expected oceanic $^{236}U/^{238}U$ signal are calculated. Since the half-life of ^{236}U is much longer than its residence time, the oceans should have a $^{236}U/^{238}U$ ratio that reflects the inputs of ^{236}U. During the phase of atmospheric bomb testings (1945–1980) approximately 900 kg of ^{236}U had been released into the atmosphere (Sakaguchi et al., 2009). To assess the $^{236}U/^{238}U$ ratio in the modern ocean surface we assume that 70% (relative Earth's surface area covered by the oceans) of the globally released ^{236}U had been incorporated at once into the surface layer of the oceans (neglecting the atmospheric residence time of about 1 year (Buesseler and Sholkovitz, 1987)). If we further assume that this amount (since then) has homogenously mixed with the upper 700–800 m (e.g. assessed from the average global penetration depth of anthropogenic CO_2 (Sabine et al., 2004)), a $^{236}U/^{238}U$ ratio of about 1×10^{-9} is calculated for modern ocean surface waters. Given the unknown but certainly large uncertainty of the global input value the above number is highly uncertain as well.

In addition to the ^{236}U from global fallout, significant amounts of anthropogenic radionuclides are released into the North Sea region by nuclear reprocessing plants since 1952 (Sellafield) and 1966 (La Hague) (SEPA, 2010). Measurements of $^{236}U/^{238}U$ in ocean water samples close to Sellafield (Irish Sea) document ratios at the order of 10^{-6} (Lee et al., 2008). Based on the available U release data (compiled by J. Herrmann, BSH-Hamburg, Germany based on the OSPAR Commission reports, e.g. (OSPAR, 2009)) it is suspected that in the 1980s the annual ^{238}U (producing ^{234}U) input had been about five times larger than in 2009. The maximum occurs in the 1980s because the $^{236}U/^{238}U$ release ratio still tends to increase (more reprocessed fuel is being used in the reactors) while the total U release decreases. Therefore, the ^{236}U input from nuclear reprocessing is significantly different from, for example, ^{129}I that reaches a maximum input around the year 2000 (Alfimov et al., 2006).

In contrast to the anthropogenic ^{236}U input that roughly started after 1945 the natural ^{236}U signal is expected to have reached steady state in the ocean. The natural signal of ^{236}U consists of two constituents. Both, nucleogenic and cosmogenic ^{236}U are mobilized by continental weathering and enter the ocean via riverine input carrying the average $^{236}U/^{238}U$ ratio of the weathering components. Because the energy released in the (n, γ)-reaction producing ^{236}U is low compared to the α-decay of ^{236}U no preferential mobilization of ^{236}U compared to ^{235}U from the host rock is expected (in contrast to ^{234}U compared to ^{238}U).

The production of nucleogenic ^{236}U depends on the U concentration in the host rock itself. For example, in U-rich ores $^{236}U/^{238}U$ ratios of up to 2×10^{-10} have been measured (Wilcken et al., 2008). In contrast to the heterogeneous distribution of ^{236}U in the lithosphere, pre-anthropogenic ocean water is expected to reflect the global average of the natural $^{236}U/^{238}U$ signal. Following previous estimates (Steier et al., 2008) and using a global average U and Th concentration of 2–3 ppm in the weathering host rock leads to a very low average oceanic $^{236}U/^{238}U$ ratio at the order of 10^{-14} from nucleogenic ^{236}U production.

A quantitative assessment of the average cosmogenic $^{236}U/^{238}U$ signal in the ocean is complicated by the fact that the in-situ production of cosmogenic nuclides strongly depends on geomagnetic latitude and atmospheric depth (i.e. elevation) (Lal, 1988). As a rough estimate we use the

analogy of cosmogenic ^{36}Cl production from ^{35}Cl. The average global production of cosmogenic ^{236}U is calculated from the average ^{36}Cl production given for different host rock compositions (Fabryka-Martin, 1988) and using the relative difference in the respective cross sections for neutron capture. Assuming an average U concentration of a few ppm in the weathering host rock leads to an estimated oceanic $^{236}U/^{238}U$ ratio at the level of 10^{-13}. The uncertainty of this estimation is probably very large taking into account the number of rough assumptions made. Given that more than 50% of the global riverine U-flux into the ocean is carried by rivers transporting the weathering signal of the highly elevated and U-rich lithologies of the Himalayan region (Dunk et al., 2002; Singh et al., 2003) the above estimations might be systematically too low. Recently, a first experimental upper limit for the pre anthropogenic $^{236}U/^{238}U$ ratio was set to 4×10^{-12} (Winkler et al., 2011). In summary, the natural oceanic $^{236}U/^{238}U$ ratio is expected to be dominated by cosmogenic ^{236}U. Therefore, on a million year timescale, the average cosmogenic $^{236}U/^{238}U$ ratio, as recorded in pre-anthropogenic ocean water, carries information about both, changes in the average continental erosion rate and/or relative changes in the U supply from different source regions to the ocean.

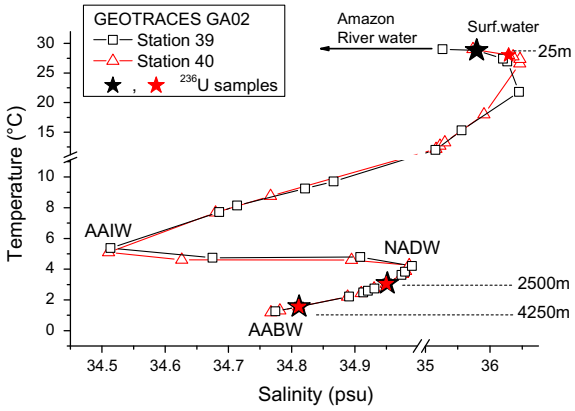

Fig. 1. Hydrographic data (temperature, T vs. salinity, S; bottle data) of stations 39 (open black squares) and 40 (open red triangles) in the western equatorial Atlantic Ocean sampled during GEOTRACES cruise GA02. The T–S data of the ^{236}U samples are marked with stars, the respective sampling depth is labeled on the right side of the diagram. Further, the characteristic water masses at this location are indicated (AAIW: Antarctic Intermediate Water, NADW: North Atlantic Deep Water, AABW: Antarctic Bottom Water). (For interpretation of the references to color in this figure legend, the reader is referred to the web version of this article.)

3. METHODS

3.1. Sampling location, hydrography

During the GEOTRACES cruise GA02 in 2010 two depth profiles (six samples of 13–22 kg sea water) were collected at stations 39 (latitude: 2°5′45.127″ N, longitude: 41°7′0.307″ W) and 40 (lat.: 1°1′47.228″ N, lon.: 39°6′86.035″ W) in the western equatorial Atlantic Ocean for ^{236}U-analysis (Table 1). The local hydrography at the selected location is reflected by the temperature and salinity (T–S) data (Fig. 1). The surface waters are dominated by the westward flowing equatorial counter current with some contributions of low saline Amazon River water plumes. The salinity minimum at about 750 m depth reflects the northward flowing Antarctic Intermediate Waters (AAIW), the following salinity maximum at a depth of about 2000 m is characteristic for the southward flowing North Atlantic Deep Water (NADW). A pronounced silicate maximum below about 4000 m depth (not shown here) clearly indicates the presence of cold and less saline Antarctic Bottom Water (AABW) (Rijkenberg, 2010). The water samples for ^{236}U were collected at 25, 2500, and 4250 m depth (Fig. 1) and therefore should reflect the U-isotopic signatures of the local surface waters, of NADW, and of AABW in the western equatorial Atlantic Ocean. While the T–S-signature of the deep water samples (for corresponding depths) is virtually identical, the surface samples have a significantly different salinity probably caused by a varying admixture from the Amazon freshwater plumes (Fig. 1).

Table 1
Water sample locations, hydrographic parameters, and measured ^{236}U-data.

Sample depth (m)	Sample mass (kg)	Pot. temperature (°C)	Salinity (psu)	^{236}U concentration (at/kg) × 10^6	±1σ (at/kg) × 10^6	^{238}U concentration (μg/g)	±1σ (μg/g)	$^{236}U/^{238}U$ × 10^{-12}	±1σ × 10^{-12}
Station: 39, latitude (deg. min. milli): N 2°5′45.127″, longitude (deg. min. milli): W 41°7′0.307									
25	21.695	28.8275	35.7933	6.33	0.33	3.37	0.07	683	25
2501	12.890	3.0682	34.9515	1.60	0.06	3.04	0.07	189	6
4252	18.135	1.5603	34.8117	1.15	0.12	3.14	0.09	128	9
Station: 40, latitude (deg. min. milli): N 1°1′47.228″, longitude (deg. min. milli): W 39°6′86.035″									
25	18.600	28.0224	36.2881	36.25	10.53	3.36	0.07	3567	678
2503	17.860	3.0389	34.9498	1.89	0.08	3.34	0.24	191	10
4247	21.025	1.5618	34.8112	0.80	0.09	3.32	0.16	91	5

Blanks	^{236}U (at) × 10^6	±1σ (at) × 10^6	^{238}U (μg)	±1σ (μg)
BL_1	1.7	0.2	0.16	0.07
BL_2	5.1	1.4	0.27	0.08

3.2. Sample preparation and AMS measurement

The ^{236}U-samples were filtered (142 mm Nuclepore filter, 1 μm pore size) on board, transferred into 20 l polyethylene cubitainer® boxes and acidified with HNO_3. At AWI-Bremerhaven about 25–30 pg of a certified ^{233}U reference material (IRMM058) was added to the samples. The use of a ^{233}U spike allows determining the ratio of ^{236}U/^{238}U in the sample material and the concentration of both ^{236}U and ^{238}U during only one AMS-measurement. Details of sample preparation and AMS measurement will be described in a separate publication, here only. The main points are summarized.

U is extracted from the sea water by a Fe-hydroxide co-precipitation that is followed by anion exchange cleaning step using UTEVA® resin. The cleaned U-sample is co-precipitated with Fe-hydroxide again, oxidized at 650 °C, mixed with Nb powder and finally pressed into the AMS target holders. The AMS measurements were performed at ETH-Zurich with the compact 0.5 MV AMS system TANDY (Synal et al., 2000; Stocker et al., 2005). The AMS system was recently upgraded and equipped with an additional magnet on the high energy side (Müller et al., 2010). The performance of the upgraded AMS system for ^{236}U was thoroughly investigated and systematic background studies demonstrate that ^{236}U/^{238}U measurements in the 10^{-12} range are possible with a high detection efficiency of $>10^{-4}$ (Vockenhuber et al., 2011). In other words, the ^{236}U content of a 3 l seawater sample (approx. 10 μg U) with a ^{236}U/^{238}U ratio of 10^{-11} can be determined with an analytical precision of less than 10% (assuming 100% sample preparation efficiency). The compact ETH-TANDY system therefore ranges among three AMS facilities in the world that report a ^{236}U/^{238}U machine background of 10^{-12} and below (Steier et al., 2010).

The AMS measurement sequence, including the measurement of samples, standards and blanks, was repeated ten times (10 passes). From each pass the standard normalized and processing blank corrected values for the ^{236}U-conc., the ^{238}U-conc., and the ^{236}U/^{238}U ratio are calculated. The final values (Table 1) represent the blank corrected and error weighted mean of all 10 measurements including the 1σ-uncertainty.

The data is reported relative to the in house standard ZUTRI with a nominal ^{236}U/^{238}U ratio of $(4.05 \pm 0.10) \times 10^{-9}$ and a nominal ^{233}U/^{238}U ratio of $(3.32 \pm 0.08) \times 10^{-8}$. To control the machine background a diluted sample of the Vienna-KkU-standard (Steier et al., 2008) with a nominal ^{236}U/^{238}U ratio of $(69.8 \pm 3.2) \times 10^{-12}$ was measured during each run. For this sample, the U-oxide sample material was diluted with Nb powder to match the expected U-currents from the 20 l sea water samples (containing not more than 66 μg U). From these analyses and from the systematic background studies (Vockenhuber et al., 2011) we conclude that the AMS machine background was below 5×10^{-12} during all measurements (Fig. 2). Using the average U-concentration in sea water the above value translates into a ^{236}U machine background of 0.04×10^6 at/kg for this study. Two samples solely containing Nb powder were measured always directly after the ZUTRI-standard. The ^{236}U counting rates of these samples indicate that the maximum memory in the ion source was below 10^{-4} and therefore negligible.

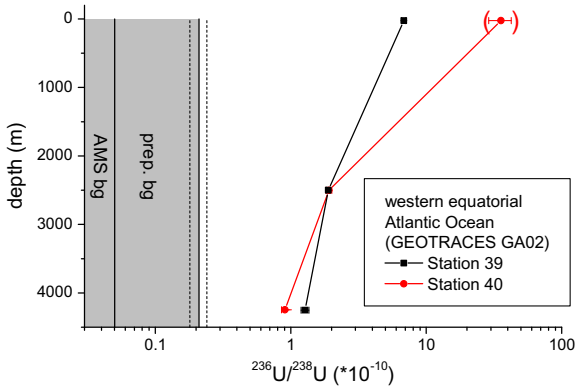

Fig. 2. The measured ^{236}U/^{238}U ratios plotted vs. depth at stations 39 (black squares) and 40 (red dots) in the western equatorial Atlantic Ocean on a logarithmic scale. The shaded regions indicate the machine background of the AMS system and the sample preparation background deduced from the blank measurements, respectively. The surface data point from station 40 is shown in brackets but excluded from the discussion because it showed clear indications for a contamination during the AMS measurements. (For interpretation of the references to color in this figure legend, the reader is referred to the web version of this article.)

3.3. Blanks, background correction

Two processing blanks were prepared together with the samples (Table 1). A negligible amount of ^{236}U (about 3×10^3 at ^{236}U) is expected to be introduced with the ^{233}U spike (^{236}U/^{233}U $= 4.3 \times 10^{-8}$, IRMM058). However, a considerable amount of ^{236}U (weighted average: $(2.6 \pm 0.4) \times 10^6$ at/sample) was measured in the blanks (Table 1). This indicates that ^{236}U was picked up during the sample preparation. The origin of the contamination is not exactly known but we suspect that it was picked up in the AMS chemistry lab where a ^{236}U/^{233}U double spike material ($N(^{236}U) \approx 10^{12}$ at) had been processed before. Although the lab was carefully cleaned afterwards, an accidental contamination at the ppm level would explain the observed blank levels. For a 15 kg sea water sample the average blank level translates into an average ^{236}U/^{238}U preparation background for this batch of samples of $(2.1 \pm 0.3) \times 10^{-11}$(prep. bg in Fig. 2) corresponding to an average ^{236}U background concentration of $(0.17 \pm 0.03) \times 10^6$ at/kg. The average ^{238}U blank of 0.2 ± 0.1 μg/sample causes background corrections for the ^{238}U-concentrations at the per mill level, which is well within the uncertainty of the ^{238}U-data. The data presented in this study (Table 1) includes all background corrections discussed above. The maximum relative background corrections for ^{236}U are 13% and 16% for the two lowermost (4250 m) samples.

4. DATA AND DISCUSSION

4.1. ^{236}U in the western equatorial Atlantic Ocean – data

Both ^{236}U concentration and ^{236}U/^{238}U ratio show a decreasing trend with depth of a factor of 6–7 (Table 1). The ^{236}U/^{238}U ratios decrease from 700×10^{-12} to about 100×10^{-12} (Fig. 2), while the ^{236}U concentrations fall from 6×10^6 at/kg at 25 m depth down to about 1×10^6 at/kg at 4250 m depth (Table 1). The surface sample from station 40 is shown but excluded from the following discussion because this AMS target showed strong indications for a particulate contamination with ^{236}U (largely varying counting rates during the measurement at almost constant ^{238}U current). Such a behavior was not observed with any of the other ^{236}U samples. We therefore exclude the possibility of such a contamination for the other samples. The good agreement of both ^{236}U-concentration and ^{236}U/^{238}U ratio between hydrographically identical samples (with respect to their temperature and salinity signature, Fig. 1) further supports the good quality of the ^{236}U-data.

The measured ^{236}U/^{238}U ratios are all at least three orders of magnitude larger than the pre-anthropogenic signal estimated above. We therefore conclude that the whole water column down to 4250 m is dominated by anthropogenic ^{236}U. The surface ^{236}U/^{238}U ratio of 0.7×10^{-9} is lower but still in agreement with the estimated signal from global fallout, especially when considering the large uncertainty of the global fallout inventory. It is also in rough agreement with a not further specified surface sample from the Atlantic Ocean (^{236}U/^{238}U $= (1.9 \pm 0.6) \times 10^{-9}$) recently presented by Eigl et al. (2011). At 2500 m depth a ^{236}U/^{238}U signature of 2×10^{-10} is found for local NADW. Possible explanations involving deep water formation in the North Atlantic region and/or the transport of U with sinking particles are discussed in the following section.

At a depth of 4250 m in the western equatorial Atlantic Ocean ^{236}U/^{238}U ratios of about 1×10^{-10} are found. At this location NADW entrains northward penetrating AABW. Hydrographical and phosphate data suggest a 50% NADW, 50% AABW mixing ratio below 4000 m depth at this location (Broecker et al., 1998). The assumption that a 50:50 binary mixing is also valid for the ^{236}U data suggests that pristine AABW does not contain any anthropogenic ^{236}U. This result is consistent with measured and modeled radiocarbon ages of >300 yr for AABW in the equatorial Atlantic Ocean (Broecker and Peng, 1982; Campin et al., 1999). We conclude that the observed ^{236}U/^{238}U ratio at 4250 m depth results from a simple mixing of pristine (no anthropogenic ^{236}U) AABW with NADW. Therefore, the explanation of the local AABW signal is tightly connected with the explanation of the local NADW signal at 2500 m depth (see Section 4.2).

Assuming that the ^{236}U concentration decreases exponentially with depth ($R^2 = 0.95$, not shown) a ^{236}U inventory of 1.1×10^9 at/cm^2 is calculated. Extrapolating from these five data points to a global scale an oceanic input of about 1.5 t ^{236}U would be necessary to explain the observed inventory. If no other source of ^{236}U was involved, this number translates into an alternative assessment for the total amount of ^{236}U from global fallout, resulting in a value of about 2100 kg. This is more than a factor of two higher than previous estimates (Sakaguchi et al., 2009). However, the uncertainty of this estimation is large because the calculated ^{236}U inventory strongly depends on the quality of one single surface data point as a representative for the global SML and because the calculated inventory also depends on the applied fit function. Additionally, the ^{236}U inventory might be systematically biased by ^{236}U transported by southward flowing NADW, which in turn might contain significant amounts of ^{236}U from nuclear reprocessing (see Section 4.2).

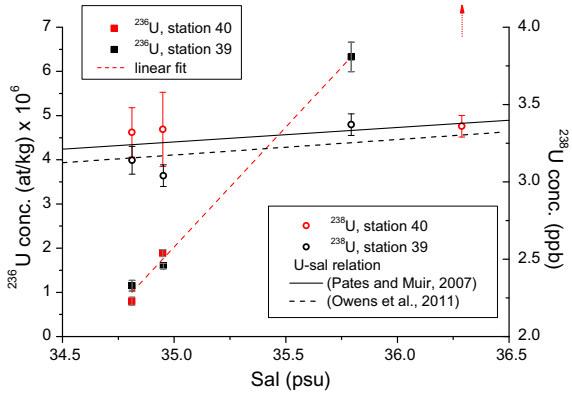

Fig. 3. Measured ^{236}U concentration (filled squares) and ^{238}U concentration (open circles) vs. salinity at stations 39 (black symbols) and 40 (red symbols). Different U-salinity relations for the open ocean are shown: black straight line (Pates and Muir, 2007), black dashed line (Owens et al., 2011). The red dashed line represents a linear fit to the ^{236}U data ($R^2 = 0.997$). The measured surface ^{236}U concentration at station 40 (indicated by the red dotted arrow) is regarded as an outlier and therefore neglected in the fit. (For interpretation of the references to color in this figure legend, the reader is referred to the web version of this article.)

The measured ^{238}U concentrations at stations 39 and 40 (Fig. 3, right axis) are in good agreement with the generally observed relation between U-concentration and salinity (Pates and Muir, 2007; Owens et al., 2011) in the open ocean (black lines in Fig. 3). The ^{236}U-concentration also exhibits a significant ($R^2 = 0.997$) but much steeper correlation with salinity (Fig. 3, left axis, red dashed line). The tight correlation, however, is dominated by one (high saline) surface data point. On the base of the current data set it is not clear if the observed correlation is accidental. An apparent ^{236}U-salinity correlation could simply be caused by the fact that a two component mixing of a pre-anthropogenic and a single anthropogenic ^{236}U signal is observed.

4.2. ^{236}U in the western equatorial Atlantic Ocean – modeling results

A main conclusion from the ^{236}U data presented above is that the whole examined water column in the western equatorial Atlantic Ocean is influenced by anthropogenic ^{236}U. A major question therefore is: how has the anthropogenic ^{236}U signal propagated into the deep ocean over the

past 50–60 yr? There are two different transport processes that may be involved. First, sinking particles may transport U from the biologically active surface layer into the deep ocean where it is released due to remineralization. Second, deep water production in the North Atlantic Ocean supplies fresh surface waters to the deep Atlantic Ocean via NADW formation. In the following, three simple conceptual models (Fig. 4) are used to simulate particle flux and NADW production in order to identify the transport mechanism for ^{236}U into the deep ocean.

4.2.1. The input function

In all three box models ^{236}U is introduced into the surface mixed layer (SML) box (Fig. 4). To estimate the $^{236}U/^{238}U$ level in the SML box including its temporal evolution it is assumed that 70% of the 900 kg ^{236}U, which were supposedly released during atmospheric bomb explosions, were at once deposited into the surface ocean in the year 1957 (roughly representing the median of the atmospheric bomb tests). In addition, the spatially heterogeneous deposition pattern of atmospheric fallout (southern vs. northern hemisphere = 1:3.8, (Hardy et al., 1973)) is considered. According to these assumptions more than 700 kg ^{236}U were deposited on the northern hemisphere, with 432 kg thereof directly entering the SML. Using this input value two different simulations are run assuming two different average SML depths (150 and 50 m; SML150 and SML50 in Fig. 5). The SML depths of 50 and 150 m represent typical minimal/maximal annual mean values for the subpolar and equatorial ocean (Monterey and Levitus, 1997).

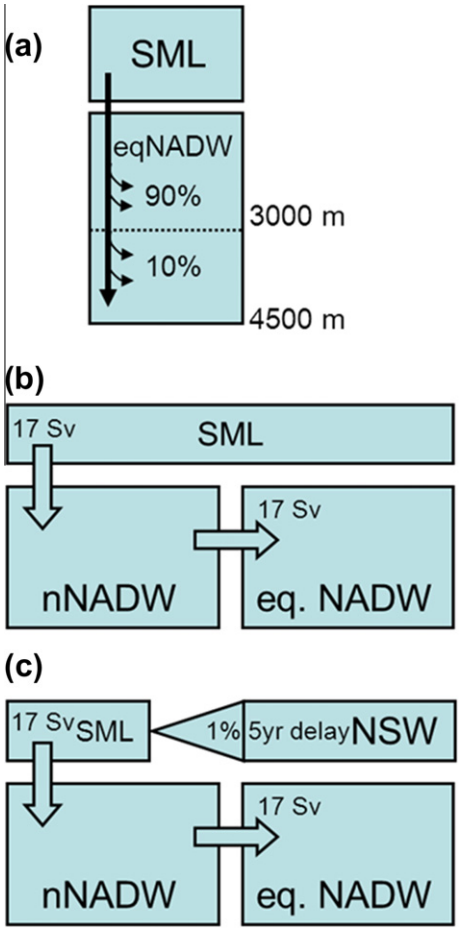

Fig. 4. Box models used for the different simulations; (a) three box model to investigate the effect of vertical transport of U with sinking particles (SML: surface mixed layer). The deep ocean box is divided at 3000 m depth to separate eqNADW from AABW. In the simulation 90% of the particulate U is remineralized in the eqNADW box, with the remainder remineralizing in the AABW box; (b) three box model for the simulation of NADW formation and export, nNADW: northern NADW, eqNADW: equatorial NADW. The arrows indicate the flow direction, the labels give the volume rate; (c) the same model as in (b) with an additional and delayed input of 1% North Sea Water (NSW).

The smaller the mixed layer in the model the higher is the calculated initial $^{236}U/^{238}U$ ratio. The SML50 scenario represents a maximum estimate for the modeled $^{236}U/^{238}U$ ratio in all simulations because in this scenario always a higher $^{236}U/^{238}U$ ratio is exported from the SML into the deep ocean than in the SML150 simulation. The above assumptions result in initial $^{236}U/^{238}U$ ratios (in the model year 1957) of 5.6×10^{-9} and 1.7×10^{-8} for the SML150 and SML50 scenarios, respectively.

In these transient scenarios it is further assumed that from year to year the initial ^{236}U signal in the SML penetrates deeper into the ocean where it then mixes with water masses that do not contain anthropogenic ^{236}U. The average yearly penetration rate of the signal is determined under the assumption that the simulated $^{236}U/^{238}U$ ratio in the surface box (dashed lines in Fig. 5) equals the measured $^{236}U/^{238}U$ ratio at 25 m depth in the year 2010 (filled circle in Fig. 5). For a SML depth of 150 m (50 m) an average signal penetration rate of 20.7 m/yr (22.5 m/yr) is determined. This implies that in both input scenarios the calculated $^{236}U/^{238}U$ surface ratios decrease with time and per definition reach a value of 6.8×10^{-10} in the model year 2010. An average penetration rate of 21 m/yr further implies that in the model year 2010 the ^{236}U signal has homogenized with the uppermost 1200 m of the water column. Further, an annual penetration length of $L = 21$ m corresponds to a vertical eddy diffusivity of $D = 0.14\ cm^2\ s^{-1}$ (with $L = (Dt)^{1/2}$), which is well within the range of observational data (Garrett, 1984).

4.2.2. Particle flux

In the surface waters of the open ocean dissolved U may be fixed to predominantly organic particles and exported to the bathypelagic layer (ca. 1000–4000 m) where it then remineralizes (Anderson, 1982). In general, this process also transports ^{236}U from the surface layer into the deep ocean. To simulate the vertical transport of particulate U a simple conceptual model is applied (Fig. 4a). In this model U is exported (e.g. by sinking particles) from the surface box and completely remineralized in the two deep ocean boxes below. For the surface layer we apply the two (SML50 and SML150) input scenarios described above. Measured export rates of particle bound bio-authigenic U range from 0.1 to 5.6 $ng\ cm^{-2}\ yr^{-1}$ (Anderson, 1982). A strict additional constraint for the maximum flux of particulate U is given by the U – salinity relation in the open ocean. Since

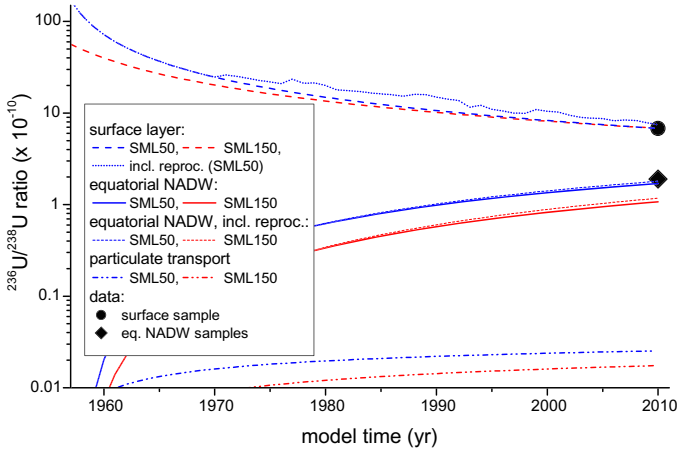

Fig. 5. The simulated $^{236}U/^{238}U$ ratio in the eqNADW given for different input scenarios and for different transport mechanisms on a logarithmic scale. Four different input scenarios are realized for the simulation of NADW production and export (upper dashed and dotted lines): (i) a transient $^{236}U/^{238}U$ scenario with an initial SML depth of 50 m (SML50, blue dashed line), (ii) a transient $^{236}U/^{238}U$ scenario with an initial SML depth of 150 m (SML150, red dashed line), (iii) and (iv) input scenarios (i) and (ii) plus an additional contribution of ^{236}U from nuclear reprocessing. For better visibility only one input scenario (iii): SML50 (blue dotted line) is shown that includes ^{236}U from reprocessing. The calculated $^{236}U/^{238}U$ ratios in the eqNADW-box for the four different input scenarios are indicated by the red and blue straight lines (without reprocessing) and by the red and blue short dotted lines (including reprocessing) in the middle of the plot. The color reflects the respective input scenario. The calculated $^{236}U/^{238}U$ ratio in the eqNADW box caused by the vertical transport of particulate U is indicated by the red and blue dashed-dotted lines in the lower part of the diagram. The filled circle and diamond mark the measured $^{236}U/^{238}U$ ratios (sampled in 2010) in the surface layer and in eqNADW, respectively. (For interpretation of the references to color in this figure legend, the reader is referred to the web version of this article.)

no vertical gradient of the salinity normalized U-concentration is observed in the open ocean (Pates and Muir, 2007) the flux of remineralized bio-authigenic U to the deep sea must be insufficient to measurably change the uranium concentration within the mixing time of the ocean (Anderson, 1982).

To realize a maximum estimate of the vertical ^{236}U flux in the model it is assumed that 90% of the particulate U remineralizes in the eqNADW box. Under the restriction that the U concentration in this box is allowed to change by not more than 2% per 1000 yr a maximum U export flux of 20 ng cm^{-2} yr^{-1} is calculated. If particulate U export from the surface is the sole mechanism transporting ^{236}U into the deep ocean the above constraint implies that (assuming a constant $^{236}U/^{238}U$ ratio in the SML) only 1.1‰ (i.e. 2% × 53 yr/1000 yr) of the $^{236}U/^{238}U$ signal at the surface reaches the deep ocean (the resulting $^{236}U/^{238}U$ ratio in eqNADW would not even be visible on the logarithmic scale of Fig. 5). The non-steady state simulations use a transient $^{236}U/^{238}U$ signal as input function (SML50 and SML150). The results (blue and red dashed dotted lines in Fig. 5) clearly indicate that the export and the subsequent remineralization of particulate U is not a significant source of ^{236}U in the deep ocean, neither in eqNADW nor in AABW.

We note that the $^{236}U/^{238}U$ signal in the deep ocean reacts much more sensitive to vertical transport processes than, for example, $^{234}U/^{238}U$ since the ^{236}U signal is not at steady state. It may therefore provide a powerful tool to quantify the particulate transport of U in oceanic regions where deep water formation does not play a significant role (e.g. the Pacific Ocean).

4.2.3. NADW formation

To simulate the temporal evolution of the $^{236}U/^{238}U$ ratio in the deep equatorial Atlantic Ocean a simple three box model is used (Fig. 4b). In this model pristine (northern) nNADW is produced from the surface layer at a volume rate of 17 Sv, which is in accordance with estimates from hydrographic section data at 24 N (Roemmich and Wunsch, 1985). Simulating the advective southward transport via the Deep Western Boundary Current (DWBC) the nNADW is transported into the equatorial NADW box (eqNADW) assuming the same volume rate (corresponding to a renewal time of 150 yr for each box). Since the modeled time period (53 yr) is much shorter than the oceanic mixing time (about 1000 yr) the box model does not conserve water (i.e. there is no return flux of water leaving the eqNADW box).

The results of the box model simulations (straight lines in Fig. 5) show that only the SML50 simulation is able to explain the observed $^{236}U/^{238}U$ ratio in eqNADW quantitatively (filled diamond in Fig. 5). The SML150 simulation produces $^{236}U/^{238}U$ ratios that are almost a factor of 2 lower than the measured data in eqNADW. Regarding all the assumptions made and the simplicity of the model the SML50 simulation is in reasonable agreement with the observations.

We are aware of the fact that the application of a box model to simulate the spatial propagation of a tracer signal a priori represents a maximum approach since no constraints for the maximal mixing lengths are given. To transport the anthropogenic ^{236}U signal within about 50 yr from the region of deep water formation (Labrador and Nordic Seas) to the sampling location (6000–8000 km further

south)a minimum average current velocity of 0.4–0.5 cm/s would be necessary. For the DWBC very variable velocities reaching values of up to 20 cm/s have been reported (Joyce et al., 1986).

Further, a rapid spreading of ^{236}U into the deep equatorial Atlantic Ocean is consistent with tritium and chlorofluorocarbon (CFC) data. For example, Jenkins and Rhines (1980) found a southward flowing tritium jet flow in the DWBC at 3500 m depth (originating from nuclear weapons testing in the atmosphere). More recently, attempt has been made to access the transit time for the NADW pathway from the Labrador and Nordic Seas to the tropics using CFCs (Andrié et al., 2002). In this study a mean transit time of 25 yr (27 yr) was determined for upper (lower) NADW to reach the equatorial Atlantic Ocean.

All these results support the interpretation that, on a time scale of several decades, it is generally possible to transport significant amounts of anthropogenic ^{236}U from the SML into the deep western equatorial Atlantic Ocean via NADW formation.

4.2.4. NADW formation and nuclear reprocessing

A contribution of anthropogenic ^{236}U from the nuclear reprocessing plants in northwestern Europe might represent an additional source of ^{236}U in the eqNADW. Although the releases started more than 50 yr ago the spatial distance from the North Sea to the western equatorial Atlantic Ocean is even larger. Therefore it seems unlikely that much of the ^{236}U from nuclear reprocessing has reached the deep equatorial Atlantic Ocean. Yet on the other hand, even small contributions of North Sea Water (NSW) to the North Atlantic regions would significantly increase the $^{236}U/^{238}U$ ratio of the NADW forming surface waters. Furthermore, there is evidence for the presence of anthropogenic ^{129}I from nuclear reprocessing in the North East Atlantic Deep Water (NEADW) (Edmonds et al., 2001) and in the Deep Western Boundary Current (DWBC) (Santschi et al., 1996; Orre et al., 2010). Taking into account the different input functions (^{129}I releases peak around the year 2000 while the ^{236}U release peak was about 20 yr earlier) it might become possible that ^{236}U from nuclear reprocessing is already present in the eqNADW.

To test this assumption, a second simulation was run to assess the contribution of ^{236}U from nuclear reprocessing. The additional ^{236}U input is included in the model under the following two assumptions. The relative contribution of NSW to the deep water forming SML is 1% and the NSW signal arrives at the location of deep water formation (e.g. in the Greenland Sea) with a 5 yr time lag (Fig. 4b). The above numbers are chosen arbitrarily to assess the sensitivity of the model to an additional input by nuclear reprocessing plants. The additional ^{236}U input is added to the SML50 and SML150 scenario, respectively (for better visibility only the SML50 plus reprocessing input is shown; blue short dotted line in Fig. 5). The results of these simulations (short dashed lines in Fig. 5) show that the incorporation of ^{236}U from nuclear reprocessing increases the $^{236}U/^{238}U$ ratio in eqNADW by not more than 10%. From this result we conclude that the incorporation of ^{236}U from nuclear reprocessing only marginally improves the agreement between data and simulation.

We note that all model simulations above were based on a global inventory of 900 kg ^{236}U from global fallout. As discussed above, this number is not well known and might reflect a source of systematic uncertainty for the simulations. A higher value, as suggested above, would improve the agreement between model and data, particularly for the SML 150 simulation. In summary, the box model simulations suggest that the distribution of ^{236}U in the deep western equatorial Atlantic Ocean most probably can be explained by deep water formation in the North Atlantic Ocean.

5. CONCLUSION

The first two oceanic depth profiles of ^{236}U sampled in the western equatorial Atlantic Ocean have been presented and discussed in detail. The data show that anthropogenic ^{236}U is present throughout the water column down to more than 4000 m depth. The local AABW samples and the 2500 m eqNADW samples reflect a binary mixing with about 50% contribution of each water mass, which agrees well with other oceanographic data and tracers from that location.

Simple conceptual models were used to identify the mechanism transporting ^{236}U into the deep ocean. The model results suggest that deep water formation in the North Atlantic Ocean is the likeliest source of ^{236}U in the eqNADW, maybe with small contributions of anthropogenic ^{236}U from nuclear reprocessing. According to the model simulations, the transport of U with sinking particles can be neglected as a significant source of ^{236}U in the deep open ocean.

^{236}U provides the transient twin isotope for natural U in the open ocean. Based on our results we conclude that ^{236}U has a large potential to become a new, transient, conservative, and therefore powerful tracer for future oceanic studies.

ACKNOWLEDGEMENTS

The authors want to thank Hendrik M. van Aken (NIOZ, Physical Oceanography Department) for providing and processing the hydrographic data, Michael Rüttimann (ETHZ) for carefully handling the ^{236}U samples in the chemistry lab, and Jürgen Herrmann (BSH-Hamburg) for compiling the ^{236}U release data. Gideon Henderson and three anonymous reviewers are acknowledged for their constructive comments that significantly improved the quality of the manuscript. This study used sample material from GEOTRACES section GA02. The Laboratory of Ion Beam Physics, ETH is partially supported by its consortium partners EAWAG, EMPA, and PSI.

REFERENCES

Alfimov V., Possnert G. and Aldahan A. (2006) Anthropogenic iodine-129 in the Arctic Ocean and Nordic Seas: numerical modeling and prognoses. *Marine Pollut. Bull.* **52**, 380–385.

Andersen M. B., Stirling C. H., Zimmermann B. and Halliday A. N. (2010) Precise determination of the open ocean $^{234}U/^{238}U$ composition. *Geochem. Geophys. Geosyst.* **11**, 8.

Anderson R. F. (1982) Concentration, vertical flux, and remineralization of particulate uranium in seawater. *Geochim. Cosmochim. Acta* **46**, 1293–1299.

Andrié C., Rhein M., Freudenthal S. and Plähn O. (2002) CFC time series in the deep water masses of the western tropical Atlantic, 1990–1999. *Deep Sea Res. Part I: Oceanogr. Res. Papers* **49**, 281–304.

Bloch S. (1980) Some factors controlling the concentration of uranium in the world ocean. *Geochim. Cosmochim. Acta* **44**, 373–377.

Boulyga S. F. and Becker J. S. (2002) Isotopic analysis of uranium and plutonium using ICP-MS and estimation of burn-up of spent uranium in contaminated environmental samples. *J. Anal. At. Spectrom.* **17**, 1143–1147.

Boulyga S. F. and Heumann K. G. (2006) Determination of extremely low $^{236}U/^{238}U$ isotope ratios in environmental samples by sector-field inductively coupled plasma mass spectrometry using high-efficiency sample introduction. *J. Environ. Radioactiv.* **88**, 1–10.

Boulyga S. F., Becker J. S., Matusevitch J. L. and Dietze H.-J. (2000) Isotope ratio measurements of spent reactor uranium in environmental samples by using inductively coupled plasma mass spectrometry. *Int. J. Mass Spectrom.* **203**, 143–154.

Broecker W. S. and Peng T. H. (1982) *Tracers in the Sea*. Columbia University, New York.

Broecker W. S., Peacock S. L., Walker S., Weiss R., Fahrbach E., Schroeder M., Mikolajewicz U., Heinze C., Key R., Peng T. H. and Rubin S. (1998) How much deep water is formed in the Southern Ocean? *J. Geophys. Res.* **103**, 15833–15843.

Buesseler K. O. and Sholkovitz E. R. (1987) The geochemistry of fallout plutonium in the North Atlantic: II. $^{240}Pu/^{239}Pu$ ratios and their significance. *Geochim. Cosmochim. Acta* **51**, 2623–2637.

Campin J.-M., Fichefet T. and Duplessy J.-C. (1999) Problems with using radiocarbon to infer ocean ventilation rates for past and present climates. *Earth Planet. Sci. Lett.* **165**, 17–24.

Chen J. H., Lawrence Edwards R. and Wasserburg G. J. (1986) ^{238}U, ^{234}U and ^{232}Th in seawater. *Earth Planet. Sci. Lett.* **80**, 241–251.

Dunk R. M., Mills R. A. and Jenkins W. J. (2002) A reevaluation of the oceanic uranium budget for the Holocene. *Chem. Geol.* **190**, 45–67.

Edmonds H. N., Zhou Z. Q., Raisbeck G. M., Yiou F., Kilius L. and Edmond J. M. (2001) Distribution and behavior of anthropogenic ^{129}I in water masses ventilating the North Atlantic Ocean. *J. Geophys. Res.* **106**, 6881–6894.

Eigl R., Wallner M., Srncik M., Steier P. and Winkler S. (2011) Goldschmidt abstracts 2011. *Mineral. Mag.* **75**, 796–824.

Fabryka-Martin J. T. (1988) *Production of Radionuclides in the Earth and their Hydrologic Significance, with Emphasis on Chlorine-36 and Iodine-129*. Department of Hydrology and Water Resources, University of Arizona, p. 400.

Fifield L. K. (2008a) Accelerator mass spectrometry of long-lived heavy radionuclides. In *Radioactivity in the Environment* (ed. P. Povinec). Elsevier, pp. 263–293.

Fifield L. K. (2008b) Accelerator mass spectrometry of the actinides. *Quat. Geochronol.* **3**, 276–290.

Gargett A. E. (1984) Vertical eddy diffusivity in the ocean interior. *J. Mar. Res.* **42**, 359–393.

Hardy E. P., Krey P. W. and Volchok H. L. (1973) Global inventory and distribution of fallout plutonium. *Nature* **241**, 444–445.

Henderson G. M. (2002) Seawater (U-234/U-238) during the last 800,000 years. *Earth Planet. Sci. Lett.* **199**, 97–110.

Henderson G. M. and Anderson R. F. (2003) The U-series toolbox for paleoceanography. In *Uranium-series Geochemistry* (eds. B. Bourdon, G. M. Henderson, C. C. Lundstrom and S. P. Turner). Mineralogical Society of America (Chapter 12).

Ivanovich M. and Harmon R. S. (1992) *Uranium-series Disequilibrium, Applications to Earth, Marine, and Environmental Sciences*. Oxford Science Publications, Oxford.

Jenkins W. J. and Rhines P. B. (1980) Tritium in the deep North Atlantic Ocean. *Nature* **286**, 877–880.

Joyce T. M., Wunsch C. and Pierce S. D. (1986) Synoptic Gulf Stream velocity profiles through simultaneous inversion of hydrographic and acoustic Doppler data. *J. Geophys. Res.* **91**, 7573–7585.

Lal D. (1988) Theoretically expected variations in the terrestrial cosmic-ray production rates of isotopes. Soc. Italiana di Fisica-Bologna-Italy XCV corso, pp. 216–233.

Lee S. H., Povinec P. P., Wyse E. and Hotchkis M. A. C. (2008) Ultra-low-level determination of ^{236}U in IAEA marine reference materials by ICPMS and AMS. *Appl. Radiat. Isot.* **66**, 823–828.

Mangini A., Sonntag C., Bertsch G. and Müller E. (1979) Evidence for a higher natural U-content in world rivers. *Nature* **79**, 337–339.

Marsden O. J., Livens F. R., Day J. P., Fifield L. K. and Goodall P. S. (2001) Determination of U-236 in sediment samples by accelerator mass spectrometry. *Analyst* **126**, 633–636.

Monterey G. and Levitus S. (1997) Seasonal Variability of Mixed Layer Depth for the World Ocean. NOAA Atlas NESDIS, vol. 14. Available from: <ftp://ftp.nodc.noaa.gov/pub/data.nodc/woa/PUBLICATIONS/Atlas14.pdf>.

Müller A. M., Christl M., Lachner J., Suter M. and Synal H.-A. (2010) Competitive ^{10}Be measurements below 1 MeV with the upgraded ETH-TANDY AMS facility. *Nucl. Instrum. Methods B* **268**, 2801–2807.

Orre S., Smith J., Alfimov V. and Bentsen M. (2010) Simulating transport of ^{129}I and idealized tracers in the northern North Atlantic Ocean. *Environ. Fluid Mech.* **10**, 213–233.

OSPAR (2009) OSPAR Commission Work Areas/Radioactive Substances/Publications. ISBN 978-1-907390-84-5, Publication No.: 543/2011. Available from: <http://www.ospar.org/>.

Owens S. A., Buesseler K. O. and Sims K. W. W. (2011) Re-evaluating the 238U-salinity relationship in seawater: implications for the 238U–234Th disequilibrium method. *Mar. Chem.* **127**, 31–39.

Pates J. M. and Muir G. K. P. (2007) U-salinity relationships in the Mediterranean: implications for ^{234}Th: ^{238}U particle flux studies. *Mar. Chem.* **106**, 530–545.

Purser K. H., Kilius L. R., Litherland A. E. and Zhao X. (1996) Detection of ^{236}U: a possible 100-million year neutron flux integrator. *NIM B* **113**, 445–452.

Rijkenberg M. (2010) RV Pelagia PE321 Cruise summary report. In (ed. B.O.D. Centre). Available from: <https://www.bodc.ac.uk/data/information_and_inventories/cruise_inventory/report/10002/>.

Robinson L. F., Belshaw N. S. and Henderson G. M. (2004) U and Th concentrations and isotope ratios in modern carbonates and waters from the Bahamas. *Geochim. Cosmochim. Acta* **68**, 1777–1789.

Roemmich D. and Wunsch C. (1985) Two transatlantic sections: meridional circulation and heat flux in the subtropical North Atlantic Ocean. *Deep Sea Res. Part A: Oceanogr. Res. Papers* **32**, 619–664.

Sabine C. L., Feely R. A., Gruber N., Key R. M., Lee K., Bullister J. L., Wanninkhof R., Wong C. S., Wallace D. W. R., Tilbrook B., Millero F. J., Peng T.-H., Kozyr A., Ono T. and Rios A. F. (2004) The oceanic sink for anthropogenic CO_2. *Science* **305**, 367–371.

Sackett W., Mo T., Spalding R., Exner M. (1973) A revaluation of the marine geochemistry of uranium. IAEA SM-158/51, pp. 757–769.

Sakaguchi A., Kawai K., Steier P., Quinto F., Mino K., Tomita J., Hoshi M., Whitehead N. and Yamamoto M. (2009) First results on ^{236}U levels in global fallout. *Sci. Total Environ.* **407**, 4238–4242.

Santschi P. H., Schink D. R., Corapcioglu O., Oktay-Marshall S., Fehn U. and Sharma P. (1996) Evidence for elevated levels of iodine-129 in the Deep Western Boundary Current in the Middle Atlantic Bight. *Deep Sea Res. Part I: Oceanogr. Res. Papers* **43**, 259–265.

SEPA (Scottish Environment Protection Agency) (2010) Radioactivity in Food and the Environment (RIFE). **15**, Available from: <http://www.food.gov.uk/multimedia/pdfs/publication/rife2009.pdf>.

Singh S. K., Dalai T. K. and Krishnaswami S. (2003) ^{238}U series isotopes and ^{232}Th in carbonates and black shales from the Lesser Himalaya: implications to dissolved uranium abundances in Ganga-Indus source waters. *J. Environ. Radioactiv.* **67**, 69–90.

Srncik M., Steier P. and Wallner G. (2009) Determination of the isotopic ratio ^{236}U/^{238}U in Austrian water samples. *NIM B* **268**, 1146–1149.

Steier P., Bichler M., Keith Fifield L., Golser R., Kutschera W., Priller A., Quinto F., Richter S., Srncik M., Terrasi P., Wacker L., Wallner A., Wallner G., Wilcken K. M. and Maria Wild E. (2008) Natural and anthropogenic ^{236}U in environmental samples. *NIM B* **266**, 2246–2250.

Steier P., Dellinger F., Forstner O., Golser R., Knie K., Kutschera W., Priller A., Quinto F., Srncik M., Terrasi F., Vockenhuber C., Wallner A., Wallner G. and Wild E. M. (2010) Analysis and application of heavy isotopes in the environment. *NIM B* **268**, 1045–1049.

Stocker M., Döbeli M., Grajcar M., Suter M., Synal H. A. and Wacker L. (2005) A universal and competitive compact AMS facility. *Nucl. Instrum. Methods B* **240**, 483–489.

Synal H. A., Jacob S. and Suter M. (2000) The PSI/ETH small radiocarbon dating system. *Nucl. Instrum. Methods B* **172**, 1–7.

Vockenhuber C., Christl M., Hofmann C., Lachner J., Müller A. M. and Synal H.-A. (2011) Accelerator mass spectrometry of ^{236}U at low energies. *NIM B* **269**, 3199–3203.

Wilcken K. M., Fifield L. K., Barrows T. T., Tims S. G. and Gladkis L. G. (2008) Nucleogenic ^{36}Cl, ^{236}U and ^{239}Pu in uranium ores. *NIM B* **266**, 3614–3624.

Winkler S., Steier P. and Carilli J. (2011) Goldschmidt abstracts 2011. *Mineral. Mag.* **75**, 796–824.

Zhao X. L., Nadeau M. J., Kilius L. R. and Litherland A. E. (1994) The first detection of naturally-occurring ^{236}U with accelerator mass spectrometry. *NIM B* **92**, 249–253.

Associate editor: James McManus

Biogeosciences, 9, 1935–1955, 2012
www.biogeosciences.net/9/1935/2012/
doi:10.5194/bg-9-1935-2012

Biogeosciences

A molecular perspective on the ageing of marine dissolved organic matter

R. Flerus[1,*], O. J. Lechtenfeld[1,*], B. P. Koch[1,2,*], S. L. McCallister[3], P. Schmitt-Kopplin[4,6], R. Benner[5], K. Kaiser[5], and G. Kattner[1]

[1]Alfred Wegener Institute for Polar and Marine Research, Ecological Chemistry, Bremerhaven, Germany
[2]University of Applied Sciences, Bremerhaven, Germany
[3]Virginia Commonwealth University, Department of Biology, Center for Environmental Studies, Richmond, VA, USA
[4]Helmholtz Zentrum München, German Research Center for Environmental Health, Analytical BioGeoChemistry, Neuherberg, Germany
[5]University of South Carolina, Marine Science Program, Columbia, SC, USA
[6]Chair of Analytical Food Chemistry, Technische Universität München, 85354 Freising-Weihenstephan, Germany
[*]These authors equally contributed to this work

Correspondence to: B. P. Koch (boris.koch@awi.de)

Received: 27 October 2011 – Published in Biogeosciences Discuss.: 29 November 2011
Revised: 3 April 2012 – Accepted: 5 April 2012 – Published: 1 June 2012

Abstract. Dissolved organic matter (DOM) was extracted by solid-phase extraction (SPE) from 137 water samples from different climate zones and different depths along an eastern Atlantic Ocean transect. The extracts were analyzed with Fourier transform ion cyclotron resonance mass spectrometry (FT-ICR MS) with electrospray ionization (ESI). $\Delta^{14}C$ analyses were performed on subsamples of the SPE-DOM. In addition, the amount of dissolved organic carbon was determined for all water and SPE-DOM samples as well as the yield of amino sugars for selected samples. Linear correlations were observed between the magnitudes of 43 % of the FT-ICR mass peaks and the extract $\Delta^{14}C$ values. Decreasing SPE-DOM $\Delta^{14}C$ values went along with a shift in the molecular composition to higher average masses (*m/z*) and lower hydrogen/carbon (H/C) ratios. The correlation was used to model the SPE-DOM $\Delta^{14}C$ distribution for all 137 samples. Based on single mass peaks, a degradation index (I_{DEG}) was developed to compare the degradation state of marine SPE-DOM samples analyzed with FT-ICR MS. A correlation between $\Delta^{14}C$, I_{DEG}, DOC values and amino sugar yield supports that SPE-DOM analyzed with FT-ICR MS reflects trends of bulk DOM. DOM weighted normalized mass peak magnitudes were used to compare aged and recent SPE-DOM on a semi-quantitative molecular basis. The magnitude comparison showed a continuum of different degradation rates for the detected compounds. A high proportion of the compounds should persist, possibly modified by partial degradation, in the course of thermohaline circulation. Prokaryotic (bacterial) production, transformation and accumulation of this very stable DOM occur primarily in the upper ocean. This DOM is an important contribution to very old DOM, showing that production and degradation are dynamic processes.

1 Introduction

Marine dissolved organic matter (DOM) is one of the major active reservoirs of the global carbon cycle. The amount of marine dissolved organic carbon (DOC) is estimated to be 662 Gt, which is comparable to the amount of carbon in atmospheric CO_2 (Hedges, 1992; Hansell et al., 2009; Tans, 2010). Since the average age of bulk DOC below the thermocline is about 4000 yr in the Sargasso Sea and about 6000 yr in the central North Pacific, marine DOM plays an important role in long-term carbon storage and sequestration of atmospheric CO_2 (Williams and Druffel, 1987; Bauer, 2002). This older DOM pool represents a refractory background with concentrations of

35–45 µmol kg^{-1} (Hansell and Carlson, 1998; Ogawa et al., 1999), upon which labile and semi-labile pools of DOM are superimposed in the upper ocean. Numerous studies have examined the fluxes, remineralization and temporal variability of accumulated DOC (e.g. Goldberg et al., 2009; Hansell et al., 2009; Carlson et al., 2010). Jiao et al. (2010) proposed the concept of the microbial carbon pump as a potential process for the production of refractory DOM in surface waters. Hereby, microbes produce the very stable DOM, which persists over very long time scales in the world oceans. However, the mechanisms of production, diagenesis and preservation of highly stable DOM are still unknown. The molecular analysis is particularly challenging as only a minor fraction of the DOM can be analyzed molecularly and identified as carbohydrates, lipids, amino acids and amino sugars (Benner, 2002).

Ultrahigh resolution Fourier transform ion cyclotron resonance mass spectrometry (FT-ICR MS) with electrospray ionization (ESI) was successfully applied to distinguish thousands of compounds of different elemental compositions in ultra-filtered and solid-phase extracted marine DOM (SPE-DOM) (Koch et al., 2005; Hertkorn et al., 2006; Kujawinski et al., 2009). Ultrahigh resolution allows elemental formulas to be assigned for individual mass peaks (Stenson et al., 2003). Water samples of different spatial origin can be distinguished based on the molecular information from FT-ICR MS analysis. However, to date only a few samples have been compared with this technique, preventing a systematic comparison of FT-ICR MS data and additional analytical parameters.

Radiocarbon age and amino sugars are critical diagnostic parameters to assess the production of refractory DOM. The analysis of amino sugars in seawater provides very valuable information on the early diagenesis of DOM (Benner and Kaiser, 2003; Davis et al., 2009; Kaiser and Benner, 2009). Radiocarbon age provides a timeline from carbon fixation in the upper ocean and its subsequent turnover and flux to the deep ocean for bulk DOC and individual components and compound classes (Druffel et al., 1992; Aluwihare et al., 1997; Loh et al., 2004; Repeta and Aluwihare, 2006). Due to the analytical challenge of radiocarbon analysis of bulk DOC, the radiocarbon age has only been determined for a few samples at some locations, including the central North Pacific (Williams and Druffel, 1987; Druffel et al., 1992), the Southern Ocean (Druffel and Bauer, 2000) and the Sargasso Sea (Bauer et al., 1992; Druffel et al., 1992). A handful of additional studies have been performed on $\Delta^{14}C$ of marine DOM fractions of differing size or chemical components, such as humic isolates, lipid extracts, carbohydrate-like DOM and protein-like DOM. The high molecular weight (>10 kD) DOM is of recent age, suggesting greater lability and faster turnover, whereas the low molecular weight (<1 kD) DOM is apparently older (Santschi et al., 1995; Loh et al., 2004). Humic substances isolated with XAD resins are similar to bulk C pools, with radiocarbon ages only slightly older (Druffel et al., 1989). The oldest age (up to 17 000 yr BP) was determined in lipid extracts (Loh et al., 2004). However, each DOM fraction still consists of multiple compounds with a continuum of ages, and consequently the bulk age of DOM represents an average of all the individual compounds. To date, a direct linkage between radiocarbon age and DOM on a molecular level has not been reported.

The aim of this study is to investigate the ageing, processes and associated molecular changes of DOM along an eastern Atlantic Ocean transect. Our combination of FT-ICR MS with radiocarbon age analysis of SPE-DOM from different depths and biogeochemical regions provided a unique opportunity to investigate the age composition and related molecular signatures of a large ocean system. To discuss the data in a broader ecological and biogeochemical context, FT-ICR MS data were combined for the first time with environmental parameters, DOC, amino sugars and bacterial activity, each determined independently. Our ultimate goal was to elucidate molecular trends that are characteristic for the entire Atlantic Ocean.

2 Materials and methods

2.1 Sampling

Water samples were collected along a transect from 50.2° N to 31.4° S in the eastern Atlantic Ocean in November 2008 during the cruise ANT-XXV/1 of R/V *Polarstern*. Surface water was sampled three times per day with a fish sampler, which was fixed alongside the ship, providing a continuous flow of surface water (∼2 m water depth). Water from 200 m and the fluorescence maximum was sampled daily with a rosette sampler connected to a CTD, as well as water from seven selected stations from surface to bottom (Fig. 1). Samples for the analysis of DOC and amino sugars were filtered through GF/F filters (Whatman, pre-combusted for 4 h, 450 °C) and stored in pre-combusted glass ampoules at −20 °C.

2.2 DOM extraction

FT-ICR MS measurement requires the concentration and desalting of marine DOM. Therefore, DOM was extracted on board using solid-phase extraction (SPE), for which the term SPE-DOM will be used in the following. Filtered samples were acidified with HCl (hydrochloric acid, p.a. grade, Merck) to pH 2. The DOM was extracted using SPE cartridges (PPL, 1g, Varian, Mega Bond Elut) according to Dittmar et al. (2008). The cartridges were rinsed with methanol (LiChrosolv; Merck), followed by acidified ultra-pure water (Milli-Q, pH 2, HCl) and then 5 l of seawater was gravity passed through each cartridge. Subsequently, remaining salt was removed with acidified ultra-pure water. After drying with nitrogen gas, DOM was eluted with 5 ml methanol into pre-combusted glass ampoules and stored at −20 °C.

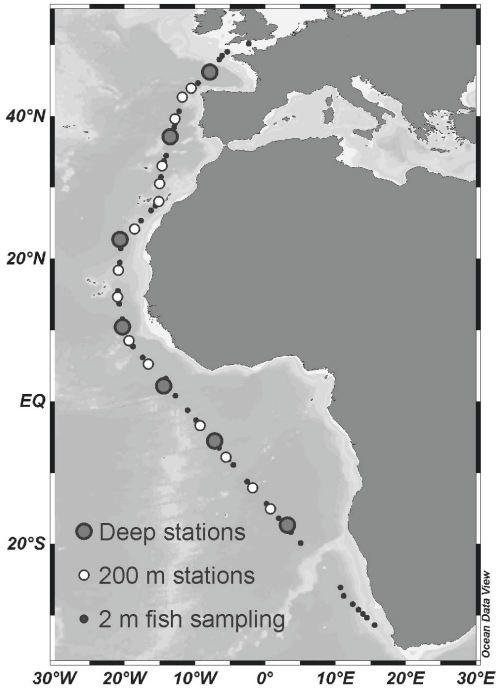

Fig. 1. Map of the sampling locations on the cruise ANT-XXV/1 of RV Polarstern.

2.3 Analyses

The DOC concentration was determined by high temperature catalytic oxidation with a Shimadzu TOC-VCPN analyzer. Before analysis water samples were acidified in the auto-sampler and purged with O_2 for 5 min. The DOC content of the SPE-DOM was determined by evaporation of 50 µl methanol extract re-dissolved in 6.5 ml ultra-pure water.

Bacterioplankton production was estimated by ^{3}H-leucine uptake (Smith and Azam, 1992). Triplicate subsamples (1.5 ml) and one trichloroacetic acid-killed control were amended with 5 nM ^{3}H-leucine (Amersham, specific activity 160 Ci mmol^{-1}) and incubated at in situ temperature (±2 °C) in the dark. Incubation time varied depending on depth: ∼2 h for upper waters (up to 200 m) and up to 12 h (below 200 m). Samples were processed according to Smith and Azam (1992) and radioassayed with a Wallac scintillation counter after addition of 1 ml of Ultima Gold AB scintillation cocktail. The disintegrations per minute (DPM) of the killed control were subtracted from the mean DPM of the corresponding duplicate samples and converted to leucine incorporation rates. A conversion factor of 3.1 kg C mol^{-1} was applied (Kirchman, 1993).

Concentrations of galactosamine (GalN), mannosamine (ManN) and glucosamine (GlcN) were determined by high-performance anion-exchange chromatography coupled to a pulsed amperometric detector (Kaiser and Benner, 2000). After hydrolysis in 3 M HCl (5 h, 100 °C), samples were neutralized with a self-absorbed ion retardation resin (AG11 A8, Biorad) and stored frozen until analysis. Samples were desalted by solid-phase extraction using Biorad's AG50 X8 resin in the Na^+-form before chromatographic separation. Subsequently, GalN, ManN and GlcN were separated isocratically on a Dionex PA20 anion-exchange column with 2 mM NaOH at a flow rate of 1 ml min^{-1}.

Subsamples of SPE-DOM (0.2–1 mg C) were quantitatively transferred to combusted (500 °C) quartz tubes (6 mm diameter), evaporated under a stream of N_2, sealed under vacuum and combusted at 900 °C to CO_2 using a CuO/Ag metal catalyst (Sofer, 1980). The CO_2 from break seals was subsequently reduced to graphite in an atmosphere of H_2 over a cobalt catalyst (Vogel et al., 1987). Graphite targets were analyzed at the Center for Accelerator Mass Spectrometry at Lawrence Livermore National Laboratory. Δ^{14}C is defined as the (per mil) deviation of a sample from the ^{14}C activity of a 1950 standard, corrected for fractionation according to Stuvier and Polach (1977). Total measurement uncertainties for Δ^{14}C analyses of these samples were typically ±4 ‰. A blank analysis of a SPE cartridge was determined before and no measurable amount of CO_2 was found (<1 µg).

FT-ICR MS analysis of 137 SPE-DOM samples was performed with an Apex Qe mass spectrometer (Bruker Daltonics), equipped with a 12 T superconducting magnet (Bruker Biospin) and an Apollo II Dual electrospray source (Bruker). Prior to analysis, SPE-DOM was adjusted to similar DOC concentrations by dilution with methanol (factor 3.1–9.7). The diluted extracts were analysed with ESI in negative ion mode (capillary voltage −4.2 kV, infusion flow rate 2 µl min^{-1}). Spectra were calibrated internally with compounds, which were repeatedly identified in marine DOM samples (*m/z* 339.10854, 369.11911, 411.12967, 469.13515, 541.15628; Schmidt et al., 2009; Flerus et al., 2011). 512 scans were added to acquire one spectrum. All ions were singly charged and the mass accuracy was below 0.2 ppm > mass accuracy > −0.2 ppm for the ions used for the internal calibration.

2.4 FT-ICR MS data evaluation

The mass spectra were evaluated in the range *m/z* 200–600. For each identified peak in the spectra (signal to noise > 3; Data analysis 3.4; Bruker Daltonics), elemental formulas were calculated in the mass accuracy range of ±0.5 ppm (e.g. Koch et al., 2005, 2007). The isotopes included for the formula calculation were as follows: ^{12}C (0–∞), ^{13}C (0–1), ^{1}H (0–∞), ^{16}O (0–∞), ^{14}N (0–2), ^{32}S (0–1). The average mass accuracy for all assigned peaks was < ±0.2 ppm. For unambiguous elemental formula assignment, the "nitrogen-rule" and following thresholds were applied: O/C ≤ 1.2 and H/C ≤ 2C + 2 + N (Koch et al., 2005). All formulas with ^{13}C isotopes were removed from the data set as they represent duplicates of the ^{12}C parent molecules.

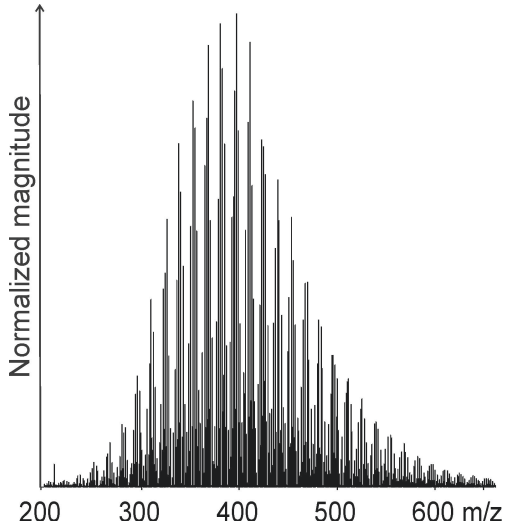

Fig. 2. Negative ESI FT-ICR mass spectrum of a representative marine SPE-DOM sample from the eastern Atlantic Ocean.

Prior to mass spectra comparison, the mass peak magnitudes of each spectrum were normalized to the sum of all identified mass peak magnitudes of the respective spectrum. These relative peak magnitudes are presented in per mill (‰) and a magnitude cutoff of 0.05 ‰ was applied. All mass peaks present in less than five mass spectra were excluded from the final data set, in favor of identifying bulk trends. Since masses with low signal to noise ratios tend to show less mass accuracy, this procedure allowed an improved formula assignment. Ambiguously identified mass peaks were checked according to the "chemical building block" approach (Koch et al., 2007). Each oxygen atom in a molecular formula could be replaced with a CH_4-fragment, forming a pseudo-homologous series with a mass difference, $\Delta m = 36.4$ mDa. Therefore, the number of oxygen atoms in a molecular formula must exceed the number of "CH_4-O" pseudo-homologous series members; otherwise it is considered as falsely assigned.

Finally, an evaluation data set was obtained showing 2850 mass peaks with only few doubly-assigned molecular formulas (average: 2 ± 1 double assignments per sample). On a presence-absence basis and the 0.05 ‰ cutoff, 54 % of the detected molecular formulas were present in more than 135 samples, while 74 % were present in at least 100 samples showing the typical peak magnitude distribution of marine SPE-DOM (Fig. 2). Most mass peaks, which were not present in all samples, showed normalized magnitudes close to the cutoff limit. Due to the high degree of similarity between all samples, our data evaluation was based on normalized peak magnitudes instead of a presence/absence-based approach as previously applied for biomarker approaches in glacial or riverine DOM (Bhatia et al., 2010; Sleighter and Hatcher, 2008).

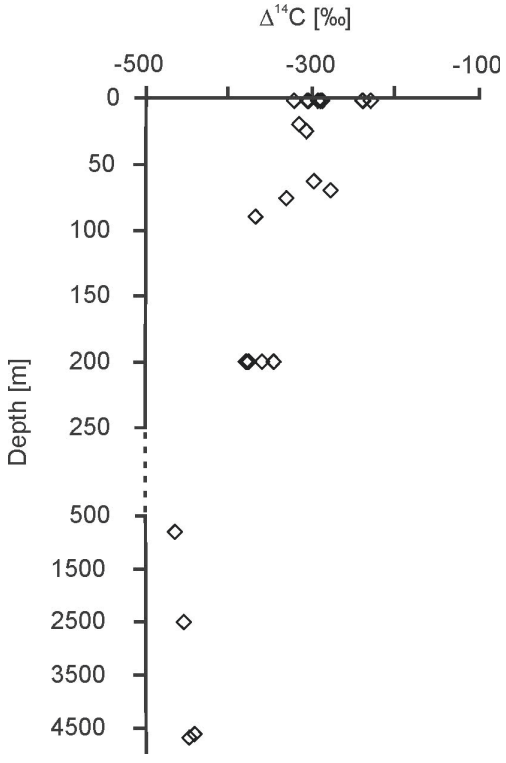

Fig. 3. $\Delta^{14}C$ values of marine SPE-DOM from the eastern Atlantic Ocean.

2.5 Statistical analysis

For statistical analysis we performed a non-parametric two-sided Mann-Whitney U-test for the comparison of weighted average parameters of SPE-DOM samples and two groups of peaks. The null hypothesis was that two groups differ by a location shift of "0" and the significance level α is 0.01.

3 Results and discussion

$\Delta^{14}C$ values ranged from a maximum of -229 ‰ in surface water extracts (2 m) to -464 ‰ in deep water extracts (>2500 m, Fig. 3). The highest surface $\Delta^{14}C$ values were comparable with the surface (3 m) $\Delta^{14}C$ value determined by Druffel and Bauer (1992) in the Sargasso Sea (-238 ‰). In comparison to the reported values from the Sargasso Sea, our $\Delta^{14}C$ values in deeper water (>2 m) were slightly more negative, ranging between that of bulk DOC and XAD isolates (Bauer et al., 1992), pointing to an almost representative extraction. However, from polarity-driven reversed-phase chromatography and the lower extraction efficiency for organic nitrogen compared to organic carbon, we know that the method discriminates against highly polar (and presumably small) compounds.

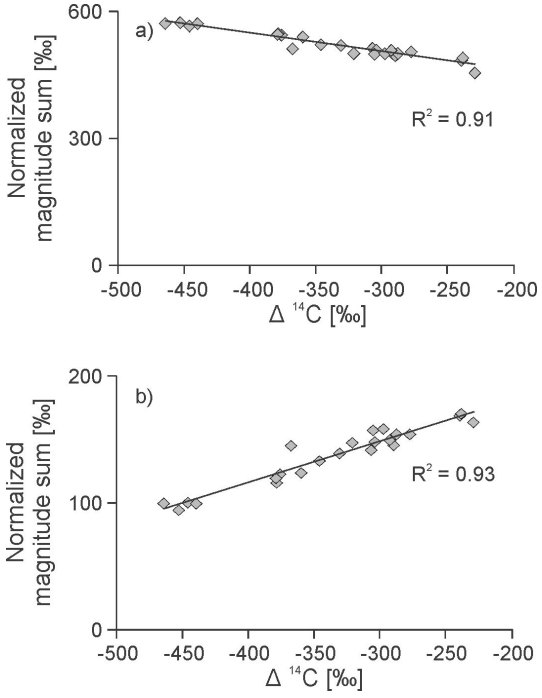

Fig. 4. Normalized magnitude sum [‰] of **(a)** negatively and **(b)** positively correlated FT-ICR mass peaks of eastern Atlantic Ocean SPE-DOM versus $\Delta^{14}C$ values of the SPE-DOM. The sums ($\sum$NEG, $\sum$POS) were built by adding the normalized magnitudes of the single with $\Delta^{14}C$ highly negatively or positively correlating mass peaks for each sample.

43 % of the normalized FT-ICR mass peak magnitudes showed either a significantly linear positive (POS) or negative (NEG) correlation with $\Delta^{14}C$ ($R > 0.5$, $p < 0.01$) (peaks and elemental formulas are presented in Tables A1 and A2 in Appendix A). The magnitudes of all significantly POS and NEG correlating mass peaks were summed up separately ($\sum$POS, $\sum$NEG), resulting in two average calibration functions (Fig. 4a, b). The $\sum$POS and $\sum$NEG mass peaks account for 61 ± 1 % of the summed magnitudes of all peaks in each spectrum, therefore representing a large and consistent fraction of peaks for the complete sample set. The two individual calibration functions were then used to calculate two different $\Delta^{14}C$ values for any of the 137 SPE-DOM samples, both resulting in almost identical $\Delta^{14}C$ values. Hence, the arithmetic mean of the two calculated $\Delta^{14}C$ values was used as the final $\Delta^{14}C$ value ($\Delta^{14}C_{Cal}$) for each sample. $\Delta^{14}C_{Cal}$ values for the upper 200 m are presented as depth-section (Fig. 5), and for the few deep water samples as individual values (Table 1).

This approach enabled us to apply calculated $\Delta^{14}C_{Cal}$ values for the whole sample set, allowing to define the groups of "recent" ($\Delta^{14}C_{Cal}$: > -280 ‰, $n = 29$) and "aged" samples ($\Delta^{14}C_{Cal}$: < -450, $n = 10$). Within both groups, the peak magnitude distributions were similar. To obtain a semi-quantitative approach of the reactivity of individual

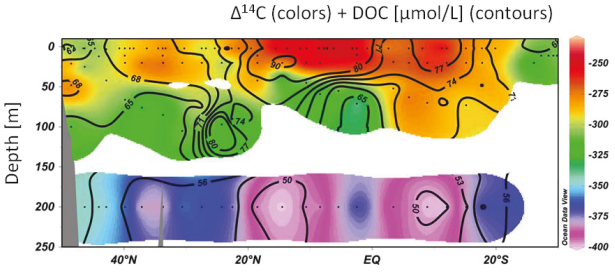

Fig. 5. Calculated SPE-DOM $\Delta^{14}C$ values (colors) and measured bulk DOC concentrations (contours) in the upper 250 m of the water column in the eastern Atlantic Ocean. The $\Delta^{14}C_{Cal}$ values and the DOC concentrations are significantly positively correlated.

DOM compounds in our Atlantic Ocean sample set, the normalized mass peak magnitudes were weighted by the respective bulk seawater DOC concentration. The relative changes in the magnitudes were calculated using a linear regression model (ordinary least squares, all 137 samples), resulting in predicted decreases of 22 to 167 %. A rate of 100 % or more is here defined as compounds with magnitudes falling below the 0.05 ‰ threshold. Since 100–167 % was a result of the definition and these compounds were still visible as very small mass peaks in the spectra, we will use the term "highly degraded" for this group. The compounds with estimated decreases >100 % were yet observed to be highly degraded in the oldest SPE-DOM in the Atlantic Ocean. This applied for only 4 % (number %) of the compounds. The magnitude weighting resulted in the disappearance of the negative correlations of magnitudes with $\Delta^{14}C$. In fact, the NEG peaks now exhibited a positive correlation with $\Delta^{14}C$ as well, suggesting that both, POS and (formerly) NEG correlating compounds detected by FT-ICR MS decrease with age.

3.1 Molecular characteristics of DOM diagenesis

We observed clear differences in the molecular characteristics between POS and NEG compounds. The peak magnitudes of the POS compounds were generally much lower than those of the NEG compounds and the average *m/z* was inversely correlated with $\Delta^{14}C$ values (Fig. 6). Comparing recent and aged samples revealed a highly significant difference (Mann-Whitney U-test; $p < 0.01$) in the weighted average *m/z* values of 11.1 Da. The magnitude average *m/z* therefore slightly increased from 407.8 ± 2.1 for recent to 417.9 ± 0.8 for aged SPE-DOM. Previous studies showed a decrease in molecular size from high molecular weight DOM (>1 kDa) to low molecular weight DOM (<1 kDa) as a result of increased diagenetic processing (Kaiser and Benner, 2009) and a decreasing bioreactivity (Amon and Benner, 1996). Dittmar and Kattner (2003) also suggested a comparatively higher refractory character for small DOM molecules. However, these previous results were

Table 1. Calculated SPE-DOM $\Delta^{14}C_{Cal}$ values [‰] and bulk DOC values [$\mu mol\,L^{-1}$] in the deep water layers of the eastern Atlantic Ocean.

Depth (m)	Parameter	46° N 8° W	37° N 14° W	23° N 20° W	11° N 20° W	2° S 14° W	5° S 7° W	17° S 3° W	24° S 9° W
400–500	$\Delta^{14}C$ (‰)		−402						
800–900	$\Delta^{14}C$ (‰)				−456	−465	−448	−451	
1100–1800	$\Delta^{14}C$ (‰)		−436	−459				−449	
2500	$\Delta^{14}C$ (‰)			−462					
4000–5000	$\Delta^{14}C$ (‰)	−443	−463	−456	−450	−451	−454		
400–500	DOC ($\mu mol\,L^{-1}$)	56	58						
800–900	DOC ($\mu mol\,L^{-1}$)				45	47	46	49	
1100–1800	DOC ($\mu mol\,L^{-1}$)	50	48			52	54	47	
2500	DOC ($\mu mol\,L^{-1}$)	48		45					
4000–5000	DOC ($\mu mol\,L^{-1}$)	48	45		47		41	47	45

obtained using size-related separations such as ultrafiltration and gel permeation chromatography. In contrast, we used absorbent enriched samples (SPE-DOM), preventing a direct comparison with the previous studies. Based on SPE-DOM samples Hertkorn et al. (2012) obtained results that also suggested a similar trend of decreasing SPE-DOM molecular size with depth.

The van Krevelen diagram (Kim et al., 2003) showed differences in the elemental composition of the POS and NEG formulas (Fig. 7). The majority of CHO compounds of the POS formulas showed high H/C ratios (1.53 ± 0.2), whereas the NEG CHO formulas showed medium to low H/C ratios (1.15 ± 0.2, Fig. 7a, b). Within the region of H/C ≤ 1.4 of the van Krevelen diagram, the average mass for NEG and POS formulas was *m/z* 441 and *m/z* 300, respectively. Most of the POS formulas containing nitrogen (CHON) showed higher H/C ratios (1.43 ± 0.2). CHON compounds of NEG formulas occurred only in the low H/C region, similarly to the CHO compounds (1.16 ± 0.2, Fig. 7c, d). The H/C ratio shift also affected the DBE, ranging between 2 and 11 for the POS formulas and between 7 and 14 for the NEG formulas.

Although it is well known that the efficiency of microbial degradation is often related to the polarity of the substrate, we did not observe a shift in the O/C ratios with increasing age of the samples. For both NEG and POS groups, CHO and CHON compounds showed average O/C values of 0.48 ± 0.3 and 0.49 ± 0.2, respectively, showing no significant differences. With the exception of two mass peaks, CHOS compounds only occurred in the POS formulas having similar H/C values as the POS CHO and CHON compounds (Fig. 7e, f) with slightly higher O/C ratios (0.6 ± 0.2). However, only little is known about the role of CHOS compounds in DOM and a considerable contribution of anthropogenic input to these compounds cannot be excluded.

The strong molecular similarity, as detected in this and other studies using FT-ICR MS, is considered to represent the refractory molecular background of marine DOM (Koch

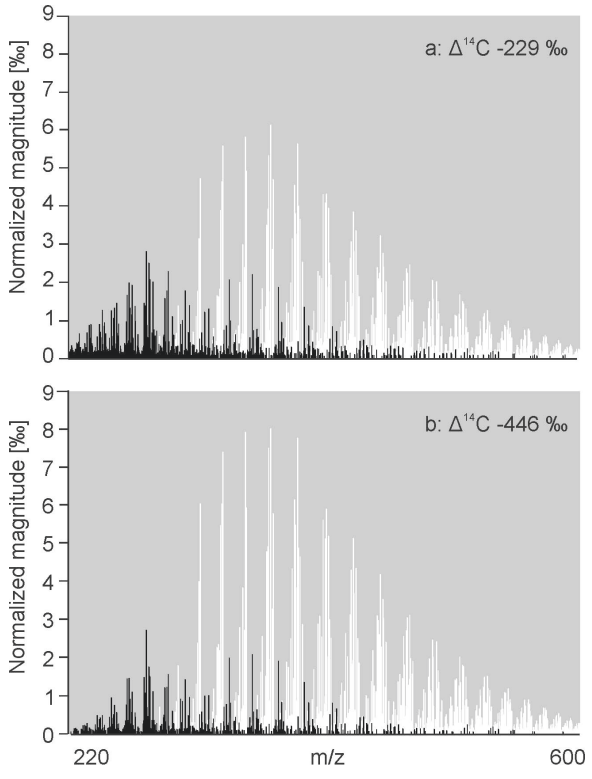

Fig. 6. Selected normalized FT-ICR mass peaks of eastern Atlantic Ocean SPE-DOM. The mass peaks show a significant linear correlation with $\Delta^{14}C$. **(a)** Surface sample extract with $\Delta^{14}C = -229$ ‰ and **(b)** deep sea sample extract with $\Delta^{14}C = -446$ ‰. The black colored masses are positively correlated with $\Delta^{14}C$ and are present in a higher proportion in the more recent SPE-DOM, whereas the white colored masses are negatively correlated with $\Delta^{14}C$ and present in a higher proportion in the aged SPE-DOM. The difference in the *m/z* between black and white masses is also reflected in the weighted average *m/z* of the whole SPE-DOM spectra and shifts from 407 (surface sample, $\Delta^{14}C = -229$) to 413 (deep sea sample, $\Delta^{14}C = -446$).

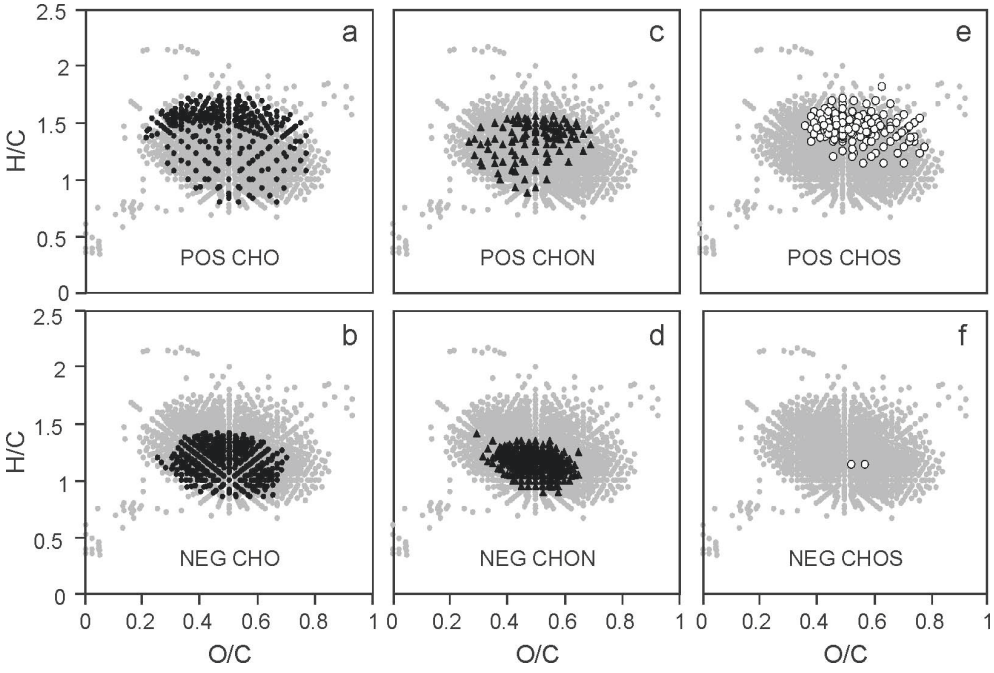

Fig. 7. Van Krevelen diagrams of compounds in eastern Atlantic Ocean SPE-DOM that are significantly correlated with $\Delta^{14}C$ ($p < 0.01$): **(a)** positively with CHO compounds; **(b)** negatively with CHO compounds; **(c)** positively with CHON compounds; **(d)** negatively with CHON compounds; **(e)** positively with CHOS compounds; **(f)** negatively with CHOS compounds. The grey dots in the background show all compounds found in the majority of Atlantic Ocean water extracts.

et al., 2005; Hertkorn et al., 2006; Gonsior et al., 2011). In our study, we observed depth and age-related trends in the total average elemental composition of the spectra. These trends were similar to the trends observed for the POS and NEG formulas. We found a highly significant difference in the weighted average H/C ratios between recent and aged samples (Mann-Whitney U-test, $p < 0.01$). The magnitude-averaged H/C ratios decreased from 1.268 ± 0.006 in recent to 1.245 ± 0.003 in aged SPE-DOM. Accordingly, the magnitude-averaged DBE increased from 8.03 ± 0.06 in recent to 8.43 ± 0.03 in aged SPE-DOM. Again, no clear trend was found in the magnitude-averaged O/C ratios, and we are currently examining potential reasons for this disparity.

Hertkorn et al. (2006) analysed surface and deep UDOM from the Pacific Ocean using NMR and FT-ICR MS. They identified carboxyl-rich alicyclic molecules (CRAM) as a major constituent in surface and deep UDOM, which was suggested to resist biodegradation. The region occupied by CRAM in the van Krevelen diagram corresponds well with the region of our NEG mass peaks, which are assumed to be compounds resistant to degradation. Hence, CRAM could also be a significant contributor to SPE-DOM. However, it has to be pointed out that the elemental composition can represent a large variety of possible structural isomers (Hertkorn et al., 2007). Nevertheless, a recent study by Witt et al. (2009) demonstrated that the structural variability represented by a single elemental formula in the FT-ICR mass spectra is probably not as high as expected for natural organic matter.

3.2 East Atlantic Ocean DOM degradation state

The linear correlation between single mass peaks and SPE-DOM $\Delta^{14}C$ allows to compare SPE-DOM samples in terms of their degradation state. Since FT-ICR MS is increasingly used for marine DOM studies, we present a degradation index that can be easily used to estimate and compare the degradation state of marine SPE-DOM. To calculate the degradation index, we selected 5 POS (POS_{Ideg}) and 5 NEG (NEG_{Ideg}) formulas (Table 2) with a particularly high correlation with the radiocarbon age. The 10 selected masses were also present in ∼400 previously analyzed samples from other locations and environments and therefore suitable to be implemented in a versatile index describing the relative degradation state of an individual sample within a given set of samples. The index I_{DEG} was calculated using the molecular formulas given in Table 2 and can be directly applied to the raw peak magnitudes:

$$I_{DEG} = \Sigma(\text{magnitudes}\, NEG_{Ideg}) / \Sigma(\text{magnitudes}\, (NEG_{Ideg} + POS_{Ideg})) \quad (1)$$

The value of I_{DEG} ranges between 0–1 and increases with the degradation state of the sample, because the magnitude contribution of NEG formulas increases. We observed

Table 2. Formulas utilized for magnitude summation in order to calculate the degradation index I_{DEG}.

NEG correlating compounds	POS correlating compounds
$C_{21}\,H_{26}\,O_{11}$	$C_{13}\,H_{18}\,O_{7}$
$C_{17}\,H_{20}\,O_{9}$	$C_{14}\,H_{20}\,O_{7}$
$C_{19}\,H_{22}\,O_{10}$	$C_{15}\,H_{22}\,O_{7}$
$C_{20}\,H_{22}\,O_{10}$	$C_{15}\,H_{22}\,O_{8}$
$C_{20}\,H_{24}\,O_{11}$	$C_{16}\,H_{24}\,O_{8}$

however from our database that the absolute value of I_{DEG} is dependent on instrument, extraction technique and environment. For example, samples from soils and sediments had generally lower values for I_{DEG} than samples from ocean water (data not shown). If similar sample extracts are measured with the same instrument in series, the I_{DEG} trends are comparable. However, since no comparable data exist, $\Delta^{14}C$ values should only be calculated using I_{DEG} in combination with measured reference $\Delta^{14}C$ values. Also, C18 extracted samples did not reliably show the respective peaks for the I_{DEG} calculation.

For our eastern Atlantic Ocean samples, I_{DEG} was in the range from 0.628–0.756 for the surface samples (Fig. 8a) and 0.756–0.808 for deeper water >200 m (Table 3). I_{DEG} showed a strong correlation with the $\Delta^{14}C$ values and the bulk DOC concentrations. In particular, in the upper 200 m changes in DOC concentrations were reflected in the I_{DEG}. The lowest I_{DEG} was found in the area with the youngest SPE-DOM, in the upper 25 m between 2–12° N along with the highest DOC concentrations. This was the most stratified region with thermocline depths of 25–30 m. The accumulation of freshly produced DOC in highly stratified surface water was also reported by Carlson et al. (1994) and Goldberg et al. (2009). At 200 m depth the lowest I_{DEG} and the youngest SPE-DOM were calculated north of 40° N. The highest I_{DEG} as well as the oldest SPE-DOM and lowest bulk DOC concentrations matched with the tropical divergences around 15° N and 10° S, which are upwelling areas. The location of the tropical divergences was obtained from CTD temperature profiles of the cruise. So far, the narrow range and small number of data points of $\Delta^{14}C$ values, DOC concentrations and FT-ICR MS spectra for deep (>500 m) and bottom water samples circumvent a detailed oceanographic discussion of abyssal water masses of terms of DOM degradation.

To support the differentiation in fresh and old DOM, amino sugars were determined directly in bulk water samples as an independent measurement. Amino sugars are bioactive compounds and the DOC-normalized yield of amino sugars is an indicator for the degradation state of DOM (Benner and Kaiser, 2003; Kaiser and Benner, 2009). The significant

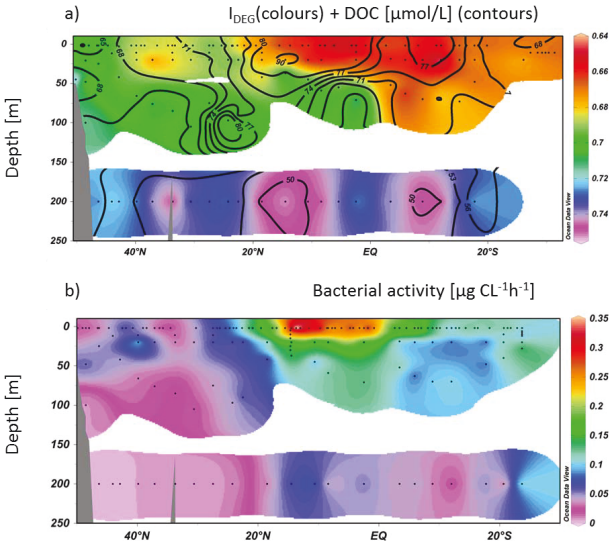

Fig. 8. **(a)** Values of the degradation index I_{DEG} for SPE-DOM samples from the eastern Atlantic Ocean (colors) and bulk DOC concentrations (contours); **(b)** the bacterial activity determined as utilized µg C l^{-1} h^{-1} in the upper 250 m of the water column in the eastern Atlantic Ocean. I_{DEG} can be easily calculated and used to estimate and compare the degradation state of marine FT-ICR MS analyzed SPE-DOM. The higher the values of I_{DEG}, the more degraded is the SPE-DOM. I_{DEG} and the DOC concentrations are significantly correlated. The bacterial activity maximum coincides with the lowest I_{DEG}, the DOC maximum and the youngest SPE-DOM (Fig. 4).

correlation between $\Delta^{14}C_{Cal}$ and the yield of amino sugars is consistent with previous observations, indicating that they are more reactive than bulk DOC. These independent results are a good indication that our mass peak magnitude-based $\Delta^{14}C$ calculation is reasonable (Fig. 9). The exponential relation between the amino sugar yield and $\Delta^{14}C_{Cal}$ also suggests that a fraction of the youngest and most bioavailable compounds was not recovered by SPE or was not detected by FT-ICR MS analysis.

3.3 Degradation continuum and the microbial carbon pump

Several studies present strategies to explain mechanisms of redistribution of DOM in the water column, based on their $\Delta^{14}C$ values and two or three component models (Beaupre and Druffel, 2009; Beaupre and Aluwihare, 2010; Hansell et al., 2009; Williams and Druffel, 1987). The models suggest a refractory DOM background fraction and labile or semi-labile fractions with distinct isotopic compositions. Beaupre and Druffel (2009) used 2-component Keeling plots to estimate the radiocarbon age of the background and the fresh DOM fractions. Applying the Keeling plot method to the SPE-DOM samples from the seven deep stations results in similar values for the fresh SPE-DOM fraction

Table 3. I_{DEG} values for deep water layers.

Depth [m]	46° N 8° W	37° N 14° W	23° N 20° W	11° N 20° W	2° S 14° W	5° S 7° W	17° S 3° W
400–500		0.756					
800–900				0.793	0.790	0.777	0.776
1100–1800		0.787	0.801				0.779
2500			0.807				
4000–5000	0.798	0.808	0.805	0.787	0.785	0.788	

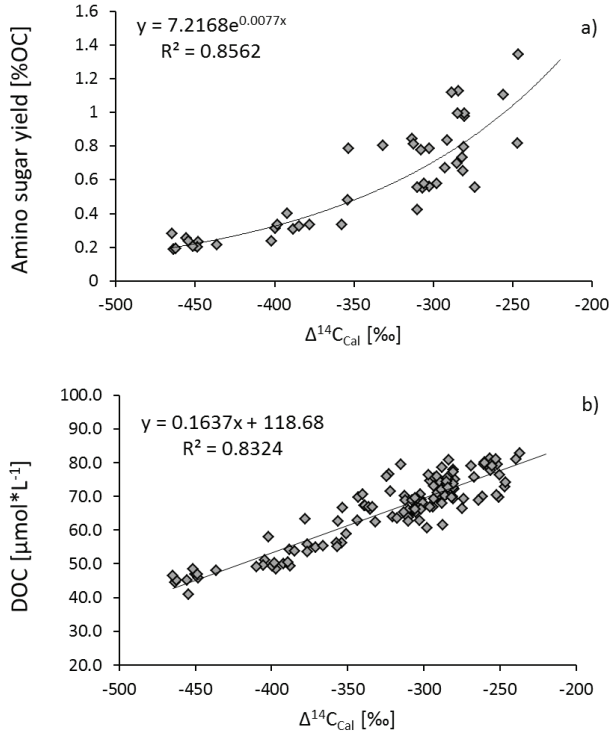

Fig. 9. Correlation and equations of **(a)** bulk amino sugar yields and **(b)** bulk DOC concentrations of Atlantic Ocean water and calculated $\Delta^{14}C$ values of the corresponding SPE-DOM. The correlations indicate the reasonability of the trend in $\Delta^{14}C_{Cal}$. The exponential relation between the amino sugar yield and $\Delta^{14}C_{Cal}$ also suggests that a fraction of the youngest and most bioavailable compounds was not recovered by SPE or was not detected by FT-ICR MS analysis.

at every station (Table 4). The values are slightly lower than the values reported for the Sargasso Sea (Beaupre and Aluwihare, 2010), but the variation is within the range of reported values for the Pacific Ocean (Beaupre and Druffel, 2009). This provides further evidence that the trends in radiocarbon age of SPE-DOM are comparable to that for the bulk DOC. Beaupre and Druffel (2009) calculated $\Delta^{14}C$ for the background DOM, but since $\Delta^{14}C$ was too low for the oldest water sample, they considered a multiple component system.

Our results indeed showed a wide spectrum of DOM reactivity represented by varying slopes of magnitude change with age, supporting our hypothesis of a continuum of DOM reactivity and age. As mentioned above, we assume that the compounds in the FT-ICR mass spectra have been degraded over time, but to varying extents. In the north Central Pacific Ocean (NCP), the lowest $\Delta^{14}C$ value of bulk DOC is −546 ‰ (Druffel et al., 1992), which is older than the oldest SPE-DOM in the Atlantic Ocean. Coinciding with the oldest water masses, the DOC concentration in the deep NCP is only ∼34 µmol kg^{-1} (Hansell et al., 2009), supporting the hypothesis of a very slow degradation (remineralization) of refractory DOC (Hansell et al., 2012). Based on the correlation between $\Delta^{14}C_{Cal}$ of SPE-DOM and DOC concentration (Fig. 9b), we estimated the $\Delta^{14}C$ values and molecular degradation trends of SPE-DOM during thermohaline circulation. Applying this correlation, the SPE-DOM $\Delta^{14}C$ in the NCP calculates to −518 ‰, which is in good agreement with the values reported by Williams and Druffel (1987) and Druffel et al. (1992). To elucidate at which point during the thermohaline circulation a single compound would be highly degraded, we performed a rough estimate using the following assumptions: (i) each mass peak either represents one compound or several compounds with similar degradation rates. This is based on a recent study by Witt et al. (2009) suggesting that the structural variability of a single elemental formula in the FT-ICR mass spectra is probably not as high as expected for natural organic matter; (ii) a compound is regarded as highly degraded when the relative magnitude falls below the cutoff of 0.05 ‰. Using the calibration functions resulting from the correlation between the bulk DOC weighted magnitudes and $\Delta^{14}C_{cal}$, a theoretical SPE-DOM $\Delta^{14}C$ limit ($\Delta^{14}C_{Lim}$) was calculated at which each compound is considered to be highly degraded. Thus, the proportion of mass peaks can be estimated, which will be highly degraded in the NCP. Since we were interested in general trends, this calculation was performed for compounds that were present in 27–29 of all "young" samples. All compounds with $\Delta^{14}C_{Lim} >$ −518 ‰ are expected to be highly degradable, as they are not supposed to be present in the NCP. This applied for 16 % (number %) of the compounds. Portions of the remaining compounds will persist for long periods of time (Fig. 10)

Table 4. Calculated $\Delta^{14}C$ values of excess SPE-DOM and corresponding Keeling slope values for the seven deep stations of the eastern Atlantic Ocean.

Station	$\Delta^{14}C$ of excess SPE-DOM	Keeling slope
46° N, 8° W	−121	−6880
37° N, 14° W	108	−11 394
23° N, 20° W	17	−10 050
11° N, 20° W	50	−9938
2° S, 14° W	68	−10 203
5° S, 7° W	76	−10 550
17° S, 3° W	44	−10239

and are supposed to contribute to the high average age of DOM. The FT-ICR MS analyzed SPE-DOM represents a fraction of the marine DOM, for which a high portion of 84 % of the compounds (number %) is expected to persist, possibly modified by partially degradation, during one or more thermohaline cycles through the global ocean circulation. At the same time the compounds are expected to degrade very slowly with a continuum of different rates in the range from 22–167 % (Fig. 10). The relative decreases were calculated using a linear regression model (ordinary least squares, all 137 samples), resulting in predicted decreases >100 % for some compounds. These compounds were yet observed to be highly degraded in the oldest SPE-DOM in the Atlantic Ocean.

Our results support the hypothesis of a broad and continuous distribution of $\Delta^{14}C$ ages, as proposed by Bauer et al. (1992). Since only few of the compounds were identified to be highly degraded in the oldest Atlantic Ocean SPE-DOM, compounds of moderate reactivity, which are degraded within month to decades and expected to be present in SPE-DOM, are potentially underrepresented in the FT-ICR mass spectra. Also, the presence of an absolute refractory fraction (i.e. ^{14}C depleted), which is hidden in a mixture with degrading compounds, cannot be excluded. However, since the $\Delta^{14}C$ trends in SPE-DOM are similar to $\Delta^{14}C$ trends of bulk DOM, we propose the degradation continuum shown for FT-ICR MS analysed SPE-DOM to be one important pathway in marine DOM degradation. Operational terms such as "labile", "semi-labile", "refractory (recalcitrant)", "background" or "excess" DOM, as used in different studies (Beaupre and Druffel, 2009; Beaupre and Aluwihare, 2010; Hansell et al., 2009; William and Druffel, 1987; Jiao et al., 2010), are generally useful to distinguish among the reactivities of different DOM fractions, but the complexity of DOM reactivity is better described as a continuum.

The microbial carbon pump provides a conceptual framework for a better understanding of the role of microbial processes in the generation of recalcitrant DOM and carbon storage in the ocean (Ogawa et al., 2001; Jiao et al., 2010).

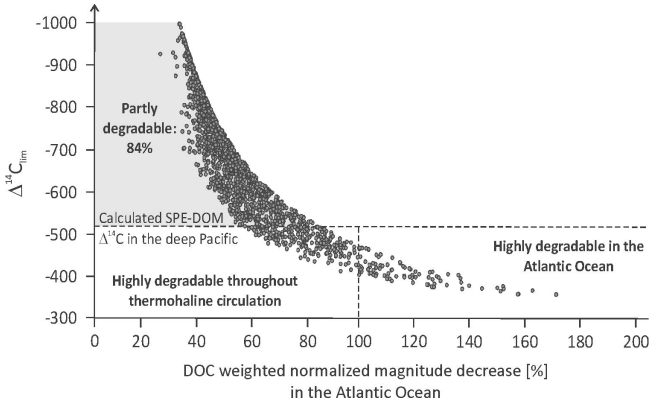

Fig. 10. Calculated limit of $\Delta^{14}C$ ($\Delta^{14}C_{Lim}$) for Atlantic Ocean SPE-DOM compounds, represented by FT-ICR mass peaks versus the calculated, DOC weighted normalized magnitude decrease of SPE-DOM in the Atlantic Ocean (x-axis, [%]). All compounds are expected to decrease with increasing SPE-DOM age, but with different rates (between 22–167 %). The relative decreases were calculated using a linear regression model (ordinary least squares, all 137 samples), resulting in predicted decreases > 100 % for some compounds. These compounds are yet observed to be highly degraded in the oldest SPE-DOM in the Atlantic Ocean. $\Delta^{14}C_{Lim}$ is a theoretical SPE-DOM $\Delta^{14}C$ value, at which a compound is regarded to be highly degraded. All compounds with a $\Delta^{14}C_{Lim} > -518$ ‰ (SPE-DOM $\Delta^{14}C$ value estimated for the CNP) are expected to be highly degraded in the oldest water masses. 84 % (number %) of the compounds should persist, possibly modified by partial degradation throughout thermohaline circulation. The variability of decreasing rates as well as the $\Delta^{14}C_{Lim}$ values represent a continuum of different degradation rates for the individual compounds.

It is hypothesized that the transformation of labile and semi-labile DOM through microbial processes leads to the accumulation of recalcitrant DOM in the ocean. Indeed, the highest bacterial activity as well as the maximum abundance of the reactive parameters (DOC, amino sugars and I_{DEG}) was determined in surface waters of the highly stratified region between 0–15° N (Fig. 7b). The primary production was supposed to have only a minor contribution. A comparison of I_{DEG} with the TChl-a fluorescence data from the discrete stations (Taylor et al., 2011) showed no clear relationship. Out of all mass peaks, the estimated fraction of the least reactive compounds is at least 61 %, accounting for 94 % of the summed magnitudes per sample. We hypothesize that this low reactivity fraction is produced and accumulates in the euphotic zone. Fresh and highly reactive DOM is rapidly consumed by prokaryotes (Carlson and Ducklow, 1996) and partially converted to low reactivity DOM (Ogawa et al., 2001). These recently produced refractory and younger compounds mix with older refractory compounds of similar reactivity in the epipelagic zone. This mixture is then further degraded by bacterial activity (Ogawa and Tanoue, 2003) and thereby aged during the thermohaline circulation.

4 Conclusions

Trends in bulk DOC radiocarbon ages were reflected in the radiocarbon age, determined from a correlation between selected FT-ICR mass peaks and SPE-DOM $\Delta^{14}C$ values. With this knowledge the degradation state of other marine DOM samples can be estimated by comparing FT-ICR mass peaks. Since this method was only applied for the Atlantic Ocean, it is important to continue these studies in other oceanic regions. For this, the degradation index I_{DEG} was introduced as a simple tool to evaluate relative degradation states in a set of similarly treated samples. So far, I_{DEG} is only applied for SPE-DOM samples (PPL extracts) from the Atlantic Ocean and thus has to be further verified.

We propose a degradation continuum of the compounds represented in the FT-ICR mass spectra, but only a minor portion of them are expected to be highly degraded during thermohaline circulation. Prokaryotic (bacterial) production, transformation and accumulation of the very stable DOM occur probably primarily in the upper ocean (Benner and Herndl, 2011). This DOM is an important contribution to very old DOM, showing that production and degradation are dynamic processes. Since bacterial growth, bacterial production or enzymatic activities are influenced by parameters, e.g. temperature or CO_2 (Piontek et al., 2009, 2010), a change of these parameters could also influence the processes of refractory DOM production or degradation and as a consequence also the amount of DOM in the world oceans.

It is likely that the microbial carbon pump and the proposed degradation continuum of microbially-produced DOM are parts of several processes taking place concurrently, resulting in the observed average age of DOM samples. To elucidate these complex processes, it is important to further investigate sources, transformations and fates of DOM in the ocean. The FT-ICR MS data provide novel insights into the molecular composition of highly degraded DOM. Microbial degradation experiments and studies of aggregation processes combined with FT-ICR MS will help to gain a better understanding of DOM cycling in the ocean.

Acknowledgements. The authors gratefully acknowledge Anne Stuart for lab assistance, two anonymous reviewers for their helpful comments and the crew of the research vessel "Polarstern" for professional assistance during sample collection.

This work was partially funded by the German Academic Exchange Service (DAAD, project 50023021), the German Science Foundation (KO 2164/8-1), and a National Science Foundation-Ocean Sciences grant OCE-0825403 to S. L. M. and NSF 0713915.

Edited by: G. Herndl

Table A1. POS molecular formulas: complete list of mass peaks and assigned molecular formulas that showed a highly significant positive correlation ($p < 0.01$) with SPE-DOM $\Delta^{14}C$.

Elemental Formula	M	Elemental Formula	M	Elemental Formula	M
C_{12} H_{14} O_4	222.089209	C_{14} H_{14} O_8	310.068867	C_{18} H_{27} O_8 N_1	385.173667
C_{13} H_{18} O_3	222.125594	C_{16} H_{22} O_6	310.141638	C_{16} H_{22} O_9 N_2	386.13253
C_{11} H_{12} O_5	224.068474	C_{17} H_{26} O_5	310.178024	C_{18} H_{26} O_7 S_1	386.139924
C_{12} H_{16} O_4	224.104859	C_{13} H_{12} O_9	312.048132	C_{19} H_{30} O_8	386.194068
C_{13} H_{20} O_3	224.141245	C_{14} H_{16} O_8	312.084518	C_{17} H_{25} O_9 N_1	387.152931
C_{11} H_{14} O_5	226.084124	C_{13} H_{16} O_7 N_2	312.095751	C_{15} H_{20} O_8 N_2 S_1	388.094036
C_{12} H_{18} O_4	226.120509	C_{15} H_{20} O_7	312.120903	C_{17} H_{24} O_8 S_1	388.119188
C_{10} H_{12} O_6	228.063388	C_{16} H_{24} O_6	312.157289	C_{19} H_{20} O_7 N_2	388.127051
C_{11} H_{16} O_5	228.099774	C_{13} H_{15} O_8 N_1	313.079767	C_{17} H_{24} O_{10}	388.136947
C_{10} H_{14} O_6	230.079038	C_{14} H_{19} O_7 N_1	313.116152	C_{18} H_{28} O_7 S_1	388.155574
C_{11} H_{18} O_5	230.115424	C_{15} H_{23} O_6 N_1	313.152538	C_{18} H_{28} O_9	388.173333
C_{10} H_{16} O_6	232.094688	C_{13} H_{14} O_9	314.063782	C_{19} H_{32} O_8	388.209718
C_{13} H_{14} O_4	234.089209	C_{14} H_{18} O_8	314.100168	C_{16} H_{23} O_8 N_1 S_1	389.114437
C_{12} H_{12} O_5	236.068474	C_{13} H_{18} O_7 N_2	314.111401	C_{16} H_{23} O_{10} N_1	389.132196
C_{13} H_{16} O_4	236.104859	C_{15} H_{22} O_7	314.136553	C_{16} H_{22} O_9 S_1	390.098453
C_{14} H_{20} O_3	236.141245	C_{16} H_{26} O_6	314.172939	C_{16} H_{22} O_{11}	390.116212
C_{12} H_{14} O_5	238.084124	C_{13} H_{17} O_8 N_1	315.095417	C_{17} H_{26} O_8 S_1	390.134839
C_{13} H_{18} O_4	238.120509	C_{14} H_{21} O_7 N_1	315.131802	C_{17} H_{26} O_{10}	390.152597
C_{11} H_{13} O_5 N_1	239.079373	C_{13} H_{16} O_7 S_1	316.061674	C_{18} H_{30} O_9	390.188983
C_{11} H_{12} O_6	240.063388	C_{13} H_{16} O_9	316.079432	C_{15} H_{21} O_9 N_1 S_1	391.093702
C_{12} H_{16} O_5	240.099774	C_{14} H_{20} O_6 S_1	316.098059	C_{16} H_{25} O_8 N_1 S_1	391.130088
C_{13} H_{20} O_4	240.136159	C_{14} H_{20} O_8	316.115818	C_{15} H_{20} O_{10} S_1	392.077718
C_{11} H_{15} O_5 N_1	241.095023	C_{15} H_{24} O_7	316.152203	C_{16} H_{24} O_9 S_1	392.114103
C_{11} H_{14} O_6	242.079038	C_{13} H_{19} O_8 N_1	317.111067	C_{16} H_{24} O_{11}	392.131862
C_{12} H_{18} O_5	242.115424	C_{13} H_{18} O_7 S_1	318.077324	C_{17} H_{28} O_{10}	392.168247
C_{10} H_{12} O_7	244.058303	C_{13} H_{18} O_9	318.095082	C_{22} H_{32} O_6	392.219889
C_{11} H_{16} O_6	244.094688	C_{14} H_{22} O_6 S_1	318.113709	C_{14} H_{18} O_{11} S_1	394.056982
C_{12} H_{20} O_5	244.131074	C_{16} H_{18} O_5 N_2	318.121572	C_{15} H_{22} O_{10} S_1	394.093368
C_{10} H_{14} O_7	246.073953	C_{14} H_{22} O_8	318.131468	C_{21} H_{32} O_7	396.214803
C_{11} H_{18} O_6	246.110338	C_{15} H_{26} O_7	318.167853	C_{21} H_{34} O_7	398.230453
C_{13} H_{12} O_5	248.068474	C_{19} H_{26} O_4	318.183109	C_{19} H_{29} O_8 N_1	399.189317
C_{14} H_{16} O_4	248.104859	C_{15} H_{12} O_8	320.053217	C_{16} H_{20} O_8 N_2 S_1	400.094036
C_{13} H_{15} O_4 N_1	249.100108	C_{12} H_{16} O_8 S_1	320.056588	C_{17} H_{24} O_9 N_2	400.14818
C_{12} H_{10} O_6	250.047738	C_{13} H_{20} O_7 S_1	320.092974	C_{19} H_{28} O_7 S_1	400.155574
C_{13} H_{14} O_5	250.084124	C_{13} H_{20} O_9	320.110732	C_{20} H_{32} O_8	400.209718
C_{14} H_{18} O_4	250.120509	C_{14} H_{24} O_8	320.147118	C_{17} H_{23} O_8 N_1 S_1	401.114437
C_{12} H_{13} O_5 N_1	251.079373	C_{15} H_{14} O_8	322.068867	C_{17} H_{23} O_{10} N_1	401.132196
C_{13} H_{17} O_4 N_1	251.115758	C_{12} H_{18} O_8 S_1	322.072238	C_{18} H_{27} O_9 N_1	401.168582
C_{12} H_{12} O_6	252.063388	C_{13} H_{22} O_7 S_1	322.108624	C_{16} H_{22} O_{10} N_2	402.127445
C_{13} H_{16} O_5	252.099774	C_{18} H_{26} O_5	322.178024	C_{18} H_{26} O_8 S_1	402.134839
C_{12} H_{16} O_4 N_2	252.111007	C_{14} H_{12} O_9	324.048132	C_{18} H_{26} O_{10}	402.152597
C_{14} H_{20} O_4	252.136159	C_{12} H_{20} O_8 S_1	324.087888	C_{19} H_{30} O_9	402.188983
C_{12} H_{15} O_5 N_1	253.095023	C_{18} H_{28} O_5	324.193674	C_{17} H_{25} O_{10} N_1	403.147846
C_{13} H_{19} O_4 N_1	253.131408	C_{17} H_{26} O_6	326.172939	C_{17} H_{24} O_9 S_1	404.114103
C_{12} H_{14} O_6	254.079038	C_{15} H_{21} O_7 N_1	327.131802	C_{17} H_{24} O_{11}	404.131862
C_{13} H_{18} O_5	254.115424	C_{14} H_{20} O_7 N_2	328.127051	C_{18} H_{28} O_8 S_1	404.150489
C_{14} H_{22} O_4	254.151809	C_{16} H_{24} O_7	328.152203	C_{18} H_{28} O_{10}	404.168247
C_{11} H_{13} O_6 N_1	255.074287	C_{17} H_{28} O_6	328.188589	C_{19} H_{32} O_9	404.204633
C_{12} H_{17} O_5 N_1	255.110673	C_{14} H_{19} O_8 N_1	329.111067	C_{16} H_{23} O_9 N_1 S_1	405.109352
C_{11} H_{12} O_7	256.058303	C_{15} H_{23} O_7 N_1	329.147452	C_{16} H_{23} O_{11} N_1	405.127111
C_{12} H_{16} O_6	256.094688	C_{13} H_{14} O_{10}	330.058697	C_{17} H_{26} O_9 S_1	406.129753
C_{13} H_{20} O_5	256.131074	C_{14} H_{18} O_9	330.095082	C_{17} H_{26} O_{11}	406.147512
C_{11} H_{15} O_6 N_1	257.089937	C_{15} H_{22} O_6 S_1	330.113709	C_{18} H_{30} O_{10}	406.183897
C_{11} H_{14} O_7	258.073953	C_{15} H_{22} O_8	330.131468	C_{15} H_{20} O_{11} S_1	408.072632

Table A1. Continued.

Elemental Formula	M	Elemental Formula	M	Elemental Formula	M
$C_{12}H_{18}O_6$	258.110338	$C_{16}H_{26}O_7$	330.167853	$C_{16}H_{24}O_{10}S_1$	408.109018
$C_{13}H_{22}O_5$	258.146724	$C_{13}H_{17}O_9N_1$	331.090331	$C_{15}H_{22}O_{11}S_1$	410.088282
$C_{11}H_{16}O_7$	260.089603	$C_{14}H_{21}O_8N_1$	331.126717	$C_{22}H_{34}O_7$	410.230453
$C_{12}H_{20}O_6$	260.125988	$C_{13}H_{16}O_8S_1$	332.056588	$C_{21}H_{32}O_8$	412.209718
$C_{14}H_{14}O_5$	262.084124	$C_{13}H_{16}O_{10}$	332.074347	$C_{19}H_{26}O_8S_1$	414.134839
$C_{11}H_{18}O_5S_1$	262.087494	$C_{14}H_{20}O_7S_1$	332.092974	$C_{18}H_{26}O_9N_2$	414.16383
$C_{11}H_{18}O_7$	262.105253	$C_{16}H_{16}O_6N_2$	332.100836	$C_{21}H_{34}O_8$	414.225368
$C_{14}H_{17}O_4N_1$	263.115758	$C_{14}H_{20}O_9$	332.110732	$C_{19}H_{29}O_9N_1$	415.184232
$C_{13}H_{12}O_6$	264.063388	$C_{15}H_{24}O_6S_1$	332.129359	$C_{17}H_{24}O_{10}N_2$	416.143095
$C_{10}H_{16}O_6S_1$	264.066759	$C_{15}H_{24}O_8$	332.147118	$C_{19}H_{28}O_8S_1$	416.150489
$C_{14}H_{16}O_5$	264.099774	$C_{16}H_{14}O_8$	334.068867	$C_{19}H_{28}O_{10}$	416.168247
$C_{13}H_{15}O_5N_1$	265.095023	$C_{13}H_{18}O_8S_1$	334.072238	$C_{20}H_{32}O_9$	416.204633
$C_{14}H_{19}O_4N_1$	265.131408	$C_{13}H_{18}O_{10}$	334.089997	$C_{18}H_{27}O_{10}N_1$	417.163496
$C_{12}H_{10}O_7$	266.042653	$C_{14}H_{22}O_7S_1$	334.108624	$C_{18}H_{26}O_9S_1$	418.129753
$C_{13}H_{14}O_6$	266.079038	$C_{14}H_{22}O_9$	334.126382	$C_{18}H_{26}O_{11}$	418.147512
$C_{14}H_{18}O_5$	266.115424	$C_{15}H_{26}O_8$	334.162768	$C_{19}H_{30}O_8S_1$	418.166139
$C_{15}H_{22}O_4$	266.151809	$C_{12}H_{16}O_9S_1$	336.051503	$C_{19}H_{30}O_{10}$	418.183897
$C_{12}H_{13}O_6N_1$	267.074287	$C_{13}H_{20}O_8S_1$	336.087888	$C_{17}H_{25}O_9N_1S_1$	419.125002
$C_{13}H_{17}O_5N_1$	267.110673	$C_{14}H_{24}O_7S_1$	336.124274	$C_{17}H_{25}O_{11}N_1$	419.142761
$C_{12}H_{12}O_7$	268.058303	$C_{19}H_{28}O_5$	336.193674	$C_{17}H_{24}O_{10}S_1$	420.109018
$C_{13}H_{16}O_6$	268.094688	$C_{12}H_{18}O_9S_1$	338.067153	$C_{17}H_{24}O_{12}$	420.126776
$C_{12}H_{16}O_5N_2$	268.105922	$C_{13}H_{22}O_8S_1$	338.103538	$C_{18}H_{28}O_9S_1$	420.145403
$C_{14}H_{20}O_5$	268.131074	$C_{18}H_{26}O_6$	338.172939	$C_{18}H_{28}O_{11}$	420.163162
$C_{15}H_{24}O_4$	268.167459	$C_{19}H_{30}O_5$	338.209324	$C_{19}H_{32}O_{10}$	420.199547
$C_{12}H_{15}O_6N_1$	269.089937	$C_{18}H_{28}O_6$	340.188589	$C_{16}H_{22}O_{11}S_1$	422.088282
$C_{13}H_{19}O_5N_1$	269.126323	$C_{15}H_{18}O_7S_1$	342.077324	$C_{17}H_{26}O_{10}S_1$	422.124668
$C_{12}H_{14}O_7$	270.073953	$C_{17}H_{26}O_7$	342.167853	$C_{17}H_{26}O_{12}$	422.142426
$C_{13}H_{18}O_6$	270.110338	$C_{18}H_{30}O_6$	342.204239	$C_{23}H_{34}O_7$	422.230453
$C_{14}H_{22}O_5$	270.146724	$C_{16}H_{25}O_7N_1$	343.163102	$C_{16}H_{24}O_{11}S_1$	424.103932
$C_{12}H_{17}O_6N_1$	271.105587	$C_{14}H_{16}O_8S_1$	344.056588	$C_{23}H_{36}O_7$	424.246104
$C_{11}H_{12}O_8$	272.053217	$C_{15}H_{20}O_7S_1$	344.092974	$C_{22}H_{34}O_8$	426.225368
$C_{12}H_{16}O_7$	272.089603	$C_{14}H_{20}O_8N_2$	344.121966	$C_{20}H_{28}O_8S_1$	428.150489
$C_{13}H_{20}O_6$	272.125988	$C_{16}H_{24}O_8$	344.147118	$C_{21}H_{32}O_9$	428.204633
$C_{14}H_{24}O_5$	272.162374	$C_{17}H_{28}O_7$	344.183503	$C_{20}H_{30}O_8S_1$	430.166139
$C_{11}H_{14}O_8$	274.068867	$C_{14}H_{19}O_7N_1S_1$	345.088223	$C_{20}H_{30}O_{10}$	430.183897
$C_{12}H_{18}O_7$	274.105253	$C_{14}H_{19}O_9N_1$	345.105981	$C_{21}H_{34}O_9$	430.220283
$C_{13}H_{22}O_6$	274.141638	$C_{15}H_{23}O_8N_1$	345.142367	$C_{18}H_{25}O_9N_1S_1$	431.125002
$C_{11}H_{16}O_6S_1$	276.066759	$C_{14}H_{18}O_8S_1$	346.072238	$C_{19}H_{29}O_{10}N_1$	431.179146
$C_{11}H_{16}O_8$	276.084518	$C_{14}H_{18}O_{10}$	346.089997	$C_{19}H_{28}O_9S_1$	432.145403
$C_{12}H_{20}O_7$	276.120903	$C_{15}H_{22}O_7S_1$	346.108624	$C_{19}H_{28}O_{11}$	432.163162
$C_{14}H_{14}O_6$	278.079038	$C_{15}H_{22}O_9$	346.126382	$C_{20}H_{32}O_{10}$	432.199547
$C_{13}H_{13}O_6N_1$	279.074287	$C_{16}H_{26}O_8$	346.162768	$C_{18}H_{27}O_{11}N_1$	433.158411
$C_{14}H_{17}O_5N_1$	279.110673	$C_{14}H_{21}O_9N_1$	347.121631	$C_{18}H_{26}O_{12}$	434.142426
$C_{13}H_{12}O_7$	280.058303	$C_{13}H_{16}O_9S_1$	348.051503	$C_{19}H_{30}O_9S_1$	434.161053
$C_{14}H_{16}O_6$	280.094688	$C_{14}H_{20}O_8S_1$	348.087888	$C_{19}H_{30}O_{11}$	434.178812
$C_{16}H_{24}O_4$	280.167459	$C_{14}H_{20}O_{10}$	348.105647	$C_{17}H_{24}O_{11}S_1$	436.103932
$C_{13}H_{15}O_6N_1$	281.089937	$C_{15}H_{24}O_7S_1$	348.124274	$C_{18}H_{28}O_{10}S_1$	436.140318
$C_{14}H_{19}O_5N_1$	281.126323	$C_{15}H_{24}O_9$	348.142032	$C_{18}H_{28}O_{12}$	436.158076
$C_{13}H_{14}O_7$	282.073953	$C_{20}H_{28}O_5$	348.193674	$C_{24}H_{36}O_7$	436.246104
$C_{14}H_{18}O_6$	282.110338	$C_{13}H_{18}O_9S_1$	350.067153	$C_{16}H_{22}O_{12}S_1$	438.083197
$C_{15}H_{22}O_5$	282.146724	$C_{14}H_{22}O_8S_1$	350.103538	$C_{23}H_{36}O_8$	440.241018
$C_{13}H_{17}O_6N_1$	283.105587	$C_{14}H_{22}O_{10}$	350.121297	$C_{22}H_{34}O_9$	442.220283
$C_{14}H_{21}O_5N_1$	283.141973	$C_{20}H_{30}O_5$	350.209324	$C_{20}H_{29}O_{10}N_1$	443.179146
$C_{12}H_{12}O_8$	284.053217	$C_{15}H_{12}O_{10}$	352.043047	$C_{20}H_{28}O_9S_1$	444.145403
$C_{13}H_{16}O_7$	284.089603	$C_{13}H_{20}O_9S_1$	352.082803	$C_{21}H_{32}O_{10}$	444.199547
$C_{12}H_{16}O_6N_2$	284.100836	$C_{19}H_{28}O_6$	352.188589	$C_{22}H_{36}O_9$	444.235933

Table A1. Continued.

Elemental Formula	M	Elemental Formula	M	Elemental Formula	M
$C_{14}H_{20}O_6$	284.125988	$C_{19}H_{30}O_6$	354.204239	$C_{20}H_{30}O_9S_1$	446.161053
$C_{15}H_{24}O_5$	284.162374	$C_{16}H_{24}O_7N_2$	356.158351	$C_{20}H_{30}O_{11}$	446.178812
$C_{12}H_{15}O_7N_1$	285.084852	$C_{18}H_{28}O_7$	356.183503	$C_{21}H_{34}O_{10}$	446.215197
$C_{13}H_{19}O_6N_1$	285.121237	$C_{16}H_{23}O_8N_1$	357.142367	$C_{19}H_{28}O_{10}S_1$	448.140318
$C_{12}H_{14}O_8$	286.068867	$C_{15}H_{18}O_8S_1$	358.072238	$C_{19}H_{28}O_{12}$	448.158076
$C_{13}H_{18}O_7$	286.105253	$C_{16}H_{22}O_7S_1$	358.108624	$C_{20}H_{32}O_9S_1$	448.176703
$C_{14}H_{22}O_6$	286.141638	$C_{15}H_{22}O_8N_2$	358.137616	$C_{20}H_{32}O_{11}$	448.194462
$C_{12}H_{17}O_7N_1$	287.100502	$C_{17}H_{26}O_8$	358.162768	$C_{18}H_{26}O_{11}S_1$	450.119582
$C_{12}H_{16}O_6S_1$	288.066759	$C_{18}H_{30}O_7$	358.199153	$C_{18}H_{26}O_{13}$	450.137341
$C_{12}H_{16}O_8$	288.084518	$C_{15}H_{21}O_7N_1S_1$	359.103873	$C_{19}H_{30}O_{12}$	450.173726
$C_{13}H_{20}O_7$	288.120903	$C_{15}H_{21}O_9N_1$	359.121631	$C_{17}H_{24}O_{12}S_1$	452.098847
$C_{14}H_{24}O_6$	288.157289	$C_{16}H_{25}O_8N_1$	359.158017	$C_{24}H_{38}O_8$	454.256668
$C_{15}H_{14}O_6$	290.079038	$C_{14}H_{16}O_9S_1$	360.051503	$C_{23}H_{36}O_9$	456.235933
$C_{12}H_{18}O_6S_1$	290.082409	$C_{15}H_{20}O_8S_1$	360.087888	$C_{21}H_{31}O_{10}N_1$	457.194796
$C_{12}H_{18}O_8$	290.100168	$C_{16}H_{24}O_7S_1$	360.124274	$C_{19}H_{26}O_{11}N_2$	458.15366
$C_{13}H_{22}O_7$	290.136553	$C_{16}H_{24}O_9$	360.142032	$C_{22}H_{34}O_{10}$	458.215197
$C_{14}H_{13}O_6N_1$	291.074287	$C_{17}H_{28}O_8$	360.178418	$C_{20}H_{29}O_{11}N_1$	459.174061
$C_{14}H_{12}O_7$	292.058303	$C_{17}H_{15}O_8N_1$	361.079767	$C_{21}H_{32}O_9S_1$	460.176703
$C_{11}H_{16}O_7S_1$	292.061674	$C_{15}H_{23}O_7N_1S_1$	361.119523	$C_{21}H_{32}O_{11}$	460.194462
$C_{12}H_{20}O_6S_1$	292.098059	$C_{15}H_{23}O_9N_1$	361.137281	$C_{19}H_{27}O_{12}N_1$	461.153325
$C_{14}H_{16}O_5N_2$	292.105922	$C_{14}H_{18}O_9S_1$	362.067153	$C_{20}H_{30}O_{10}S_1$	462.155968
$C_{15}H_{20}O_4N_2$	292.142307	$C_{15}H_{22}O_8S_1$	362.103538	$C_{20}H_{30}O_{12}$	462.173726
$C_{14}H_{15}O_6N_1$	293.089937	$C_{15}H_{22}O_{10}$	362.121297	$C_{21}H_{34}O_{11}$	462.210112
$C_{15}H_{19}O_5N_1$	293.126323	$C_{16}H_{26}O_7S_1$	362.139924	$C_{19}H_{28}O_{11}S_1$	464.135232
$C_{14}H_{14}O_7$	294.073953	$C_{16}H_{26}O_9$	362.157682	$C_{19}H_{28}O_{13}$	464.152991
$C_{13}H_{13}O_7N_1$	295.069202	$C_{14}H_{21}O_8N_1S_1$	363.098787	$C_{20}H_{32}O_{12}$	464.189377
$C_{14}H_{17}O_6N_1$	295.105587	$C_{13}H_{16}O_{10}S_1$	364.046417	$C_{18}H_{26}O_{12}S_1$	466.114497
$C_{13}H_{12}O_8$	296.053217	$C_{14}H_{20}O_9S_1$	364.082803	$C_{24}H_{38}O_9$	470.251583
$C_{14}H_{16}O_7$	296.089603	$C_{15}H_{24}O_8S_1$	364.119188	$C_{22}H_{32}O_9S_1$	472.176703
$C_{11}H_{20}O_7S_1$	296.092974	$C_{15}H_{24}O_{10}$	364.136947	$C_{23}H_{36}O_{10}$	472.230847
$C_{15}H_{20}O_6$	296.125988	$C_{14}H_{22}O_9S_1$	366.098453	$C_{21}H_{31}O_{11}N_1$	473.189711
$C_{16}H_{24}O_5$	296.162374	$C_{20}H_{30}O_6$	366.204239	$C_{22}H_{34}O_{11}$	474.210112
$C_{13}H_{15}O_7N_1$	297.084852	$C_{13}H_{20}O_{10}S_1$	368.077718	$C_{21}H_{32}O_{10}S_1$	476.171618
$C_{14}H_{19}O_6N_1$	297.121237	$C_{20}H_{32}O_6$	368.219889	$C_{21}H_{32}O_{12}$	476.189377
$C_{13}H_{14}O_8$	298.068867	$C_{19}H_{30}O_7$	370.199153	$C_{20}H_{30}O_{11}S_1$	478.150883
$C_{14}H_{18}O_7$	298.105253	$C_{16}H_{21}O_9N_1$	371.121631	$C_{20}H_{30}O_{13}$	478.168641
$C_{13}H_{18}O_6N_2$	298.116486	$C_{17}H_{25}O_8N_1$	371.158017	$C_{19}H_{28}O_{12}S_1$	480.130147
$C_{15}H_{22}O_6$	298.141638	$C_{17}H_{24}O_7S_1$	372.124274	$C_{25}H_{38}O_9$	482.251583
$C_{16}H_{26}O_5$	298.178024	$C_{16}H_{24}O_8N_2$	372.153266	$C_{24}H_{38}O_{10}$	486.246497
$C_{13}H_{17}O_7N_1$	299.100502	$C_{18}H_{28}O_8$	372.178418	$C_{22}H_{32}O_{10}S_1$	488.171618
$C_{14}H_{21}O_6N_1$	299.136887	$C_{19}H_{32}O_7$	372.214803	$C_{23}H_{36}O_{11}$	488.225762
$C_{13}H_{16}O_8$	300.084518	$C_{15}H_{19}O_8N_1S_1$	373.083137	$C_{22}H_{34}O_{12}$	490.205027
$C_{14}H_{20}O_7$	300.120903	$C_{16}H_{23}O_9N_1$	373.137281	$C_{21}H_{32}O_{11}S_1$	492.166533
$C_{13}H_{20}O_6N_2$	300.132136	$C_{15}H_{18}O_9S_1$	374.067153	$C_{21}H_{32}O_{13}$	492.184291
$C_{15}H_{24}O_6$	300.157289	$C_{16}H_{22}O_8S_1$	374.103538	$C_{27}H_{40}O_8$	492.272318
$C_{12}H_{15}O_8N_1$	301.079767	$C_{16}H_{22}O_{10}$	374.121297	$C_{20}H_{30}O_{12}S_1$	494.145797
$C_{13}H_{19}O_7N_1$	301.116152	$C_{17}H_{26}O_7S_1$	374.139924	$C_{26}H_{40}O_9$	496.267233
$C_{12}H_{14}O_9$	302.063782	$C_{17}H_{26}O_9$	374.157682	$C_{25}H_{38}O_{10}$	498.246497
$C_{13}H_{18}O_6S_1$	302.082409	$C_{18}H_{30}O_8$	374.194068	$C_{24}H_{36}O_{11}$	500.225762
$C_{13}H_{18}O_8$	302.100168	$C_{15}H_{21}O_8N_1S_1$	375.098787	$C_{23}H_{34}O_{10}S_1$	502.187268
$C_{14}H_{22}O_7$	302.136553	$C_{15}H_{21}O_{10}N_1$	375.116546	$C_{24}H_{38}O_{11}$	502.241412
$C_{15}H_{26}O_6$	302.172939	$C_{16}H_{25}O_9N_1$	375.152931	$C_{23}H_{36}O_{12}$	504.220677
$C_{15}H_{12}O_7$	304.058303	$C_{14}H_{16}O_{10}S_1$	376.046417	$C_{22}H_{34}O_{13}$	506.199941
$C_{12}H_{16}O_7S_1$	304.061674	$C_{15}H_{20}O_9S_1$	376.082803	$C_{19}H_{26}O_{14}S_1$	510.104326
$C_{12}H_{16}O_9$	304.079432	$C_{15}H_{20}O_{11}$	376.100562	$C_{26}H_{40}O_{10}$	512.262148
$C_{13}H_{20}O_6S_1$	304.098059	$C_{16}H_{24}O_8S_1$	376.119188	$C_{25}H_{38}O_{11}$	514.241412
$C_{13}H_{20}O_8$	304.115818	$C_{16}H_{24}O_{10}$	376.136947	$C_{24}H_{36}O_{12}$	516.220677

Table A1. Continued.

Elemental Formula	M	Elemental Formula	M	Elemental Formula	M
C_{14} H_{24} O_7	304.152203	C_{17} H_{28} O_9	376.173333	C_{23} H_{34} O_{11} S_1	518.182183
C_{15} H_{14} O_7	306.073953	C_{15} H_{23} O_8 N_1 S_1	377.114437	C_{22} H_{32} O_{12} S_1	520.161447
C_{12} H_{18} O_7 S_1	306.077324	C_{14} H_{18} O_{10} S_1	378.062068	C_{26} H_{40} O_{11}	528.257062
C_{12} H_{18} O_9	306.095082	C_{15} H_{22} O_9 S_1	378.098453	C_{25} H_{38} O_{12}	530.236327
C_{13} H_{22} O_6 S_1	306.113709	C_{15} H_{22} O_{11}	378.116212	C_{24} H_{36} O_{13}	532.215591
C_{13} H_{22} O_8	306.131468	C_{16} H_{26} O_8 S_1	378.134839	C_{27} H_{42} O_{11}	542.272712
C_{18} H_{26} O_4	306.183109	C_{16} H_{26} O_{10}	378.152597	C_{26} H_{40} O_{12}	544.251977
C_{14} H_{13} O_7 N_1	307.069202	C_{14} H_{20} O_{10} S_1	380.077718	C_{25} H_{38} O_{13}	546.231241
C_{14} H_{12} O_8	308.053217	C_{15} H_{24} O_9 S_1	380.114103	C_{24} H_{36} O_{14}	548.210506
C_{11} H_{16} O_8 S_1	308.056588	C_{21} H_{32} O_6	380.219889	C_{26} H_{40} O_{13}	560.246891
C_{12} H_{20} O_7 S_1	308.092974	C_{14} H_{22} O_{10} S_1	382.093368	C_{25} H_{36} O_{13} S_1	576.187662
C_{14} H_{16} O_6 N_2	308.100836	C_{18} H_{24} O_7 S_1	384.124274	C_{46} H_{24}	576.187801
C_{17} H_{24} O_5	308.162374	C_{20} H_{32} O_7	384.214803	C_{24} H_{34} O_{14} S_1	578.166927

Table A2. NEG molecular formulas: complete list of mass peaks and assigned molecular formulas that showed a highly significant negative correlation ($p < 0.01$) with SPE-DOM $\Delta^{14}C$.

Elemental Formula	M	Elemental Formula	M	Elemental Formula	M
C_{17} H_{16} O_6	316.094688	C_{22} H_{23} O_9 N_1	445.137281	C_{23} H_{25} O_{12} N_1	507.137675
C_{18} H_{20} O_5	316.131074	C_{21} H_{18} O_{11}	446.084911	C_{24} H_{29} O_{11} N_1	507.174061
C_{17} H_{18} O_6	318.110338	C_{22} H_{22} O_{10}	446.121297	C_{23} H_{24} O_{13}	508.121691
C_{17} H_{20} O_6	320.125988	C_{21} H_{22} O_9 N_2	446.13253	C_{22} H_{24} O_{12} N_2	508.132924
C_{18} H_{18} O_6	330.110338	C_{23} H_{26} O_9	446.157682	C_{24} H_{28} O_{12}	508.158076
C_{19} H_{22} O_5	330.146724	C_{24} H_{30} O_8	446.194068	C_{25} H_{32} O_{11}	508.194462
C_{17} H_{16} O_7	332.089603	C_{21} H_{21} O_{10} N_1	447.116546	C_{26} H_{36} O_{10}	508.230847
C_{18} H_{20} O_6	332.125988	C_{22} H_{25} O_9 N_1	447.152931	C_{22} H_{23} O_{13} N_1	509.11694
C_{17} H_{18} O_7	334.105253	C_{21} H_{20} O_{11}	448.100562	C_{23} H_{27} O_{12} N_1	509.153325
C_{18} H_{22} O_6	334.141638	C_{20} H_{20} O_{10} N_2	448.111795	C_{24} H_{31} O_{11} N_1	509.189711
C_{17} H_{20} O_7	336.120903	C_{22} H_{24} O_{10}	448.136947	C_{22} H_{22} O_{14}	510.100955
C_{17} H_{24} O_5 N_2	336.168522	C_{21} H_{24} O_9 N_2	448.14818	C_{23} H_{26} O_{13}	510.137341
C_{19} H_{20} O_6	344.125988	C_{23} H_{28} O_9	448.173333	C_{22} H_{26} O_{12} N_2	510.148574
C_{20} H_{24} O_5	344.162374	C_{20} H_{19} O_{11} N_1	449.09581	C_{24} H_{30} O_{12}	510.173726
C_{18} H_{18} O_7	346.105253	C_{21} H_{23} O_{10} N_1	449.132196	C_{23} H_{30} O_{11} N_2	510.18496
C_{19} H_{22} O_6	346.141638	C_{22} H_{27} O_9 N_1	449.168582	C_{25} H_{34} O_{11}	510.210112
C_{18} H_{21} O_6 N_1	347.136887	C_{20} H_{18} O_{12}	450.079826	C_{22} H_{25} O_{13} N_1	511.13259
C_{17} H_{16} O_8	348.084518	C_{19} H_{18} O_{11} N_2	450.091059	C_{23} H_{29} O_{12} N_1	511.168975
C_{18} H_{20} O_7	348.120903	C_{21} H_{22} O_{11}	450.116212	C_{22} H_{24} O_{14}	512.116605
C_{17} H_{19} O_7 N_1	349.116152	C_{20} H_{22} O_{10} N_2	450.127445	C_{21} H_{24} O_{13} N_2	512.127839
C_{18} H_{23} O_6 N_1	349.152538	C_{22} H_{26} O_{10}	450.152597	C_{23} H_{28} O_{13}	512.152991
C_{17} H_{18} O_8	350.100168	C_{21} H_{26} O_9 N_2	450.16383	C_{22} H_{28} O_{12} N_2	512.164224
C_{18} H_{22} O_7	350.136553	C_{23} H_{30} O_9	450.188983	C_{24} H_{32} O_{12}	512.189377
C_{17} H_{20} O_8	352.115818	C_{20} H_{21} O_{11} N_1	451.111461	C_{22} H_{27} O_{13} N_1	513.14824
C_{16} H_{18} O_9	354.095082	C_{21} H_{25} O_{10} N_1	451.147846	C_{22} H_{26} O_{14}	514.132256
C_{17} H_{22} O_8	354.131468	C_{22} H_{29} O_9 N_1	451.184232	C_{23} H_{30} O_{13}	514.168641
C_{19} H_{18} O_7	358.105253	C_{20} H_{20} O_{12}	452.095476	C_{24} H_{34} O_{12}	514.205027
C_{20} H_{22} O_6	358.141638	C_{19} H_{20} O_{11} N_2	452.10671	C_{25} H_{24} O_{12}	516.126776
C_{18} H_{16} O_8	360.084518	C_{21} H_{24} O_{11}	452.131862	C_{22} H_{28} O_{14}	516.147906
C_{19} H_{20} O_7	360.120903	C_{20} H_{24} O_{10} N_2	452.143095	C_{26} H_{28} O_{11}	516.163162
C_{20} H_{24} O_6	360.157289	C_{22} H_{28} O_{10}	452.168247	C_{27} H_{32} O_{10}	516.199547
C_{18} H_{19} O_7 N_1	361.116152	C_{23} H_{32} O_9	452.204633	C_{28} H_{36} O_9	516.235933
C_{19} H_{23} O_6 N_1	361.152538	C_{20} H_{23} O_{11} N_1	453.127111	C_{24} H_{22} O_{13}	518.106041
C_{18} H_{18} O_8	362.100168	C_{21} H_{27} O_{10} N_1	453.163496	C_{25} H_{26} O_{12}	518.142426

Table A2. Continued.

Elemental Formula	M	Elemental Formula	M	Elemental Formula	M
$C_{19}H_{22}O_7$	362.136553	$C_{20}H_{22}O_{12}$	454.111126	$C_{24}H_{26}O_{11}N_2$	518.15366
$C_{18}H_{21}O_7N_1$	363.131802	$C_{19}H_{22}O_{11}N_2$	454.12236	$C_{26}H_{30}O_{11}$	518.178812
$C_{17}H_{16}O_9$	364.079432	$C_{21}H_{26}O_{11}$	454.147512	$C_{27}H_{34}O_{10}$	518.215197
$C_{18}H_{20}O_8$	364.115818	$C_{20}H_{26}O_{10}N_2$	454.158745	$C_{24}H_{25}O_{12}N_1$	519.137675
$C_{19}H_{24}O_7$	364.152203	$C_{22}H_{30}O_{10}$	454.183897	$C_{25}H_{29}O_{11}N_1$	519.174061
$C_{17}H_{19}O_8N_1$	365.111067	$C_{19}H_{21}O_{12}N_1$	455.106375	$C_{24}H_{24}O_{13}$	520.121691
$C_{18}H_{23}O_7N_1$	365.147452	$C_{20}H_{25}O_{11}N_1$	455.142761	$C_{23}H_{24}O_{12}N_2$	520.132924
$C_{17}H_{18}O_9$	366.095082	$C_{20}H_{24}O_{12}$	456.126776	$C_{25}H_{28}O_{12}$	520.158076
$C_{18}H_{22}O_8$	366.131468	$C_{21}H_{28}O_{11}$	456.163162	$C_{24}H_{28}O_{11}N_2$	520.16931
$C_{17}H_{21}O_8N_1$	367.126717	$C_{20}H_{27}O_{11}N_1$	457.158411	$C_{26}H_{32}O_{11}$	520.194462
$C_{17}H_{20}O_9$	368.110732	$C_{19}H_{22}O_{13}$	458.106041	$C_{27}H_{36}O_{10}$	520.230847
$C_{17}H_{22}O_9$	370.126382	$C_{23}H_{22}O_{10}$	458.121297	$C_{24}H_{27}O_{12}N_1$	521.153325
$C_{14}H_{16}O_8N_2S_1$	372.062736	$C_{20}H_{26}O_{12}$	458.142426	$C_{25}H_{31}O_{11}N_1$	521.189711
$C_{20}H_{20}O_7$	372.120903	$C_{24}H_{26}O_9$	458.157682	$C_{23}H_{22}O_{14}$	522.100955
$C_{19}H_{18}O_8$	374.100168	$C_{25}H_{30}O_8$	458.194068	$C_{24}H_{26}O_{13}$	522.137341
$C_{20}H_{22}O_7$	374.136553	$C_{22}H_{20}O_{11}$	460.100562	$C_{23}H_{26}O_{12}N_2$	522.148574
$C_{19}H_{21}O_7N_1$	375.131802	$C_{19}H_{24}O_{13}$	460.121691	$C_{25}H_{30}O_{12}$	522.173726
$C_{18}H_{16}O_9$	376.079432	$C_{23}H_{24}O_{10}$	460.136947	$C_{24}H_{30}O_{11}N_2$	522.18496
$C_{19}H_{20}O_8$	376.115818	$C_{24}H_{28}O_9$	460.173333	$C_{26}H_{34}O_{11}$	522.210112
$C_{20}H_{24}O_7$	376.152203	$C_{22}H_{23}O_{10}N_1$	461.132196	$C_{23}H_{25}O_{13}N_1$	523.13259
$C_{18}H_{19}O_8N_1$	377.111067	$C_{23}H_{27}O_9N_1$	461.168582	$C_{24}H_{29}O_{12}N_1$	523.168975
$C_{19}H_{23}O_7N_1$	377.147452	$C_{21}H_{18}O_{12}$	462.079826	$C_{23}H_{24}O_{14}$	524.116605
$C_{18}H_{18}O_9$	378.095082	$C_{22}H_{22}O_{11}$	462.116212	$C_{24}H_{28}O_{13}$	524.152991
$C_{19}H_{22}O_8$	378.131468	$C_{21}H_{22}O_{10}N_2$	462.127445	$C_{23}H_{28}O_{12}N_2$	524.164224
$C_{17}H_{17}O_9N_1$	379.090331	$C_{23}H_{26}O_{10}$	462.152597	$C_{25}H_{32}O_{12}$	524.189377
$C_{18}H_{21}O_8N_1$	379.126717	$C_{22}H_{26}O_9N_2$	462.16383	$C_{26}H_{36}O_{11}$	524.225762
$C_{17}H_{16}O_{10}$	380.074347	$C_{24}H_{30}O_9$	462.188983	$C_{22}H_{23}O_{14}N_1$	525.111854
$C_{18}H_{20}O_9$	380.110732	$C_{21}H_{21}O_{11}N_1$	463.111461	$C_{23}H_{27}O_{13}N_1$	525.14824
$C_{17}H_{20}O_8N_2$	380.121966	$C_{22}H_{25}O_{10}N_1$	463.147846	$C_{24}H_{31}O_{12}N_1$	525.184625
$C_{17}H_{19}O_9N_1$	381.105981	$C_{23}H_{29}O_9N_1$	463.184232	$C_{23}H_{26}O_{14}$	526.132256
$C_{17}H_{18}O_{10}$	382.089997	$C_{21}H_{20}O_{12}$	464.095476	$C_{22}H_{26}O_{13}N_2$	526.143489
$C_{18}H_{22}O_9$	382.126382	$C_{20}H_{20}O_{11}N_2$	464.10671	$C_{24}H_{30}O_{13}$	526.168641
$C_{17}H_{21}O_9N_1$	383.121631	$C_{22}H_{24}O_{11}$	464.131862	$C_{25}H_{34}O_{12}$	526.205027
$C_{17}H_{20}O_{10}$	384.105647	$C_{21}H_{24}O_{10}N_2$	464.143095	$C_{22}H_{25}O_{14}N_1$	527.127505
$C_{20}H_{18}O_8$	386.100168	$C_{23}H_{28}O_{10}$	464.168247	$C_{22}H_{24}O_{15}$	528.11152
$C_{21}H_{22}O_7$	386.136553	$C_{22}H_{28}O_9N_2$	464.179481	$C_{23}H_{28}O_{14}$	528.147906
$C_{20}H_{20}O_8$	388.115818	$C_{24}H_{32}O_9$	464.204633	$C_{24}H_{32}O_{13}$	528.184291
$C_{21}H_{24}O_7$	388.152203	$C_{21}H_{23}O_{11}N_1$	465.127111	$C_{26}H_{26}O_{12}$	530.142426
$C_{19}H_{19}O_8N_1$	389.111067	$C_{22}H_{27}O_{10}N_1$	465.163496	$C_{23}H_{30}O_{14}$	530.163556
$C_{20}H_{23}O_7N_1$	389.147452	$C_{21}H_{22}O_{12}$	466.111126	$C_{27}H_{30}O_{11}$	530.178812
$C_{19}H_{18}O_9$	390.095082	$C_{20}H_{22}O_{11}N_2$	466.12236	$C_{28}H_{34}O_{10}$	530.215197
$C_{20}H_{22}O_8$	390.131468	$C_{22}H_{26}O_{11}$	466.147512	$C_{25}H_{24}O_{13}$	532.121691
$C_{19}H_{21}O_8N_1$	391.126717	$C_{21}H_{26}O_{10}N_2$	466.158745	$C_{26}H_{28}O_{12}$	532.158076
$C_{19}H_{20}O_9$	392.110732	$C_{23}H_{30}O_{10}$	466.183897	$C_{27}H_{32}O_{11}$	532.194462
$C_{18}H_{20}O_8N_2$	392.121966	$C_{20}H_{21}O_{12}N_1$	467.106375	$C_{28}H_{36}O_{10}$	532.230847
$C_{20}H_{24}O_8$	392.147118	$C_{21}H_{25}O_{11}N_1$	467.142761	$C_{25}H_{27}O_{12}N_1$	533.153325
$C_{19}H_{24}O_7N_2$	392.158351	$C_{22}H_{29}O_{10}N_1$	467.179146	$C_{26}H_{31}O_{11}N_1$	533.189711
$C_{18}H_{19}O_9N_1$	393.105981	$C_{20}H_{20}O_{13}$	468.090391	$C_{24}H_{22}O_{14}$	534.100955
$C_{19}H_{23}O_8N_1$	393.142367	$C_{21}H_{24}O_{12}$	468.126776	$C_{25}H_{26}O_{13}$	534.137341
$C_{20}H_{27}O_7N_1$	393.178752	$C_{20}H_{24}O_{11}N_2$	468.13801	$C_{26}H_{30}O_{12}$	534.173726
$C_{18}H_{18}O_{10}$	394.089997	$C_{22}H_{28}O_{11}$	468.163162	$C_{25}H_{30}O_{11}N_2$	534.18496
$C_{19}H_{22}O_9$	394.126382	$C_{21}H_{28}O_{10}N_2$	468.174395	$C_{27}H_{34}O_{11}$	534.210112
$C_{18}H_{22}O_8N_2$	394.137616	$C_{23}H_{32}O_{10}$	468.199547	$C_{28}H_{38}O_{10}$	534.246497
$C_{18}H_{21}O_9N_1$	395.121631	$C_{20}H_{23}O_{12}N_1$	469.122025	$C_{25}H_{29}O_{12}N_1$	535.168975

Table A2. Continued.

Elemental Formula	M	Elemental Formula	M	Elemental Formula	M
$C_{18}H_{20}O_{10}$	396.105647	$C_{21}H_{27}O_{11}N_1$	469.158411	$C_{26}H_{33}O_{11}N_1$	535.205361
$C_{17}H_{20}O_9N_2$	396.11688	$C_{20}H_{22}O_{13}$	470.106041	$C_{23}H_{20}O_{15}$	536.08022
$C_{19}H_{24}O_9$	396.142032	$C_{21}H_{26}O_{12}$	470.142426	$C_{24}H_{24}O_{14}$	536.116605
$C_{17}H_{19}O_{10}N_1$	397.100896	$C_{20}H_{26}O_{11}N_2$	470.15366	$C_{23}H_{24}O_{13}N_2$	536.127839
$C_{18}H_{23}O_9N_1$	397.137281	$C_{22}H_{30}O_{11}$	470.178812	$C_{25}H_{28}O_{13}$	536.152991
$C_{17}H_{18}O_{11}$	398.084911	$C_{20}H_{25}O_{12}N_1$	471.137675	$C_{24}H_{28}O_{12}N_2$	536.164224
$C_{18}H_{22}O_{10}$	398.121297	$C_{20}H_{24}O_{13}$	472.121691	$C_{26}H_{32}O_{12}$	536.189377
$C_{17}H_{20}O_{11}$	400.100562	$C_{24}H_{24}O_{10}$	472.136947	$C_{27}H_{36}O_{11}$	536.225762
$C_{21}H_{20}O_8$	400.115818	$C_{21}H_{28}O_{12}$	472.158076	$C_{24}H_{27}O_{13}N_1$	537.14824
$C_{18}H_{24}O_{10}$	400.136947	$C_{25}H_{28}O_9$	472.173333	$C_{25}H_{31}O_{12}N_1$	537.184625
$C_{22}H_{24}O_7$	400.152203	$C_{26}H_{32}O_8$	472.209718	$C_{23}H_{22}O_{15}$	538.09587
$C_{20}H_{18}O_9$	402.095082	$C_{23}H_{22}O_{11}$	474.116212	$C_{24}H_{26}O_{14}$	538.132256
$C_{21}H_{22}O_8$	402.131468	$C_{24}H_{26}O_{10}$	474.152597	$C_{23}H_{26}O_{13}N_2$	538.143489
$C_{22}H_{26}O_7$	402.167853	$C_{25}H_{30}O_9$	474.188983	$C_{25}H_{30}O_{13}$	538.168641
$C_{20}H_{21}O_8N_1$	403.126717	$C_{23}H_{25}O_{10}N_1$	475.147846	$C_{24}H_{30}O_{12}N_2$	538.179874
$C_{20}H_{20}O_9$	404.110732	$C_{22}H_{20}O_{12}$	476.095476	$C_{26}H_{34}O_{12}$	538.205027
$C_{19}H_{20}O_8N_2$	404.121966	$C_{21}H_{20}O_{11}N_2$	476.10671	$C_{27}H_{38}O_{11}$	538.241412
$C_{21}H_{24}O_8$	404.147118	$C_{23}H_{24}O_{11}$	476.131862	$C_{23}H_{25}O_{14}N_1$	539.127505
$C_{20}H_{24}O_7N_2$	404.158351	$C_{22}H_{24}O_{10}N_2$	476.143095	$C_{24}H_{29}O_{13}N_1$	539.16389
$C_{19}H_{19}O_9N_1$	405.105981	$C_{24}H_{28}O_{10}$	476.168247	$C_{25}H_{33}O_{12}N_1$	539.200276
$C_{20}H_{23}O_8N_1$	405.142367	$C_{23}H_{28}O_9N_2$	476.179481	$C_{23}H_{24}O_{15}$	540.11152
$C_{19}H_{18}O_{10}$	406.089997	$C_{25}H_{32}O_9$	476.204633	$C_{24}H_{28}O_{14}$	540.147906
$C_{18}H_{18}O_9N_2$	406.10123	$C_{22}H_{23}O_{11}N_1$	477.127111	$C_{25}H_{32}O_{13}$	540.184291
$C_{20}H_{22}O_9$	406.126382	$C_{23}H_{27}O_{10}N_1$	477.163496	$C_{26}H_{36}O_{12}$	540.220677
$C_{19}H_{22}O_8N_2$	406.137616	$C_{24}H_{31}O_9N_1$	477.199882	$C_{23}H_{27}O_{14}N_1$	541.143155
$C_{21}H_{26}O_8$	406.162768	$C_{21}H_{18}O_{13}$	478.074741	$C_{24}H_{30}O_{14}$	542.163556
$C_{18}H_{17}O_{10}N_1$	407.085246	$C_{22}H_{22}O_{12}$	478.111126	$C_{25}H_{34}O_{13}$	542.199941
$C_{19}H_{21}O_9N_1$	407.121631	$C_{21}H_{22}O_{11}N_2$	478.12236	$C_{23}H_{28}O_{15}$	544.14282
$C_{20}H_{25}O_8N_1$	407.158017	$C_{23}H_{26}O_{11}$	478.147512	$C_{27}H_{28}O_{12}$	544.158076
$C_{19}H_{20}O_{10}$	408.105647	$C_{22}H_{26}O_{10}N_2$	478.158745	$C_{24}H_{32}O_{14}$	544.179206
$C_{18}H_{20}O_9N_2$	408.11688	$C_{24}H_{30}O_{10}$	478.183897	$C_{28}H_{32}O_{11}$	544.194462
$C_{20}H_{24}O_9$	408.142032	$C_{23}H_{30}O_9N_2$	478.195131	$C_{26}H_{26}O_{13}$	546.137341
$C_{19}H_{24}O_8N_2$	408.153266	$C_{21}H_{21}O_{12}N_1$	479.106375	$C_{27}H_{30}O_{12}$	546.173726
$C_{18}H_{19}O_{10}N_1$	409.100896	$C_{22}H_{25}O_{11}N_1$	479.142761	$C_{28}H_{34}O_{11}$	546.210112
$C_{19}H_{23}O_9N_1$	409.137281	$C_{23}H_{29}O_{10}N_1$	479.179146	$C_{29}H_{38}O_{10}$	546.246497
$C_{18}H_{18}O_{11}$	410.084911	$C_{21}H_{20}O_{13}$	480.090391	$C_{25}H_{24}O_{14}$	548.116605
$C_{19}H_{22}O_{10}$	410.121297	$C_{20}H_{20}O_{12}N_2$	480.101624	$C_{26}H_{28}O_{13}$	548.152991
$C_{18}H_{22}O_9N_2$	410.13253	$C_{22}H_{24}O_{12}$	480.126776	$C_{25}H_{28}O_{12}N_2$	548.164224
$C_{20}H_{26}O_9$	410.157682	$C_{21}H_{24}O_{11}N_2$	480.13801	$C_{27}H_{32}O_{12}$	548.189377
$C_{18}H_{21}O_{10}N_1$	411.116546	$C_{23}H_{28}O_{11}$	480.163162	$C_{28}H_{36}O_{11}$	548.225762
$C_{19}H_{25}O_9N_1$	411.152931	$C_{22}H_{28}O_{10}N_2$	480.174395	$C_{29}H_{40}O_{10}$	548.262148
$C_{18}H_{20}O_{11}$	412.100562	$C_{24}H_{32}O_{10}$	480.199547	$C_{25}H_{27}O_{13}N_1$	549.14824
$C_{19}H_{24}O_{10}$	412.136947	$C_{21}H_{23}O_{12}N_1$	481.122025	$C_{26}H_{31}O_{12}N_1$	549.184625
$C_{18}H_{23}O_{10}N_1$	413.132196	$C_{22}H_{27}O_{11}N_1$	481.158411	$C_{24}H_{22}O_{15}$	550.09587
$C_{18}H_{22}O_{11}$	414.116212	$C_{23}H_{31}O_{10}N_1$	481.194796	$C_{25}H_{26}O_{14}$	550.132256
$C_{22}H_{22}O_8$	414.131468	$C_{21}H_{22}O_{13}$	482.106041	$C_{26}H_{30}O_{13}$	550.168641
$C_{19}H_{26}O_{10}$	414.152597	$C_{22}H_{26}O_{12}$	482.142426	$C_{25}H_{30}O_{12}N_2$	550.179874
$C_{23}H_{26}O_7$	414.167853	$C_{21}H_{26}O_{11}N_2$	482.15366	$C_{27}H_{34}O_{12}$	550.205027
$C_{21}H_{20}O_9$	416.110732	$C_{23}H_{30}O_{11}$	482.178812	$C_{28}H_{38}O_{11}$	550.241412
$C_{18}H_{24}O_{11}$	416.131862	$C_{24}H_{34}O_{10}$	482.215197	$C_{24}H_{25}O_{14}N_1$	551.127505
$C_{22}H_{24}O_8$	416.147118	$C_{20}H_{21}O_{13}N_1$	483.10129	$C_{25}H_{29}O_{13}N_1$	551.16389
$C_{23}H_{28}O_7$	416.183503	$C_{21}H_{25}O_{12}N_1$	483.137675	$C_{26}H_{33}O_{12}N_1$	551.200276
$C_{20}H_{19}O_9N_1$	417.105981	$C_{22}H_{29}O_{11}N_1$	483.174061	$C_{24}H_{24}O_{15}$	552.11152
$C_{21}H_{23}O_8N_1$	417.142367	$C_{21}H_{24}O_{11}S_1$	484.103932	$C_{25}H_{28}O_{14}$	552.147906
$C_{20}H_{18}O_{10}$	418.089997	$C_{21}H_{24}O_{13}$	484.121691	$C_{26}H_{32}O_{13}$	552.184291

Table A2. Continued.

Elemental Formula	M	Elemental Formula	M	Elemental Formula	M
$C_{19}H_{18}O_9N_2$	418.10123	$C_{22}H_{28}O_{12}$	484.158076	$C_{27}H_{36}O_{12}$	552.220677
$C_{21}H_{22}O_9$	418.126382	$C_{23}H_{32}O_{11}$	484.194462	$C_{25}H_{31}O_{13}N_1$	553.17954
$C_{22}H_{26}O_8$	418.162768	$C_{21}H_{27}O_{12}N_1$	485.153325	$C_{24}H_{26}O_{15}$	554.12717
$C_{19}H_{17}O_{10}N_1$	419.085246	$C_{21}H_{26}O_{13}$	486.137341	$C_{25}H_{30}O_{14}$	554.163556
$C_{20}H_{21}O_9N_1$	419.121631	$C_{25}H_{26}O_{10}$	486.152597	$C_{24}H_{30}O_{13}N_2$	554.174789
$C_{21}H_{25}O_8N_1$	419.158017	$C_{22}H_{30}O_{12}$	486.173726	$C_{26}H_{34}O_{13}$	554.199941
$C_{20}H_{20}O_{10}$	420.105647	$C_{26}H_{30}O_9$	486.188983	$C_{25}H_{32}O_{14}$	556.179206
$C_{19}H_{20}O_9N_2$	420.11688	$C_{20}H_{25}O_{13}N_1$	487.13259	$C_{26}H_{36}O_{13}$	556.215591
$C_{21}H_{24}O_9$	420.142032	$C_{23}H_{20}O_{12}$	488.095476	$C_{24}H_{30}O_{15}$	558.15847
$C_{20}H_{24}O_8N_2$	420.153266	$C_{20}H_{24}O_{14}$	488.116605	$C_{25}H_{34}O_{14}$	558.194856
$C_{20}H_{23}O_9N_1$	421.137281	$C_{24}H_{24}O_{11}$	488.131862	$C_{29}H_{34}O_{11}$	558.210112
$C_{21}H_{27}O_8N_1$	421.173667	$C_{21}H_{28}O_{13}$	488.152991	$C_{27}H_{28}O_{13}$	560.152991
$C_{19}H_{18}O_{11}$	422.084911	$C_{25}H_{28}O_{10}$	488.168247	$C_{28}H_{32}O_{12}$	560.189377
$C_{18}H_{18}O_{10}N_2$	422.096145	$C_{26}H_{32}O_9$	488.204633	$C_{29}H_{36}O_{11}$	560.225762
$C_{20}H_{22}O_{10}$	422.121297	$C_{23}H_{23}O_{11}N_1$	489.127111	$C_{26}H_{26}O_{14}$	562.132256
$C_{19}H_{22}O_9N_2$	422.13253	$C_{24}H_{27}O_{10}N_1$	489.163496	$C_{27}H_{30}O_{13}$	562.168641
$C_{21}H_{26}O_9$	422.157682	$C_{23}H_{22}O_{12}$	490.111126	$C_{28}H_{34}O_{12}$	562.205027
$C_{20}H_{26}O_8N_2$	422.168916	$C_{22}H_{22}O_{11}N_2$	490.12236	$C_{29}H_{38}O_{11}$	562.241412
$C_{19}H_{21}O_{10}N_1$	423.116546	$C_{24}H_{26}O_{11}$	490.147512	$C_{26}H_{29}O_{13}N_1$	563.16389
$C_{20}H_{25}O_9N_1$	423.152931	$C_{23}H_{26}O_{10}N_2$	490.158745	$C_{25}H_{24}O_{15}$	564.11152
$C_{19}H_{20}O_{11}$	424.100562	$C_{25}H_{30}O_{10}$	490.183897	$C_{26}H_{28}O_{14}$	564.147906
$C_{18}H_{20}O_{10}N_2$	424.111795	$C_{26}H_{34}O_9$	490.220283	$C_{25}H_{28}O_{13}N_2$	564.159139
$C_{20}H_{24}O_{10}$	424.136947	$C_{22}H_{21}O_{12}N_1$	491.106375	$C_{27}H_{32}O_{13}$	564.184291
$C_{19}H_{24}O_9N_2$	424.14818	$C_{23}H_{25}O_{11}N_1$	491.142761	$C_{28}H_{36}O_{12}$	564.220677
$C_{19}H_{23}O_{10}N_1$	425.132196	$C_{24}H_{29}O_{10}N_1$	491.179146	$C_{29}H_{40}O_{11}$	564.257062
$C_{20}H_{27}O_9N_1$	425.168582	$C_{22}H_{20}O_{13}$	492.090391	$C_{25}H_{27}O_{14}N_1$	565.143155
$C_{18}H_{18}O_{12}$	426.079826	$C_{21}H_{20}O_{12}N_2$	492.101624	$C_{26}H_{31}O_{13}N_1$	565.17954
$C_{19}H_{22}O_{11}$	426.116212	$C_{23}H_{24}O_{12}$	492.126776	$C_{25}H_{26}O_{15}$	566.12717
$C_{18}H_{22}O_{10}N_2$	426.127445	$C_{22}H_{24}O_{11}N_2$	492.13801	$C_{26}H_{30}O_{14}$	566.163556
$C_{20}H_{26}O_{10}$	426.152597	$C_{24}H_{28}O_{11}$	492.163162	$C_{27}H_{34}O_{13}$	566.199941
$C_{18}H_{21}O_{11}N_1$	427.111461	$C_{23}H_{28}O_{10}N_2$	492.174395	$C_{28}H_{38}O_{12}$	566.236327
$C_{19}H_{25}O_{10}N_1$	427.147846	$C_{25}H_{32}O_{10}$	492.199547	$C_{24}H_{25}O_{15}N_1$	567.122419
$C_{18}H_{20}O_{12}$	428.095476	$C_{22}H_{23}O_{12}N_1$	493.122025	$C_{26}H_{33}O_{13}N_1$	567.19519
$C_{19}H_{24}O_{11}$	428.131862	$C_{23}H_{27}O_{11}N_1$	493.158411	$C_{25}H_{28}O_{15}$	568.14282
$C_{20}H_{28}O_{10}$	428.168247	$C_{24}H_{31}O_{10}N_1$	493.194796	$C_{26}H_{32}O_{14}$	568.179206
$C_{21}H_{18}O_{10}$	430.089997	$C_{22}H_{22}O_{13}$	494.106041	$C_{27}H_{36}O_{13}$	568.215591
$C_{22}H_{22}O_9$	430.126382	$C_{21}H_{22}O_{12}N_2$	494.117274	$C_{25}H_{31}O_{14}N_1$	569.174455
$C_{19}H_{26}O_{11}$	430.147512	$C_{23}H_{26}O_{12}$	494.142426	$C_{25}H_{30}O_{15}$	570.15847
$C_{23}H_{26}O_8$	430.162768	$C_{22}H_{26}O_{11}N_2$	494.15366	$C_{26}H_{34}O_{14}$	570.194856
$C_{21}H_{21}O_9N_1$	431.121631	$C_{24}H_{30}O_{11}$	494.178812	$C_{28}H_{30}O_{13}$	574.168641
$C_{21}H_{20}O_{10}$	432.105647	$C_{23}H_{30}O_{10}N_2$	494.190045	$C_{29}H_{34}O_{12}$	574.205027
$C_{20}H_{20}O_9N_2$	432.11688	$C_{25}H_{34}O_{10}$	494.215197	$C_{30}H_{38}O_{11}$	574.241412
$C_{22}H_{24}O_9$	432.142032	$C_{21}H_{21}O_{13}N_1$	495.10129	$C_{27}H_{28}O_{14}$	576.147906
$C_{21}H_{24}O_8N_2$	432.153266	$C_{22}H_{25}O_{12}N_1$	495.137675	$C_{28}H_{32}O_{13}$	576.184291
$C_{23}H_{28}O_8$	432.178418	$C_{23}H_{29}O_{11}N_1$	495.174061	$C_{29}H_{36}O_{12}$	576.220677
$C_{20}H_{19}O_{10}N_1$	433.100896	$C_{22}H_{24}O_{13}$	496.121691	$C_{30}H_{40}O_{11}$	576.257062
$C_{21}H_{23}O_9N_1$	433.137281	$C_{21}H_{24}O_{12}N_2$	496.132924	$C_{26}H_{26}O_{15}$	578.12717
$C_{22}H_{27}O_8N_1$	433.173667	$C_{23}H_{28}O_{12}$	496.158076	$C_{27}H_{30}O_{14}$	578.163556
$C_{20}H_{18}O_{11}$	434.084911	$C_{22}H_{28}O_{11}N_2$	496.16931	$C_{28}H_{34}O_{13}$	578.199941
$C_{19}H_{18}O_{10}N_2$	434.096145	$C_{24}H_{32}O_{11}$	496.194462	$C_{29}H_{38}O_{12}$	578.236327
$C_{21}H_{22}O_{10}$	434.121297	$C_{21}H_{23}O_{13}N_1$	497.11694	$C_{26}H_{29}O_{14}N_1$	579.158805
$C_{20}H_{22}O_9N_2$	434.13253	$C_{22}H_{27}O_{12}N_1$	497.153325	$C_{26}H_{28}O_{15}$	580.14282
$C_{22}H_{26}O_9$	434.157682	$C_{21}H_{22}O_{14}$	498.100955	$C_{27}H_{32}O_{14}$	580.179206
$C_{21}H_{26}O_8N_2$	434.168916	$C_{22}H_{26}O_{13}$	498.137341	$C_{28}H_{36}O_{13}$	580.215591
$C_{19}H_{17}O_{11}N_1$	435.08016	$C_{21}H_{26}O_{12}N_2$	498.148574	$C_{29}H_{40}O_{12}$	580.251977
$C_{20}H_{21}O_{10}N_1$	435.116546	$C_{23}H_{30}O_{12}$	498.173726	$C_{25}H_{27}O_{15}N_1$	581.138069

Table A2. Continued.

Elemental Formula	M	Elemental Formula	M	Elemental Formula	M
$C_{21}H_{25}O_9N_1$	435.152931	$C_{24}H_{34}O_{11}$	498.210112	$C_{26}H_{31}O_{14}N_1$	581.174455
$C_{20}H_{20}O_{11}$	436.100562	$C_{21}H_{25}O_{13}N_1$	499.13259	$C_{25}H_{26}O_{16}$	582.122085
$C_{19}H_{20}O_{10}N_2$	436.111795	$C_{22}H_{29}O_{12}N_1$	499.168975	$C_{26}H_{30}O_{15}$	582.15847
$C_{21}H_{24}O_{10}$	436.136947	$C_{21}H_{24}O_{14}$	500.116605	$C_{25}H_{30}O_{14}N_2$	582.169704
$C_{20}H_{24}O_9N_2$	436.14818	$C_{22}H_{28}O_{13}$	500.152991	$C_{27}H_{34}O_{14}$	582.194856
$C_{22}H_{28}O_9$	436.173333	$C_{26}H_{28}O_{10}$	500.168247	$C_{28}H_{38}O_{13}$	582.231241
$C_{19}H_{19}O_{11}N_1$	437.09581	$C_{23}H_{32}O_{12}$	500.189377	$C_{26}H_{32}O_{15}$	584.17412
$C_{20}H_{23}O_{10}N_1$	437.132196	$C_{24}H_{22}O_{12}$	502.111126	$C_{27}H_{36}O_{14}$	584.210506
$C_{21}H_{27}O_9N_1$	437.168582	$C_{21}H_{26}O_{14}$	502.132256	$C_{26}H_{34}O_{15}$	586.18977
$C_{19}H_{18}O_{12}$	438.079826	$C_{25}H_{26}O_{11}$	502.147512	$C_{29}H_{32}O_{13}$	588.184291
$C_{20}H_{22}O_{11}$	438.116212	$C_{26}H_{30}O_{10}$	502.183897	$C_{30}H_{36}O_{12}$	588.220677
$C_{19}H_{22}O_{10}N_2$	438.127445	$C_{27}H_{34}O_9$	502.220283	$C_{28}H_{30}O_{14}$	590.163556
$C_{21}H_{26}O_{10}$	438.152597	$C_{23}H_{20}O_{13}$	504.090391	$C_{29}H_{34}O_{13}$	590.199941
$C_{22}H_{30}O_9$	438.188983	$C_{24}H_{24}O_{12}$	504.126776	$C_{30}H_{38}O_{12}$	590.236327
$C_{19}H_{21}O_{11}N_1$	439.111461	$C_{23}H_{24}O_{11}N_2$	504.13801	$C_{27}H_{28}O_{15}$	592.14282
$C_{20}H_{25}O_{10}N_1$	439.147846	$C_{25}H_{28}O_{11}$	504.163162	$C_{28}H_{32}O_{14}$	592.179206
$C_{19}H_{20}O_{12}$	440.095476	$C_{24}H_{28}O_{10}N_2$	504.174395	$C_{29}H_{36}O_{13}$	592.215591
$C_{20}H_{24}O_{11}$	440.131862	$C_{26}H_{32}O_{10}$	504.199547	$C_{30}H_{40}O_{12}$	592.251977
$C_{19}H_{24}O_{10}N_2$	440.143095	$C_{27}H_{36}O_9$	504.235933	$C_{27}H_{30}O_{15}$	594.15847
$C_{21}H_{28}O_{10}$	440.168247	$C_{23}H_{23}O_{12}N_1$	505.122025	$C_{28}H_{34}O_{14}$	594.194856
$C_{19}H_{23}O_{11}N_1$	441.127111	$C_{24}H_{27}O_{11}N_1$	505.158411	$C_{29}H_{38}O_{13}$	594.231241
$C_{20}H_{27}O_{10}N_1$	441.163496	$C_{25}H_{31}O_{10}N_1$	505.194796	$C_{27}H_{33}O_{14}N_1$	595.190105
$C_{19}H_{22}O_{12}$	442.111126	$C_{23}H_{22}O_{13}$	506.106041	$C_{26}H_{28}O_{16}$	596.137735
$C_{20}H_{26}O_{11}$	442.147512	$C_{22}H_{22}O_{12}N_2$	506.117274	$C_{27}H_{32}O_{15}$	596.17412
$C_{22}H_{20}O_{10}$	444.105647	$C_{24}H_{26}O_{12}$	506.142426	$C_{28}H_{36}O_{14}$	596.210506
$C_{19}H_{24}O_{12}$	444.126776	$C_{23}H_{26}O_{11}N_2$	506.15366	$C_{26}H_{30}O_{16}$	598.153385
$C_{23}H_{24}O_9$	444.142032	$C_{25}H_{30}O_{11}$	506.178812	$C_{27}H_{34}O_{15}$	598.18977
$C_{20}H_{28}O_{11}$	444.163162	$C_{24}H_{30}O_{10}N_2$	506.190045		
$C_{24}H_{28}O_8$	444.178418	$C_{26}H_{34}O_{10}$	506.215197		

References

Aluwihare, L. I., Repta, D. J., and Chen, R. F.: A major biopolymeric component to dissolved organic carbon in surface water, Nature, 387, 166–169, 1997.

Amon, R. M. W. and Benner, R.: Bacterial utilization of different size classes of dissolved organic matter, Limnol. Oceanogr., 41, 41–51, 1996.

Bauer, J. E.: Carbon isotopic composition of DOM, in: Biogeochemistry of marine dissolved organic matter, edited by: Hansell, D. A. and Carlson, C. A., Amsterdam, Academic Press, 405–446, 2002.

Bauer, J. E., Williams, P. M., and Druffel, E. R. M.: ^{14}C activity of dissolved organic carbon fractions in north-central Pacific and Sargasso Sea, Nature, 357, 667–670, 1992.

Beaupre, S. R. and Aluwihare, L.: Constraining the 2-component model of marine dissolved organic radiocarbon, Deep-Sea Res. II, 57, 1494–1503, 2010.

Beaupre, S. R. and Druffel, E. R. M.: Constraining the propagation of bomb-radiocarbon through the dissolved organic carbon (DOC) pool in the northeast Pacific Ocean, Deep-Sea Res. I, 56, 1717–1726, 2009.

Benner, R.: Chemical composition and reactivity, in: Biogeochemistry of marine dissolved organic matter, edited by: Hansell, D. A. and Carlson, C. A., Amsterdam, Academic Press, 59–85, 2002.

Benner, R. and Herndl, G. J.: Bacterially derived dissolved organic matter in the microbial carbon pump, in: Microbial Carbon Pump in the Ocean, edited by: Jiao, N., Azam, F., and Sanders, S.,, Science/AAAS, Washington, DC, Science/AAAS, 46–48, 2011.

Benner, R. and Kaiser, K.: Abundance of amino sugars and peptidoglycan in marine particulate and dissolved organic matter, Limnol. Oceanogr., 48, 118–128, 2003.

Bhatia, M. P., Das, S. B., Longnecker, K., Charette, M. A., and Kujawinski, L. E.: Molecular characterization of dissolved organic matter associated with the Greenland ice sheet, Geochim. Cosmochim. Acta, 74, 3768–3784, 2010.

Carlson, C. A. and Ducklow, H. W.: Growth of bacterioplankton and consumption of dissolved organic carbon in the oligotrophic Sargasso Sea, Aquat. Microb. Ecol., 10, 69–85, 1996.

Carlson, C. A., Ducklow, H. W., and Michaels, A. F.: Annual flux of dissolved organic carbon from the euphotic zone in the northwestern Sargasso Sea, Nature, 371, 405–408, 1994.

Carlson, C. A., Hansell, D. A., Nelson, N. B., Siegel, D. A., Smethie, W. M., Khatiwala, S., Meyers, M. M., and Halewood, E.: Dissolved organic carbon export and subsequent remineralization in the mesopelagic and bathypelagic realms of the North Atlantic basin, Deep-Sea Res. II, 57, 1433–1445, 2010.

Davis, J., Kaiser, K., and Benner, R.: Amino acid and amino sugar yields and compositions as indicators of dissolved organic matter diagenesis, Org. Geochem., 40, 343–352, 2009.

Dittmar, T. and Kattner, G.: Recalcitrant dissolved organic matter in the ocean: major contribution of small amphiphilics, Mar. Chem., 82, 115–123, 2003.

Dittmar, T., Koch, B. P., Hertkorn, N., and Kattner, G.: A simple and efficient method for the solid-phase extraction of dissolved organic matter (SPE-DOM) from seawater, Limnol. Oceanogr.-Methods, 6, 230–235, 2008.

Druffel, E. R. M. and Bauer, J. E., Radiocarbon distributions in Southern Ocean dissolved and particulate organic matter, Geophys. Res. Lett., 27, 1495–1498, 2000.

Druffel, E. R. M., Williams, P. M., and Suzuki, Y.: Concentrations and radiocarbon signatures of dissolved organic matter in the Pacific Ocean, Geophys. Res. Lett., 16, 991–994, 1989.

Druffel, E. R. M., Williams, P. M., Bauer, J. E., and Ertel, J. R.: Cycling of dissolved and particulate organic matter in the open ocean, J. Geophys. Res., 97, 15639–15659, 1992.

Flerus, R., Koch, B. P., Schmitt-Kopplin, P., Witt, M., and Kattner, G.: Molecular level investigation of reactions between dissolved organic matter and extraction solvents using FT-ICR MS, Mar. Chem., 124, 100–107, 2011.

Goldberg, S. J., Carlson, C. A., Hansell, D. A., Nelson, N. B., and Siegel, D. A.: Temporal dynamics of dissolved combined neutral sugars and the quality of dissolved organic matter in the Northwestern Sargasso Sea, Deep-Sea Res. I., 56, 672–685, 2009.

Gonsior, M., Peake, B. M., Cooper, W. T., Podgorski, D. C., D'Andrilli, J., Dittmar, T., and Cooper, W. J.: Characterization of dissolved organic matter across the Subtropical Convergence off the South Island, New Zealand, Mar. Chem., 123, 99–110, 2011.

Hansell, D. A. and Carlson, C. A.: Deep-ocean gradients in the concentration of dissolved organic carbon, Nature, 395, 263–266, 1998.

Hansell, D. A., Carlson, C. A., Repeta, D. J., and Schlitzer, R.: Dissolved organic matter in the ocean, Oceanogr., 22, 202–211, 2009.

Hansell, D. A., Carlson, C. A., and Schlitzer, R.: Net removal of major marine dissolved organic carbon fractions in the subsurface ocean, Global Biogeochem. Cy., 26, GB1016, doi:10.1029/2011GB004069, 2012.

Hedges, J. I.: Global biogeochemical cycles: progress and problems, Mar. Chem., 39, 67–93, 1992.

Hertkorn, N., Benner, R., Frommberger, M., Schmitt-Kopplin, P., Witt, M., Kaiser, K., Kettrup, A., and Hedges, J. I.: Characterization of a major refractory component of marine dissolved organic matter, Geochim. Cosmochim. Acta, 70, 2990–3010, 2006.

Hertkorn, N., Ruecker, C., Meringer, M., Gugisch, R., Frommberger, M., Perdue, E. M., Witt, M., and Schmitt-Kopplin, P.: High-precision frequency measurements: indispensable tools at the core of the molecular-level analysis of complex systems, Anal. Bioanal. Chem., 389, 1311–1327, 2007.

Hertkorn, N., Harir, M., Koch, B. P., Michalke, B., Grill, P., and Schmitt-Kopplin, P.: High field NMR spectroscopy and FTICR mass spectrometry: powerful discovery tools for the molecular level characterization of marine dissolved organic matter from the South Atlantic Ocean, Biogeosciences Discuss., 9, 745–833, doi:10.5194/bgd-9-745-2012, 2012.

Jiao, N., Herndl, G. J., Hansell, D. A., Benner, R., Kattner, G., Wilhelm, S. W., Kirchman, D., Weinbauer, M. G., Luo, T., Chen, F., and Azam, F.: Microbial production of recalcitrant dissolved organic matter: long-term carbon storage in the global ocean, Nature Rev. Microbiol., 8, 593–599, 2010.

Kaiser, K. and Benner, R.: Determination of amino sugars in environmental samples with high salt content by high-performance anion-exchange chromatography and pulsed amperometric detection, Anal. Chem., 72, 2566–2572, 2000.

Kaiser, K. and Benner, R.: Biochemical composition and size distribution of organic matter at the Pacific and Atlantic time-series stations, Mar. Chem., 113, 63–77, 2009.

Kim, S., Simpson, A. J., Kujawinski, E. B., Freitas, M. A., and Hatcher, P. G.: High resolution electrospray ionization mass spectrometry and 2D solution NMR for the analysis of DOM extracted by C18 solid phase disk, Org. Geochem., 34, 1324–1335, 2003.

Kirchman, D. L.: Leucine incorporation as a measure of biomass production by heterotrophic bacteria, in: Handbook of Methods in Aquatic Microbial Ecology, edited by: Kemp, P. F., Sherr, B. F., Sherr, B. E., Cole, J. J, Boca Raton: Lewis Publishers, 509–512, 1993.

Koch, B. P., Witt, M. R., Engbrodt, R., Dittmar, T., and Kattner, G.: Molecular formulae of marine and terrigenous dissolved organic matter detected by electrospray ionization Fourier transform ion cyclotron resonance mass spectrometry, Geochim. Cosmochim. Acta, 69, 3299–3308, 2005.

Koch, B. P., Dittmar, T., Witt, M., and Kattner, G.: Fundamentals of molecular formula assignment to ultrahigh resolution mass data of natural organic matter, Anal. Chem., 79, 1758–1763, 2007.

Kujawinski, E. B., Longnecker, K., Blough, N. V., Del Vecchio, R., Finlay, L., Kitner, J. B., and Giovannoni, S. J.: Identification of possible source markers in marine dissolved organic matter using ultra high resolution mass spectrometry, Geochim. Cosmochim. Acta, 73, 4384–4399, 2009.

Loh, A. N., Bauer, J. E., and Druffel, E. R. M.: Variable ageing and storage of dissolved organic components, Nature, 430, 877–881, 2004.

Ogawa, H. and Tanoue, E..: Dissolved organic matter in oceanic waters, J. Oceanogr., 59, 129–147, 2003.

Ogawa, H., Fukuda, R., and Koike, I.: Vertical distributions of dissolved organic carbon and nitrogen in the Southern Ocean, Deep-Sea Res. I, 46, 1809–1826, 1999.

Ogawa, H., Amagai, Y., Koike, I., Kaiser, K., and Benner, R.: Production of refractory dissolved organic matter by bacteria, Science, 292, 917–920, 2001.

Piontek, J., Händel, N., Langer, G., Wohlers, J., Riebesell, U.,and Engel, A.: Effects of rising temperature on the formation and microbial degradation of marine diatom aggregates, Aquat. Microb. Ecol., 54, 305–318 2009.

Piontek, J., Lunau, M., Händel, N., Borchard, C., Wurst, M., and Engel, A.: Acidification increases microbial polysaccharide degradation in the ocean, Biogeosci., 7, 1615–1624, 2010.

Repeta, D. J. and Aluwihare, L. I.: Radiocarbon analysis of neutral sugars in high-molecular-weight dissolved organic carbon: implications for organic carbon cycling, Limnol. Oceanogr., 51, 1045–1053, 2006.

Santschi, P. H., Guo, L. D., Baskaran, M., Trumbore, S., Southon, J., Bianchi, T. S., Honeyman, B., and Cifuentes, L.: Isotopic evidence for the contemporary origin of high-molecular weight organic matter in oceanic environments, Geochim. Cosmochim. Acta, 59, 625–631, 1995.

Schmidt, F., Elvert, M., Koch, B. P., Witt, M., and Hinrichs, K.-U.: Molecular characterization of dissolved organic matter in pore water of continental shelf sediments, Geochim. Cosmochim. Acta, 73, 3337–3358, 2009.

Sleighter, R. L. and Hatcher, P. G.: Molecular characterization of dissolved organic matter (DOM) along a river to ocean transect of the lower Chesapeake Bay by ultrahigh resolution electrospray ionization Fourier transform ion cyclotron resonance mass spectrometry, Mar. Chem., 110, 140–152, 2008.

Smith, D. C. and Azam, F.: A simple, economical method for measuring bacterial protein synthesis rates in seawater using ^{3}H-leucine, Mar. Microb. Food Webs, 6, 107–114, 1992.

Sofer, Z.: Preparation of carbon dioxide for stable carbon isotope analysis of petroleum fractions, Anal. Chem., 52, 1389–1391, 1980.

Stenson, A. C., Marshall, A. G., and Cooper, W. T.: Exact masses and chemical formulas of individual Suwanee river fulvic acids from ultrahigh resolution electrospray ionisation Fourier transform ion cyclotron resonance mass spectra, Anal. Chem., 75, 1275–1284, 2003.

Stuiver, M. and Polach, H. A.: Discussion: Reporting of ^{14}C data, Radiocarb., 19, 355–363, 1977.

Tans, P., NOAA/ESRL; available at: www.esrl.noaa.gov/gmd/ccgg/trends, 2010.

Taylor, B. B., Torrecilla, E., Bernhardt, A., Taylor, M. H., Peeken, I., Röttgers, R., Piera, J., and Bracher, A.: Bio-optical provinces in the eastern Atlantic Ocean and their biogeographical relevance, Biogeosciences, 8, 3609–3629, doi:10.5194/bg-8-3609-2011, 2011.

Vogel, J. S., Nelson, D. E., and Southon, J. R.: ^{14}C background levels in an accelerator mass spectrometry system, Radiocarb., 29, 323–333, 1987.

Williams, P. M. and Druffel, E. R. M.: Radiocarbon in dissolved organic matter in the central North Pacific Ocean, Nature, 330, 246–248, 1987.

Witt, M., Fuchser, J., and Koch, B. P.: Fragmentation studies of fulvic acids using collision induced dissociation Fourier transform ion cyclotron resonance mass spectrometry, Anal. Chem., 81, 2688–2694, 2009.

Supporting information for manuscript 5: Molecular transformation and degradation of refractory dissolved organic matter and role of the Weddell Sea for global carbon cycling

Oliver J. Lechtenfeld,[1] Boris P. Koch,[1,2,*] Ruth Flerus,[1,#] S. Leigh McCallister,[3] Philippe Schmitt-Kopplin,[4,5] and Gerhard Kattner[1]

[1] Alfred Wegener Institute for Polar and Marine Research, Ecological Chemistry, Am Handelshafen 12, D-27570 Bremerhaven, Germany

[2] University of Applied Sciences, An der Karlstadt 8, D-27568 Bremerhaven, Germany

[3] Virginia Commonwealth University, Department of Biology, Center for Environmental Studies, 1000 West Cary Street, Richmond, Virginia 23284, USA

[4] Helmholtz Zentrum München, German Research Center for Environmental Health, Analytical BioGeoChemistry, Ingolstädter Landstraße 1, D-85764 Neuherberg, Germany

[5] Technische Universität München, Chair of analytical food chemistry, Alte Akademie 10, D-85354 Freising, Germany

[#] Present address: GEOMAR Helmholtz Centre for Ocean Research, Biological Oceanography, Düsternbrooker Weg 20, D-24105 Kiel, Germany

[*] To whom correspondence should be addressed: E-mail: boris.koch@awi.de

Text SI

Outliers. We had to exclude different outliers at different stages of the model calculations. First, there were two out of 206 FT-ICR mass spectra that showed abnormal low total intensities, resulting in a low number of assigned peaks. For 13 samples where the FT-ICR mass spectrum was included in the data set, no DOC concentration was measured, these samples were excluded from the model (7 East Atlantic and 6 Southern Ocean samples). In the DOC concentration vs. age plot (main text Figure VI.5-3), a total of 6 samples were excluded deviating from the overall regression pattern (tested with a two step iterative regression starting with all samples). These samples were also excluded from the model calculation (4 East Atlantic and 2 Southern Ocean samples).

Figures SI

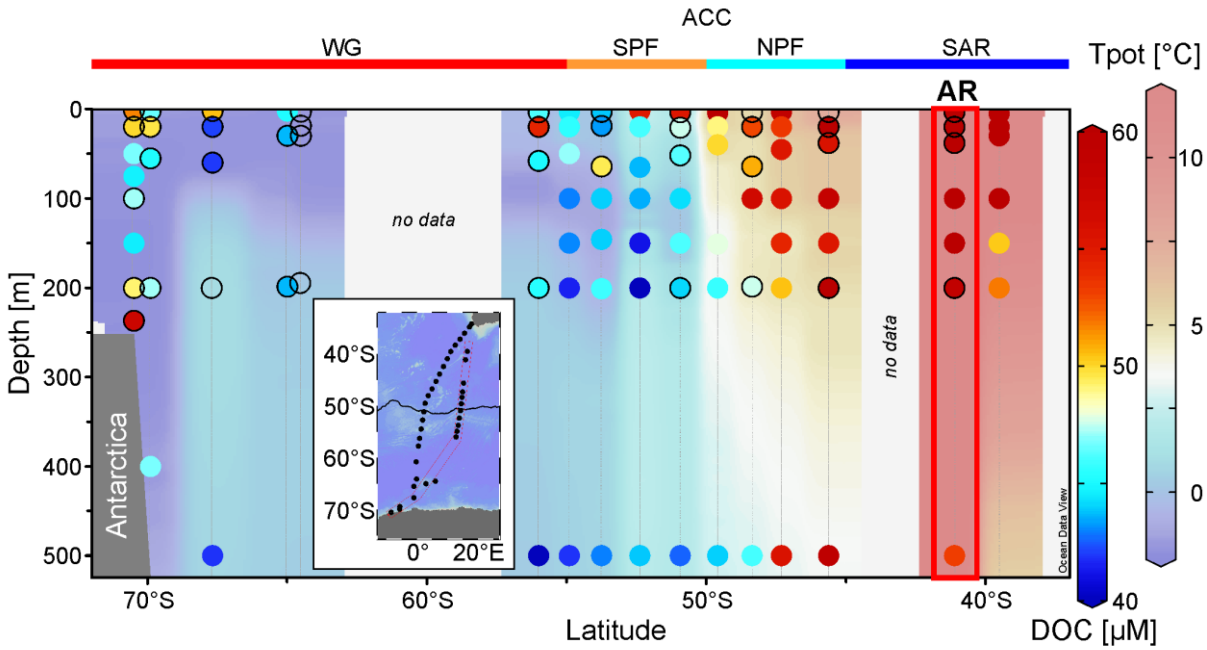

Figure S1. Upper 500 m potential temperature (Tpot, background gridded light colors) and DOC concentration (µM, dark color dots) of the Weddell Sea between 37 and 72° S along the eastern section shown in the small insert. Sampling depths for SPE-DOM are marked with black circles. The geographical grouping follows the description in the main article and Figure VI.5-1 with the red box indicating the warm Agulhas ring (AR) station.

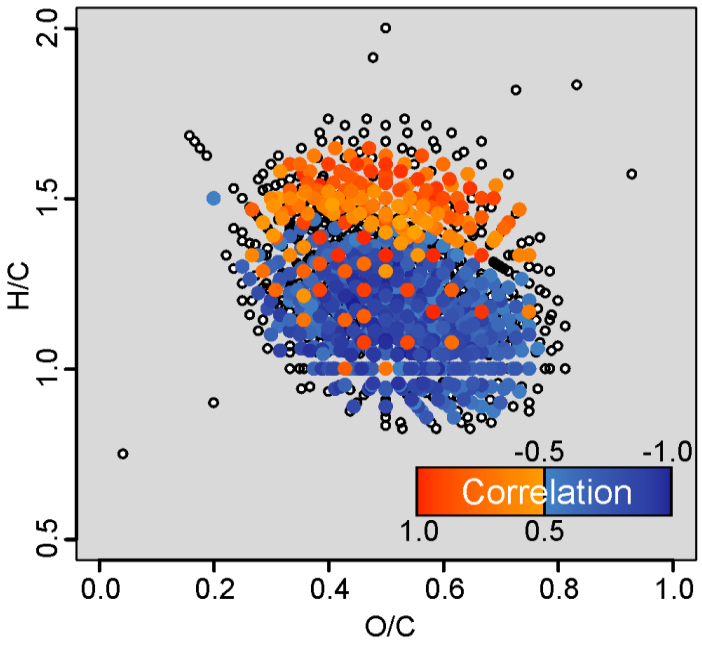

Figure S2. All FT-ICR MS masses used in the combined age model AM^{EA+SO} to calculate the SPE-DOM $\Delta^{14}C$ values. 187 POS (red) and 633 NEG (blue) masses encompass the full range of molecular oxygen to carbon (O/C) and hydrogen to carbon (H/C) ratios, defined by all peaks from all 197 samples (peaks present in ≥ 25 samples, small dots, n = 1,725). Darker colors refer to a higher correlation coefficient r between normalized peak magnitude and $\Delta^{14}C$ value of the sample and only peaks with $|r| \geq 0.5$ were considered for the model.

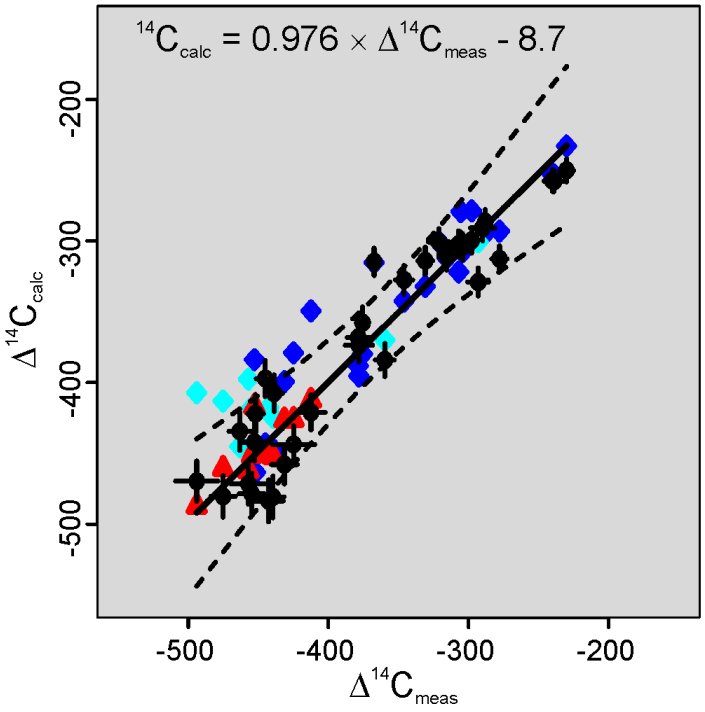

Figure S3. Comparison of the three age models AM^{EA}_{ext}, AM^{SO} and AM^{EA+SO}; calculated ($\Delta^{14}C_{calc}$) vs. measured ($\Delta^{14}C_{meas}$) values of 34 SPE-DOM radiocarbon samples. The original model AM^{EA} (blue, n_s = 24) was extended to the Southern Ocean (SO) samples, using the same POS and NEG masses (AM^{EA}_{ext}, cyan, approach **a**). Only the new SPE-DOM $\Delta^{14}C_{meas}$ values were used to construct an age model for the 60 SO samples (AM^{SO}, red, n_s = 10, approach **b**). All SPE-DOM $\Delta^{14}C_{meas}$ values were combined for the AM^{EA+SO} model (black circles, n_s = 34, approach **c**). Error bars indicate $\Delta^{14}C_{meas}$-SD or model $\Delta^{14}C_{calc}$-SEM and the model II regression fit and equation for AM^{EA+SO} is shown with 95% confidence intervals (black curves, only AM^{EA+SO}).

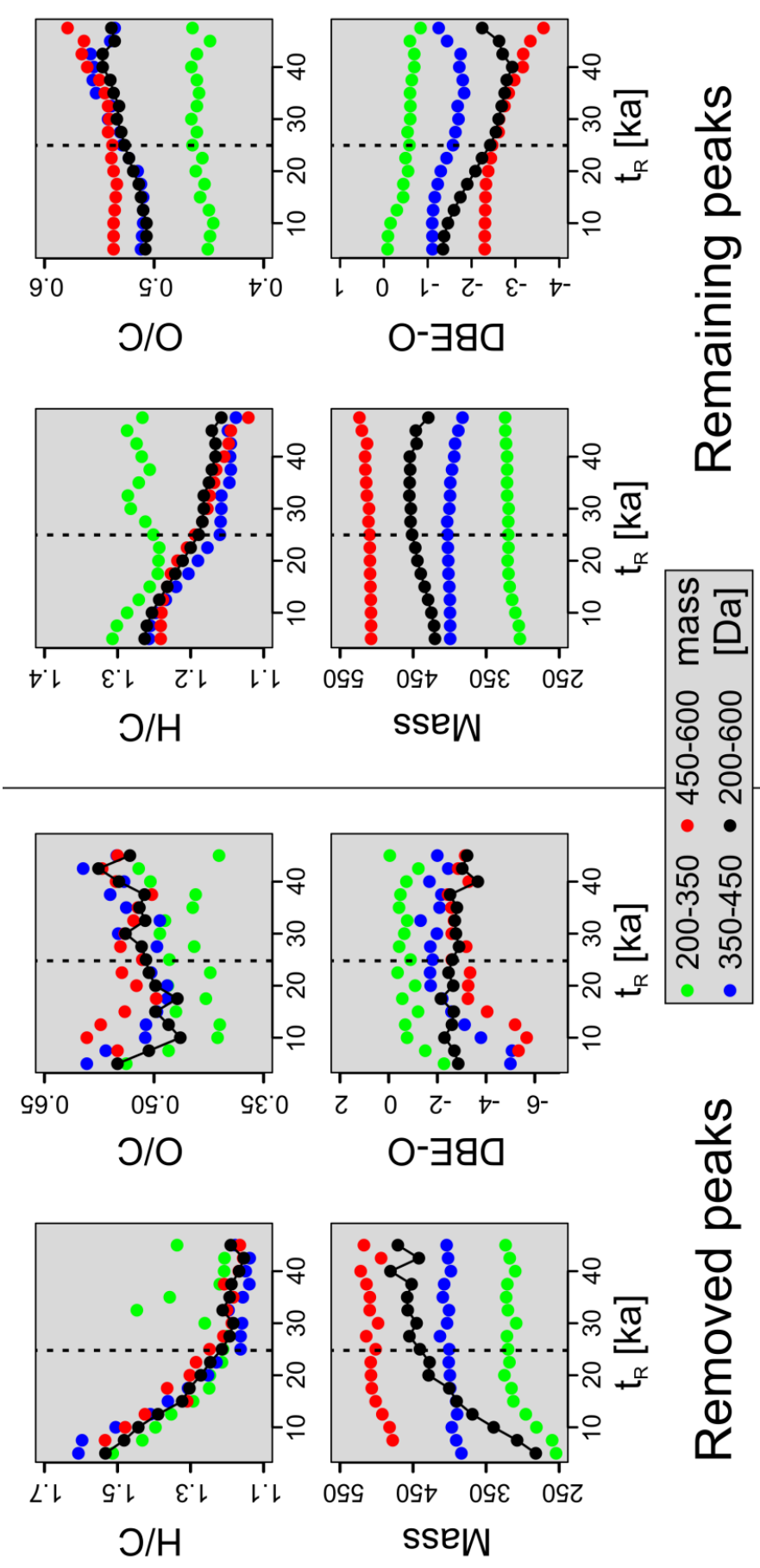

Figure S4. Trends of mean molecular mass, H/C and O/C ratios and DBE-O for all peaks with an assigned residence time t_R (n = 1,664). Starting from 5,000 a, peaks were removed in 2,500 a steps from the data set (number of peaks per step: 20 – 180) and the mean values for the removed (left) and remaining (right) peaks were calculated. All peaks were further divided in molecular mass bins (200 – 350: green, 350 – 450; blue, 450 – 600: red) to account for the different trends in the full mass range (200 – 600: black). The dashed line represents the calculated residence time of DOC, t_{DOC} (~24 ka). While only small changes in the removed peaks after t_{DOC} occur, the trend of the mean values of the remaining peaks still persists. DBE-O is the sum of all rings plus double bonds minus the number of oxygen atoms in a molecular formula. Negative values indicate that not all oxygen atoms are bound in carboxylic groups.

Table S1. Mean physico-chemical parameters of selected water masses (abbreviations see main text). Weddell gyre (WG) water mass definitions according to Foldvik et al. (1985) shown with salinity (S) ranges. For the Antarctic Circumpolar Current (ACC), only the means of the upper 200 m are shown because no deeper samples were extracted for FT-ICR MS. The nutrients (nitrate, phosphate, silicate) were depleted on the Antarctic shelf throughout the whole water column (nitrate < 30 µM, phosphate < 2 µM) compared to deep Weddell Gyre values. Nitrate and phosphate concentrations were also lower in the top 20 to 50 m within the Weddell Gyre (AASW), but the distribution was patchy. Further north nitrate and phosphate depletion was observed down to 150 m in the SPF, but the DOC concentrations in this layer were insignificantly higher than in deeper waters. Pronounced surface depletion of nitrate and phosphate occurred in the NPF coinciding with the increased subsurface DOC concentrations at these stations.

			ACC		WG			
	SAR (0 – 200 m) 35 to 45° S	AR (0 – 200 m) 41° S, 16° E	NPF (0 – 200 m) 45 to 50° S	SPF (0 – 200 m) 50 to 55° S	AASW (S ≤ 34.3)	LSSW (34.28 ≤ S ≤ 34.44)	WDW (34.64 ≤ S ≤ 34.72)	WSDW (34.64 ≤ S ≤ 34.68)
T [°C]	15.0 ± 4.2	16.4 ± 3.2	5.0 ± 1.3	0.6 ± 1.2	-1.4 ± 0.4	-1.8 ± 0.1	0.5 ± 0.3	-0.5 ± 0.2
DOC [µM]	55.6 ± 11.5	65.8 ± 8.5	53.0 ± 5.0	45.7 ± 3.7	47.5 ± 3.0	47.5 ± 5.4	43.0 ± 2.1	44.0 ± 4.4
Nitrate [µM]	5.4 ± 6.5	4.6 ± 6.2	21.8 ± 2.8	28.8 ± 3.4	26.1 ± 3.8	29.3 ± 2.0	33.6 ± 1.1	33.8 ± 0.6
Silicate [µM]	3.3 ± 3.0	3.9 ± 2.9	6.9 ± 2.7	53.9 ± 22.6	69.3 ± 8.3	64.4 ± 8.5	109.9 ± 9.5	123.2 ± 3.4
Phosphate [µM]	0.4 ± 0.4	0.3 ± 0.4	1.4 ± 0.2	1.9 ± 0.2	1.9 ± 0.2	2.1 ± 0.0	2.2 ± 0.0	2.2 ± 0.0
DOC/DON	17.4 ± 3.7	18.7 ± 2.0	24.0 ± 10.9	17.0 ± 9.2	14.9 ± 8.8	17.6 ± 12.9	17.4 ± 5.4	23.1 ± 11.7

Table S2. Sample location and depth and weighted average (wa) FT-ICR MS parameter for the 60 Southern Ocean samples: Molecular hydrogen to carbon (H/C), oxygen to carbon (O/C), nitrogen to carbon (N/C) and sulfur to carbon (S/C) ratios and molecular degradation index I_{DEG} (Flerus et al. 2012).

Latitude [°S]	Longitude [°E]	Depth [m]	Assigned peaks	wa mass [Da]	wa H/C	wa O/C	wa N/C	wa S/C	I_{DEG}
17.2	-34.8	11	1507	406.7	1.260	0.506	0.011	0.002	0.653
15.6	-36.0	11	1493	407.8	1.261	0.508	0.011	0.002	0.643
14.1	-37.2	11	1500	406.7	1.263	0.509	0.011	0.002	0.623
12.5	-38.3	11	1522	406.9	1.255	0.511	0.011	0.002	0.635
11.1	-39.5	11	1484	408.5	1.252	0.512	0.011	0.002	0.660
9.9	-40.9	11	1469	408.0	1.256	0.509	0.011	0.002	0.655
8.7	-42.4	11	1427	409.4	1.250	0.511	0.011	0.001	0.674
7.5	-43.9	11	1440	410.2	1.253	0.510	0.011	0.002	0.677
4.9	-46.7	11	1439	411.6	1.248	0.511	0.011	0.001	0.697
3.7	-48.0	11	1436	410.9	1.249	0.510	0.011	0.001	0.694
2.3	-51.1	11	1429	409.5	1.239	0.516	0.011	0.002	0.715
1.9	-52.7	11	1413	409.3	1.238	0.514	0.011	0.002	0.731
1.4	-54.5	11	1417	409.2	1.241	0.515	0.011	0.002	0.723
0.9	-56.2	11	1415	409.3	1.239	0.515	0.011	0.002	0.735
0.5	-57.8	11	1421	410.3	1.243	0.512	0.010	0.002	0.730
-0.2	-60.8	1	1373	406.8	1.240	0.509	0.011	0.001	0.734
-0.1	-64.1	1	1394	407.8	1.241	0.511	0.011	0.002	0.735
-5.5	-69.4	1	1395	408.3	1.244	0.512	0.011	0.002	0.723
-8.4	-70.5	1	1379	406.2	1.240	0.514	0.011	0.002	0.725
-8.4	-70.5	20	1406	406.4	1.238	0.513	0.011	0.002	0.725
-8.4	-70.5	100	1381	406.3	1.241	0.512	0.011	0.002	0.724
-8.4	-70.5	200	1397	407.1	1.240	0.512	0.011	0.002	0.729
-8.4	-70.5	237	1407	408.3	1.240	0.512	0.011	0.002	0.722
-5.5	-69.9	2	1351	402.6	1.242	0.510	0.011	0.001	0.707
-5.5	-69.9	20	1355	406.2	1.238	0.510	0.011	0.002	0.717
-5.5	-69.9	55	1375	406.4	1.239	0.510	0.011	0.002	0.721
-5.5	-69.9	200	1385	406.9	1.241	0.512	0.011	0.001	0.717
-5.5	-69.9	800	1377	407.7	1.239	0.512	0.011	0.001	0.733
-5.5	-69.9	1975	1364	407.8	1.236	0.512	0.011	0.001	0.741
-1.0	-67.7	2	1371	406.5	1.240	0.510	0.011	0.002	0.722
-1.0	-67.7	20	1365	410.3	1.239	0.510	0.011	0.001	0.748
-1.0	-67.7	60	1386	407.7	1.234	0.509	0.011	0.001	0.734
-1.0	-67.7	1996	1379	407.2	1.237	0.509	0.012	0.001	0.733

Latitude [°S]	Longitude [°E]	Depth [m]	Assigned peaks	wa mass [Da]	wa H/C	wa O/C	wa N/C	wa S/C	I_{DEG}
-1.0	-67.7	4528	1346	407.2	1.239	0.510	0.011	0.001	0.729
-1.0	-65.0	20	1381	405.8	1.240	0.509	0.011	0.002	0.723
-1.0	-65.0	200	1370	406.1	1.235	0.509	0.011	0.001	0.735
3.0	-65.0	2	1311	399.4	1.249	0.503	0.012	0.001	0.706
3.0	-65.0	30	1342	402.5	1.249	0.500	0.011	0.001	0.710
3.0	-65.0	199	1334	403.8	1.244	0.503	0.011	0.001	0.724
12.8	-56.0	3	1349	401.3	1.244	0.510	0.012	0.002	0.717
12.8	-56.0	20	1357	403.1	1.241	0.510	0.011	0.002	0.719
12.8	-56.0	58	1386	402.6	1.241	0.509	0.012	0.002	0.713
12.8	-56.0	200	1351	403.5	1.238	0.514	0.012	0.002	0.736
13.5	-53.8	3	1355	401.9	1.248	0.506	0.011	0.001	0.710
13.5	-53.8	19	1323	399.5	1.250	0.503	0.012	0.001	0.704
13.5	-53.8	64	1308	397.2	1.258	0.490	0.012	0.001	0.694
14.2	-50.9	3	1391	401.8	1.244	0.512	0.012	0.002	0.711
14.2	-50.9	21	1342	400.3	1.246	0.512	0.011	0.002	0.705
14.2	-50.9	52	1345	403.9	1.240	0.508	0.011	0.001	0.711
14.2	-50.9	200	1359	403.2	1.244	0.512	0.011	0.001	0.726
14.7	-48.4	3	1395	401.3	1.247	0.511	0.012	0.002	0.685
14.7	-48.4	20	1334	397.9	1.257	0.498	0.012	0.001	0.665
14.7	-48.4	64	1326	397.8	1.255	0.500	0.012	0.001	0.670
14.7	-48.4	199	1348	400.2	1.249	0.511	0.011	0.001	0.685
15.2	-45.6	20	1410	400.3	1.251	0.508	0.011	0.002	0.671
15.2	-45.6	38	1398	400.6	1.251	0.510	0.011	0.002	0.673
15.9	-41.1	3	1424	391.3	1.259	0.511	0.012	0.002	0.589
15.9	-41.1	20	1443	392.4	1.260	0.510	0.012	0.002	0.591
15.9	-41.1	38	1420	391.6	1.258	0.511	0.012	0.002	0.596
15.9	-41.1	200	1404	397.9	1.254	0.512	0.011	0.002	0.625

Table S3. Summary of the age model (**a** – **c**) comparison. Three different subsets of $\Delta^{14}C_{meas}$ values were used to construct the age models (only EA: AM^{EA}_{ext} (**a**), only SO: AM^{SO} (**b**), and combined data set: AM^{EA+SO} (**c**)). Different significance levels *p* (corresponding to an r_{min}) were used to account for the different number of samples in each model. Each model was constructed with a set of positive (POS) and negative (NEG) correlating peaks and the model results ($\Delta^{14}C_{calc}$) compared to the training data $\Delta^{14}C_{meas}$. The goodness of the fit was tested with a model II regression (DF refers to the total number of observations minus number of fit parameters) and expressed as Pearson's correlation coefficient *r*, slope (perfect fit: 1) and intercept (perfect fit: 0). The last column shows the goodness of fit parameters between measured and calculated values, if the AM^{EA} and AM^{SO} model results were independently applied to both sample sets and thereafter combined (AM^{EA}+AM^{SO}). The regression yielded similar parameters to the combined model **c** but it was not used further as both individual models combine different peaks for the calculation, different samples sizes and different age and error ranges.

Age model (required # of samples/peak)	AM^{EA}_{ext} (**a**) (≥20)	AM^{SO} (**b**) (=10)	AM^{EA+SO} (**c**) (≥25)	AM^{EA}+AM^{SO}
r_{min} for correlation peak magnitude vs. $\Delta^{14}C_{meas}$	±0.56 ($p < 0.01$)	±0.65 ($p < 0.05$)	±0.5 ($p < 0.01$)	
# all peaks with $r > r_{min}$	677	152	820	
# POS / # NEG peaks	233/444	52/46	187/633	
Correlation coef. *r* ($\Delta^{14}C_{meas}$ vs. $\Delta^{14}C_{calc}$)	0.933 ($p < 0.001$)	0.833 ($p < 0.005$)	0.950 ($p < 0.001$)	0.979 ($p < 0.001$)
Degrees of freedom (DF)	32	8	32	32
Slope ($\Delta^{14}C_{meas}$ vs. $\Delta^{14}C_{calc}$)	0.818	0.965	0.976	0.993
Intercept ($\Delta^{14}C_{meas}$ vs. $\Delta^{14}C_{calc}$)	-52.4	-15.6	-8.7	-2.4

Table S4. DOC degradation rates and predicted DOC ages ($\Delta^{14}C_{pred}$) for the North Central Pacific (NCP). For predicting the age of the remaining DOC when SPE-DOC concentration is < 1 µM C, ordinary least squares (OLS) regression was used. DOC values were corrected for outliers. A comparison of the regression [DOC] vs. age using only the 34 $\Delta^{14}C_{meas}$ values yielded a nearly identical DOC degradation rate and predicted residence times. Using only the data from the East Atlantic resulted in substantially lower calculated age of the NCP DOC, consistent with observation of the apparent age difference $DO^{14}C$ and $DI^{14}C$ between Sargasso Sea and North Central Pacific (Bauer 2002).

SPE-DOM data	Degrees of freedom	Correlation log([DOC]) vs. age	intercept a^0_{DOC} at t = 0 a	decay rate k_{DOC} [a^{-1}]	NCP (34 µM DOC) age and $\Delta^{14}C_{pred}$	SPE-DOM decay to 1 µM DOC age and $\Delta^{14}C_{pred}$
only measured values (two outliers)	30	-0.82 ($p < 10^{-4}$)	129 ± 1	2.18×10^{-4} $\pm 1.9\times10^{-5}$	6,400 ± 660 a -549 ± 37‰	24,400 ± 2,500 a 952 ± 15‰
calculated values (six outliers)	185	-0.86 ($p < 10^{-4}$)	131 ± 1	2.23×10^{-4} $\pm 8.7\times10^{-6}$	6,410 ± 290 a -553 ± 16‰	24,400 ± 1,100 a 953 ± 7‰
calculated values, only East Atlantic	120	-0.88 ($p < 10^{-4}$)	168 ± 1	3.12×10^{-4} $\pm 1.4\times10^{-5}$	5,350 ± 270 a -486 ± 18‰	18,100 ± 920 a 894 ± 12‰

Table S5. Exact masses and molecular formulas of the Southern Ocean ultra refractory (SOUR) compounds. Three hundred thirty-nine peaks were identified in the Southern Ocean samples that possibly contribute to an increased DOC concentration compared to the standard model of DOC degradation with overturning circulation.

Molecular formula	IUPAC Mass	Molecular formula	IUPAC Mass	Molecular formula	IUPAC Mass
$C_{10}H_{15}N_1O_2S_1$	213.082349	$C_{14}H_{16}O_{10}$	344.074347	$C_{18}H_{16}O_9$	376.079432
$C_{14}H_{16}O_4$	248.104859	$C_{19}H_{20}O_6$	344.125988	$C_{15}H_{20}O_9S_1$	376.082803
$C_{14}H_{20}O_4$	252.136159	$C_{16}H_{24}O_8$	344.147118	$C_{19}H_{20}O_8$	376.115818
$C_{13}H_{20}O_5$	256.131074	$C_{17}H_{28}O_7$	344.183503	$C_{16}H_{24}O_8S_1$	376.119188
$C_{12}H_{18}O_6$	258.110338	$C_{14}H_{18}O_8S_1$	346.072238	$C_{18}H_{20}N_2O_7$	376.127051
$C_{14}H_{16}O_5$	264.099774	$C_{18}H_{18}O_7$	346.105253	$C_{16}H_{24}O_{10}$	376.136947
$C_{13}H_{14}O_6$	266.079038	$C_{19}H_{22}O_6$	346.141638	$C_{20}H_{24}O_7$	376.152203
$C_{13}H_{16}O_6$	268.094688	$C_{20}H_{26}O_5$	346.178024	$C_{21}H_{28}O_6$	376.188589
$C_{14}H_{20}O_5$	268.131074	$C_{17}H_{17}N_1O_7$	347.100502	$C_{18}H_{19}N_1O_8$	377.111067
$C_{14}H_{22}O_5$	270.146724	$C_{18}H_{21}N_1O_6$	347.136887	$C_{19}H_{23}N_1O_7$	377.147452
$C_{14}H_{14}O_6$	278.079038	$C_{17}H_{16}O_8$	348.084518	$C_{17}H_{14}O_{10}$	378.058697
$C_{15}H_{18}O_5$	278.115424	$C_{14}H_{20}O_8S_1$	348.087888	$C_{14}H_{18}O_{10}S_1$	378.062068
$C_{14}H_{18}N_2O_4$	278.126657	$C_{16}H_{16}N_2O_7$	348.095751	$C_{18}H_{18}O_9$	378.095082
$C_{16}H_{22}O_4$	278.151809	$C_{18}H_{20}O_7$	348.120903	$C_{15}H_{22}O_9S_1$	378.098453
$C_{14}H_{17}N_1O_5$	279.110673	$C_{17}H_{20}N_2O_6$	348.132136	$C_{19}H_{22}O_8$	378.131468
$C_{13}H_{14}O_7$	282.073953	$C_{19}H_{24}O_6$	348.157289	$C_{18}H_{22}N_2O_7$	378.142701
$C_{14}H_{18}O_6$	282.110338	$C_{20}H_{28}O_5$	348.193674	$C_{20}H_{26}O_7$	378.167853
$C_{13}H_{18}N_2O_5$	282.121572	$C_{16}H_{15}N_1O_8$	349.079767	$C_{21}H_{30}O_6$	378.204239
$C_{15}H_{22}O_5$	282.146724	$C_{17}H_{19}N_1O_7$	349.116152	$C_{18}H_{21}N_1O_8$	379.126717
$C_{13}H_{16}O_7$	284.089603	$C_{18}H_{23}N_1O_6$	349.152538	$C_{17}H_{16}O_{10}$	380.074347
$C_{14}H_{20}O_6$	284.125988	$C_{17}H_{18}O_8$	350.100168	$C_{14}H_{20}O_{10}S_1$	380.077718
$C_{15}H_{24}O_5$	284.162374	$C_{14}H_{22}O_8S_1$	350.103538	$C_{16}H_{16}N_2O_9$	380.08558
$C_{13}H_{19}N_1O_6$	285.121237	$C_{16}H_{18}N_2O_7$	350.111401	$C_{18}H_{20}O_9$	380.110732
$C_{16}H_{18}O_5$	290.115424	$C_{18}H_{22}O_7$	350.136553	$C_{17}H_{20}N_2O_8$	380.121966
$C_{17}H_{22}O_4$	290.151809	$C_{17}H_{22}N_2O_6$	350.147786	$C_{19}H_{24}O_8$	380.147118
$C_{15}H_{16}O_6$	292.094688	$C_{19}H_{26}O_6$	350.172939	$C_{18}H_{24}N_2O_7$	380.158351
$C_{16}H_{20}O_5$	292.131074	$C_{16}H_{17}N_1O_8$	351.095417	$C_{20}H_{28}O_7$	380.183503
$C_{11}H_{18}O_7S_1$	294.077324	$C_{16}H_{16}O_9$	352.079432	$C_{16}H_{15}N_1O_{10}$	381.069596
$C_{15}H_{21}N_1O_5$	295.141973	$C_{15}H_{16}N_2O_8$	352.090666	$C_{18}H_{23}N_1O_8$	381.142367
$C_{14}H_{16}O_7$	296.089603	$C_{17}H_{20}O_8$	352.115818	$C_{17}H_{18}O_{10}$	382.089997
$C_{15}H_{20}O_6$	296.125988	$C_{16}H_{20}N_2O_7$	352.127051	$C_{18}H_{22}O_9$	382.126382
$C_{16}H_{24}O_5$	296.162374	$C_{18}H_{24}O_7$	352.152203	$C_{17}H_{22}N_2O_8$	382.137616
$C_{14}H_{18}O_7$	298.105253	$C_{19}H_{28}O_6$	352.188589	$C_{19}H_{26}O_8$	382.162768
$C_{15}H_{22}O_6$	298.141638	$C_{15}H_{15}N_1O_9$	353.074681	$C_{20}H_{30}O_7$	382.199153
$C_{16}H_{16}O_6$	304.094688	$C_{16}H_{19}N_1O_8$	353.111067	$C_{18}H_{25}N_1O_8$	383.158017
$C_{17}H_{20}O_5$	304.131074	$C_{15}H_{14}O_{10}$	354.058697	$C_{17}H_{20}O_{10}$	384.105647

Molecular formula	IUPAC Mass	Molecular formula	IUPAC Mass	Molecular formula	IUPAC Mass
$C_{15}H_{14}O_7$	306.073953	$C_{16}H_{18}O_9$	354.095082	$C_{18}H_{24}O_9$	384.142032
$C_{16}H_{18}O_6$	306.110338	$C_{15}H_{18}N_2O_8$	354.106316	$C_{17}H_{24}N_2O_8$	384.153266
$C_{17}H_{22}O_5$	306.146724	$C_{18}H_{26}O_7$	354.167853	$C_{19}H_{28}O_8$	384.178418
$C_{16}H_{21}N_1O_5$	307.141973	$C_{19}H_{30}O_6$	354.204239	$C_{20}H_{32}O_7$	384.214803
$C_{17}H_{24}O_5$	308.162374	$C_{15}H_{17}N_1O_9$	355.090331	$C_{17}H_{23}N_1O_9$	385.137281
$C_{14}H_{18}N_2O_6$	310.116486	$C_{15}H_{16}O_{10}$	356.074347	$C_{18}H_{27}N_1O_8$	385.173667
$C_{14}H_{20}N_2O_6$	312.132136	$C_{15}H_{20}N_2O_8$	356.121966	$C_{16}H_{18}O_9S_1$	386.067153
$C_{16}H_{24}O_6$	312.157289	$C_{18}H_{28}O_7$	356.183503	$C_{17}H_{22}O_8S_1$	386.103538
$C_{16}H_{26}O_6$	314.172939	$C_{15}H_{19}N_1O_9$	357.105981	$C_{17}H_{22}O_{10}$	386.121297
$C_{18}H_{20}O_5$	316.131074	$C_{15}H_{18}O_8S_1$	358.072238	$C_{18}H_{26}O_9$	386.157682
$C_{17}H_{18}O_6$	318.110338	$C_{15}H_{18}O_{10}$	358.089997	$C_{19}H_{30}O_8$	386.194068
$C_{18}H_{22}O_5$	318.146724	$C_{16}H_{22}O_7S_1$	358.108624	$C_{17}H_{25}N_1O_9$	387.152931
$C_{15}H_{16}N_2O_6$	320.100836	$C_{16}H_{22}O_9$	358.126382	$C_{16}H_{20}O_9S_1$	388.082803
$C_{17}H_{20}O_6$	320.125988	$C_{20}H_{22}O_6$	358.141638	$C_{17}H_{24}O_8S_1$	388.119188
$C_{16}H_{20}N_2O_5$	320.137222	$C_{17}H_{26}O_8$	358.162768	$C_{17}H_{24}O_{10}$	388.136947
$C_{15}H_{15}N_1O_7$	321.084852	$C_{14}H_{16}O_{11}$	360.069261	$C_{18}H_{28}O_9$	388.173333
$C_{16}H_{19}N_1O_6$	321.121237	$C_{18}H_{16}O_8$	360.084518	$C_{16}H_{23}N_1O_{10}$	389.132196
$C_{16}H_{18}O_7$	322.105253	$C_{15}H_{20}O_8S_1$	360.087888	$C_{15}H_{18}O_{10}S_1$	390.062068
$C_{15}H_{18}N_2O_6$	322.116486	$C_{19}H_{20}O_7$	360.120903	$C_{19}H_{18}O_9$	390.095082
$C_{17}H_{22}O_6$	322.141638	$C_{16}H_{24}O_7S_1$	360.124274	$C_{16}H_{22}O_9S_1$	390.098453
$C_{16}H_{22}N_2O_5$	322.152872	$C_{16}H_{24}O_9$	360.142032	$C_{20}H_{22}O_8$	390.131468
$C_{18}H_{26}O_5$	322.178024	$C_{20}H_{24}O_6$	360.157289	$C_{17}H_{26}O_8S_1$	390.134839
$C_{15}H_{17}N_1O_7$	323.100502	$C_{17}H_{28}O_8$	360.178418	$C_{19}H_{22}N_2O_7$	390.142701
$C_{16}H_{21}N_1O_6$	323.136887	$C_{14}H_{18}O_9S_1$	362.067153	$C_{17}H_{26}O_{10}$	390.152597
$C_{15}H_{16}O_8$	324.084518	$C_{18}H_{18}O_8$	362.100168	$C_{22}H_{30}O_6$	390.204239
$C_{14}H_{16}N_2O_7$	324.095751	$C_{15}H_{22}O_8S_1$	362.103538	$C_{18}H_{17}N_1O_9$	391.090331
$C_{16}H_{20}O_7$	324.120903	$C_{19}H_{22}O_7$	362.136553	$C_{20}H_{25}N_1O_7$	391.163102
$C_{15}H_{20}N_2O_6$	324.132136	$C_{16}H_{26}O_9$	362.157682	$C_{18}H_{16}O_{10}$	392.074347
$C_{17}H_{24}O_6$	324.157289	$C_{20}H_{26}O_6$	362.172939	$C_{15}H_{20}O_{10}S_1$	392.077718
$C_{18}H_{28}O_5$	324.193674	$C_{17}H_{17}N_1O_8$	363.095417	$C_{19}H_{20}O_9$	392.110732
$C_{14}H_{15}N_1O_8$	325.079767	$C_{17}H_{16}O_9$	364.079432	$C_{16}H_{24}O_9S_1$	392.114103
$C_{15}H_{19}N_1O_7$	325.116152	$C_{14}H_{20}O_9S_1$	364.082803	$C_{18}H_{20}N_2O_8$	392.121966
$C_{16}H_{23}N_1O_6$	325.152538	$C_{18}H_{20}O_8$	364.115818	$C_{20}H_{24}O_8$	392.147118
$C_{14}H_{14}O_9$	326.063782	$C_{17}H_{20}N_2O_7$	364.127051	$C_{19}H_{24}N_2O_7$	392.158351
$C_{15}H_{18}O_8$	326.100168	$C_{19}H_{24}O_7$	364.152203	$C_{19}H_{23}N_1O_8$	393.142367
$C_{14}H_{18}N_2O_7$	326.111401	$C_{18}H_{24}N_2O_6$	364.163437	$C_{15}H_{22}O_{10}S_1$	394.093368
$C_{15}H_{22}N_2O_6$	326.147786	$C_{20}H_{28}O_6$	364.188589	$C_{18}H_{22}N_2O_8$	394.137616
$C_{17}H_{26}O_6$	326.172939	$C_{16}H_{15}N_1O_9$	365.074681	$C_{19}H_{26}N_2O_7$	394.174001
$C_{14}H_{17}N_1O_8$	327.095417	$C_{18}H_{23}N_1O_7$	365.147452	$C_{19}H_{25}N_1O_8$	395.158017

Molecular formula	IUPAC Mass	Molecular formula	IUPAC Mass	Molecular formula	IUPAC Mass
$C_{14}H_{16}O_9$	328.079432	$C_{17}H_{18}O_9$	366.095082	$C_{18}H_{20}O_{10}$	396.105647
$C_{18}H_{18}O_6$	330.110338	$C_{16}H_{18}N_2O_8$	366.106316	$C_{18}H_{24}N_2O_8$	396.153266
$C_{17}H_{16}O_7$	332.089603	$C_{18}H_{22}O_8$	366.131468	$C_{21}H_{32}O_7$	396.214803
$C_{18}H_{20}O_6$	332.125988	$C_{17}H_{22}N_2O_7$	366.142701	$C_{18}H_{23}N_1O_9$	397.137281
$C_{17}H_{19}N_1O_6$	333.121237	$C_{19}H_{26}O_7$	366.167853	$C_{17}H_{22}N_2O_9$	398.13253
$C_{17}H_{18}O_7$	334.105253	$C_{20}H_{30}O_6$	366.204239	$C_{18}H_{25}N_1O_9$	399.152931
$C_{16}H_{18}N_2O_6$	334.116486	$C_{17}H_{21}N_1O_8$	367.126717	$C_{17}H_{20}O_9S_1$	400.082803
$C_{18}H_{22}O_6$	334.141638	$C_{18}H_{25}N_1O_7$	367.163102	$C_{18}H_{24}O_8S_1$	400.119188
$C_{19}H_{26}O_5$	334.178024	$C_{16}H_{16}O_{10}$	368.074347	$C_{19}H_{28}O_9$	400.173333
$C_{16}H_{17}N_1O_7$	335.100502	$C_{15}H_{16}N_2O_9$	368.08558	$C_{17}H_{23}N_1O_{10}$	401.132196
$C_{17}H_{21}N_1O_6$	335.136887	$C_{17}H_{20}O_9$	368.110732	$C_{17}H_{22}O_9S_1$	402.098453
$C_{16}H_{16}O_8$	336.084518	$C_{16}H_{20}N_2O_8$	368.121966	$C_{18}H_{26}O_8S_1$	402.134839
$C_{15}H_{16}N_2O_7$	336.095751	$C_{18}H_{24}O_8$	368.147118	$C_{18}H_{26}O_{10}$	402.152597
$C_{17}H_{20}O_7$	336.120903	$C_{17}H_{24}N_2O_7$	368.158351	$C_{17}H_{24}O_9S_1$	404.114103
$C_{16}H_{20}N_2O_6$	336.132136	$C_{19}H_{28}O_7$	368.183503	$C_{18}H_{28}O_8S_1$	404.150489
$C_{19}H_{28}O_5$	336.193674	$C_{15}H_{15}N_1O_{10}$	369.069596	$C_{18}H_{28}O_{10}$	404.168247
$C_{15}H_{15}N_1O_8$	337.079767	$C_{17}H_{23}N_1O_8$	369.142367	$C_{19}H_{28}O_8S_1$	416.150489
$C_{16}H_{19}N_1O_7$	337.116152	$C_{15}H_{14}O_{11}$	370.053611	$C_{18}H_{28}O_{11}$	420.163162
$C_{17}H_{23}N_1O_6$	337.152538	$C_{17}H_{22}O_9$	370.126382	$C_{23}H_{34}O_7$	422.230453
$C_{15}H_{14}O_9$	338.063782	$C_{16}H_{22}N_2O_8$	370.137616	$C_{20}H_{26}O_9S_1$	442.129753
$C_{16}H_{18}O_8$	338.100168	$C_{18}H_{26}O_8$	370.162768	$C_{20}H_{30}O_9S_1$	446.161053
$C_{15}H_{18}N_2O_7$	338.111401	$C_{19}H_{30}O_7$	370.199153	$C_{21}H_{18}O_{12}$	462.079826
$C_{17}H_{22}O_7$	338.136553	$C_{17}H_{25}N_1O_8$	371.158017	$C_{21}H_{26}O_{10}S_1$	470.124668
$C_{16}H_{22}N_2O_6$	338.147786	$C_{15}H_{16}O_{11}$	372.069261	$C_{20}H_{18}O_{14}$	482.069655
$C_{15}H_{17}N_1O_8$	339.095417	$C_{16}H_{20}O_8S_1$	372.087888	$C_{21}H_{20}O_{14}$	496.085305
$C_{16}H_{21}N_1O_7$	339.131802	$C_{15}H_{20}N_2O_7S_1$	372.099122	$C_{20}H_{20}O_{15}$	500.08022
$C_{15}H_{16}O_9$	340.079432	$C_{16}H_{20}O_{10}$	372.105647	$C_{21}H_{24}O_{12}S_1$	500.098847
$C_{14}H_{16}N_2O_8$	340.090666	$C_{17}H_{24}O_9$	372.142032	$C_{20}H_{22}O_{15}$	502.09587
$C_{16}H_{20}O_8$	340.115818	$C_{18}H_{28}O_8$	372.178418	$C_{21}H_{20}O_{15}$	512.08022
$C_{15}H_{20}N_2O_7$	340.127051	$C_{16}H_{23}N_1O_9$	373.137281	$C_{22}H_{22}O_{15}$	526.09587
$C_{18}H_{28}O_6$	340.188589	$C_{15}H_{18}O_9S_1$	374.067153	$C_{24}H_{22}O_{14}$	534.100955
$C_{14}H_{15}N_1O_9$	341.074681	$C_{19}H_{18}O_8$	374.100168	$C_{23}H_{24}N_2O_{13}$	536.127839
$C_{15}H_{19}N_1O_8$	341.111067	$C_{16}H_{22}O_8S_1$	374.103538	$C_{23}H_{22}O_{15}$	538.09587
$C_{14}H_{14}O_{10}$	342.058697	$C_{16}H_{22}O_{10}$	374.121297	$C_{23}H_{24}O_{15}$	540.11152
$C_{15}H_{18}O_9$	342.095082	$C_{20}H_{22}O_7$	374.136553	$C_{22}H_{22}O_{16}$	542.090785
$C_{14}H_{18}N_2O_8$	342.106316	$C_{17}H_{26}O_9$	374.157682	$C_{22}H_{24}O_{16}$	544.106435
$C_{17}H_{26}O_7$	342.167853	$C_{21}H_{26}O_6$	374.172939	$C_{24}H_{24}O_{16}$	568.106435
$C_{14}H_{17}N_1O_9$	343.090331	$C_{19}H_{21}N_1O_7$	375.131802	$C_{25}H_{26}O_{16}$	582.122085

Hiermit versichere ich,

dass ich die vorliegende Arbeit mit dem Titel "Biogeochemistry of marine dissolved organic matter: molecular composition, reactivity and new methods" selbstständig und ohne unerlaubte fremde Hilfe angefertigt habe. Ich habe keine anderen als die von mir angegebenen Quellen und Hilfsmittel verwendet, sowie die aus benutzen Werken wörtlich oder inhaltlich übernommenen Stellen als solche kenntlich gemacht.

Es erfolgte keine inhaltliche Änderung dieser Version gegenüber der zur Begutachtung vorgelegten Fassung. Diese Fassung wurde lediglich hinsichtlich Formatierung, Orthografie und Grammatik überarbeitet sowie die im Peer-Review Verfahren revidierte und nun zur Publikation akzeptierte Version des dritten Manuskripts übernommen.

Oliver Lechtenfeld